

Point-of-Care Ultrasound for the Neonatal and Pediatric Intensivist

A Practical Guide on
the Use of POCUS

Yogen Singh
Cécile Tissot
María Victoria Fraga
Thomas Conlon
Editors



Point-of-Care Ultrasound for the Neonatal and Pediatric Intensivist

Yogen Singh • Cécile Tissot
María Victoria Fraga • Thomas Conlon
Editors

Point-of-Care Ultrasound for the Neonatal and Pediatric Intensivist

A Practical Guide on the Use
of POCUS

 Springer

Editors

Yogen Singh
Department of Pediatrics
Division of Neonatology
Loma Linda University School of
Medicine
California, CA, USA

María Victoria Fraga
Department of Pediatrics
Division of Neonatology
Children's Hospital of Philadelphia
Perelman School of Medicine
University of Pennsylvania
Philadelphia, PA, USA

Cécile Tissot
Pediatric Cardiology
Hirslanden Clinique des Grangettes
Chene-Bougeries/Geneva, Switzerland

Thomas Conlon
Department of Anesthesiology and
Critical Care Medicine
Perelman School of Medicine, The
University of Pennsylvania
Philadelphia, PA, USA

ISBN 978-3-031-26537-2 ISBN 978-3-031-26538-9 (eBook)
<https://doi.org/10.1007/978-3-031-26538-9>

© The Editor(s) (if applicable) and The Author(s), under exclusive license to Springer Nature Switzerland AG 2023, corrected publication 2023

This work is subject to copyright. All rights are solely and exclusively licensed by the Publisher, whether the whole or part of the material is concerned, specifically the rights of translation, reprinting, reuse of illustrations, recitation, broadcasting, reproduction on microfilms or in any other physical way, and transmission or information storage and retrieval, electronic adaptation, computer software, or by similar or dissimilar methodology now known or hereafter developed. The use of general descriptive names, registered names, trademarks, service marks, etc. in this publication does not imply, even in the absence of a specific statement, that such names are exempt from the relevant protective laws and regulations and therefore free for general use.

The publisher, the authors, and the editors are safe to assume that the advice and information in this book are believed to be true and accurate at the date of publication. Neither the publisher nor the authors or the editors give a warranty, expressed or implied, with respect to the material contained herein or for any errors or omissions that may have been made. The publisher remains neutral with regard to jurisdictional claims in published maps and institutional affiliations.

This Springer imprint is published by the registered company Springer Nature Switzerland AG
The registered company address is: Gewerbestrasse 11, 6330 Cham, Switzerland

“Seeing is believing but eyes see only what your brain knows”

Yogen Singh

Foreword

Understanding pathophysiology to ensure an accurate diagnosis is key to optimizing therapeutic management. Monitoring bedside vital signs such as heart rate, temperature, blood pressure, respiratory rate, and oxygen saturation by pulse oximetry is routine practice in intensive care units (ICUs). Imaging using X-rays is helpful in diagnosing neonatal and pediatric diseases but can only assess anatomical abnormalities, be performed periodically, and involves radiation. It is increasingly recognized that bedside assessment of neonates and children by point-of-care ultrasound (POCUS) provides longitudinal anatomical and physiological assessment of the patient, and the data considerably adds to the clinician's diagnostic accuracy and ability to determine optimal management strategy. In many countries, POCUS is standard of practice, and training in these techniques is part of routine curriculum during neonatal and pediatric critical care fellowship.

The textbook *point-of-Care Ultrasound for the Neonatal and Pediatric Intensivist* by Drs. Singh, Tissot, Fraga, and Conlon is an excellent resource to guide both novice and experienced clinicians new to POCUS and a valuable refresher for the trained expert. The editors and authors have extensive experience in the field and are internationally recognized authorities.

This book begins with a well-written introduction and an overview of physics unique to the small size of neonates and children. In comparison to comprehensive echocardiography and neonatologist performed echocardiography, POCUS is primarily focused at answering a specific question for specific indications and mostly used in the acute care setting. This textbook, written for a global audience, enhances in-depth theoretical knowledge and understanding of echocardiography for pediatric and neonatal intensivists through chapters on basic views, evaluation of left ventricular dysfunction, shock and hypotension, and right ventricular dysfunction and pulmonary hypertension. Although not the focus of a bedside POCUS program, the authors discuss the identification of critical congenital heart disease, advanced echocardiography and hemodynamic evaluation, and the importance of pediatric cardiology consultation for timely intervention.

Bedside assessment of thoracic, abdominal, and neurological pathophysiology by POCUS can be lifesaving in conditions such as pneumothorax or acute hemorrhage, and chapters within this book discuss both the indications and technique for performing nonprocedural diagnostic POCUS applications. Procedural POCUS applications, including vascular access and drainage techniques, are deeply explored as it is well recognized that procedural accu-

racy is improved with ultrasound integration. Portable ultrasound devices have enhanced our ability to assess neonatal and pediatric patients in the field and also on transport. These important topics are beautifully covered with plenty of images to guide the clinician.

Finally, practical considerations regarding the establishment of a POCUS program, both in high-income countries and resource-limited settings, are covered in this later chapters within the textbook.

The editors should be congratulated on providing this comprehensive resource to neonatal and pediatric clinicians. We are confident that this book will stimulate further interest and enhance knowledge of the bedside clinician. This will undoubtedly lead to saving and improving the lives of our tiniest and most fragile patients.

Satyan Lakshminrusimha
UC Davis Children's Hospital
Sacramento, CA, USA

Ramasamy Ramanathan
Keck School of Medicine of USC
Los Angeles, CA, USA

Acknowledgments

Writing a textbook is a journey that requires determination, patience, guidance, support, and encouragement from various highly talented individuals. I am extremely grateful to my wonderful Co-Editors and friends, *Dr Cécile Tissot, Dr María Victoria Fraga, and Dr Thomas Conlon*, who have worked relentlessly to ensure that this book is completed to the highest standard—thank you for your camaraderie, intellectual stimulation, excellent teamwork, and friendship. To all the authors, thank you for writing such high-quality chapters and sharing your knowledge. Point-of-care ultrasound (POCUS) is growing across all pediatric practice settings, and we are proud to have contributions from distinguished writers representing international perspectives and diverse clinical experiences. I extend my appreciation to the main illustrator of our book, *Sheen Gahlaut*, who produced beautiful illustrations and figures with her creativity. And to the Springer team, your guidance, dedication, and professionalism have been instrumental in bringing this book to publication.

I also extend my deepest appreciation to my family, whose unwavering love, support, and sacrifice have been a constant source of inspiration. Their belief in me and my abilities have been a driving force behind the completion of this endeavor. I am forever indebted to their sacrifice and the support they have provided throughout the writing of this book and my career, especially my wife *Renu Gahlaut* who has always pushed me to strive for excellence.

Finally, I would like to extend heartfelt thanks to all the neonatal and pediatric intensivists readers and colleagues with interest in functional echocardiography or POCUS. Wherever you are on your educational journeys, I hope this book inspires you to continue exploring new ideas that may translate to the improved care of sick children everywhere.

Yogen Singh

Professor of Pediatrics, Division of Neonatology
Loma Linda University School of Clinical Medicine
Loma Linda, CA, USA

Adjunct Clinical Professor
Division of Neonatal and Developmental Medicine
Stanford University School of Medicine
Stanford, CA, USA

Adjunct Clinical Professor of Pediatrics,
Division of Neonatology
Keck School of Medicine
University of Southern California (USC)
Los Angeles, CA, USA

Contents

Part I Basics in Critical Care and Neonatal Point of Care Ultrasound

- Introduction to Point of Care Ultrasound** 3
Thomas Conlon, Cécile Tissot, María Victoria Fraga, and Yogen Singh
- Physics, Knobology, and Transducers: Imaging Optimization.** 9
Jason Z. Stoller, Yogen Singh, and Cécile Tissot

Part II Cardiovascular System Assessment

- Basic Echocardiographic Views for the Intensivist** 31
Cécile Tissot and Yogen Singh
- POCUS in Shock and Hypotension** 47
Saul Flores, Fabio Savorgnan, and David Kantor
- Echocardiographic Evaluation of Left Ventricular Function and Hemodynamic Status** 57
Cécile Tissot, Nicole Sekarski, and Yogen Singh
- Focused Ultrasound in Right Ventricular Function and Pulmonary Hypertension** 71
Shazia Bhombal, Shahab Noori, Yogen Singh, and María Victoria Fraga
- Focused Assessment of Pericardial Effusion and Cardiac Tamponade** 85
Yogen Singh, Farha Vora, and Cécile Tissot
- Advanced Functional Echocardiographic Views Including PDA Assessment and Hemodynamic Evaluation** 97
Yogen Singh, Sebastien Joye, and Cécile Tissot
- Comprehensive Echocardiography and Diagnosis of Major Common Congenital Heart Defects.** 111
Nicole Sekarski, Yogen Singh, and Cécile Tissot

Part III Thoracic Assessment

- Basic Lung Ultrasound for the Intensivist** 133
Adam S. Himebauch and Akira Nishisaki

Airway Ultrasound	141
Erik Su and Bereketiab Haileselassie	
Diaphragmatic Ultrasound	149
Joel K. B. Lim, Jan Hau Lee, and Mark D. Weber	
Clinical Applications in Lung Point-of-Care Ultrasound	
Assessment in Neonates	163
Nadya Yousef and Daniele De Luca	
Part IV Abdominal Assessment	
Abdominal Point-of-Care Ultrasound in Neonatal and Pediatric Populations	179
Yasser Elsayed and Vidit Bhargava	
Part V Neurosonology	
Focused Cranial Ultrasound for Neurointensive Care	207
Marlina Lovett, Kerri LaRovere, and Nicole O'Brien	
Cranial Ultrasound	227
Pradeep Suryawanshi, Reema Garegrat, and Yogen Singh	
Part VI Use of Point of Care Ultrasound in Transport Setting	
Role of Point of Care Ultrasound in the Transport Setting for Evaluating Infants and Children with Shock	243
Sajeev Job, Michael J. Griksaitis, and Yogen Singh	
Part VII Procedural Ultrasound	
Vascular Access Considerations in Children and Neonates	253
Mark D. Weber, Benjamin Kozyak, and María Victoria Fraga	
Ultrasound-Guided Procedures Beyond Vascular Access	277
Jesse Wenger and Grace Chong	
Use of Ultrasound in ECMO	291
Ivanna Maxson and Erik Su	
Part VIII Programmatic Considerations and Moving Forward	
POCUS Guidelines, Training Curriculum, and Education	301
Thomas Conlon, Sam Rosenblatt, Adam S. Himebauch, Christie Glau, Yogen Singh, and Akira Nishisaki	

**Current and Future Challenges to Ultrasound Adoption
in Clinical Practice** 309
Thomas Conlon, Yogen Singh, Cécile Tissot,
and María Victoria Fraga

**Correction to: Echocardiographic Evaluation of
Left Ventricular Function and Hemodynamic Status** C1
Cécile Tissot, Nicole Sekarski, and Yogen Singh

Appendix: Learning Outcomes 319

Editors and Contributors

Editors

Yogen Singh, MD, MA, FASE, DCH, FRCPCH Department of Pediatrics, Loma Linda University School of Clinical Medicine, Loma Linda, CA, USA
Adjunct Clinical Professor of Pediatrics, Division of Neonatal and Developmental Medicine, Stanford University School of Medicine, Palo Alto, CA, USA

Adjunct Clinici Professor, Keck School of Medicine, University of Southern California (USC), Los Angeles, CA, USA

Chair, ESPNIC Cardiovascular Dynamics Section and POCUS Working Group, Geneva, Switzerland

Pediatrics, Neonatology and Pediatric Cardiology, Cambridge University Hospitals NHS Foundation Trust, Cambridge, UK

Cécile Tissot, MD ESPNIC POCUS Working Group, Geneva, Switzerland
Centre de Pédiatrie, Clinique des Grangettes, Chêne Bougeries, Geneva, Switzerland

Maria Victoria Fraga, MD Department of Pediatrics, Division of Neonatology, Children's Hospital of Philadelphia, Perelman School of Medicine University of Pennsylvania, Philadelphia, PA, USA

The Children's Hospital of Philadelphia, Philadelphia, PA, USA

Thomas Conlon, MD Assistant Professor, Department of Anesthesiology and Critical Care Medicine, Children's Hospital of Philadelphia, Perelman School of Medicine University of Pennsylvania, Philadelphia, PA, USA

The Children's Hospital of Philadelphia, Philadelphia, PA, USA

Contributors

Vidit Bhargava, MD Division of Pediatric Critical Care, University of Alabama at Birmingham, Birmingham, AL, USA

Shazia Bhombal, MD Pediatrics, Division of Neonatology, Emory University, Atlanta, GA, USA

Erik Brandsma, MD Clinical Pediatrics, Perelman School of Medicine at the University of Pennsylvania, Philadelphia, PA, USA

Division of Neonatology, Children's Hospital of Philadelphia, Philadelphia, PA, USA

Grace Chong, MD Division of Pediatric Critical Care Medicine, Comer Children's Hospital, The University of Chicago School of Medicine, Chicago, IL, USA

Daniele De Luca, MD, PhD Neonatology, Division of Pediatrics and Neonatal Critical Care, "A.Béclère" Medical Center, Paris Saclay University Hospitals, APHP, Paris, France

Yasser El Sayed, MD, PhD Section of Neonatology, Department of Pediatrics, University of Manitoba, Winnipeg, MB, Canada
Royal College of Physicians and Surgeons, Ottawa, MB, Canada

Saul Flores, MD Divisions of Critical Care and Cardiology, Texas Children's Hospital, Baylor College of Medicine, Houston, TX, USA

Sheen Gahlaut The Perse school, Cambridge, UK

Reema Garegrat, MBBS, DNB Pediatrics and Neonatology, Sahyadri Hospital, Pune, India

Christie Glau, MD Anesthesiology and Critical Care Medicine, The Children's Hospital of Philadelphia, Philadelphia, PA, USA

Michael J. Griksaitis, MRCPCH, MSc, FFICM Southampton Children's Hospital, Southampton, UK

Bereketeab Haileselassie, MD Pediatric Critical Care Medicine, Stanford Lucile Packard Children's Hospital, Palo Alto, CA, USA

Adam S. Himebauch, MD Anesthesiology and Critical Care Medicine, The Children's Hospital of Philadelphia, Philadelphia, PA, USA

Sajeev Job, MRCPCH Pediatric and Neonatal Decision Support and Retrieval Service (PaNDR), Cambridge University Hospitals NHS Foundation Trust, Cambridge, UK

Sebastien Joye, MD Department of Neonatology, Centre Hospitalier Universitaire Romand (CHUV), Lausanne, Switzerland

David Kantor, MD, PhD Department of Anesthesiology, Critical Care and Pain Medicine, Harvard Medical School, Boston, MA

Benjamin Kozyak, MD Division of Cardiac Critical Care Medicine, Department of Anesthesiology and Critical Care Medicine, Children's Hospital of Philadelphia, Perelman School of Medicine at the University of Pennsylvania, Philadelphia, PA, USA

Kerri LaRovere, MD Department of Neurology, Boston Children's Hospital, Boston, MA, USA

Jan Hau Lee, MBBS, MRCPCH MCI Children's Intensive Care Unit, Department of Pediatric Subspecialties, KK Women's and Children's Hospital, Singapore, Singapore

Joel K. B. Lim, MBBS, MRCPCH Children's Intensive Care Unit, Department of Pediatric Subspecialties, KK Women's and Children's Hospital, Singapore, Singapore

Marlina Lovett, MD Clinical Medicine, The Ohio State University, Columbus, OH, USA

Division of Pediatric Critical Care Medicine, Nationwide Children's Hospital, Columbus, OH, USA

Ivanna Maxson, MD Division of Critical Care Medicine, Department of Pediatrics, Baylor College of Medicine, Texas Children's Hospital, Houston, TX, USA

Akira Nishisaki, MD, MSCE, FAAP Clinical Implementation Programs, Department of Anesthesiology and Critical Care Medicine, The Children's Hospital of Philadelphia, Philadelphia, PA, USA

Shahab Noori, MD Pediatrics, Keck School of Medicine, University of Southern California, Los Angeles, CA, USA

Division of Neonatology, Children's Hospital Los Angeles, Los Angeles, CA, USA

Nicole O'Brien, MD Clinical Medicine, The Ohio State University, Columbus, OH, USA

Division of Pediatric Critical Care Medicine, Nationwide Children's Hospital, Columbus, OH, USA

Sam Rosenblatt, MD Department of Anesthesiology and Critical Care Medicine, Children's Hospital of Philadelphia, Perelman School of Medicine at the University of Pennsylvania, Philadelphia, PA, USA

Fabio Savorgnan, MD Divisions of Critical Care and Cardiology, Texas Children's Hospital, Baylor College of Medicine, Houston, TX, USA

Nicole Sekarski, MD Pediatric Cardiology, Department of Pediatrics, Centre Hospitalier Universitaire Romand (CHUV), Lausanne, Switzerland

Jason Z. Stoller, MD Clinical Pediatrics, Perelman School of Medicine at the University of Pennsylvania, Philadelphia, PA, USA

Division of Neonatology, Children's Hospital of Philadelphia, Philadelphia, PA, USA

Erik Su, MD Division of Critical Care Medicine, Department of Pediatrics
Baylor College of Medicine, Texas Children's Hospital, Houston, TX, USA

Pradeep Suryawanshi, MD Neonatology, Bharati Vidyapeeth University
Medical College, Pune, India

Farha Vora, MD Department of Pediatrics, Division of Neonatology, Loma
Linda University School of Clinical Medicine, Loma Linda, CA, USA

Mark D. Weber, RN, CPNP-AC, FCCM Department of Anesthesiology
and Critical Care Medicine, Children's Hospital of Philadelphia, University
of Pennsylvania, Philadelphia, PA, USA

Jesse Wenger, MD Division of Pediatric Critical Care Medicine, Seattle
Children's Hospital, University of Washington, Seattle, WA, USA

Nadya Yousef, MD, MSc Division of Pediatrics and Neonatal Critical Care,
"A.Bécélère" Medical Center, Paris Saclay University Hospitals, APHP, Paris,
France

List of Videos

Chapter 9

- Video 1.** HLHS, PSAX, hypoplastic left ventricle (posterior) with dilated right ventricle (anterior)
- Video 2.** HLHS, 4C, hypoplastic left ventricle (LV) and left atrium (LA), dilated right ventricle (RV) and right atrium (RA), interatrial left to right shunt
- Video 3.** Critical AS, PLAX, very little opening of aortic valve, decreased left ventricular function
- Video 4.** Critical AS, A4C, very little high-velocity flow through aortic valve, severe left ventricular dysfunction, moderate to severe mitral regurgitation
- Video 5.** CoA, suprasternal, narrowing of the descending aorta in the juxtaductal position with aliasing of flow and increased blood flow velocity
- Video 6.** PS, PSAX, pulmonary valve thickened and doming with aliasing of flow
- Video 7.** Truncus arteriosus, subcostal, single vessel coming off heart and dividing into aorta and PA
- Video 8.** Tetralogy of Fallot, PSAX, pulmonary valve stenosis with aliasing of flow and high-velocity flow, hypoplastic pulmonary trunk
- Video 9.** TAPVR, high suprasternal, flow from pulmonary vein collector through vertical vein into innominate vein
- Video 10.** Tricuspid atresia, 4C, echogenic band in the position of the tricuspid valve with no opening of the valve and no forward flow from right atrium (RA) to right ventricle (RV), ventricular septal defect (VSD)
- Video 11.** Tricuspid atresia, subcostal, no opening of tricuspid valve, right to left obligatory interatrial shunt
- Video 12.** PDA, PSAX, left to right shunt through PDA between aorta and pulmonary artery
- Video 13.** VSD, 4C, echolucent space in the muscular (trabecular VSD) interventricular septum with high velocity left to right shunt
- Video 14.** VSD, 5C, echolucent space in the perimembranous sub-aortic interventricular septum with high velocity left to right shunt
- Video 15.** ASD, 4C, echolucent space in the ostium secundum interatrial septum with left to right shunt

Video 16. ASD, subcostal, left to right interatrial shunt

Video 17. AVSD, 4C, inlet ventricular septal defect and primum atrial septal defect with common atrioventricular valve (defect of the crux of the heart), moderate right AV valve regurgitation (multiples jets)

Chapter 10

Video 1. Linear probe 2D ultrasound clip demonstrating lung sliding in a normal lung. An A-line is also visualized

Video 2. Linear probe 2D ultrasound clip demonstrating diffuse B-lines which characteristically originate at the pleural line, extend vertically deep into the ultrasound field, are synchronous with lung sliding, and obscure A-lines

Video 3. Linear probe 2D ultrasound clip demonstrating a complex pleural effusion

Video 4. Linear probe 2D ultrasound clip demonstrating a lung point, a sign very specific for pneumothorax in the area underlying the ultrasound probe

Part I

**Basics in Critical Care and Neonatal
Point of Care Ultrasound**



Introduction to Point of Care Ultrasound

Thomas Conlon, Cécile Tissot,
María Victoria Fraga, and Yogen Singh

Contents

Point of Care Ultrasound—Is It Time to Adopt in Routine Clinical Practice?	3
References	6

T. Conlon (✉)

Department of Anesthesiology and Critical Care
Medicine, Children’s Hospital of Philadelphia,
Perelman School of Medicine University
of Pennsylvania, Philadelphia, PA, USA

The Children’s Hospital of Philadelphia,
Philadelphia, PA, USA
e-mail: Conlont@chop.edu

C. Tissot

Department of Pediatrics, Clinique des Grangettes,
Chêne-Bougeries, Geneva, Switzerland

M. V. Fraga

Department of Pediatrics, Division of Neonatology,
Children’s Hospital of Philadelphia, Perelman School
of Medicine, University of Pennsylvania,
Philadelphia, PA, USA

The Children’s Hospital of Philadelphia,
Philadelphia, PA, USA

e-mail: fragam@chop.edu

Y. Singh

Department of Pediatrics, Division of Neonatology,
Loma Linda University School of Medicine,
California, USA

Department of Pediatrics, Division of Neonatal and
Developmental Medicine, Stanford University School
of Medicine, California, UK

Department of Pediatrics, Division of Neonatology,
University of Southern California, California, UK

ESPNIC Cardiovascular Dynamics Section and
POCUS Working Group, Geneva, Switzerland
e-mail: YSingh@llu.edu

Point of Care Ultrasound—Is It Time to Adopt in Routine Clinical Practice?

Throughout the past two decades, portable ultrasound machines emerged at the bedside of acutely ill children. Incorporation of diagnostic and procedural ultrasound applications by non-cardiology/non-radiology providers, specifically pediatric emergency medicine, critical care, and neonatology clinicians, challenges and changes practice paradigms. As portable ultrasound machines are now ubiquitous across pediatric acute care settings, the pediatric field is now tasked with the question of how to optimize the integration of technology in clinical care.

This book is structured to provide readers an extensive assessment of current ultrasound applications specific to the care of neonatal and pediatric patients with critical illness. Experts from around the world share their knowledge regarding the technique and integrate relevant literature to answer both “why” and “why not” ultrasound. Later chapters attempt to move beyond clinical applications and introduce challenges related to

training and program development. We must, upfront, acknowledge that we are at the beginning of ultrasound's journey in pediatric practice. Many ultrasound applications that may greatly impact patient outcomes have yet to be discovered or standardized within care. We recognize that the incorporation of new technologies and novel ideas takes time and patience before attaining widespread acceptance.

“That it will ever come into general use, notwithstanding its value, is extremely doubtful; because its beneficial application requires much time and gives a good bit of trouble both to the patient and the practitioner; because its hue and character are foreign and opposed to all our habits and associations.”

John Forbes, physician to Queen Victoria, wrote this in 1821 as a preface to his translation of René-Théophile-Hyacinthe Laënnec's 1816 book describing a new device: the stethoscope [1]. Over two hundred years later, this device remains a diagnostic mainstay, draped around the neck of every medical student reciting their Hippocratic Oath and at the bedside of every critically ill child undergoing care. Is the story of the stethoscope one of success given its elevated position among medical devices? Or is the continued reliance upon a 200-years-old technology the story of our failure to develop, explore, or adopt other technologies?

This book is not meant to answer those questions, and importantly, this book is not meant to declare the superiority of ultrasound to any currently utilized technologies or practices. This book is meant to *expose* readers to ultrasound and present arguments for (and against!) its incorporation in pediatric clinical practice by non-radiology/non-cardiology providers. In fact, within neonatal and pediatric critical care specialty POCUS guidelines the vast majority of pediatric-specific statements have moderate, low, or very low (B, C, D) quality of supporting evidence [2–4].

Despite limitations in accumulated evidence, POCUS use is proliferating across pediatric practice settings [5–7]. There is tremendous face validity to the technology; pathophysiologic pro-

cesses are now *visualized in real time!* Signs and symptoms and constellations of datapoints requiring interpretation beyond human capabilities [8] can be encapsulated in a single image. The “art” of medicine is now digitalized pixels on a screen. And the ability to acquire those pixels ourselves, at the bedside of our critically ill patients, complements our developed clinical expertise. Pixels change our assessments, change our management, and change our outcomes.

Concern appropriately exists when introducing any new technology in clinical practice. The success of the stethoscope as a technology integrated in practice can be contrasted by the downfall of the pulmonary arterial catheter due to poor implementation processes and resultant unforeseen harm [9]. Providers learning ultrasound require thorough training across knowledge, psychomotor and interpretative domains for successful translation of skill in clinical practice. This takes considerable time and effort, and it is particularly burdensome in the early stages of technology integration where training infrastructure is sparse. So, is it worth the effort to learn ultrasound?

First, let us assess whether ultrasound technology adheres to our goals and values as “modern” clinicians. Though authors and readers arise from different countries, practice in different settings, and have different clinical experiences, there are common ties to the practice of medicine. The Institute of Medicine (now called the National Academy of Medicine) is a nonprofit evidence-based United States scientific advisory organization with global scope dedicated to “catalyzing action and achieving impact” [10]. In 2001, the organization published *Crossing The Quality Chasm: A New Health System for the twenty-first Century* and defined six aims for idealized care: Safety, Efficacy, Patient-centeredness, Timeliness, Efficiency, and Equitability [11]. Any new technology we seek to introduce within our clinical practice should *strengthen* our ability to deliver ideal, value-based care to patients.

Ultrasound technology embraces a culture of *safety*. First, providers may now use ultrasound to assess catheter positioning or diagnostics pre-

viously performed using radiating technologies such as CT or plain radiography. There is also ample evidence that the incorporation of ultrasound improves provider performance and reduces complications across the spectrum of procedures performed by pediatric acute care providers [12–18]. Finally, and most importantly, ultrasound may protect both us and our patients from ourselves. By improving the accuracy of diagnosis, we can align therapeutics to target a specific diagnosis. Administrators and regulators may raise concerns regarding institutional protection from “rogue” non-cardiology/non-radiology providers performing bedside POCUS studies, but there have not been reported incidents of medical malpractice associated with the point of care ultrasonography use. In fact, the only medical-legal incidents reported in the literature related to POCUS ultrasound is the *lack of use* of the technology when the equipment was available and the provider had the capability to use it within the scope of care [19–21]. Thus, ultrasound provides safety for patients, providers, and institutions when implemented effectively.

Ultrasound technology demonstrates *efficacy*. Although there may be limited POCUS evidence in pediatric acute care disciplines, literature and experience are robust in cardiology and radiology disciplines supporting benefits to clinical care. While ultrasound may be “new” to many, the technology has actually been present in medicine for the better part of the past century. Whether used by physical therapists in the 1920s, neuroradiologists in the 1940s, or cardiologists in the 1950s and 60s, there is expertise in the use of the technology both within the greater context of medical practice as well as locally within our radiology and cardiology practice partners [22]. Applications specific to other subspecialty domains of practice continue to emerge, such as fluid responsiveness in shock in pediatric critical care or indication for surfactant in neonates with respiratory distress syndrome. Enough experience with the technology exists within our global medical practice rendering new questions answerable using preexisting skills and methodological frameworks.

Ultrasound technology is *patient-centered*. Our current practice environment embraces pathways and algorithms often driven by population-based data. Standardization of care demonstrates benefit for the masses and quality improvement strategies in pediatric care embrace its principles [23]. But the patient that presents to the pediatric emergency department is not a population, they are an individual child. And our physical exams, our laboratory values, and our monitor data all have respective limitations in accuracy, precision, sensitivities, and specificities when applied in care. Standardization of approaches through pathways and algorithms only embraces patient-centeredness if there is a willingness to continually revisit data we use to optimize downstream diagnostics and therapeutics. Support for the inclusion of ultrasound in standardized hemodynamic assessments now embraced by both adult and pediatric specialists [24, 25] lends support to the idea that ultrasound data has value both to individual patients and collective populations, and may improve our own clinical performance.

Ultrasound technology is *timely*. Ultrasound devices are now more portable, though retain much of the imaging capabilities of older, larger machines. Some are now pocket size and images can be assessed in real time by providers or housed within institutional servers for near real-time assessment by remote experts. Point of care ultrasonography is not only available at clinical presentation but can be repeated throughout a clinical course to assess responsiveness to therapeutic intervention or reevaluate protean physiologies. Data continue to suggest that time to appropriate therapies is associated with outcomes, whether early antibiotics in sepsis [26, 27] or reperfusion in stroke or acute coronary syndromes [28, 29]. Ultrasound facilitates diagnostics at the bedside, therapeutics in management, and reassessment in ongoing care.

Ultrasound technology is *efficient*. With smaller sized machines comes greater portability to expand capabilities across varied practice settings. Ultrasound has now even found itself used in space [30]! But beyond the economy of machine presence, ultrasound efficiency is opti-

mized by the *context* of its use. Clinicians trained in acquiring and interpreting images no longer rely on an order, a technician to come to the bedside for image acquisition, and a remote imaging-based specialist for interpretation. Further, the real-time information gathered is not being processed in a dark reading room, but rather within the presence of the patient and the surrounding clinical data. Emergency medicine studies consistently demonstrate reduced time spent in the hospital for patients and families as well as greater satisfaction [31].

Ultrasound use is *equitable*. Our larger society as well as profession strives to create systems and render care that is fair and just to individuals. We know that inequalities exist across medicine which result in disproportionate outcomes between groups based upon sex, race, ethnicity, and socioeconomic status [32–34]. Ultrasound may help to remove some of the deeply rooted, systemic biases knowingly or unknowingly entangled within our clinical care. Ultrasound is simply white and black dots with many shades of gray in between. In some ways, the technology itself defines respect for equitability. How we incorporate the technology and translate it within care is yet to be assessed for this important clinical aim.

Clearly, ultrasound can provide care that adheres to our clinical goals and values. So we ask again, is it worth the effort to learn ultrasound? We definitely think so... which is why we write this book.

References

1. A treatise on the diseases of the chest by Laennec RTH, translated from French to English by John Forbes, Translator's Preface by John Forbes, Start Page i, Quote Page xviii-xix, Printed for T. and C. Underwood, London. [Facsimile of the London 1821 Edition Published in 1962 by Hafner Publishing, New York].
2. Singh Y, Tissot C, Fraga MV, et al. International evidence-based guidelines on point of care ultrasound (POCUS) for critically ill neonates and children issued by the POCUS Working Group of the European Society of Paediatric and Neonatal Intensive Care (ESPNIC). *Crit Care*. 2020;24:65.
3. Frankel HL, Kirkpatrick AW, Elbarbary M, et al. Guidelines for the appropriate use of bedside general and cardiac ultrasonography in the evaluation of critically ill patients—Part I: general ultrasonography. *Crit Care Med*. 2015;43:2479–502.
4. Levitov A, Frankel HL, Blaivas M, et al. Guidelines for the appropriate use of bedside general and cardiac ultrasonography in the evaluation of critically ill patients—Part II: cardiac ultrasonography. *Crit Care Med*. 2016;44:1206–27.
5. Conlon TW, Kantor DB, Su ER, et al. Diagnostic bedside ultrasound program development in pediatric critical care medicine: results of a national survey. *Pediatr Crit Care Med*. 2018;19:e561–8.
6. Chamberlain MC, Reid SR, Madhok M. Utilization of emergency ultrasound in pediatric emergency departments. *Pediatr Emerg Care*. 2011;27:628–32.
7. Nguyen J, Amirmovin R, Ramanathan R, et al. The state of point-of-care ultrasonography use and training in neonatal-perinatal medicine and pediatric critical care medicine fellowship programs. *J Perinatol*. 2016;36:972–6.
8. Szulewski A, Howes D, van Merriënboer JGG, et al. From load theory to practice: the application of cognitive load theory to the practice of medicine. *Acad Med*. 2021;96:24–30.
9. Marik PE. Obituary: pulmonary artery catheter 1970–2013. *Ann Intensive Care*. 2013;3:38.
10. As found on <https://nam.edu/about-the-nam/>. May 20, 2021.
11. Institute of Medicine (US) Committee on Quality of Health Care in America. *Crossing the quality chasm: a new health system for the 21st century*. Washington (DC): National Academies Press (US); 2001.
12. de Souza TH, Brandão MB, Nadal JAH, et al. Ultrasound guidance for pediatric central venous catheterization: a meta-analysis. *Pediatrics*. 2018;142:e20181719.
13. Hanada S, Van Winkle MT, Subramani S, et al. Dynamic ultrasound-guided short-axis needle tip navigation technique vs. landmark technique for difficult saphenous vein access in children: a randomised study. *Anaesthesia*. 2017;72:1508–15.
14. Takeshita J, Yoshida T, Nakajima Y, et al. Superiority of dynamic needle tip positioning for ultrasound-guided peripheral venous catheterization in patients younger than 2 years old: a randomized controlled trial. *Pediatr Crit Care Med*. 2019;20:e410–4.
15. Kantor DB, Su E, Milliren CE, et al. Ultrasound guidance and other determinants of successful peripheral artery catheterization in critically ill children. *Pediatr Crit Care Med*. 2016;17:1124–30.
16. Katheria AC, Fleming SE, Kim JH. A randomized controlled trial of ultrasound-guided peripherally inserted central catheters compared with standard radiograph in neonates. *J Perinatol*. 2013;33:791–4.
17. Helgeson SA, Fritz AV, Tatari MM, et al. Reducing iatrogenic pneumothoraces: using real-time ultrasound guidance for pleural procedures. *Crit Care Med*. 2019;47:903–9.

18. Hayes J, Borges B, Armstrong D, et al. Accuracy of manual palpation vs ultrasound for identifying the L3-L4 intervertebral space level in children. *Paediatr Anaesth*. 2014;24:510–5.
19. Nguyen J, Cascione M, Noori S. Analysis of lawsuits related to point-of-care ultrasonography in neonatology and pediatric subspecialties. *J Perinatol*. 2016;36:784–6.
20. Blaivas M, Pawl R. Analysis of lawsuits filed against emergency physicians for point-of-care emergency ultrasound examination performance and interpretation over a 20-year period. *Am J Emerg Med*. 2012;30:338–41.
21. Reaume M, Farishta M, Costello JA, Gibb T, Melgar TA. Analysis of lawsuits related to diagnostic errors from point-of-care ultrasound in internal medicine, paediatrics, family medicine and critical care in the USA. *Postgrad Med J*. 2021;97:55–8.
22. Newman PG, Rozycki GS. The history of ultrasound. *Surg Clin North Am*. 1998;78:179–95.
23. Lavelle J, Schast A, Keren R. Standardizing care processes and improving quality using pathways and continuous quality improvement. *Curr Treat Options Peds*. 2015;1:347–58.
24. Singh Y, Villaescusa JU, da Cruz EM, et al. Recommendations for hemodynamic monitoring for critically ill children—expert consensus statement issued by the cardiovascular dynamics section of the European Society of Paediatric and Neonatal Intensive Care (ESPNIC). *Crit Care*. 2020;24:620.
25. Cecconi M, De Backer D, Antonelli M, et al. Consensus on circulatory shock and hemodynamic monitoring. Task force of the European Society of Intensive Care Medicine. *Intensive Care Med*. 2014;40:1795–815.
26. Liu VX, Fielding-Singh V, Greene JD, et al. The timing of early antibiotics and hospital mortality in sepsis. *Am J Respir Crit Care Med*. 2017;196:856–63.
27. Weiss SL, Fitzgerald JC, Balamuth F, et al. Delayed antimicrobial therapy increases mortality and organ dysfunction duration in pediatric sepsis. *Crit Care Med*. 2014;42:2409–17.
28. Rathore SS, Curtis JP, Chen J, et al.; National Cardiovascular Data Registry. Association of door-to-balloon time and mortality in patients admitted to hospital with ST elevation myocardial infarction: national cohort study. *BMJ*. 2009;338:b1807.
29. Mazighi M, Chaudhry SA, Ribo M, et al. Impact of onset-to-reperfusion time on stroke mortality: a collaborative pooled analysis. *Circulation*. 2013;127:1980–5.
30. Garcia KM, Harrison MF, Sargsyan AE, et al. Real-time ultrasound assessment of astronaut spinal anatomy and disorders on the International Space Station. *J Ultrasound Med*. 2018;37:987–99.
31. Lin MJ, Neuman MI, Monuteaux M, et al. Does point-of-care ultrasound affect patient and caregiver satisfaction for children presenting to the pediatric emergency department? *AEM Educ Train*. 2017;2:33–9.
32. Allen-Dicker J, Auerbach A, Herzig SJ. Perceived safety and value of inpatient “very important person” services. *J Hosp Med*. 2017;12:177–9.
33. Hawkins RB, Charles EJ, Mehaffey JH. Socio-economic status and COVID-19-related cases and fatalities. *Public Health*. 2020;189:129–34.
34. Adler NE, Rehkopf DH. U.S. disparities in health: descriptions, causes, and mechanisms. *Annu Rev Public Health*. 2008;29:235–52.



Physics, Knobology, and Transducers: Imaging Optimization

Jason Z. Stoller, Yogen Singh, and Cécile Tissot

Contents

Principles of Ultrasound	10
Sound Is a Wave	10
Sound Frequencies	10
Piezoelectric Effect	10
How Is an Image Formed?	11
What Determines Echogenicity (Brightness)?	12
Image Optimization and Knobology	14
2D Gain	14
Active Gain	14
Depth	16
Resolution	16
Focal Zone	16
Transducers	17
Two-Dimensional Ultrasound	18

J. Z. Stoller (✉)

Division of Neonatology, Department of Pediatrics,
Children's Hospital of Philadelphia,
Philadelphia, PA, USA

Perelman School of Medicine at the University of
Pennsylvania, Philadelphia, PA, USA
e-mail: stoller@chop.edu

Y. Singh
Department of Pediatrics, Division of Neonatology,
Loma Linda University School of Medicine,
California, USA

Department of Pediatrics, Division of Neonatal and
Developmental Medicine, Stanford University School
of Medicine, California, UK

Department of Pediatrics, Division of Neonatology,
University of Southern California, California, UK

ESPNIC Cardiovascular Dynamics Section and
POCUS Working Group, Geneva, Switzerland
e-mail: YSingh@llu.edu

C. Tissot
Centre de Pédiatrie, Clinique des Grangettes, Geneva,
Switzerland
e-mail: cecile.tissot@hirslanden.ch

Doppler Ultrasound 19
 The Doppler Effect 19
 Clinical Applications of Color Doppler 22
Tissue Doppler 24
Artifacts 25
 Gain Artifact 25
 Posterior Acoustic Shadowing 25
 Posterior Acoustic Enhancement 25
 Reverberation and Contact Artifacts 26
References 27

Principles of Ultrasound

Sound Is a Wave

The most fundamental properties of sound are those of a wave. As with all waves, sound waves have an amplitude, a wavelength, a frequency, and they propagate at a specific velocity (Fig. 1). The amplitude of a sound wave corresponds to its energy or “power.” The wavelength is defined as the distance traveled in one cycle and the frequency is the number of waves per unit time, usually measured in cycles per second (Hz). Wavelength (λ) is inversely proportional to frequency (f):

$$\lambda \propto \frac{1}{f}$$

This relationship is particularly important when considering the choice of the ultrasound transducer and adjusting imaging settings as it directly affects the image resolution and how deep the sound waves will penetrate.

Sound Frequencies

The wide range of sound frequencies is commonly divided into infrasound, acoustic range,

and ultrasound (Fig. 2). Infrasound includes frequencies extending below 20 Hz. Sounds in this range are not perceptible to humans. The acoustic range of human hearing is from 20 Hz to 20 kHz. Frequencies above 20 kHz are considered ultrasound. These sounds are not perceptible to the human ear but are perceptible to animals such as bats, dogs, and porpoises. Typically, the range of frequencies utilized for medical ultrasound is 2–20 MHz with some recent transducers operating up to 70 MHz. The ultrasound transducer frequency is adjustable and has a direct effect on image resolution and depth of sound wave penetration.

Piezoelectric Effect

Ultrasound imaging is made possible by leveraging the piezoelectric effect. The piezoelectric effect is the ability of oscillating crystals to convert electrical energy into kinetic energy (ultrasound waves) and back again. The ultrasound machine sends an electrical signal to an array of crystals at the edge of the transducer. The electrical signal is converted to ultrasound waves that are emitted from the transducer. The reflected ultrasound wave echoes returning from subcuta-



Fig. 1 Properties of a sound wave. All sound waves have a wavelength (λ), amplitude, and propagation velocity (v_w). The frequency (f) is inversely proportional to the wavelength

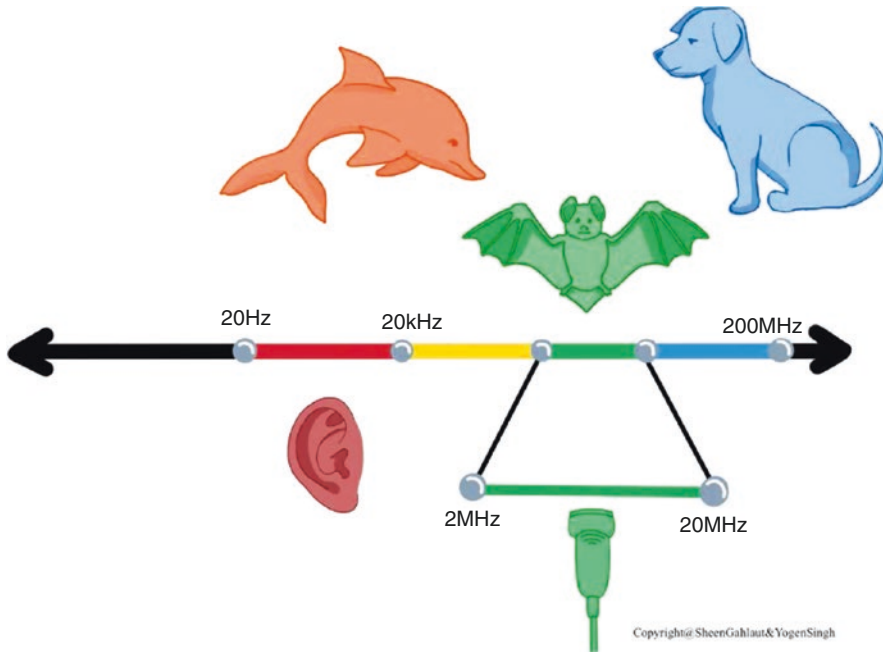


Fig. 2 Range of sound frequencies. The acoustic range (red), perceptible to humans, is from 20 Hz to 20 kHz. The ultrasound range above 20 kHz is perceptible to some animals. This includes the approximate range,

2–20 MHz, used in medical ultrasound (green). Below 20 Hz is considered infrasound. (Courtesy: Sheen Gahlaut and Yogen Singh)

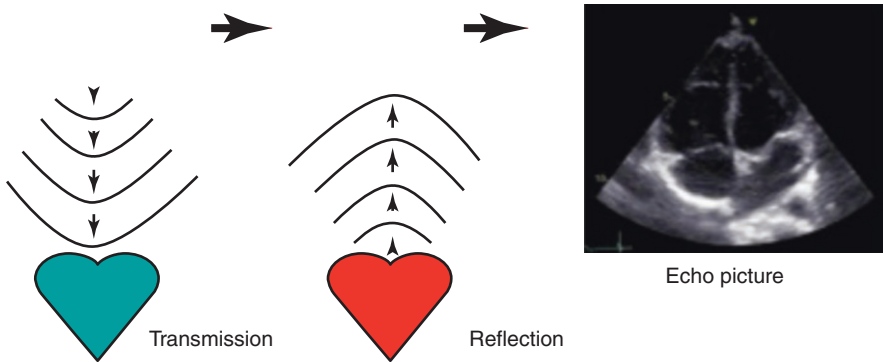


Fig. 3 Schematic representation of the ultrasound principle and piezoelectric effect: electricity is applied to the crystals and generates kinetic energy (ultrasound wave), transmitted to the heart. The returning ultrasound wave is

converted back to electrical energy to give a cross-sectional 2D image. Echoes are reflected differently depending on the tissue properties. The transducer is both a transmitter and a receiver

neous structures deform these same crystals to generate electrical energy which is transmitted back to the ultrasound machine. The signals are then processed to generate ultrasound images (Fig. 3).

How Is an Image Formed?

The ultrasound waves emitted from the transducer are reflected off various tissues, received by the transducer, and processed by the ultra-

sound machine software. To generate an image, the returning echoes are analyzed in two fundamental ways: depth determination and wave amplitude measurement.

Depth: The depth of the different structures is determined by using the pulse-echo principle. When considering the equation for velocity:

$$v = \frac{x}{t}$$

where v is velocity, x and t are distance and time respectively, from the transducer to a structure and back again. The velocity of ultrasound in most human tissues is similar to its velocity in water 1540 m/s. Therefore, the velocity of ultrasound in water is used to approximate depth calculations. By rearranging the equation above, by measuring the time elapsed between emitting and receiving the ultrasound wave, the round-trip distance can be calculated:

$$x = 1540 \cdot t$$

The depth of the reflecting structure is half this distance, $x/2$.

Amplitude: There are several techniques to analyze and visualize the amplitude of the reflected ultrasound waves. In A-mode (Amplitude-mode) ultrasound, the amplitude is plotted over time to visualize the ultrasound echoes along a single path [1]. This mode is not typically used in point-of-care ultrasound (POCUS) assessment. B-mode, or **B**rightness-mode, is vastly more common and useful for POCUS and is often referred to as gray-scale ultrasound or 2D ultrasound. The amplitude of the reflected wave is translated to gray-scale, whereby a high amplitude wave is depicted as white and a low amplitude wave is black.

It can be useful to conceptualize this analysis by imagining the emitted ultrasound waves as a two-dimensional plane. This plane can be split into individual slices, each slice with its own depth and amplitude data. These tiny slices are assembled side-by-side to generate a two-dimensional image displayed on the ultrasound machine.

What Determines Echogenicity (Brightness)?

There are several factors that determine the echogenicity, or brightness, of a tissue or anatomic structure. The first important concept is acoustic impedance. Acoustic impedance refers to the resistance an ultrasound wave encounters as it travels through a medium and can be described mathematically using the following equation:

$$Z = \rho \cdot c$$

where Z is acoustic impedance, ρ is density of a medium, and c is the ultrasound wave propagation velocity. If two adjacent tissues have different acoustic impedance, they are said to have acoustic impedance mismatch. The greater the mismatch, the greater the percentage of the ultrasound wave that is reflected back to the transducer from the interface between the two tissues thus resulting in a highly echogenic signal. A commonly encountered example of acoustic impedance mismatch is the highly echogenic signal created when soft tissue is adjacent to bone (Fig. 4). The acoustic impedance of non-fatty tissue and bone are 1.66×10^6 and 6.98×10^6 kg/(m²s), respectively [2]. This high discrepancy causes a highly echogenic (white) appearance at the interface. The acoustic impedance of many biological tissues (e.g., water, blood, fat, muscle) are quite similar, and hence the echogenicity is only slightly different (Table 1). Learners are often taught the BAD mnemonic to remember this: **B**ones and **A**ir are **B**Ad for ultrasound imaging.

The second factor, and one particularly important for novice POCUS providers to understand, is the angle of insonation. The angle of insonation is defined as the angle between the direction of wave propagation and the structure of interest (Fig. 5). The ideal angle, at which the greatest percentage of ultrasound waves will be reflected back to the transducer, is 90°. Thus, it is at this angle that the sonographer will observe the highest echogenicity (highest amplitude). As this angle varies from 90°, a diminishing fraction of the reflected waves will

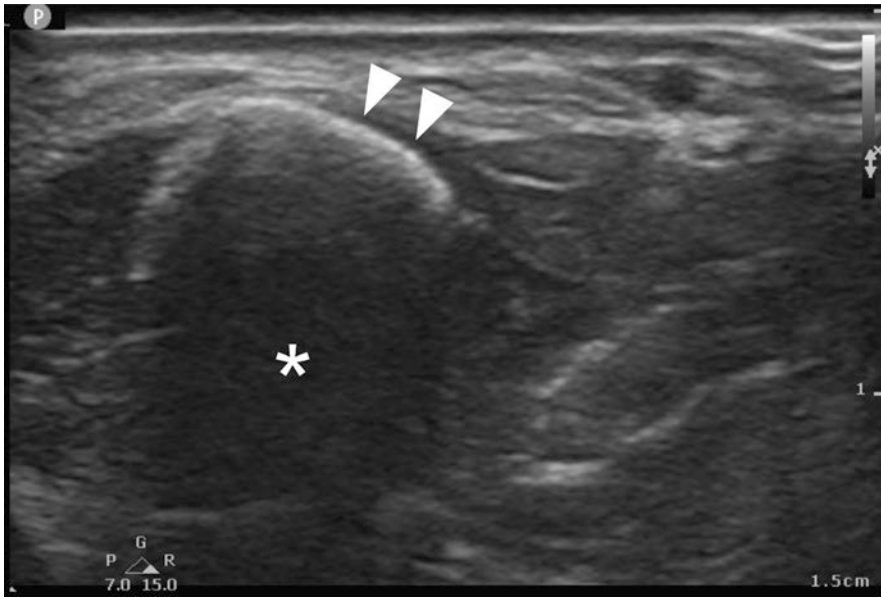


Fig. 4 Acoustic impedance mismatch. Transverse view of the distal radius is shown. A large mismatch between the acoustic impedance of bone and soft tissue results in

the highly echogenic appearance of the radius (arrow-heads). Deep to the bone cortex, a hypoechoic posterior acoustic shadowing artifact is observed (*)

Table 1 Acoustic impedance: properties of representative biological tissues

Tissue	Propagation speed (m s ⁻¹)	Characteristic acoustic impedance (10 ⁶ kg m ⁻² s ⁻¹)
Cortical bone	3635	6.98
Non-fatty tissue	1575	1.66
Fat	1465	1.44
Blood	1584	1.68

Adapted from [2]

be detected by the transducer and hence there will be decreased echogenicity. This is clearly apparent when observing the appearance of a needle at varying angles of insonation.

The last factor, discussed here, that results in high echogenicity are good specular reflectors. These can be thought of as structures that have a relatively smooth surface, such as the pleura (Fig. 21) or diaphragm. When encountering these structures, a high percentage of the incident wave is reflected back to the transducer resulting in a highly echogenic appearance. Conversely, structures that are not “smooth” result in scattering of the incident ultrasound wave with a relatively low percentage of the reflected wave returning to the transducer. Specular reflectors are relatively uncommon and most tissues encountered in POCUS studies do not have dramatically high echogenicity.

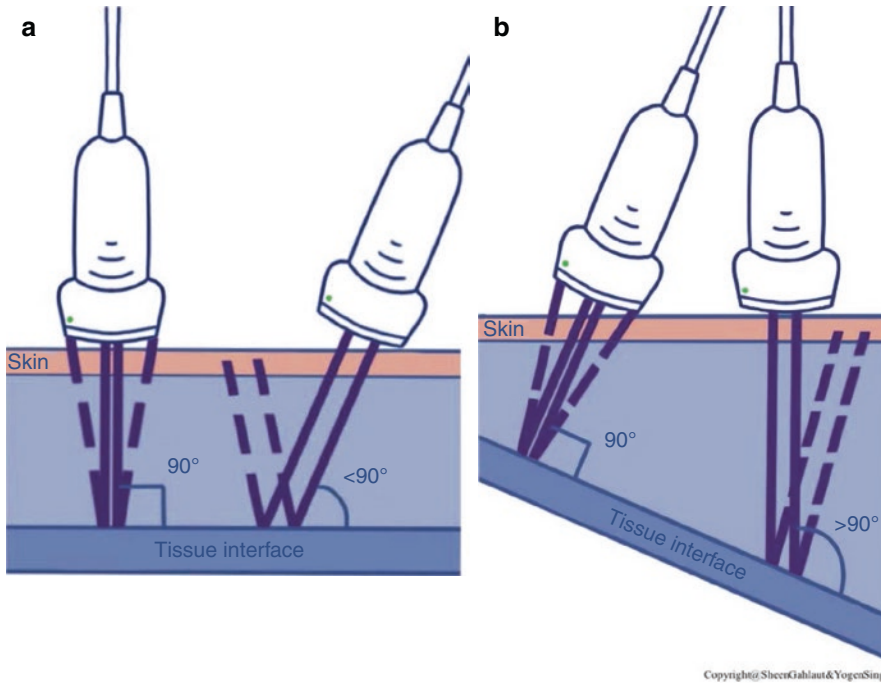


Fig. 5 Angle of insonation. The highest echogenicity is obtained when there is a 90° angle (a) between the direction of sound wave propagation and the structure of interest (angle of insonation). At this angle, the greatest percentage of the sound waves are reflected to the trans-

ducer. When the angle is less than 90° , reflected sound waves cannot be detected by the transducer. If the structure of interest is not parallel to the skin, the sonographer must tilt or rock the transducer (b) to obtain a 90° angle. (Courtesy: Sheen Gahlaut)

Image Optimization and Knobology

There are numerous settings that can be adjusted to achieve an optimal ultrasound image. Some of these settings are common to all ultrasound machines while others may be manufacturer-specific and proprietary. In this section, the most fundamental settings available on all ultrasound machines are discussed. The settings every sonographer should be familiar with include gain, depth, resolution, and focus.

2D Gain

Adjusting the gain modulates the intensity of the reflected sound waves throughout the entire image. If the *gain is set too low*, the entire *screen will be dark*, and the sonographer will not be able to distinguish individual structures (Fig. 6a). If

the gain is set too high, the observer will also not be able to distinguish individual structures and may result in gain artifacts whereby artifacts appear in areas that should normally be anechoic (Fig. 6c). Finer adjustments to the gain can be achieved with Lateral Gain Compensation (LGC) and Time-Gain Compensation (TGC). LGC allows for adjustments to the gain in one specific vertically segmented area of the image (e.g., the left half of the image) while TGC (Fig. 7) allows for adjustments to the gain in one specific horizontally segmented area of the image (e.g., the image segment furthest from the transducer).

Active Gain

Similar to 2D gain, active gain is used for color flow mapping and Doppler settings. Increasing too much active gain in color flow mapping may

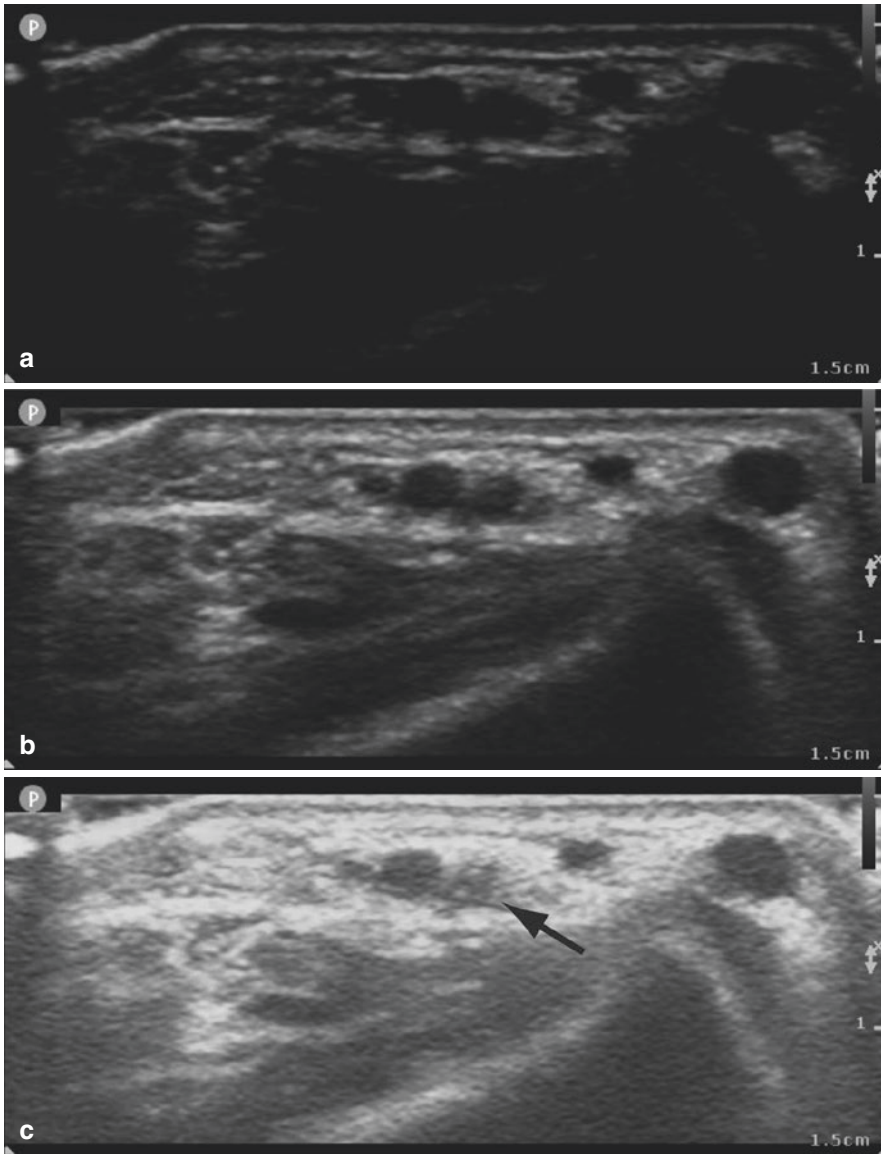


Fig. 6 Optimizing gain. Transverse view of superficial blood vessels is shown. If the gain is set too low (a), it is difficult differentiate structures from one another. The gain

is adjusted so that structures known to be anechoic (e.g., vessel lumen) appear black (b). If the gain is set too high (c), gain artifacts appear in anechoic structures (arrow)

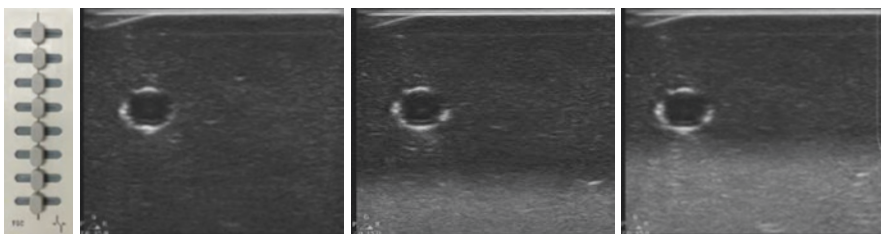


Fig. 7 Time-Gain Compensation (TGC). Transverse view of a blood vessel within a phantom simulator is shown. TGC sliders allow for adjustment of the amplification of the reflected sound waves at a specific depth

lead to too many speckles in the area of interest while too less gain may have little color flow mapping. This is particularly important when measuring structures on color Doppler such as measuring the size of patent ductus arteriosus (PDA). If the active gain setting is not optimized, then it can lead to over- or underestimation of size.

Depth

Depth, as the name implies, allows the sonographer to change how shallow or deep the target area is. The depth should *initially* be overestimated or adjusted to be deeper than the expected depth of the structure(s) of interest. This allows for the identification of any unexpected findings deep to the structure of interest. After the structure of interest is visualized, the depth should be gradually adjusted to a shallower setting until the region of interest is as large as possible (Fig. 8). When the depth is too deep, there is “wasted real estate” on the screen, deep to the structure of interest and visualization is suboptimal. Learners are often taught to adjust the depth to “use all the real estate” on the screen. It is important to distinguish depth adjustment from zoom. With many ultrasound machines, adjusting the zoom will result in a larger image, but will sacrifice resolution. Zoom can be used to visualize small structures like coronary arteries or visualizing annulus attachment while measuring annular diameter.

Resolution

Many modern transducers are dynamic, made to operate at a variable range of frequencies. These can be adjusted by the sonographer. Often the transducer is labeled with the range of frequencies (e.g., L15–8, 8–15 MHz). Although the vast majority of transducers allow for resolution adjustments, novice sonographers frequently overlook this option when optimizing image quality. Understanding the effects of resolution adjustments is critical. To understand the effect, one needs to remember that wavelength is inversely proportional to frequency. At **high frequencies**, the ultrasound wave has a short wavelength and thus the **resolution is very good**. The trade-off of adjusting to a high frequency is a **decreased depth of penetration**. If the region of interest is a superficial structure (e.g., peripheral blood vessel), it is most appropriate to change the settings and choose a transducer with a high frequency which will result in very good resolution but only shallow penetration (Fig. 9a, b). Conversely, if the goal is to visualize a deeper structure (e.g., IVC in a subcostal longitudinal view), it is most appropriate to choose a transducer that allows for the sonographer to adjust to a low frequency which will result in very good penetration but sacrificing resolution (Fig. 9c, d).

Focal Zone

The ultrasound beam is commonly depicted as a two-dimensional (2D) plane emanating from the

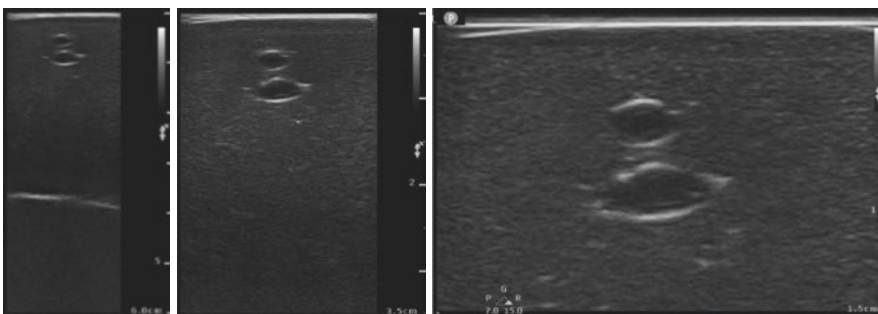


Fig. 8 Optimizing depth. Transverse view of blood vessels within a phantom simulator is shown. After adjusting the depth to view deep structures, it is adjusted to the shal-

lowest setting that still allows for visualization of the structure(s) of interest

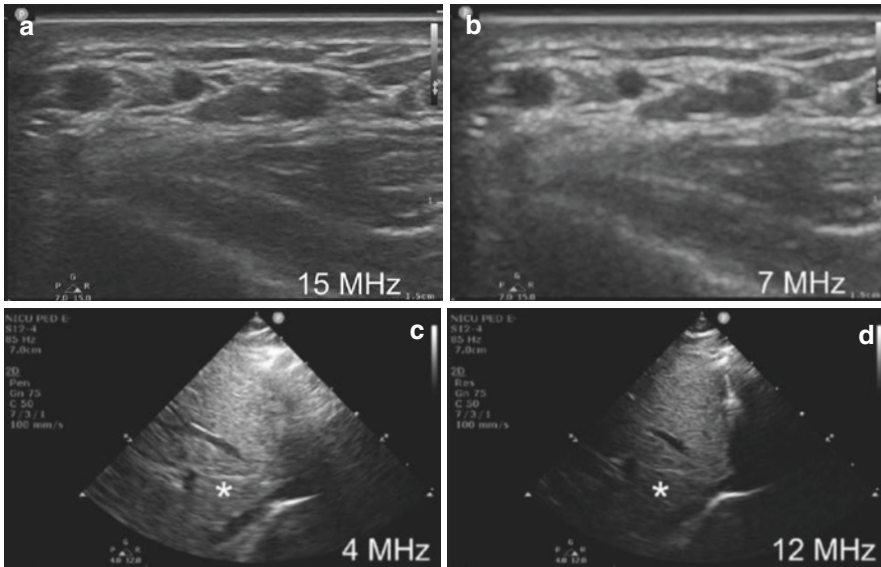


Fig. 9 Optimizing frequency. Transverse view of superficial blood vessels is shown (a, b). There is improved resolution of superficial structures when adjusting to a higher frequency (a) compared to a lower frequency (b).

Longitudinal inferior vena cava view is shown (c, d). Adjusting to a lower frequency (c) allows for improved penetration to visualize deep structures (*) compared to a higher frequency (d)

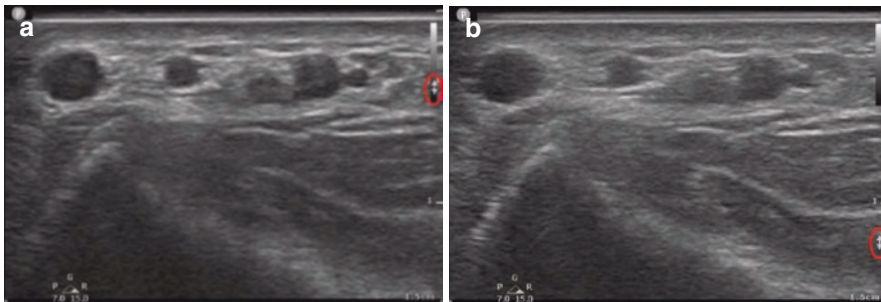


Fig. 10 Focal zone adjustment. Transverse view of superficial blood vessels is shown. The focal point (red ellipse) of the sound beam can be adjusted to allow for the highest resolution at the level of superficial (a) or deep (b) structures

transducer. In reality, the ultrasound waves form a three-dimensional column of sound. Many ultrasound manufacturers offer the ability to focus the sound beam at a specified depth (Fig. 10). Conceptually this is similar to ophthalmology where the lens is able to focus light precisely on the retina. This setting allows for **higher resolution in a limited region** of interest (e.g., at the exact depth of a blood vessel) and can be adjusted to the desired depth. Some ultrasound machines have the ability to designate multiple focal zones simultaneously. While this may improve the resolution at several depths, there is a trade-off. With multiple focal zones, there will be

a significantly worse temporal resolution and resulting degradation of the motion quality.

Transducers

Various transducers are used depending on the structure that needs to be imaged (Fig. 11). The three types of transducers commonly used for POCUS are:

- Linear transducers: the ultrasound beam is stepped sideways by a fraction of beam width between each transmission, all the beams stay-



Fig. 11 The different kinds of transducers and their applications for ultrasound imaging

ing parallel to each other. These transducers give a wide field of view close to the surface and are typically used for vascular or lung imaging.

- Sector transducers (or phased array): the ultrasound beams fan out from a fixed point at or near the body surface. These transducers are useful when gas or bone structures (e.g., ribs and lungs) restrict the acoustic window and are typically used for cardiac imaging.
- Curvilinear transducers are a cross between linear and sector transducers and provide a wide field of view both close to the transducer and at depth. They are typically used for abdominal imaging.

Two-Dimensional Ultrasound

In two-dimensional ultrasound, a cross-sectional image of a structure is built up by sweeping an ultrasound beam through a chosen scan plane.

The beam is transmitted down a scan line and echoes from any targets are detected and plotted as brightness modulation. Each structure has different echo brightness giving rise to the anatomical 2D ultrasound image.

M-mode, or motion mode, imaging interrogates a single straight line and reveals movements of interfaces along that line over time. Each structure of variable brightness traces out a line. M-mode is used for cardiac and lung ultrasound. In echocardiography, M-mode imaging is obtained from the parasternal long or short-axis view [3]. The image is produced by a single line of interrogation and is shown with time on the x-axis and distance from the transducer, or depth, along the y-axis. M-mode is mainly used in echocardiography to estimate left ventricular function (shortening fraction) by measuring the left ventricular dimension and wall thickness during systole and diastole (Fig. 12).

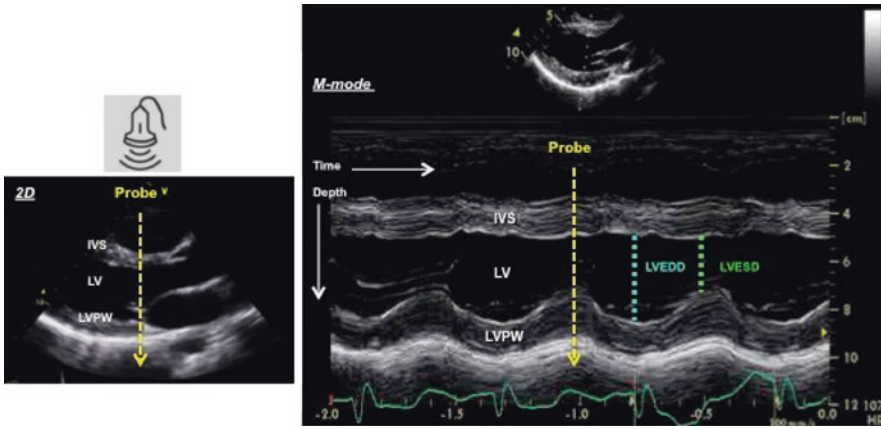


Fig. 12 M-mode echocardiography obtained from the parasternal long-axis view through the left ventricular chambers at the tip of the mitral valve leaflets. *IVS* inter-ventricular septum, *LV* left ventricle, *LVEDD* left ventric-

ular end-diastolic dimension, *LVESD* left ventricular end-systolic dimension, *LVPW* left ventricle posterior wall

Doppler Ultrasound

The Doppler ultrasound modes allow for measurement and color visualization of blood flow velocity and myocardial movement. The ability to estimate velocity is possible due to the Doppler shift phenomenon. Moving objects change the frequency of the Doppler shift according to the direction and velocity with which they are moving in relation to the transducer [4]. Doppler ultrasound modes include color flow Doppler, pulsed-wave (PW) Doppler, continuous-wave (CW) Doppler, high-pulsed repetition frequency (HPRF) Doppler, and Tissue Doppler modes.

The Doppler Effect

Ultrasound waves emitted from the transducer have a single frequency but upon reflection off a moving structure, such as blood, the frequency is altered (Fig. 13a). This shift in frequency, termed the Doppler shift (Δf), is dependent upon several factors and is calculated using the following formula:

$$\Delta f = f_R - f_T = \frac{2 \cdot v \cdot f_T \cdot \cos(\theta)}{c}$$

where f_T and f_R are the frequencies of the ultrasound waves transmitted from the transducer and reflected off the moving blood, respectively, v is the blood flow velocity, c is the ultrasound wave propagation velocity in the medium, and θ is the angle between the ultrasound beam and the axis of blood flow (i.e., the angle of insonation) (Fig. 13b). There are several important aspects of this equation to point out. First, if the ultrasound beam is perpendicular to the direction of blood flow, a 90° angle of insonation, the frequency shift will be zero ($\cos(90^\circ) = 0$) and the velocity will be incalculable. If the blood flow is parallel and moving directly toward the transducer, a 0° angle of insonation, the Doppler shift will be positive and of the greatest magnitude ($\cos(0^\circ) = 1$). If the same angle is maintained but the blood is flowing away from the transducer, a 180° angle of insonation, the Doppler shift will be negative but still of the greatest magnitude ($\cos(180^\circ) = -1$). By examining the rearranged equation to calculate blood flow velocity (v):

$$v = \frac{\Delta f \cdot c}{2 \cdot f_T \cdot \cos(\theta)}$$

We see that a positive Doppler shift, Δf , results in a positive calculated velocity. When using spectral Doppler imaging, the convention is that

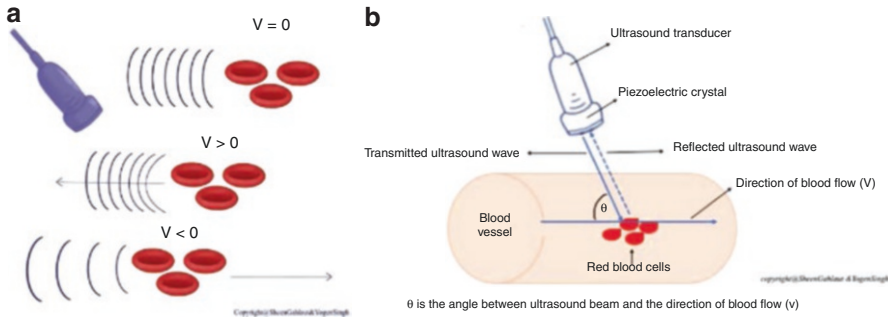


Fig. 13 Doppler shift. (a) The frequency of reflected sound waves is altered upon reflection off a moving structure (e.g., blood). When the movement is toward the transducer ($v > 0$), there is a shift toward a higher frequency—a

positive Doppler shift. Conversely, movement away ($v < 0$) results in a negative Doppler shift. (b) The Doppler shift is dependent upon the angle of insonation (θ). (Courtesy: Sheen Gahlaut)

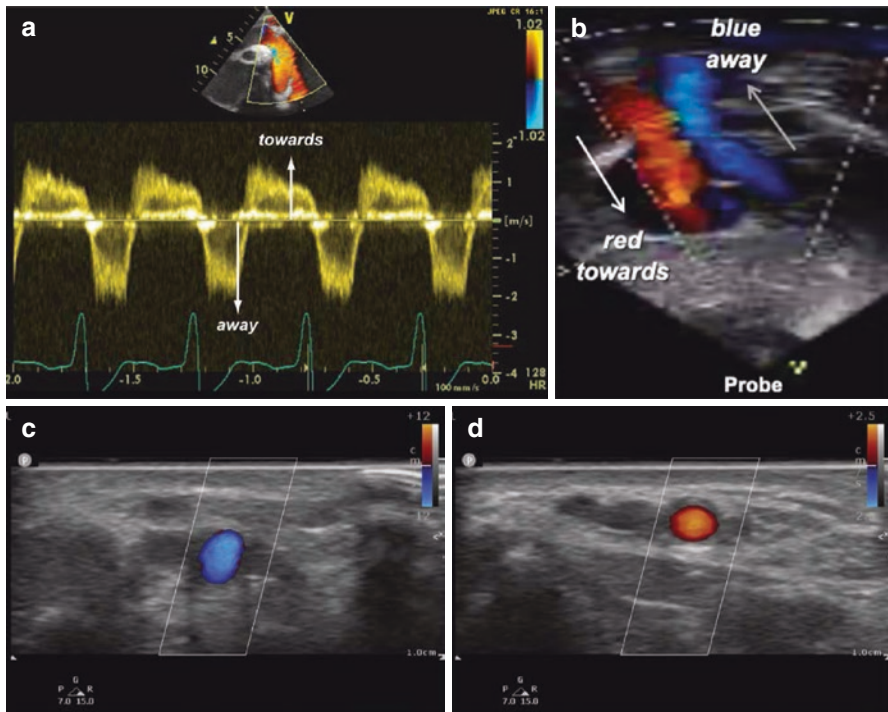


Fig. 14 Spectral and color Doppler imaging. (a) Spectral Doppler obtained in the descending aorta with positive Doppler shift representing flow moving toward the transducer and negative Doppler shift representing flow moving away from the transducer. (b) Color Doppler with flow moving toward the transducer represented in red and flow

moving away from the transducer represented in blue. Transverse view of a superficial blood vessel with color Doppler with flow moving away (blue) the transducer (c) and, after tilting the transducer, flow toward (red) the transducer (d)

blood flowing away from the transducer is displayed as a negative velocity and blood flowing toward the transducer as a positive velocity

(Fig. 14). A *positive velocity* (i.e., toward the transducer and above the baseline) is typically represented in red on color Doppler. Conversely,

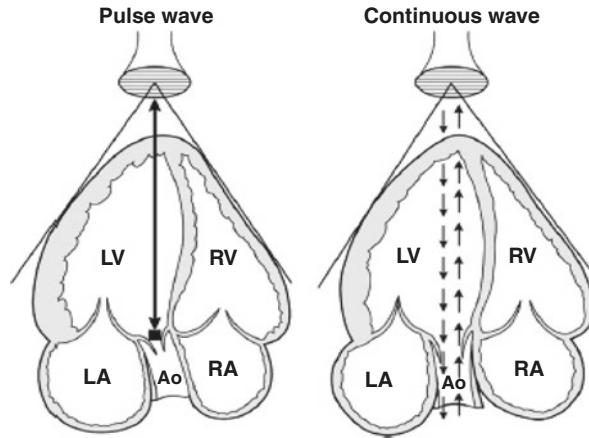


Fig. 15 Schematic representation of pulsed-wave and continuous-wave Doppler at the level of the aorta from apical 5-chamber view. *Ao* aorta, *LA* left atrium, *LV* left

ventricle, *RA* right atrium, *RV* right ventricle. (From Anavekar NS, Oh JK, Doppler echocardiography: a contemporary review. *J Cardiol* 2009;54(3):347–58, Fig. 2)

blood *flow away from the transducer, a negative Doppler* shift and velocity (below the baseline), is **represented in blue** (Fig. 14). It should be noted that red and blue have no correlation with artery or vein, only the direction of flow (Fig. 14). Learners are often taught the BART mnemonic to remember this: **Blue Away, Red Toward**.

During PW Doppler, the transducer transmits short bursts of ultrasound waves at regular intervals (the pulse repetition frequency, PRF). PW Doppler's main advantage is that it allows the measurement of blood flow velocity at a precise location (Fig. 15).

However, the main disadvantage of PW doppler is the ability to accurately determine blood flow direction or velocity when there is high-velocity blood flow. There is a limit in the ability to accurately measure the Doppler shift, termed the Nyquist limit. The Nyquist limit is equal to half the sampling rate, or PRF. **PW** is then limited by the Nyquist limit making *it unsuitable for high-velocity flow quantification*.

In contrast, CW Doppler is not constrained by velocity limits. CW Doppler can record velocities exceeding those of PW Doppler but interrogates all points along a given ultrasound beam rather than at a single location (Fig. 15). The disadvantage is that knowledge of anatomy must

already be determined to identify the precise location of the maximum velocity.

PW is used to record the velocity across the valves, by placing the sample volume slightly proximal to the valve. During Doppler imaging, it is important that the beam should be perfectly aligned with the line of flow to avoid distortion of data. An angle of interrogation of less than 20° is essential to ensure clinically accurate information.

The pulmonary and aortic valve Doppler tracing is a unique envelope with a peak velocity of approximately 1 m/s while the tricuspid and mitral valve inflow Doppler show two phases (Fig. 16).

Flow in early diastole, representing early passive ventricular filling, is characterized by a peak wave called the E wave. It is followed by the A wave, representing late ventricular filling during atrial contraction [5]. The mitral valve peak velocity is slightly higher than that of the tricuspid valve [6]. The flow in the pulmonary vein is continuous with diastolic (D wave) and systolic peak (S wave) (Fig. 17).

The diastolic peak velocity is usually higher than the systolic. Often, flow reversal (AR wave) can be seen during atrial contraction. This flow pattern does not vary with respiration [7]. Vena

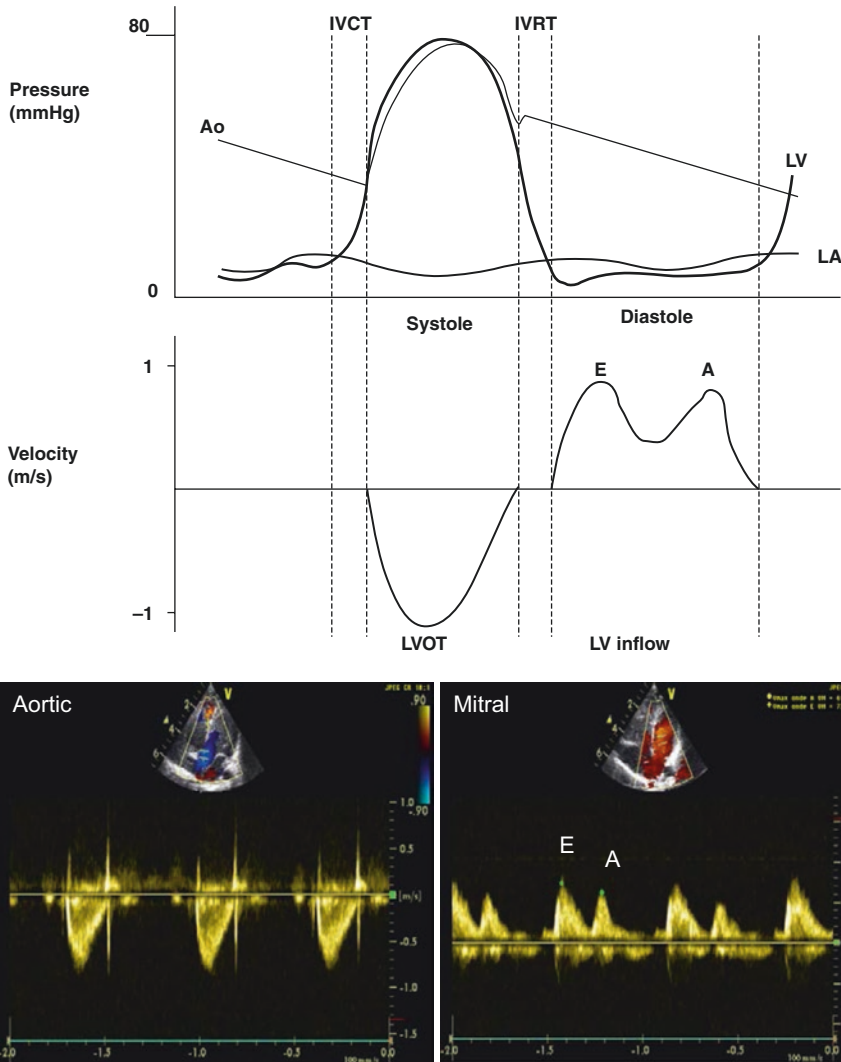


Fig. 16 Comparison of pressure curve of the aorta (Ao), left ventricle (LV, left atrium (LA) and velocity across the left ventricular outflow tract (LVOT) and left ventricular inflow (LV inflow) and spectral Doppler from pulsed-wave across the LVOT (aortic valve) from apical 5-chamber view and LV inflow (mitral valve) from apical

4-chamber view. *E* early diastolic ventricular filling, *A* late diastolic ventricular filling during atrial contraction. (Adapted from Echocardiography for the Neonatologist, Ed Kinner, Alverson, Hunter, Churchill-Livingston 2000, page 115)

caval flow is a continuous low-velocity flow but the peak velocity is greater in systole. Flow reversal during atrial contraction (AR wave) occurs less often in children compared to adults. Respiratory variation is seen with the augmentation of flow velocities during inspiration [5]. Hepatic venous flow shows a predominantly systolic biphasic flow pattern [8].

Clinical Applications of Color Doppler

Color flow Doppler mapping allows velocity information to be overlaid on a two-dimensional image providing data about intracardiac and extracardiac shunts, insufficiency or stenosis of valves, and vessel obstruction. By convention, shades of red are utilized in identifying blood

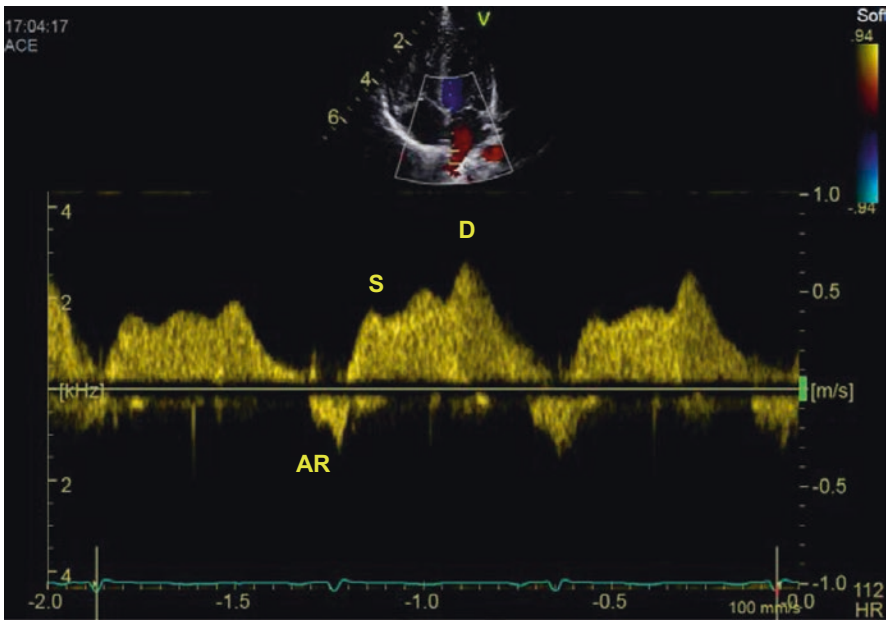
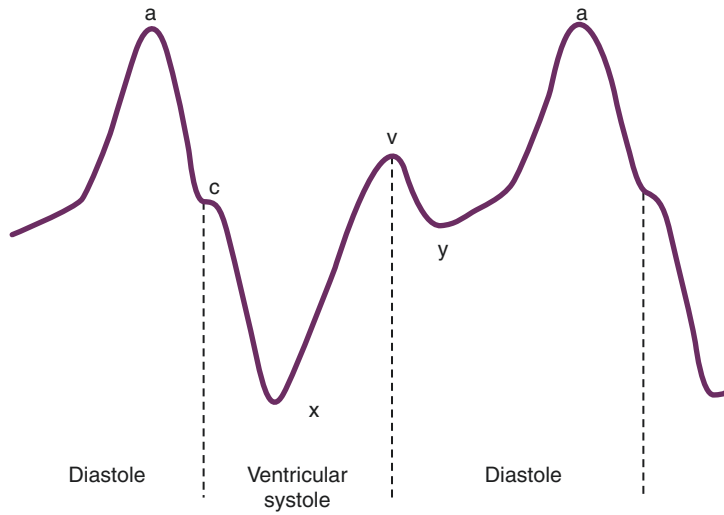


Fig. 17 Comparison of the pressure curve and spectral Doppler tracing from the pulmonary veins. The *a wave* corresponds to the atrial contraction, the *c wave* to the ventricular contraction, the *v wave* to the venous filling when the mitral/tricuspid are closed and venous pressure increases from venous return. The *x descent* corresponds

to ventricular systole (ventricular ejection/atrial relaxation) and the *y descent* to the rapid emptying of the atrium into the ventricle following the opening of the mitral/tricuspid valve. *S* systolic flow, *D* diastolic flow, *AR* flow related to atrial contraction (atrial-reversal)

flowing toward the transducer and blue to indicate blood flowing away from the transducer. Therefore, color flow Doppler defines the pres-

ence and direction of shunts and is used to grade the severity of valvar regurgitation (see cardiac Chaps. 3 and 4).

Tissue Doppler

Tissue Doppler Imaging (TDI) allows recording of the Doppler velocities generated by the ventricular wall motion (myocardium). A PW Doppler cursor is placed on the myocardial wall (mitral, septal, or tricuspid annulus) to record the peak myocardial velocities. Three waveforms are obtained: a peak systolic wave (S'), an early diastolic wave (E'), and an end-diastolic wave (A') produced by atrial contraction

(Fig. 18) [9]. The Tissue Doppler systolic mitral annular velocity has been shown to correlate with global left ventricular myocardial function [10]. TDI has also been used to estimate diastolic function, and is relatively independent of preload condition, as opposed to the Doppler evaluation [11, 12]. TDI assessment is out of the scope of POCUS assessment but it is part of the echocardiography protocols including neonatologist-performed echocardiography (NPE) assessments.

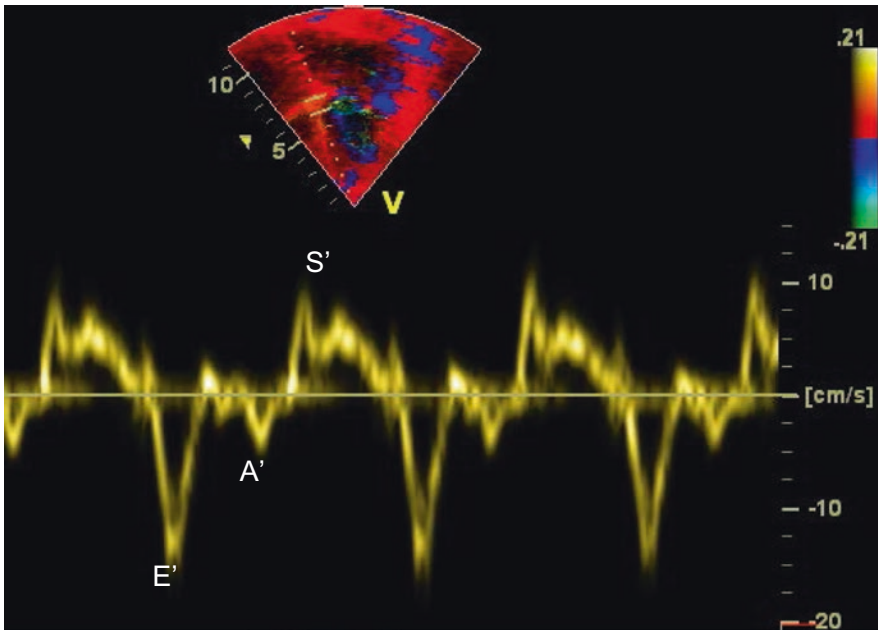


Fig. 18 Tissue Doppler Imaging (TDI) at the level of the interventricular septum from apical 4-chamber view demonstrating the E' , A' , and S' waves. A' late diastolic ven-

tricular filling during atrial contraction, E' early ventricular filling, S' systolic wave

Artifacts

Artifacts are inherent to ultrasound imaging. The software embedded into modern ultrasound machines incorporates sophisticated artifact suppression algorithms to filter out many of these artifacts in real time. A clear understanding of the remaining unfiltered artifacts allows the sonographer to obtain additional information that would otherwise be unavailable. In some cases, the sonographer must disable the artifact suppression algorithms to obtain the desired information (e.g., lung ultrasound). Here we discuss several important categories of artifacts. There are many artifacts that will not be discussed here and the reader is referred to a recent comprehensive review [13].

Gain Artifact

To optimize an image, the gain is either adjusted manually or using automated algorithms (the “automatic” button in some ultrasound machines). This artifact is common among novice sonographers when the gain has not been adjusted properly. When the gain is turned up too high, echogenic foci begin to appear within regions that should be anechoic. For example, when imaging a blood vessel, small echogenic foci may appear in the lumen in the absence of any true thrombi or emboli (Fig. 6). To avoid this artifact, the sonographer should locate a structure in the field of view that is known to be anechoic (e.g., vessel lumen) and decrease the gain until the region of interest appears anechoic. Learners are commonly taught to adjust the gain until “black is black.”

Posterior Acoustic Shadowing

This is a common artifact caused by the reflection of ultrasound waves at the interface between two tissues with high acoustic impedance mismatch. A very high percentage of ultrasound waves are reflected and thus, due to this “obstruction,” relatively few continue to penetrate deeper tissues (Fig. 4). Several common structures that cause this are air, bone, and foreign bodies. The lack of sound waves returning from deeper structures results in the ultrasound machine displaying an anechoic, or black, region during B-mode imaging. Occasionally the structure causing the posterior acoustic shadowing is not sonographically obvious and the only clue to its presence is the shadowing itself. For example, by identifying posterior acoustic shadowing, the sonographer can infer the presence of a foreign body, even if the foreign body itself is not apparent.

Posterior Acoustic Enhancement

Posterior acoustic enhancement is a diffuse highly echogenic artifact occurring deep to a fluid-filled structure. To understand this artifact, it is critical to appreciate the phenomenon of ultrasound wave attenuation. Attenuation refers to the gradual decrease in wave amplitude as the wave travels through a medium. To compensate for this and allow for a homogenous tissue to appear homogenous on the screen, the ultrasound machine software uses correction algorithms to gradually increase the amplitude of the reflected echoes corresponding to the far field (Fig. 19). The sonographer can manually adjust this ampli-

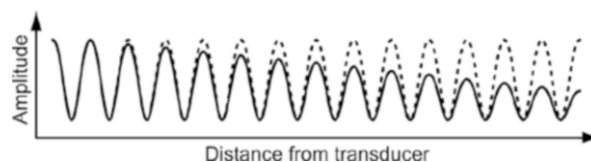


Fig. 19 Amplitude attenuation and compensation. The sound wave amplitude becomes attenuated (solid line) while traveling through a medium. Ultrasound machine

software compensates for this phenomenon by gradually increasing the amplitude (dashed line) resulting in the isoechoic appearance of homogenous tissue

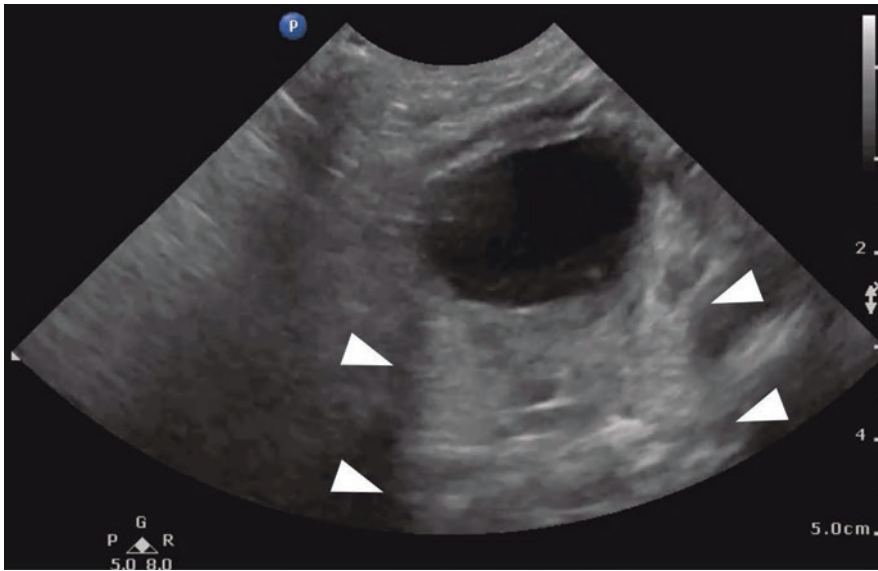


Fig. 20 Posterior acoustic enhancement artifact. Transverse view of the bladder is shown. Tissue deep into the bladder falsely appears more echogenic (arrowheads) than the surrounding tissue

fication using the time-gain compensation (TGC) settings. Posterior acoustic enhancement can be recognized as a diffuse hyperechoic signal in regions where it is unexpected. A common example of this is cystic structures such as the bladder (Fig. 20), gallbladder, and abscess cavities. As sound waves pass through an anechoic fluid-filled cavity (e.g., bladder), the degree of attenuation is significantly less than normally predicted in biological tissues. As the sound waves progress past the cavity, the wave amplitude is higher than adjacent waves that did not pass through the cavity. The software correction algorithm continues to compensate for attenuation thus overcompensating without “realizing” there was less attenuation. Thus, the tissue deep into the cavity falsely appears more echogenic than the surrounding tissue.

Reverberation and Contact Artifacts

Reverberation artifact occurs when an ultrasound wave repeatedly echoes between two highly echogenic specular reflectors (e.g., the pleura and skin). With each echo, a fraction of the reflected ultrasound wave returns to the transducer and

appears as a horizontal line. The remaining reflected ultrasound waves continue to echo between the specular reflectors, and with each subsequent echo, a fraction of waves returns to be detected by the transducer. The time required for the ultrasound wave to travel between the specular reflectors is fixed and hence the horizontal lines are equidistant from each other, a hallmark of this artifact. Reverberation artifact is commonly observed in lung imaging where it manifests in two distinctly different forms. The first, A-lines, are caused by reverberations between the pleura and the skin (Fig. 21a). The second, B-lines or “comet-tails,” are caused by intra-pulmonary reverberation and originate at the pleural line extending to the far field edge of the screen (Fig. 21b) [14].

Contact artifact is similar to reverberation artifact and is a common occurrence among novice sonographers. This form of reverberation artifact is caused by not maintaining contact between the transducer surface and the skin resulting in the interposition of air between the two surfaces. The ultrasound waves reverberate between the skin surface and the surface of the transducer resulting in a series of horizontal echogenic lines (Fig. 21c). This is often due to inadvertent sliding, tilting, or

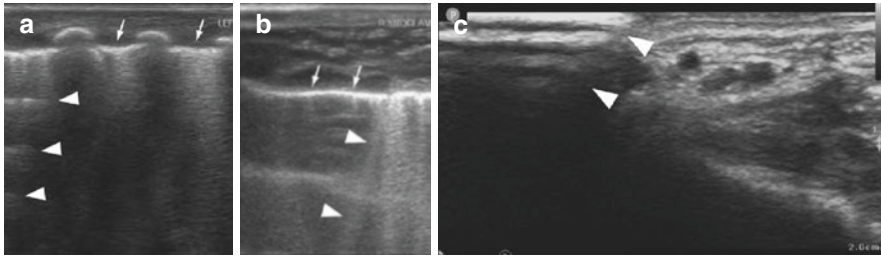


Fig. 21 Forms of reverberation artifact. Lung ultrasound images showing (a) equidistant horizontal A-lines (arrowheads) and (b) vertical B-lines or comet-tails (arrow-

heads). The pleural line is indicated (arrows). (c) Contact artifact is shown (arrowheads) where the transducer loses contact with the skin

rocking of the transducer but may also be due to insufficient gel. The sonographer can avoid inadvertent transducer movement by anchoring the fingers or heel of the hand to the bed or to the patient's skin while performing the ultrasound. This allows the sonographer to maintain their focus on the screen and to feel the inadvertent movement without looking at the transducer.

References

1. Shung KK. Diagnostic ultrasound: imaging and blood flow measurements. 2nd ed. Boca Raton: CRC Press; 2015.
2. Duck FA. The propagation of ultrasound through tissue. In: Haar G, editor. The safe use of ultrasound in medical diagnosis. 3rd ed. London: British Institute of Radiology; 2012.
3. Solinger R, Elbl F, Minhas K. Echocardiography in the normal neonate. *Circulation*. 1973;47(1):108–18. <https://doi.org/10.1161/01.cir.47.1.108>.
4. Franklin DL, Schlegel W, Rushmer RF. Blood flow measured by Doppler frequency shift of back-scattered ultrasound. *Science*. 1961;134(3478):564–5. <https://doi.org/10.1126/science.134.3478.564>.
5. Riggs TW, Rodriguez R, Snider AR, Batton D, Pollock J, Sharp EJ. Doppler echocardiographic evaluation of right and left ventricular diastolic function in normal neonates. *J Am Coll Cardiol*. 1989;13(3):700–5. [https://doi.org/10.1016/0735-1097\(89\)90614-1](https://doi.org/10.1016/0735-1097(89)90614-1).
6. Cohen GI, Pietrolungo JF, Thomas JD, Klein AL. A practical guide to assessment of ventricular diastolic function using Doppler echocardiography. *J Am Coll Cardiol*. 1996;27(7):1753–60. [https://doi.org/10.1016/0735-1097\(96\)00088-5](https://doi.org/10.1016/0735-1097(96)00088-5).
7. Minich LL, Tani LY, Hawkins JA, McGough EC, Shaddy RE. Abnormal Doppler pulmonary venous flow patterns in children after repaired total anomalous pulmonary venous connection. *Am J Cardiol*. 1995;75(8):606–10. [https://doi.org/10.1016/s0002-9149\(99\)80626-2](https://doi.org/10.1016/s0002-9149(99)80626-2).
8. Meyer RJ, Goldberg SJ, Donnerstein RL. Superior vena cava and hepatic vein velocity patterns in normal children. *Am J Cardiol*. 1993;72(2):238–40. [https://doi.org/10.1016/0002-9149\(93\)90170-h](https://doi.org/10.1016/0002-9149(93)90170-h).
9. Dokainish H. Tissue Doppler imaging in the evaluation of left ventricular diastolic function. *Curr Opin Cardiol*. 2004;19(5):437–41. <https://doi.org/10.1097/01.hco.0000131538.55528.8f>.
10. Gulati VK, Katz WE, Follansbee WP, Gorcsan J 3rd. Mitral annular descent velocity by tissue Doppler echocardiography as an index of global left ventricular function. *Am J Cardiol*. 1996;77(11):979–84. [https://doi.org/10.1016/s0002-9149\(96\)00033-1](https://doi.org/10.1016/s0002-9149(96)00033-1).
11. Vignon P, Allot V, Lesage J, Martaille JF, Aldigier JC, Francois B, et al. Diagnosis of left ventricular diastolic dysfunction in the setting of acute changes in loading conditions. *Crit Care*. 2007;11(2):R43. <https://doi.org/10.1186/cc5736>.
12. Eidem BW, McMahon CJ, Ayres NA, Kovalchin JP, Denfield SW, Altman CA, et al. Impact of chronic left ventricular preload and afterload on Doppler tissue imaging velocities: a study in congenital heart disease. *J Am Soc Echocardiogr*. 2005;18(8):830–8. <https://doi.org/10.1016/j.echo.2004.09.011>.
13. Baad M, Lu ZF, Reiser I, Paushter D. Clinical significance of US artifacts. *Radiographics*. 2017;37(5):1408–23. <https://doi.org/10.1148/rg.2017160175>.
14. Dietrich CF, Mathis G, Blaivas M, Volpicelli G, Seibel A, Wastl D, et al. Lung B-line artefacts and their use. *J Thorac Dis*. 2016;8(6):1356–65. <https://doi.org/10.21037/jtd.2016.04.55>.

Part II

Cardiovascular System Assessment



Basic Echocardiographic Views for the Intensivist

Cécile Tissot and Yogen Singh

Contents

Introduction	31
Basic Anatomy of the Heart for Cardiac Ultrasound	32
Major Indications for Functional Echocardiography and Cardiac POCUS Assessment	32
Echocardiography Windows and Basic Views for the Neonatal and Pediatric Intensivist	33
Parasternal Window	34
Apical Window	37
Subcostal Window	39
Suprasternal Window	41
Conclusion	45
References	45

C. Tissot (✉)

Department of Pediatrics, Clinique des Grangettes,
Chêne-Bougeries, Geneva, Switzerland

Y. Singh

Department of Pediatrics, Division of Neonatology,
Loma Linda University School of Medicine,
California, USA

Department of Pediatrics, Division of Neonatal and
Developmental Medicine, Stanford University School
of Medicine, California, UK

Department of Pediatrics, Division of Neonatology,
University of Southern California, California, UK

ESPNIC Cardiovascular Dynamics Section and
POCUS Working Group, Geneva, Switzerland
e-mail: YSingh@llu.edu

Introduction

Echocardiography has become an invaluable tool in the pediatric and neonatal intensive care units [1–4]. In conjunction with clinical examination and cardiovascular monitoring techniques, echocardiography and point of care ultrasound (POCUS) can provide real-time, rapid, noninvasive, and reliable diagnostic answers that are invaluable to patient care.

Echocardiography, as typically performed by trained cardiologists, provides a comprehensive qualitative and quantitative assessment of anatomy and physiology in various neonatal and pediatric conditions. Cardiac POCUS provides discrete qualitative assessments (present/absent, mild/

Table 1 Advantages and disadvantages to cardiac point of care ultrasound (POCUS)

• Advantages	• Disadvantages
▫ Fast and immediate results	▫ Highly user-dependent
▫ Non-invasive exam	▫ Does not provide quantitative analysis
▫ Dynamic assessments	
▫ Serial monitoring	

moderate/ severe, etc.) to answer specific questions at the patient bedside. *Cardiac POCUS should not be used for the screening of congenital heart diseases (CHDs) in all children or for comprehensive hemodynamic evaluation in neonatal patients.*

Both cardiac POCUS and complete echocardiography can be performed at the patient's bedside, can be used in acute clinical situations, and provide rapid assessments in order to aid in making a diagnosis or to help in assessing responsiveness to treatment. In clinical practice they have different indications and involve different training. However, basic echocardiography views are required in both cardiac POCUS as well as complete echocardiography. Cardiac POCUS should also be distinguished from targeted neonatal echocardiography (TNE, also referred to as neonatologist performed echocardiography or NPE), an emerging field of imaging for neonatologists requiring more expansive views similar to functional echocardiography, as well a unique understanding of neonatal circulation and hemodynamics. The advantages and disadvantages of cardiac POCUS are summarized in Table 1. The primary barrier to the universal adoption of this "stethoscope of the future" is that it is operator-dependent, therefore adequate training is needed in order to understand its limitations prior to relying on the information it provides.

Basic Anatomy of the Heart for Cardiac Ultrasound

The normal heart is situated in the left hemithorax with its apex pointing anterior and inferior towards the left side of the body. The base of the heart is anchored by the great vessels: the aorta, the main pulmonary artery, and the superior vena cava. The heart consists of four chambers: two thin walled atria and two thicker walled ventricles, separated by four valves: the atrioventricu-

lar valves (the tricuspid and mitral valves) and the semilunar valves (pulmonary and aortic valves). The blood flows from the vena cava into the right atrium and then flows through the tri-leaflet tricuspid valve (recognizable by its more apical insertion and by its septal leaflet) into the trabeculated thin-walled right ventricle (recognizable by its moderator band) to be pumped into the lungs. The left atrium is connected to the four pulmonary veins and blood flows through the anterior and posterior leaflets of the mitral valve into the smooth thick-walled left ventricle to be pumped into the aorta through the aortic valve.

Major Indications for Functional Echocardiography and Cardiac POCUS Assessment

Over the last few decades, echocardiography has been used primarily by pediatric cardiologists to diagnose or rule out congenital heart defect (CHD). While a comprehensive structural and functional assessment remains the remit of a pediatric cardiologist or clinician formally trained in echocardiography, pediatric cardiac POCUS can be used by a trained person for the indications below. Given the complex cardiovascular physiology and risk of duct dependent CHDs, the scope of cardiac POCUS is further limited in the neonatal period and should be mainly used for emergency situations such as detection of pericardial effusion and cardiac tamponade, qualitative assessment of cardiac function on 'eyeballing', evaluation of line tip position and initial rapid assessment in a crashing infant. Children with abnormalities identified with cardiac POCUS should have comprehensive assessment by an expert [5]. Suggested cardiac POCUS (including NPE) assessments include:

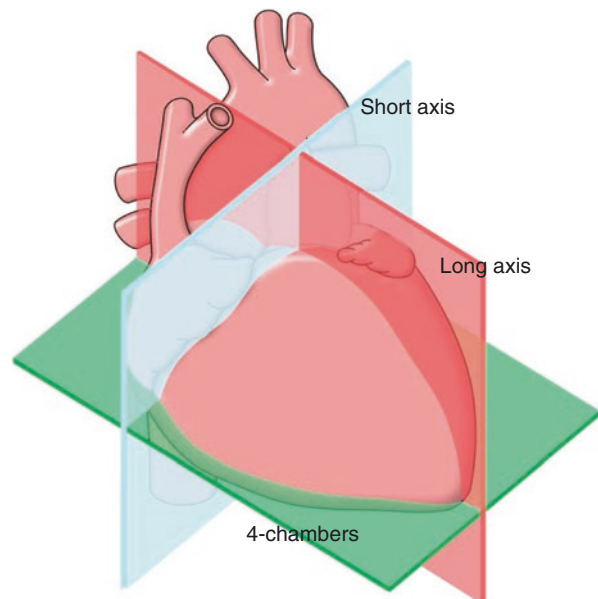
1. Qualitative and semi-quantitative evaluation of cardiac function
2. Evaluation of filling pressure and fluid responsiveness
3. Diagnosis of pericardial effusion and tamponade
4. Guidance for interventions (pericardiocentesis)

5. Recognition of pulmonary hypertension and estimation of pulmonary artery systolic pressure (PASP) (comprehensive assessment is out of the scope of POCUS)
6. Patency of ductus arteriosus on POCUS (a comprehensive evaluation of ductus arteriosus is out of the scope of POCUS and is performed on neonatologist-performed echocardiography (NPE) or advanced functional echocardiography)
7. Evaluation of transitional circulation of the newborn (on NPE or advanced functional echocardiography, and out of the scope of POCUS)
8. Evaluation of cardiac output and hemodynamics (advanced functional echocardiography, out of the scope of POCUS)
9. Evaluation of central line tip position

Echocardiography Windows and Basic Views for the Neonatal and Pediatric Intensivist

In order to limit respiration artifacts, the patient should be placed in a left lateral decubitus position with the neck slightly extended if possible.

Fig. 1 Echocardiography views refer to the axis of the heart with parasternal long axis (red), parasternal short axis (blue), and apical 4-chamber (green)



All planes refer to the axis of the heart and not to its position within the body (Fig. 1).

The different views are obtained from the four standard windows (Fig. 2).

For each window, different movements of the probe (translation, angulation, and rotation, see Fig. 3) will give rise to different echocardiographic views. Sweeping refers to a continuous movement of the probe made to allow imaging of the different views for one specific window in one clip.

The standard echocardiography views in the neonatal and pediatric intensive care unit include:

- the parasternal views including long axis and short axis (high left thorax just lateral to the sternum)
- the apical views (left lateral thorax just inferior and lateral to the nipple)
- the subcostal views (below the xiphoid region)
- the suprasternal views (suprasternal notch) for aortic arch assessment; it may be useful for looking at line placement (jugular or subclavian catheters) and is a crucial view for the evaluation of patent ductus arteriosus

Fig. 2 Pediatric basic echocardiographic windows: parasternal left (yellow), apical (green), subxyphoid or subcostal (red), suprasternal (blue)

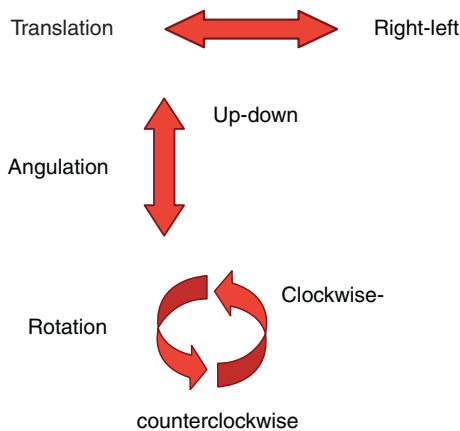
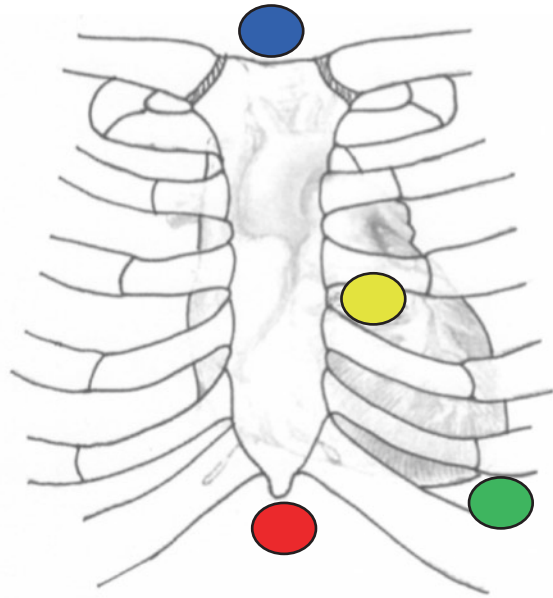


Fig. 3 Basic movements made with the probe in order to obtain the different echocardiography views for a specific window

Parasternal Window

The parasternal view evaluates the heart aligned along its long and short axis.

Parasternal long axis (PLAX): In the long axis view (Fig. 4), the left ventricular inflow and outflow tracts can be imaged. The aorta can be observed, as well as its relationship to the mitral valve (mitro-aortic continuity). The left ventricular infero-posterior wall and interventricular septum are visualized. The anterior and poste-

rior leaflets of the mitral valve can be examined.

The standard PLAX view includes the left atrium, left ventricle, aortic valve and right ventricle (middle image, Fig. 4). From this standard view, the probe can be tilted anteriorly (towards left shoulder) to achieve the right ventricular infow view (top image, Fig. 4) and posteriorly (towards right hypochondrium) for the right ventricular outflow view (bottom image, Fig. 4) (Fig. 5).

Parasternal long axis view (PLAX): This view is usually used for the assessment of the following echocardiographic parameters:

- LV size and function
- RV size and function
- Interventricular septum
- Ascending aorta
- Aortic valve
- Mitral valve
- Pericardium/pericardial effusion, and differentiating pericardial effusion from pleural effusion

Parasternal short axis (PSAX): A 90° clockwise rotation will provide the short axis views (Fig. 6), providing an evaluation of the heart chambers, the semilunar and atrioventricular valves,

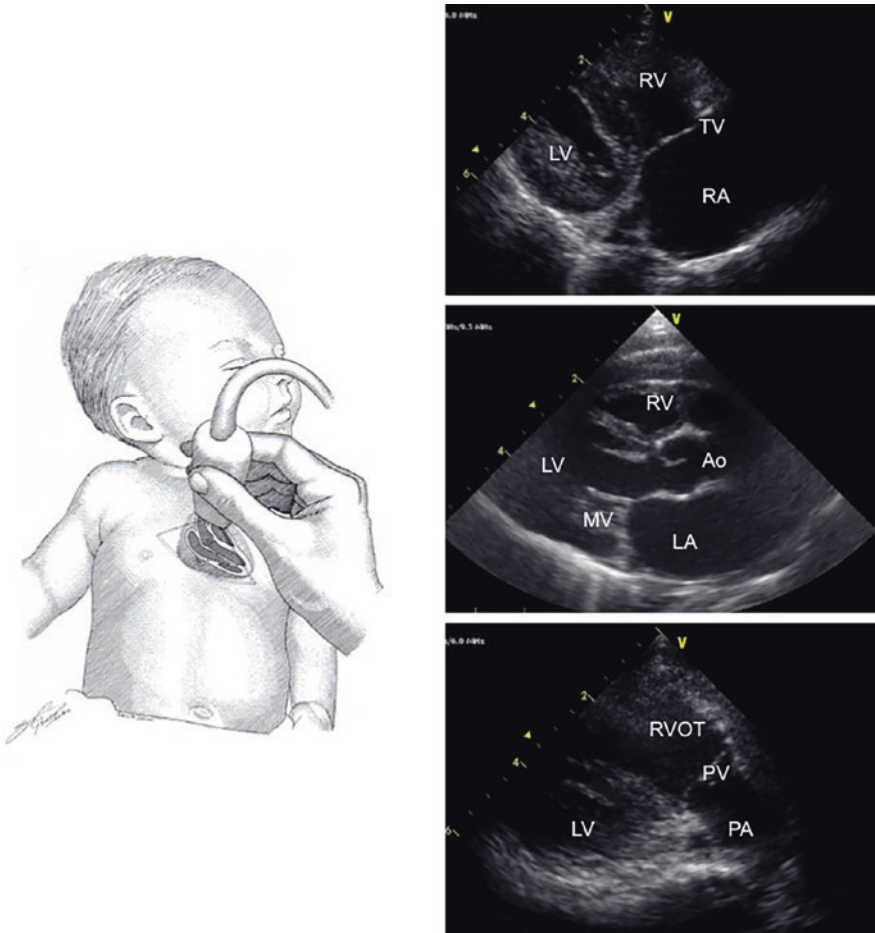
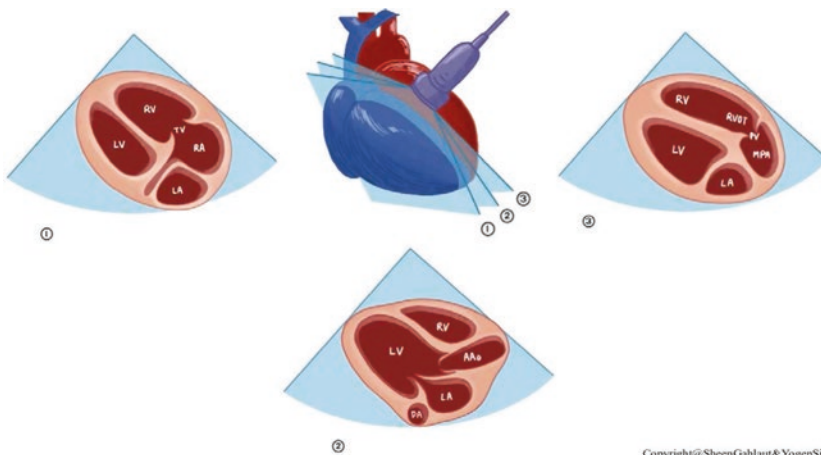


Fig. 4 Parasternal long axis view (PLAX). Standard PLAX echocardiographic image planes from the high left chest just lateral to the sternum with marker towards the right shoulder. *Ao* aortic valve, *CS* coronary sinus, *IVC* inferior vena cava, *IVS* interventricular septum, *LA* left

atrium, *LPA* left pulmonary artery, *LV* left ventricle, *MV* mitral valve, *PA* pulmonary artery, *PV* Pulmonary valve, *PVs* Pulmonary veins, *RA* right atrium, *RPA* right pulmonary artery, *RV* right ventricle, *TV* tricuspid valve, *RVOT* right ventricular outflow tract, *SVC* superior vena cava



Copyright@SheenGahlaut&YogenSingh

Fig. 5 Parasternal long axis views: (1) Right ventricular inflow view, (2) Standard parasternal long axis (PLAX) view, and (3) PLAX right ventricular inflow view. (Courtesy: Sheen Gahlaut)

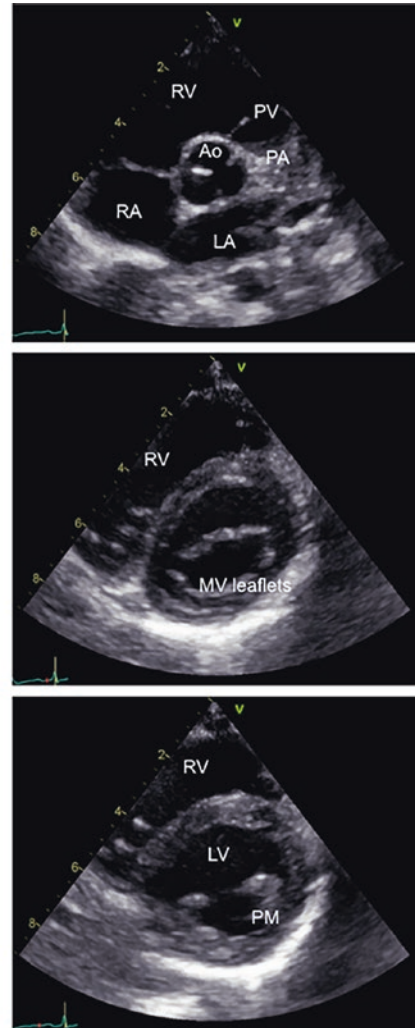
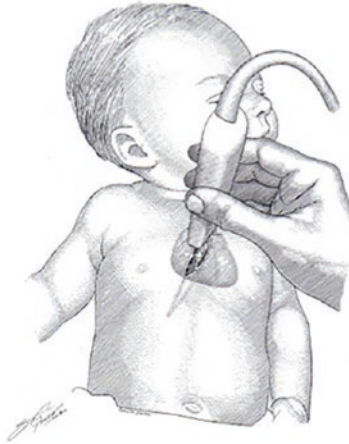


Fig. 6 Parasternal short axis view at the base, mitral valve, and papillary muscles level

and the coronary arteries. The ventricular chambers can be examined by sweeping from the apex towards the base of the heart. The left ventricle has circular geometry with symmetric contraction. The right ventricle is trabeculated and crescent-shaped in short axis views. Sweeping further to the base of the heart will show the papillary muscles followed by the mitral valve annulus. Continued sweep to the base of the heart will allow imaging of the tri-leaflet aortic valve, the right ventricular outflow tract and the pulmonary artery as it “wraps” itself anteriorly and to the left. Part of the atrial septum and the tricuspid valve may be seen.

Progressive sweep permits the examination of the branch pulmonary arteries (Fig. 7).

Parasternal short axis view (PSAX) can be used for the following echocardiographic parameters:

- LV size and function
- RV size and function
- Assessment of the interventricular septum for flattening (in cases with pulmonary hypertension or right ventricle volume overloading)
- Aortic valve
- Mitral valve

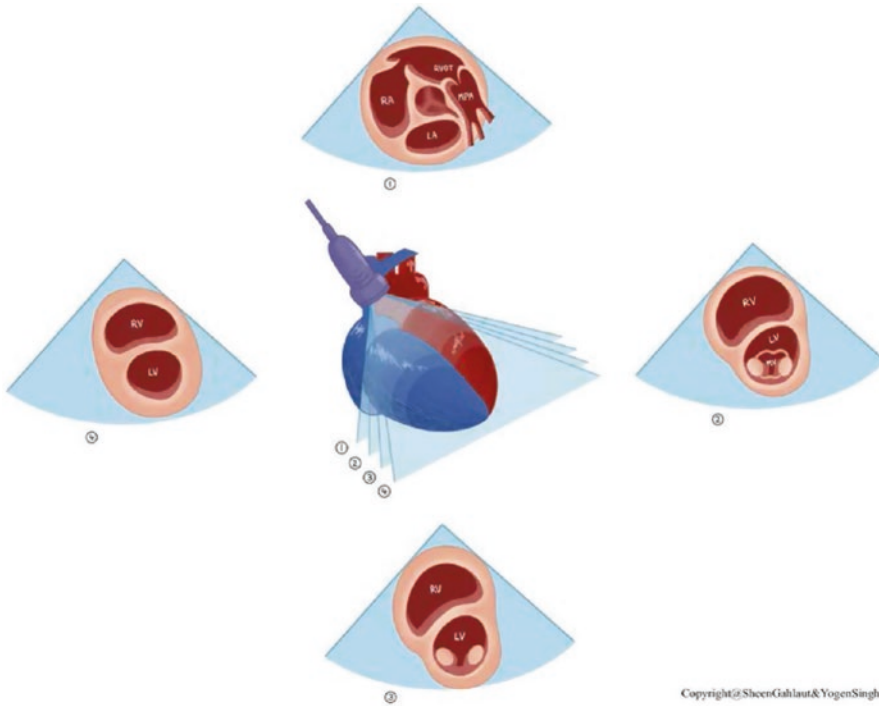


Fig. 7 Parasternal short axis sweep views at (1) base of heart, (2) mitral valve level, (3) papillary muscles level, and (4) at the apex. (Courtesy: Sheen Gahlaut and Yogen Singh)

- Eccentricity index (EI) for evaluation of pulmonary hypertension
- RV to LV ratio

Apical Window

The apical position (Fig. 8) allows visualization of all four chambers and heart valves with a left-to-right orientation. The four-chamber view identifies the anatomic right and left ventricles. The coronary sinus can be visualized from a posterior sweep while tilting the transducer anteriorly will show the apical five-chamber (A5C) view in which the atrial and ventricular septa may be imaged, and the left ventricular outflow tract and ascending aorta may also be examined. The mitral valve leaflets and pulmonary veins as they enter the left atrium can also be seen in the A5C view. Turning the transducer 60° clockwise will bring a three-chamber view which shows the sub-aortic structures and is best for Doppler measurements of the

left ventricular outflow tract. Turning the transducer 90° counterclockwise from the four-chamber view will produce a two-chamber view of the left ventricle and left atrium. This view is best to evaluate anterior and posterior left ventricular wall function.

The right ventricular outflow, A5C and posterior views should be considered advanced and are acquired by tilting the probe as demonstrated in Fig. 9.

Apical views can be used in the assessment of the following echocardiographic parameters:

- Left ventricle and atrium morphology and left ventricular function
- Right ventricle and atrium morphology and right ventricular function
- Aortic valve
- Mitral valve
- Tricuspid valve
- Estimation of pulmonary artery systolic pressure (PASP) from tricuspid regurgitation

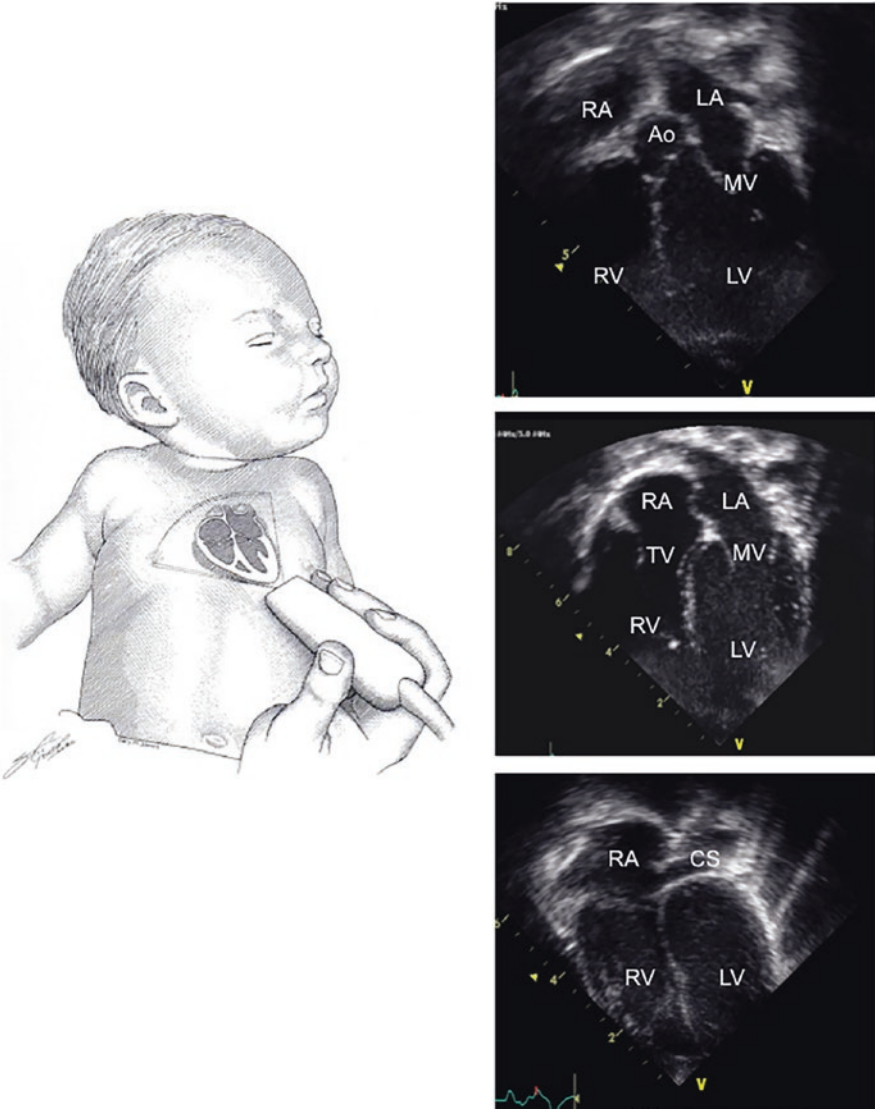


Fig. 8 Apical views from anterior to posterior (inverted picture as often used by the pediatric cardiologist)

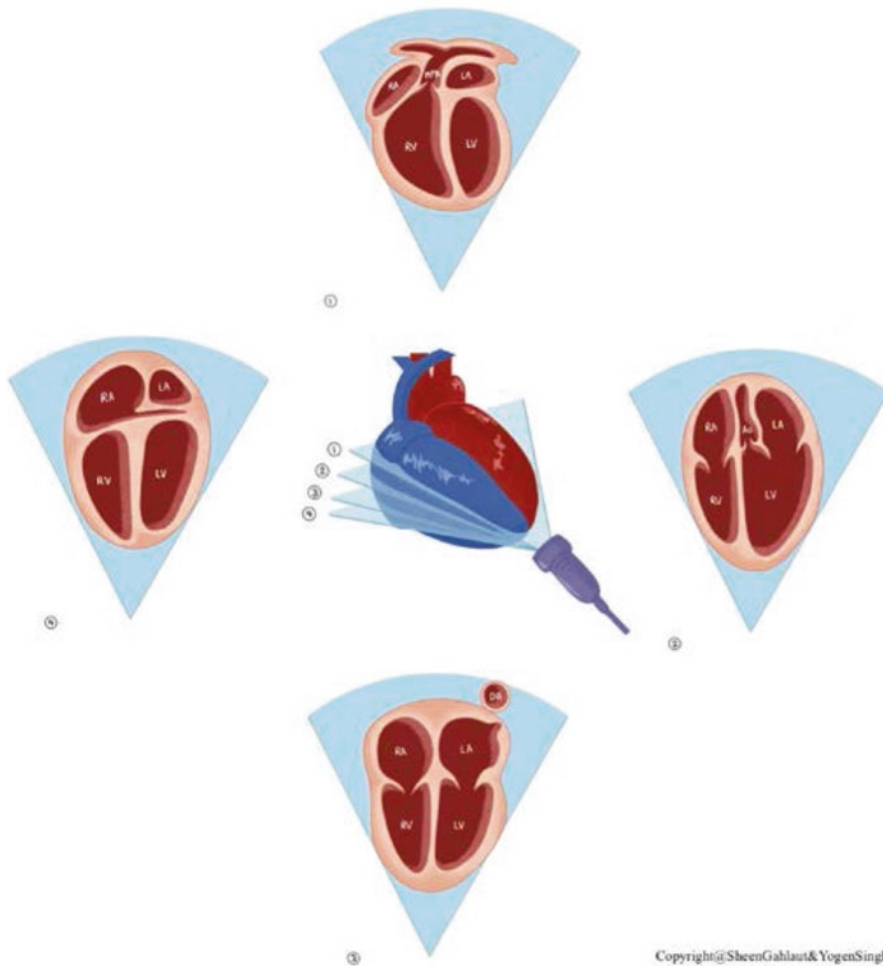


Fig. 9 Apical sweep views at level of (1) Apical right ventricular outflow tract, (2) apical left ventricular flow tract, (3) classical apical 4-chamber, and (4) apical posterior views. (Courtesy: Sheen Gahlaut and Yogen Singh)

- Tricuspid annular pan-systolic excursion (TAPSE) for right ventricle systolic function
- Left ventricular outflow velocity time integral (VTI) from apical 5-chamber view—for calculation of left ventricular cardiac output

Subcostal Window

The subcostal view provides comprehensive information, especially in the neonatal period.

Children are placed supine with the transducer in the subxiphoid position. In older cooperative children, better image quality may be achieved by having the child hold his breath allowing the heart to move downwards towards the transducer.

Subcostal views (Fig. 10) provide detailed imaging of the entire heart (atrial and ventricular septum, atrioventricular valves, atrial and ventricular chambers, and systemic venous return) though in older children cardiac views may demonstrate poorer resolution with the increased distance from

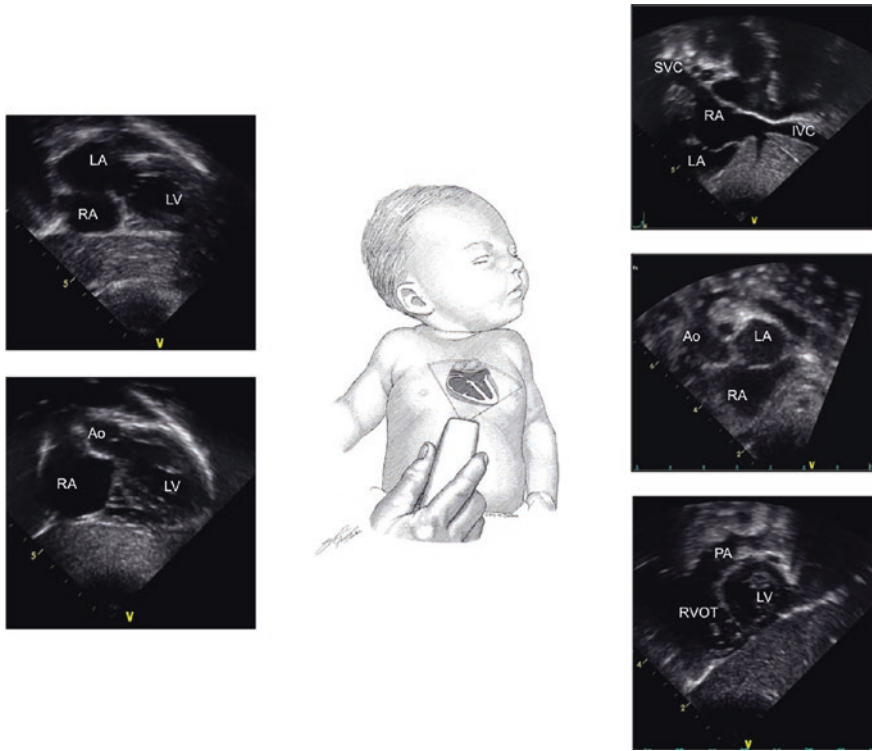


Fig. 10 Subcostal views (inverted picture used by the pediatric cardiologist)

the heart to the probe. Rotating the transducer will permit images of both ventricular outflow tracts. Even the peripheral pulmonary arteries and the aorta may be examined from this position in some patients. This view is prioritized in cardiac arrest scenarios in which the chest is unavailable for imaging due to ongoing compressions. This view may also be ideal in critically ill children with obstructive lung diseases precluding transmission of ultrasound waves due to overdistended aerated lung overlying the cardiac structure.

Subcostal sweep views may be obtained by tilting the probe at different levels as illustrated in Fig. 11.

Subcostal views are used for the assessment of the following echocardiographic parameters:

- Left ventricle and atrium morphology and left ventricular function
- Right ventricle and atrium morphology and right ventricular function
- Intra-atrial septum (and intra-atrial shunt evaluation)
- Mitral valve
- Tricuspid valve
- Pericardium and pericardial effusion
- Superior vena cava (SVC) imaging and Doppler

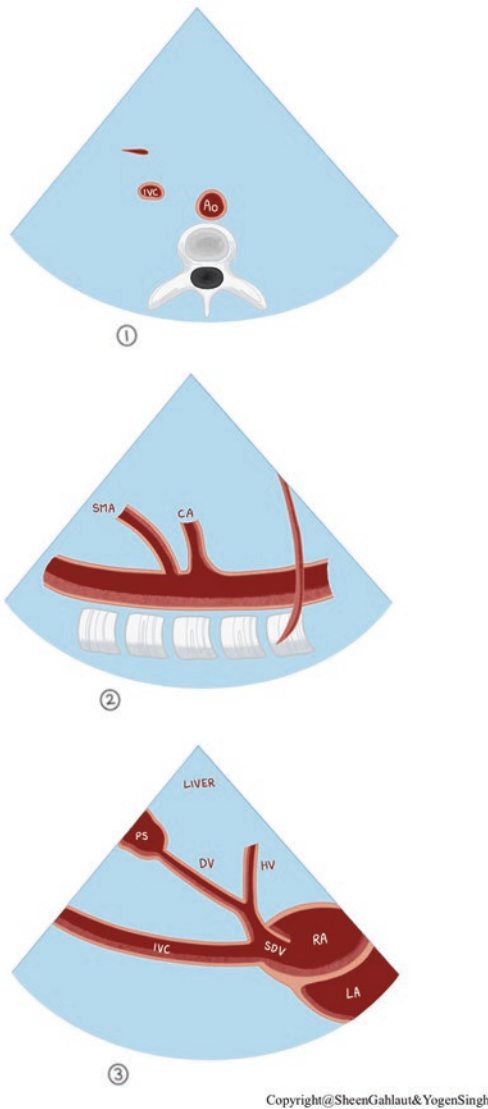


Fig. 11 Subcostal sweep views at level of (1) subcostal coronal posterior, (2) subcostal coronal anterior for superior vena cava (SVC), and (3) right ventricular outflow tract (RVOT). (Courtesy: Sheen Gahlaut and Yogen Singh)

Transverse subcostal views help to immediately determine visceral situs as well as the relationship between the inferior vena cava (right-sided) and aorta (left-sided) of the midline. Longitudinal views will allow imaging of the aorta and inferior vena cava thus allowing evaluation of the right heart filling pressure (Fig. 12).

Sob-costal longitudinal views of IVC and aorta are obtained by tilting the probe to the right and left, respectively, in a child with abdominal situs solitus as demonstrated in Fig. 13.

Subcostal coronal and longitudinal views are used to assess the following echocardiographic parameters:

- Abdominal situs
- Abdominal aorta
- Inferior vena cava
- To check the position of umbilical venous and arterial catheters

Suprasternal Window

The suprasternal views are obtained by placing the transducer in the suprasternal notch with the child's neck extended and slightly turned to the left. The suprasternal long and short axis views (Fig. 14) give information regarding the ascending and descending aorta and head and neck vessels, the branching of the pulmonary arteries, the systemic upper venous return (superior vena cava and innominate vein) as well as malformations of the pulmonary veins. A patent ductus arteriosus can also be imaged in this view via ductal cut, obtained by tilting the duct towards left and slight anti-clockwise rotation. Note that the suprasternal views become more challenging in older patients.

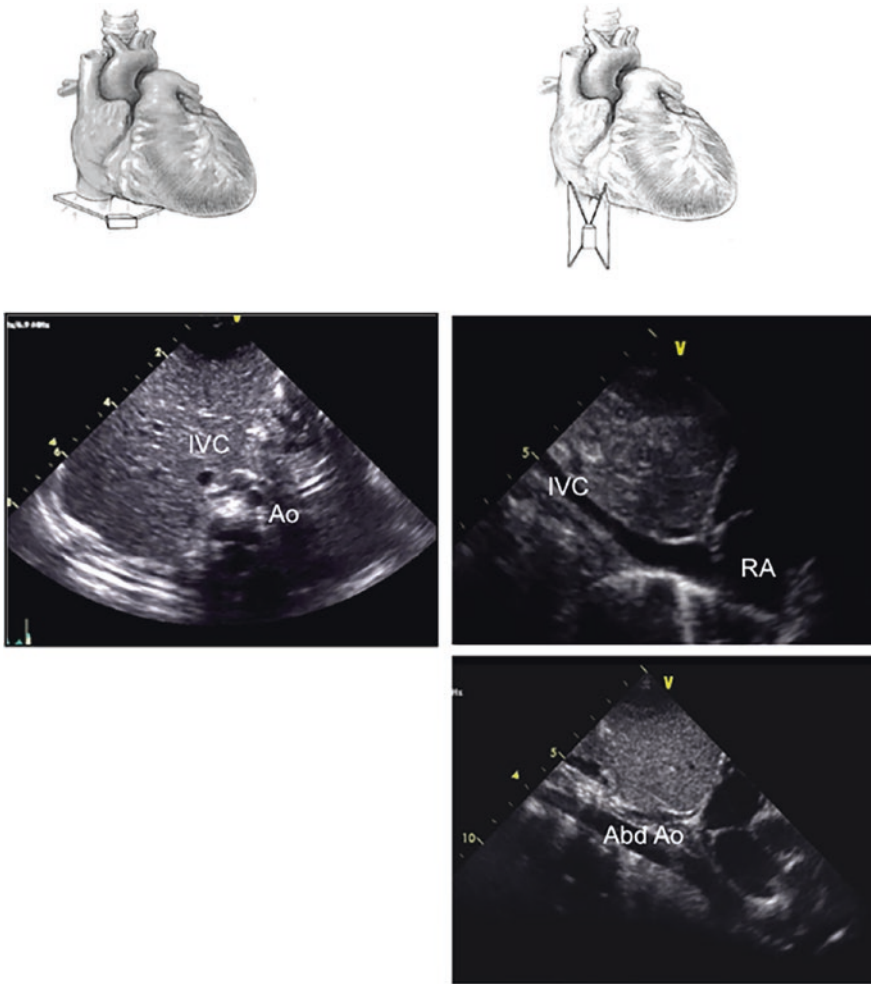


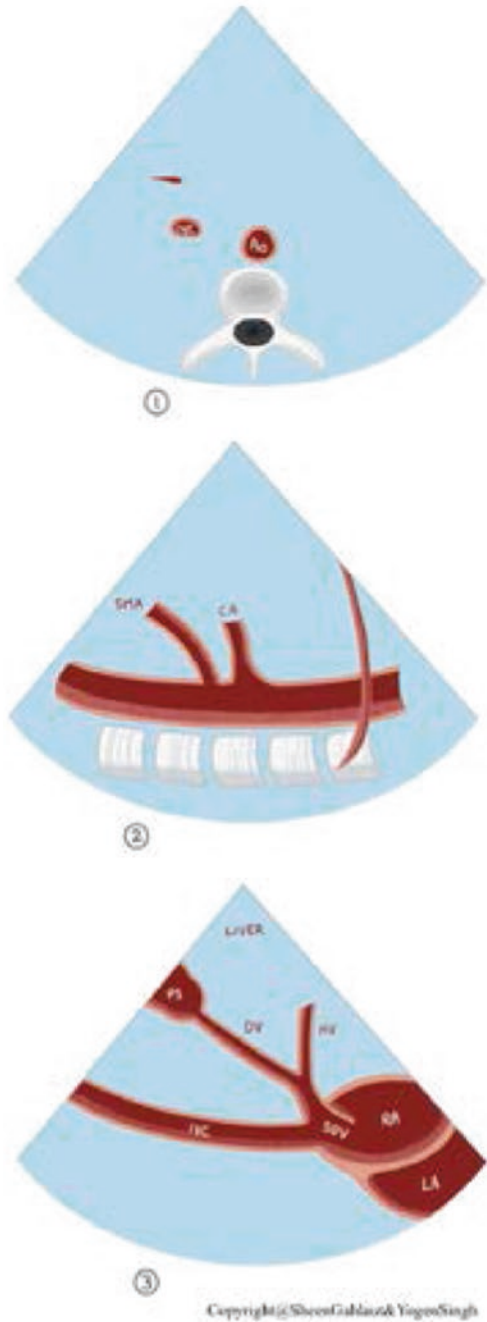
Fig. 12 Subcostal transverse and longitudinal views of aorta and IVC

In the suprasternal windows, by tilting the probe from right to left, different structures can be imaged as demonstrated in Fig. 15. By rotating the probe clockwise the “crab view” can be obtained (Fig. 16).

Suprasternal views can be used for the assessment of the following echocardiographic parameters:

- Aortic arch with head/neck vessels
- Superior vena cava and innominate vein
- Pulmonary veins to left atrium
- Patent ductus arteriosus evaluation for size, direction of shunt, and Doppler

Fig. 13 Subcostal short axis view (1) to assess abdominal situs and subcostal longitudinal (sagittal) views obtained by rotating the probe 90° counter clockwise; the aorta should be on the left side of the patient and inferior vena cava on the left), (2) descending aorta with celiac axis and superior mesenteric artery, and (3) inferior vena cava with ductus venosus and hepatic vein. (Courtesy: Sheen Gahlaut and Yogen Singh)



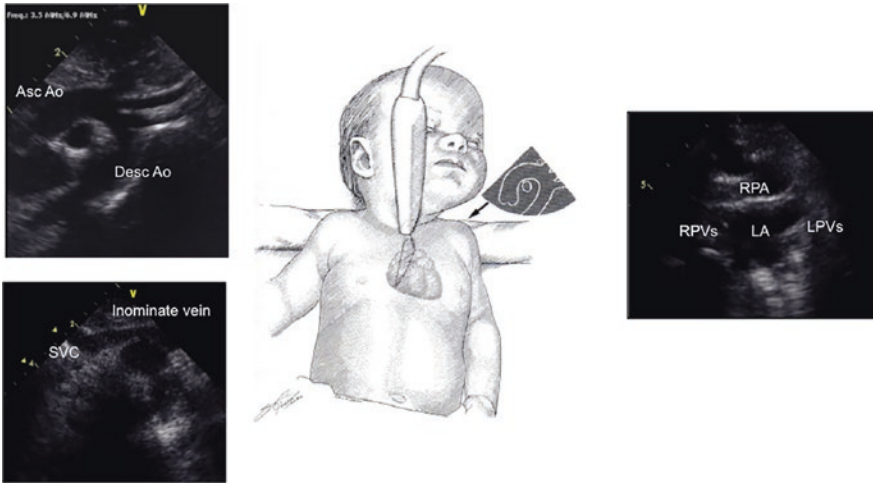


Fig. 14 Suprasternal views to visualize arch, superior vena cava (SVC), and crab view to visualize pulmonary veins

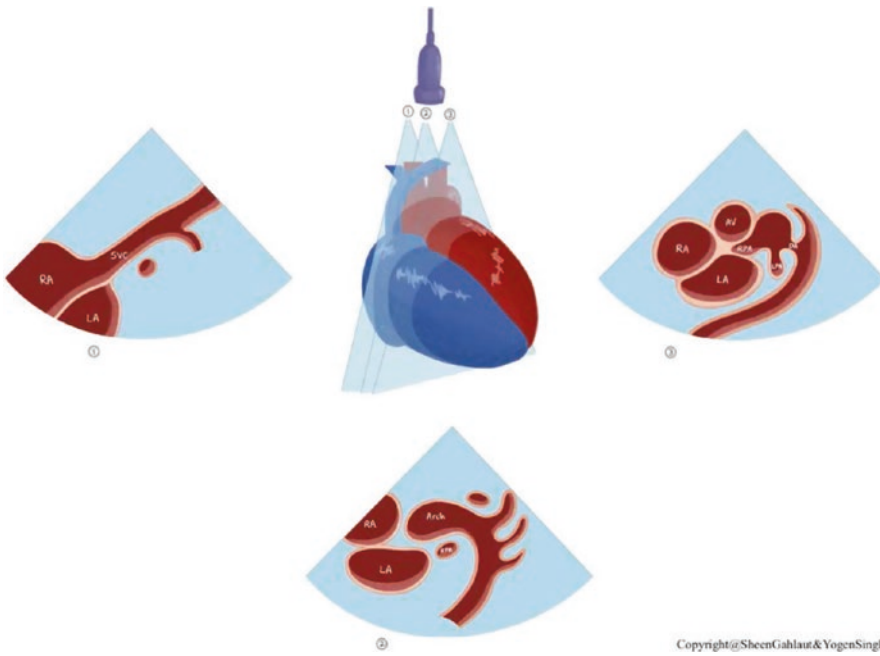


Fig. 15 Suprasternal arch views at the level of (1) superior vena cava, (2) arch, and ductal duct. (Courtesy: Sheen Gahlaut and Yogen Singh)

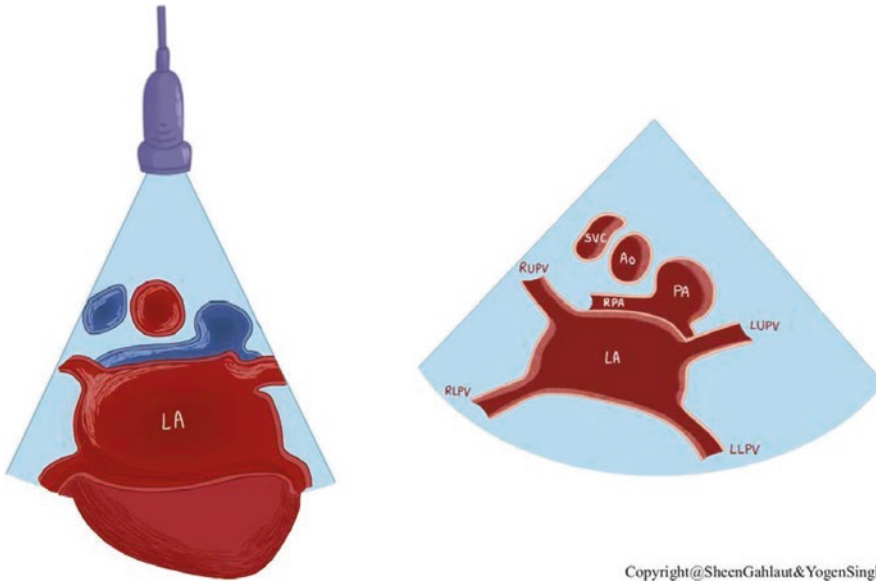


Fig. 16 “Crab view” obtained by rotating the probe clockwise until marker towards the left (3 O’clock) and then tilting posteriorly from the suprasternal view. (Courtesy: Sheen Gahlaut and Yogen Singh)

Conclusion

Quality echocardiographic imaging is crucial to obtain accurate structural and/or functional information. Sub-optimal imaging may lead to interpretative inaccuracy and inappropriate interventions. Cardiac POCUS uses standard views to answer focused questions relevant to the immediate or ongoing care of the critically ill child. Further chapters discuss the incorporation of cardiac POCUS in a number of clinical conditions.

References

1. Tissot C, Muehlethaler V, Sekarski N. Basics of functional echocardiography in children and neonates. *Front Pediatr.* 2017;5:235. <https://doi.org/10.3389/fped.2017.00235>.
2. Beaulieu Y, Marik PE. Bedside ultrasonography in the ICU. *Chest.* 2005;128:881–95.
3. Tissot C, Singh Y. Neonatal functional echocardiography. *Curr Opin Pediatr.* 2020;32(2):235–44. <https://doi.org/10.1097/MOP.0000000000000887>.
4. Singh Y, Katheria A, Tissot C. Functional echocardiography in the neonatal intensive care unit. *Indian Pediatr.* 2018;55(5):417–24.
5. Singh Y, Tissot C, Fraga M, Yousef N, Cortes RM, Lopez J, et al. International evidence-based guidelines on point of care ultrasound (POCUS) for critically ill neonates and children issued by the POCUS Working Group of the European Society of Paediatric and Neonatal Intensive Care (ESPNIC). *Crit Care.* 2020;24:65.



POCUS in Shock and Hypotension

Saul Flores, Fabio Savorgnan, and David Kantor

Contents

Introduction	47
The Concept of Fluid Responsiveness	48
Fluid Responsiveness Assessment Methods	49
Static Parameters	49
Dynamic Parameters	50
Integrating Fluid Responsiveness in the Hemodynamic Assessment of Shock	51
Types of Shock and Ultrasound Assessment	53
Clinical Considerations	54
Conclusion	54
References	55

Introduction

The use of ultrasound by non-radiology clinicians has steadily increased with now over 11,000 publications on point-of-care ultrasound (POCUS) in the national library of medicine, and over 600 in the last year. This technology is now ubiquitous in the critical care setting and most training programs will provide a curriculum for POCUS education [1–5]. One of the most used POCUS

applications in children is the assessment of hemodynamic perturbation. Hemodynamics is the complex interplay of numerous physiologic variables working together to provide oxygen and adequate perfusion to the end organs (Fig. 1). Shock is the inability of the system to balance hemodynamics such that there is inadequate end organ systemic support.

Preload, contractility, and afterload are terms characterizing conditions impacting cardiac stroke volume. Categories of shock classification such as hypovolemic, cardiogenic, obstructive, and distributive shock attempt to define distinct pathophysiologic patterns suggestive of specific therapeutic interventions. Historically, critical care physicians used the pulmonary artery catheter (PAC) to derive real-time physiologic data to assess hemodynamic profiles and guide therapies. This device has fallen out of favor in cur-

S. Flores (✉) · F. Savorgnan
Divisions of Critical Care and Cardiology, Texas
Children's Hospital, Baylor College of Medicine,
Houston, TX, USA
e-mail: saul.flores2@bcm.edu

D. Kantor
Department of Anesthesiology, Critical Care and Pain
Medicine, Harvard Medical School,
Boston, MA, USA

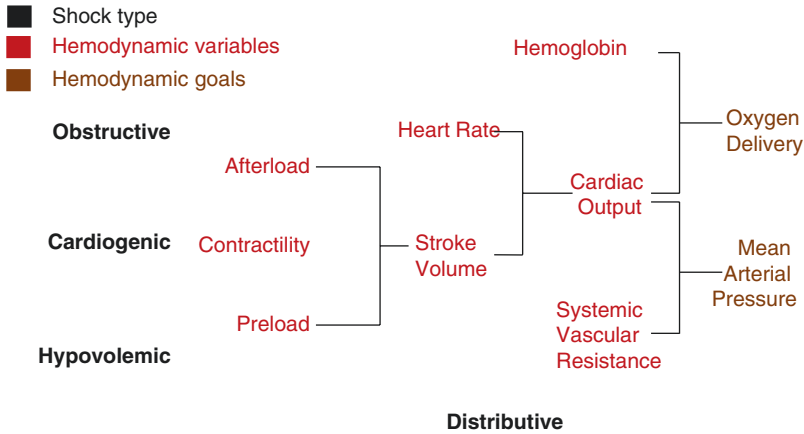


Fig. 1 The interaction between hemodynamic variables results in end organ oxygen delivery and perfusion pressure. Abnormalities in hemodynamic variables result in our simplified categorization of shock as hypovolemic, cardiogenic, obstructive, and distributive. Recognize that

rent practice as literature demonstrated no benefit in patient outcomes when integrated into care and suggested potential harm from the catheter itself [6].

Without PAC data, clinicians sought to characterize hemodynamics using less invasive technologies, laboratory values, clinical exam findings, and bedside monitor data. Early Goal-Directed Therapy (EGDT) characterized preload, contractility, and afterload by using clinical “surrogate” markers of core hemodynamic variables and demonstrated remarkable outcome success as mortality significantly declined in patients with septic shock [7]. Unfortunately, attempts at replicating this study did not achieve similar outcome benefits suggesting that the success of EGDT was likely more from the standardization of care than the clinical methods of hemodynamic characterization [8].

Despite our best attempts at characterizing physiology at the bedside, we know that many of our physical exam findings and laboratory values are inadequate in assessing individual hemodynamic profile and that surrogate markers of hemodynamic variables can lack accuracy and precision in both adults and children [9, 10]. Ultrasound allows for the direct visualization and both qualitative and quantitative assessment of many core hemodynamic variables. This chapter

these categories may be in isolation from one another, may overlap with one another, and may evolve through the course of disease. Ultrasound is a tool to improve our understanding of hemodynamic variables to inform management decisions

discusses how ultrasound can be used to assess preload (fluid responsiveness), contractility, and afterload conditions relevant to stabilizing the pediatric patient with hypotension and shock. Further, we will discuss methods of standardizing a clinical assessment of hemodynamics using ultrasound and propose an algorithmic approach to evaluation and management.

The Concept of Fluid Responsiveness

The optimal fluid status of a patient can be defined as the ideal intravascular volume to maintain adequate end organ perfusion. As a patient’s intravascular volume status changes, so do their cardiovascular, respiratory, and renal physiology. Fluid responsiveness can be defined as the ability of the left ventricle to increase its stroke volume in response to fluid administration [11]. In the research literature, fluid responsiveness is typically defined as a ≥ 10 –15% increase in stroke volume or cardiac output in response to a 10–20 mL/kg fluid bolus [12]. The European Society of Pediatric and Neonatal Intensive Care recently published evidence-based guidelines on POCUS [13]. These guidelines assessed a total of 41 recommendations with a strong agreement in

22 on the use of POCUS in neonatal and pediatric critical care. The use of POCUS to assess fluid responsiveness in neonates and children was one of the recommendations with a strong agreement.

Fluid Responsiveness Assessment Methods

Restoring the volume status of a pediatric patient in shock is important since excessive fluid administration may have deleterious effects [14]. The assessment of a patient’s response to volume expansion presents challenges for clinicians. Fluid responsiveness has been evaluated in various clinical conditions characterized by acute circulatory failure. Measurement parameters to suggest fluid responsiveness have been categorized as either static or dynamic (Table 1).

Static Parameters

Static parameters for the assessment of fluid responsiveness can be defined as a fixed or “static” measure. For example, an elevated heart rate is a static parameter that may indicate fluid respon-

siveness in the appropriate clinical setting. There are several static parameters used for the assessment of fluid responsiveness using ultrasound:

1. Areas and volumes
 - (a) Left ventricular end diastolic area
 - (b) Left ventricular end diastolic volume

Areas and volumes have been reported as reproducible indicators of preload. However, left ventricular end diastolic area and volume have been reported as poor predictors of fluid responsiveness in critically ill adult patients [15].

2. Diameters
 - (a) Inferior vena cava maximum diameter
 - (b) IVC to aorta ratio

IVC maximum diameter is a commonly used ultrasound parameter for the assessment of volume status in adults. There is evidence from adult studies suggesting that inferior vena cava diameter is lower in hypovolemic patients and that IVC size is associated with right atrial pressure [16]. Unfortunately, this relationship with central pressure does not imply volume responsiveness since there is robust literature indicating that central venous pressure is a poor predictor of intravascular volume or volume responsiveness [17]. In pediatrics, absolute measurements of size will always need to be contextual to the age and clinical condition of a patient. Obviously, the size of an IVC will be different between an infant and an adolescent as well as between a patient supported with positive pressure ventilation compared to one spontaneously breathing. Nephrologists exploring noninvasive methods of assessing dry weight measured the ratio of the IVC diameter to the aorta diameter in cross-sectional views. They identified that euvolemic children typically had an IVC to aorta ratio of ~1.2 [18]. This ratio has been validated as a relevant measure in the assessment of dehydrated children in low-resource settings but also suffers from some of the same limitations of static IVC measurements [19]. The use of both ultrasound and non-ultrasound-based static parameters is typically limited by poor specificity in the pediatric population [12].

Table 1 Examples of fluid responsiveness assessment methods

Measurement	Static parameter	Dynamic parameter
Invasive	Central venous pressure	Systolic pressure variation
	Pulmonary artery occlusion pressure	Pulse pressure variation
		Stroke volume variation
Noninvasive POCUS	Left ventricular end diastolic area	Inferior vena cava variation
	Left ventricular end diastolic volume	Superior vena cava variation
	Inferior vena cava maximum diameter	Aortic outflow variation
Clinical exam	Heart rate	Systolic blood pressure variation
	Systolic blood pressure	

Dynamic Parameters

Dynamic parameters for the assessment of fluid responsiveness can be defined as the changes induced in the cardiovascular system after provoking a change in preload. The change in preload is typically achieved by physiologic variations that occur during the respiratory cycle. The physiologic basis for the dynamic changes of preload during the respiratory cycle (both during positive and negative pressure ventilation) can be summarized as the cyclic variation of right ventricular stroke volume via changes in venous return by alterations in afterload conditions imposed by ventilatory mechanics. There are several ultrasound-based parameters used for the assessment of fluid responsiveness. The most studied measurement is the respiratory variation of inferior vena cava. Inferior vena cava variation is best assessed in the subcostal sagittal view distal to its confluence with the hepatic veins. In spontaneously breathing adults and children with normal right atrial pressure, inferior vena cava collapse of more than 50% is indicative of fluid responsiveness. A dilated inferior vena cava in spontaneously breathing patients with variation less than 50% may be a sign of elevated right atrial pressure and may not necessarily indicate fluid status in varied clinical contexts [20]. In adults, the literature supports IVC distensibility >15–20% as predictive of fluid responsiveness in paralyzed intubated patients [20, 21]. Pediatric studies have not identified optimal cutoffs for identifying fluid responsiveness in intubated children.

Flow Velocity

The measurement of systemic blood flow velocity variation during the respiratory cycle provides the highest sensitivity, specificity, and predictive value of all the dynamic parameter measurement techniques. It has been validated in both pediatric and adult patients as well as spontaneously breathing and intubated patients [13, 20, 22]. The three most common areas for assessment of the flow velocity variation are the left ventricular outflow tract, aorta, and carotid artery. The velocity time integral (VTI) is another measure utiliz-

ing blood flow velocity to identify fluid-responsive patients.

Assessing and measuring flow velocities requires advanced POCUS skills to acquire an adequate apical 5-chamber view of the heart. The image should allow for Doppler alignment minimizing the angle of insonation (less than 20°) for adequate velocity measures. The left ventricular VTI is calculated by placing the pulsed Doppler sample volume in the outflow tract below the aortic valve and recording the velocity. When the velocity signal is integrated with time, the distance blood moves with each systole is calculated in cm/systole [23]. A variation larger than 15% has been reported as helpful to assess fluid responsiveness [24].

Fluid Challenge

The fluid challenge method consists of monitoring changes in stroke volume and cardiac output in response to a fluid bolus. Stroke volume and cardiac output can be measured using invasive techniques (e.g., transpulmonary thermodilution) though this data is rarely available at the bedside in the current context of medical practice in the pediatric intensive care setting. The fluid challenge maneuvers can be classified as follows (Table 2):

1. Spontaneously breathing patients
 - (a) Passive leg raising
 - (b) Mini-fluid challenge
 - (c) Ten-second fluid challenge

Passive leg raising induces an increase in the preload via an increase in venous blood return from the lower extremities to the heart. This test utilizes the fluid present in the body and does not expose patients to unnecessary

Table 2 Fluid challenge method

Ventilation type	Type of fluid challenge
Spontaneous breathing	Passive leg rise
	Mini-fluid challenge
	Ten-second fluid challenge
Intubated patients	End expiratory occlusion
	Positive end expiratory pressure induce hemodynamic changes

exposure to excess fluid, particularly concerning for the patient who is found not to be a fluid responder. There are currently no specific guidelines in pediatric patients to detect fluid responsiveness during passive leg raising. Based on adult data the best cut-off value for detecting fluid responsiveness is a 10% increase in aortic blood flow by Doppler [25].

The mini-fluid challenge is completed by administering a colloid fluid bolus with a concomitant assessment of the aortic velocity time integral over 1 min [26]. The ten-second fluid challenge uses crystalloid solution instead of colloid solution and is administered over 10 seconds [27].

2. Intubated patients

- (a) End expiratory occlusion
- (b) Positive end expiratory pressure-induced hemodynamic changes

End expiratory occlusion is performed in intubated patients by imposing a 15 second interruption in mechanical ventilation while monitoring the stroke volume. Similar to the passive leg rising, the end expiratory occlusion tends to attenuate the effects of respiration on the venous return [28]. The measurement of positive end expiratory pressure-induced hemodynamic change was introduced in an effort to overcome the effects of the ventilator on fluid responsiveness. The principle of this maneuver is to increase the central venous pressure by increasing the positive end expiratory pressure to predict fluid responsiveness [29].

Integrating Fluid Responsiveness in the Hemodynamic Assessment of Shock

Shock is a complex clinical syndrome that often presents in children with critical illness [30]. If a child's clinical presentation is consistent with shock, a clinician should try to understand the underlying physiology before tailoring management. The pathophysiology of shock can be summarized as the failure of the cardiovascular system to deliver adequate oxygen and glucose to the cells [30, 31].

The cardiac output (CO) is calculated by multiplying the heart rate (HR) with the stroke volume (SV) (Fig. 1). In pediatric patient, CO is more dependent on heart rate (HR) than on stroke volume (SV) compared to adults due to the lack of ventricular muscle mass. Tachycardia is the child's principal means of compensation to maintain an adequate CO. As shock progresses, a further increase in HR may no longer be beneficial due to reduced ventricular diastolic filling time. Consequently, there is an increase in systemic vascular resistance through peripheral vasoconstriction mechanisms, which are mediated by the sympathetic nervous system and the renin-angiotensin-aldosterone system.

CO is maintained by optimizing preload, contractility, and afterload, which are the determinants of stroke volume SV. These neurohumoral mechanisms maintain blood pressure, tissue perfusion, and metabolic delivery, which creates a compensatory state in shock [32]. Eventually, the compensatory mechanisms become overwhelmed and pathophysiological derangements worsen, which is the progressive state of shock. In pediatric patients, blood pressure can often be preserved in the compensatory state of shock therefore blood pressure is often a late indicator of cardiovascular collapse. Thus, waiting for hypotension to develop before assessment and treatment may result in delays in necessary clinical support indicated by other clinical findings [32]. POCUS can help to gather information about preload (as previously discussed), contractility, and afterload during clinical care.

POCUS can be considered an extension of the bedside clinical assessment when used in conjunction with standard examination techniques [33]. The provider must keep in mind that shock can have more than one pathophysiologic process. For instance, sepsis can start with reduced systemic vascular resistance but can evolve into hypovolemia due to capillary leak and depressed cardiac function due to acidosis, reduced coronary perfusion, and/or primary myocyte dysfunction [32]. Therefore, sepsis can present with distributive, hypovolemic, and cardiogenic shock alone or overlapping one another. Identifying shock type early in care is important in determin-

ing steps in management in patients with circulatory failure [32]. Early integration of bedside ultrasound data may answer essential questions (Fig. 2) and inform therapeutic decisions that will impact clinical outcomes [33].

The rapid ultrasound for shock and hypotension (RUSH) protocol provides a framework for clinicians to obtain information that would help to determine the pathophysiology and subsequent management of the shock (Table 3) [34]. Given that many shock causes are age-independent, the adult

RUSH protocol can be adapted to pediatric and neonatal practice. There are some age-dependent conditions, though, which may allow pediatric clinicians to streamline assessments. For example, the burden of clots predisposing children to life-threatening pulmonary embolism is far less than in adults and exhaustive assessments for DVTs may not be valuable time spent. Further, abdominal aortic aneurysms are seen almost exclusively in adult populations rendering learning this assessment unnecessary for most pediatric providers.

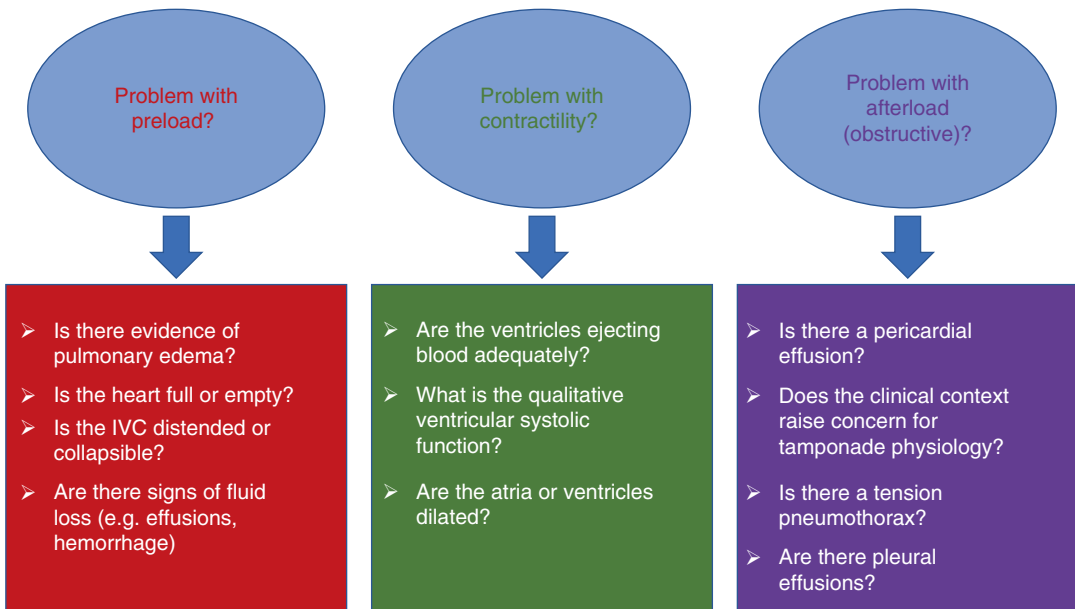


Fig. 2 Clinical questions regarding shock states that can be answered using point of care ultrasound

Table 3 Rapid Ultrasound in Shock (RUSH) protocol to assess shock state

Evaluation	Hypovolemic shock	Cardiogenic shock	Obstructive shock	Distributive shock
Pump/ Contractility	Hypercontractile heart Small cardiac chamber size	Hypocontractile heart Dilated cardiac chambers	Hyper- or hypocontractile heart Pericardial effusion with clinical concern for tamponade Right ventricular dilation Cardiac thrombus	Hypercontractile heart (early sepsis) Hypocontractile heart (late sepsis)
Tank/Preload	Flat IVC/IVC respiratory variation Peritoneal fluid (fluid loss) Pleural fluid (fluid loss)	Distended IVC Lung rockets (pulmonary edema) Pleural fluid Peritoneal fluid (ascites)	Distended IVC Absent lung sliding (pneumothorax)	Normal or small IVC (early sepsis) Peritoneal fluid (sepsis source) Pleural fluid (sepsis source)
Pipes/ Afterload	Abdominal aneurysm Aortic dissection	Normal	DVT	Normal

Types of Shock and Ultrasound Assessment

- (a) Hypovolemic
- (b) Cardiogenic
- (c) Obstructive
- (d) Distributive

Hypovolemic shock presents with a reduction in circulating volume. Examples of hypovolemic shock include hemorrhage, vomiting/diarrhea, diabetes ketoacidosis, and burn injuries [35]. We can identify multiple signs compatible with hypovolemic shock using the POCUS protocol. In a spontaneously breathing child, an elliptical or flat IVC with respiratory collapse >50% of the vessel diameter suggests a fluid responsive clinical state. Absent B-lines in the anterior and lateral aspects of the lungs are consistent with the absence of pulmonary edema. The empty left ventricle and hyperdynamic heart in at least two different views lend support to hypovolemic physiology. Evidence of intravascular fluid loss in either the abdomen or thorax following trauma may help to identify an etiology underlying the physiology. All these findings are consistent with low preload, normal contractility, and likely normal afterload physiologies. However, the afterload can be increased as the neurohumoral compensatory mechanism of shock gets activated or may be decreased due to insufficient (e.g., overwhelming sepsis) or dysregulated (e.g., adrenal insufficiency) compensatory mechanisms.

Cardiogenic shock results in a decline in cardiac output due to reduced myocardial function or cardiac damage. Examples of cardiogenic shock are myocardial infarction, cardiac failure, arrhythmias, septic shock, and post-cardiac surgery [35]. In this type of shock, clinicians may encounter the following POCUS finding in the assessment of the heart: dilated ventricle(s) and atria, reduced movement of ventricle walls, evidence of valve regurgitation, distended IVC, and well-filled ventricles among others. On the assessment of the lung, B-lines and other signs of volume overload may be found. Direct visualization of the heart will reveal decreased contractility of one or both ventricles. Similar to hypovolemic shock, the afterload may be

increased or decreased. Since qualitative and quantitative ultrasound measures of cardiac function are load dependent, frequent reassessments of contractility should be undertaken to evaluate responsiveness to therapy as well as to better define loading conditions.

Obstructive shock presents with mechanical obstruction that reduces CO. Examples of obstructive shock are cardiac tamponade, pneumothorax, and massive pulmonary embolism (PE) [35]. A distended IVC, presence of a pericardial effusion, dilated right ventricle, or bowing interventricular septum into the left ventricle among other findings may be identified in obstructive states. A distended or minimally collapsible IVC suggests a high-volume state or potential obstructive physiology. POCUS features of pneumothorax or pleural effusions may further identify the etiology of the obstructive process. Despite a distended IVC, preload to the right ventricle will be decreased in pericardial effusion and pneumothorax due to intra- and extracardiac pressure equilibration. In obstructive processes involving the pulmonary vasculature, including PE and pulmonary hypertension, preload to the left ventricle is predominant thereby limiting systemic cardiac output. Cardiac contractility of either or both ventricles may be preserved or even hyperdynamic in the early stages of obstructive shock as the heart attempts to maintain adequate cardiac output.

Distributive shock is an abnormality of blood flow distribution despite standard or high cardiac output. Examples of distributive shock are septic shock, anaphylaxis, and neurogenic shock [35]. Distributive shock is challenging to evaluate as there are currently no methods of directly visualizing vasomotor tone using ultrasound. Experientially, the diagnosis of distributive shock integrates ultrasound findings with clinical assessment and therapeutic responsiveness. For example, the spontaneously breathing child presenting to the intensive care unit with sepsis and hypotension following fluid loading may demonstrate minimal IVC respiratory variation, normal biventricular systolic function, and no evidence of an obstructive process. Therefore, the initial management strategy may be selection of a pharmacologic agent preferentially targeting vascular tone to

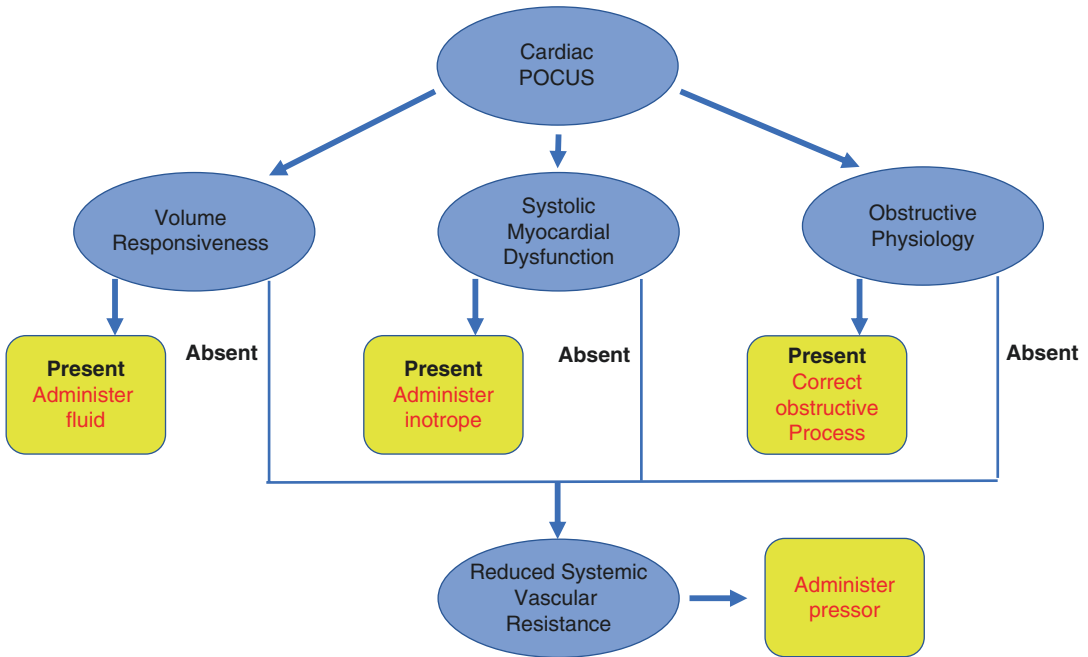


Fig. 3 Suggested algorithm for evaluation and management of pediatric shock when integrating ultrasound in clinical care

improve blood pressure. Similarly, the intubated child presenting to the intensive care unit with hypotension following cardiac arrest with diminished myocardial function may initially be treated with medications to improve inotropy. Subsequent POCUS evaluations may demonstrate improved myocardial functioning despite the recurrence of hypotension. Although post-cardiac arrest syndrome may be characterized by early myocardial dysfunction amenable to pharmacologic support, it is also characterized by an ischemic reperfusion response which may persist, and POCUS findings may identify this transition in physiology suggesting the initiation of pharmacologic agents to target vasomotor tone. Thus, distributive shock may be a diagnosis of exclusion when using ultrasound to guide management decisions in a hypotensive patient, and ultrasound findings should always be placed in the clinical context and within the scope of clinical experience.

Clinical Considerations

The management of a pediatric patient in shock should be tailored to address the underlying cause [33]. The Advanced Pediatric Life Support guide-

lines suggest a trial of volume resuscitation when we still do not know the cause of shock in the initial stages of management; however, with the information gained from POCUS, a child with myocardial dysfunction may be preferentially treated with inotropes with limited fluid administration [33, 34]. After any intervention, the POCUS examination can be repeated, and this reassessment helps confirm that the selected management is improving the physiologic perturbation. A basic evaluative and management algorithm is presented in Fig. 3. There is some evidence that a POCUS algorithm aligns to improve pediatric clinician diagnostic accuracy and patient outcome [36]. It may also reduce the number of unnecessary interventions, the time to diagnosis, and initiation of more specific management [33].

Conclusion

Pediatric acute care providers commonly encounter shock and hypotension in the clinical setting. Despite attempts at characterizing hemodynamic profiles using clinical exam, laboratory data, bedside monitoring, and other invasive devices, these data elements often lack accuracy and precision

regarding the core hemodynamic variables they are supposed to represent. Ultrasound technology allows us to directly visualize many of these variables in real time which allows for the delivery of timely and targeted therapies. POCUS studies can be longitudinally employed to monitor response to therapies as well as better understand protean physiology. Developing an ultrasound algorithm to standardize methods of assessment may improve provider identification of shock state as well as patient outcomes and is an important next-step pursuit for research within the pediatric POCUS community.

References

1. Brady AK, Spitzer CR, Kelm D, Brosnahan SB, Latifi M, Burkart KM. Pulmonary critical care fellows' use of and self-reported barriers to learning bedside ultrasound during training: results of a national survey. *Chest*. 2021;160(1):231–7. <https://doi.org/10.1016/j.chest.2021.01.068>. Epub 2021 Feb 1. PMID: 33539836.
2. Brown KA, Riley AF, Alade KH, Kyle WB, Castro D, Tchamntchi MH, Thammasitboon S. A novel tool for teaching cardiac point-of-care ultrasound: an exploratory application of the design-based research approach. *Pediatr Crit Care Med*. 2020;21(12):e1113–8. <https://doi.org/10.1097/PCC.0000000000002441>. PMID: 32701750.
3. Conlon TW, Kantor DB, Su ER, Basu S, Boyer DL, Haileselassie B, Petersen TL, Su F, Nishisaki A. Diagnostic bedside ultrasound program development in pediatric critical care medicine: results of a national survey. *Pediatr Crit Care Med*. 2018;19(11):e561–8. <https://doi.org/10.1097/PCC.0000000000001692>. PMID: 30113518.
4. Dhanani M, Hou A, Moll M, Schembri F. Introduction of an academic medical center's point-of-care ultrasound curriculum to internal medicine residents at a community-based teaching hospital. *J Community Hosp Intern Med Perspect*. 2020;10(2):93–8. <https://doi.org/10.1080/20009666.2020.1742483>. PMID: 32850043; PMCID: PMC7425611.
5. Lauerman MH, Haase DJ, Teeter W, Kufera J, Ghneim M, Betzold R, Scalea T, Murthi S. Surgical intensivists-led training in critical care ultrasound improves performance. *Am Surg*. 2021;87(8):1238–44. <https://doi.org/10.1177/0003134820972984>. Epub 2020 Dec 19. PMID: 33345585.
6. Marik PE. Obituary: pulmonary artery catheter 1970 to 2013. *Ann Intensive Care*. 2013;3(1):38. <https://doi.org/10.1186/2110-5820-3-38>. PMID: 24286266; PMCID: PMC4175482.
7. Rivers E, Nguyen B, Havstad S, Ressler J, Muzzini A, Knoblich B, Peterson E, Tomlanovich M, Early Goal-Directed Therapy Collaborative Group. Early goal-directed therapy in the treatment of severe sepsis and septic shock. *N Engl J Med*. 2001;345(19):1368–77. <https://doi.org/10.1056/NEJMoa010307>. PMID: 11794169.
8. Nguyen HB, Jaehne AK, Jayaprakash N, Semler MW, Hegab S, Yataco AC, Tatem G, Salem D, Moore S, Boka K, Gill JK, Gardner-Gray J, Pflaum J, Domecq JP, Hurst G, Belsky JB, Fowkes R, Elkin RB, Simpson SQ, Falk JL, Singer DJ, Rivers EP. Early goal-directed therapy in severe sepsis and septic shock: insights and comparisons to ProCESS, ProMISe, and ARISE. *Crit Care*. 2016;20(1):160. <https://doi.org/10.1186/s13054-016-1288-3>. PMID: 27364620; PMCID: PMC4929762.
9. Walker SB, Conlon TW, Zhang B, Mensinger JL, Fitzgerald JC, Himebauch AS, Glau C, Nishisaki A, Ranjit S, Nadkarni V, Weiss SL. Clinical signs to categorize shock and target vasoactive medications in warm versus cold pediatric septic shock. *Pediatr Crit Care Med*. 2020;21(12):1051–8. <https://doi.org/10.1097/PCC.0000000000002481>. PMID: 32740190.
10. Tibby SM, Hatherill M, Marsh MJ, Murdoch IA. Clinicians' abilities to estimate cardiac index in ventilated children and infants. *Arch Dis Child*. 1997;77(6):516–8. <https://doi.org/10.1136/adc.77.6.516>. PMID: 9496187; PMCID: PMC1717412.
11. Huang CC, Fu JY, Hu HC, Kao KC, Chen NH, Hsieh MJ, Tsai YH. Prediction of fluid responsiveness in acute respiratory distress syndrome patients ventilated with low tidal volume and high positive end-expiratory pressure. *Crit Care Med*. 2008;36(10):2810–6. <https://doi.org/10.1097/CCM.0b013e318186b74e>. PMID: 18766099.
12. Gan H, Cannesson M, Chandler JR, Ansermino JM. Predicting fluid responsiveness in children: a systematic review. *Anesth Analg*. 2013;117(6):1380–92. <https://doi.org/10.1213/ANE.0b013e3182a9557e>. PMID: 24257389.
13. Singh Y, Tissot C, Fraga MV, Yousef N, Cortes RG, Lopez J, Sanchez-de-Toledo J, Brierley J, Colunga JM, Raffaj D, Da Cruz E, Durand P, Kenderessy P, Lang HJ, Nishisaki A, Kneyber MC, Tissieres P, Conlon TW, De Luca D. International evidence-based guidelines on point of care ultrasound (POCUS) for critically ill neonates and children issued by the POCUS Working Group of the European Society of Paediatric and Neonatal Intensive Care (ESPNIC). *Crit Care*. 2020;24(1):65. <https://doi.org/10.1186/s13054-020-2787-9>. PMID: 32093763; PMCID: PMC7041196.
14. Arikan AA, Zappitelli M, Goldstein SL, Naipaul A, Jefferson LS, Loftis LL. Fluid overload is associated with impaired oxygenation and morbidity in critically ill children. *Pediatr Crit Care Med*. 2012;13(3):253–8. <https://doi.org/10.1097/PCC.0b013e31822882a3>. PMID: 21760565.
15. Coudray A, Romand JA, Treggiari M, Bendjelid K. Fluid responsiveness in spontaneously breathing patients: a review of indexes used in intensive care. *Crit Care Med*. 2005;33(12):2757–62. <https://doi.org/10.1097/01.ccm.0000189942.24113.65>. PMID: 16352956.

16. Dipti A, Soucy Z, Surana A, Chandra S. Role of inferior vena cava diameter in assessment of volume status: a meta-analysis. *Am J Emerg Med.* 2012;30(8):1414–1419.e1. <https://doi.org/10.1016/j.ajem.2011.10.017>. Epub 2012 Jan 4. PMID: 22221934.
17. Marik PE, Baram M, Vahid B. Does central venous pressure predict fluid responsiveness? A systematic review of the literature and the tale of seven mares. *Chest.* 2008;134(1):172–8. <https://doi.org/10.1378/chest.07-2331>. PMID: 18628220.
18. Kosiak W, Swieton D, Piskunowicz M. Sonographic inferior vena cava/aorta diameter index, a new approach to the body fluid status assessment in children and young adults in emergency ultrasound—preliminary study. *Am J Emerg Med.* 2008;26(3):320–5. <https://doi.org/10.1016/j.ajem.2007.07.012>. PMID: 18358944.
19. Millington SJ. Ultrasound assessment of the inferior vena cava for fluid responsiveness: easy, fun, but unlikely to be helpful. *Can J Anaesth.* 2019;66(6):633–8. <https://doi.org/10.1007/s12630-019-01357-0>. Epub 2019 Mar 27. PMID: 30919234.
20. Feissel M, Michard F, Faller JP, Teboul JL. The respiratory variation in inferior vena cava diameter as a guide to fluid therapy. *Intensive Care Med.* 2004;30(9):1834–7. <https://doi.org/10.1007/s00134-004-2233-5>. Epub 2004 Mar 25. PMID: 15045170.
21. Barbier C, Loubières Y, Schmit C, Hayon J, Ricôme JL, Jardin F, Vieillard-Baron A. Respiratory changes in inferior vena cava diameter are helpful in predicting fluid responsiveness in ventilated septic patients. *Intensive Care Med.* 2004;30(9):1740–6. <https://doi.org/10.1007/s00134-004-2259-8>. Epub 2004 Mar 18. PMID: 15034650.
22. Ficial B, Finnemore AE, Cox DJ, Broadhouse KM, Price AN, Durighel G, Ektizidou G, Hajnal JV, Edwards AD, Groves AM. Validation study of the accuracy of echocardiographic measurements of systemic blood flow volume in newborn infants. *J Am Soc Echocardiogr.* 2013;26(12):1365–71. <https://doi.org/10.1016/j.echo.2013.08.019>. Epub 2013 Sep 26. PMID: 24075229; PMCID: PMC3852205.
23. Zhou G, Zhang H, Wang X, Liu D. Variation of left ventricular outflow tract velocity time integral at different positive end-expiratory pressure levels can predict fluid responsiveness in mechanically ventilated critically ill patients. *J Cardiothorac Vasc Anesth.* 2022;36(8 Pt B):3101–8. <https://doi.org/10.1053/j.jvca.2022.04.033>. Epub 2022 Apr 29. PMID: 35599102.
24. Monnet X, Rienzo M, Osman D, Anguel N, Richard C, Pinsky MR, Teboul JL. Esophageal Doppler monitoring predicts fluid responsiveness in critically ill ventilated patients. *Intensive Care Med.* 2005;31(9):1195–201. <https://doi.org/10.1007/s00134-005-2731-0>. Epub 2005 Jul 30. PMID: 16059723.
25. Monnet X, Rienzo M, Osman D, Anguel N, Richard C, Pinsky MR, Teboul JL. Passive leg raising predicts fluid responsiveness in the critically ill. *Crit Care Med.* 2006;34(5):1402–7. <https://doi.org/10.1097/01.CCM.0000215453.11735.06>. PMID: 16540963.
26. Muller L, Toumi M, Bousquet PJ, Riu-Poulenc B, Louart G, Candela D, Zoric L, Suehs C, de La Coussaye JE, Molinari N, Lefrant JY, AzuRéa Group. An increase in aortic blood flow after an infusion of 100 ml colloid over 1 minute can predict fluid responsiveness: the mini-fluid challenge study. *Anesthesiology.* 2011;115(3):541–7. <https://doi.org/10.1097/ALN.0b013e318229a500>. PMID: 21792056.
27. Wu Y, Zhou S, Zhou Z, Liu B. A 10-second fluid challenge guided by transthoracic echocardiography can predict fluid responsiveness. *Crit Care.* 2014;18(3):R108. <https://doi.org/10.1186/cc13891>. PMID: 24886990; PMCID: PMC4075154.
28. Monnet X, Osman D, Ridel C, Lamia B, Richard C, Teboul JL. Predicting volume responsiveness by using the end-expiratory occlusion in mechanically ventilated intensive care unit patients. *Crit Care Med.* 2009;37(3):951–6. <https://doi.org/10.1097/CCM.0b013e3181968fe1>. PMID: 19237902.
29. Wilkman E, Kuitunen A, Pettilä V, Varpula M. Fluid responsiveness predicted by elevation of PEEP in patients with septic shock. *Acta Anaesthesiol Scand.* 2014;58(1):27–35. <https://doi.org/10.1111/aas.12229>. Epub 2013 Nov 11. PMID: 24341692.
30. McKiernan CA, Lieberman SA. Circulatory shock in children: an overview. *Pediatr Rev.* 2005;26(12):451–60. <https://doi.org/10.1542/pir.26-12-451>. PMID: 16327026.
31. Greer O, Shah NM, Srisikandan S, Johnson MR. Sepsis: precision-based medicine for pregnancy and the puerperium. *Int J Mol Sci.* 2019;20(21):5388. <https://doi.org/10.3390/ijms20215388>. PMID: 31671794; PMCID: PMC6861904.
32. Wheeler DS, Jeffries HE, Zimmerman JJ, Wong HR, Carcillo JA. Sepsis in the pediatric cardiac intensive care unit. *World J Pediatr Congenit Heart Surg.* 2011;2(3):393–9. <https://doi.org/10.1177/2150135111403781>. PMID: 22337571; PMCID: PMC3277844.
33. Hardwick JA, Griksaitis MJ. Fifteen-minute consultation: point of care ultrasound in the management of paediatric shock. *Arch Dis Child Educ Pract Ed.* 2021;106(3):136–41. <https://doi.org/10.1136/archdischild-2019-317972>. Epub 2020 Aug 7. PMID: 32769083.
34. Keikha M, Salehi-Marzijarani M, Soldoozi Nejat R, Sheikh Motahar Vahedi H, Mirrezaie SM. Diagnostic accuracy of rapid ultrasound in shock (RUSH) exam; a systematic review and meta-analysis. *Bull Emerg Trauma.* 2018;6(4):271–8. <https://doi.org/10.29252/beat-060402>. PMID: 30402514; PMCID: PMC6215077.
35. Kisilitsina ON, Rich JD, Wilcox JE, Pham DT, Churyla A, Vorovich EB, Ghafourian K, Yancy CW. Shock—Classification and pathophysiological principles of therapeutics. *Curr Cardiol Rev.* 2019;15(2):102–13. <https://doi.org/10.2174/1573403X15666181212125024>. PMID: 30543176; PMCID: PMC6520577.
36. Arnoldi S, Glau CL, Walker SB, Himebauch AS, Parikh DS, Udeh SC, Weiss SL, Fitzgerald JC, Nishisaki A, Conlon TW. Integrating focused cardiac ultrasound into pediatric septic shock assessment. *Pediatr Crit Care Med.* 2021;22(3):262–74. <https://doi.org/10.1097/PCC.0000000000002658>. PMID: 33657611.



Echocardiographic Evaluation of Left Ventricular Function and Hemodynamic Status

Cécile Tissot, Nicole Sekarski, and Yogen Singh

Contents

Introduction	57
Left Ventricular Anatomy and Physiology	58
Measurement of Cardiac Dimensions	60
Evaluation of Left Ventricular Systolic Function	60
Qualitative Assessment	60
Quantitative Assessment	62
Semi-quantitative Assessment	63
Evaluation of Left Ventricular Diastolic Function	66
Evaluation of Cardiac Output and Cardiac Index	67
Conclusion	69
References	69

The original version of the chapter has been revised. A correction to this chapter can be found at https://doi.org/10.1007/978-3-031-26538-9_23

C. Tissot (✉)
Department of Pediatrics, Clinique des Grangettes,
Chêne-Bougeries, Geneva, Switzerland
e-mail: cecile.tissot@hirslanden.ch

N. Sekarski
Centre Hospitalier Universitaire Vaudois (CHUV),
University of Lausanne, Lausanne, Switzerland
e-mail: Nicole.sekarski@chuv.ch

Y. Singh
Department of Pediatrics, Division of Neonatology,
Loma Linda University School of Medicine,
California, USA

Introduction

Hemodynamic instability is common in sick neonates and children requiring intensive care management. Cardiac point of care ultrasound (POCUS) can be used in assessing cardiac func-

Department of Pediatrics, Division of Neonatal and Developmental Medicine, Stanford University School of Medicine, California, UK

Department of Pediatrics, Division of Neonatology, University of Southern California, California, UK

ESPNIC Cardiovascular Dynamics Section and POCUS Working Group, Geneva, Switzerland
e-mail: YSingh@llu.edu

tion and may help in understanding the underlying pathophysiology in infants and children with hemodynamic instability [1–6]. Physiological information from cardiac POCUS, in conjunction with other clinical parameters and hemodynamic monitoring tools, can be used in choosing fluid resuscitation therapy or appropriate inotropic or vasopressor/vasodilator pharmacologic agents [7]. While some infants with septic shock or those with hemodynamic instability may need fluid resuscitation therapy, aggressive fluid boluses can be hazardous in infants with cardiogenic shock or those with poor cardiac function. Similarly, acute pulmonary hypertension is common in neonatal shock and early recognition of increased pulmonary afterload may help in early institution of pulmonary vasodilator therapy [8, 9]. A complete evaluation of pulmonary hypertension and hemodynamic assessment requires comprehensive echocardiographic evaluation in the neonatal patient. Cardiac POCUS can be used for rapid qualitative assessment of left ventricle (LV) function in emergency situations. However, the clinicians performing cardiac POCUS assessments should have good understanding of left ventricle anatomy, physiology, echocardiographic parameters used for LV function assessment and their limitations, especially when performed by a non-expert in echocardiography.

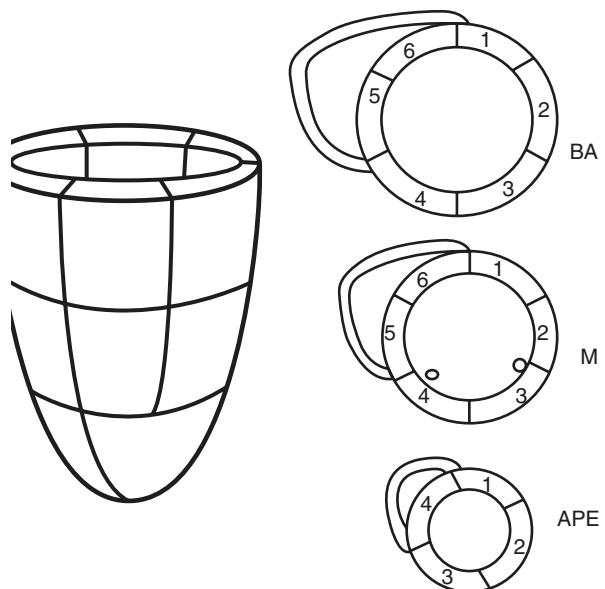
Left Ventricular Anatomy and Physiology

The left ventricle is comprised of an inlet, apical trabecular, and outlet portion. The left ventricular wall is smoother compared to the right ventricle and is thinner at the apex. The shape of the left ventricle approximates a cone (or bullet) with the crescent shaped right ventricle ‘hugging’ it and with the left ventricular outlet overlapping the inlet (Fig. 1).

The ventricular septum is curved and convex towards right ventricular cavity. The mitral valve is comprised of two leaflets different in structure (an anteromedial and a posterolateral leaflet), a fibrous ring at the atrioventricular junction known as the mitral annulus, tendinous chords, and papillary muscles. The papillary muscles are supporting the mitral valve and are an integral component of the left ventricular wall disposed in anterolateral and posteromedial locations in the short axis plane (Fig. 2).

Left ventricular systole follows the depolarization of the ventricles and is represented by the QRS complex in the electrocardiogram. At the end of atrial systole, and just prior to ventricular contraction, the left ventricle contains about 130 mL of blood in an adult which is called the left ventricle end-diastolic volume

Fig. 1 Shape of the left ventricle approximating a cone (or bullet) with the crescent shaped right ventricle “hugging” it. BA - base, M - medial, APE - apex of the heart, and 1-6 are the different segments of left ventricle posterior wall and interventricular septum (IVS)



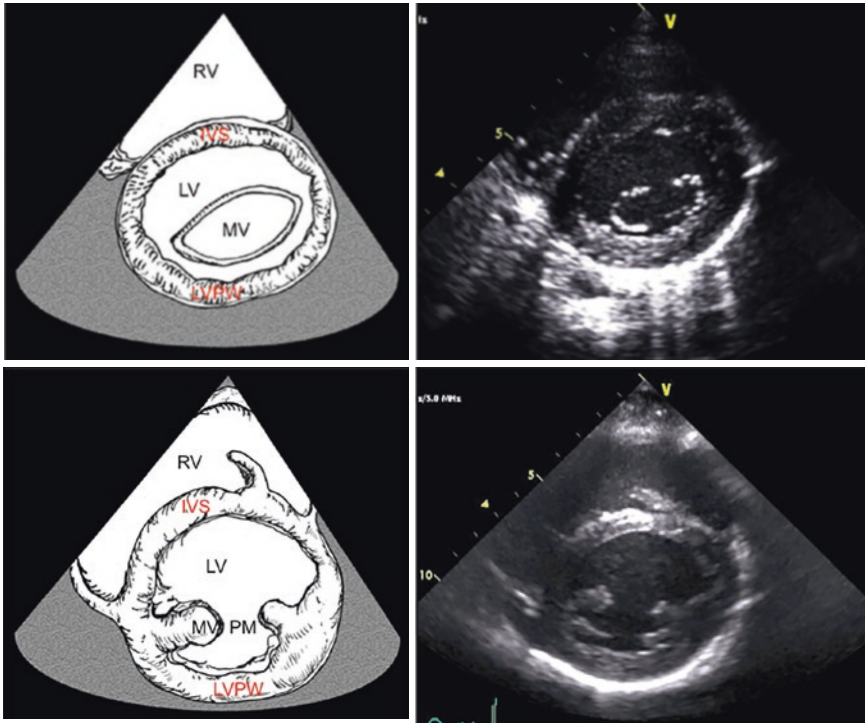


Fig. 2 Echocardiographic parasternal short axis view showing the left ventricle from the apex to the base, with the mitral valve apparatus (papillary muscles and

mitral leaflets). *IVS* interventricular septum, *LVPW* left ventricle posterior wall, *RV* - right ventricle, *LV* - left ventricle, *MV* - mitral valve, *PM* - papillary muscle

(LVEDV) or preload. As the left ventricle starts contracting, the ventricular pressure rises until it is higher than the left atrial pressure allowing for mitral valve closure (isovolumic contraction phase). When the left ventricular pressure has raised until it is higher than the aortic pressure, the aortic valve opens (ejection phase). The quantity of blood pumped into the aorta is called the stroke volume (about 70 mL for an adult) and is the same for both ventricles (in the absence of a shunting lesion), whereas some blood will stay in the left ventricle and is called the left ventricle end-systolic volume (LVESV).

Left ventricular diastole follows repolarization of the ventricles and is represented by the

T-wave of the electrocardiogram. During the early phase, the pressure within the ventricle begins to fall until it drops below the pressure of the aorta, producing the dicrotic notch (small dip) seen in blood pressure tracings. The aortic valve closes while the mitral valve remains closed at this point, allowing for no change in the left ventricular volume (isovolumic relaxation phase). During late ventricular diastole, the left ventricle continues to relax until its pressure drops below the atrial pressure, allowing for blood to flow from the left atrium into the left ventricle, pushing up and opening the mitral valve. Blood flows from the pulmonary veins into the relaxed left atrium and ventricle (Fig. 3)

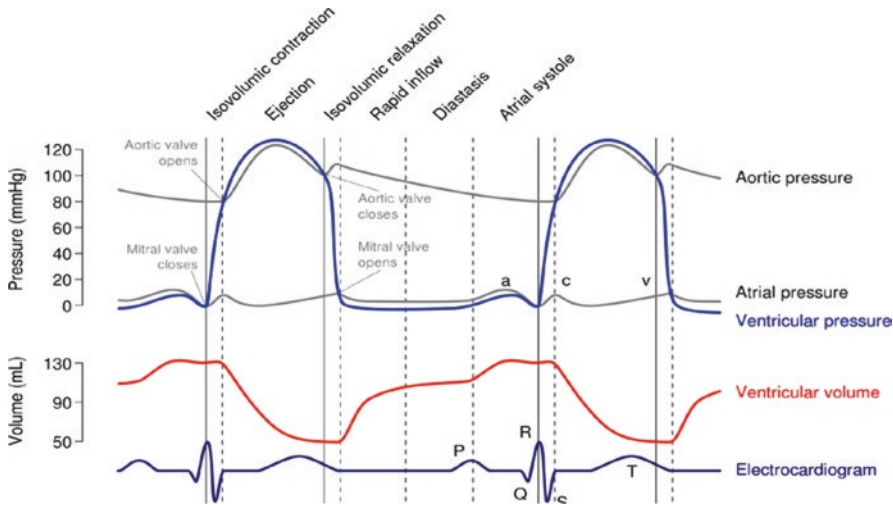


Fig. 3 Pressure and volume tracings of the left ventricle and left atrium over the cardiac cycle: (1) Isovolumic contraction indicated by the QRS wave of the ECG. (2) Opening of the aortic valve allowing for aortic ejection.

(3) Aortic valve closure allowing for isovolumic relaxation. (4) Filling of the left ventricle (diastole) with initial slow filling followed by atrial contraction-related filling

Measurement of Cardiac Dimensions

Cardiac dimensions are essential in the evaluation of ventricular function in newborns and children. The heart chambers increase progressively after birth, reaching 50% of their adult size at birth, 75% by 5 years, and 90% by 12 years of age [10].

Ventricular size is measured by M-mode and is done using the leading edge-to-leading edge technique. The left ventricular M-mode tracing is obtained from the parasternal long axis or short axis view (Fig. 4).

Accuracy and consistency of M-mode assessment site is essential because ventricular contraction is not uniform from the base to the apex. End-diastole can be measured at the beginning of the QRS complex [11] but taking the measurements at the largest and smallest ventricular diameter may be more pertinent.

Quantification of cardiac chambers and cardiac structure dimensions implies reporting the measurements as Z-scores [12, 13]. Increased left ventricular end-diastolic dimension can be seen in volume loading conditions (shunt lesions or valve regurgitation) or in left ventricular dysfunction (dilated cardiomyopathy) [7]. Increased wall

thickness can occur in pressure loading conditions (valve stenosis) or infiltrative disorders (hypertrophic cardiomyopathy, mucopolysaccharidosis).

Evaluation of Left Ventricular Systolic Function

Determination of systolic function is fundamental in the management of a hemodynamically unstable newborn or child [1]. This includes the measurement of shortening fraction (SF), ejection fraction (EF), and cardiac output (CO). Various methods can be utilized to make these assessments.

Qualitative Assessment

Visual assessment of left ventricular systolic function is the most commonly used method for the non-specialist echocardiographers but this method is prone to inter- and intra-observer variability even among experts [14]. Ejection fraction is estimated visually using multiple echocardiography views (Fig. 5 and Video clip).

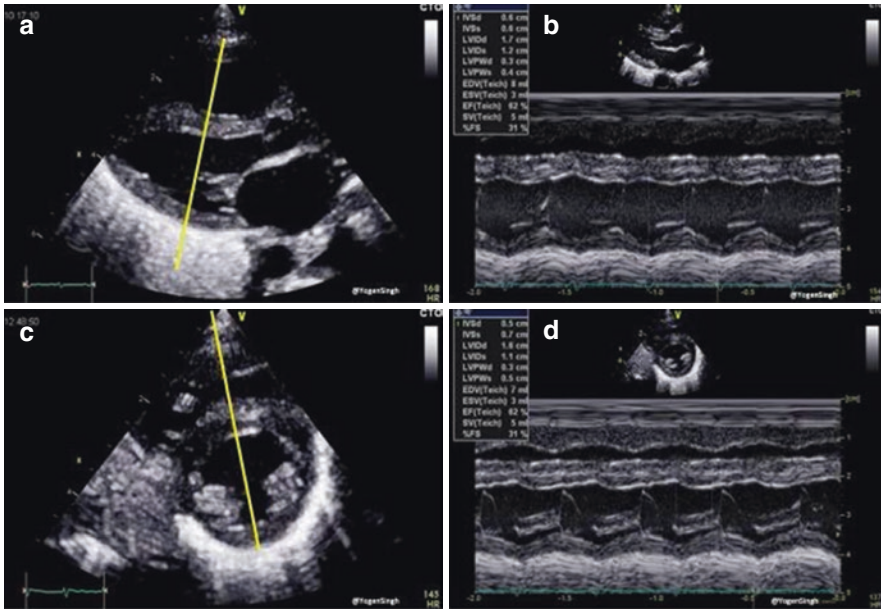


Fig. 4 M-mode imaging on parasternal long axis and short axis views showing assessment of left ventricular systolic function. Images a and b show fraction shortening (FS) assessment on parasternal long axis view; images c and d show FS assessment in parasternal short axis view

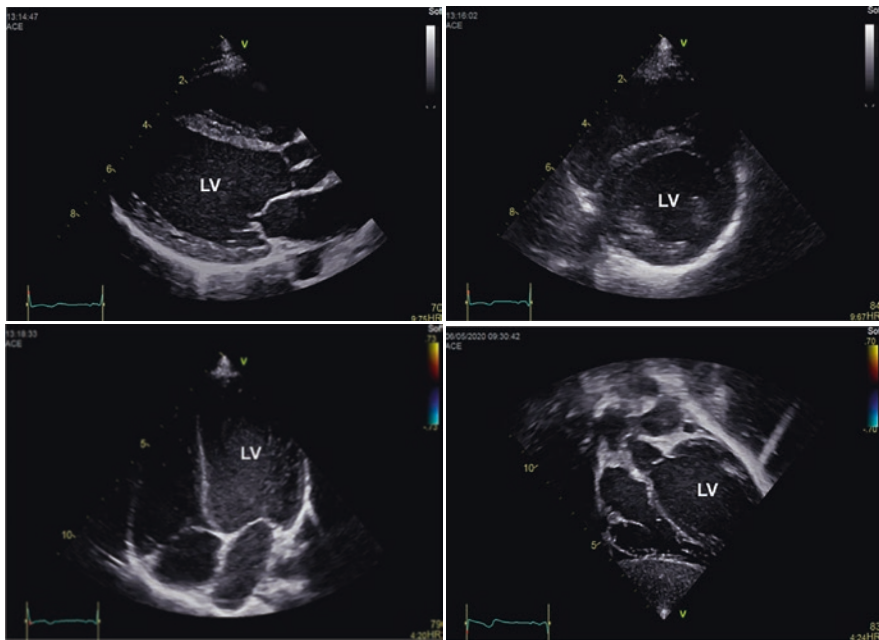


Fig. 5 Different echocardiographic views commonly used for qualitative left ventricular systolic estimation: parasternal long and short axis view, apical 4-chamber view, and subcostal view (good view to assess function during cardiac massage)

Left ventricular function is subjectively classified into normal function (EF $\geq 55\%$), mild dysfunction (EF 41–55%), moderate dysfunction

(EF 31–40%), and severe dysfunction (EF $\leq 30\%$) [15]. Adult providers will often use EF as a method of communicating their qualitative

assessment. Obviously EF is the fraction of volume ejected during systole and is only estimated as it cannot be quantified in a 2D image alone.

Quantitative Assessment

M-mode tracings are obtained in the parasternal long axis view at the tips of the mitral valve leaflets or in the parasternal short axis view at the level of the papillary muscles (Fig. 6) and enable to measurement the left ventricular end-diastolic dimension (LVEDD) and the left ventricular end-systolic dimension (LVESD) necessary for the determination of FS.

The FS is calculated using the following equation:

$$FS(\%) = \frac{LVEDD \times LVESD}{LVEDD} \times 100$$

Normal values for FS in children and infants are typically between 28 and 44% [16–18]. The disadvantage of this method is that it assumes a circular shape of the left ventricle. If this shape is

altered (related to congenital heart disease, preload and afterload changes, or ventricular interactions), it may affect the measurement of FS causing an under- or overestimation. The second method of assessing left ventricular function is the calculation of the ejection fraction (EF). The EF is a volumetric appraisal of ventricular fiber shortening. Biplane measurement of left ventricular volumes from the apical four-chamber and two-chamber views is the best method of calculating the EF (Fig. 7).

The endocardial border of the left ventricle is traced manually at end-diastole and at end-systole (planimetry) giving a value of end-diastolic volume (LVEDV) and end-systolic volume (LVESV). The Simpson method uses the method of summation of disks [19, 20]. The EF is calculated using the following equation:

$$EF(\%) = \frac{LVEDV \times LVESV}{LVEDV} \times 100$$

Normal values for EF in children are 56–78%. Calculation of the EF by the Simpson's method can sometimes be inaccurate. Variations in ven-

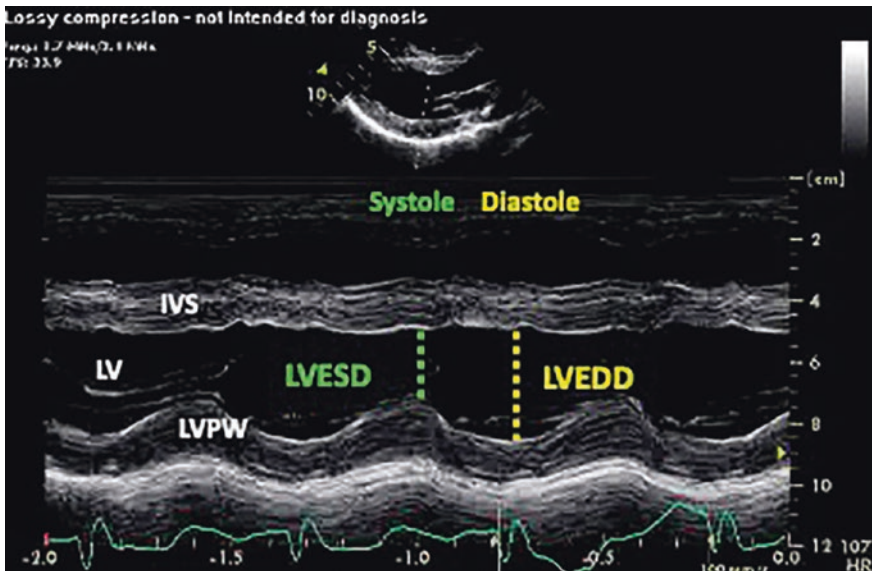


Fig. 6 M-mode echocardiography from a parasternal long axis view showing the left ventricular cavity over the cardiac cycle (see ECG tracing) during systole and diastole. *IVS* - interventricular septum, *LV* - left ventricle,

LVEDD - left ventricle end-diastolic dimension (yellow), *LVESD* - left ventricle end-systolic dimension (green), *LVPW* - left ventricle posterior wall

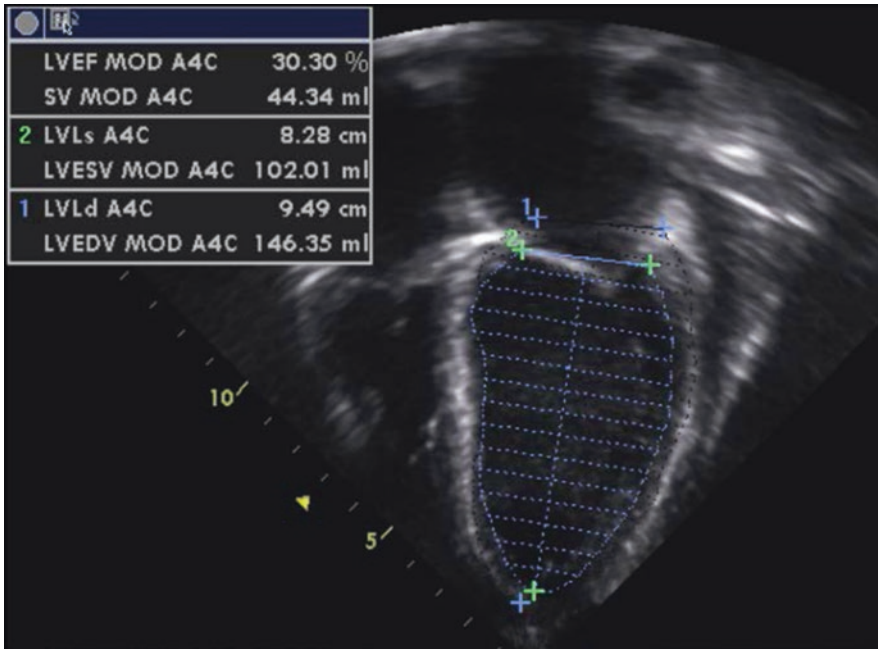


Fig. 7 Assessment of left ventricular systolic function by planimetry using the modified Simpson's method and allowing estimation of the ejection fraction (EF) by tracing the endocardial left ventricular border in end-diastole (LVEDV) and in end-systole (LVESV), obtained from a

patient with moderate left ventricular systolic dysfunction (EF = 30%). *LVEF* left ventricular ejection fraction, *LVEDV* left ventricle end-diastolic volume, *LVESV* left ventricle end-systolic volume, *SV* stroke volume

tricular shape, as seen in newborns and in congenital heart diseases, can alter the EF. Intensive care patients often have suboptimal views with difficulty in tracing the endocardial border correctly. When interpreting SF and EF, the influence of preload and afterload should be taken into account. This is especially true when comparing cardiac function before and after ductal closure in newborns and explains the usual decrease in SF and EF seen immediately after surgical duct ligation. It is also true for patients on ventricular assist devices or extracorporeal membrane oxygenation in whom the ventricular function needs to be assessed during the weaning process when the heart is unloaded. The advances in newer techniques for evaluating myocardial function (Tissue Doppler Imaging, strain and strain rate, and three-dimensional echocardiography) may be helpful in the future for the assessment of ventricular function in this setting but these methods still need to be validated in children.

Semi-quantitative Assessment

Alternative parameters for the evaluation of left ventricular systolic function should also be considered especially in critical care patients with poor imaging quality.

In patients with mitral regurgitation (MR), the rate of pressure rise in early systole (dp/dt max) represents a good evaluation of global left ventricular contractility. Mitral regurgitation jet velocity depends on the pressure gradient between the left ventricle and the left atrium. Because there are no significant changes in left atrial pressure during isovolumetric contraction (IVCT), mitral regurgitation changes reflect left ventricular pressure changes. MR dp/dt is measured from a continuous wave (CW) Doppler tracing of the mitral regurgitation jet during the time interval at which the velocity is 1 m/s and 3 m/s (Fig. 8).

Normal values ≥ 1000 – 1200 mmHg/s and value < 500 mmHg/s are indicative of severe systolic dysfunction (Fig. 9). It is important to

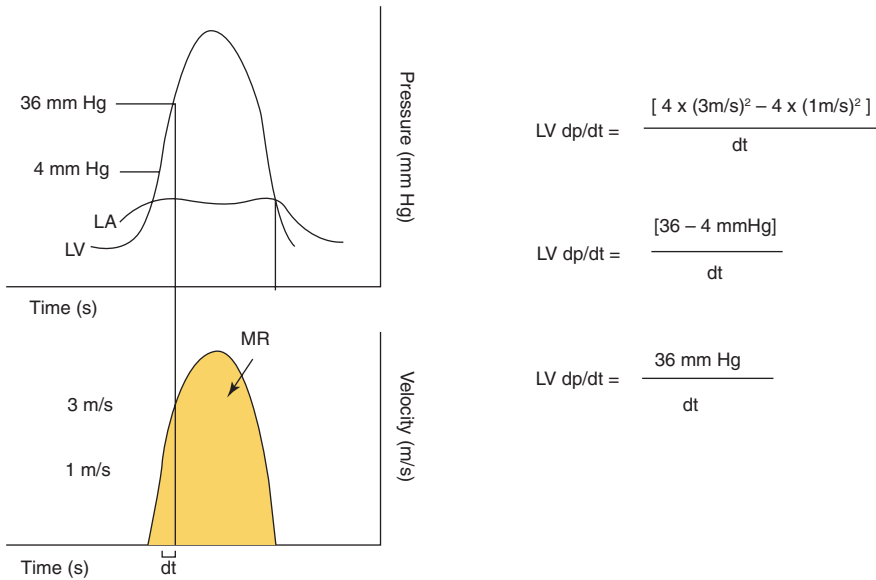


Fig. 8 Representation of the measurement of mitral regurgitation (MR) dP/dt over the cardiac cycle

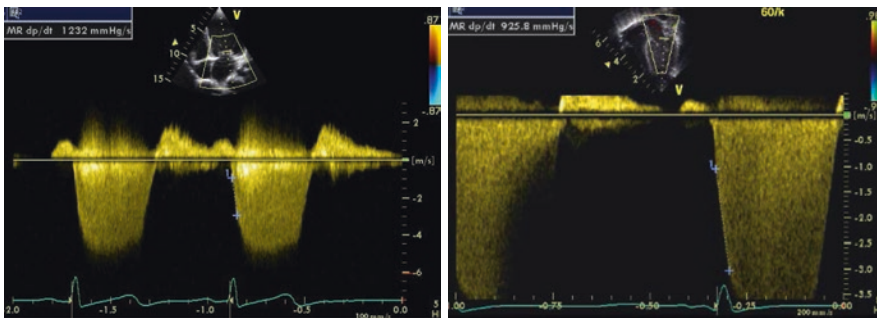


Fig. 9 Doppler tracing from mitral regurgitation allowing measurement of the mitral regurgitation MR dP/dt max obtained between 1 and 3 m/s, on a normal patient (left image) and on a patient with left ventricular dysfunction

(right image). An MR dP/dt max <500 mmHg/s is indicative of left ventricular systolic dysfunction. The same can be applied to tricuspid regurgitation (TR dP/dt max) but has to be measured between 1 and 2 m/s

note that the MR dP/dt max is influenced by preload, afterload, heart rate, and myocardial hypertrophy.

Tissue Doppler Imaging (TDI) allows the evaluation of myocardial velocities. Peak systolic annular velocity (S' wave) is measured at the level of the mitral annulus and reflects left ventricular contractility (Fig. 10) [21]. The S' has become a reliable qualitative measure of global left ventricular systolic function with a value <10 cm/s indicative of systolic dysfunction [22].

The Tei index represents an index of myocardial performance (myocardial performance index = MPI) that allows the evaluation of both

systolic and diastolic function. The disadvantage of MPI is that it is nonspecific and influenced by preload and afterload changes, making it of limited use in hemodynamically unstable patients. MPI is calculated on a pulsed wave (PW) Doppler at the mitral and aortic valve or Tissue Doppler (TDI) tracing at the lateral mitral annulus (Fig. 11) by dividing the isovolumetric relaxation time (IVRT) plus the isovolumetric contraction time (IVCT) by the ejection time (ET):

$$Tei\text{index} = \frac{IVRT + IVCT}{ET}$$

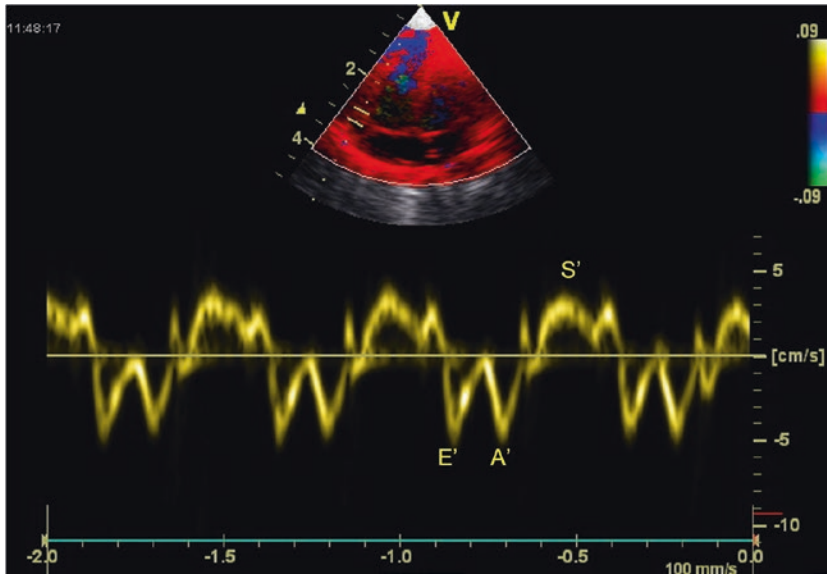


Fig. 10 Tissue Doppler Imaging (TDI) tracing obtained at the septal annulus showing S' (systolic velocity) wave, E' (early diastolic velocity) wave, and A' (late diastolic velocity related to atrial contraction) wave

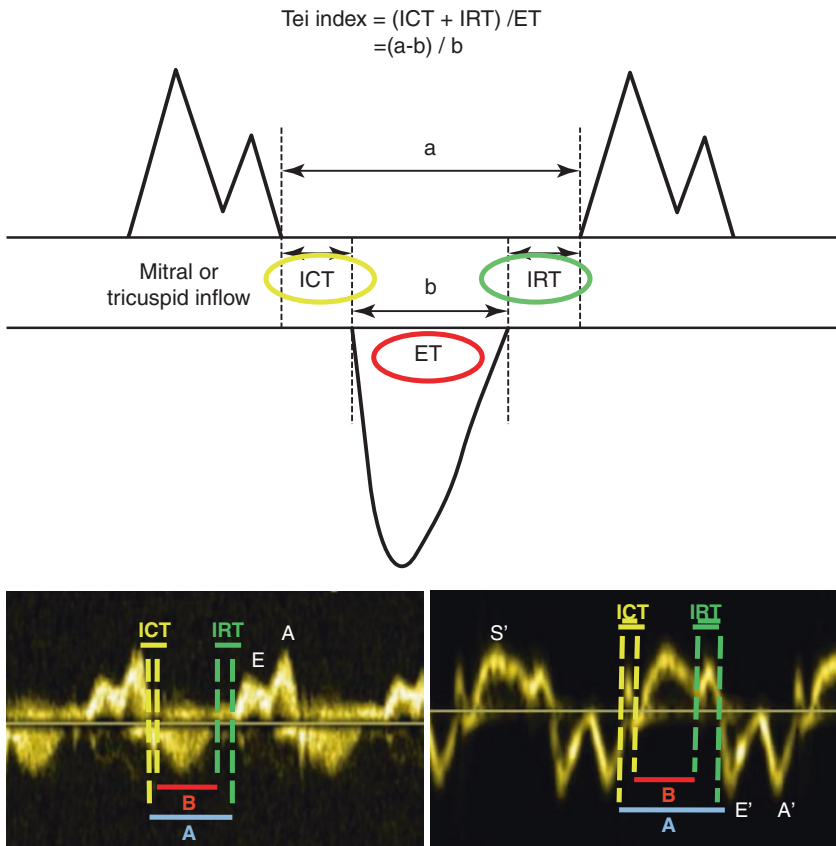


Fig. 11 Myocardial Performance Index (=MPI or Tei index) obtained from Doppler (above cartoon and bottom left image) and Tissue Doppler (below right image). The MPI is calculated as the (IVCT PLUS SPIVVRT)/ET or

(B – A)/A. The MPI allows the evaluation of systolic and diastolic ventricular function. ET ejection time, IVCT isovolumetric contraction time, IVVRT isovolumetric relaxation time

The Tei index is affected by age during the first 3 years of life, with significantly greater values (0.4 ± 0.09) at birth [23] and progressive reduction until the age of 3. There are no further changes from age 3 to 18 years, with normal values of 0.33 ± 0.02 by pulsed wave (PW) Doppler.

Evaluation of Left Ventricular Diastolic Function

Evaluation of diastolic function has become more important in the intensive care settings, especially in post-cardiac surgery patients. Spectral Doppler evaluation is the quickest method to judge diastolic function at the bedside but is highly preload dependent. A prominent pulmonary venous A wave reversal, a marker for flow reversal into the pulmonary veins during atrial systole in a noncompliant ventricle, is a hallmark of diastolic dysfunction. The mitral inflow Doppler pattern can also be used for the estimation of diastolic dysfunction. Age, arrhythmia,

conduction disturbances, and changes in loading conditions and heart rate may affect the Doppler signal and represents a major limitation, particularly in critical care patients.

The assessment of diastolic function requires the analysis of the mitral valve and pulmonary venous wave patterns using Pulsed Wave (PW) Doppler and of the lateral mitral annulus motion with Tissue Doppler Imaging (TDI). Mild diastolic dysfunction is characterized by an inversion of the mitral early and late diastolic E/A Doppler waves with a ratio <0.8 . Severe diastolic dysfunction is characterized by a mitral valve Doppler E/A ratio >2 , a deceleration time of the Doppler mitral E wave <160 ms, as well as a diastolic flow predominance in the pulmonary venous Doppler pattern (S/D <1) with prominent atrial wave reversal (AR ≥ 35 cm/s) (Fig. 12).

TDI signs of diastolic dysfunction are an early mitral annular or septal E' wave velocity <8 cm/s. The Doppler early mitral inflow velocity (E) divided by the TDI early diastolic mitral annular velocity (E') results in a ratio (E/E') that has been

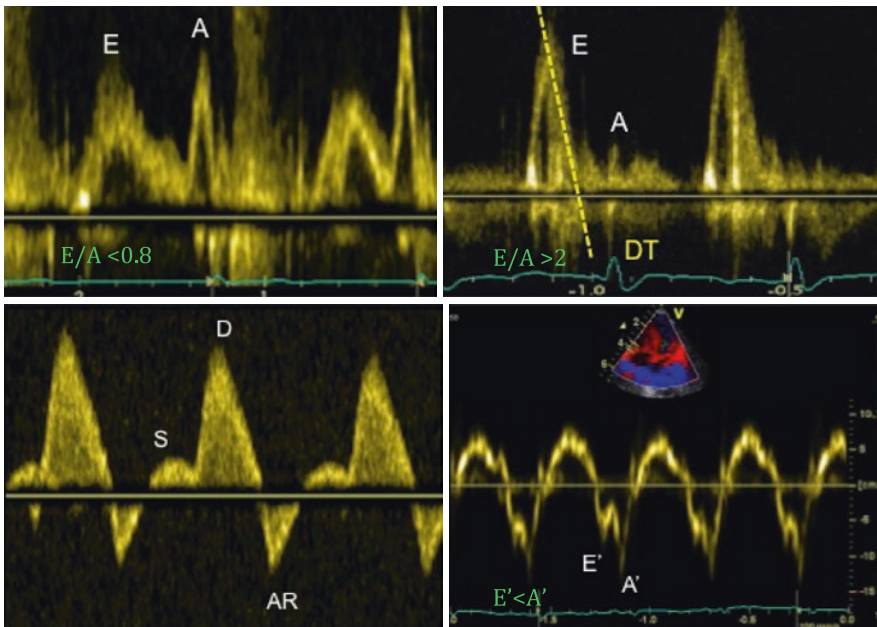


Fig. 12 Evaluation of diastolic function in a patient with severe diastolic dysfunction: (1) mitral inflow Doppler pattern with E and A wave reversal (above left image); (2) mitral inflow Doppler pattern with sharp E wave DT (above right image); (3) pulmonary venous Doppler with

prominent diastolic flow, S/D reversal and increased velocity of AR wave (below left image); (4) TDI at the mitral annulus with E'/A' reversal and decreased E' wave velocity <8 cm/s (below right image)

shown to correlate with the pulmonary capillary wedge pressure in adults [24]. The E/E' ratio is also helpful in estimating left ventricular filling pressure [25] with a value >14 indicative of increased left heart filling pressure in adults. TDI is relatively independent of preload condition, as opposed to the Doppler evaluation [26, 27], and is currently the most accurate technique to evaluate diastolic function in children, particularly in critically ill patients where loading conditions can vary widely.

In the newborn period, important changes are seen during the first weeks of life with a gradual change from a fetal filling pattern (more dependent on atrial contraction) with Doppler A > E wave toward a more mature filling pattern with E > A wave. This is characterized by a progressive increase in E wave velocity and an increase in E/A ratio. In the newborn with high heart rate, E and A waves may be fused and render the assessment of diastolic function difficult. Moreover, E wave velocity is sensitive to changes in preload. Infants with PDA and left-to-right shunt will exhibit

increased pulmonary blood flow and left atrial pressure resulting in increased mitral E wave velocity. Evaluation of left ventricle diastolic function is likely outside of the scope of basic cardiac POCUS and requires advanced training and expert consultation.

Evaluation of Cardiac Output and Cardiac Index

Echocardiographic assessment of cardiac output is a useful adjunct in the evaluation of the hemodynamically unstable infant. The most commonly used technique is the Doppler estimation of LV stroke volume, although this technique demonstrates inconsistent reproducibility. The systemic blood flow is obtained by multiplying the velocity time integral (VTI) obtained by pulsed Doppler tracing in the LV outflow tract from an apical 5-chamber view by the cross-sectional area obtained from parasternal long axis view (Fig. 13).

$$\text{Cardiac output (CO)} = \text{SV} \times \text{HR} = \text{VTI}_{\text{LVOT}} \times \text{CSA}_{\text{LVOT}} \times \text{HR}$$

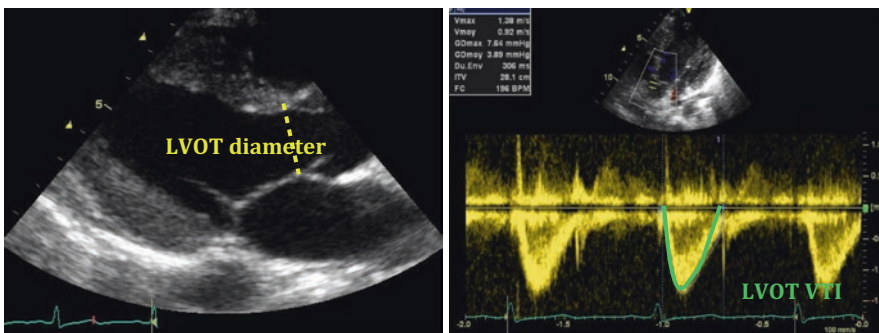


Fig. 13 Echocardiographic assessment of cardiac output: 2D echocardiography parasternal long axis view with measurement of LVOT diameter (left image), allowing for calculation of the LVOT cross sectional area (CSA) and pulse wave Doppler tracing from an apical 5-chamber

view (right image) with tracing of the LVOT velocity to obtain the LVOT velocity time integral (VTI). CSA cross-sectional area (calculated as $\pi \times r^2$ and $r = \text{radius} = \text{diameter}/2$). LVOT left ventricular outflow tract, VTI Velocity time integral (or mean velocity)

where SV is the stroke volume, VTI is the velocity time integral, CSA is the cross-sectional area ($=\pi \times r^2$ and $r = \text{diameter}/2$) and HR is the heart rate. The cardiac index can be derived by dividing the cardiac output by the body weight in kilograms according to the equation below:

$$\text{Cardiac index (CI)} = \frac{\text{VTI}_{\text{LVOT}} \times \text{CSA}_{\text{LVOT}} \times \text{HR}}{\text{BSA}}$$

where BSA is the body surface area, with normal values for LV cardiac index ranging from 1.7 to 3.5 L/min/m².

Despite various assumptions and limitations, the assessment of left ventricular output on echocardiography correlates strongly with measurements acquired by other well-established techniques such as pressure measurement by cardiac catheter, cardiac MRI and Fick's dye dilution method. The published studies showed a bias under 10% [28].

The assessment of left ventricular output is reliable in children without shunts. The trend of

serial echocardiography may be more useful than one absolute value in clinical practice. Because the CSA for any patient does not change and HR can be calculated precisely at any time, serial assessment of the VTI may help in studying the impact of any intervention on cardiac output in real time. Assessment of left ventricle cardiac output requires precise measurements and is typically reserved for providers with advanced imaging skills.

Unfortunately, this technique cannot be used in infants with a PDA where the LV output is not an appropriate surrogate of cardiac output. In those patients, the Doppler superior vena cava flow (SVC) may be a better surrogate for LV output. This measurement should be done over 5–10 cardiac beats to account for respiratory variation.

A summary of semi-quantitative systolic ventricular function evaluation is provided in Table 1 which may be used by explored in practice by clinicians with more evolved use of POCUS.

Table 1 Semi-quantitative systolic ventricular function measures that might be used by the clinician with more evolved training in cardiac POCUS (adapted from Singh Y et al. *International evidence-based guidelines on Point of Care Ultrasound (POCUS) for critically ill neonates and children issued by the POCUS Working Group of the European Society of Paediatric and Neonatal Intensive Care (ESPNIC). Critical Care 2020; 24: 65*) [29]

Echo parameter	Echo views	Measurement	Reference values
LV Fraction Shortening (FS%)	PSAX, PLAX, (2D or M-mode)	LV intraluminal diameter change	28–46% for all ages
LV Ejection Fraction (Simpson's method)	A4C, A2C	Percentage change of LV volume between end-diastole and end-systole	55–80% for all ages
E-Point Septal Separation (EPSS)	PLAX (2D or M-mode)	Distance between anterior leaflet of mitral valve and intraventricular septum during the diastolic phase. This measurement is associated with LV systolic volume	>7 mm in adults predictive of severe LV dysfunction ^a
LV output (stroke volume)	A5C, PLAX	Product of VTI measured by pulse wave Doppler at LVOT in A5C and LVOT cross-sectional area measured in PLAX	Z-scores available for different ages and should be used Neonates: 150–400 mL/kg/min
RV output (stroke volume)	PSAX or sweep PLAX	Product of VTI measured by pulsed wave Doppler at RVOT and RVOT cross-sectional area	Z-scores available for different ages and should be used Neonates: 150–400 mL/kg/min

Table 1 (continued)

Echo parameter	Echo views	Measurement	Reference values
Tricuspid annular plane systolic excursion (TAPSE)	A4C	Systolic excursion of lateral (or medial) tricuspid annulus toward apex to assess RV systolic function	Term neonates: >8 mm (8–11 mm) Children—Z-score available; generally >12 mm (12–17 mm) Adults or grown-up children >17 mm (17–25 mm)

A4C Apical 4-chamber view, A5C Apical 5-chamber view, A2C Apical 2-chamber view, PSAX Parasternal short axis view, PLAX Parasternal long axis view, *M-mode* Motion mode, LV Left ventricle, LVOT Left ventricular outflow tract, VTI velocity time integral

Conclusion

A comprehensive evaluation of cardiac function and hemodynamic status requires a depth of knowledge in echocardiography, good image quality, and using multiple echocardiographic parameters using multiple views in order to provide accurate and reliable information. However, a qualitative and semi-quantitative evaluation of systolic cardiac function can be performed using cardiac POCUS.

References

- Tissot C, Singh Y, Sekarski N. Echocardiographic evaluation of ventricular function—for the neonatologist and pediatric intensivist. *Front Pediatr.* 2018;6:79. Published online 2018 Apr 4. <https://doi.org/10.3389/fped.2018.00079>.
- Tissot C, Muehlethaler V, Sekarski N. Basics of functional echocardiography in children and neonates. *Front Pediatr.* 2017;5:235. <https://doi.org/10.3389/fped.2017.00235>. eCollection 2017. PMID: 29250515.
- Singh Y. Echocardiographic evaluation of hemodynamics in neonates and children. *Front Pediatr.* 2017;5:201. Published online 2017 Sep 15. <https://doi.org/10.3389/fped.2017.00201>.
- Tissot C, Singh Y. Neonatal functional echocardiography. *Curr Opin Pediatr.* 2020;32(2):235–44. <https://doi.org/10.1097/MOP.0000000000000887>.
- Singh Y, Katheria A, Tissot C. Functional echocardiography in the neonatal intensive care unit. *Indian Pediatr.* 2018;55(5):417–24.
- de Boode WP, van der Lee R, Horsberg Eriksen B, Nestaas E, Dempsey E, Singh Y, Austin T, El-Khuffash A, European Special Interest Group ‘Neonatologist Performed Echocardiography’ (NPE). The role of neonatologist performed echocardiography in the assessment and management of neonatal shock. *Pediatr Res.* 2018;84(Suppl 1):57–67. <https://doi.org/10.1038/s41390-018-0081-1>.
- Levy PT, Tissot C, Horsberg Eriksen B, Nestaas E, Rogerson S, McNamara PJ, El-Khuffash A, de Boode WP, European Special Interest Group ‘Neonatologist Performed Echocardiography’ (NPE). Application of neonatologist performed echocardiography in the assessment and management of neonatal heart failure unrelated to congenital heart disease. *Pediatr Res.* 2018;84(Suppl 1):78–88. <https://doi.org/10.1038/s41390-018-0075-z>.
- Singh Y, Tissot C. Echocardiographic evaluation of transitional circulation for the neonatologists. *Front Pediatr.* 2018;6:140. <https://doi.org/10.3389/fped.2018.00140>. Published online 2018 May 15. Correction in: *Front Pediatr.* 2020; 8: 600496.
- de Boode WP, Singh Y, Molnar Z, Schubert U, Savoia M, Sehgal A, Levy PT, McNamara PJ, El-Khuffash A, European Special Interest Group ‘Neonatologist Performed Echocardiography’ (NPE). Application of neonatologist performed echocardiography in the assessment and management of persistent pulmonary hypertension of the newborn. *Pediatr Res.* 2018;84(Suppl 1):68–77. <https://doi.org/10.1038/s41390-018-0082-0>.
- Nidorf SM, Picard MH, Triulzi MO, Thomas JD, Newell J, King ME, Weyman AE. New perspectives in the assessment of cardiac chamber dimensions during development and adulthood. *J Am Coll Cardiol.* 1992;19(5):983–8.
- Sahn DJ, DeMaria A, Kisslo J, Weyman A. Recommendations regarding quantitation in M-mode echocardiography: results of a survey of echocardiographic measurements. *Circulation.* 1978;58(6):1072–83.

12. Rogé CL, Silverman NH, Hart PA, Ray RM. Cardiac structure growth pattern determined by echocardiography. *Circulation*. 1978;57(2):285–90.
13. Lai WW, Geva T, Shirali GS, Frommelt PC, Humes RA, Brook MM, Pignatelli RH, Rychik J, Task Force of the Pediatric Council of the American Society of Echocardiography; Pediatric Council of the American Society of Echocardiography. Guidelines and standards for performance of a pediatric echocardiogram: a report from the task force of the Pediatric Council of the American Society of Echocardiography. *J Am Soc Echocardiogr*. 2006;19(12):1413–30. No abstract available.
14. Ünlüer E, Karagöz A, Akoglu H, Bayata S. Visual estimation of bedside echocardiography ejection fraction by emergency physicians. *Western J Emerg Med*. 2014;15(2):221–6.
15. Margossian R, Schwartz ML, Prakash A, Wruck L, Colan SD, Atz AM, Bradley TJ, Fogel MA, Hurwitz LM, Marcus E, Powell AJ, Printz BF, Puchalski MD, Rychik J, Shirali G, Williams R, Yoo SJ, Geva T, Pediatric Heart Network Investigators. Comparison of echocardiographic and cardiac magnetic resonance imaging measurements of functional single ventricular volumes, mass, and ejection fraction (from the Pediatric Heart Network Fontan Cross-Sectional Study). *Am J Cardiol*. 2009;104(3):419–28. <https://doi.org/10.1016/j.amjcard.2009.03.058>.
16. Gutgesell HP, Paquet M, Duff DF, et al. Evaluation of left ventricular size and function by echocardiography. Results in normal children. *Circulation*. 1977;56:457–62.
17. Rowland DG, Gutgesell HP. Noninvasive assessment of myocardial contractility, preload, and afterload in healthy newborns. *Am J Cardiol*. 1995;75:818–21.
18. Colan SD, Parness IA, Spevak SP. Developmental modulation of myocardial mechanics: age and growth related alterations in afterload and contractility. *J Am Coll Cardiol*. 1992;19:619–29.
19. Schiller NB, Acquatella H, Ports TA, et al. Left ventricular volume from paired biplane two dimensional echocardiography. *Circulation*. 1979;60:547–55.
20. Silverman NH, Ports TA, Snider AR, et al. Determination of left ventricular volume in children: echocardiographic and angiographic comparisons. *Circulation*. 1980;62:548–57.
21. Nestaas E, Schubert U, de Boode WP, El-Khuffash A, European Special Interest Group ‘Neonatologist Performed Echocardiography’ (NPE). Tissue Doppler velocity imaging and event timings in neonates: a guide to image acquisition, measurement, interpretation, and reference values. *Pediatr Res*. 2018;84(Suppl 1):18–29. <https://doi.org/10.1038/s41390-018-0079-8>. PMID: 30072806.
22. Gulati VK, Katz WE, Follansbee WP, et al. Mitral annular descent velocity by tissue Doppler echocardiography as an index of global left ventricular function. *Am J Cardiol*. 1996;77:979–84.
23. Eto G, Ishii M, Tei C, Tsutsumi T, Akagi T, Kato H. Assessment of global left ventricular function in normal children and in children with dilated cardiomyopathy. *J Am Soc Echocardiogr*. 1999;12:1058–64.
24. Nagueh SF, Middleton KJ, Kopelen HA, et al. Doppler tissue imaging: a noninvasive technique for evaluation of left ventricular relaxation and estimation of filling pressures. *J Am Coll Cardiol*. 1997;30:1527–33.
25. Ommen SR, Nishimura RA, Appleton CP, et al. Clinical utility of Doppler echocardiography and tissue Doppler imaging in the estimation of left ventricular filling pressures: a comparative simultaneous Doppler-catheterization study. *Circulation*. 2000;102:1788–94.
26. Vignon P, Allot V, Lesage J, et al. Diagnosis of left ventricular diastolic dysfunction in the setting of acute changes in loading conditions. *Crit Care*. 2007;11:R43.
27. Eidem BW, McMahon CJ, Ayres NA, et al. Impact of chronic left ventricular preload and afterload on Doppler tissue imaging velocities: a study in congenital heart disease. *J Am Soc Echocardiogr*. 2005;18:830–8.
28. Fical B, Finnemore AE, Cox DJ, Broadhouse KM, Price AN, Durighel G, Ekitzidou G, Hajnal JV, Edwards AD, Groves AM. Validation study of the accuracy of echocardiographic measurements of systemic blood flow volume in newborn infants. *J Am Soc Echocardiogr*. 2013;26(12):1365–71. <https://doi.org/10.1016/j.echo.2013.08.019>. Epub 2013 Sep 26.
29. Singh Y, Tissot C, Fraga M, Yousef N, Cortes RM, Lopez J, et al. International evidence-based guidelines on point of care ultrasound (POCUS) for critically ill neonates and children issued by the POCUS Working Group of the European Society of Paediatric and Neonatal Intensive Care (ESPNIC). *Crit Care*. 2020;24:65.



Focused Ultrasound in Right Ventricular Function and Pulmonary Hypertension

Shazia Bhombal, Shahab Noori, Yogen Singh, and María Victoria Fraga

Contents

Introduction	72
Right Ventricular Morphology	72
Importance of Point-of-Care Assessment of Right Ventricular Function	73
Qualitative and Quantitative Assessment of the Right Ventricle	74
TAPSE.....	74
Fractional Area Change.....	75
Tei Index.....	75
Assessment of the Presence of Pulmonary Hypertension	76
Pulmonary Artery Pressure Assessment.....	77
Ductal Shunt.....	78
Septal Assessment.....	78
Assessment of Pulmonary Vascular Resistance.....	80
Right Ventricular Function.....	80
Conclusion	81
References	82

S. Bhombal (✉)
Division of Neonatology, Emory University/
Children's Healthcare of Atlanta,
Atlanta, GA, USA
e-mail: Shazia.bhombal@emory.edu

S. Noori
Division of Neonatology, Department of Pediatrics,
Fetal and Neonatal Institute, Children's Hospital Los
Angeles, Keck School of Medicine, University of
Southern California, Los Angeles, CA, USA
e-mail: snoori@chla.usc.edu

Y. Singh
Department of Pediatrics, Division of Neonatology,
Loma Linda University School of Medicine,
California, USA

Department of Pediatrics, Division of Neonatal and
Developmental Medicine, Stanford University School
of Medicine, California, UK

Department of Pediatrics, Division of Neonatology,
University of Southern California, California, UK

ESPNC Cardiovascular Dynamics Section and
POCUS Working Group, Geneva, Switzerland
e-mail: YSingh@llu.edu

M. V. Fraga
Department of Pediatrics, Division of Neonatology,
Children's Hospital of Philadelphia, Perelman School
of Medicine, University of Pennsylvania,
Philadelphia, PA, USA

The Children's Hospital of Philadelphia,
Philadelphia, PA, USA
e-mail: fragam@chop.edu

Introduction

The goal of point-of-care ultrasound (POCUS) is to answer a clinical question, with the image acquisition and analysis performed by the bedside clinician. While the scope of POCUS in imaging and evaluation of the RV is limited, in order to provide an overall understanding of the impact of pathology on the RV and the ability to interpret changes seen by ultrasound, this chapter will provide a more in-depth overview of RV morphologic and functional assessment that is beyond the scope of cardiac POCUS. However, when applicable, we will point out the RV views and assessments that could be considered part of cardiac POCUS.

Right Ventricular Morphology

The RV is the most anterior chamber of the heart, wrapping around the left ventricle (LV), and thus is the first structure the ultrasound beam will interrogate just under the sternum. The role of the RV is to act as a low resistance circuit for venous flow to enter and pump deoxygenated blood to the low resistance pulmonary vascular bed [1]. The RV function and size reflect the impact of preload, afterload, and ventricular–ventricular interactions. The morphology of the RV is tripartite. The three sections are an inlet chamber, an apex/trabecular body, and the outflow chamber. The inlet portion encompasses the area from the level of atrioventricular junction as marked by the annulus of the tricuspid valve to the insertion of the papillary muscles to the walls of the ventricle, followed by the trabecular pumping chamber. The outlet portion comprises the smooth subvalvular infundibulum to the pulmonary valve in a normally structured heart (Fig. 1). Though trabeculations are usually associated with the RV in comparison to the LV, trabeculations are not the distinguishing feature, as in some cases, the LV may be trabeculated as well. A distinguishing feature of the RV is its association with the tricuspid valve, with the

septal attachment of the tricuspid valve having a more caudal insertion compared to the mitral valve. The tricuspid valve is always associated with the RV.

The RV is also distinguished from the left by its fiber orientation. Fibers in the RV are mainly arranged in a longitudinal direction, compared to approximately 60% circumferential, 20% longitudinal, and 20% oblique arrangement in the LV [2]. In a normally structured heart, the RV pumps blood to a low resistance circuit and its thin wall wraps partially around the LV (Fig. 2). As the RV encounters increasing afterload, the ventricle may dilate and thicken, changing its morphology. RV failure may result from a combination of decreased RV contractility, increased RV pressure, and RV volume overload [3]. The longitudinal orientation of the RV fibers provides mechanisms for functional assessment, such as the tricuspid annular plane systolic excursion (TAPSE). Of note, the right and left ventricles share fiber arrangement at the interventricular septum; thus, ventricular–ventricular interactions are an important consideration as decreased RV function can impact the LV function and vice versa.

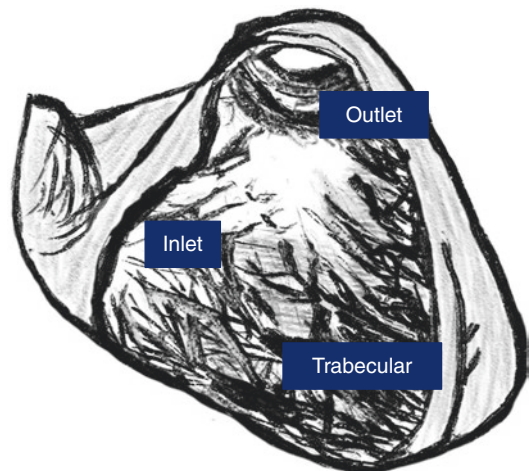


Fig. 1 Composition of the right ventricle with three sections; inlet, trabeculated chamber, and smooth outlet portion

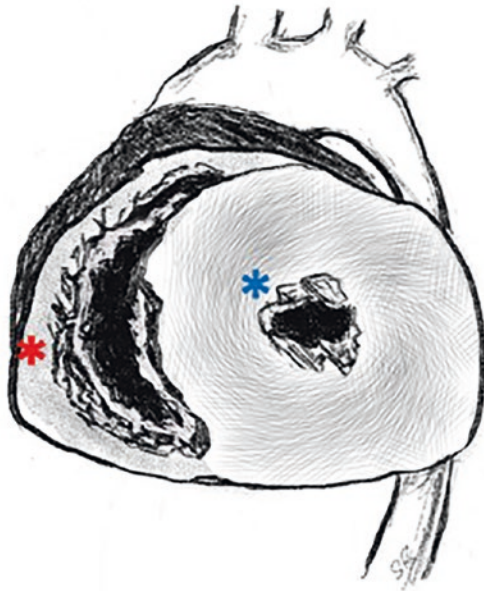


Fig. 2 Short axis image of the right ventricle (red star) wrapping around the left ventricle (blue star)

Importance of Point-of-Care Assessment of Right Ventricular Function

As mentioned earlier, the scope of POCUS in the assessment of RV function is evolving and somewhat limited in neonates by the extensive training required in neonatal hemodynamics. In adult critical care medicine, POCUS has been recommended to assess for evidence of acute RV failure [4] (Fig. 3). Acute RV failure recognized by bedside cardiac ultrasound allows for earlier diagnosis and dedicated management strategies that can impact outcomes [5]. Indeed, bedside cardiac ultrasound has become increasingly utilized in the critical care setting. A plethora of research has been published in the field of RV functional assessment [6]. A multitude of disease processes can be assessed, particularly in patients with the potential for increase RV afterload, such as pulmonary embolism and acute respiratory distress

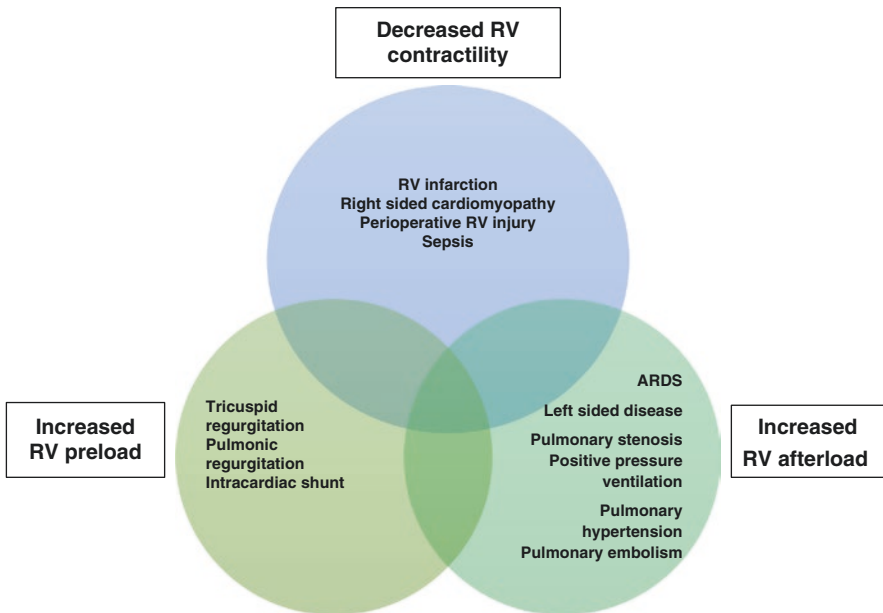


Fig. 3 Etiologies for acute right ventricular failure. *RV* right ventricle, *ARDS* acute respiratory distress syndrome

syndrome. RV dysfunction in the critically ill infant has been associated with increased morbidity and mortality [7].

Functional evaluation of the RV includes assessment of longitudinal motion with TAPSE and global functional assessment with fractional area change (FAC). In a systematic review of studies performed in the critical care setting that reported RV function as a measure, TAPSE was the most frequent index used to assess RV function, followed by FAC. The mechanism of hemodynamic pathophysiology due to RV dysfunction is multifactorial. In the case of a pulmonary hypertensive crisis, the RV end-diastolic pressure and volume increase with the potential for compromised coronary perfusion leading to RV ischemia and failure. In addition, increased RV end-diastolic pressure and volume can lead to a shift in the interventricular septal position into the LV, which could decrease LV end-diastolic volume and thus decrease cardiac output. Mortality from pulmonary hypertension is directly related to RV function. Timely assessment of the RV can be of particular importance in certain conditions, particularly those in patients with a normal RV that suffers from an acute increase in RV afterload.

Qualitative and Quantitative Assessment of the Right Ventricle

Evaluation of the RV includes RV size assessment as well as a qualitative and quantitative functional assessment. Qualitative measures of the RV include assessment of RV/LV ratio and qualitative functional assessment. In pediatric and adult literature, qualitative RV to LV size comparison (typically the diameter of each respective ventricle in the apical four chamber view) has been utilized to assess RV dilation, with a normal RV size being two-thirds of LV. Therefore, the finding of an RV larger than

the LV is considered a sign of severe RV enlargement. In a pediatric population of patients with pulmonary hypertension (PH), an RV/LV ratio > 1 was associated with an adverse clinical event, such as disease progression necessitating initiation of pulmonary vasodilators, death, or transplant [8]. Qualitative RV functional assessment includes “eyeballing” the function by assessing movement and dilation in the parasternal short axis. This qualitative assessment could be integrated as part of cardiac POCUS. In the setting of volume overload conditions such as a ventricular septal defect, the RV will become dilated and demonstrate septal flattening in diastole. In true RV pressure overload conditions such as pulmonary arterial hypertension the interventricular septum flattens at end systole/early diastole as the RV contracts against a higher resistance pulmonary vasculature.

TAPSE

Quantitative assessment of RV systolic function includes measuring TAPSE and FAC. As the RV fibers contract primarily by longitudinal movement, measurement of the distance the tricuspid valve moves along the lateral wall of the RV provides a measure of the longitudinal contractile ability of the RV. In the 4-chamber apical view with the apex visible, the M-mode cursor is placed at the lateral annulus of the tricuspid valve with the line as parallel as possible to the lateral wall (Fig. 4). TAPSE is the most frequently utilized index to report RV function, with normal reference values published for infants and children (Table 1) [6, 9]. However, TAPSE focuses on the longitudinal, not global, assessment of the RV. Assessment of global function will account for regional wall motion of the RV and can be obtained through multiple measures, including FAC, Tei index, and tissue Doppler.

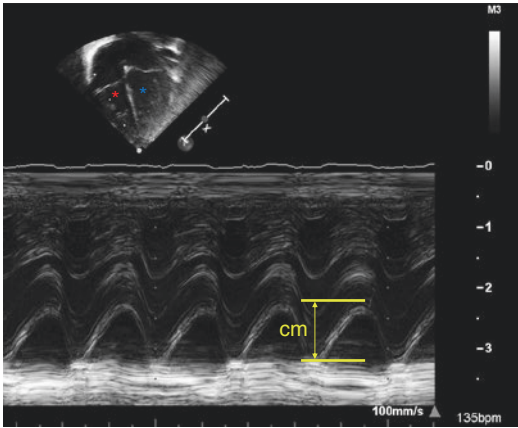


Fig. 4 M-mode measured TAPSE—Tricuspid Annular Plane Systolic Excursion. White dotted line measuring tricuspid valve movement through systole and diastole along the lateral wall of the right ventricle with apex in view; yellow lines outline displacement of tricuspid valve; yellow arrow denotes measurement in centimeters. Right ventricle (red star) wraps around LV (blue star)

Table 1 Tricuspid annular plane systolic excursion (TAPSE) values in cm by age group, reported as mean and ± 2 SD (95%). (Based on data from Koestenberger et al. 2009)

Age	Mean (cm)	± 2 SD (95%) (cm)	
0–30 days	0.91	0.68	1.15
1–3 months	1.14	0.85	1.42
4–6 months	1.31	1.01	1.65
7–12 months	1.44	1.13	1.77
1 year	1.55	1.25	1.88
2 years	1.65	1.36	1.94
5 years	1.87	1.60	2.13
10 years	2.05	1.79	2.31
18 years	2.47	2.05	2.91

Fractional Area Change

The geometric morphology of the RV compared with the LV can make the assessment of function challenging; however, fractional area change (FAC %) by echo correlates with RV ejection fraction by MRI [10, 11]. FAC is obtained by tracing the RV endocardial border in the 4-chamber apical view at end diastole (EDA) and end systole (ESA), subtracting ESA from EDA and dividing by EDA to get a fraction of change in RV size from systole to diastole (Fig. 5). Levy

et al. noted that FAC in preterm neonates increased almost twice as rapidly in the first month compared with healthy term infants [12]. Limitations of FAC include acquiring a high-quality image of the RV for chamber size calculation, and noninclusion of the right ventricular outflow tract in the assessment.

Tei Index

The Tei index, also referred to as the myocardial performance index, offers a quantitative measure of global function and incorporates systolic and diastolic functional assessments. It is calculated from a ratio of time intervals—measuring changes in the time interval of isovolumic contraction time (IVCT) and isovolumic relaxation time (IVRT) in comparison to the RV ejection time (RVET). These measurements are similar to those previously discussed in Chap. 5 for assessment of the left ventricle. Following the P wave, signaling the point of active filling of the ventricle from the atria, the tricuspid valve closes. The isovolumic contraction time precedes the opening of the pulmonary valve and RV ventricular ejection, which is followed by a period of tricuspid and pulmonary valve closure (isovolumic relaxation time). The myocardial performance index represents the time from tricuspid valve closure to opening minus the RVET, over the RVET. A shortened ejection time due to a prolonged IVCT is indicative of systolic dysfunction and a shortened ejection time due to a prolonged IVRT is consistent with diastolic dysfunction. The Tei index is assessed through tissue Doppler or flow Doppler at the level of the tricuspid and pulmonary valve and has the advantage of being heart rate and geometry independent (Fig. 6). Due to the challenges of obtaining multiple measures and the need for adequate Doppler measures, it has not been utilized significantly in the critical care literature.

Finally, tissue Doppler imaging (TDI), assessing myocardial velocities, is utilized as another measure of RV function in the 4-chamber apical view with RV focus.

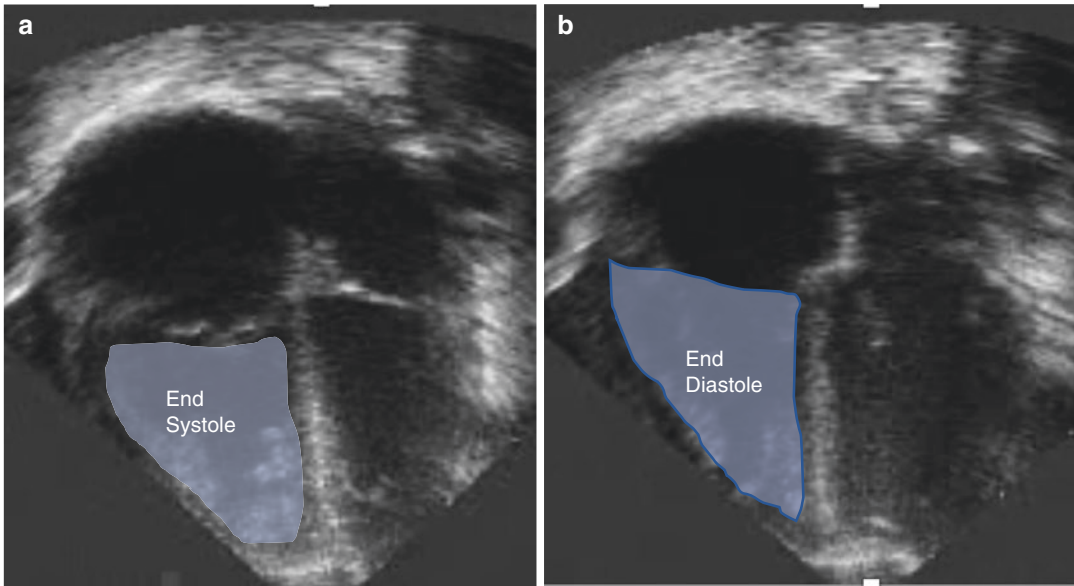


Fig. 5 Fractional area change (FAC); measurement of right ventricular size in systole (a) and diastole (b)

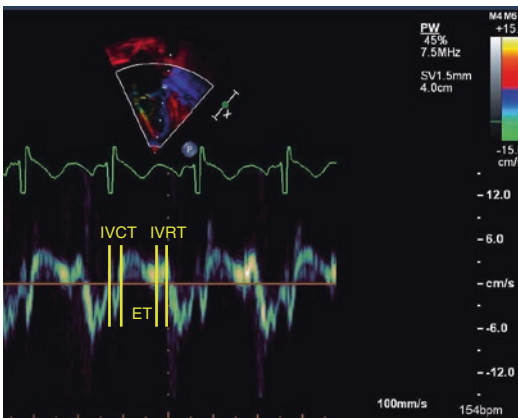


Fig. 6 Tei index, also called myocardial performance index, measures global function incorporating systolic and diastolic function. *IVCT* isovolumic contraction time, *IVRT* isovolumic relaxation time, *ET* ejection time. Tei index = $(IVCT + IVRT)/ET$

Assessment of the Presence of Pulmonary Hypertension

Echocardiography is utilized as a noninvasive method to assess pulmonary hypertension. Using traditional conventions for measuring pulmonary hypertension by echo, such as tricuspid regurgitation and septal flattening, echocardiog-

raphy has been found to be a reasonable noninvasive technique to identify patients with pulmonary hypertension, though not necessarily to quantify severity. A study by Mourani et al. demonstrated that echocardiography correctly diagnosed pulmonary hypertension in 79% of patients in which pulmonary pressures could be estimated, though was correct in severity for 47% of the patients [13].

Recognition and quantification of pulmonary hypertension by echocardiography include estimating pulmonary artery pressures and evaluating pulmonary vascular resistance. Subjective “eyeballing” of the RV is commonly utilized for bedside assessment, particularly in the intensive care units, with a fair agreement between subjective and objective measures. Eyeballing is potentially not as reliable for the reassessment of subtle changes following interventions [14]. Thus, while basic cardiac imaging may be able to assess the presence of pulmonary hypertension, comprehensive echocardiography is needed for qualitatively and quantitatively assessing pulmonary hypertension. This section will focus on basic cardiac views and will introduce advanced views for the assessment of pulmonary hypertension.

Comprehensive echocardiography for pulmonary hypertension includes the estimation of pul-

monary artery pressures, assessment of pulmonary vascular resistance, as well as evaluation of cardiac function to assess the impact of elevated pulmonary pressures upon the heart. As this chapter is focused on right ventricular assessment, left ventricular function will not be discussed; however, it is important to assess the left ventricular function due to the important contribution of ventricular–ventricular interactions on RV function, and decreased LV filling from decreased left-sided preload in the setting of pulmonary hypertension. Obtaining standard echocardiographic views including parasternal long and short axis, 4- and 5-chamber apical, subcostal, and suprasternal views will provide information for adequate assessment. Conventional parameters to estimate pulmonary artery pressures includes the assessment of tricuspid regurgitation peak velocity, pulmonary insufficiency peak velocity, shunt direction, velocity through the ductus arteriosus or ventricular septal defect if present, and interventricular

septal geometry. Evaluation of pulmonary vascular resistance includes recognition of abnormalities of pulmonary artery waveforms and assessment of pulmonary time intervals. In addition, the evaluation of right ventricular strain and 3D evaluation of RV volumes provide additional information on the right ventricular functional assessment of pulmonary hypertension.

Pulmonary Artery Pressure Assessment

Pulmonary artery pressure can be obtained with the estimation of an adequate tricuspid regurgitation (TR) peak velocity, pulmonary insufficiency peak velocity, shunt direction, and velocity and septal geometry. TR peak velocity estimates pulmonary artery pressures using the modified Bernoulli equation:

$$\text{Right Ventricular Pressure} = 4(\text{Tricuspid Regurgitation Velocity})^2 + \text{Right atrial pressure (estimate } \sim 5 \text{ mmHg)}$$

Estimation of pulmonary artery systolic pressures by echocardiographic assessment of TR peak velocity has demonstrated reasonable accuracy when compared to cardiac catheterization. However, in up to 40% of echocardiography studies, it may be difficult to obtain an interpretable TR jet or a jet may be completely absent [13, 15]. When obtaining the TR jet velocity, it is key to maintain angle of insonation minimal (as parallel as possible to the jet, <20° angle of insonation) to avoid underestimating the velocity of regurgitation and thus the estimation of pulmonary pressures. Continuous wave Doppler should be utilized for this measurement, as the velocity is usually too high for the pulse wave Doppler assessment (>2 m/s). Multiple views should be utilized to obtain the maximum or best TR jet velocity, including the 4-chamber apical view, parasternal long axis RV inflow view, or parasternal short axis view (Fig. 7). It is important to consider

that this measurement may be under- or overestimated by decreased RV function and RV outflow tract obstruction, respectively [16]. Pulmonary hypertension is defined as a mean pulmonary blood pressure >20 mmHg at rest in infants >3 months of age, and in neonates, elevated pulmonary pressure is often defined in relation to systemic blood pressure. Increased afterload on the RV leads to remodeling with the development of hypertrophy to reduce wall stress, which can be reversible. In the setting of volume overload, the RV dilates and can maintain a normal Frank-Starling curve with preserved RV function [17]. A pulmonary insufficiency jet velocity provides an estimation of the mean pulmonary artery pressure. Continuous wave Doppler of the peak pulmonary regurgitant jet in parasternal short axis view during diastole will provide an estimation of mean PA pressure again using the modified Bernoulli equation:

$$\text{mPAP} = 4(\text{VmaxPR})^2 + \text{RA pressure} (\sim 5 \text{ mmHg})$$

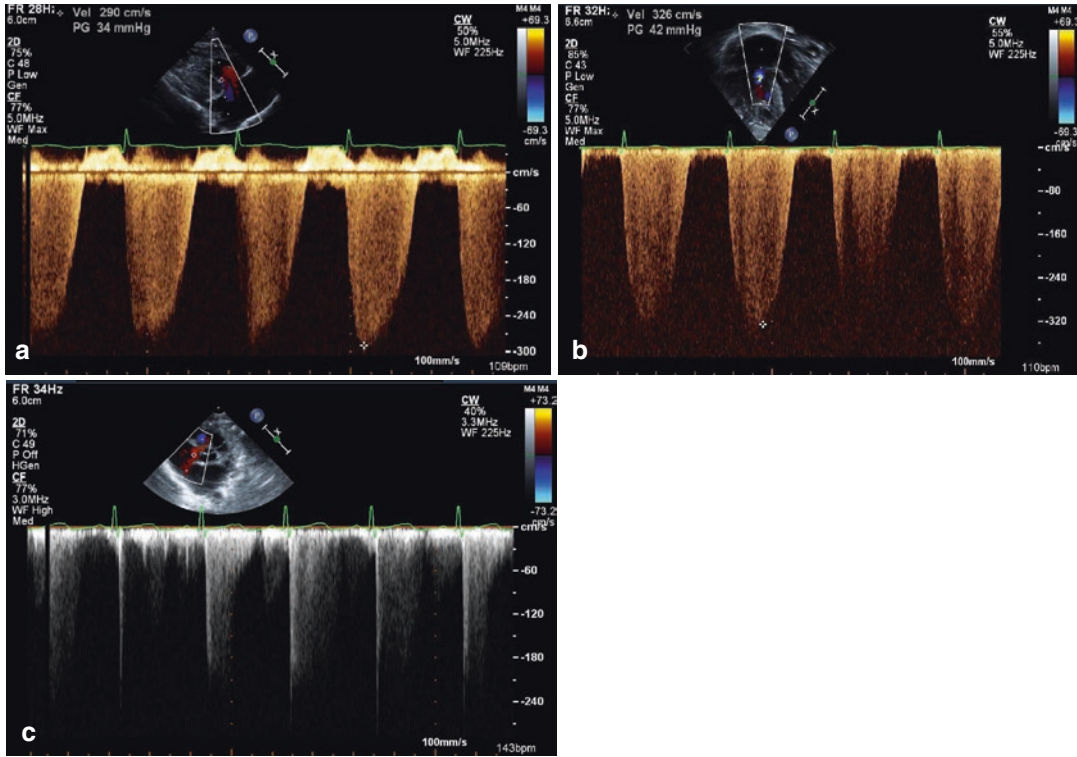


Fig. 7 Tricuspid regurgitation jet velocity, (a) Parasternal long axis right heart view with full envelope; (b) Apical 4-chamber view with full envelope; (c) Parasternal short

axis base view with incomplete tricuspid regurgitation envelope

Ductal Shunt

The presence of a patent ductus arteriosus (PDA) provides quantitative measurement of pulmonary hypertension through the assessment of the direction and flow velocity of the PDA shunt. A pure right to left shunt across the PDA (flow directing from the pulmonary artery to the aorta) correlates with suprasystemic pulmonary pressures, while a bidirectional shunt, with right to left shunting in systole and left to right shunting in diastole, is consistent with systemic pulmonary pressures (Fig. 8). The velocity of the transductal flow correlates with catheterization measures of pressure; however, location of the Doppler sample is important. Peak velocity of both right to left and left to right shunts vary compared with catheterization data depending on the location of the Doppler within the PDA. For a right to left shunt,

suggesting suprasystemic pulmonary pressures, maximal velocity occurs at the aortic end of the PDA, while in left to right shunt, peak velocity is noted at the point of maximal constriction at the pulmonary end [18].

Septal Assessment

The interventricular ventricular septum is rounded in systole and diastole in hemodynamically stable conditions with normal systemic vascular resistance (SVR) and pulmonary vascular resistance (PVR). The left ventricular systolic pressure equals the arterial systolic blood pressure in a patient without outflow tract obstruction. RV systolic pressure is typically lower than that of the LV, thus in systole and diastole the LV is a rounded structure relative to the RV. In patients with volume overload

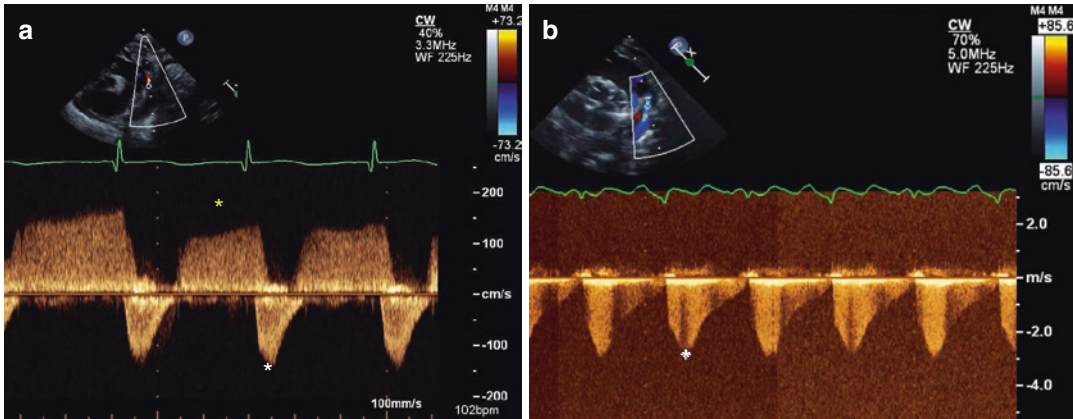


Fig. 8 PDA Doppler. (a) Bidirectional PDA shunt with flow above (yellow star) and below the baseline; (b) Pure right to left flow (white star) across the PDA consistent with suprasystemic pulmonary pressures

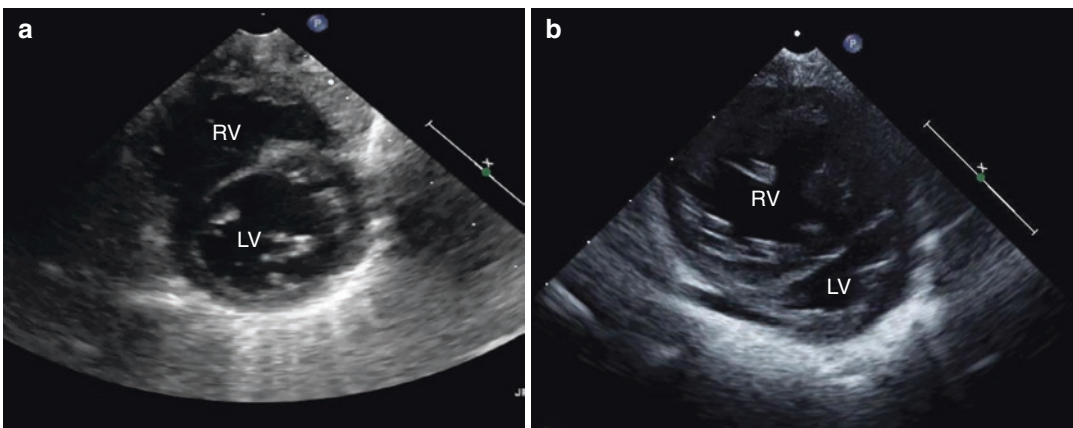


Fig. 9 Assessment of septal flattening in parasternal short axis view. (a) Normal rounded septum consistent with normal RV pressures, (b) Flattened septum, consistent with elevated pulmonary pressures

from a shunt or pressure overload from elevated PVR, the interventricular septum may be flattened or even crescent-shaped or bowed in the parasternal short axis view (Fig. 9). A flattened septum during diastole is consistent with volume overload, whereas in systole with RV pressure overload. However, foreshortening the LV by ultrasound can result in a flat septum from technical error rather than patient conditions. Thus, it is prudent to assess other parameters in addition to septal flattening when determining elevated pulmonary pressures.

Eccentricity index is utilized as an objective measure of septal flattening. For assessing pul-

monary hypertension, it is obtained by measuring the LV dimension ratio parallel (D1) and perpendicular (D2) to the septum in parasternal short axis in end systole (Fig. 10):

$$\text{Eccentricity index} = D1 / D2$$

In adult literature, an eccentricity index >1 is consistent with elevated RV pressures. Simultaneous catheterization and echocardiography studies in the pediatric population demonstrated a correlation between eccentricity index and pulmonary hypertension and are less prone to variability in measures [19].

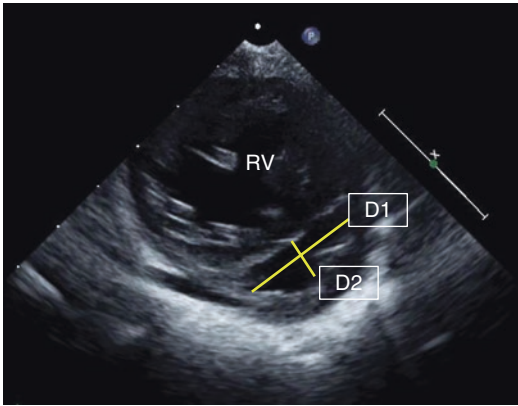


Fig. 10 Eccentricity index as quantitative measurement of septal flattening. *D1* LV dimension parallel to septum, *D2* LV dimension perpendicular to the septum, *RV* right ventricle

Assessment of Pulmonary Vascular Resistance

Catheterization is considered the gold standard method of calculating pulmonary vascular resistance, with a PVR >3 Wood units consistent with elevated pulmonary vascular resistance. However, echocardiography can be utilized to noninvasively assess PVR and can aid in differentiation between precapillary pulmonary hypertension, occurring in the lungs, versus postcapillary pulmonary hypertension due to pathology beyond the capillary bed, such as pulmonary vein stenosis or left heart disease. Evaluation of PVR by echocardiography includes the assessment of pulmonary valve Doppler waveforms and systolic time intervals of pulmonary flow. The pulmonary valve Doppler flow waveform in the presence of normal PVR is dome-shaped with a steady increase and decrease in flow. In the presence of elevated PVR, the time to peak velocity flow is short, as the pressure necessary to push blood out the pulmonary valve to overcome the elevated resistance is higher than normal. Once the valve opens, there is a rapid increase in velocity. In the presence of increased PVR as well as decreased vascular compliance, a flying “W” sign may be present, with the presence of a pulmonary mid-systolic notch (Fig. 11). Systolic time intervals of the RV provide an indirect assessment of PVR. RV time intervals include

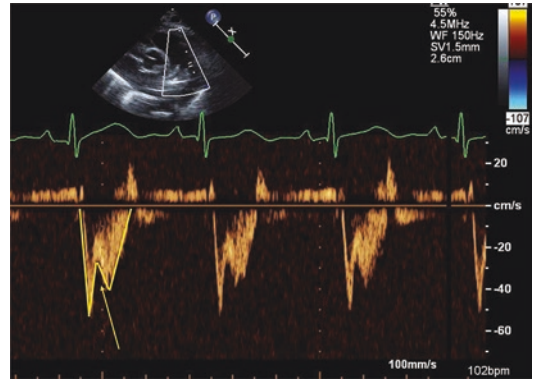


Fig. 11 Pulmonary doppler demonstrating Flying “W” sign (outlined in yellow) with a pulmonary mid-systolic notch (arrow), consistent with elevated pulmonary vascular resistance and decreased vascular compliance

the pre-ejection period (RPEP), RV ejection time (RVET), and the time to peak velocity (TPV), also referred to as the pulmonary artery acceleration time (PAAT). At any given heart rate, the RVET is directly related to stroke volume and indirectly related to contractility, and thus low contractility results in longer ejection time. In the presence of pulmonary hypertension, as described above, there is a higher RPEP:RVET ratio, as the RV is pushing against a higher afterload thus prolonging the pre-ejection period. Pulmonary artery acceleration time measures the time interval from the onset of ejection to the peak flow velocity. With elevated PVR, the PAAT shortens and the PAAT:RVET ratio decreases, with simultaneous catheterization and echocardiography studies demonstrating a PAAT <90 ms and PAAT:RVET ratio <0.31 correlated with pulmonary hypertension [20].

Right Ventricular Function

Both right and left ventricular function may be affected in the presence of pulmonary hypertension. The increased afterload of the RV can impact the function, and the LV may be impaired through ventricular–ventricular interactions as well as potential myocardial ischemia [16]. Qualitative assessment of cardiac function in the setting of pulmonary hypertension includes

RV:LV size comparisons as described above, though more comprehensive assessment is warranted, particularly with longitudinal assessment following interventions. Measures used for quantitative RV functional assessment in the presence of pulmonary hypertension are TAPSE and FAC, as described above. TAPSE reference values and z-scores are available in infants and pediatric patients, as well as for preterm and term neonates, with a noted linear increase in TAPSE values from 26 to 41 weeks gestational age [9, 21]. In adults with pulmonary hypertension, low TAPSE has been associated with worse survival outcomes [22]. Low TAPSE has also been noted in pediatric patients with pulmonary hypertension. As such, it is recommended to obtain TAPSE for longitudinal assessment of RV function at each routine echo in pediatric patients with pulmonary hypertension [23].

Fractional area change %, Tei index, and tissue Doppler imaging have been noted to be significantly lower in infants with moderate/severe bronchopulmonary dysplasia (BPD) compared with a non-BPD cohort, and can be utilized to assess for pulmonary hypertension in the neonatal population [24].

Additional advanced tools for assessment of pulmonary hypertension by echocardiography include assessment of right heart size with 3D echocardiography to better assess the complexities of RV geometry. 3D echocardiography has been validated with cardiac MRI, and in pediatric patients with pulmonary hypertension may provide a better assessment of volume and function than 2D echocardiography. Pediatric patients with pulmonary hypertension have higher RV volumes and lower RV ejection fractions than normal controls by 3D measures [25, 26]. In addition, right atrial and RV strain provides additional information on the impact of elevated pulmonary pressures. Strain and strain rate are increasingly reported as RV functional measures to detect regional wall motion abnormalities, with strain reporting the change in length and strain rate as the rate of deformation per second [27, 28]. In a population of preterm patients with severe BPD, infants with pulmonary hypertension at 6 months had lower global longitudinal

strain than those with BPD without pulmonary hypertension.

Comprehensive echocardiography for assessment includes estimates of pulmonary pressures, evaluation of pulmonary vascular resistance, and measures of RV, as well as left ventricular function. With adequate training, initial and longitudinal assessment can provide guidance for patient care.

Conclusion

RV assessment by point-of-care ultrasound is an evolving field. In the adult literature, the most common measures of RV function are TAPSE and FAC, with subjective quantitative measures, such as RV/LV size and assessment of septal flattening, often reported. Neonatal cardiac POCUS is performed to answer a specific question, for example, identifying the presence of pulmonary hypertension. Cardiac POCUS may be utilized to “eyeball” systolic function, compare RV with LV size, assess septal flattening, and determine the direction of PDA shunt. When performing neonatal point-of-care cardiac ultrasound, it is crucial to keep in mind that neonates have a complex dynamic transitional cardiovascular physiology and a risk of undiagnosed critical congenital heart disease, if a prior comprehensive echocardiography has not been performed to establish normal cardiac anatomy. Significant right heart dilation and decreased function can occur in the setting of congenital heart disease such as critical pulmonary stenosis. The ability to rapidly recognize abnormalities on basic RV evaluation may result in an earlier cardiology consult if abnormalities are noted. Cardiac POCUS should be focused, short in duration, and performed to understand the underlying clinical problem. Cardiac POCUS should not be used as a screening tool for congenital heart diseases. A comprehensive echocardiogram performed by a cardiologist prior to or around the time of a point-of-care ultrasound should be considered to carefully rule out congenital heart disease. Similarly, a comprehensive assessment of RV function, pulmonary hypertension evaluation and complex

transitional cardiovascular physiologic assessment should be undertaken by experienced imaging specialists.

References

- Bleeker GB. Assessing right ventricular function: the role of echocardiography and complementary technologies. *Heart*. 2006;92:i19–26.
- Sengupta PP, Krishnamoorthy VK, Korinek J, Narula J, Vannan MA, Lester SJ, Tajik JA, Seward JB, Khandheria BK, Belohlavek M. Left ventricular form and function revisited: applied translational science to cardiovascular ultrasound imaging. *J Am Soc Echocardiogr*. 2007;20:539–51.
- Piazza G, Goldhaber SZ. The acutely decompensated right ventricle. *Chest*. 2005;128:1836–52.
- Levitov A, Frankel HL, Blaivas M, Kirkpatrick AW, Su E, Evans D, Summerfield DT, Slonim A, Breikreutz R, Price S, McLaughlin M, Marik PE, Elbarbary M. Guidelines for the appropriate use of bedside general and cardiac ultrasonography in the evaluation of critically ill patients-part II: cardiac ultrasonography. *Crit Care Med*. 2016;44:1206–27.
- Filopei J, Acquah SO, Bondarsky EE, Steiger DJ, Ramesh N, Ehrlich M, Patrawalla P. Diagnostic accuracy of point-of-care ultrasound performed by pulmonary critical care physicians for right ventricle assessment in patients with acute pulmonary embolism*. *Crit Care Med*. 2017;45:2040–5.
- Huang SJ, Nalos M, Smith L, Rajamani A, McLean AS. The use of echocardiographic indices in defining and assessing right ventricular systolic function in critical care research. *Intensive Care Med*. 2018;44:868–83.
- Malowitz JR, Forsha DE, Smith PB, Cotten CM, Barker PC, Tatum GH. Right ventricular echocardiographic indices predict poor outcomes in infants with persistent pulmonary hypertension of the newborn. *Eur Heart J Cardiovasc Imaging*. 2015;16:1224–31.
- Jone P-N, Hinzman J, Wagner BD, Ivy DD, Younoszai A. Right ventricular to left ventricular diameter ratio at end-systole in evaluating outcomes in children with pulmonary hypertension. *J Am Soc Echocardiogr*. 2014;27:172–8.
- Koestenberger M, Ravekes W, Everett AD, Stueger HP, Heinzl B, Gamillscheg A, Cvirm G, Boysen A, Fandl A, Nagel B. Right ventricular function in infants, children and adolescents: reference values of the tricuspid annular plane systolic excursion (TAPSE) in 640 healthy patients and calculation of z score values. *J Am Soc Echocardiogr*. 2009;22:715–9.
- Breatnach CR, Levy PT, James AT, Franklin O, El-Khuffash A. Novel echocardiography methods in the functional assessment of the newborn heart. *Neonatology*. 2016;110:248–60.
- Lee JZ, Low S-W, Pasha AK, Howe CL, Lee KS, Suryanarayana PG. Comparison of tricuspid annular plane systolic excursion with fractional area change for the evaluation of right ventricular systolic function: a meta-analysis. *Open Heart*. 2018;5:e000667.
- Levy PT, Dioneda B, Holland MR, Sekarski TJ, Lee CK, Mathur A, Cade WT, Cahill AG, Hamvas A, Singh GK. Right ventricular function in preterm and term neonates: reference values for right ventricle areas and fractional area of change. *J Am Soc Echocardiogr*. 2015;28:559–69.
- Mourani PM, Sontag MK, Younoszai A, Ivy DD, Abman SH. Clinical utility of echocardiography for the diagnosis and management of pulmonary vascular disease in young children with chronic lung disease. *Pediatrics*. 2008;121:317–25.
- Orde S, Slama M, Yastrebov K, Mclean A, Huang S. Subjective right ventricle assessment by echo qualified intensive care specialists: assessing agreement with objective measures. *Crit Care*. 2019;23:70.
- Currie PJ, Seward JB, Chan K-L, Fyfe DA, Hagler DJ, Mair DD, Reeder GS, Nishimura RA, Tajik AJ. Continuous wave doppler determination of right ventricular pressure: a simultaneous Doppler-catheterization study in 127 patients. *J Am Coll Cardiol*. 1985;6:750–6.
- de Boode WP, Singh Y, Molnar Z, Schubert U, Savoia M, Sehgal A, Levy PT, McNamara PJ, El-Khuffash A, European Special Interest Group ‘Neonatologist Performed Echocardiography’ (NPE). Application of neonatologist performed echocardiography in the assessment and management of persistent pulmonary hypertension of the newborn. *Pediatr Res*. 2018;84:68–77.
- Kovács A, Lakatos B, Tokodi M, Merkely B. Right ventricular mechanical pattern in health and disease: beyond longitudinal shortening. *Heart Fail Rev*. 2019;24:511–20.
- Musewe NN, Smallhorn JF, Benson LN, Burrows PE, Freedom RM. Validation of Doppler-derived pulmonary arterial pressure in patients with ductus arteriosus under different hemodynamic states. *Circulation*. 1987;76:1081–91.
- Burkett DA, Patel SS, Mertens L, Friedberg MK, Ivy DD. Relationship between left ventricular geometry and invasive hemodynamics in pediatric pulmonary hypertension. *Circ Cardiovasc Imaging*. 2020;13:e009825.
- Levy PT, Patel MD, Groh G, Choudhry S, Murphy J, Holland MR, Hamvas A, Grady MR, Singh GK. Pulmonary artery acceleration time provides a reliable estimate of invasive pulmonary hemodynamics in children. *J Am Soc Echocardiogr*. 2016;29:1056–65.
- Koestenberger M, Nagel B, Ravekes W, Urlesberger B, Raith W, Avian A, Halb V, Cvirm G, Fritsch P, Gamillscheg A. Systolic right ventricular function in preterm and term neonates: reference values of the tricuspid annular plane systolic excursion (TAPSE)

- in 258 patients and calculation of Z-score values. *Neonatology*. 2011;100:85–92.
22. Forfia PR, Fisher MR, Mathai SC, Houston-Harris T, Hemnes AR, Borlaug BA, Chamera E, Corretti MC, Champion HC, Abraham TP. Tricuspid annular displacement predicts survival in pulmonary hypertension. *Am J Respir Crit Care Med*. 2006;174:1034–41.
 23. Koestenberger M, Aplitz C, Abdul-Khaliq H, Hansmann G. Transthoracic echocardiography for the evaluation of children and adolescents with suspected or confirmed pulmonary hypertension. Expert consensus statement on the diagnosis and treatment of paediatric pulmonary hypertension. The European Paediatric Pulmonary Vascular Disease Network, endorsed by ISHLT and D6PK. *Heart*. 2016;102:ii14–22.
 24. Sehgal A, Malikiwi A, Paul E, Tan K, Menahem S. Right ventricular function in infants with bronchopulmonary dysplasia: association with respiratory sequelae. *Neonatology*. 2016;109:289–96.
 25. Jone P-N, Patel SS, Cassidy C, Ivy DD. Three-dimensional echocardiography of right ventricular function correlates with severity of pediatric pulmonary hypertension. *Congenit Heart Dis*. 2016;11:562–9.
 26. Jone P-N, Schäfer M, Pan Z, Bremen C, Ivy DD. 3D echocardiographic evaluation of right ventricular function and strain: a prognostic study in paediatric pulmonary hypertension. *Eur Heart J Cardiovasc Imaging*. 2018;19:1026–33.
 27. Koestenberger M, Friedberg MK, Nestaas E, Michel-Behnke I, Hansmann G. Transthoracic echocardiography in the evaluation of pediatric pulmonary hypertension and ventricular dysfunction. *Pulm Circ*. 2016;6:15–29.
 28. Jone P-N, Ivy DD. Comprehensive noninvasive evaluation of right ventricle-pulmonary circulation axis in pediatric patients with pulmonary hypertension. *Curr Treat Options Cardiovasc Med*. 2019;21:6.



Focused Assessment of Pericardial Effusion and Cardiac Tamponade

Yogen Singh, Farha Vora, and Cécile Tissot

Contents

Anatomy of Pericardium	85
Physiology	86
Assessment of Pericardial Effusion on Ultrasonography	88
Ultrasound (Echocardiography) Views	88
Cardiac Tamponade	90
Comprehensive Assessment of Cardiac Tamponade on Echocardiography Using 2D and M-Mode	90
Doppler Echocardiography in Pericardial Effusion and Cardiac Tamponade	92
Pericardiocentesis	92
References	93

Y. Singh (✉)

Department of Pediatrics, Division of Neonatology,
Loma Linda University School of Medicine,
California, USA

Department of Pediatrics, Division of Neonatal and
Developmental Medicine, Stanford University School
of Medicine, California, UK

Department of Pediatrics, Division of Neonatology,
University of Southern California, California, UK

ESPNIC Cardiovascular Dynamics Section and
POCUS Working Group, Geneva, Switzerland
e-mail: YSingh@llu.edu

F. Vora

Department of Pediatrics, Division of Neonatology,
Loma Linda University School of Clinical Medicine,
Loma Linda, CA, USA
e-mail: FVora@llu.edu

C. Tissot

Department of Pediatrics, Clinique des Grangettes,
Chêne-Bougeries, Geneva, Switzerland

Anatomy of Pericardium

The pericardium is a fibroelastic sac surrounding the heart and is comprised of two layers—a thin inner visceral layer called the *serous (visceral) pericardium or epicardium*, and a thick outer layer called the *fibrous (parietal) pericardium* [1]. The pericardiac sac contains a small amount of fluid (<30 mL), which is considerably less in infants and young children. The pericardial fluid is an ultrafiltrate of plasma produced by the visceral pericardium. The pericardial fluid normally drains through the right lymphatic duct via the right pleural space, and through the thoracic duct via the parietal pericardium [2].

The pericardium envelops the heart and great vessels forming pericardial recesses and sinuses and it is anchored to the diaphragm by the pericardiophrenic ligament and to the sternum by the sterno-pericardial ligament, providing support for the heart within the thoracic cage [1, 2].

The pericardium plays an important role in preserving normal cardiac physiology including limitation of intrathoracic cardiac motion and acute cardiac dilatation, preservation of diastolic and systolic interactions between the right and left ventricles, lubricant effect that minimizes friction between cardiac chambers and surrounding structures, and lymphatic and immunological functions, helping prevent the spread of infection from contiguous structures, especially the lungs [3, 4].

Physiology

The normal pericardium limits cardiac distension by coupling the ventricles and enhancing their positive interactions. The pericardial sac also helps to balance the right and left ventricular output by influencing diastolic pressure and dimension of the ventricles. The normal intrapericardial pressure is sub-atmospheric and less than the right atrial (RA) pressure. As the right ventricle (RV) fills, this passively increases pericardial pressure, which restricts further ventricular filling due to the limited extensibility of the pericardium near end diastole [3, 4].

The intrapericardial pressure varies with the pleural pressure: the inspiratory decrease in pleural pressure slightly reduces the pericardial, RA, RV, and systemic arterial pressures. Under physiologic conditions, the respiratory phase influences cardiac filling and hemodynamics, but their effects on the right and left heart are different due

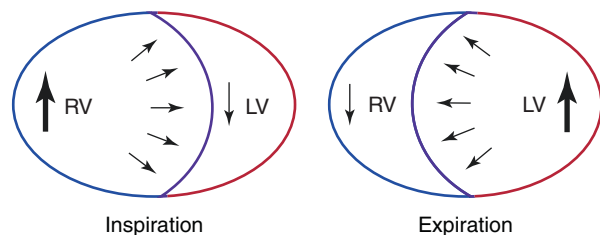
to the differences in the anatomic relationship of the venous return to the intrapleural space [5]. The systemic venous system is extrapleural while the pulmonary venous return is intrapleural. Hence, a decrease in intrathoracic pressure (ITP) during inspiration has a different effect on systemic and pulmonary venous return. During inspiration, the systemic venous return is increased by around 50%, which increases right heart filling and output. On the other hand, there is minimal change in left heart filling and output throughout the respiratory cycle as pulmonary venous return is intrathoracic leading to evenly distributed pleural pressure changes on the left heart chambers and pulmonary veins. During the expiration phase, there is an increased ITP leading to decreased RV filling and hence a relatively increased LV filling because of interventricular dependence of ventricles via shared interventricular septum [6] (Fig. 1).

Increased pericardial fluid production is usually secondary to injury (such as postoperative pericardial effusion) or inflammation (acute pericarditis or post-pericardiotomy syndrome). Pericardial effusion can be transudative or exudative. Transudative pericardial effusions result from obstruction of fluid drainage, while exudative fluid is secondary to inflammatory, infectious, malignant, or autoimmune processes.

The hemodynamic impact of a pericardial effusion is highly dependent upon the rate of accumulation of the fluid in the pericardial sac. A rapid accumulation of pericardial fluid causes a sudden increase in intrapericardial pressure and hemodynamic compromise while slow accumulation can be entirely asymptomatic even when a large amount of fluid is present [7] (Fig. 2).

A rapid accumulation of pericardial fluid beyond a threshold leads to a sudden increase in

Fig. 1 Ventricular interdependence and impact of respiratory cycle on the ventricular filling



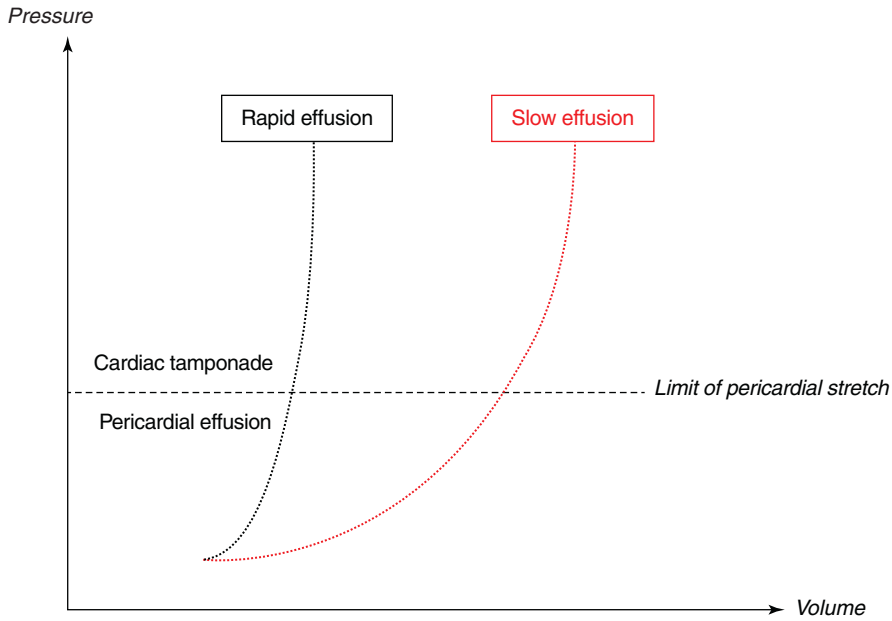


Fig. 2 Effect of rapid and slow accumulation of pericardial fluid on pericardial pressure over time (Pericardial pressure-volume curve)

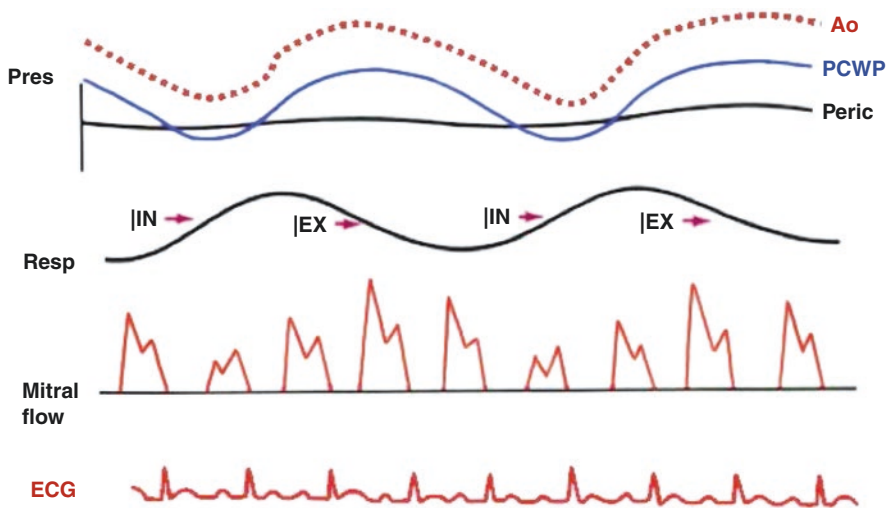


Fig. 3 Mechanism of pulsus paradoxus with exaggeration of inspiratory decrease in blood pressure, as seen in pericardial effusion and tamponade. ECG electrocardiogram

Pres pressure, *Ao* aortic pressure, *PCWP* pulmonary capillary wedge pressure, *Peric* intrapericardial pressure

intrapericardial pressure leading to cardiac tamponade and drastic hemodynamic effects.

Cardiac tamponade results from a markedly diminished diastolic filling that occurs when intracardiac (atrial and ventricular) distending pressures are insufficient to overcome the

increased intrapericardial pressure. During tamponade, inspiration increases inflow to RV, causing an abrupt expansion of the RV during diastole at the expense of the left ventricle. Conversely during expiration, left ventricular expansion causes RV and RA diastolic collapse (Fig. 3).

This reciprocating behavior of the ventricles during respiration is responsible for a *paradoxical pulse*, defined as an exaggeration (>10 mmHg) of the normal inspiratory decrease in systolic blood pressure [8].

Assessment of Pericardial Effusion on Ultrasonography

Ultrasonography (echocardiography) is safe, low cost, portable, and readily available at bedside in urgent situations, and hence an excellent tool for assessment of pericardial effusion and its effects on hemodynamic compromise, as recommended by the 2015 European Society of Cardiology (ESC) guidelines as well as a 2003 task force comprising of American College of Cardiology (ACC), the American Heart Association (AHA), and the American Society of Echocardiography (ASE) [9, 10].

POCUS can not only assess the presence of pericardial fluid (pericardial effusion) but also help determine the physiologic and hemodynamic effects of such an effusion (cardiac tamponade) and aid in drainage (pericardiocentesis) [11]. Focused POCUS imaging can be extremely helpful during a period of acute decompensation if cardiac tamponade is suspected. However, a more comprehensive exam is recommended after hemodynamic stabilization to find the cause and under pathophysiology. For neonates, practice guidelines and application of targeted neonatal echocardiography for the diagnosis and management of pleural effusion have been published [12] and the use of POCUS has been recommended for the assessment of pericardial effusion and pericardiocentesis by the International evidence-based guidelines on the use of POCUS endorsed by the European Society of Paediatric and Neonatal Intensive Care (ESPNIC) [11].

The role of POCUS is to assess the presence of pericardial effusion and if the child is hemodynamically stable then full echocardiography

should be solicited by the pediatric cardiologist or clinician formally trained in performing pediatric echocardiography.

A pericardial effusion appears as the echolucent space between the visceral and parietal pericardium on echocardiography. 2D echocardiography (ultrasonography) can offer a qualitative and quantitative assessment of pericardial fluid. Pericardial effusion can be appreciated on parasternal long, parasternal short, apical and subcostal views, and its assessment should utilize multiple views if the patient's condition allows.

Ultrasound (Echocardiography) Views

A left-sided pleural effusion can mimic pericardial effusion. However, this can easily be distinguished on 2D parasternal long axis view with pericardial effusion appearing as fluid between the descending aorta and heart. Left pleural effusion, on the other hand, is seen posterior to the descending aorta (Fig. 4).

Effusion can be further differentiated into global or localized effusion (Fig. 5). Parasternal short axis and subcostal views are commonly used for this. However, it should be remembered that with a subcostal view, the angle of the probe can easily alter the estimation of the size of the effusion. More importantly, repeated measurements should be obtained in the same area, and from the same view to allow for consistent quantitative and qualitative comparison.

Quantitative assessment can be made by measuring fluid collection on 2D imaging from the epicardial surface of the heart to its maximum dimension at end diastole, with identification of the location [11]. Traditionally, pericardial effusion has been classified as trivial (only visible during systole), small (<10 mm), moderate (10–20 mm), large (>20 mm), or very large (>25 mm) in adults [13]. However, size by

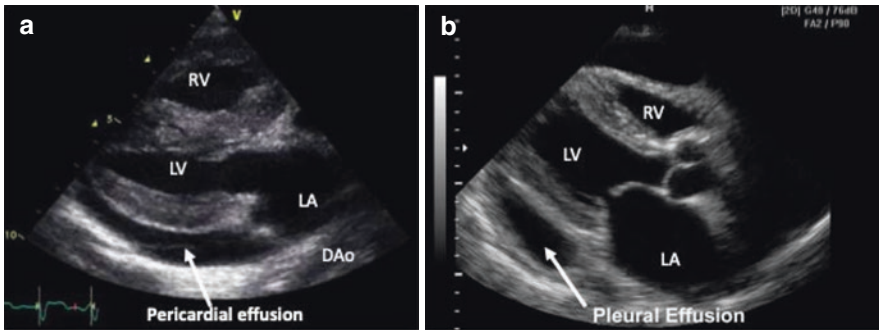


Fig. 4 Differentiating pericardial effusion from pleural effusion on 2D parasternal long axis (PLAX) view. (a) Pericardial fluid anterior to descending aorta (DAo) while

pleural effusion (b) is seen posterior to DAo. *LV* left ventricle, *RV* right ventricle, *LA* left atrium, *DAo* descending aorta

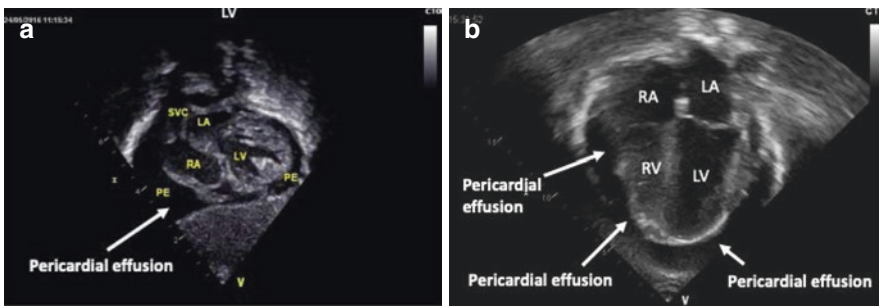


Fig. 5 Pericardial effusion. (a) Pericardial effusion (PE) in subcostal view with effusion primarily around the right atrium (RA). (b) Global pericardial effusion in apical

4-chamber view. *LV* left ventricle, *RV* right ventricle, *LA* left atrium, *RA* right atrium, *PE* pericardial effusion

itself may not entirely be the predictor of hemodynamic significance, as this may also depend on how rapidly the fluid accumulates. Of note, there are no validated methods of accurately quantifying volume of effusion using ultrasound.

Qualitative assessment of pericardial effusion should be prioritized by the POCUS provider. The size of the effusion can be accurately estimated qualitatively using the eyeball technique. Trace effusions can be physiologic in many infants and children. Moderate and large effusions are typically circumferential. Presence of stranding, swirling echoes, adhesions, or uneven distribution may be reflective of the exudative

nature of effusion. In contrast, transudates show a more echo-free signal, characterized by sinusoid image in M-mode echocardiography. Hemorrhagic products may be identified by swirling echoes due to blood clots [14].

In addition to the standard 2D images, M-mode and Doppler analysis on echocardiography offer important information regarding the physiologic impact of a pericardial effusion. The pericardial space normally difficult to visualize on M-mode echocardiography. In the presence of an effusion, an echo lucent space can be appreciated either anterior to the RV or behind the posterior wall of the LV [14] (Fig. 6).

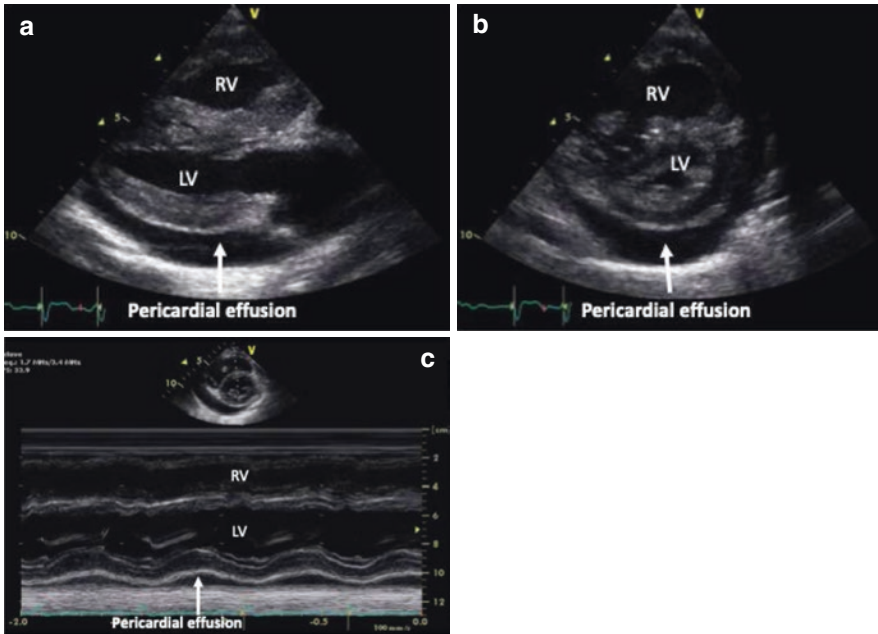


Fig. 6 Pericardial effusion on 2D parasternal long axis (PLAX) view (a), parasternal short axis (PSAX) view (b), and in M-mode in PSAX view (c). *LV* left ventricle, *RV* right ventricle, *LA* left atrium

Cardiac Tamponade

Cardiac tamponade is a clinical diagnosis. The physiologic features of cardiac tamponade result from the increase in intrapericardial pressure due to the effusion, leading to impaired cardiac filling and adverse effect on cardiac function [1, 15–17]. The amount and the rate of fluid collection relative to pericardial stretch predict the hemodynamic significance [7].

The clinical features associated with cardiac tamponade are hypotension with narrow pulse pressure, muffled heart sounds, and pulsus paradoxus. Ventricular interdependence (as discussed above in anatomy and physiology) is the phenomenon in which an increase in the volume of one of the ventricles leads to a decrease in the volume of the contralateral ventricle, as seen in constrictive pericarditis or cardiac tamponade. This leads to a marked exaggeration of the phasic changes in right and left ventricular filling and, consequently, stroke volume and systolic arterial blood pressures with inspiration. This forms the basis of pathologic pulsus paradoxus seen in cardiac tamponade [18].

2D ultrasonography can offer important data regarding the hemodynamic significance of peri-

cardial effusion and can further guide immediate evacuation and hemodynamic stabilization. If the clinical condition allows, urgent detailed echocardiography should be solicited but if the child is decompensated then POCUS can help in guiding pericardiocentesis by the clinician on the bedside. Ultrasonographic evidence of tamponade physiology may even be evident prior to clinical instability though providers must remember that pulsus paradoxus can present with other physiologies as well. Therefore, ultrasound findings must be interpreted within the clinical context.

Comprehensive Assessment of Cardiac Tamponade on Echocardiography Using 2D and M-Mode

POCUS is an excellent tool for qualitative assessment and detecting pericardial effusion or cardiac tamponade. However, a comprehensive and quantitative assessment of cardiac tamponade requires advanced training and expertise beyond basic POCUS applications.

A quantitative assessment of pericardial effusion can be made, as described earlier. Swinging of the heart within the effusion can be seen in a moderate to large effusion in suspected cardiac tamponade. An increase in this ventricular interdependence is seen in the form of septal bounce, a paradoxical movement of the interventricular septum during early diastole, initially directed towards and then away from the left ventricle (Fig. 7) [19, 20]. This can be appreciated on M-mode in parasternal long and short axis views. This is a nonspecific finding and may also be seen in constrictive pericarditis.

Chamber collapse can occur when the intrapericardial pressure exceeds intracardiac

pressure. Right-sided chambers are particularly susceptible to such collapse. Right atrial collapse during early systole, early diastolic collapse of the right ventricle, and left-sided chamber collapse are associated with cardiac tamponade (Fig. 8). It is important to remember that right atrial collapse in the presence of collapsed IVC is indicative of hypovolemia and the IVC should be dilated in tamponade physiology. Sustained right atrial collapse, lasting from more than one-third of the cardiac cycle is both sensitive and specific for cardiac tamponade [21]. RV diastolic collapse is less sensitive but more specific for cardiac tamponade [22]. Left atrial collapse is very specific for cardiac tamponade. Left ventricular collapse,

Fig. 7 Paradoxical septal movement in cardiac tamponade. Notched interventricular septum seen during early diastole

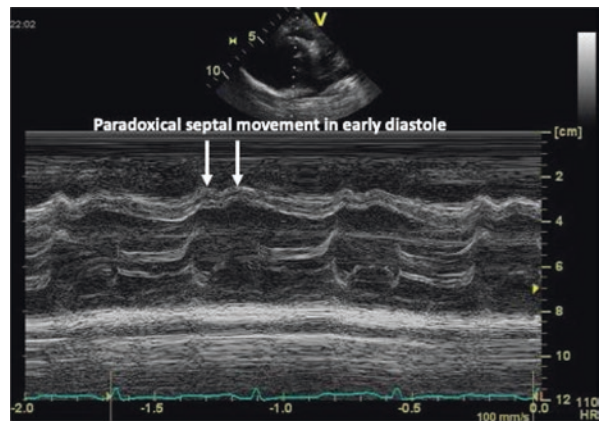


Image showing paradoxical septal movement in cardiac tamponade

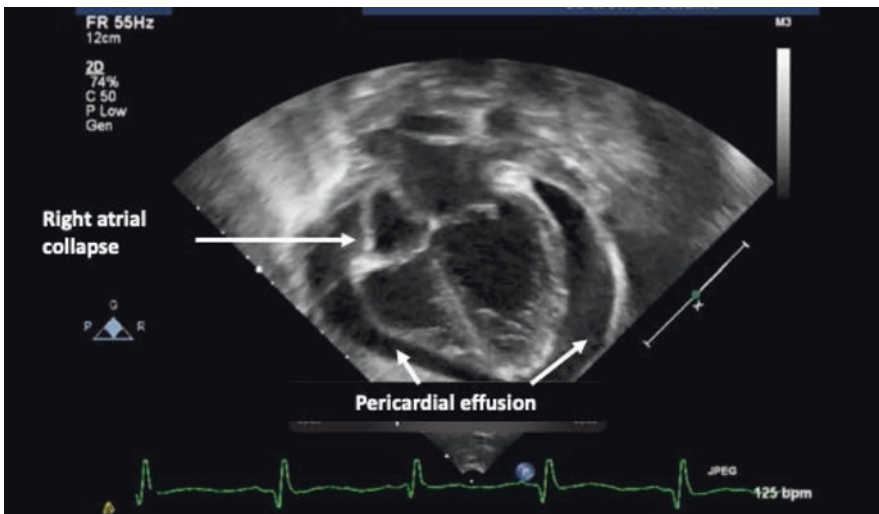


Fig. 8 Cardiac tamponade leading to right atrial wall collapse during early diastole

on the other hand, is less commonly seen due to its thicker wall [7, 23, 24]. Chamber collapse may be affected by the presence of factors that cause RV dysfunction and/or increase RV diastolic pressure such as pulmonary hypertension, positive pressure ventilation, or severe LV dysfunction [15, 25, 26]. The combination of right atrial and ventricular collapse plus abnormal venous flow offers highest specificity (98%) for cardiac tamponade [27]. In a study involving 50 patients with pericardial effusion, right atrial collapse was seen in 92% and right ventricular collapse in 57% of the patients, respectively [28].

An enlarged nonpulsatile vena cava with lack of inspiratory collapse is a sensitive sign of cardiac tamponade. Significant pericardial effusion leads to elevation in pericardial pressure and hence elevation of central venous pressure can lead to dilation of IVC. A dilated IVC predicts tamponade with 97% sensitivity [29]. However, this is a nonspecific sign and may be present in other clinical conditions.

Doppler Echocardiography in Pericardial Effusion and Cardiac Tamponade

Pulsed wave Doppler can offer assessment of respiratory variation in flows and volumes. Respiration may be normally associated with variation in the amplitude of inflow and outflow signals across the mitral and tricuspid valves, usually not more than 20–25% variation. Normal inspiratory variation in peak tricuspid E-wave velocity may be up to 25% and mitral up to 10% in spontaneously breathing infants (Fig. 3) [30]. In cardiac tamponade, decreased left ventricular filling with inspiration can lead to delay of mitral valve opening, lengthened isovolumic relaxation time, and decreased mitral E velocity. Opposite changes occur on expiration and reciprocal changes on the right side [31]. Consequently, mitral flow variation may exceed 30% and tricuspid valve flow variation may exceed 60% in the presence of cardiac tamponade [9]. However, this variation may be affected by mechanical ventilation (intrathoracic pressures in general) and preload.

Similarly, >10% variation in the peak velocities of right and left ventricular outflow tracts during inspiration are additional signs associated with significant pericardial effusion [18] (Fig. 9).

Other findings associated with cardiac tamponade are inspiratory decrease and expiratory increase in pulmonary venous diastolic forward flow as well as expiratory increase in hepatic venous diastolic flow reversal. Findings of predominantly systolic forward flow in the superior vena cava, with a decrease or loss of diastolic component and increased flow reversals on expiration, also offer additional evidence of tamponade [31].

Pericardiocentesis

Drainage of pericardial fluid is indicated in cardiac tamponade or in large effusions for diagnostic purposes. This can be achieved via surgical or percutaneous approaches. This discussion will focus on the percutaneous approach using ultrasound. Ultrasound can help diagnose the presence and hemodynamic significance of pericardial effusion and guide pericardiocentesis. In a series involving 245 procedures in 208 patients with pericardial effusion, echo-guided pericardiocentesis as the initial management strategy was successful in 97% of the cases and it was the only form of therapy necessary for 82% of the patients [32]. Further studies have shown a success rate of 97% with an overall complication rate of 4.7%. Success rates are much higher with anterior effusions >10 mm (93%) vs small, posterior effusions (58%) [32, 33]. Guidelines and standards for such a procedure have been published in adults [34]. In addition, the safety and efficacy of this procedure have been established in adults and pediatric patients [31, 32, 35].

Recently published POCUS guidelines by the European Society of Pediatric and Neonatal Intensive Care (ESPNIC) suggest strong agreement for the use of POCUS for the detection of pericardial effusion and diagnosis of cardiac tamponade in neonates and children, and literature suggests a lower rate of complications with ultrasound-guided pericardiocentesis noted compared to the traditional landmark technique [11, 32, 36, 37].

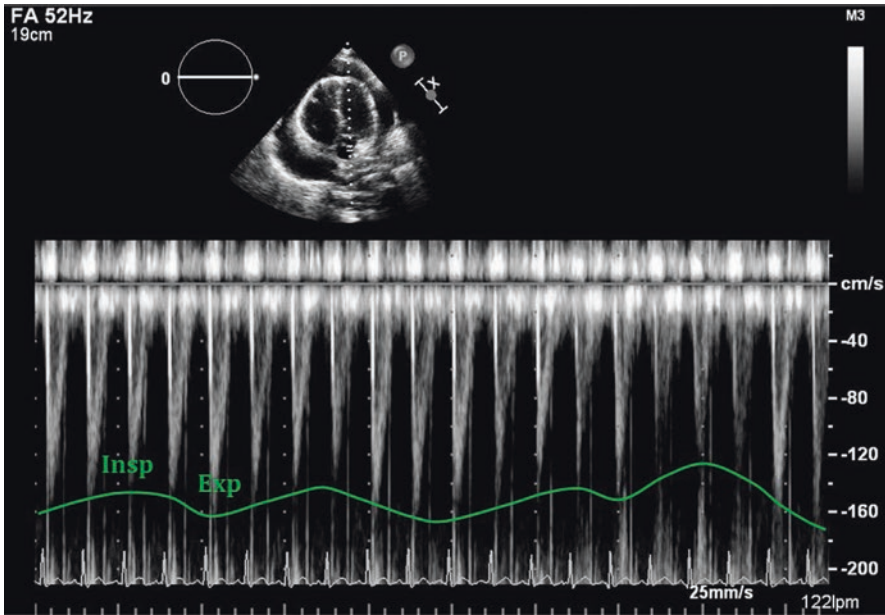


Fig. 9 Doppler assessment across left ventricular outflow tract (LVOT) showing significant variation during inspiration and expiration

The largest pocket of effusion that is closest to the transducer should be identified on ultrasound. Although subcostal, apical or parasternal axis views can be used to visualize effusion, the subcostal view is most commonly described for the purpose of drainage. Pericardiocentesis can be performed using either static or dynamic methods of ultrasound guidance. For the former, the area with the largest fluid collection and thinnest anterior chest wall is identified with ultrasound, marked, and then the needle is introduced at that site into the pocket for drainage without sonographic guidance. Ultrasound can also be used to determine the depth of insertion of the needle. Real-time ultrasonography can be used to direct dynamic drainage whereby insertion of the needle into the chest is actively followed under direct visualization as it enters into the pericardial space. Dynamic guidance correctly performed ensures that the needle tip is continuously visualized to avoid trauma to the vital organs.

For both a blind and ultrasound guided subcostal approach, an angiocath is inserted between the xiphoid process and left costal margin at a shallow angle (<30°) to pass under the costal margin. The needle should be advanced towards the left shoulder while aspirating. Major compli-

cations associated with the procedure are cardiac perforation, pneumothorax, coronary perforation, injury to abdominal organs, and death. As noted earlier, these are significantly reduced with ultrasound guidance.

Success is largely dependent on the operator’s comfort and experience with the procedure. Additionally, transducer placement and site of needle entry may be limited by the small size of the child. Caution should be exercised to avoid the internal mammary artery (3–5 cm lateral to lower sternal border) and the neurovascular bundles that run below each rib. Side-to-side manipulation of the needle during needle entry should also be avoided to prevent inadvertent laceration of myocardial tissue or vessels [38].

References

1. Spodick DH. The normal and diseased pericardium: current concepts of pericardial physiology, diagnosis and treatment. *J Am Coll Cardiol.* 1983;1(1):240–51.
2. Holt JP. The normal pericardium. *Am J Cardiol.* 1970;26(5):455–65.
3. Shabetai R. Pericardial and cardiac pressure. *Circulation.* 1988;77(1):1–5.
4. Glantz SA, et al. The pericardium substantially affects the left ventricular diastolic pressure-volume relationship in the dog. *Circ Res.* 1978;42(3):433–41.

5. Higano ST, et al. Hemodynamic rounds series II: hemodynamics of constrictive physiology: influence of respiratory dynamics on ventricular pressures. *Catheter Cardiovasc Interv.* 1999;46(4):473–86.
6. Goldstein JA. Cardiac tamponade, constrictive pericarditis, and restrictive cardiomyopathy. *Curr Probl Cardiol.* 2004;29(9):503–67.
7. Spodick DH. Acute cardiac tamponade. *N Engl J Med.* 2003;349(7):684–90.
8. Guntheroth WG, Morgan BC, Mullins GL. Effect of respiration on venous return and stroke volume in cardiac tamponade. Mechanism of pulsus paradoxus. *Circ Res.* 1967;20(4):381–90.
9. Klein AL, Abbata S, Agler DA, Appleton CP, Asher CR, Hoit B, Hung J, et al. American Society of Echocardiography clinical recommendations for multimodality cardiovascular imaging of patients with pericardial disease: endorsed by the Society for Cardiovascular Magnetic Resonance and Society of Cardiovascular Computed Tomography. *J Am Soc Echocardiogr.* 2013;26(9):965–1012.e15.
10. Adler Y, Charron P, Imazio M, Badano L, Barón-Esquivias G, Bogaert J, Brucato A, et al. 2015 ESC guidelines for the diagnosis and management of pericardial diseases: the task force for the diagnosis and management of pericardial diseases of the European Society of Cardiology (ESC) endorsed by: the European Association for Cardio-Thoracic Surgery (EACTS). *Eur Heart J.* 2015;36(42):2921–64.
11. Singh Y, Tissot C, Fraga MV, Yousef N, Cortes RG, Lopez J, Sanchez-de-Toledo J, et al. International evidence-based guidelines on point of care ultrasound (POCUS) for critically ill neonates and children issued by the POCUS working group of the European Society of Paediatric and Neonatal Intensive Care (ESPNIC). *Crit Care.* 2020;24(1):65.
12. Mertens L, Seri I, Marek J, Arlettaz R, Barker P, McNamara P, Moon-Grady AJ, et al. Targeted neonatal echocardiography in the neonatal intensive care unit: practice guidelines and recommendations for training. Writing Group of the American Society of Echocardiography (ASE) in Collaboration with the European Association of Echocardiography (EAE) and the Association for European Pediatric Cardiologists (AEPC). *J Am Soc Echocardiogr.* 2011;24(10):1057–78.
13. Weitzman LB, et al. The incidence and natural history of pericardial effusion after cardiac surgery—an echocardiographic study. *Circulation.* 1984;69:506–11.
14. Horowitz MS, et al. Sensitivity and specificity of echocardiographic diagnosis of pericardial effusion. *Circulation.* 1974;50(2):239–47.
15. Fowler NO. Cardiac tamponade. A clinical or an echocardiographic diagnosis? *Circulation.* 1993;87(5):1738–41.
16. Roy CL, Minor MA, Alan Brookhart M, Choudhry NK. Does this patient with a pericardial effusion have cardiac tamponade? *JAMA.* 2007;297(16):1810–8.
17. Reddy PS, Curtiss EI, O’Toole JD, Shaver JA. Cardiac tamponade: hemodynamic observations in man. *Circulation.* 1978;58(2):265–72.
18. Armstrong WF, Ryan T. Feigenbaum’s echocardiography. Lippincott Williams & Wilkins. 2012.
19. Walker CM, Chung JH, Reddy GP. Septal bounce. *J Thorac Imaging.* 2012;27(1):W1.
20. Chong HH, Plotnick GD. Pericardial effusion and tamponade: evaluation, imaging modalities, and management. *Compr Ther.* 1995;21(7):378–85.
21. Gillam LD, Guyer DE, Gibson TC, King ME, Marshall JE, Weyman AE. Hydrodynamic compression of the right atrium: a new echocardiographic sign of cardiac tamponade. *Circulation.* 1983;68(2):294–301.
22. Kerber RE, Gascho JA, Litchfield R, Wolfson P, Ott D, Pandian NG. Hemodynamic effects of volume expansion and nitroprusside compared with pericardiocentesis in patients with acute cardiac tamponade. *N Engl J Med.* 1982;307(15):929–31.
23. Reydel B, Spodick DH. Frequency and significance of chamber collapses during cardiac tamponade. *Am Heart J.* 1990;119(5):1160–3.
24. Fusman B, Schwinger ME, Charney R, Ausubel K, Cohen MV. Isolated collapse of left-sided heart chambers in cardiac tamponade: demonstration by two-dimensional echocardiography. *Am Heart J.* 1991;121(2 Pt 1):613–6.
25. Hoit BD, Fowler NO. Influence of acute right ventricular dysfunction on cardiac tamponade. *J Am Coll Cardiol.* 1991;18(7):1787–93.
26. Hoit BD, Gabel M, Fowler NO. Cardiac tamponade in left ventricular dysfunction. *Circulation.* 1990;82(4):1370–6.
27. Mercé J, Sagristà-Sauleda J, Permanyer-Miralda G, Evangelista A, Soler-Soler J. Correlation between clinical and Doppler echocardiographic findings in patients with moderate and large pericardial effusion: implications for the diagnosis of cardiac tamponade. *Am Heart J.* 1999;138(4 Pt 1):759–64.
28. Levine MJ, Lorell BH, Diver DJ, Come PC. Implications of echocardiographically assisted diagnosis of pericardial tamponade in contemporary medical patients: detection before hemodynamic embarrassment. *J Am Coll Cardiol.* 1991;17(1):59–65.
29. Himelman RB, Kircher B, Rockey DC, Schiller NB. Inferior vena cava plethora with blunted respiratory response: a sensitive echocardiography sign of cardiac tamponade. *J Am Coll Cardiol.* 1988;12(6):1470–7.
30. Riggs TW, Rodriguez R, Snider AR, Batton D. Doppler echocardiographic evaluation of right and left ventricular diastolic function in normal neonates. *J Am Coll Cardiol.* 1989;13(3):700–5.
31. Tsang TSM, Enriquez-Sarano M, Freeman WK, Barnes ME, Sinak LJ, Gersh BJ, Bailey KR, Seward JB. Consecutive 1127 therapeutic echocardiographically guided pericardiocenteses: clinical profile, practice patterns, and outcomes spanning 21 years. *Mayo Clinic Proc.* 2002;77(5):429–36.

32. Tsang TS, Barnes ME, Hayes SN, Freeman WK, Dearani JA, Butler SL, Seward JB. Clinical and echocardiographic characteristics of significant pericardial effusions following cardiothoracic surgery and outcomes of echo-guided pericardiocentesis for management: Mayo Clinic experience, 1979-1998. *Chest*. 1999;116(2):322-31.
33. Tsang TS, Freeman WK, Sinak LJ, Seward JB. Echocardiographically guided pericardiocentesis: evolution and state-of-the-art technique. *Mayo Clinic Proc*. 1998;73(7):647-52.
34. Silvestry FE, Kerber RE, Brook MM, Carroll JD, Eberman KM, Goldstein SA, Herrmann HC, et al. Echocardiography-guided interventions. *J Am Soc Echocardiogr*. 2009;22(3):213-31; quiz 316-17.
35. Tsang TS, El-Najdawi EK, Seward JB, Hagler DJ, Freeman WK, O'Leary PW. Percutaneous echocardiographically guided pericardiocentesis in pediatric patients: evaluation of safety and efficacy. *J Am Soc Echocardiogr*. 1998;11(11):1072-7.
36. Spurney CF, Sable CA, Berger JT, Martin GR. Use of a hand-carried ultrasound device by critical care physicians for the diagnosis of pericardial effusions, decreased cardiac function, and left ventricular enlargement in pediatric patients. *J Am Soc Echocardiogr*. 2005;18(4):313-9.
37. Nagdev A, Mantuani D. A novel in-plane technique for ultrasound-guided pericardiocentesis. *Am J Emerg Med*. 2013;31(1424.e9):1424.e5-9.
38. Marin JR, Abo AM, Arroyo AC, Doniger SJ, Fischer JW, Rempell R, Gary B, et al. Pediatric emergency medicine point-of-care ultrasound: summary of the evidence. *Crit Ultrasound J*. 2016;8(1):16.



Advanced Functional Echocardiographic Views Including PDA Assessment and Hemodynamic Evaluation

Yogen Singh, Sebastien Joye, and Cécile Tissot

Contents

Echocardiographic Diagnosis and Hemodynamic Evaluation of the Patent Ductus Arteriosus.....	98
Echocardiographic Assessment of Ductal Characteristics.....	98
Echocardiographic Evaluation of Pulmonary Over-Circulation.....	99
Echocardiographic Evaluation of Systemic Hypoperfusion.....	102
Advanced Hemodynamic Evaluation—Measurement of Blood Flow and Cardiac Output.....	104
Assessment of Cardiac Output and Blood Flow on Echocardiography.....	104
Estimation of Left Ventricular Output.....	105
Estimation of Right Ventricular Output.....	106
Limitations of LVO and RVO Measurement Using Echocardiography.....	107
Superior Vena Cava (SVC) Blood Flow.....	107
References.....	109

Y. Singh (✉)

Department of Pediatrics, Division of Neonatology,
Loma Linda University School of Medicine,
California, USA

Department of Pediatrics, Division of Neonatal and
Developmental Medicine, Stanford University School
of Medicine, California, UK

Department of Pediatrics, Division of Neonatology,
University of Southern California, California, UK

ESPNIC Cardiovascular Dynamics Section and
POCUS Working Group, Geneva, Switzerland
e-mail: YSingh@llu.edu

S. Joye

Department of Neonatology, Centre
Hospitalier Universitaire Vaudois (CHUV),
University of Lausanne, Lausanne,
Switzerland

e-mail: Sebastien.Joye@chuv.ch

C. Tissot

Department of Pediatrics, Clinique des
Grangettes, Chêne-Bougeries, Geneva,
Switzerland

Echocardiographic Diagnosis and Hemodynamic Evaluation of the Patent Ductus Arteriosus

Echocardiography is the gold standard non invasive bedside imaging modality to evaluate a patent ductus arteriosus (PDA). In addition to make a confirmative diagnosis of PDA and exclude/diagnose any associated congenital heart defect (CHD), it can help in estimating the magnitude of shunt volume and assessing its hemodynamic significance—it can be used to assess the hemodynamic impact from pulmonary over-circulation and systemic hypoperfusion due to shunt volume [1–3]. This could be systematically achieved by assessing: (a) ductal characteristics, (b) parameters of pulmonary over-circulation, and (c) signs of systemic hypoperfusion (Fig. 1).

Various echocardiographic parameters have been described in the research setting as well as complex staging/scoring systems [3, 4]. In this chapter, we will focus on the parameters which can help clinicians in making a clinical decision at the bedside.

Echocardiographic Assessment of Ductal Characteristics

Echocardiography can be used to assess the size of PDA by measuring transductal diame-

ter. Interrogation of shunt direction, and velocity of blood flow across the ductus arteriosus can be measured by using Doppler technique.

Measuring Transductal Diameter

Although the PDA can be visualized from many windows, the high left-sided parasternal “ductal” view and suprasternal arch view are preferred to obtain a clear 2D image and accurately measure the size of the ductus arteriosus. PDA size is measured from the transductal diameter at the site of maximum constriction (narrowest dimension), which is usually at the pulmonary end. Many studies have described measuring the PDA size using color Doppler, although measuring its diameter in 2D is more accurate. However, to avoid an over or under-estimation, it is important to know the shape of the PDA [2, 5]. It will therefore be important to carry out a sweep starting at the level of the aortic arch up to the pulmonary artery.

If color Doppler is used to measure the ductal size, the gain setting should be adequately optimized to minimize the risk of over-estimation. Color comparison or simultaneous mode, which allows 2D and color Doppler images side by side, can be applied to measure ductal size in both modes using frame-by-frame technique [1] (Fig. 2).

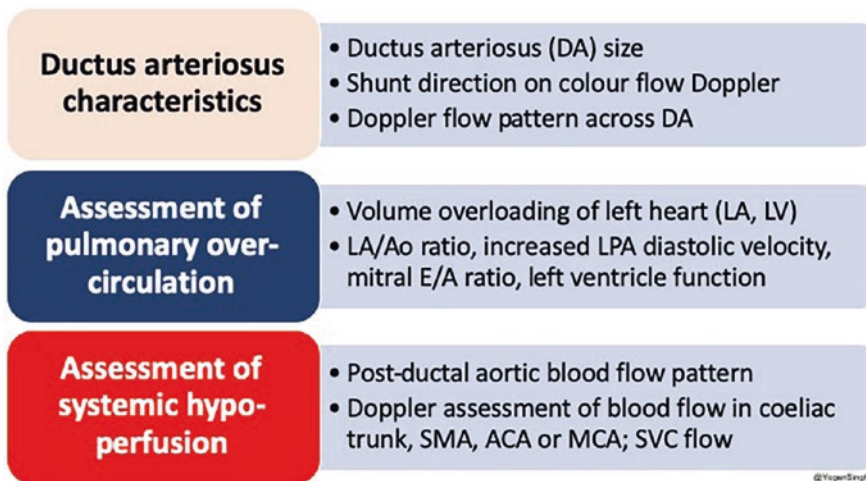


Fig. 1 Summary of an approach to the echocardiographic assessment of PDA and hemodynamic evaluation. LA left atrium, LV left ventricle, DA ductus arteriosus, Ao aorta, SMA

superior mesenteric artery, ACA anterior cerebral artery, MCA middle cerebral artery, SVC superior vena cava, LPA left pulmonary artery (copyright—Dr. Yogen Singh)

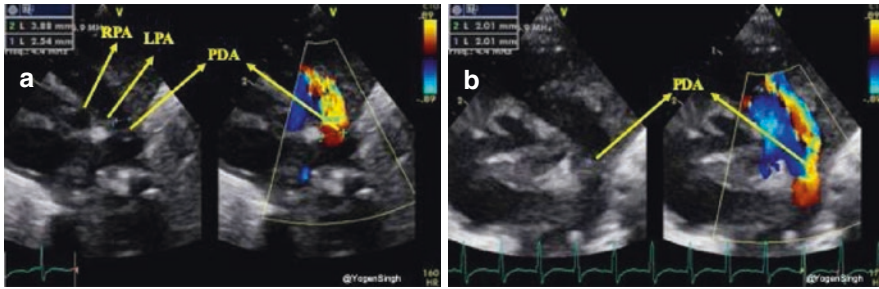


Fig. 2 Measurement of ductal size on 2D and color Doppler on high left parasternal “ductal view.” (a) A significant discrepancy between ductal diameter measurement on 2D and color Doppler—over-estimation of ductal size on color Doppler due to gain setting; (b) no significant

discrepancy between ductal diameter measurement on 2D and color Doppler after optimization of gain setting. *LPA* left pulmonary artery, *RPA* right pulmonary artery, *PDA* patent ductus arteriosus (copyright—Dr. Yogen Singh)

Direction of Shunt Across the Ductus Arteriosus

The direction of the ductal shunt depends upon the relationship between the pulmonary and systemic pressures. It is assessed using color Doppler. The direction of blood flow across the ductus arteriosus is normally left to right, from the aorta (high systemic pressure) to the pulmonary artery (low pulmonary pressure) but it can be right to left or bidirectional when there is high pulmonary vascular resistance or when there is an anatomical cause (due to certain CHDs). With the conventional setting of the Nyquist scale, left to right shunt is seen as a red jet while right to left shunt is seen as blue [1, 6]. A right to left shunt across the PDA is more difficult to see because the color Doppler will show it as a blue jet, blood going towards aorta from pulmonary end, similar to branch pulmonary arteries. Color comparison or simultaneous mode can be very helpful in this situation. Bidirectional flow is often seen during transitional circulation or when the pulmonary artery pressures are equal to the systemic pressures [2, 6]. Shunt direction can also be assessed using pulse or continuous wave Doppler, where left to right shunt is seen above the baseline (blood coming towards the probe) while right to left shunt is seen below the baseline (blood going away from the probe) [1, 6] (Fig. 3).

Velocity of Shunt Across PDA and Its Significance

The shunt velocity across the PDA during the cardiac cycle can be obtained by applying pulse or

continuous wave Doppler in the ductus arteriosus. The maximum velocity during systole and diastole can be measured. Nonrestrictive shunts have a low peak systolic velocity with a high systolic to end-diastolic velocity gradient while restrictive shunts have a high peak systolic velocity and a low systolic to diastolic velocity gradient. A ratio of >2 between peak systolic and end-diastolic velocity is considered as a pulsatile flow pattern while a ratio of <2 is described as a restrictive shunt suggestive of a closing PDA [7, 8] (Fig. 4).

Echocardiographic Evaluation of Pulmonary Over-Circulation

The increased pulmonary blood flow from a significant left to right ductal shunt leads to pulmonary overcirculation and therefore, increased pulmonary venous return. This volume overload to the left atrium (LA) gradually dilates this chamber. If this significant left to right shunt persists over time then dilatation of the left ventricle from increased preload, especially in absence of a large intra-atrial shunt also occurs. As the aortic valve annulus (Ao) is a relatively fixed structure and it does not get dilated due to left heart overloading, the LA/Ao ratio can be used as a surrogate of increased pulmonary venous return [9, 10]. Similarly, the left ventricular end-diastolic diameter (LVEDD) can be used as a surrogate marker for pulmonary venous return. In clinical practice, the volume overload of the left heart can be subjectively assessed by “eyeballing” [11] (Fig. 5).

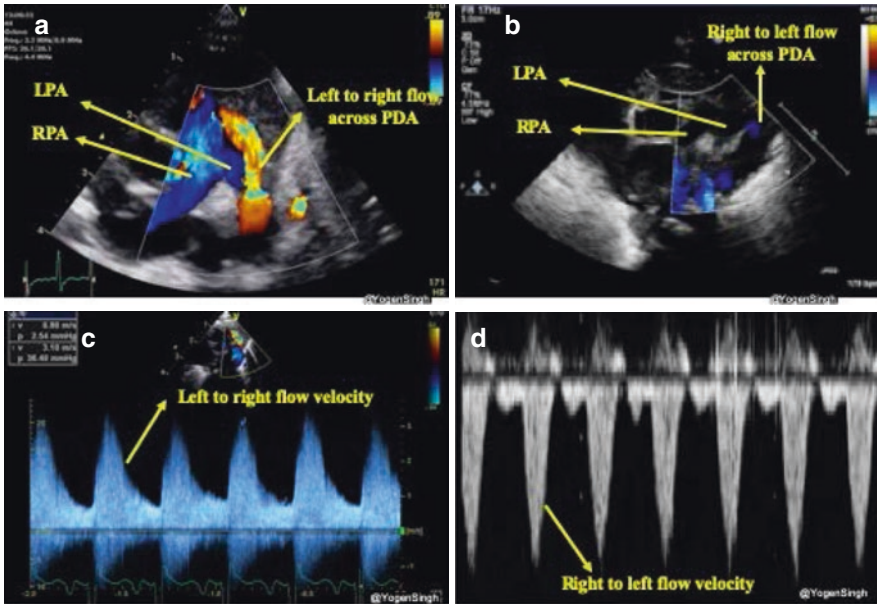


Fig. 3 Assessment of PDA shunt direction on color flow and spectral Doppler. (a) Left to right shunt seen as red (blood coming towards probe) while blood in branch pulmonary arteries is seen as blue (blood going away from the probe); (b) right to left shunt seen as blue color—similar to branch pulmonary arteries in a view “three legged trouser”; (c) Pulsed Wave Doppler assessment showing

left to right shunt (above the baseline as blood coming towards the probe) and (d) Doppler assessment showing right to left shunt (below the baseline as blood going away from the probe). *LPA* left pulmonary artery, *RPA* right pulmonary artery, *PDA* patent ductus arteriosus (copyright—Dr. Yogen Singh)

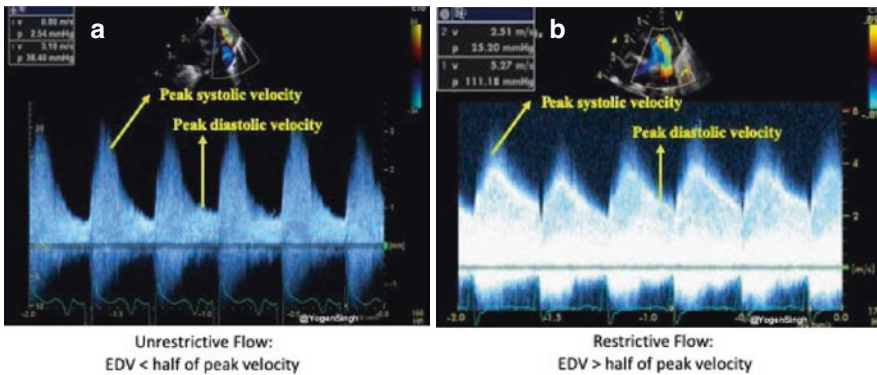


Fig. 4 Assessment of restrictive and unrestrictive flow pattern on Doppler assessment of PDA. (a) Unrestrictive flow pattern with end-diastolic velocity (EDV) less than

half of the peak systolic velocity and (b) A restrictive flow pattern with end-diastolic velocity (EDV) more than half of the peak systolic velocity. (copyright—Dr. Yogen Singh)

Both LA/Ao ratio and LVEDD can be measured from the parasternal long axis view using M-mode with the cursor perpendicular to the aorta at the level of the aortic valve or at the tip of the mitral valve leaflets, respectively (Fig. 6). LA/Ao ratio of >1.4 is considered significant and has been used as a cut-off value in many

clinical trials [11]. The normal reference ranges for LVEDD in preterm infants in relation to body weight and postnatal age have been published and z-scores should be used for LVEDD [12].

Variable degree of mitral valve insufficiency is often seen in infants with a persistently large

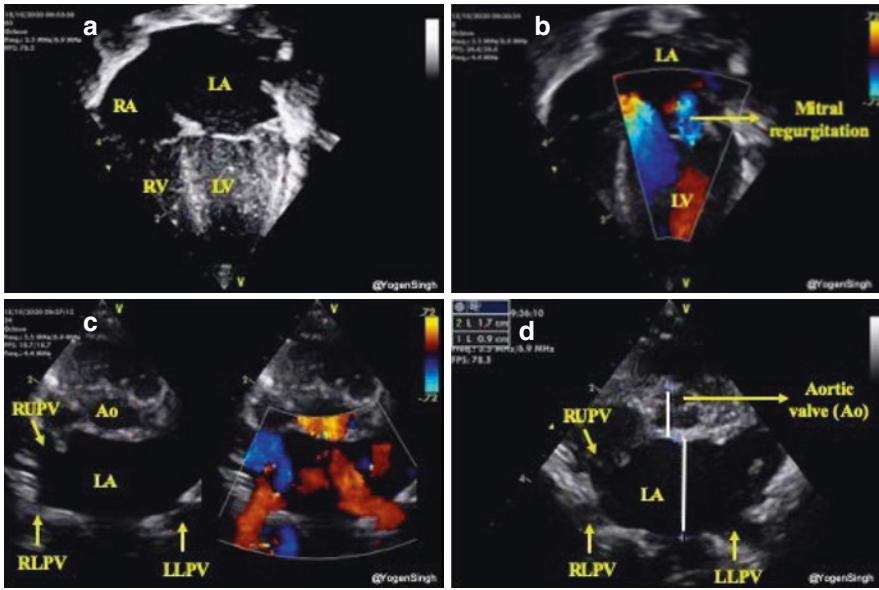
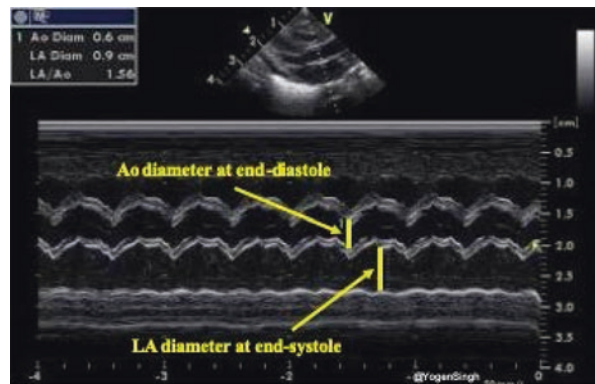


Fig. 5 Assessment of left heart volume overload on visual inspection “eyeballing.” (a) Apical 4-chamber view in 2D showing dilated left side of the heart (dilated left atrium and left ventricle); (b) Mitral regurgitation on color flow mapping as blue jet going back to the left atrium (see explanation in text); (c) “Crab view” showing dilated pulmonary veins reflecting increased pulmonary venous

return and (d) Dilated left atrium in parasternal short axis view—on visual inspection LA looks double the size of the aortic valve (Ao). LA left atrium, LV left ventricle, RA right atrium, RV right ventricle, Ao aortic valve, RUPV right upper pulmonary vein, RLPV right lower pulmonary vein, LLPV left lower upper pulmonary vein (copyright—Dr. Yogen Singh)

Fig. 6 Assessment of left atrium (LA) to aorta (Ao) ratio in parasternal long axis view. LA and Ao diameter measurement shown using M-mode. (copyright—Dr. Yogen Singh)



Left atrium (LA) / Aorta (Ao) ratio measurement

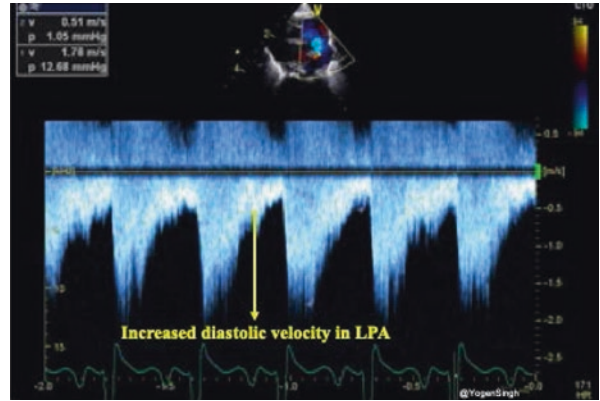
PDA and significant left heart dilatation. It occurs due to left atrial dilatation resulting in stretching of mitral valve and left ventricular volume overload. The mitral valve regurgitation usually improves significantly with normalization of left atrial size and resolves completely within weeks after PDA closure [13].

While assessing left heart volume overload one should be mindful of intra-atrial shunts. A large left to right shunt through the foramen ovale

or atrial septal defect can “offload” the left side of the heart even in the presence of a significant ductal shunt leading to an artificially low/normal LA/Ao ratio or low LVEDD.

The presence of forward pulmonary flow in diastole in the left pulmonary artery (LPA) has been described as a sign of significant left to right shunt through the PDA. Using pulsed wave Doppler in the LPA, mean and end-diastolic velocity can be measured and cut-off points of

Fig. 7 Doppler assessment of blood flow in left pulmonary artery (LPA) showing increased diastolic velocity indicative of significant ductal shunt in diastole leading to turbulence and increased velocity. (copyright—Dr. Yogen Singh)



0.42 m/s and 0.20 m/s, respectively have been described as indicative of significant ductal shunt [14] (Fig. 7).

The mitral valve E/A ratio refers to the ratio of the velocity of the early (E) diastolic phase of ventricular filling versus the late atrial (A) contraction component. Mitral valve E/A ratio can be obtained from apical 4-chamber view with the pulse Doppler range gate set slightly below the mitral valve annulus. In preterm infants, mitral valve E/A ratio is usually <1 due to poor compliance of the myocardium leading to moderate impairment of diastolic performance and low early diastolic filling velocity. In the presence of a hemodynamically significant PDA (hsPDA), atrial pressure increases because of high pulmonary venous return and this leads to a reversal of the E/A ratio >1 [2].

Various other echocardiographic parameters have been studied and described to assess pulmonary circulation such as left ventricular output (LVO) to superior vena cava flow (SVC) ratio and decreased isovolumic relaxation time (IVRT) using tissue Doppler Imaging (TDI) [14]. However, echocardiographic assessments (such as SVC flow and LVO estimation) that need multiple measurements are not only time-consuming but also has the potential to make errors in measurements and they have significant intra- and inter-observer variability [15–17]. Hence, the common echocardiographic parameters often

used in clinical decision-making at the bedside remain qualitative assessment on visual inspection “eyeballing,” LA/Ao ratio, LPA diastolic velocity and LVEDD measurement. Mitral E/A ratio is easy to measure but one should be mindful that even in preterm infants with no hsPDA E/A ratio gradually become >1 with time as myocardium compliance improves.

Echocardiographic Evaluation of Systemic Hypoperfusion

In the presence of a large PDA, blood shunts away from the systemic circulation throughout the cardiac cycle; however, this becomes more apparent during diastole and it can be studied using pulsed wave Doppler on echocardiography [11, 16]. Retrograde or absent blood flow during diastole in descending aorta below the ductal ampulla, in the coeliac axis or in the superior mesenteric artery have been described as indicators of significant PDA shunt leading to systemic blood steal (systemic hypoperfusion) [9, 17]. Doppler flow patterns from the descending aorta can be obtained from a suprasternal or high parasternal view with the pulsed wave Doppler sample gate placed distal to the origin of ductus arteriosus (ductal ampulla) (Fig. 8).

Similarly, celiac trunk or superior mesenteric artery can be interrogated using pulsed wave

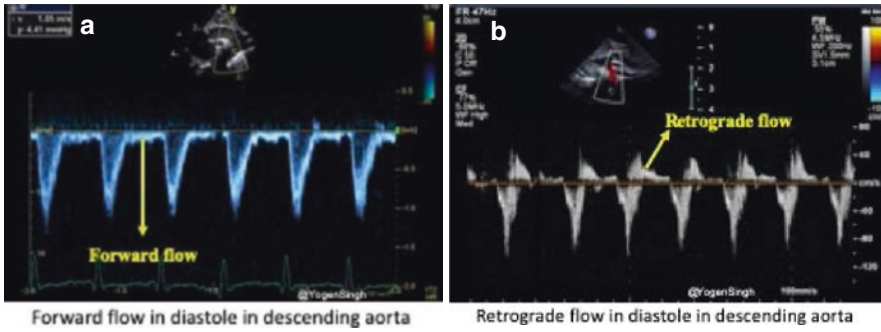


Fig. 8 Pulsed Wave Doppler assessment of blood flow in descending aorta (Post-ductal flow). (a) Forward blood flow during diastole and (b) Retrograde blood flow during

diastole indicating “ductal steal” in the presence of a large PDA. (copyright—Dr. Yogen Singh)

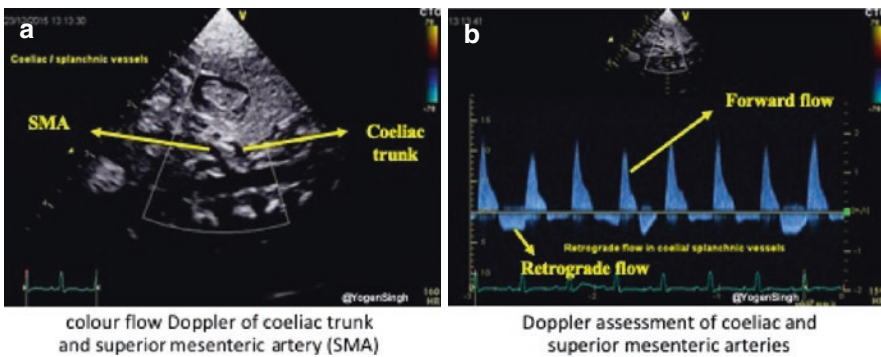


Fig. 9 Color flow mapping and pulsed wave Doppler assessment of blood flow in the coeliac trunk and superior mesenteric artery in sub-costal sagittal view. (a) Color flow mapping of the coeliac and superior mesenteric

artery and (b) Retrograde blood flow during diastole in the coeliac and superior mesenteric artery indicating “ductal steal” in the presence of a large PDA. (copyright—Dr. Yogen Singh)

Doppler in the sagittal abdominal view (Fig. 9). Doppler assessment of the anterior cerebral artery in the mid-sagittal view of brain ultrasound can be performed and retrograde flow during diastole would suggest significant ductal shunt—similar to coeliac or superior mesentery artery Doppler assessment. However, to date, the clinical relevance and long-term outcomes of the deranged cerebral Doppler flow patterns remain unknown [1, 18] (Fig. 9).

Based upon the clinical and echocardiographic criteria various staging systems have been described and have been shown to help in

decision-making for intervention [3, 19]. Recently, van Laere et al. (2018) suggested essential various echocardiographic parameters including measuring left ventricular output in all infants needing assessment of PDA [4]. However, these staging systems that require extensive echocardiographic measurements have not been widely adopted in pediatric cardiology clinical practice. We have summarized the most commonly used measurements which help clinicians in assessing the PDA and its hemodynamic significance on echocardiography (Table 1).

Table 1 Summary of the most common echocardiographic parameters used for assessment and hemodynamic evaluation of PDA

PDA evaluation criteria	Essential echocardiographic parameters for assessment of PDA and hemodynamic evaluation
Ductal characteristics	<ul style="list-style-type: none"> • PDA size (small <1.5 mm, moderate 1.51–2 mm, large >2 mm) and • Flow direction (Left to right, right to left, or bidirectional), and • Doppler assessment with maximum velocity (Vmax) in systole and end diastole
Assessment of pulmonary over-circulation	<ul style="list-style-type: none"> • Dilated left side of the heart on visual inspection “eyeballing” and • LA/Ao ratio (mild <1.4, moderate 1.41–1.6, severe >1.6) OR • LVEDD (correlate with z-scores) OR • LPA diastolic velocity—mean velocity >0.42 m/s, end diastolic velocity >0.2 m/s OR • Reversal of mitral E/A ratio
Assessment of systemic hyperperfusion	<ul style="list-style-type: none"> • Retrograde or absent blood flow during diastole in: <ul style="list-style-type: none"> – descending aorta OR – coeliac trunk or superior mesenteric artery (SMA) OR – anterior or middle cerebral artery

A comprehensive echocardiographic assessment should be performed to rule out any underlying congenital heart defect or pulmonary hypertension and delineate orientation of the arch (left or right sidedness) before any intervention to close the PDA

Advanced Hemodynamic Evaluation—Measurement of Blood Flow and Cardiac Output

Echocardiography can help in the advanced hemodynamic evaluation including measurement of cardiac output, superior vena cava flow, and fluid responsiveness. Evaluation of fluid responsiveness has been discussed in the chapter on assessment of neonatal shock (chapter “POCUS in Shock and Hypotension”) and a detailed assessment of pulmonary hypertension has been described in chapter “Focused Ultrasound in Right Ventricular Function and Pulmonary Hypertension” on pulmonary hypertension. We have discussed the estimation of left ventricular output, right ventricular output, and superior vena cava flow, which have not been

discussed elsewhere in this book. However, advanced hemodynamic evaluation and these measurements are out of the scope of POCUS applications.

Assessment of Cardiac Output and Blood Flow on Echocardiography

The echocardiographic assessment of blood flow across any “vessel or outflow tract” can be estimated by multiplying the cross-sectional area (CSA) of the vessel with the velocity time integral (VTI) of the blood flow across a specific point where CSA is calculated and the heart rate (HR), applying these values in the following equation below [20, 21].

$$\text{Blood flow (mL / kg / min)} = \frac{\text{CSA} \times \text{VTI (incm)} \times \text{HR}}{\text{Body weight (inkg)}}$$

It is applied in clinical practice to estimate left ventricular cardiac output (LVO), right ventricu-

lar output (RVO), and superior vena flow in children.

Estimation of Left Ventricular Output

The CSA for LVO is calculated by measuring the diameter at the level of aortic valve (AV) annulus at end systole in the parasternal long axis view

(PLAX) and the VTI is measured just distal to the AV valve by using pulsed wave Doppler in the apical 5-chamber view. HR is calculated automatically by the ultrasound machine from the ECG recording (Fig. 10).

$$\text{Left ventricular output (mL / kg / min)} = \frac{\text{CSA (at AV annulus)} \times \text{VTI} \times \text{LVOT (incm)} \times \text{HR}}{\text{Body weight (in kg)}}$$

Despite various assumptions and limitations (discussed below), the assessment of LVO on echocardiography correlates strongly to the measurements acquired by other well-established techniques such as pressure measurement by cardiac catheter and Fick’s dye dilution

method. The published studies showed a bias under 10%. A recently published study on the estimation of left ventricular cardiac output on echocardiography correlated strongly with the assessment by phase contrast MRI, which is very reassuring [22, 23].

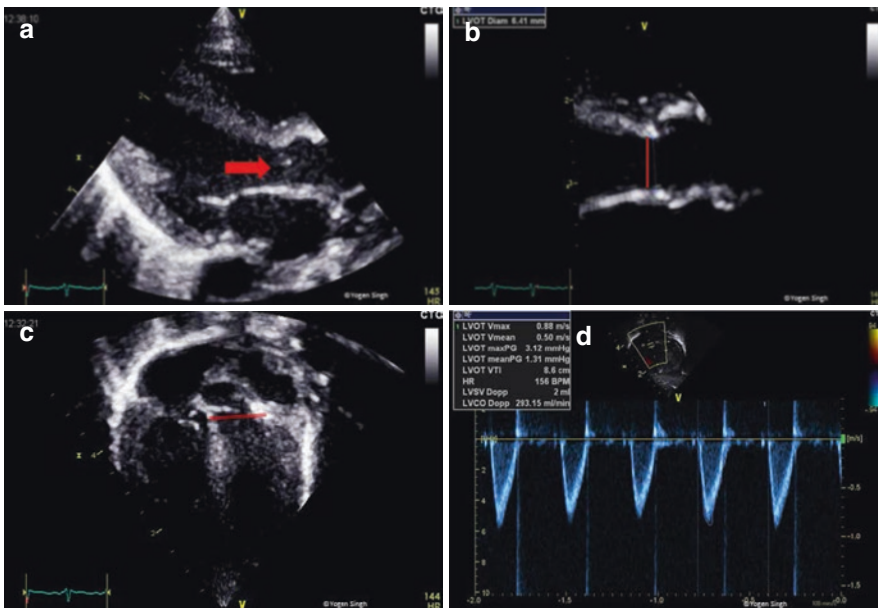


Fig. 10 Assessment of left ventricular output (LVO) on echocardiography. (a) LV outflow tract (red arrow) and AV annulus (red line), which has been zoomed in (b) to measure diameter at the hinge point of AV valve. (c) LV outflow tract and the site for pulsed wave Doppler to mea-

sure VTI (red line showing pulsed wave sample gate). (d) LVO in mL/min. AV aortic valve, LV left ventricle (copyright @Yogen Singh, adopted from Singh, Y. Echocardiographic evaluation of hemodynamic in neonates and children. Front Pediatr 2017)

Estimation of Right Ventricular Output

The RV output equals systemic venous return in the absence of cardiac shunts. RV output can be easily assessed on echocardiography. The CSA is calculated by measuring the diameter at the hinge point of pulmonary valve (PV) annulus at end-

systole in the parasternal long axis sweep view (PLAX) or parasternal short axis view (PSAX), and VTI is measured just proximal to the pulmonary valve by using PW Doppler in the same views. HR is calculated automatically by the ultrasound machine from the ECG recording (Fig. 11).

$$\text{Right ventricular output (mL/kg/min)} = \frac{\text{CSA (at PV annulus)} \times \text{VTI} \times \text{RVOT (incm)} \times \text{HR}}{\text{Body weight (in kg)}}$$

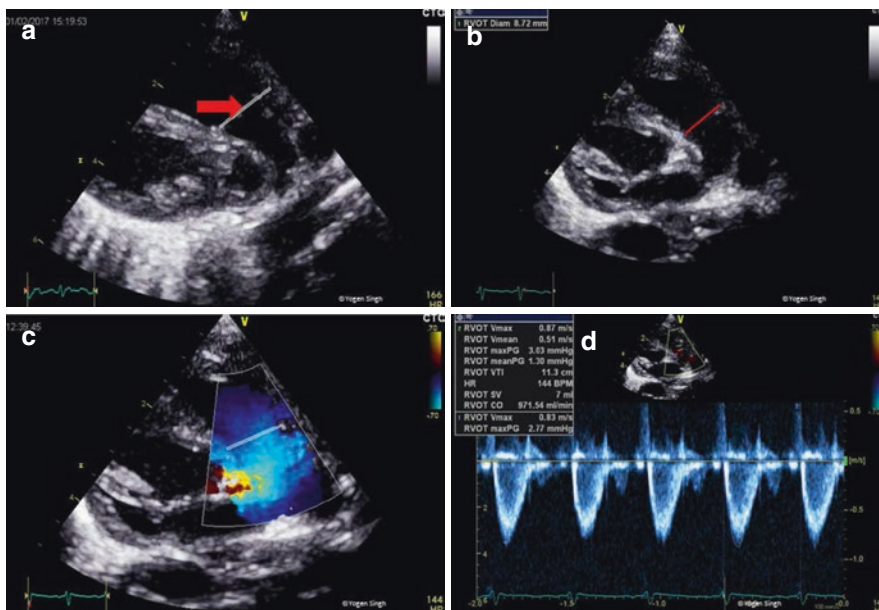


Fig. 11 Assessment of right ventricular output (RVO) on echocardiography. (a) RV outflow tract (red arrow) and (b) measurement of PV annulus (red line) at the hinge point of AV valve. (c) RV outflow tract and the site for PW Doppler to measure VTI (red line showing PW sample

gate). (d) RVO in mL/min. PV aortic valve, PW pulse wave, RV right ventricle (copyright @Yogen Singh, adopted from Singh, Y. *Echocardiographic evaluation of hemodynamic in neonates and children*. *Front Pediatr* 2017)

Limitations of LVO and RVO Measurement Using Echocardiography

The measurement of LVO and RVO using echocardiography has various limitations including [1]:

1. LVO and RVO assessment may be contaminated by trans-atrial and ductus arteriosus shunts, which are quite common in neonates during transitional circulation and those with congenital heart defects. In the presence of a PDA, LVO reflects systemic blood flow plus the amount of ductal shunt. Similarly, in the presence of trans-atrial shunt (via persistent foramen ovale (PFO) or atrial septal defect), RVO reflects the systemic blood flow plus atrial shunt volume.
2. Measurement of AV diameter is prone to mistake and CSA is calculated by squaring the diameter, any error in measurement is multiplied.
3. Measurement of VTI (stroke distance) is also prone to errors. The angle of insonation, angle between the ultrasound waves and the blood flow, during Doppler assessment, should be minimal. If the angle of insonation is $>10^\circ$ it would underestimate the cardiac output.

The echocardiographer should be aware of these limitations and precautions should be taken

to minimize such errors. In clinical practice, considering the trend of measurement values by serial echocardiography may be more useful than the absolute values.

Superior Vena Cava (SVC) Blood Flow

SVC flow has been proposed as a surrogate measure of cerebral blood flow, and it has been associated with short-term and long-term outcomes in neonates [24, 25]. Several studies have reported an association between low SVC flow in the first 24 h and intraventricular hemorrhage (IVH) and/or neonatal death in preterm infants [24, 25]. However, other studies could not demonstrate such association [26].

CSA is calculated by measuring SVC diameter in a modified PSAX view, and VTI is measured just proximal to its connection to RA by using PW Doppler in the sub-costal view. The SVC is a venous structure that is D-shaped and collapsible. Hence, measuring CSA of superior vena cava is prone to increased error as compared to a relatively noncollapsible AV or PV annulus. It is recommended that SVC diameter should be averaged over 5–10 heart cycles and best measured in M-mode. Similarly, VTI is also averaged over 5–10 cardiac cycles. HR is calculated automatically by the ultrasound machine from the ECG recording (Fig. 12).

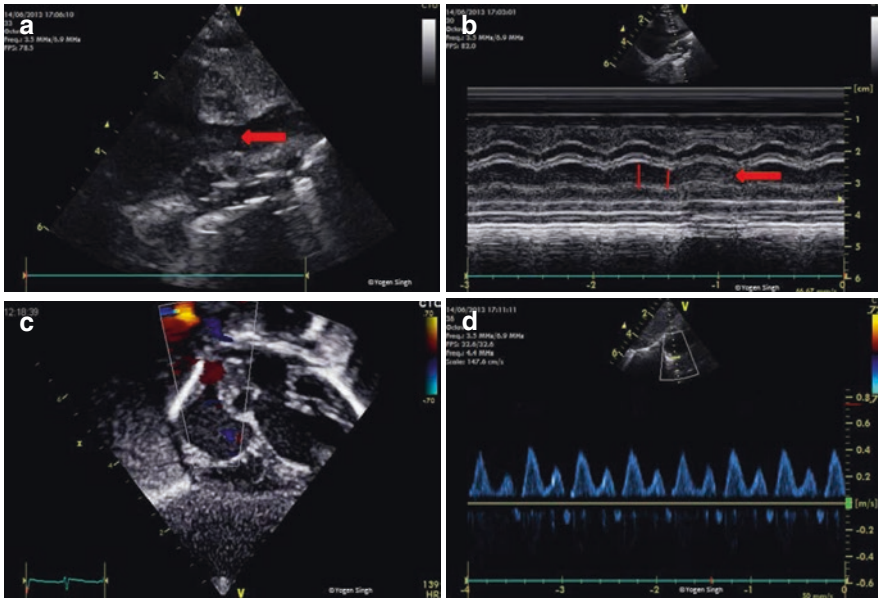


Fig. 12 Measurement of superior vena cava (SVC) flow on echocardiography. (a) SVC in modified parasternal short axis view (PSAX) on 2D and (b) measurement of SVC diameter in M-mode. (c) Acquisition of color flow Doppler in sub-costal view and (d) SVC flow in mL/min

calculated after measuring velocity time integral. (copyright @Yogen Singh, adopted from Singh, Y. *Echocardiographic evaluation of hemodynamic in neonates and children*. *Front Pediatr* 2017)

$$\text{SVC blood flow (mL / kg / min)} = \frac{\text{CSA (SVC in M} \times \text{mode)} \times \text{VTI (in cm)} \times \text{HR}}{\text{Body weight (in kg)}}$$

The reference values for SVC flow in term and preterm infants have been published with considerable variations [15, 27, 28]. However, given the risk of errors in measuring SVC diameter accurately, there is no surprise that the validation studies on estimating SVC blood flow by using echocardiography in neonates showed poor correlation when compared to MRI [22]. The studies have reported high intra- and inter-observer variability, a significant bias, and an error percentage of up to 55% [15, 22, 27, 28]. With the current published evidence, it is hard to recommend using SVC flow in clinical decision-making; however, a trend in SVC flow can be useful in clinical practice to assess the impact of any intervention.

Advanced echocardiographic techniques and views can be applied for detailed hemodynamic evaluation in neonates and children including evaluation of cardiac output, preload, afterload, cardiac contractility/function, fluid responsiveness, diagnosis, and hemodynamic evaluation of patent ductus arteriosus and pulmonary hypertension. This advanced evaluation needs a depth of knowledge and high-quality echocardiography skills, and they are out of the scope of POCUS practice. This protocol-based evaluation using advanced echocardiographic parameters is often used by clinicians formally trained in neonatologist-performed echocardiography.

References

- Singh Y. Echocardiographic evaluation of Hemodynamics in neonates and children. *Front Pediatr.* 2017;5:201. <https://doi.org/10.3389/fped.2017.00201>.
- Singh Y, Fraisse A, Erdevé O, Atasay B. Echocardiographic diagnosis and hemodynamic evaluation of patent ductus arteriosus in extremely low gestational age newborn (ELGAN) infants. *Front Pediatr.* 2020;8:573627. <https://doi.org/10.3389/fped.2020.573627>.
- McNamara PJ, Sehgal A. Towards rational management of the patent ductus arteriosus: the need for disease staging. *Arch Dis Child Fetal Neonatal Ed.* 2007;92:F424–7. <https://doi.org/10.1136/adc.2007.118117>.
- van Laere D, van Overmeire B, Gupta S, El Khuffash A, Savoia M, McNamara PJ, et al. Application of NPE in the assessment of a patent ductus arteriosus. *Pediatr Res.* 2018;84:S46–56. <https://doi.org/10.1038/s41390-018-0077-x>.
- Fraisse A, Bautista C, Burmester M, Lane M, Singh Y. Transcatheter closure of patent ductus arteriosus in infants with weight under 1,500 grams. *Front Pediatr.* 2020;8:558256.
- Singh Y, Tissot C. Echocardiographic evaluation of transitional circulation for the neonatologists. *TINEC research article.* *Front Pediatr.* 2018;6:79. <https://doi.org/10.3389/fped.2018.00140>.
- Condo M, Evans N, Bellu R, Kluckow M. Echocardiographic assessment of ductal significance: retrospective comparison of two methods. *Arch Dis Child Fetal Neonatal Ed.* 2012;97:F35–8. <https://doi.org/10.1136/adc.2010.207233>.
- Smith A, Maguire M, Livingstone V, Dempsey EM. Peak systolic to end diastolic flow velocity ratio is associated with ductal patency in infants below 32 weeks of gestation. *Arch Dis Child Fetal Neonatal Ed.* 2015;100:F132–6. <https://doi.org/10.1136/archdischild-2014-306439>.
- El Hajjar M, Vaksmann G, Rakza T, Kongolo G, Storme L. Severity of the ductal shunt: a comparison of different markers. *Arch Dis Child Fetal Neonatal Ed.* 2005;90:F419–22. <https://doi.org/10.1136/adc.2003.027698>.
- Iyer P, Evans N. Re-evaluation of the left atrial to aortic root ratio as a marker of patent ductus arteriosus. *Arch Dis Child Fetal Neonatal Ed.* 1994;70:F112–7. <https://doi.org/10.1136/fn.70.2.F112>.
- Singh Y, Katheria A, Tissot C. Functional echocardiography in the neonatal intensive care unit. *Indian Pediatr.* 2018;14:417–25. <https://doi.org/10.1007/s13312-018-1286-4>.
- Abushaban L, Vel MT, Rathinasamy J, Sharma P. Normal reference ranges for left ventricular dimensions in preterm infants. *Ann Pediatr Cardiol.* 2014;7:180–6. <https://doi.org/10.4103/0974-2069.140832>.
- Kheiwā A, Ross RD, Kobayashi D. Reversal of severe mitral regurgitation by device closure of a large patent ductus arteriosus in a premature infant. *Cardiol Young.* 2017;27:189–92. <https://doi.org/10.1017/S1047951116000998>.
- Walther FJ, Kim DH, Ebrahimi M, Siassi B. Pulsed Doppler measurement of left ventricular output as early predictor of symptomatic patent ductus arteriosus in very preterm infants. *Biol Neonate.* 1989;56:121–8. <https://doi.org/10.1159/000243112>.
- Lee A, Liestøl K, Nestaas E, Brunvand L, Lindemann R, Fugelseth D. Superior vena cava flow: feasibility and reliability of the off-line analyses. *Arch Dis Child Fetal Neonatal Ed.* 2010;95:F121–5. <https://doi.org/10.1136/adc.2009.176883>.
- Mertens L, Seri I, Marek J, Arlettz R, Barker P, McNamara P, et al. Targeted neonatal echocardiography in the neonatal intensive care unit: practice guidelines and recommendations for training. Writing Group of the American Society of Echocardiography (ASE) in collaboration with the European Association of Echocardiography (EAE) and the Association for European Pediatric Cardiologists (AEPC). *J Am Soc Echocardiogr.* 2011;24:1057–78. <https://doi.org/10.1016/j.echo.2011.07.014>.
- Broadhouse KM, Price AN, Durighel G, Cox DJ, Finnemore AE, Edwards AD, et al. Assessment of PDA shunt and systemic blood flow in newborns using cardiac MRI. *NMR Biomed.* 2013;26:1135–41. <https://doi.org/10.1002/nbm.2927>.
- Ecury-Goossen GM, Raets MMA, Camfferman FA, Vos RHJ, van Rosmalen J, Reiss IRM, et al. Resistive indices of cerebral arteries in very preterm infants: values throughout stay in the neonatal intensive care unit and impact of patent ductus arteriosus. *Pediatr Radiol.* 2016;46:1291–300. <https://doi.org/10.1007/s00247-016-3615-x>.
- El-Khuffash A, James AT, Corcoran JD, Dicker P, Franklin O, Elsayed YN, et al. A patent ductus arteriosus severity score predicts chronic lung disease or death before discharge. *J Pediatr.* 2015;167:1354–61. <https://doi.org/10.1016/j.jpeds.2015.09.028>.
- Alverson DC, Eldridge M, Dillon T, Yabek SM, Berman W Jr. Noninvasive pulsed Doppler determination of cardiac output in neonates and children. *J Pediatr.* 1982;101:46–50.
- Alverson DC. Neonatal cardiac output measurement using pulsed Doppler ultrasound. *Clin Perinatol.* 1985;12:101–27.
- Ficial B, Finnemore AE, Cox DJ, Broadhouse KM, Price AN, Durighel G, et al. Validation study of the accuracy of echocardiographic measurements of systemic blood flow volume in newborn infants. *J Am Soc Echocardiogr.* 2013;26:1365–71.
- Groves AM, Chiesa G, Durighel G, et al. Functional cardiac MRI in preterm and term newborns. *Arch Dis Child Fetal Neonatal Ed.* 2011;96:F86–91.
- Osborn DA, Evans N, Kluckow M, Bowen JR, Rieger I. Low superior vena cava flow and effect of inotropes

- on neurodevelopment to 3 years in preterm infants. *Pediatrics*. 2007;120:372–80.
25. Miletin J, Dempsey EM. Low superior vena cava flow on day 1 and adverse outcome in the very low birthweight infant. *Arch Dis Child Fetal Neonatal Ed*. 2008;93:F368–71.
 26. El-Khuffash AF, Jain A, Weisz D, Mertens L, McNamara PJ. Assessment and treatment of post patent ductus arteriosus ligation syndrome. *J Pediatr*. 2014;165:46–52.
 27. Kluckow M, Evans N. Superior vena cava flow in newborn infants: a novel marker of systemic blood flow. *Arch Dis Child Fetal Neonatal Ed*. 2000;82:F182–7.
 28. Groves AM, Kuschel CA, Knight DB, Skinner JR. Echocardiographic assessment of blood flow volume in the superior vena cava and descending aorta in the newborn infant. *Arch Dis Child Fetal Neonatal Ed*. 2008;93:F24–8.



Comprehensive Echocardiography and Diagnosis of Major Common Congenital Heart Defects

Nicole Sekarski, Yogen Singh, and Cécile Tissot

Contents

Introduction	112
Classification of Congenital Heart Defects	115
Identifying Newborns with Critical Congenital Heart Disease	116
1. Shock (The Grey Neonate).....	117
Common Key Echocardiography Feature: Poorly Functioning Left Ventricle.....	117
2. Cyanosis (The Blue Neonate).....	120
Ductal-Dependent Lesions.....	120
Transposition of the great arteries (Figs. 17, 18, and 19).....	122
Non-ductal-Dependent Lesions.....	123
3. The Tachypneic Neonate (Respiratory Symptoms).....	124
Patent Ductus Arteriosus (Figs. 27 and 28; Video 12).....	125
Ventricular Septal Defect (Figs. 29, 30, 31, and 32; Videos 13 and 14).....	126
Atrial Septal Defect (Figs. 33 and 34; Videos 15 and 16).....	127
Atrioventricular Septal Defect (Fig. 35; Video 17).....	128
Conclusion	129
References	129

Supplementary Information The online version contains supplementary material available at https://doi.org/10.1007/978-3-031-26538-9_9.

N. Sekarski (✉)
Centre Hospitalier Universitaire Vaudois (CHUV),
University of Lausanne, Lausanne, Switzerland
e-mail: Nicole.sekarski@chuv.ch

Y. Singh
Department of Pediatrics, Division of Neonatology,
Loma Linda University School of Medicine,
California, USA

Department of Pediatrics, Division of Neonatal and
Developmental Medicine, Stanford University School
of Medicine, California, UK

Department of Pediatrics, Division of Neonatology,
University of Southern California, California, UK

ESPNIC Cardiovascular Dynamics Section and
POCUS Working Group, Geneva, Switzerland
e-mail: YSingh@llu.edu

C. Tissot
Department of Pediatrics, Clinique des Grangettes,
Chêne-Bougeries, Geneva, Switzerland

Introduction

Congenital heart diseases (CHD) are structural anomalies of the heart and great vessels. They represent the most frequent congenital anomalies with an incidence of 0.8–1 per 100 live newborns [1, 2]. Every year one million children worldwide are born with CHD and they are the first cause of mortality due to congenital anomalies [3, 4]. CHD develops early in fetal life as the heart is the first functional organ in the embryo. It is therefore of paramount importance to understand basic cardiac embryology and its disruption leading to CHD.

Basic cardiac embryology—a brief overview is summarized below and illustrated in Fig. 1 [5, 6].

(a) *Formation of the heart tube*

In the second week of gestation, the human embryo consists of a disc within the amniotic fluid. Cardiogenic precursors in the epiblast will migrate through the primitive streak to form the mesodermal bilateral cardiogenic areas. These will merge cranially to form a horseshoe-shaped field. The embryonic disc will then undergo lateral folding, bringing together the two precursor areas creating the primitive heart tube. The heart starts to beat around day 21. From superior to inferior, the heart tube consists of the aortic sinuses, the truncus arteriosus, the bulbus cordis, the ventricle, the atrium, and the sinus venosus.

(b) *Looping*

At day 23 the heart tube begins to loop with the bulbus cordis moving ventrally, caudally, and to the right (d-loop) and the primitive ventricle moving dorsally, cranially, and to the left.

(c) *Septation*

Septation occurs between the fourth and fifth week of development. Two endocardial cushions develop from the dorsal and ventral surface of the atrioventricular canal and fuse, separating the atrium from the ventricle. Two other endocardial cushions on the lateral walls will ultimately form the tricuspid and mitral valve.

Septation of the atria begins with membranous tissue, the septum primum, growing from the roof of the atrium moving towards the endocardial cushions. Perforations in the center of the septum primum give rise to the

foramen secundum. A muscular septum secundum grows to the right of the septum primum and will overlap the foramen secundum gradually. The remainder of the opening is called the foramen ovale.

The septation of the ventricles starts with a muscular interventricular ridge developing at the apex and ultimately fusing with the endocardial cushions.

(d) *Systemic and pulmonary veins*

The right horn of the sinus venosus increases giving rise to the superior vena cava (SVC) and the inferior vena cava (IVC), the left sinus horn regresses and ultimately will become the coronary sinus. The primordial pulmonary vein is formed in the dorsal wall of the left atrium (LA) and the branches of the pulmonary veins become incorporated into the LA.

(e) *Outflow tracts*

Neural crest mesenchymal cells in the bulbus cordis proliferate during the fifth week and form a bulbar ridge which continues in the truncus arteriosus. These cells migrate to reach the outflow tract. The ridges operate a 180-degree spiral movement to form the aortopulmonary septum which will then divide into the aorta and pulmonary trunk.

(f) *Heart valves*

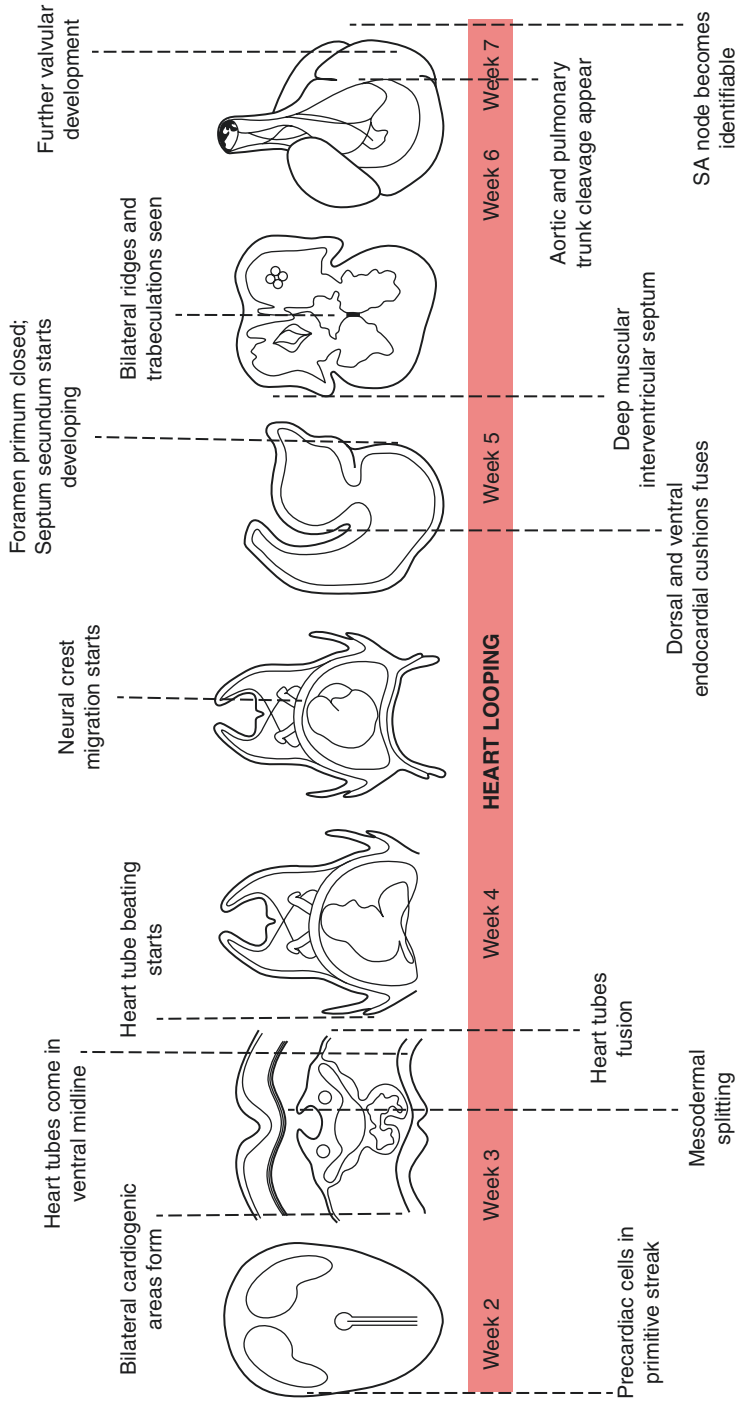
The atrioventricular valves develop between the fifth and eighth week of gestation. The left atrioventricular valve, the mitral valve has an anterior and posterior leaflet, the right atrioventricular valve, the tricuspid valve also has a septal leaflet. The valves are attached to the septum by thin fibrous chords inserted into the papillary muscles. The semilunar valves (aortic and pulmonary valves) are formed from the bulbar ridges and subendocardial tissue.

(g) *Arterial system*

The arterial system consists initially of bilateral symmetric aortic arches which will undergo major changes to create the great arteries.

(h) *Conduction system*

Cardiac development is a highly regulated process implicating complex molecular pathways at each step of development. A multitude of genes involved in this process has been described (Fig. 2) [7].



Copyright © SheenGahlaut & YogenSingh

Fig. 1 Heart formation in the embryo (Courtesy: Sheen Gahlaut and Yogen Singh)

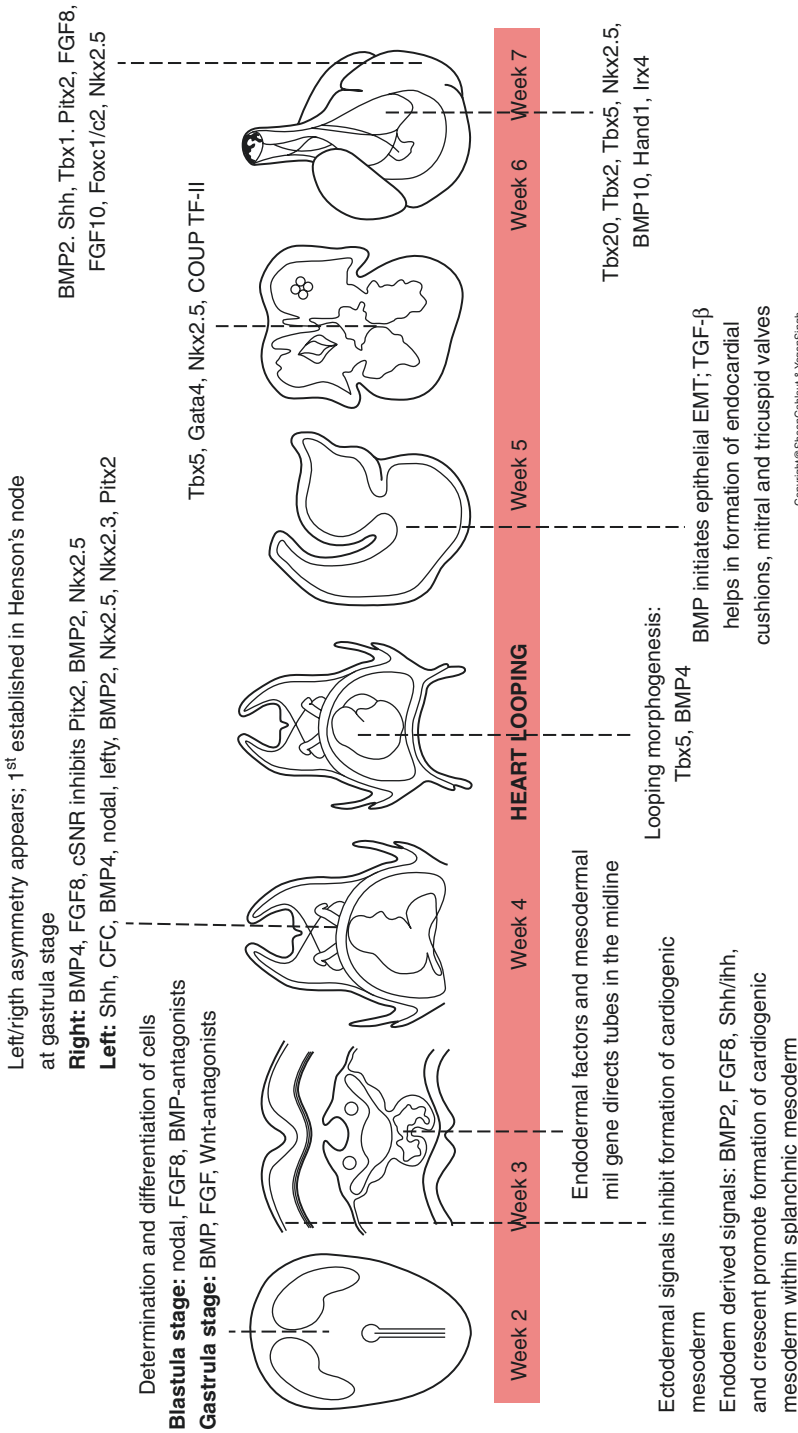


Fig. 2 Genes involved in cardiac development (Courtesy: Sheen Gahlaut and Yogen Singh)

Disruption of this process by different genetic, maternal, environmental, or most often unknown factors can lead to CHD in the fetus. During the heart development, earlier the disruption occurs, the more severe the heart malformation will be [5, 6].

includes two major categories, non-cyanotic and cyanotic congenital heart defects (CHD). The non-cyanotic category can be subdivided into two groups: CHD with increased pulmonary blood flow and CHD with obstructive blood flow from the ventricles. The cyanotic category can be subdivided into CHD with decreased pulmonary blood flow and CHD with mixed blood flow [8, 9] (Fig. 3).

Classification of Congenital Heart Defects

To this date, there is no universally accepted classification for congenital heart defects, but the one most used is based on pathophysiology and it

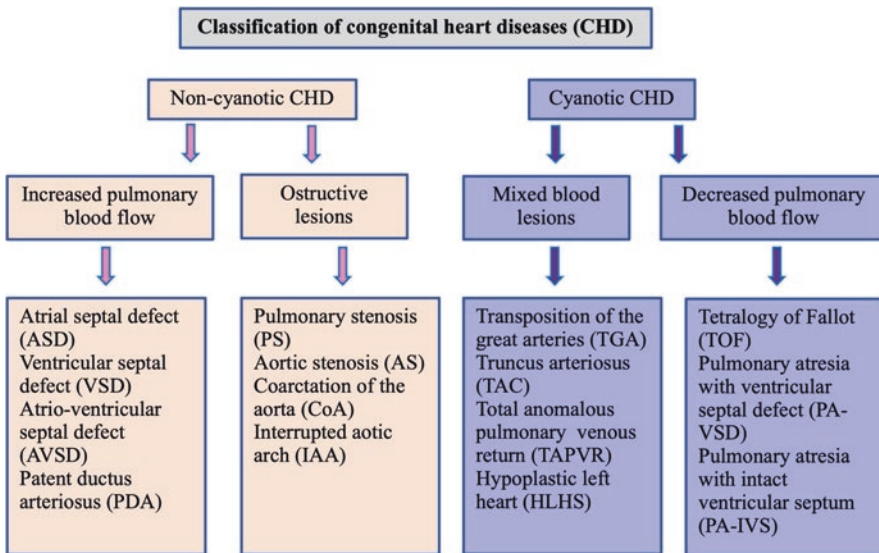


Fig. 3 A simple classification of congenital heart disease based on cyanosis and amount of pulmonary blood flow

Identifying Newborns with Critical Congenital Heart Disease

As many as 25–33% of infants born with CHD are considered to have critical CHD, which is defined as having a cardiac lesion requiring surgical or catheter-based intervention [3]. In these infants, any delay in diagnosis will increase morbidity and mortality [10, 11]. It is therefore important for neonatologist or intensivist performing echocardiography to be able to recognize these defects as early as possible.

Neonatologist performed echocardiography (NPE) or targeted neonatal echocardiography (TNE) should be performed by accredited neonatologists according to the guidelines of the European Society of Pediatric and Neonatal Intensive Care (ESPNIC) and American Society of Echocardiography (ASE)/Association for European Pediatric Cardiology (AEPC) [12, 13] (Tables 1, 2, and 3).

Table 1 Indications for performing NPE include (but not exhaustive list as there may be many more indications depending upon the clinical indications and NPE service availability):

Suspicion of PDA in premature baby (24–72 h of life)
Evaluation of a perinatal asphyxia
Abnormal cardiovascular adaptation in the first 24 h of life
Suspicion of persistent pulmonary hypertension
Congenital diaphragmatic hernia
Shock

Table 2 The first echocardiography should include a complete morphologic and functional examination using a segmental approach [14–17]

Atrial situs and position of the heart in the thorax
Systemic venous return
Size and morphology of the atria
Presence of atrial communication and direction of shunt
Atrioventricular connection and function of AV valves
Ventricular morphology, size, and function
Ventricular septal anatomy
Ventriculo-arterial connection and function of semilunar valves
Presence/absence of PDA and shunting
Coronary anatomy
Aortic arch and pulmonary artery anatomy
Pulmonary venous return

Table 3 The standard echocardiography required for NPE core examination

1. Anatomy
(a) Cardiac anatomy including
• Inflow
• Outflow
• Cardiac valves
• Cardiac chambers
(b) Skills
• 2D images of the neonatal heart in long axis, short axis, high parasternal, PDA and aortic arch view, apical and subcostal
• Mode M to measure LA/Ao ratio
• Pulsed and color Doppler to demonstrate normal blood flow across valves and outflow tracts
• Continuous Doppler (CW) to measure tricuspid regurgitation (TR)
2. Systolic LV function
(a) End-diastolic and end-systolic dimension of the LV (2D or M-Mode)
(b) End-diastolic and end-systolic thickness of the posterior LV wall (2D, M-Mode)
(c) End-diastolic and end-systolic thickness of the interventricular septum (2D, M-Mode)
(d) Shortening fraction (M-Mode)
(e) Ejection fraction (M-Mode or 2D Simpson)
3. Diastolic LV function
(a) Mitral valve max velocity of E wave (PW Doppler)
(b) Mitral valve max velocity of A wave (PW Doppler)
4. Evaluation of pulmonary hypertension
(a) Max velocity of TR (CW Doppler)
(b) End-diastolic velocity of pulmonary regurgitation (PR) (PW/CW Doppler)
5. Evaluation of PDA
(a) Minimal dimension of the PDA (2D)
(b) Shunt direction (color Doppler, PW, CW)
(c) Max and mean gradient of ductal flow (CW, PW)
6. Evaluation of an interatrial shunt:
(a) Direction of shunt (color Doppler)
7. Evaluation of pericardial effusion
(a) Measure of the effusion in diastole (2D)

Compared to comprehensive NPE evaluation, cardiac POCUS assessment is limited and focused at answering specific clinical question or target specific intervention. Indications for the cardiac POCUS, especially in neonates, are limited and it should NOT be used as a screening tool for the CHDs, although abnormality can be detected while performing cardiac POCUS for

other indications. If any CHD or cardiac abnormality suspected on cardiac POCUS performed by the neonatologist or intensivist, these cases should be urgently discussed with the pediatric cardiology service for a formal structural echocardiography and cardiac consultation. Although cardiac POCUS is not aimed at screening or diagnosing CHDs, still its important for the neonatal and pediatric intensivist performing cardiac POCUS to have a good knowledge of cardiovascular physiology and echocardiographic aspects of critical CHDs.

The majority of newborns with critical CHDs present with the one of the following 3 clinical presentations: 1) shock, 2) cyanosis, and 3) tachypnea (or respiratory symptoms). Each presentation is associated with certain types of CHDs. Infants with critical CHDs can be asymptomatic or can present with non-specific signs and symptoms, especially early in the clinical course while ductus arteriosus is still patent and / or pulmonary vascular resistance is high. Specific CHD will have some key echocardiographic features helping to pinpoint the diagnosis which will then have to be precisely determined on a comprehensive echocardiography by the pediatric cardiologist.

A summary of the most frequent critical CHD according to clinical symptoms, with their echocardiography features and best echocardiography views to suspect the diagnosis have been described below.

1. Shock (The Grey Neonate)

The main clinical signs will be poor peripheral perfusion, decreased or absent pulses, tachycardia, tachypnea, and respiratory distress syndrome as the ductus arteriosus closes and systemic perfusion decreases [18].

Main Cardiac Lesions

- Hypoplastic left heart syndrome
- Critical aortic stenosis
- Coarctation of the aorta
- Interrupted aortic arch

Common Key Echocardiography Feature: Poorly Functioning Left Ventricle

HLHS Echo Features and Best Views (Figs. 4, 5, 6, and 7; Videos 1 and 2)

Key echo feature: hypoplastic left ventricle

	PLAX	PSAX	A4/5C	SC	SS
Very small hyperechogenic ventricle with poor contraction	X	X	X	X	
No or very reduced flow through mitral valve	X		X		
No or very minimal flow through aortic valve	X		X	X	X
Small LA	X		X		
Small aortic annulus, very small ascending aorta, and arch	X		X		X
Retrograde flow in ascending aorta					X
PDA with right to left flow					X
Left to right shunt through PFO, sometimes restrictive (high velocity)				X	

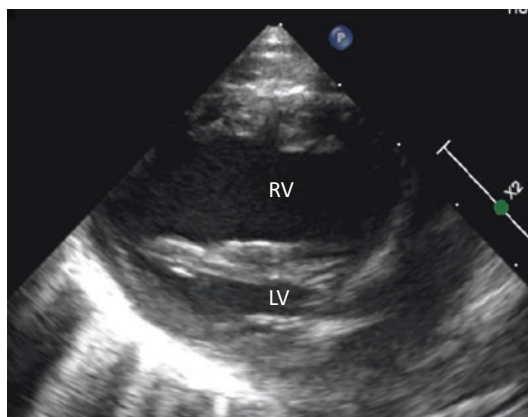


Fig. 4 PLAX: hypoplasia of the LV, dilated RV

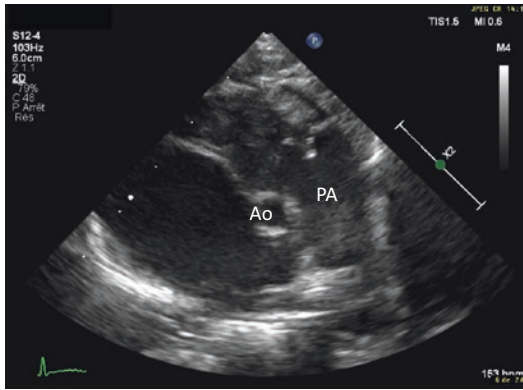


Fig. 5 PSAX : very small aorta (Ao), dilated pulmonary artery (PA)

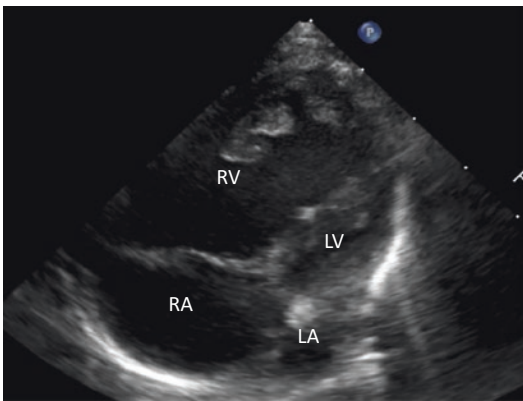


Fig. 6 4C: dilated RA and RV, hypoplastic LV, small LA, mitral atresia

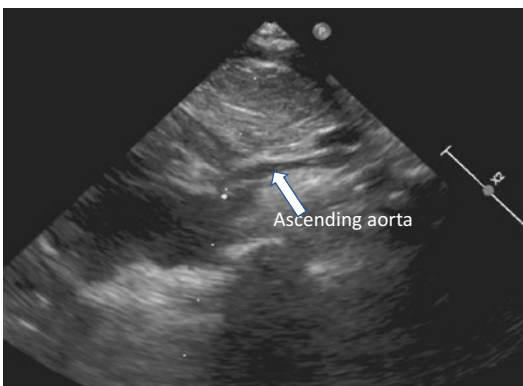


Fig. 7 Suprasternal: very hypoplastic ascending aorta

Critical Aortic Stenosis (Figs. 8 and 9; Videos 1–4)

Key echo feature: minimal antegrade flow through aortic valve

	PLAX	PSAX	A4/5C	SC	SS
Small or normal sized aortic annulus	X				
Very thickened aortic leaflets with decreased mobility	X	X			
Dilated, poorly contractile LV	X	X	X	X	
Hyperechogenic endocardium (endocardial fibroelastosis)	X	X	X	X	
Mitral regurgitation, dilated LA	X		X		
In severe cases retrograde flow in ascending aorta					X
Pulmonary hypertension	X		X		
Accelerated L-R shunt through PFO					X

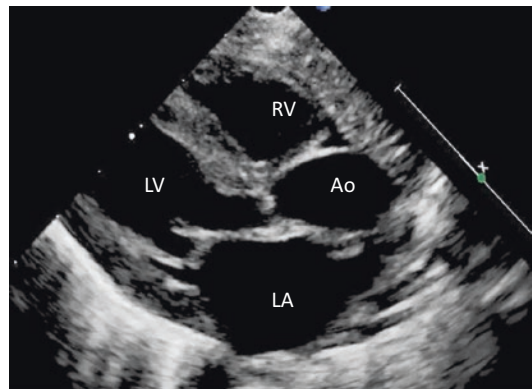


Fig. 8 PLAX: thickened aortic valve, post-stenotic dilation of the ascending aorta, globular dilated LV with hypertrophy

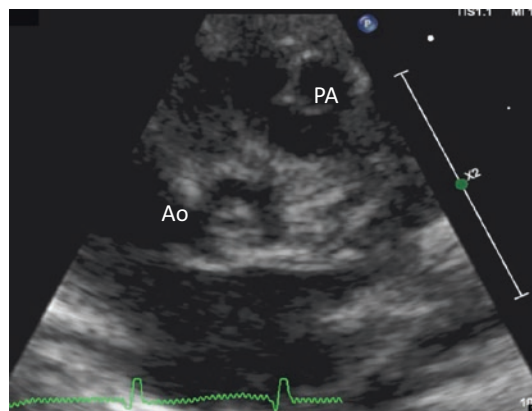


Fig. 9 PSAX: thickened aortic valve with minimal opening

Critical Aortic Coarctation (Figs. 10 and 11; Video 5)

Key echo feature: accelerated flow in descending aorta with run-off in diastole

	PLAX	PSAX	A4/5C	SC	SS
Dilated, poorly contractile LV	X	X	X	X	
Hypoplastic transverse aortic arch					X

	PLAX	PSAX	A4/5C	SC	SS
Hypoplastic aortic isthmus					X
Bicuspid aortic valve		X			
PDA with left to right shunt		X			
Pulmonary hypertension	X	X	X		

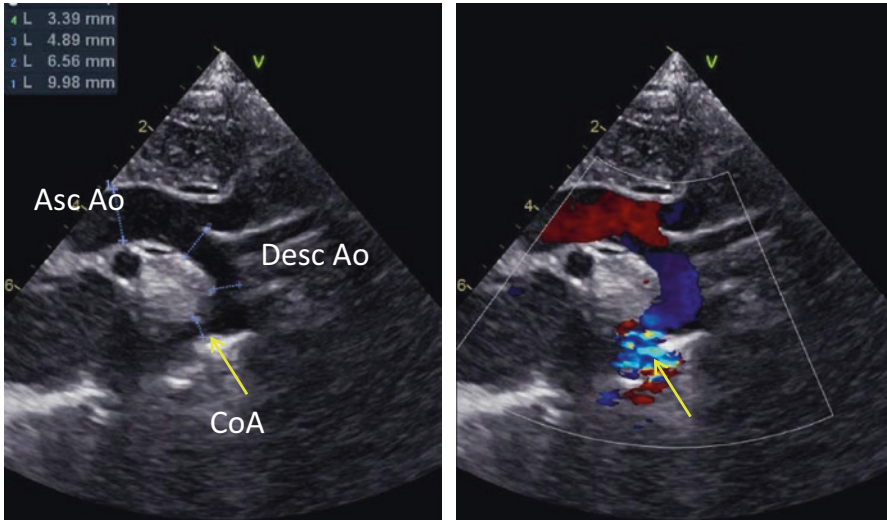


Fig. 10 Suprasternal: narrowing of the descending aorta (arrow = coarctation) in juxtaductal position with aliasing of flow by color Doppler

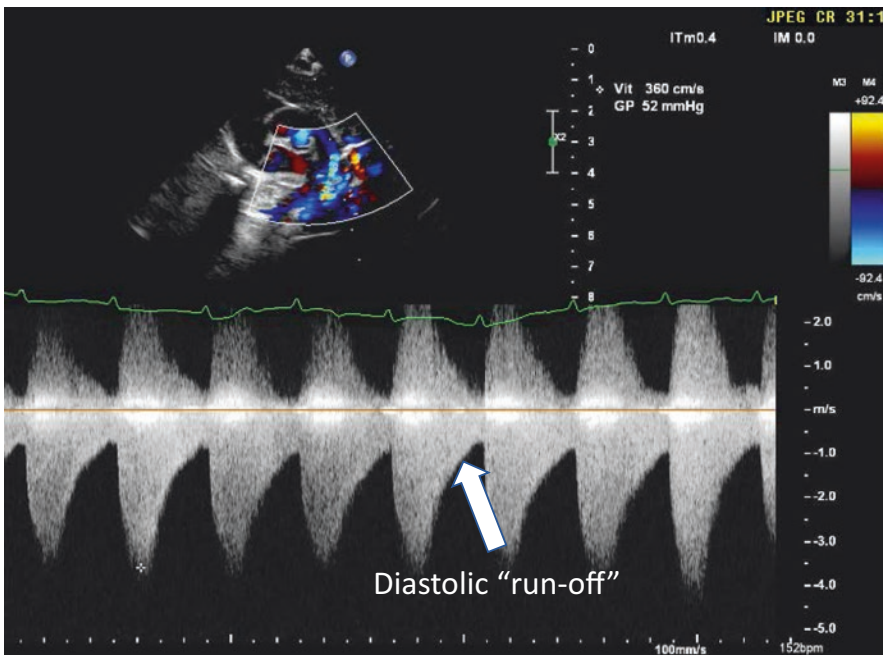


Fig. 11 Suprasternal Doppler: high-velocity flow with diastolic “run-off”

Interrupted Aortic Arch (Fig. 12)

Key echo feature: unable to visualize entire aortic arch

	PLAX	PSAX	A4/5C	SC	SS
Dilated brachiocephalic artery					X
Inability to image the entire arch in suprasternal view					X
PDA with right to left shunt		X			X
VSD	X		X	X	

2. Cyanosis (The Blue Neonate)

The main clinical signs will be central cyanosis, sometimes associated with signs of shock.

Ductal and non-ductal dependent lesions can cause cyanosis in the newborn. In some cases, there will be differential cyanosis with lower saturations in the lower extremities compared to the upper extremities (left heart obstructive lesions) or reverse differential saturation with higher saturations in the upper extremities compared to the lower extremities (Transposition of the great vessels with coarctation and pulmonary hypertension) [19, 20].

Ductal-Dependent Lesions

- Right heart obstructive lesions: severe pulmonary valve stenosis or pulmonary atresia with intact ventricular septum (PA-VSD), tetralogy of Fallot’s

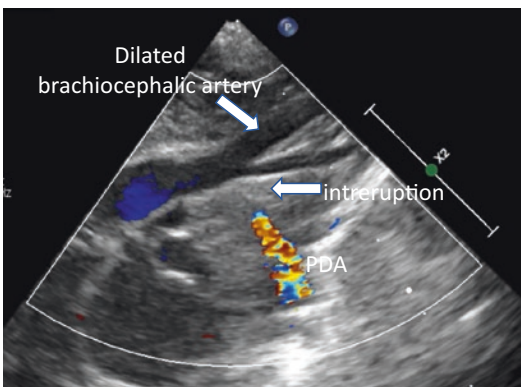


Fig. 12 Suprasternal: dilated brachiocephalic artery, descending aorta perfused through PDA

- Parallel circulation: transposition of the great arteries (TGA)

Severe Pulmonary Valve Stenosis (Fig. 13; Video 6)

Key echo feature: thickened and doming pulmonary valve with post-stenotic dilatation of pulmonary trunk

	PLAX	PSAX	A4/5C	SC	SS
Pulmonary valve thickened and doming, restricted opening		X		X	
Aliasing of flow into pulmonary artery		X		X	
Post-stenotic dilatation of pulmonary trunk		X		X	

Pulmonary Atresia with Intact Septum (Figs. 14, 15, and 16)

Key echo feature: hypoplastic, poorly contractile RV

	PLAX	PSAX	A4/5C	SC	SS
Small, hypertrophied RV, often not tripartite with decreased function	X		X	X	
Pulmonary valve thickened, restricted, or no opening		X		X	
No antegrade flow or very little antegrade flow into pulmonary artery		X		X	
Retrograde flow into pulmonary artery from PDA		X			X
Severe tricuspid regurgitation	X		X		
PFO with right to left shunt				X	

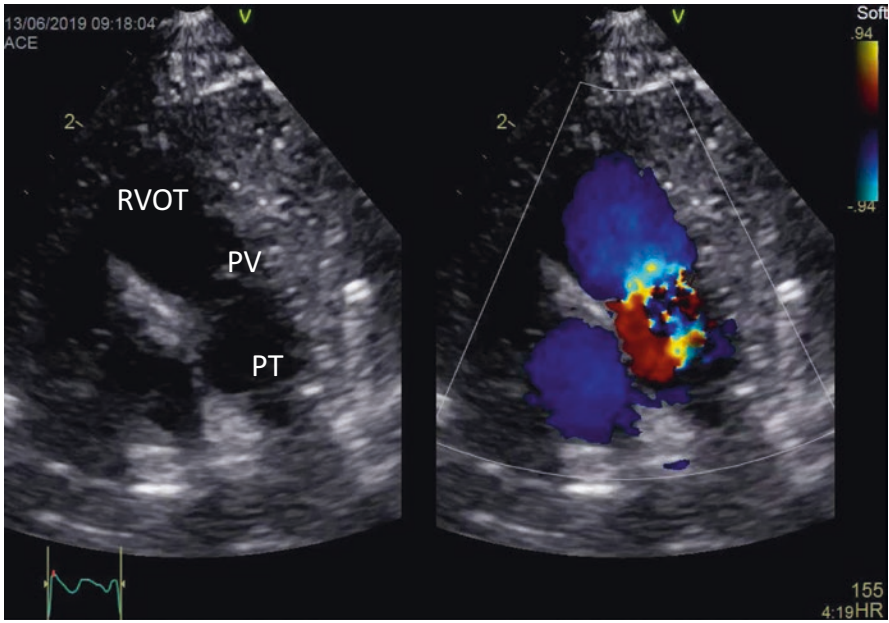


Fig. 13 PSAX: pulmonary valve (PV) thickened, doming with restricted opening and aliasing of flow, post-stenotic dilatation of pulmonary trunk (PT)

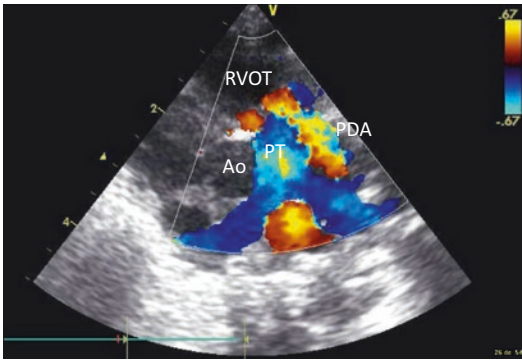


Fig. 14 PSAX: absent flow across pulmonary valve, retrograde flow in pulmonary trunk (PT) through patent ductus arteriosus (PDA)

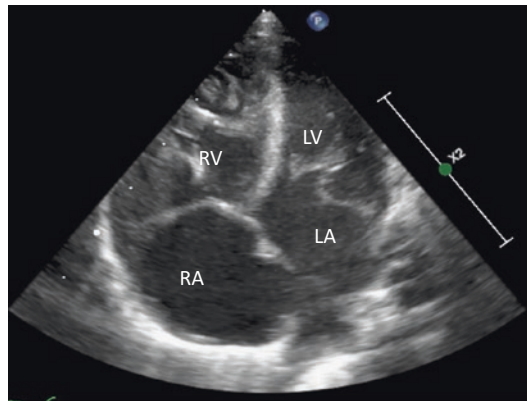


Fig. 15 4C: Hypertrophied and small RV, interatrial septum bulging to the left (and obligatory right to left interatrial shunt)

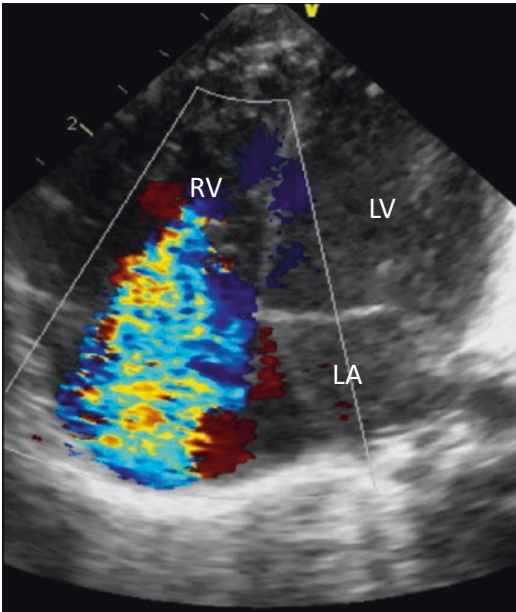


Fig. 16 4C: severe tricuspid regurgitation (TR)

Transposition of the great arteries (Figs. 17, 18, and 19)

Key echo feature: parallel arrangement of great vessels

	PLAX	PSAX	A4/5C	SC	SS
RV giving rise to straight vessel (aorta)	X			X	
LV giving rise to vessel bifurcating (pulmonary artery)	X			X	
Parallel arrangement of great vessels (cannonball)	X			X	
Aorta anterior and to left of pulmonary artery		X			
PDA with left to right flow		X			X

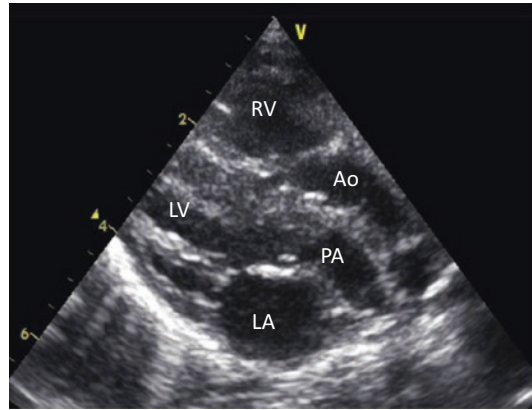


Fig. 17 PLAX: Pulmonary artery (PA) coming from LV, aorta (AO) coming from RV, parallel arrangement of the great vessels

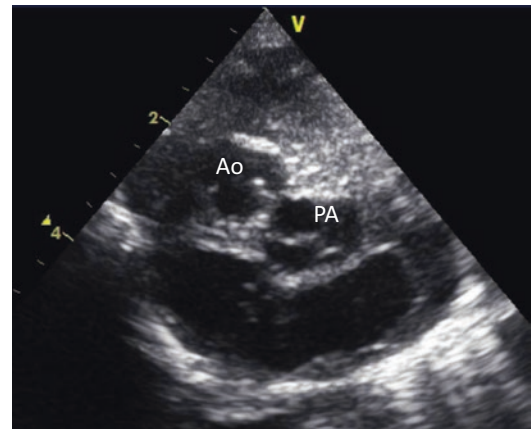


Fig. 18 PSAX: Aorta anterior right, pulmonary artery (PA) posterior left

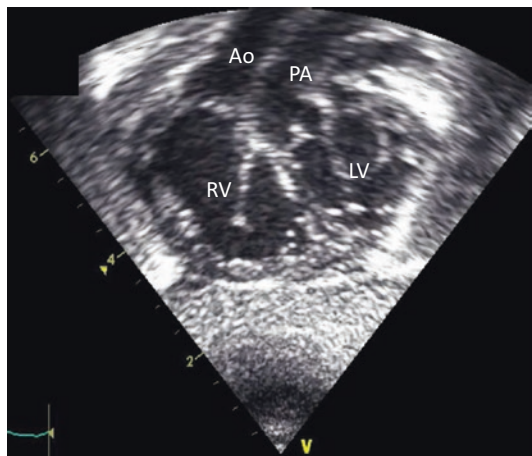


Fig. 19 Subcostal: Parallel arrangement of the great vessels, aorta anterior right and pulmonary artery (PA) posterior left bifurcating into branches

	PLAX	PSAX	A4/5C	SC	SS
PFO with bidirectional flow				X	

Non-ductal-Dependent Lesions

- Truncus arteriosus
- Tetralogy of Fallot
- Total anomalous pulmonary venous return
- Tricuspid atresia

Truncus Arteriosus (Figs. 20 and 21; Video 7)

Key echo feature: only one great vessel exiting heart

	PLAX	PSAX	A4/5C	SC	SS
Large perimembranous VSD	X		X	X	
Single large arterial vessel overriding VSD giving rise to aorta and pulmonary arteries	X	X		X	
Absent PDA		X			X
Truncal valve thickened with stenosis and/or regurgitation, sometimes quadricuspid		X			

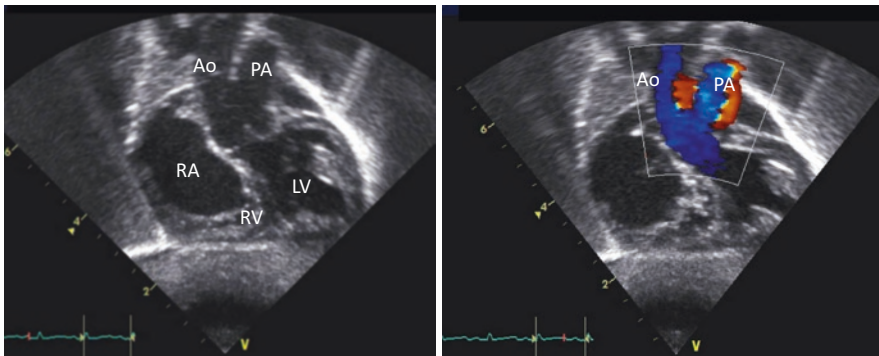


Fig. 20 Subcostal: Single artery coming from LV giving rise to aorta and pulmonary artery (PA)

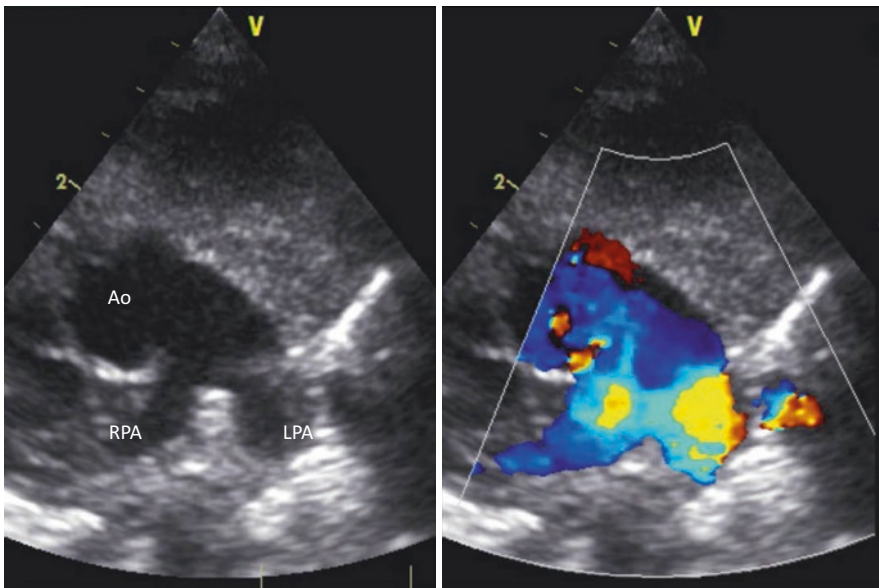


Fig. 21 PSAX: Branch right (RPA) and left (LPA) pulmonary arteries coming from aorta (AO)

Tetralogy of Fallot (Figs. 22 and 23; Video 8)

Key echo feature: VSD and overriding aorta

	PLAX	PSAX	A4/5C	SC	SS
Large perimembranous VSD	X		X	X	
Large overriding aorta	X	X		X	
RV hypertrophy		X		X	
Infundibular and valvar/supravalvar pulmonary stenosis		X		X	
Some degree of pulmonary hypoplasia		X		X	
Right aortic arch (25%)					X

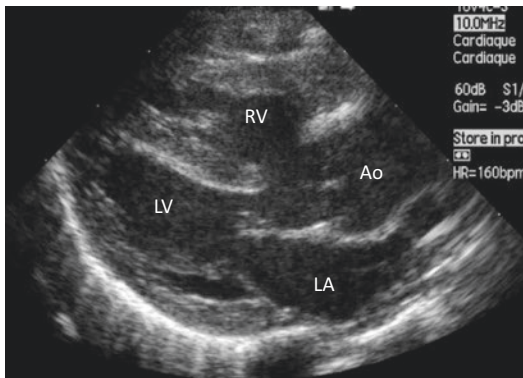


Fig. 22 PLAX: Large ventricular septal defect (VSD) and overriding aorta

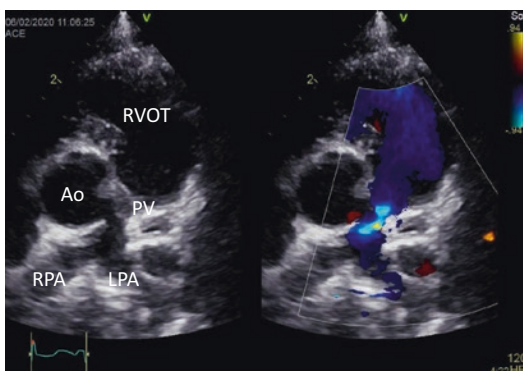


Fig. 23 PSAX: Hypoplasia of pulmonary valve (PV) annulus, trunk (PT), and branch left (LPA) and right (RPA) pulmonary arteries with aliasing of flow through PV

Total Anomalous Pulmonary Venous Return (TAPVR) (Figs. 24 and 25; Video 9)

Key echo feature: very small LA, right to left shunt through PFO

	PLAX	PSAX	A4/5C	SC	SS
Inability to visualize pulmonary veins entering LA			X		X
Very small LA	X		X	X	
Very dilated right-sided cavities	X	X	X	X	
PFO with right to left shunt				X	
Pulmonary hypertension		X	X		
Either dilated SVC, IVC, or coronary sinus			X	X	X
Vertical vein to innominate vein					X
Dilated portal vein (infradiaphragmatic TAPVR)				X	

Tricuspid Atresia (Fig. 26; Videos 10 and 11)

Key echo feature: only one AV valve present (left)

	PLAX	PSAX	A4/5C	SC	SS
Absent tricuspid valve (echogenic band)			X	X	
No flow through tricuspid valve			X		
Some degree of RV hypoplasia	X		X	X	
PFO with right to left shunt				X	
Associated with VSD, pulmonary stenosis/atresia, transposed great vessels depending on subtype	X	X	X	X	

3. The Tachypneic Neonate (Respiratory Symptoms)

Tachypnea is usually due to pulmonary edema secondary to increased pulmonary blood flow as pulmonary vascular resistance decreases after birth. The main clinical signs of increased pulmo-

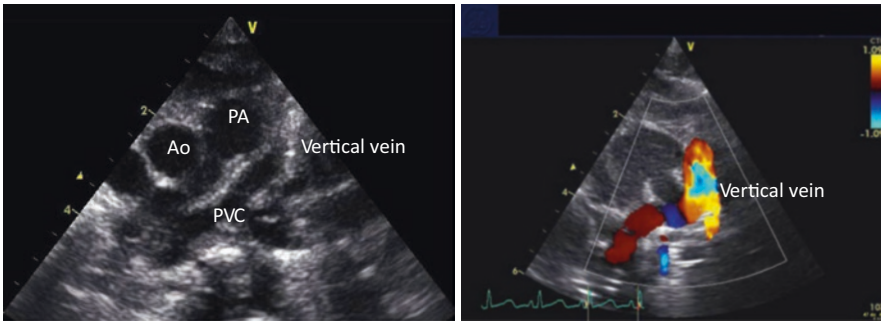


Fig. 24 High left parasternal: Pulmonary vein collector (PVC) and vertical vein (red flow, right-sided picture)

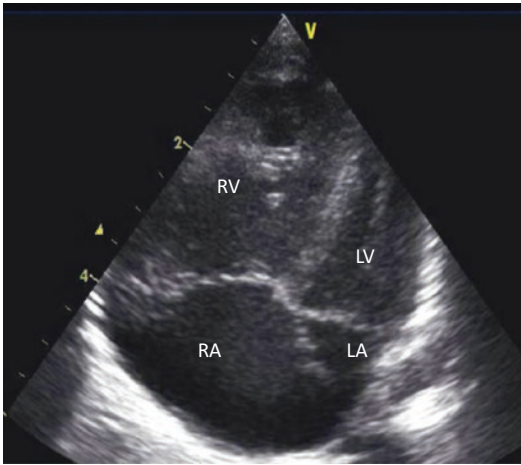


Fig. 25 4C: small LA, dilated RA and RV

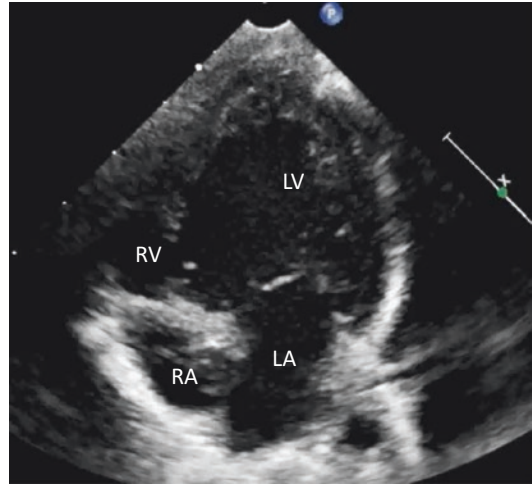


Fig. 26 4C: Echogenic band at place of tricuspid valve, hypoplastic RV

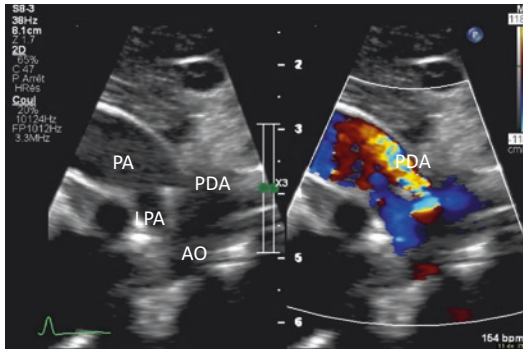
nary blood flow are tachypnea, increased work of breathing or respiratory distress. Respiratory distress can also be due to elevated pulmonary venous pressures or pulmonary venous congestion [21].

Main Cardiac Lesions

- Truncus arteriosus (cf above)
- Patent ductus arteriosus in premature infants
- Large ventricular septal defects
- Atrio-ventricular septal defects (AVSD)
- Total anomalous pulmonary venous return with obstruction - pulmonary blood flow is not increased in this lesion but obstruction leads to deranged pulmonary venous return and pulmonary venous congestion

Patent Ductus Arteriosus (Figs. 27 and 28; Video 12)

	PLAX	PSAX	A4/5C	SC	SS
Flow from descending aorta to pulmonary artery		X			X
Dilated LA/LV	X		X		
Retrograde flow in descending aorta					X
Retrograde flow in abdominal aorta				X	



Ventricular Septal Defect (Figs. 29, 30, 31, and 32; Videos 13 and 14)

	PLAX	PSAX	A4/5C	SC	SS
Echolucent space in interventricular septum	X	X	X	X	
Left to right systolic flow through VSD	X	X	X	X	
Dilated LA/LV	X		X		

Fig. 27 PSAX: PDA is seen connecting the PA and the descending aorta

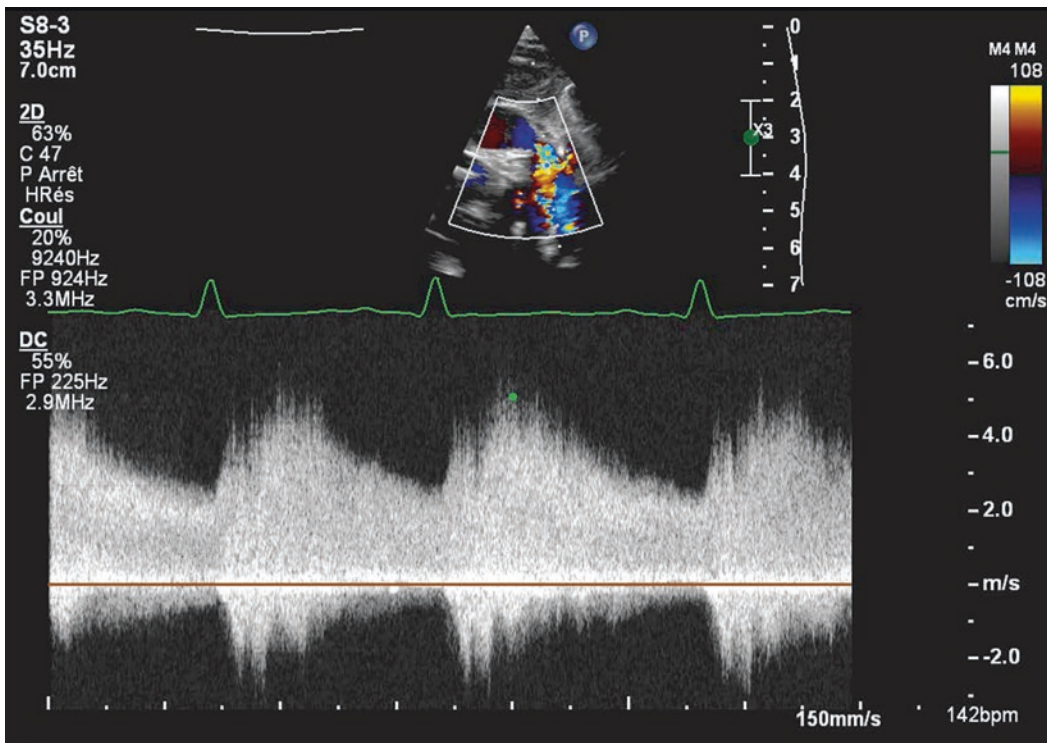


Fig. 28 Doppler high velocity left to right shunt (5 m/s) through the PDA, allowing to estimate a systolic pressure gradient of 100 mmHg (Bernoulli = $4 \times V^2$) between aorta and PA (restrictive PDA)

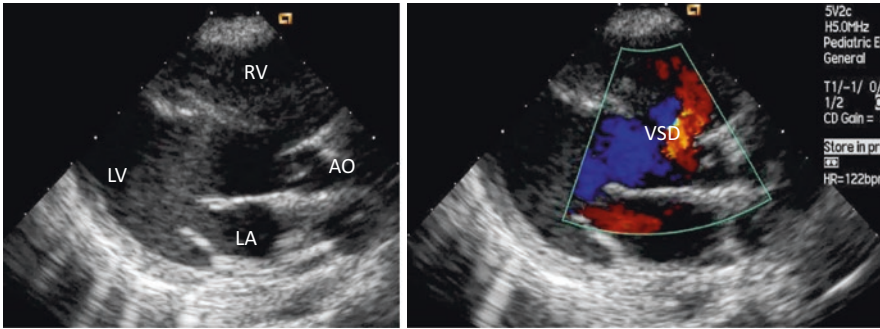


Fig. 29 PLAX: Echolucent space between the two ventricles = perimembranous VSD with low velocity left to right shunt

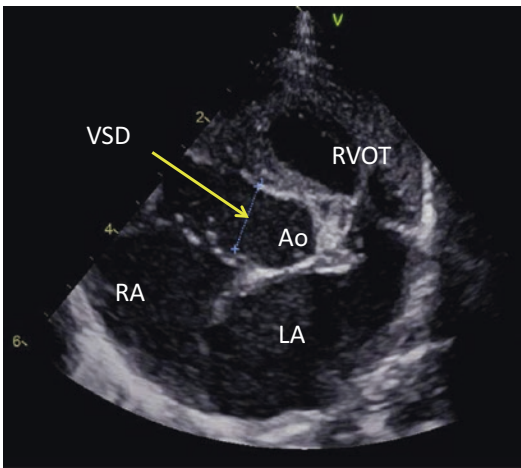


Fig. 30 PSAX: Echolucent space in the sub-aortic inter-ventricular septum

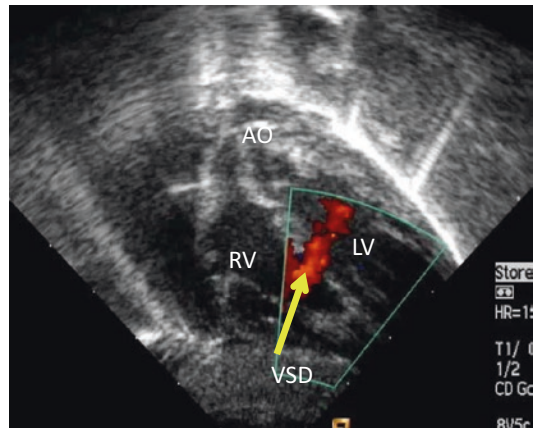


Fig. 32 Subcostal: left to right flow through muscular VSD

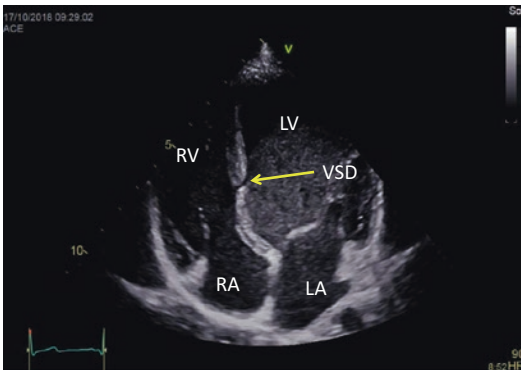


Fig. 31 4C: echolucent space in the muscular interventricular septum (arrow) = trabecular VSD with dilated LV

Atrial Septal Defect (Figs. 33 and 34; Videos 15 and 16)

	PLAX	PSAX	A4/5C	SC	SS
Echolucent space in secundum interatrial septum		X	X	X	
Left to right flow through VSD and ASD		X	X	X	
Aliasing of flow through pulmonary valve (PV)		X		X	
Dilated RV and RA	X	X	X	X	

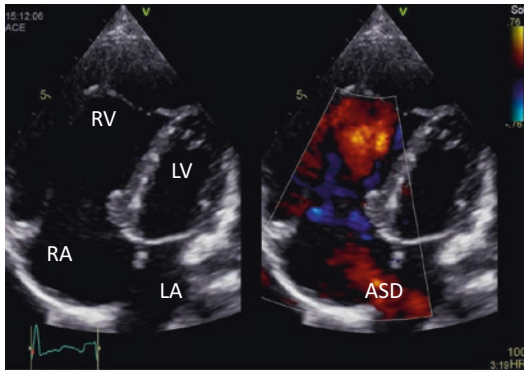


Fig. 33 4C: echolucent space in the interatrial septum with left to right shunt, dilated RA and RV

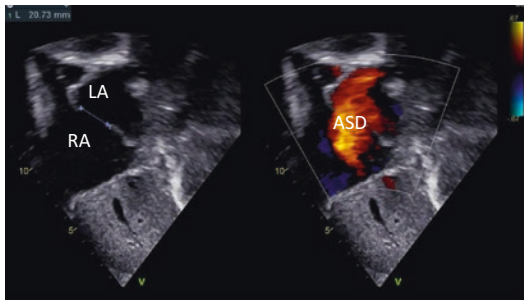


Fig. 34 Subcostal: left to right shunt through atrial septal defect (ASD)

Atrioventricular Septal Defect (Fig. 35; Video 17)

Key echo feature: crux of the heart defect

	PLAX	PSAX	A4/5C	SC	SS
Echolucent space in inlet interventricular septum		X	X	X	
Common atrioventricular valve	X	X	X	X	
Echolucent space in primum interatrial septum		X	X	X	
Left to right flow through VSD and ASD		X	X	X	
Dilated left and right heart chambers	X	X	X	X	
Atrioventricular valve regurgitation frequent	X	X	X	X	

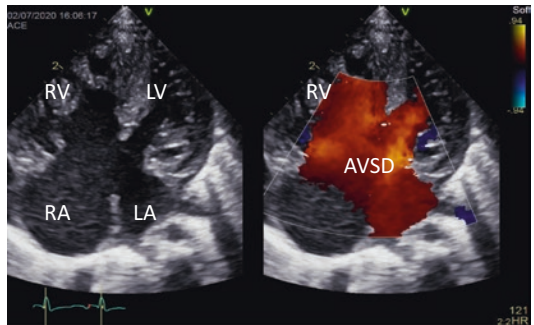


Fig. 35 4C: Echolucent space in primum atrial septum and inlet ventricular septum (AVSD: defect of the crux of the heart) with common atrioventricular valve

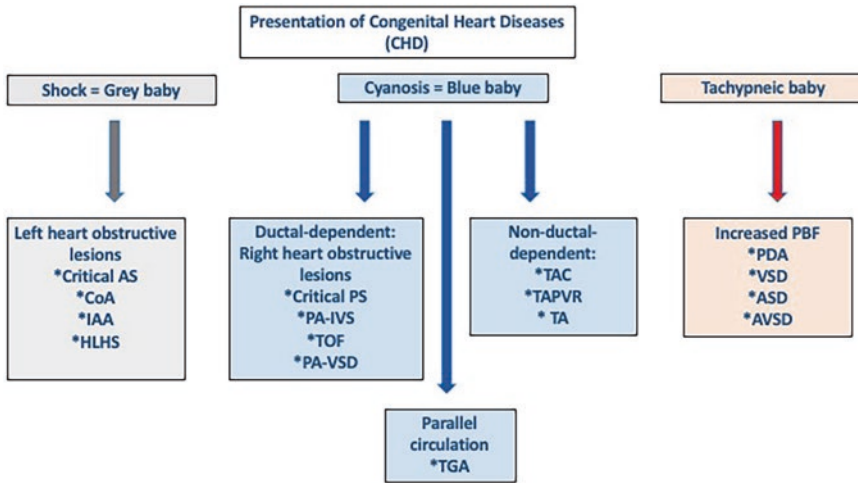


Fig. 36 Clinical presentation of congenital Heart Diseases (CHD), some CHD may show overlapping between the different categories. Abbreviations: AS: aortic stenosis; ASD: atrial septal defect; AVSD: atrio-ventricular septal defect; CoA: coarctation of the aorta; HLHS: hypoplastic left heart syndrome; IAA: interrupted aortic arch PA-IVS: pulmonary atresia intact ventricular septum;

PA-VSD: pulmonary atresia with ventricular septal defect; PBF: pulmonar blood flow; PDA: patent ductus arteriosus; PS: pulmonry stenosis; TA: tricuspid atresia TAC: truncus arteriosus (common arterial trunk); TAPVR: total anomalous pulmonary venous return; TGA: transposition of the great arteries; TOP: Tetralogy of Fallot; VSD: ventricular septal defect

Conclusion

In well-trained hands, echocardiography is a great tool allowing the detection and diagnosis of almost all congenital heart defects. Early recognition of critical CHD may be lifesaving, especially for ductal-dependent lesions or for those when adequate mixing between the pulmonary and systemic circulation is crucial for survival. Some of these infants with inadequate central mixing of blood may need urgent atrial septostomy. A simple classification of critical CHDs based upon their clinical presentation is summarized in Fig. 36 above. When such lesions are encountered, prompt treatment should be initiated but for any newborn with suspected CHD, pediatric cardiology referral is mandatory in order to make the best medical and surgical therapeutic plan for the child.

References

- Hoffman JL, Kaplan S. The incidence of congenital heart disease. *J Am Coll Cardiol.* 2002;39(12):1890–900.
- Reller MD, Strickland MJ, Riehle-Colarusso T, Mahle WT, Correa A. Prevalence of congenital heart defects in Atlanta, 1998-2005. *J Pediatr.* 2008;153:807–13.
- Wu W, He J, Shao X. Incidence and mortality trend of congenital heart disease at the global, regional, and national level, 1990-2017. *Medicine (Baltimore).* 2020;99(23):e20593.
- Sable C. Global, regional, and national burden of congenital heart disease, 1990–2017: a systematic analysis for the global burden of disease study 2017. *Lancet Child Adolesc Health.* 2020;4:185–200.
- Kloesel B, DiNardo JA, Body SC. Cardiac embryology and molecular mechanisms of congenital heart disease—a primer for anesthesiologists. *Anesth Analg.* 2016;123(3):551–69.
- Shiraishi I. Basic and comprehensive outlines of cardiovascular embryology and morphogenesis. *J Pediatr Cardiol Cardiac Surg.* 2020;4(2):63–74.

7. Bruneau BG. The developmental genetics of congenital heart disease. *Nature*. 2008;451:943–8.
8. Arvind B, Saxena A. Timing of interventions in infants and children with congenital heart defects. *Indian J Pediatr*. 2020;87:289–94.
9. Maude E. Atlas of congenital cardiac disease. Abbot, ed 2006.
10. Oster ME, Lee KA, Honein MA, Riehle-Colarusso T, Shin M, Correa A. Temporal trends in survival among infants with critical congenital heart defects. *Pediatrics*. 2013;131(5):e1502–8. <https://doi.org/10.1542/peds.2012-3435>. Epub 2013 Apr 22. PMID: 23610203; PMCID: PMC4471949.
11. Altman CA. Identifying newborns with critical congenital heart disease. Uptodate. 2016.
12. Mertens L, Seri I, Marek J, et al. Targeted neonatal echocardiography in the neonatal intensive care unit: practice guidelines and recommendations for training. *J Am Soc Echocardiogr*. 2011;24:1057–78.
13. De Boode WP, Singh A, Gupta S et al. Recommendations for neonatologist performed echocardiography in Europe: consensus statement endorsed by European Society for Paediatric Research(ESPR) and European Society for Neonatology (ESN). *Pediatric Research*.
14. Sekarski N, Tissot C, Muehlethaler V et al. Ausbildung in targeted neonatal echocardiography in der Schweiz. *Paediatrica*. 2017;28(4).
15. Tissot C, Muehlethaler V, Sekarski N. Basics of functional echocardiography in children and neonates. *Front Pediatr*. 2017;5:235.
16. Tissot C, Singh Y, Sekarski N. Echocardiographic evaluation of ventricular function—for the neonatologist and pediatric intensivist. *Front Pediatr*. 2017;6:79.
17. Lai WW, Geva T, Shirali GS, et al. Guidelines and standards for performance of a pediatric echocardiogram: a report from the task force of the pediatric council of the American Society of Echocardiography. *J Am Soc Echocardiogr*. 2006;19:4013–30.
18. Singh Y, Katheria AC, Vora F. Advances in diagnosis and management of hemodynamic instability in neonatal shock. *Front Pediatr*. 2018;(6):2.
19. Eichewald E. Uptodate 2021. www.uptodate.com.
20. Pammi M, Airas-Shah AM. *BMJ Best Practice*. 2021.
21. Silberbach M, Hannon D. Presentation of congenital heart disease in the neonate and young infant. *Pediatr Rev*. 2007;28(4):121–31.

Part III

Thoracic Assessment



Basic Lung Ultrasound for the Intensivist

Adam S. Himebauch and Akira Nishisaki

Contents

Introduction	133
Anatomic Considerations	134
Ultrasound Transducer Selection, Orientation, and Performance	135
Lung Sliding	136
Common Ultrasound Artifacts	136
Evaluation for Pleural Effusion	137
Evaluation for Pneumothorax	137
Differential Diagnosis of B-Lines	138
Evaluation of Consolidated or Atelectatic Lung	139
Summary	139
References	140

Supplementary Information The online version contains supplementary material available at https://doi.org/10.1007/978-3-031-26538-9_10.

A. S. Himebauch (✉) · A. Nishisaki
Department of Anesthesiology and Critical Care
Medicine, Perelman School of Medicine at the
University of Pennsylvania, The Children's Hospital
of Philadelphia, Philadelphia, PA, USA
e-mail: himebaucha@chop.edu; nishisaki@chop.edu

Introduction

Point-of-care ultrasound (POCUS) is a fundamental tool for the assessment of the lungs and thoracic cavity in critically ill neonatal and pediatric patients. Visualization and interpretation of pathology are largely dependent on the generation and recognition of ultrasound artifacts. Lung ultrasound is extremely helpful in acute situations such as shock and respiratory failure (Table 1). International evidence-based recommendations for POCUS in critically ill neonates and children included 11 consensus

Table 1 Essential diagnostic and therapeutic applications of lung and thoracic ultrasound

Diagnostic applications	Therapeutic applications
Evaluation for pneumothorax	Guidance for thoracentesis
Clarification of radiograph findings	Guidance for thoracostomy tube placement
Qualitative evaluation of pleural effusion	Confirming location of chest tube
Aid in differential diagnosis of lung pathology	
Aid in differential diagnosis of undifferentiated shock	
Adjunct for detection of mainstem intubation	

recommendations for lung POCUS [1]. The goals of this chapter are to discuss methods of POCUS interrogation of the thoracic cavity, describe how ultrasound artifacts play important roles in the assessment of lung pathophysiology, describe how to differentiate pleural effusions from atelectatic or consolidated lung, describe the assessment for a pneumothorax, discuss how to avoid common interpretation pitfalls, and to review relevant ultrasound scientific literature.

Anatomic Considerations

It is important to understand how different anatomical structures of the chest wall can affect ultrasound wave transduction. As reviewed in the earlier chapter on physics of ultrasound (Chap. 2), the interface between different tissue densities contributes to the quality and characteristics of the displayed ultrasound image (i.e., impedance mismatch). Subcutaneous fat and tissue are usually a good medium for the transduction of waves. Conversely, air is a poor medium for transduction resulting in an impedance mismatch at its interface with the soft tissue whereby ultrasound waves are reflected. This is not only an important consideration when identifying the pleural line

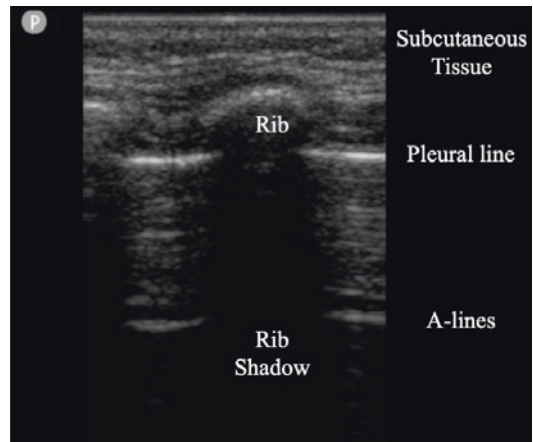


Fig. 1 The linear probe indicator is located on the upper left portion of this image and denotes the cranial direction. The pleural line is hyperechoic line and is located just deep to adjacent ribs. The rib shadow and A-line artifacts are demonstrated

(the soft tissue/air interface in healthy children), but also in disease processes resulting in the presence of subcutaneous air. Ultrasound waves reflected by impedance mismatch will not be transmitted to deeper structures. Therefore, caution must be taken during the interpretation of any ultrasound imaging when subcutaneous air is suspected (e.g., status asthmaticus with air leak).

Ribs are highly reflective and have poor ultrasound wave transduction. This creates shadowing that can inhibit the imaging of deeper structures in the thoracic cavity (Fig. 1). For neonates, infants, and patients with poor bone mineralization, rib shadowing may be minimal and a pleural line may be visualized below the unossified ribs (Fig. 2). The parietal and visceral pleura are both highly reflective and transduce ultrasound waves to deeper air-filled lung tissue. They are arguably the most important structures to visualize and interpret for many applications of lung and thoracic POCUS. The ultrasound artifacts generated by the parietal and visceral pleura and their relationship to the underlying contents within the thoracic cavity are used to identify lung pathology.

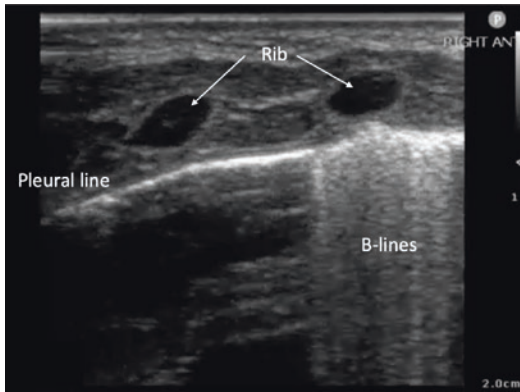


Fig. 2 Linear probe 2D ultrasound image for thoracic imaging in an infant identifies minimal rib shadowing because of immature bones with less calcification. Coalescent B-lines are also demonstrated

Ultrasound Transducer Selection, Orientation, and Performance

For neonatal and pediatric patients, most of the pulmonary disease processes extend to the surfaces of the lung or involve the pleura. This, along with the size of patients, contributes to the decision of which type of ultrasound probe to choose for imaging the lung and thoracic cavity. Higher frequency linear probes allow for a detailed examination of the superficial structures and pleura as well as higher axial and lateral resolution which may be helpful for procedural applications. However, especially for small children, rib interference can be a problem. For larger children and adolescents, phased array (i.e., cardiac) or curvilinear (i.e., abdominal) probes can also be used. These lower frequency probes allow for greater penetration resulting in improved visualization in patients with thicker chest walls or if imaging the lung and thoracic cavity from a subcostal view. Lower frequency probes also allow for imaging extension into the cardiac or abdominal fields during acute resuscitations.

Patients are often supine in the neonatal, cardiac, or pediatric intensive care unit but providers should attempt to completely evaluate each hemithorax, including the posterior regions, for the presence of pathology. By convention, the transducer should initially be placed in the longitudinal

or long-axis plane and perpendicular to the skin with the probe indicator cranial in orientation. This is a systematic evaluation and practitioners advocate for dividing the thoracic cavity into segments or lines. Various neonatal, pediatric, and adult emergency and critical care protocols are published [2–4]. For a complete ultrasound evaluation, the evaluator should include, at a minimum, both anterior and lateral views of both lungs. Clinicians should record or clip dynamic processes while moving the probe from the apex to the base of the lung. If there are difficulties with visualization between ribs or if there is a desire to focus on one part of the thoracic cavity, a short-axis (i.e., horizontal) view can supplement the initial long-axis evaluation. Lung and thoracic cavity ultrasound imaging can also be evaluated from subcostal and abdominal views (Fig. 3).

Patterns and generation of artifacts are often dependent on imaging of the pleural line (Figs. 1 and 2). For this reason, the angle of insonation and gain should be adjusted to optimize the brightness and visualization of the pleural line and any imaging smoothing algorithms should be turned off. Practically, “air rises” and “fluid falls” so dedicated and focused imaging based on the clinical scenario should also drive the imaging priorities and views. As will be discussed further, both two-dimensional (2D) B-mode and M-mode can be utilized.



Fig. 3 Abdominal and subcostal views using a phased array or curvilinear probe may also be used to image the lung and thoracic cavity. In this example, the right upper quadrant abdominal view using a phased array probe identified a small, simple hypoechoic right-sided pleural effusion

Lung Sliding

Lung sliding is a normal finding during lung POCUS with 2D B-mode ultrasound. It is the result of the movement of the parietal and visceral pleura against one another that coincides with the respiratory cycle (Video 1). It is important to remember that the presence of lung sliding RULES OUT a pneumothorax in the area of the visualized lung. The absence of lung sliding is less useful as there are many causes, including pneumothorax, bronchial occlusion (mucus plug, mainstem intubation), severe pneumonia or during acute respiratory distress syndrome, and the presence of pleural adhesions or prior pleurodesis. A related imaging finding is an M-mode pattern known as the “Seashore sign” (Fig. 4). The pleural line is identified (“the shore-line”). Superficial structures should be motionless (as long as the patient is not moving) and have a pattern of a series of horizontal hyperechoic and hypoechoic lines (“the waves”). Motion of the visceral and parietal pleura is inferred by the structures deep to the pleural line appearing granular (“the sand”). This pattern RULES OUT pneumothorax in the area underlying the ultrasound probe.

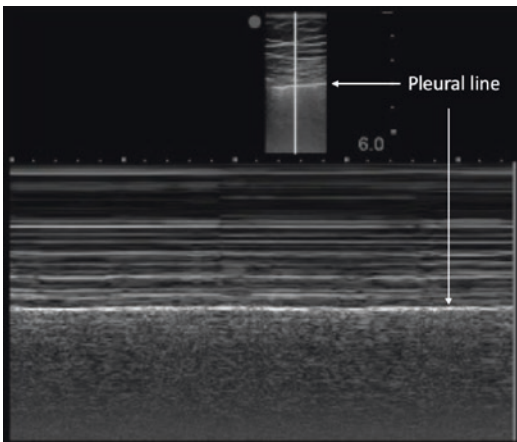


Fig. 4 Linear probe M-mode ultrasound image demonstrating the “Seashore sign” (lower image). The upper image is the corresponding 2D ultrasound view

Common Ultrasound Artifacts

A-lines are reverberation artifacts visualized deep to the pleural line that result from the reflection of ultrasound waves between the parietal pleura and intrathoracic air [5]. A-lines can be readily recognized as horizontal in orientation, linear, and the distance between lines is the same as the distance between the chest wall and pleural line (Fig. 1). A-lines require air deep into the parietal pleura. They are therefore visible in both normal lungs as well as if there is a pneumothorax, but they are not visible in the presence of pleural effusions or consolidated lung (thoracic pathologies characterized by tissue or fluid below the pleural line allowing for ultrasound wave transduction).

B-lines are also reverberation artifacts that result from the reflection of ultrasound waves due to air/water interfaces present in consolidated or atelectatic lungs [5–7]. B-lines originate at the pleural line, extend vertically into the ultrasound field, are synchronous with lung sliding, and obscure A-lines (Figs. 2, 5, and 6) (Video 2). As these artifacts require apposition of the visceral and parietal pleura, their presence RULES OUT a pneumothorax in the area underlying the ultra-

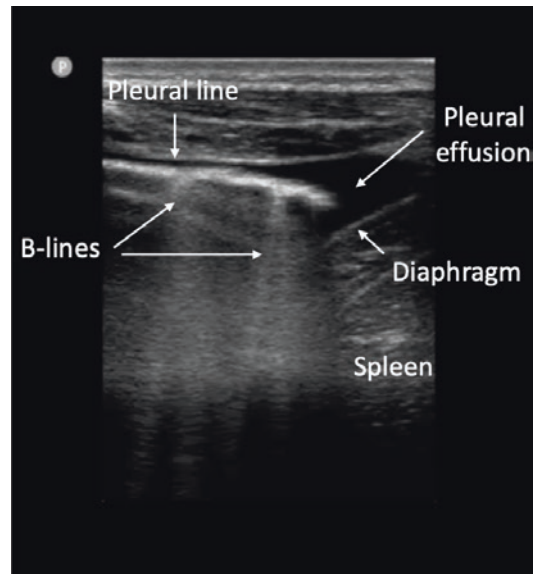


Fig. 5 Linear probe 2D ultrasound image at the costophrenic angle demonstrates a few scattered B-lines in the left lower lung and a small, simple hypoechoic pleural effusion

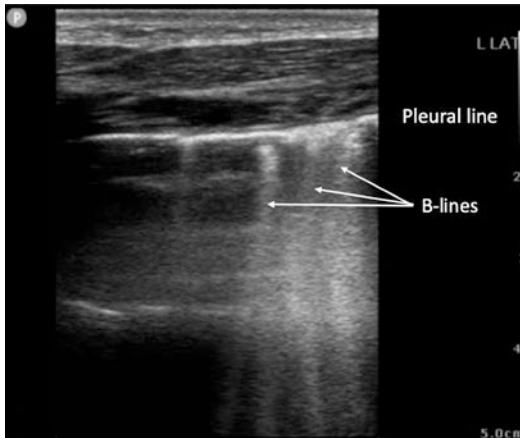


Fig. 6 Linear probe 2D ultrasound image demonstrating B-lines

sound probe. Although a few scattered B-lines can be found in the dependent areas of the lung in otherwise healthy persons, they are generally considered pathologic. The differential diagnosis of B-lines is broad and further discussion is provided in later sections of this chapter and other chapters (Chaps. 12–13) of this book.

Z-lines are artifacts that are also vertical in orientation and originate from the pleural line. They can be differentiated from B-lines as they extend only a short distance into the viewing field deep to the pleural line and have no known associated pathologic conditions. Similar to B-lines, Z-lines should also be synchronous with lung sliding. As with B-lines, the presence of Z-lines also RULES OUT a pneumothorax in the area underneath the ultrasound probe.

Evaluation for Pleural Effusion

Lung ultrasound in the intensive care setting has the capability to characterize equivocal findings within plain chest radiographs. Pleural effusions are easily recognized as hypoechoic areas that separate the visceral and parietal pleura. It is not possible to accurately quantify the volume of pleural fluid by ultrasound therefore we rely on discrete qualitative designations such as small, moderate, or large.

Both the appearance and location of pleural fluid should be characterized. When visualizing a

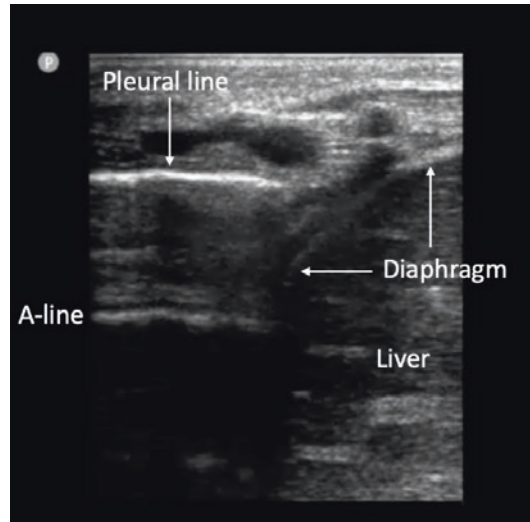


Fig. 7 For the detection of pleural effusions and to help differentiate fluid that may be in the peritoneal cavity versus the pleural cavity, it is important to demonstrate anatomic boundaries, including the diaphragm, chest wall, and lung. This figure demonstrates these boundaries when a pleural effusion or peritoneal fluid is not present. (See Fig. 5 for demonstration of the same structures with a small pleural effusion)

pleural effusion, it is very important to first identify the anatomic boundaries of the diaphragm, chest wall, and lung to accurately differentiate pleural effusion from ascites (Fig. 7). Simple effusions are hypoechoic (black) in appearance and are best detected at dependent areas of the thoracic cavity (Figs. 3 and 5). Complex effusions are heteroechoic; septations and fibrin strands may be visible, and swirling debris may be noted that is agitated by cardiac or respiratory motion (Video 3). Pleural effusions can easily be recognized from subcostal, subxiphoid, and abdominal views (Fig. 3). As discussed in later chapters, ultrasound has a clear role in improving the safety of thoracic procedures (including thoracentesis and chest tube placement) by identifying the superior diaphragm border to localize optimal insertion sites.

Evaluation for Pneumothorax

A very important and practical application of lung ultrasound is the acute assessment of a pneumothorax. Lung ultrasound has been shown

to be faster and more accurate for the detection of pneumothorax in neonatal, pediatric, and adult populations [8–12]. The visualization of lung sliding, B-lines, Z-lines, and a lung pulse all **RULE OUT** a pneumothorax within the ultrasound-interrogated region of the chest. Lung pulse is most often seen in the setting of left-sided lung atelectasis and can be recognized as the rhythmic pulsation of the lung in synchrony with the heartbeat that is transmitted through the lung parenchyma to the pleural surface. Lung sliding, B-lines, Z-lines, and a lung pulse all require apposition of the visceral and parietal pleura for visualization. Given the many possible reasons for losing lung sliding, B-lines or Z-lines, the absence of lung sliding, B-lines, or Z-lines are highly sensitive but not specific to pneumothorax [13].

Alternatively, the lung point is an ultrasound finding that is specific (**RULE IN**) for pneumothorax in the right clinical scenario. A lung point can be visualized in 2D B-mode at the point of transition between the presence of lung sliding (with apposed visceral and parietal pleura) and absence of lung sliding (where air is located between the visceral and parietal pleura) (Video 4). In 2D M-mode, visualization of the “barcode,” also known as “stratosphere” sign can help to detect pneumothorax. If there is no movement below the pleural line, the appearance of the M-mode image is horizontal hyperechoic and hypoechoic lines above AND below the pleural line (Fig. 8).

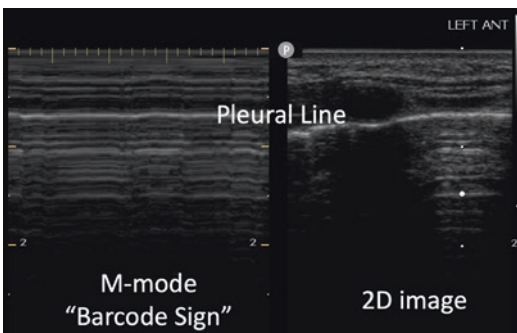


Fig. 8 Linear probe M-mode ultrasound image (left) demonstrating the “barcode sign,” which is suggestive of a pneumothorax located in the area under the ultrasound probe. The corresponding 2D ultrasound image is shown on the right side

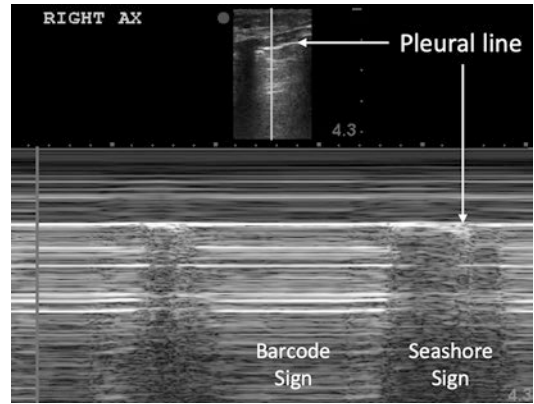


Fig. 9 Linear probe M-mode ultrasound image at the site of a lung point, which is very specific sign for pneumothorax in the area under the ultrasound probe. In this image, there is intermittent “Seashore sign” and “Barcode sign” as the lung point comes in and out of the plane of the M-mode

M-mode can also visualize a lung point as alternating “barcode” and “seashore” signs under the ultrasound probe (Fig. 9). While a lung point is very specific for identifying a pneumothorax, in a rare situation it can also be visualized in other pathologic conditions such as pulmonary blebs [14]. Importantly, the lung point is typically not identified in patients with a large pneumothorax because the transition point between pneumothorax and normally apposed pleura often does not exist (i.e., sensitivity of lung points for diagnosing pneumothorax is low). In a practical sense, when the clinical suspicion is high for pneumothorax, and lung sliding and B- or Z-lines are not present on POCUS, clinical intervention should be made to evacuate the pneumothorax without spending additional time to look for lung points.

Differential Diagnosis of B-Lines

As noted previously in this chapter, the differential diagnosis of B-lines is wide and requires clinical data for accurate interpretation. The presence of scattered B-lines can occur in neonates and in otherwise healthy lungs in children, particularly in dependent regions. During the ultrasound evaluation of lungs, the sonographer needs to interpret both the density and location of B-lines.

Coalescent B-lines, defined as multiple B-lines “fused” together, can be seen in many neonatal, pediatric, and adult disease states, including cardiogenic pulmonary edema, non-cardiogenic pulmonary edema, viral pneumonia or bronchiolitis, transient tachypnea of the newborn, respiratory distress syndrome, interstitial lung disease, acute respiratory distress syndrome, and chronic lung disease (Fig. 2). Focal B-lines can be seen in pathologies including atelectasis, lobar pneumonia, pulmonary contusions, pulmonary infarcts from pulmonary emboli, and, though rare in pediatrics, associated with lung masses [1, 5, 7].

Adult emergency medicine and critical care literature describe protocols and algorithms using B-line patterns to help differentiate cardiogenic pulmonary edema from other causes of dyspnea, sometimes in combination with a multimodal POCUS assessment [15–19]. Similarly, while algorithms have been published for neonatal and pediatric populations, [20] they are currently not as well developed or tested but the experience is increasing. This is particularly the case in neonatal lung ultrasound and is discussed more extensively in Chap. 13.

Evaluation of Consolidated or Atelectatic Lung

The appearance of consolidated or atelectatic areas of lung result from various densities of air, fluid, and lung tissue. Dynamic or static air bronchograms are often visualized and the lung itself may have a similar sonographic appearance to the liver (so-called hepatization of the lung). Dynamic air bronchograms are highly specific for pneumonia and are identified by hyperechoic and often linear structures that have a “sparkly” appearance during the respiratory cycle [21, 22]. Alternatively, static air bronchograms do not have a variable appearance with the respiratory cycle (i.e., indicating no airway flow in small bronchial branches) and can indicate either atelectasis or pneumonia.

Lung consolidations are easily detected by POCUS and have proven more sensitive than chest radiograph in the diagnosis of pneumonia

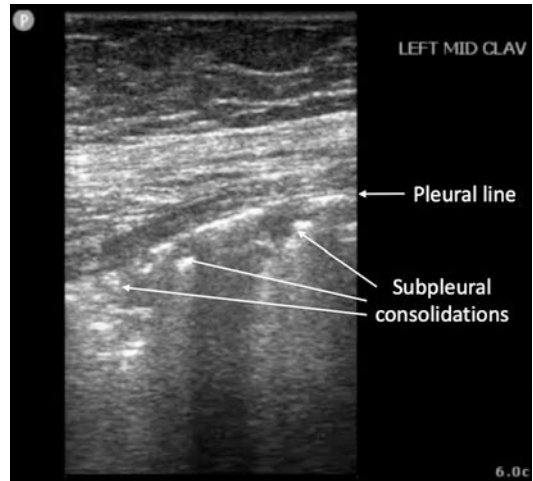


Fig. 10 Linear probe 2D ultrasound image demonstrating subpleural consolidations

in the Emergency Department setting, especially when a consolidation with a diameter <10 mm is identified [23]. While the diagnosis of pneumonia using POCUS is more sensitive than chest radiograph, antibiotic treatment of pneumonia only detectable by lung POCUS remains controversial. Subpleural consolidations can appear as small (i.e., less than 5 mm), irregular hypoechoic structures that are adjacent to the pleura (Fig. 10). These can be seen in a variety of neonatal and pediatric diseases, including meconium aspiration syndrome, bronchiolitis, chronic lung disease of prematurity, and areas of infarction associated with pulmonary emboli.

Summary

The performance and interpretation of lung and thoracic ultrasound are increasingly important skills for the practitioner who cares for critically ill and injured neonates and children. Being systematic in the assessment, learning how to identify and visualize important anatomic boundaries, knowing how to interpret ultrasound artifacts, developing pattern recognition of different pathologic processes, and knowing the limitations of the techniques will allow for successful incorporation into clinical practice.

References

1. Singh Y, Tissot C, Fraga MV, et al. International evidence-based guidelines on point of care ultrasound (POCUS) for critically ill neonates and children issued by the POCUS working group of the European Society of Paediatric and Neonatal Intensive Care (ESPNIC). *Crit Care*. 2020;24:65.
2. Tsung JW, Kessler DO, Shah VP. Prospective application of clinician-performed lung ultrasonography during the 2009 H1N1 influenza A pandemic: distinguishing viral from bacterial pneumonia. *Crit Ultrasound J*. 2012;4(1):16.
3. Volpicelli G, Mussa A, Garafalo G, et al. Bedside lung ultrasound in the assessment of alveolar-interstitial syndrome. *Am J Emerg Med*. 2006;24:689–96.
4. Brat R, Yousef N, Klifa R, et al. Lung ultrasonography score to evaluate oxygenation and surfactant need in neonates with continuous positive airway pressure. *JAMA Pediatr*. 2015;169(8):e151797.
5. Lichtenstein DA, Meziere GA, Lagoueyte JF, et al. A-lines and B-lines: lung ultrasound as a bedside tool for predicting pulmonary artery occlusion pressure in the critically ill. *Chest*. 2009;136:1014–20.
6. Volpicelli G, Elbarbary M, Blaivas M, et al. International evidence-based recommendations for point-of-care lung ultrasound. *Intensive Care Med*. 2012;38:577–91.
7. Dietrich CF, Mathis G, Blaivas M, et al. B-lines artefacts and their use. *J Thorac Dis*. 2016;8:1356–65.
8. Blaivas M, Lyon M, Duggal S. A prospective comparison of supine chest radiography and bedside ultrasound for the diagnosis of traumatic pneumothorax. *Acad Emerg Med*. 2005;12:844–9.
9. Soldati G, Testa A, Sher S, et al. Occult traumatic pneumothorax: diagnostic accuracy of lung ultrasonography in the emergency department. *Chest*. 2008;133:204–2011.
10. Zhang M, Liu ZH, Yang JX, et al. Rapid detection of pneumothorax by ultrasonography in patients with multiple trauma. *Crit Care*. 2006;10:R112.
11. Raimondi F, Fanjul JR, Aversa S, et al. Lung ultrasound for diagnosing pneumothorax in the critically ill neonate. *J Pediatr*. 2016;175:74–8.
12. Cattarossi L, Copetti R, Brusa G, Pintaldi S. Lung ultrasound diagnostic accuracy in neonatal pneumothorax. *Can Respir J*. 2016;2016:6515069.
13. Lichtenstein D, Mezière G, Biderman P, Gepner A. The comet-tail artifact: an ultrasound sign ruling out pneumothorax. *Intensive Care Med*. 1999;25:383–8.
14. Gelabert C, Nelson M. Bleb point: mimicker of pneumothorax in bullous lung disease. *West J Emerg Med*. 2015;16:447–9.
15. Lichtenstein DA, Mezière GA. Relevance of lung ultrasound in the diagnosis of acute respiratory failure: the BLUE protocol. *Chest*. 2008;134:117–25.
16. Zanobetti M, Scorpinti M, Gigli C, et al. Point-of-care ultrasound for the evaluation of acute dyspnea in the ED. *Chest*. 2017;151:1295–301.
17. Volpicelli G, Lamorte A, Tullio M, et al. Point-of-care multiorgan ultrasonography for the evaluation of undifferentiated hypotension in the emergency department. *Intensive Care Med*. 2013;39:1290–8.
18. Shokoohi H, Boniface KS, Pourmand A, et al. Bedside ultrasound reduces diagnostic uncertainty and guides resuscitation in patients with undifferentiated hypotension. *Crit Care Med*. 2015;43:2562–9.
19. Lichtenstein DA, Karakitsos D. Integrating lung ultrasound in the hemodynamic evaluation of circulatory failure (the fluid administration limited by lung sonography protocol). *J Crit Care*. 2012;27:e11–9.
20. Kurepa D, Zaghoul N, Watkins L, Liu J. Neonatal lung ultrasound exam guidelines. *J Perinatol*. 2018;38(1):11–22.
21. Lichtenstein D, Mezière GA, Seitz J. The dynamic air bronchogram: a lung ultrasound sign of alveolar consolidation ruling out atelectasis. *Chest*. 2009;135:1421–5.
22. Gillman LM, Panebianco N, Alkadi A, et al. The dynamic sonographic air bronchogram: a simple and immediate bedside diagnosis of alveolar consolidation in severe respiratory failure. *J Trauma*. 2011;70:760.
23. Jones BP, Tay ET, Elikashvili I, et al. Feasibility and safety of substituting lung ultrasonography for chest radiography when diagnosing pneumonia in children: a randomized controlled trial. *Chest*. 2016;150:131–8.



Airway Ultrasound

Erik Su and Bereketeab Haileselassie

Contents

Airway Ultrasound	141
Applications	141
Conclusion	146
References	146

Airway Ultrasound

Imaging of the airway is amenable to probes with linear or curvilinear faces to provide detailed imaging near the skin surface. Since the region of ultrasound interrogation is relatively superficial, high-frequency probes including linear or micro-convex curvilinear probes are preferred for this purpose. Musculoskeletal or small parts imaging settings with higher frequency presets permit high-resolution imaging of small throat structures and appropriate frame averaging smooths images and reduces noise. Given the importance of airway diagnosis, recording of imaging as a

part of the medical record is highly recommended.

Applications

Evaluation of Intubation

Measurement of Tracheal Diameter

In older pediatric populations through adulthood, direct visualization of the endotracheal tube has been described with the probe held transversely over the trachea inferior to the cricothyroid membrane [1–11]. In a study of 50 children with congenital scoliosis undergoing surgery [3], an ultrasound-based protocol demonstrated a strong correlation between predicted and required endotracheal tube (ETT) size confirmed by the presence of an appropriate leak. In patients with cervical scoliosis there was a moderate correlation, with ultrasound frequently overestimating tube size. The authors suggest this overestima-

E. Su (✉)

Division of Critical Care Medicine in the Department of Pediatrics, Baylor College of Medicine at Texas Children's Hospital, Houston, TX, USA
e-mail: erik.su@bcm.edu

B. Haileselassie

Division of Critical Care Medicine in the Department of Pediatrics, Stanford University School of Medicine, Palo Alto, CA, USA

tion occurs because the trachea appears ellipsoid in this view and measurements did not capture the smallest diameter of the trachea. A study of 152 children receiving adenotonsillar surgery demonstrated that airway ultrasound accurately determined ideal ETT size in 88% of patients, with 15 patients requiring larger and 3 requiring smaller tube diameters [1]. Evidence suggests practice is needed to develop a reliable technique of measurement as only 10 of 16 (62.5%) anesthesiology residents performing airway ultrasound were proficient in appropriately measuring tracheal diameter appropriately after 30 examinations [12]. With focused attention to training and skill development, this technique may benefit children with normal airway anatomy. In the setting of airway pathology such as subglottic stenosis, cephalad to caudal sweep of the airway is likely necessary to attain a complete assessment. However, there is limited data of the efficacy of this metric in patients with subglottic stenosis or other airway irregularities therefore no recommendation can be made for standardized evaluation.

To assess the airway, in a transverse view:

1. Visualize the trachea: normally the air artifact within the cylindrical trachea only permits a semicircular view of its anterior surface bounded by air behind it. The homogenous thyroid gland is visible surrounding the trachea, and the great vessels of the neck may also be seen (Fig. 1).
2. Angle the probe such that it is held slightly left of midline. This permits views of the esophagus, which appears as a collapsed ellipsoid in profile. Because the esophagus can be visualized in this profile, this view has been proposed as a method of assessing adequacy of cricoid pressure though further studies are necessary to demonstrate efficacy in children [13, 14].
3. From this view, it is potentially possible to monitor intubation. Changes during intubation can be subtle as the endotracheal tube, similar to the trachea, is an air-filled cylinder. Therefore, most authors who endorse this technique suggest that one visualizes the tra-

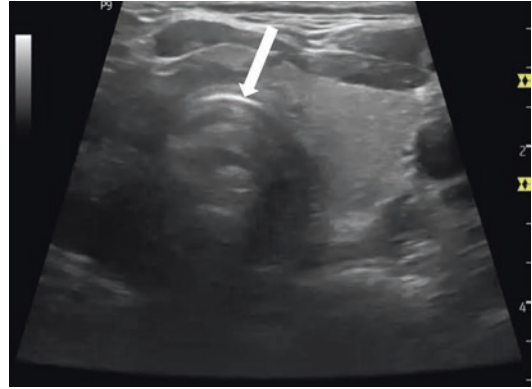


Fig. 1 Transverse trachea (arrow)

chea during the intubation process for confirming that the endotracheal tube is passing into the airway [15, 16]. A probe placed on the neck for monitoring during intubation can obviously confound applying and/or maintaining cricoid pressure during intubation.

Direct Visualization of Endotracheal Tube Cuff

After intubation, confirmation of tube placement depth has also been described where ultrasound imaging of the endotracheal tube cuff is confirmed at the suprasternal notch. This technique was first described by Tessaro et al. (compared to fiberoptic bronchoscope) and Uya et al. (compared to fluoroscopy) [17, 18]. To date, a study comparing ultrasound assessment of cuff position to chest radiography remains lacking and complications including malpositioned ETTs remaining above the glottis cannot be assessed using ultrasound. Identification of the ETT cuff in the suprasternal notch can be particularly challenging with air-filled cuffs due to obscuring effects of air, and therefore both studies cited used a saline-filled cuff in a perioperative setting. It is unclear whether longer dwelling endotracheal tube cuffs in the ICU require different considerations regarding saline injection.

Using this method:

1. Place the probe again transversely but at the level of the suprasternal notch.

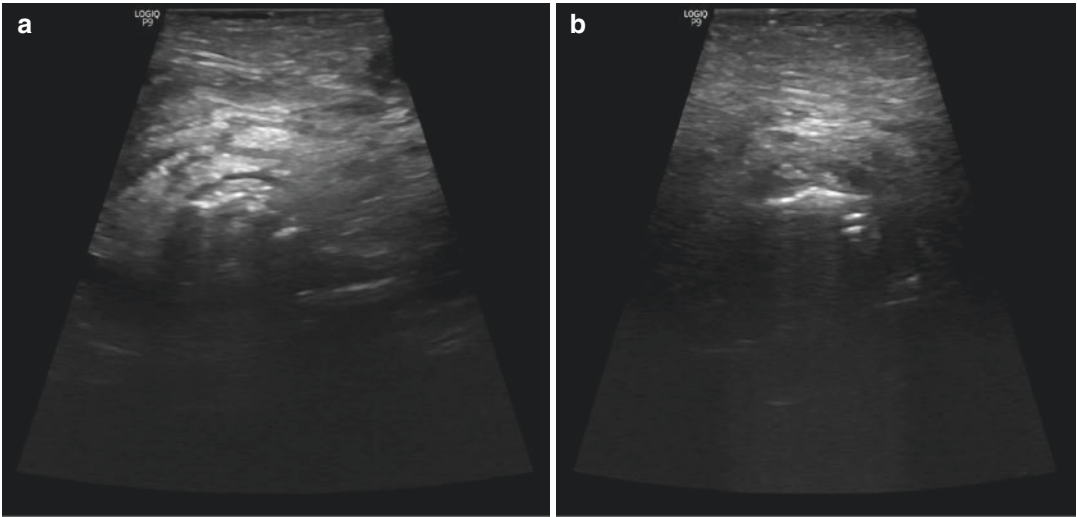


Fig. 2 (a) Transverse trachea, cuff up; note the rounded form of the anterior tracheal wall. (b) Transverse trachea, cuff down

- Inflation of the cuff is performed, and pre- and post-inflation images demonstrate a change in the diameter of the air shadow caused by the cuff. A common strategy to improve visualization of the cuff profile is to inflate the cuff with saline. Protocols regarding routine use of saline inflation in the ICU have not been described. Confirmation of cuff location at the notch is considered an appropriate position of the ETT (Fig. 2a and b).

Direct Visualization of Endotracheal Tube Tip

To varying degrees, endotracheal tubes can be visualized within the airway as they displace normal anatomy. In the neonatal population, visualization of the endotracheal tube has been described in a longitudinal orientation by placing a linear array probe over the length of the sternum and aligning it with the trachea. Slovis and colleagues described this in a series of 16 newborns where the endotracheal tube was identified in all patients with a good correlation between chest X-ray and ultrasound [19]. This method has been replicated by other authors [20–25].

In the method described by Dennington et al., a linear array transducer is placed sagittally along the length of the sternum, preferably with the probe indicator towards the patient's head.

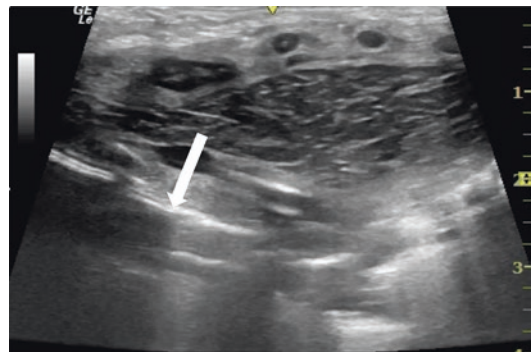


Fig. 3 Longitudinal view of endotracheal tube in a neonate; the tip of the tube is indicated by the arrow and can be identified by the shadowing artifact distal to the tube (right brace)

(Fig. 3; [26]) The beam is aimed to align with the endotracheal tube such that shadowing artifact caused by the tube can be used to determine the tube tip, optimally around 2 cm proximal to the right pulmonary artery seen in cross-section and used as a landmark approximating the level of the carina. Beyond the neonatal period, direct visualization of the endotracheal tube becomes more difficult due to air artifact, sternal ossification, and patient size. Therefore, this technique is practical in few patients and confounded by difficulties in conceptualizing the endotracheal tube only in terms of artifacts.

Diaphragmatic Ultrasound for Confirmation of Intubation

Intubation can also be indirectly assessed using diaphragmatic ultrasound. After intubation, providers can image the diaphragm from a transverse subxiphoid position with sufficient depth to visualize the spine and include interrogation of the anterior sagittal or lateral coronal planes (Fig. 4). Differential or lack of movement of diaphragm leaflets suggests mainstem intubation or failure to intubate the trachea. Ultrasound assessment of diaphragm movement has been explored by multiple authors in the pediatric population [27, 28]. In the PICU setting, efficacy has been demonstrated in a population of 59 children where all intubations were correctly identified as successful or not successful, including failed intubation and right mainstem intubation [27].

To perform this technique after attempted endotracheal intubation:

1. For the anterior subxiphoid approach, place a phased array or curvilinear probe below the xiphoid process and aim it cephalad at an approximately 45° angle to the skin to visualize the bright diaphragm leaflets. Gastric contents may obscure the view of the left hemidiaphragm (Fig. 4).
2. For a lateral coronal approach, the diaphragms can be visualized independently from the flanks of the patient at the level of thoracic ribs 10–12 with the probe oriented coronally and parallel to the spine. The imaging target is the bright arc of the hemidiaphragm on each side

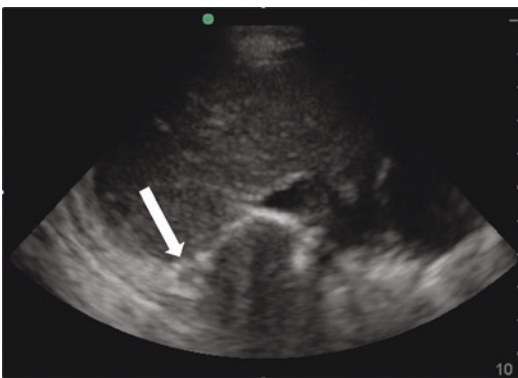


Fig. 4 Subcostal diaphragm view (arrow indicates right hemidiaphragm)

of the patient. A limitation to this approach is that both diaphragms cannot be viewed at the same time, though the image of the diaphragm architecture and movement will be clearer compared to the subxiphoid approach.

3. Alternatively, each hemidiaphragm can also be imaged in the anterior sagittal plane at the lower margin of the ribcage in line with the midclavicular line. This may be possible for patients where lateral views can be difficult due to patient habitus but is problematic when the stomach contains air or solids.
4. With manual bagging ventilation of the endotracheal tube, both diaphragm leaflets should move towards the ultrasound probe as the lungs inflate in the subcostal view or past the probe in the lateral or anterior views.
5. Preferential inflation of one side indicates possible mainstem intubation of that respective bronchus.
6. No movement suggests failure to intubate the trachea.

Though this technique cannot detect the position of the endotracheal tube tip, it can identify aeration of the lungs readily while keeping the ultrasound away from the neck in the event of a failed intubation when other manipulations may be required.

An alternative technique has also been described using a linear probe for identifying lung sliding in the aforementioned lateral coronal and anterior sagittal planes but higher in the chest [29]. Using the same manual ventilation technique, differential or absent movement may suggest mainstem or failed intubation, respectively.

Cricothyroid Imaging

In the sagittal plane, a linear ultrasound probe can be placed longitudinally over the larynx and trachea to identify the cricoid membrane for guidance of percutaneous or surgical cricothyroidotomy. This technique has been described by Walsh et al. successfully identifying the membrane on ultrasound in comparison to MRI, though a test of practicality is stymied by the rarity of the procedure and has not been described [30].

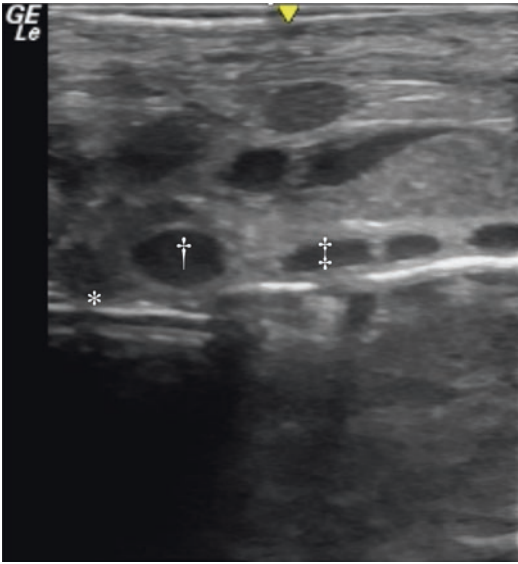


Fig. 5 Sagittal cricothyroid membrane view. * Cricothyroid membrane; † cricoid cartilage; ‡ first tracheal ring

To accomplish this:

1. Place the probe longitudinally over the thyroid cartilage and trachea. By convention the probe indicator goes towards the head. A variety of imaging presets can be used for this modality.
2. Elements of the upper airway can be identified longitudinally including the thyroid cartilage, the cricothyroid membrane, the cricoid cartilage, and the tracheal rings (Fig. 5).

Vocal Cord Imaging

Assessment of the vocal cords can be performed at the level of the cricothyroid membrane tilting the plane of the transducer cephalad for visualization. This technique has been reported by multiple authors as a reliable method of evaluating vocal cord dysfunction. Though primarily described in the patient who has received cardiac surgery in the vicinity of the aortic arch, it has also been mentioned in the evaluation of patients with primary thyroid malignancy as well as

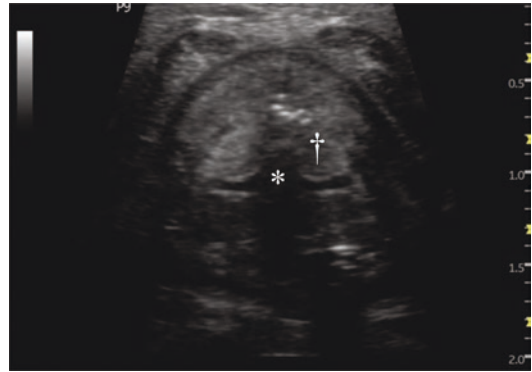


Fig. 6 Vocal fold imaging. * True vocal folds are in this anechoic area; † false focal folds

laryngeal trauma [31–36]. A recently published meta-analysis revealed a pooled sensitivity for laryngeal ultrasound in detecting vocal cord immobility of 91% (95% CI, 83–95%) and specificity of 97% (95% CI, 82–100%) across varied pediatric practice settings [37].

In imaging the vocal cords:

1. The transducer is oriented transversely and angled cephalad to visualize the true and false vocal cords at the level of apposition to minimize air interference.
2. From this vantage, the vocal folds and the arytenoid cartilages can be imaged. (Fig. 6).
3. Note that the angle of the probe to the skin may be shallow.

Evaluating the Difficult Airway

To date, a number of authors have published information on preintubation ultrasound assessments yielding measurements potentially predictive for difficult intubation. None of these have been readily translated to clinical practice in the neonatal and pediatric population. These methods identify a panel of assessments of anterior neck tissue thickness or distances from the chin to neck structures such as the hyoid bone. Further study is necessary to determine a practical set of measurements for ultrasound-based difficult airway assessment in infants and children.

Conclusion

Visualization of the airway is practical in point-of-care ultrasound and ultimately yields useful information for clinical care. It is gaining attention as a modality for evaluating airway procedures as well as airway pathology. As it is a relatively new area of interest in clinical ultrasound, airway ultrasound will continue to evolve with insights from promising emerging research and clinical application.

References

- Altun D, Orhan-Sungur M, Ali A, Özkan-Seyhan T, Sivriköz N, Çamcı E. The role of ultrasound in appropriate endotracheal tube size selection in pediatric patients. *Paediatr Anaesth.* 2017;27(10):1015–20. <https://doi.org/10.1111/pan.13220>. Epub 2017 Aug 28. PMID: 28846176.
- Gollu G, Onat Bermede A, Khanmammadov F, Ates U, Genc S, Selvi Can O, Fitoz S, Alanoglu Z, Yagmurlu A. Use of ultrasonography as a noninvasive decisive tool to determine the accurate endotracheal tube size in anesthetized children. *Arch Argent Pediatr.* 2018;116(3):172–8. <https://doi.org/10.5546/aap.2018.eng.172>. English, Spanish. PMID: 29756700.
- Hao J, Zhang J, Dong B, Luo Z. The accuracy of ultrasound to predict endotracheal tube size for pediatric patients with congenital scoliosis. *BMC Anesthesiol.* 2020;20(1):183. <https://doi.org/10.1186/s12871-020-01106-7>. PMID: 32736523; PMCID: PMC7394693.
- Hao J, Zhang J, Wu Z, Cai W, Dong B, Luo Z. Accuracy of ultrasound to measure the cricoid cartilage diameter in children. *Acta Anaesthesiol Scand.* 2020;64(10):1426–30. <https://doi.org/10.1111/aas.13687>. Epub 2020 Sep 13. PMID: 32803771.
- Kim EJ, Kim SY, Kim WO, Kim H, Kil HK. Ultrasound measurement of subglottic diameter and an empirical formula for proper endotracheal tube fitting in children. *Acta Anaesthesiol Scand.* 2013;57(9):1124–30. <https://doi.org/10.1111/aas.12167>. Epub 2013 Aug 2. PMID: 23909603.
- Makireddy R, Cherian A, Elakkumanan LB, Bidkar PU, Kundra P. Correlation between correctly sized uncuffed endotracheal tube and ultrasonographically determined subglottic diameter in paediatric population. *Indian J Anaesth.* 2020;64(2):103–8. https://doi.org/10.4103/ija.IJA_619_19. Epub 2020 Feb 4. PMID: 32139927; PMCID: PMC7017658.
- Pillai R, Kumaran S, Jeyaseelan L, George SP, Sahajanandan R. Usefulness of ultrasound-guided measurement of minimal transverse diameter of subglottic airway in determining the endotracheal tube size in children with congenital heart disease: a prospective observational study. *Ann Card Anaesth.* 2018;21(4):382–7. https://doi.org/10.4103/aca.ACA_220_17. PMID: 30333331; PMCID: PMC6206798.
- Schramm C, Knop J, Jensen K, Plaschke K. Role of ultrasound compared to age-related formulas for uncuffed endotracheal intubation in a pediatric population. *Paediatr Anaesth.* 2012;22(8):781–6. <https://doi.org/10.1111/j.1460-9592.2012.03889.x>. Epub 2012 May 21. PMID: 22612446.
- Shibasaki M, Nakajima Y, Ishii S, Shimizu F, Shime N, Sessler DI. Prediction of pediatric endotracheal tube size by ultrasonography. *Anesthesiology.* 2010;113(4):819–24. <https://doi.org/10.1097/ALN.0b013e3181ef6757>. PMID: 20808208.
- Sutagatti JG, Raja R, Kurdi MS. Ultrasonographic estimation of endotracheal tube size in paediatric patients and its comparison with physical indices based formulae: a prospective study. *J Clin Diagn Res.* 2017;11(5):UC05–8. <https://doi.org/10.7860/JCDR/2017/25905.9838>. Epub 2017 May 1. PMID: 28658880; PMCID: PMC5483782.
- Zhang K, Ma RJ, Zheng JJ, Chen YQ, Zhang MZ. Selection of cuffed endotracheal tube for children with congenital heart disease based on an ultrasound-based linear regression formula. *J Clin Monit Comput.* 2019;33(4):687–94. <https://doi.org/10.1007/s10877-018-0203-7>. Epub 2018 Sep 28. PMID: 30264220.
- Orhan-Sungur M, Altun D, Özkan-Seyhan T, Aygün E, Koltka K, Çamcı E. Learning curve of ultrasound measurement of subglottic diameter for endotracheal tube selection in pediatric patients. *Paediatr Anaesth.* 2019;29(12):1194–200. <https://doi.org/10.1111/pan.13751>. Epub 2019 Oct 20. PMID: 31583796.
- Andruszkiewicz P, Wojtczak J, Wroblewski L, Kaczor M, Sobczyk D, Kowalik I. Ultrasound evaluation of the impact of cricoid pressure versus novel ‘paralaryngeal pressure’ on anteroposterior oesophageal diameter. *Anaesthesia.* 2016;71(9):1024–9. <https://doi.org/10.1111/anae.13518>. PMID: 27523050.
- Kim H, Chang JE, Won D, Lee JM, Jung JY, Choi S, Min SW, Hwang JY. The effect of cricoid and paralaryngeal force on upper oesophageal occlusion during induction of anaesthesia: a randomised, crossover study. *Anaesthesia.* 2020;75(2):179–86. <https://doi.org/10.1111/anae.14873>. Epub 2019 Oct 21. PMID: 31631314.
- Galiciniao J, Bush AJ, Godambe SA. Use of bedside ultrasonography for endotracheal tube placement in pediatric patients: a feasibility study. *Pediatrics.* 2007;120(6):1297–303. <https://doi.org/10.1542/peds.2006-2959>. PMID: 18055679.
- Tsung JW, Fenster D, Kessler DO, Novik J. Dynamic anatomic relationship of the esophagus and trachea on sonography: implications for endotracheal tube confirmation in children. *J Ultrasound Med.* 2012;31(9):1365–70. <https://doi.org/10.7863/jum.2012.31.9.1365>. PMID: 22922616.
- Tessaro MO, Salant EP, Arroyo AC, Haines LE, Dickman E. Tracheal rapid ultrasound saline test

- (T.R.U.S.T.) for confirming correct endotracheal tube depth in children. *Resuscitation*. 2015;89:8–12. <https://doi.org/10.1016/j.resuscitation.2014.08.033>. Epub 2014 Sep 17. PMID: 25238740.
18. Uya A, Gautam NK, Rafique MB, Pawelek O, Patnana SR, Gupta-Malhotra M, Balaguru D, Numan MT, Hill MJ, Miller SK. Point-of-care ultrasound in sternal notch confirms depth of endotracheal tube in children. *Pediatr Crit Care Med*. 2020;21(7):e393–8. <https://doi.org/10.1097/PCC.0000000000002311>. PMID: 32168296.
 19. Slovis TL, Poland RL. Endotracheal tubes in neonates: sonographic positioning. *Radiology*. 1986;160(1):262–3. <https://doi.org/10.1148/radiology.160.1.3520649>. PMID: 3520649.
 20. Sethi A, Nimbalkar A, Patel D, Kungwani A, Nimbalkar S. Point of care ultrasonography for position of tip of endotracheal tube in neonates. *Indian Pediatr*. 2014;51(2):119–21. <https://doi.org/10.1007/s13312-014-0353-8>. PMID: 24632693.
 21. Chowdhry R, Dangman B, Pinheiro JM. The concordance of ultrasound technique versus X-ray to confirm endotracheal tube position in neonates. *J Perinatol*. 2015;35(7):481–4. <https://doi.org/10.1038/jp.2014.240>. Epub 2015 Jan 22. PMID: 25611791.
 22. Najib K, Pishva N, Amoozegar H, Pishdad P, Fallahzadeh E. Ultrasonographic confirmation of endotracheal tube position in neonates. *Indian Pediatr*. 2016;53(10):886–8. <https://doi.org/10.1007/s13312-016-0953-6>. PMID: 27771669.
 23. Oulego-Erroz I, Alonso-Quintela P, Rodríguez-Blanco S, Mata-Zubillaga D, Fernández-Miaja M. Verification of endotracheal tube placement using ultrasound during emergent intubation of a preterm infant. *Resuscitation*. 2012;83(6):e143–4. <https://doi.org/10.1016/j.resuscitation.2012.02.014>. Epub 2012 Mar 2. PMID: 22387919.
 24. Zaytseva A, Kurepa D, Ahn S, Weinberger B. Determination of optimal endotracheal tube tip depth from the gum in neonates by X-ray and ultrasound. *J Matern Fetal Neonatal Med*. 2020;33(12):2075–80. <https://doi.org/10.1080/14767058.2018.1538350>. Epub 2019 Apr 22. PMID: 30332898.
 25. Singh P, Thakur A, Garg P, Aggarwal N, Kler N. Normative data of optimally placed endotracheal tube by point-of-care ultrasound in neonates. *Indian Pediatr*. 2019;56(5):374–80. PMID: 31102379.
 26. Dennington D, Vali P, Finer NN, Kim JH. Ultrasound confirmation of endotracheal tube position in neonates. *Neonatology*. 2012;102(3):185–9. <https://doi.org/10.1159/000338585>. Epub 2012 Jul 6. PMID: 22777009.
 27. Hsieh KS, Lee CL, Lin CC, Huang TC, Weng KP, Lu WH. Secondary confirmation of endotracheal tube position by ultrasound image. *Crit Care Med*. 2004;32(9 Suppl):S374–7. <https://doi.org/10.1097/01.ccm.0000134354.20449.b2>. PMID: 15508663.
 28. Kerrey BT, Geis GL, Quinn AM, Hornung RW, Ruddy RM. A prospective comparison of diaphragmatic ultrasound and chest radiography to determine endotracheal tube position in a pediatric emergency department. *Pediatrics*. 2009;123(6):e1039–44. <https://doi.org/10.1542/peds.2008-2828>. Epub 2009 May 4. PMID: 19414520.
 29. Lin MJ, Gurley K, Hoffmann B. Bedside ultrasound for tracheal tube verification in pediatric emergency department and ICU patients: a systematic review. *Pediatr Crit Care Med*. 2016;17(10):e469–76. <https://doi.org/10.1097/PCC.0000000000000907>.
 30. Walsh B, Fennessy P, Ni Mhuircheartaigh R, Snow A, McCarthy KF, McCaul CL. Accuracy of ultrasound in measurement of the pediatric cricothyroid membrane. *Paediatr Anaesth*. 2019;29(7):744–52. <https://doi.org/10.1111/pan.13658>. Epub 2019 May 27. PMID: 31063634.
 31. Lee MGY, Millar J, Rose E, Jones A, Wood D, Luitingh TL, Zannino D, Brink J, Konstantinov IE, Brizard CP, d'Udekem Y. Laryngeal ultrasound detects a high incidence of vocal cord paresis after aortic arch repair in neonates and young children. *J Thorac Cardiovasc Surg*. 2018;155(6):2579–87. <https://doi.org/10.1016/j.jtcvs.2017.12.133>. Epub 2018 Feb 9. PMID: 29510943.
 32. Ongkasuwan J, Ocampo E, Tran B. Laryngeal ultrasound and vocal fold movement in the pediatric cardiovascular intensive care unit. *Laryngoscope*. 2017;127(1):167–72. <https://doi.org/10.1002/lary.26051>. Epub 2016 Apr 23. PMID: 27107409.
 33. Sayyid Z, Vendra V, Meister KD, Krawczeski CD, Speiser NJ, Sidell DR. Application-based translaryngeal ultrasound for the assessment of vocal fold mobility in children. *Otolaryngol Head Neck Surg*. 2019;161(6):1031–5. <https://doi.org/10.1177/0194599819877650>. Epub 2019 Sep 24. PMID: 31547773.
 34. Shaath GA, Jijeh A, Alkurdi A, Ismail S, Elbarbary M, Kabbani MS. Ultrasonography assessment of vocal cords mobility in children after cardiac surgery. *J Saudi Heart Assoc*. 2012;24(3):187–90. <https://doi.org/10.1016/j.jsha.2012.02.009>. Epub 2012 Mar 15. PMID: 23960693; PMCID: PMC3727376.
 35. Wang LM, Zhu Q, Ma T, Li JP, Hu R, Rong XY, Xu W, Wang ZC. Value of ultrasonography in diagnosis of pediatric vocal fold paralysis. *Int J Pediatr Otorhinolaryngol*. 2011;75(9):1186–90. <https://doi.org/10.1016/j.ijporl.2011.06.017>. Epub 2011 Jul 18. PMID: 21763007.
 36. Zhang WQ, Lambert EM, Ongkasuwan J. Point of care, clinician-performed laryngeal ultrasound and pediatric vocal fold movement impairment. *Int J Pediatr Otorhinolaryngol*. 2020;129:109773. <https://doi.org/10.1016/j.ijporl.2019.109773>. Epub 2019 Nov 9. PMID: 31790923.
 37. Hamilton CE, Su E, Tawfik D, Fernandez E, Veten A, Conlon T, Ginsburg S, Mariano K, Sidell D, Haileselassie B, Pediatric Research Collaborative on Critical Ultrasound (PeRCCUS). Assessment of vocal cord motion using laryngeal ultrasound in children: a systematic review and meta-analysis. *Pediatr Crit Care Med*. 2021;22(10):e532–9. <https://doi.org/10.1097/PCC.0000000000002734>. PMID: 33833204.



Diaphragmatic Ultrasound

Joel K. B. Lim, Jan Hau Lee, and Mark D. Weber

Contents

Functional Anatomy of the Diaphragm	149
Diaphragmatic Dysfunction	150
Ultrasound Views for Diaphragmatic Assessment	151
Reference Values for Diaphragm Ultrasound in Children	153
Assessment of Pathophysiology	154
Future Directions	156
Conclusion	158
References	159

Functional Anatomy of the Diaphragm

The diaphragm, the main muscle of respiration, is comprised of a dome-shaped muscle and central tendon with a convex upper surface forming the floor of the thoracic cavity, and a concave under-surface forming the roof of the abdominal cavity. The diaphragm originates superiorly and anteriorly from the xiphoid process, inferiorly from the first two lumbar vertebrae, and laterally

from the lower six thoracic costal cartilages. The muscle fibers from these origins converge to form the central tendon, forming the crest of the dome. The area where the diaphragm muscle fibers attach to the lateral lower thorax is called the zone of apposition (ZOA).

The thickness of the diaphragm is variable, tapering from the anterior to posterior costal regions and from its costal insertions to the central tendon. The diaphragm is also asymmetric, with the right side slightly superior to the left, due to the presence of the liver. During diaphragmatic contraction the central tendon is pulled caudally, effectively increasing the vertical diameter of the thoracic cavity.

J. K. B. Lim (✉) · J. H. Lee
Children's Intensive Care Unit, Department of
Pediatric Subspecialties, KK Women's and Children's
Hospital, Singapore, Singapore
e-mail: joel.lim.k.b@singhealth.com.sg

M. D. Weber
Department of Anesthesiology and Critical Care
Medicine, Children's Hospital of Philadelphia,
University of Pennsylvania, Philadelphia, PA, USA

Diaphragmatic Dysfunction

Diaphragmatic dysfunction (DD) classifications include eventration, weakness, and paralysis [1]. Eventration is a permanent elevation of part or all of the hemidiaphragm caused by congenital thinning of the muscle. Diaphragm weakness refers to the partial loss of muscle strength required to generate sufficient pressure for ventilation. Paralysis refers to the complete absence of movement of the diaphragm. Diaphragm weakness or paralysis typically causes elevation of an entire hemidiaphragm, while eventration usually causes elevation of only a focal part of the hemidiaphragm [1]. Paradoxical diaphragm movement refers to a cephalad movement of the hemidiaphragm during inspiration. In the presence of a weak or paralyzed hemidiaphragm, inspiratory force generated by the external intercostal and accessory muscles expands the thoracic cavity, creating a negative intrathoracic pressure and pulling the diaphragm and abdominal viscera cephalad toward the thorax.

The clinical manifestations and severity of DD can vary widely. Clinically, patients with DD may be asymptomatic or may present with reduced exercise tolerance, orthopnea, paradoxical breathing, unexplained respiratory distress, recurrent pneumonia, atelectasis, unexplained supplementary oxygen dependence, or difficulty weaning from mechanical ventilation [2, 3]. Symptoms of DD can also be exacerbated by cardiac or pulmonary diseases, disorders that increase intra-abdominal pressure or changes in posture, such as being in the supine position [4]. The wide spectrum of clinical manifestations makes recognition of DD challenging and it is even more difficult when the work of breathing is being supported by mechanical ventilation. Consequently, the sequelae associated with DD include prolonged duration of mechanical ventilation, increased risk of nosocomial infection, increased length of intensive care unit and hospital stay, poorer functional outcomes, and increased mortality [2, 5]. Depending on the severity and cause of DD, management may be conservative or may include noninvasive ventila-

tion, tracheostomy creation with invasive mechanical ventilation, diaphragm plication, or diaphragm pacing [1, 4].

Apart from diaphragmatic eventration, DD can be caused by disorders of diaphragm innervation, diaphragm muscle weakness or atrophy, and disorders of the chest wall [6]. In children, the most frequently reported cause of DD is due to phrenic nerve injury after congenital heart surgery, with an incidence ranging between 0.3 and 20% [2, 7, 8]. Mechanisms of nerve injury include direct traumatic injury or transient neuropraxia due to traction, exposure to cold solutions, and excessive heat from diathermy use [2, 7]. The second most common cause of DD in infants is birth trauma [7]. This frequently affects the right hemidiaphragm and affected infants often also present with an ipsilateral brachial plexus palsy [9]. Other traumatic causes of DD include chest tube insertion and subclavian or jugular venous cannulation. Extravasation of parenteral nutrition around the phrenic nerve from a peripherally inserted central catheter has also been reported to cause DD [7].

In the intensive care unit, there is increasing recognition that DD occurs in association with critical illness neuromyopathy or due to mechanical ventilation, which is known as ventilator-induced DD and has been reported to occur within as little as 18–69 hours of mechanical ventilation [5, 10–12]. There may be a degree of overlap between critical illness neuromyopathy and ventilator-induced DD and data suggests that about 30–80% of critically ill children and adults are affected [5, 13–17]. Other contributing factors to DD in the critically ill child include sepsis, malnutrition, and the use of corticosteroids, aminoglycosides, and neuromuscular blocking agents [5, 14, 15]. Rarer causes of DD in infants and children include neuromuscular disease, spinal cord injury, mediastinal or pulmonary infections or mass lesions, brainstem disorders, cervicobrachial surgery, abdominal surgery, inflammatory polyneuropathies such as Guillain-Barre syndrome and infectious neuropathies secondary to congenital Zika syndrome and congenital cytomegalovirus infection [8, 18–20].

Ultrasound Views for Diaphragmatic Assessment

In diaphragmatic assessment using ultrasound, there are two parameters which can be assessed from two main views. The first parameter, diaphragm thickness (DT), should be measured at the zone of apposition (ZOA) in end-inspiration and end-expiration. This is then used to calculate the diaphragm thickening fraction (DTF), which is the percentage increase in thickness during inspiration, using the formula: $(\text{End-inspiratory DT} - \text{End-expiratory DT}) / \text{End-expiratory DT} \times 100\%$. The second parameter, diaphragmatic excursion (DE), should be measured via a view of the dome of the hemidiaphragm.

Prior to diaphragm assessment, ultrasound should be used to screen the lower thoracic and upper abdominal regions to exclude pathologies which are adjacent to, and may impact upon, diaphragm function such as pleural effusion, pulmonary consolidation, atelectasis, thoracic or abdominal mass lesions, or ascites. This screening view may be achieved by using a curvilinear or phased array transducer placed in an oblique transverse plane at the subxiphoid area to facilitate simultaneous imaging and comparison of both hemidiaphragms [2, 3, 21–23] (Fig. 1).

To acquire a view of the ZOA with the best visual resolution, a high-frequency linear trans-

ducer should be placed perpendicularly to the orientation of the ribs, in a longitudinal, semi-coronal plane, between the eighth and tenth intercostal spaces and between the anterior and mid-axillary lines [24–30] (Fig. 2). Some reports have proposed more posterior transducer placement, either between the anterior and posterior axillary lines or at the posterior axillary line [2, 3, 31, 32]. At high resolution, the diaphragm appears as a three-layered structure, with a non-echogenic muscular layer bounded by the echo-



Fig. 2 A high-frequency linear transducer placed perpendicularly to the chest wall, in a longitudinal, semi-coronal plane, between the eighth and tenth intercostal spaces and between the anterior and mid-axillary lines to acquire an image of the zone of apposition

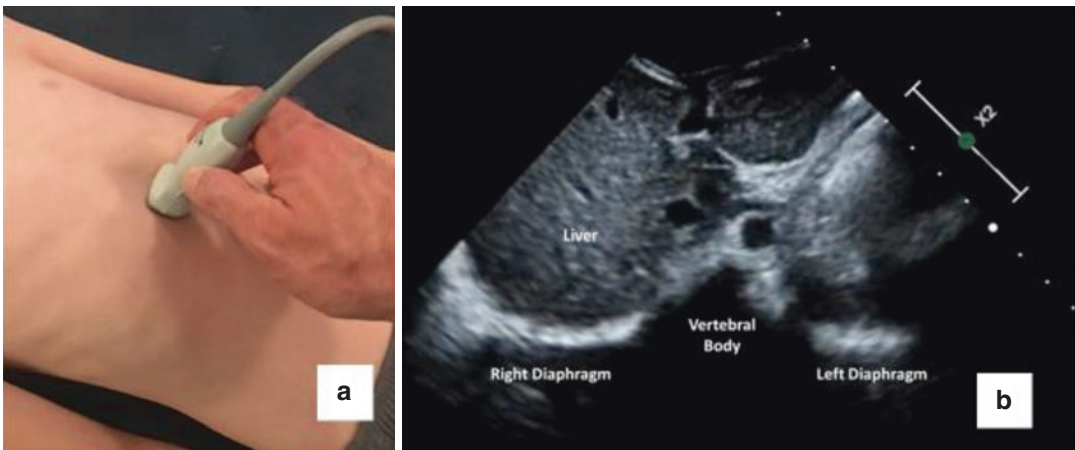


Fig. 1 Phased array transducer placed in an oblique transverse plane at the subxiphoid area (a) facilitating simultaneous imaging and comparison of both hemidiaphragms (b)

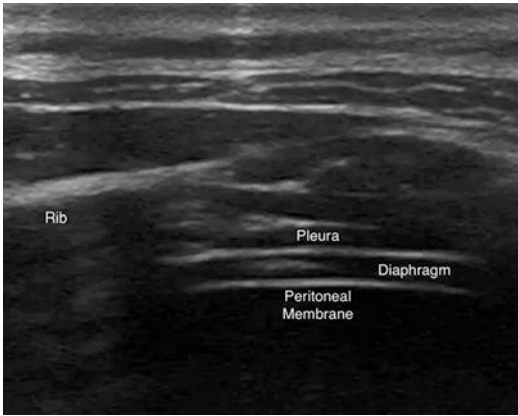


Fig. 3 An image of the diaphragm revealing the three-layered structure, with a non-echogenic muscular layer bounded by the echogenic parietal pleura and peritoneal membrane

genic parietal pleura and peritoneum (Fig. 3). In this view, the diaphragm may sometimes be obliterated by the edge of the inflated lung during inspiration. DT, measured as the perpendicular distance between the pleural and peritoneal layers, should be assessed in end-inspiration and end-expiration using M-mode. However, there is no consensus regarding the inclusion of the full thickness of the pleural and peritoneal layers in the measurement of DT. Many authors measure the perpendicular distance between the midpoints of the pleura and peritoneum [24, 27, 28], while others include or exclude the thickness of the pleura and peritoneum [29–32].

To acquire a view of the dome of the hemidiaphragm, a lower frequency curvilinear or phased array transducer should be placed in a sagittal plane in the subcostal area, between the mid-clavicular and anterior axillary lines for the right hemidiaphragm and between the anterior and mid-axillary lines for the left hemidiaphragm. The transducer should be directed cranially using the liver or spleen as acoustic windows so that the ultrasound beam reaches the posterior aspect of the right and left hemidiaphragms, respectively [22–27, 33] (Fig. 4). Since the diaphragm is assessed at a greater distance from the point of transducer-skin contact using a lower frequency phased array probe, the resolution using this view is poorer compared to the assessment at the

ZOA. At this lower resolution, the diaphragm appears as a single echogenic line due to the tightly adherent parietal pleura. During inspiration in the spontaneously breathing child, the normal diaphragm moves caudally, toward the transducer, while in expiration, the diaphragm moves cephalad, away from the transducer.

During diaphragm ultrasound, movement of the diaphragm must be correlated with the phases of the respiratory cycle, which can be distinguished according to their timing. Normal inspiration typically occurs after a respiratory pause after the end of expiration, whereas expiration begins immediately at the end of inspiration. Correlating diaphragm movements with the respiratory cycle may be further enhanced by placing a free hand on the patient's chest to correlate chest wall movements with the M-mode tracing. After determining the direction of DE with the phases of the respiratory cycle, M-mode should be used to measure the amplitude of DE on a vertical axis of the M-mode tracing, from the baseline (at end-expiration) to the point of maximum height (at end-inspiration) on the tracing (Fig. 5).

In general, the right hemidiaphragm is easier to visualize than the left. The challenge of obtaining clear images of the left hemidiaphragm is due to the smaller acoustic window provided by the spleen and the potential for overlying bowel gas which may obscure views. This has led some investigators to limit assessments to the right hemidiaphragm [14, 15, 28–30]. Reports from adult and pediatric studies suggest that there are no significant differences in DT, DTF, or DE between the right and left hemidiaphragms [32–35]. When performing diaphragm ultrasound, the impact of postural changes on respiratory mechanics must also be considered. For the same volume inspired, DE has been reported to be greater in the supine position than in sitting or standing positions. DT has also been reported to be greater while sitting or standing than in the supine position [36]. This may suggest that the diaphragm function is more efficient in the sitting or standing positions. Hence, it would be ideal to standardize the patient's position when performing serial diaphragm ultrasound assessments.

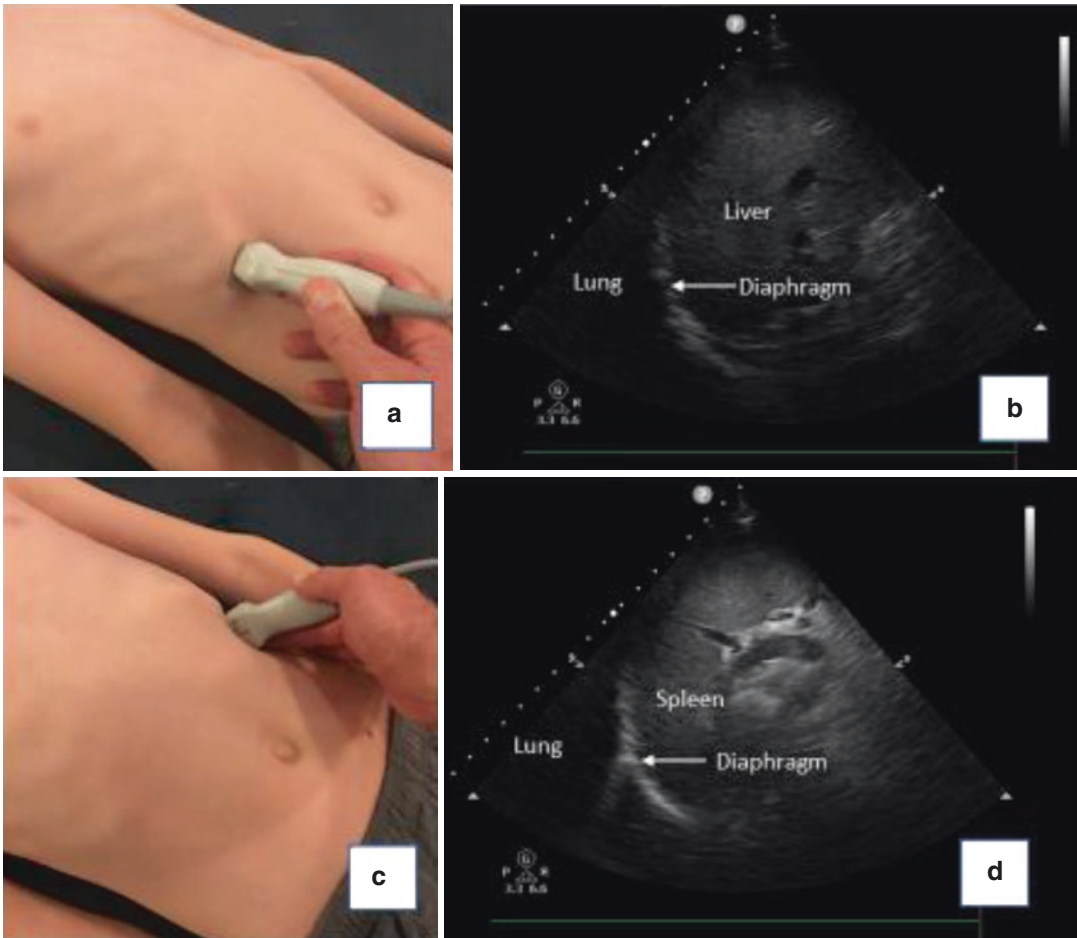


Fig. 4 Acquiring an image of the dome of the diaphragm. (a) Phased array transducer should be placed in a sagittal plane in the subcostal area, between the mid-clavicular and anterior

axillary lines for the (b) right hemidiaphragm. (c) Transducer placed between the anterior and mid-axillary lines on the left side to acquire an image of the (d) left hemidiaphragm

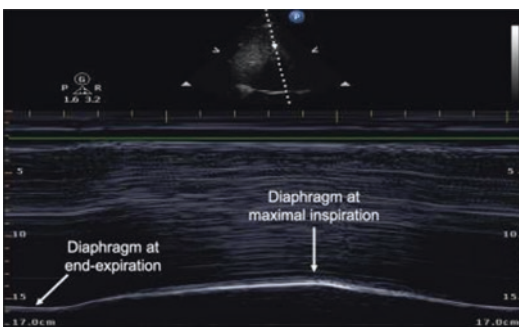


Fig. 5 M- mode image revealing the amplitude of the diaphragmatic excursion

Reference Values for Diaphragm Ultrasound in Children

There is a paucity of data for reference values for normal diaphragm dimensions or function in children. Several small studies have attempted to provide age-based normative values for diaphragm ultrasound parameters in healthy, spontaneously breathing preterm and term infants, with only one larger study including older children and adolescents [26, 27, 32, 33] (Table 1). Several

Table 2 Reference values for diaphragm ultrasound measurements in children supported on mechanical ventilation

Study/Year	Cohort	Patient Position	DT (mm)	DTF (%)
Lee 2017 ^a [28] (Mean \pm SD)	Infants and children <i>n</i> = 31	Not specified	End-expiratory 1.52 \pm 0.38 End-inspiratory 1.92 \pm 0.48	25.8 \pm 3.3
Dionisio 2019 ^{a, b} [14]	Infants and children <i>n</i> = 17	Semi-recumbent	End-expiratory 2.3 (2–3.5)	41 \pm 11 (Mean \pm SD)
Glau 2020 ^c [29]	Infants and children <i>n</i> = 56	Semi-recumbent	Within 36 h of intubation End-expiratory 2.0 (1.8–2.5) End-inspiratory 2.2 (2.0–2.7)	Within 36 h after intubation 9.7 (6.5–16.4) 24 h before extubation 14.8 (10.9–26.8)
IJland 2020 ^d [30]	Infants and children <i>n</i> = 34	Semi-recumbent	End-expiratory 1.5 (1.0–1.6)	10.7 (7.5–16.2)
Mistri 2020 ^d [37]	Children <i>n</i> = 55	Not specified	End-expiratory 1.27 (1.00–1.60) End-inspiratory 1.76 (1.35–2.10)	33.75 (26.9–44.6)
Valverde Montoro 2021 ^a [15]	Infants and children <i>n</i> = 47	Semi-recumbent	End-expiratory 1.8 (1.5–2.0) End-inspiratory 2.2 (1.8–2.5)	24.0 (8.5–36.0)

Data are presented in median (IQR) unless otherwise specified

All studies included assessed only the right diaphragm, with ultrasound studies performed within the first 24 h of intubation unless otherwise specified

DE Diaphragm excursion, DT Diaphragm thickness, DTF Diaphragm thickening fraction, IQR Interquartile range, SD Standard deviation

^a DT measurements in these studies were from the midpoint of the pleura to the midpoint of the peritoneal layer

^b Dionisio et al. also assessed DE in their cohort within the first 24 h of intubation, while on pressure support ventilation (Mean 7.8 \pm 3.9 mm) [14]

^c DT measurement in this study included the thickness of the pleura and peritoneal layers

^d DT measurements in these studies excluded the thickness of the pleural and peritoneal layers

whether patients are spontaneously breathing or receiving positive pressure ventilation support, with or without paresis/paralysis. However, the concurrent use of mechanical ventilation results in greater difficulties in interpreting results, especially in deeply sedated patients receiving full ventilatory support, which constitutes a large proportion of the critically ill population. The optimal depth of sedation, extent of ventilatory support, or timing during which diaphragm ultrasound should be performed in order to assess DD, atrophy, respiratory workload, or to predict extubation success has yet to be determined.

Assessment of Diaphragm Atrophy and Weakness

End-expiratory DT is thought to be the most appropriate indicator of muscle bulk as it represents diaphragm muscle thickness at rest or at functional residual capacity and does not depend on maintaining a patient's spontaneous respiratory effort [14, 15, 37]. Diaphragm atrophy occurs in 44–82% of critically ill children, with the onset occurring within 24–96 hours after the initiation of mechanical ventilation [5, 13–15, 28, 30]. In children, substantial reductions in mean end-expiratory DT from 1.52 to 1.50 mm

(a 1.3% decrease), mean end-inspiratory DT from 1.92 to 1.75 mm (an 8.8% decrease), and mean DTF from 25.8 to 16.4% (a 36.4% decrease) have been reported within 48 hours of mechanical ventilation [28].

Assessment of Diaphragm Paresis

In contrast to the assessment for diaphragm atrophy, an accurate assessment of DE and DTF requires the preservation of a patient's spontaneous respiratory effort [14, 15]. It is preferable to perform diaphragm ultrasound to assess DE and DTF in a standardized manner, with patients quietly breathing spontaneously in a semi-recumbent position with minimal use of sedation. In children suspected to have diaphragmatic paralysis, DE is considered normal if inspiratory motion is toward the transducer, with an amplitude >4 mm and a difference of DE between hemidiaphragms of $<50\%$. An amplitude of ≤ 4 mm and a difference of DE between hemidiaphragms $>50\%$ is considered decreased or paretic [2, 21, 22, 38, 39]. Unilateral diaphragmatic paralysis after congenital cardiac surgery can be assessed with B-mode ultrasound by placing a transducer in the subxiphoid plane, demonstrating sliding of the descending aorta toward the unaffected hemidiaphragm during respiration. In healthy patients, the descending aorta remains in the same position and does not move during respiration [40].

Assessment of Readiness for Weaning of Mechanical Ventilation

DTF is the most robust parameter for representing diaphragm contractile function and predicting successful weaning from mechanical ventilation in adults and children [15, 37, 41–45] (Table 3). These studies typically performed diaphragm ultrasound during spontaneous breathing trials (SBT). Cutoff values associated with successful extubation in children have a pre-extubation DTF ranging from >21 to 23% [44, 45]. In contrast, data on the role of DE for predicting successful weaning from mechanical ventilation is less certain. Another factor to consider is the variability of respiratory drive and muscle activity throughout the day. DTF tends to be assessed once daily and measurement at a single point in

time may be an insufficient estimate of global respiratory muscle function. Thus, it may be important to assess DTF when patients are awake and asleep.

Future Directions

There are an increasing number of techniques proposed to assess diaphragm function. New sonographic parameters, such as the product of DE and inspiratory time, the ratio between respiratory rate and DE (known as the diaphragmatic rapid shallow breathing index), and a combination of DTF with the rapid shallow breathing index have been reported to predict successful extubation in adults [46–49]. However, the utility of these parameters in children may be limited due to the wide range of inspiratory times, respiratory rates, DE, and DTF across the pediatric population.

Echocardiographic techniques are now also being applied to diaphragm assessments. Tissue doppler imaging (TDI) is a technique that measures the velocity of moving tissue. In a study that assessed diaphragm TDI during an SBT in 116 mechanically ventilated adults and 20 healthy controls, patients who were successfully weaned and healthy controls had lower peak contraction velocity, peak relaxation velocity, and TDI-maximal relaxation rate compared to patients who failed weaning [50]. Researchers proposed that higher peak contraction velocities indicate a compensatory increase in respiratory motor output in patients with progressive respiratory failure, while higher peak relaxation velocities reflect the need of the diaphragm to rapidly return to end-expiratory length, in preparation for the following inspiratory contraction.

Diaphragm TDI has also been investigated in healthy neonates [51]. The authors reported that measuring DE via M-mode ultrasound was less reliable in neonates due to their erratic breathing patterns and high respiratory rates, concluding that diaphragm TDI is a more feasible technique. While they established reference values for diaphragm peak motion velocities in a sizable cohort of 229 neonates, further studies are required to

Table 3 Comparison of diaphragm ultrasound variables between children with successful or failed weaning from mechanical ventilation

Study/Year	Cohort	Weaning result	DE (mm/kg)	End-inspiratory DT (mm/kg)	End-expiratory DT (mm/kg)	Pre-extubation DTF (%)
Xue 2019 ^a [44]	Infants and children <i>n</i> = 50	Successful <i>n</i> = 39	0.74 ± 0.75	1.07 ± 0.88	0.79 ± 0.61	30.93 ± 11.23
		Failed <i>n</i> = 11	0.45 ± 0.32	1.08 ± 0.62	0.91 ± 0.49	15.98 ± 6.65
			DE (mm)	End-inspiratory DT (mm)	End-expiratory DT (mm)	Pre-extubation DTF (%)
Abdel Rahman 2020 ^b [45]	Infants <i>n</i> = 84	Successful <i>n</i> = 44	8.21 ± 2.25	2.32 ± 0.62	1.75 ± 0.52	33.56 ± 7.81
		Failed <i>n</i> = 40	6.06 ± 1.87	1.98 ± 0.82	1.68 ± 0.74	20.06 ± 10.41
	Children <i>n</i> = 10	Successful <i>n</i> = 9	9.22 ± 2.22	2.96 ± 0.27	2.34 ± 0.41	26.49 ± 3.47
		Failed <i>n</i> = 1	4	2.8	2.3	21.74
	Adolescents <i>n</i> = 12	Successful <i>n</i> = 11	11.6 ± 1.16	2.93 ± 0.19	2.21 ± 0.13	32.58 ± 5.48
		Failed <i>n</i> = 1	14	3.1	2.3	34.78
			End-inspiratory DT (mm)	End-expiratory DT (mm)	Pre-extubation DTF (%)	Post-extubation DTF (%)
Mistri 2020 ^a [37] Median (IQR)	Children <i>n</i> = 55 ^c	Successful <i>n</i> = 30	1.61 (1.06, 1.80)	1.13 (0.82, 1.47)	30.14 (22.17, 42.00)	27.40 (20.70, 41.30)
		Failed <i>n</i> = 5	1.08 (0.96, 1.25)	0.81 (0.81, 1.05)	32.78 (19.04, 33.30)	32.50 (19.81, 34.42)
					Pre-extubation DTF (%)	Post-extubation DTF (%)
Valverde Montoro 2021 ^b [15] Median (IQR)	Infants and children <i>n</i> = 47	Successful <i>n</i> = 32	–	–	30 (25, 38)	41 (33, 57)
		Failed <i>n</i> = 13	–	–	30 (20, 63)	55 (36.5, 65.5)

Data are presented in mean ± standard deviation unless otherwise specified

All results displayed are for the right diaphragm

All studies performed diaphragm ultrasound during a spontaneous breathing trial in the semi-recumbent position, except that Mistri et al. did not specify the patient position

DE Diaphragm excursion, DT Diaphragm thickness, DTF Diaphragm thickening fraction, IQR Interquartile range

^a DT measurements in these studies excluded the thickness of the pleural and peritoneal layers

^b DT measurements in these studies were from the midpoint of the pleura to the midpoint of the peritoneal layer

^c 19 children in the study demised and 1 patient underwent tracheostomy without a trial of extubation

test the clinical utility of this parameter in critically ill neonates.

Speckle tracking imaging (STI) is a method of analysis used to determine myocardial fiber deformation or “strain” [52–54]. The STI software analyzes the relative motion of groups of pixels (known as speckles) in an ultrasound

image. Positive strain values indicate passive stretch while negative strain values indicate muscle fiber shortening. The velocity of tissue deformation is represented by the strain rate. A few studies have assessed diaphragm STI in small groups of healthy adults, but no studies have been performed in critically ill adults or in children

[36, 52–55]. Nonetheless, STI appears to be a promising technique for assessing diaphragm function, with studies reporting a good correlation between strain and strain rate with transdiaphragmatic pressure and diaphragm electrical activity, as well as good reproducibility [53, 54]. In contrast to M-mode measurements of DE, which measures tissue movement in a single plane, STI is angle-independent, measures tissue motion in two dimensions, and follows the same region of interest during diaphragm motion, which may facilitate greater accuracy in assessing diaphragm function. However, current STI technology is designed to track speckle motion related to the cardiac cycle, not the respiratory cycle. In addition, significant time is required to perform the analysis, limiting its clinical utility. Technologic advancements and software adaptations for diaphragm analysis may eventually allow for easy bedside use.

Ultrasound shear wave elastography (SWE) is a developing method of ultrasound imaging based on the measurement of the propagation velocity of shear waves through tissues. The shear wave velocity is used to calculate shear modulus, which reflects the degree of tissue stiffness and active muscle force [56, 57]. Studies in healthy adults have demonstrated good reproducibility and good correlation between diaphragm shear modulus and transdiaphragmatic pressure or inspiratory mouth pressure [56, 58, 59]. In a study of 25 mechanically ventilated adults, diaphragm shear modulus did not distinguish patients who failed or tolerated an SBT. Further studies and technological advancements are required before SWE can be recommended for use in critically ill children.

Other approaches to predict extubation failure combine diaphragm ultrasound with echocardiography, lung ultrasound, or both [55]. This alludes to the fact that extubation failure is often multifactorial and can be due to any one or a combination of factors, including high airway resistance, poor respiratory system compliance, respiratory muscle dysfunction, cardiac failure, excessive metabolic demands, excessive secretions, poor cough reflex, or depressed conscious level [36, 46, 47]. Two studies investigating inte-

grated cardiac, lung and diaphragm ultrasound in mechanically ventilated adults reported that left ventricular diastolic dysfunction and loss of lung aeration were the most predictive of extubation failure [60, 61]. Neither study assessed DT nor DTF and found that DE was poorly predictive of extubation failure. However, this may be due to the significant prevalence of cardiovascular comorbidities in these cohorts, with cardiac dysfunction potentially contributing more to extubation failure than DD. A third study reported that left ventricular diastolic dysfunction and ejection fraction predicted respiratory failure within 48 h of extubation, while DE predicted the need for reintubation within a week of extubation [62].

A large number of studies have reported the utility of combined diaphragm and lung ultrasound for predicting extubation failure in adults [63, 64]. A systematic review and meta-analysis of 19 studies found that DTF and lung ultrasound were good predictors of extubation failure, while DE was less accurate [63]. One pediatric study has also investigated the utility of combined diaphragm and lung ultrasound for predicting extubation failure in 106 children [45]. Lung ultrasound scores were assigned based on the aeration patterns of 12 zones of the lung, with scores ranging from 0 to 36. The best cutoff values for DTF, DE, and lung ultrasound scores for predicting successful extubation were >23.2%, >6.2 mm, and <12, with an area under the receiver operating characteristic curve of 0.93, 0.88, and 0.93, respectively. Although DTF, DE, and lung ultrasound scores were predictive of extubation failure in infants, only DTF was predictive in children and none of the parameters were predictive in adolescents. However, this is probably a reflection of the sample population, which included 84 neonates, 10 children, and 12 adolescents, with only 1 child and 1 adolescent failing extubation.

Conclusion

Diaphragm ultrasound is a promising technique for the assessment of diaphragm function. Assessment methods are quick, noninvasive,

reproducible, and repeatable at the bedside. At present, diaphragm thickness is an accurate measure of diaphragm atrophy while diaphragm thickening fraction is a useful measure of diaphragm contractile strength. Optimizing respiratory mechanics using diaphragm ultrasound has the potential to provide sufficient respiratory support while limiting ventilator-induced DD in order to facilitate successful weaning and extubation. While it is important to routinely monitor and prevent DD in the mechanically ventilated child, it is imperative to consider that DD and weaning failures can be multifactorial and that critically ill patients will benefit from a holistic multiorgan assessment to plan for individualized intervention and weaning.

References

- Nason LK, Walker CM, McNeeley MF, Burivong W, Fligner CL, Godwin JD. Imaging of the diaphragm: anatomy and function. *Radiographics*. 2012;32(2):E51–70. <https://doi.org/10.1148/rg.322115127>.
- Gil-Juanmiquel L, Gratacós M, Castilla-Fernández Y, Piqueras J, Baust T, Ragner N, Balcells J, Perez-Hoyos S, Abella RF, Sanchez-de-Toledo J. Bedside ultrasound for the diagnosis of abnormal diaphragmatic motion in children after heart surgery. *Pediatr Crit Care Med*. 2017;18(2):159–64. <https://doi.org/10.1097/PCC.0000000000001015>.
- Sanchez de Toledo J, Munoz R, Landsittel D, Shiderly D, Yoshida M, Komarlu R, Wearden P, Morell VO, Chrysostomou C. Diagnosis of abnormal diaphragm motion after cardiothoracic surgery: ultrasound performed by a cardiac intensivist vs. fluoroscopy. *Congenit Heart Dis*. 2010;5(6):565–72. <https://doi.org/10.1111/j.1747-0803.2010.00431.x>.
- Ricoy J, Rodríguez-Núñez N, Álvarez-Dobaño JM, Toubes ME, Riveiro V, Valdés L. Diaphragmatic dysfunction. *Pulmonology*. 2019;25(4):223–35. <https://doi.org/10.1016/j.pulmoe.2018.10.008>.
- Johnson RW, Ng KWP, Dietz AR, Hartman ME, Batty JD, Hasan N, Zaidman CM, Shoykhet M. Muscle atrophy in mechanically-ventilated critically ill children. *PLoS One*. 2018;13(12):e0207720. <https://doi.org/10.1371/journal.pone.0207720>.
- Laghi F, Tobin MJ. Disorders of the respiratory muscles. *Am J Respir Crit Care Med*. 2003;168(1):10–48. <https://doi.org/10.1164/rccm.2206020>.
- Gerard-Castaing N, Perrin T, Ohlmann C, Mainguy C, Coutier L, Buchs C, Reix P. Diaphragmatic paralysis in young children: a literature review. *Pediatr Pulmonol*. 2019;54(9):1367–73. <https://doi.org/10.1002/ppul.24383>.
- Commare MC, Kurstjens SP, Barois A. Diaphragmatic paralysis in children: a review of 11 cases. *Pediatr Pulmonol*. 1994;18(3):187–93. <https://doi.org/10.1002/ppul.1950180311>.
- Rizeq YK, Many BT, Vacek JC, Reiter AJ, Raval MV, Abdullah F, Goldstein SD. Diaphragmatic paralysis after phrenic nerve injury in newborns. *J Pediatr Surg*. 2020;55(2):240–4. <https://doi.org/10.1016/j.jpedsurg.2019.10.038>.
- Banwell BL, Mildner RJ, Hassall AC, Becker LE, Vajsar J, Shemie SD. Muscle weakness in critically ill children. *Neurology*. 2003;61(12):1779–82. <https://doi.org/10.1212/01.WNL.0000098886.90030.67>.
- Mortamet G, Crulli B, Fauroux B, Emeriaud G. Monitoring of respiratory muscle function in critically ill children. *Pediatr Crit Care Med*. 2020;21(5):e282–90. <https://doi.org/10.1097/PCC.0000000000002254>.
- Levine S, Nguyen T, Taylor N, Friscia ME, Budak MT, Rothenberg P, Zhu J, Sachdeva R, Sonnad S, Kaiser LR, et al. Rapid disuse atrophy of diaphragm fibers in mechanically ventilated humans. *N Engl J Med*. 2008;358(13):1327–35. <https://doi.org/10.1056/NEJMoa070447>.
- Xue Y, Yang CF, Ao Y, Qi J, Jia FY. A prospective observational study on critically ill children with diaphragmatic dysfunction: clinical outcomes and risk factors. *BMC Pediatr*. 2020;20(1):422. <https://doi.org/10.1186/s12887-020-02310-7>.
- Dionisio MT, Rebelo A, Pinto C, Carvalho L, Neves JF. Avaliação Ecográfica da Disfunção Diafragmática Induzida pelo Ventilador em Idade Pediátrica [Ultrasound Assessment of Ventilator-induced Diaphragmatic Dysfunction in Paediatrics]. *Acta Med Port*. 2019;32(7–8):520–528. Portuguese. <https://doi.org/10.20344/amp.10830>.
- Valverde Montoro D, García Soler P, Hernández Yuste A, Camacho Alonso JM. Ultrasound assessment of ventilator-induced diaphragmatic dysfunction in mechanically ventilated pediatric patients. *Paediatr Respir Rev*. 2021;40:58–64. <https://doi.org/10.1016/j.prrv.2020.12.002>.
- Koch S, Spuler S, Deja M, Bierbrauer J, Dimroth A, Behse F, Spies CD, Wernecke K-D, Weber-Carstens S. Critical illness myopathy is frequent: accompanying neuropathy protracts ICU discharge. *J Neurol Neurosurg Psychiatry*. 2011;82(3):287–93. <https://doi.org/10.1136/jnnp.2009.192997>.
- Jung B, Moury PH, Mahul M, de Jong A, Galia F, Prades A, Albaladejo P, Chanques G, Molinari N, Jaber S. Diaphragmatic dysfunction in patients with ICU-acquired weakness and its impact on extubation failure. *Intensive Care Med*. 2016;42(5):853–61. <https://doi.org/10.1007/s00134-015-4125-2>.
- van der Linden V, Lins OG, de Lima Petribu NC, de Melo ACMG, Moore J, Rasmussen SA, Moore CA. Diaphragmatic paralysis: evaluation in infants

- with congenital Zika syndrome. *Birth Defects Res.* 2019;111(19):1577–83. <https://doi.org/10.1002/bdr2.1597>.
19. Rajapakse NS, Ellsworth K, Liesman RM, Ho ML, Henry N, Theel ES, Wallace A, Alvino ACI, Medeiros de Mello L, Meneses J. Unilateral phrenic nerve palsy in infants with congenital Zika syndrome. *Emerg Infect Dis.* 2018;24(8):1422–7. <https://doi.org/10.3201/eid2408.180057>.
 20. Izumi K, Hokoto I, Yamaguchi S, Uezono A, Ikeda K, Rice L, McCandless SE, Craven DI. Diaphragm dysfunction with congenital cytomegalovirus infection. *J Perinatol.* 2010;30(10):691–4. <https://doi.org/10.1038/jp.2010.65>.
 21. Urvoas E, Pariente D, Fausser C, Lipsich J, Taleb R, Devictor D. Diaphragmatic paralysis in children: diagnosis by TM-mode ultrasound. *Pediatr Radiol.* 1994;24(8):564–8. <https://doi.org/10.1007/BF02012733>.
 22. Epelman M, Navarro OM, Daneman A, Miller SF. M-mode sonography of diaphragmatic motion: description of technique and experience in 278 pediatric patients. *Pediatr Radiol.* 2005;35(7):661–7. <https://doi.org/10.1007/s00247-005-1433-7>.
 23. Miller SG, Brook MM, Tacy TA. Reliability of two-dimensional echocardiography in the assessment of clinically significant abnormal hemidiaphragm motion in pediatric cardiothoracic patients: comparison with fluoroscopy. *Pediatr Crit Care Med.* 2006;7(5):441–4. <https://doi.org/10.1097/01.PCC.0000227593.63141.36>.
 24. Sferrazza Papa GF, Pellegrino GM, Di Marco F, Imeri G, Brochard L, Goligher E, Centanni S. A review of the ultrasound assessment of diaphragmatic function in clinical practice. *Respiration.* 2016;91(5):403–11. <https://doi.org/10.1159/000446518>.
 25. Zambon M, Greco M, Bocchino S, Cabrini L, Beccaria PF, Zangrillo A. Assessment of diaphragmatic dysfunction in the critically ill patient with ultrasound: a systematic review. *Intensive Care Med.* 2017;43(1):29–38. <https://doi.org/10.1007/s00134-016-4524-z>.
 26. Rehan VK, Laiprasert J, Wallach M, Rubin LP, McCool FD. Diaphragm dimensions of the healthy preterm infant. *Pediatrics.* 2001;108(5):E91. <https://doi.org/10.1542/peds.108.5.e91>.
 27. Rehan VK, McCool FD. Diaphragm dimensions of the healthy term infant. *Acta Paediatr.* 2003;92(9):1062–7.
 28. Lee E-P, Hsia S-H, Hsiao H-F, Chen M-C, Lin J-J, Chan O-W, Lin C-Y, Yang M-C, Liao S-L, Lai S-H. Evaluation of diaphragmatic function in mechanically ventilated children: an ultrasound study. *PLoS One.* 2017;12(8):e0183560. <https://doi.org/10.1371/journal.pone.0183560>.
 29. Glau CL, Conlon TW, Himebauch AS, Yehya N, Weiss SL, Berg RA, Nishisaki A. Progressive diaphragm atrophy in pediatric acute respiratory failure. *Pediatr Crit Care Med.* 2018;19(5):406–11. <https://doi.org/10.1097/PCC.0000000000001485>.
 30. Iljand MM, Lemson J, van der Hoeven JG, Heunks LMA. The impact of critical illness on the expiratory muscles and the diaphragm assessed by ultrasound in mechanical ventilated children. *Ann Intensive Care.* 2020;10(1):115. <https://doi.org/10.1186/s13613-020-00731-2>.
 31. Buonsenso D, Supino MC, Giglioni E, Battaglia M, Mesturino A, Scateni S, Scialanga B, Reale A, Musolino AMC. Point of care diaphragm ultrasound in infants with bronchiolitis: a prospective study. *Pediatr Pulmonol.* 2018;53(6):778–86. <https://doi.org/10.1002/ppul.23993>.
 32. Alonso-Ojembarrena A, Ruiz-González E, Estepa-Pedregosa L, Armenteros-López AI, Segado-Arenas A, Lubián-López SP. Reproducibility and reference values of diaphragmatic shortening fraction for term and premature infants. *Pediatr Pulmonol.* 2020;55(8):1963–8. <https://doi.org/10.1002/ppul.24866>.
 33. El-Halaby H, Abdel-Hady H, Alsawah G, Abdelrahman A, El-Tahan H. Sonographic evaluation of diaphragmatic excursion and thickness in healthy infants and children. *J Ultrasound Med.* 2016;35(1):167–75. <https://doi.org/10.7863/ultra.15.01082>.
 34. Boon AJ, Harper CJ, Ghahfarokhi LS, Strommen JA, Watson JC, Sorenson EJ. Two-dimensional ultrasound imaging of the diaphragm: quantitative values in normal subjects. *Muscle Nerve.* 2013;47(6):884–9. <https://doi.org/10.1002/mus.23702>.
 35. Goligher EC, Laghi F, Detsky ME, Farias P, Murray A, Brace D, Brochard LJ, Sebastien-Bolz S, Rubinfeld GD, Kavanagh BP, et al. Measuring diaphragm thickness with ultrasound in mechanically ventilated patients: feasibility, reproducibility and validity. *Intensive Care Med.* 2015;41(4):642–9. <https://doi.org/10.1007/s00134-015-3687-3>.
 36. Boussuges A, Rives S, Finance J, Brégeon F. Assessment of diaphragmatic function by ultrasonography: current approach and perspectives. *World J Clin Cases.* 2020;8(12):2408–24. <https://doi.org/10.12998/wjcc.v8.i12.2408>.
 37. Mistri S, Dhochak N, Jana M, Jat KR, Sankar J, Kabra SK, Lodha R. Diaphragmatic atrophy and dysfunction in critically ill mechanically ventilated children. *Pediatr Pulmonol.* 2020;55(12):3457–64. <https://doi.org/10.1002/ppul.25076>.
 38. Öztürk E, Tanıdır İC, Yıldız O, Yükcü B, Ergün S, Haydın S, Güzeltaş A. Ultrasonographic postoperative evaluation of diaphragm function of patients with congenital heart defects. *Turk Gogus Kalp Damar Cerrahisi Derg.* 2020;28(1):70–5. <https://doi.org/10.5606/tgkdc.dergisi.2020.18458>.
 39. Hamadah HK, Kabbani MS, Elbarbary M, Hijazi O, Shaath G, Ismail S, Qadi AMH, AlTaweel H, Jijeh A. Ultrasound for diaphragmatic dysfunction in postoperative cardiac children. *Cardiol Young.* 2017;27(3):452–8. <https://doi.org/10.1017/S1047951116000718>.
 40. Hosokawa T, Tanami Y, Sato Y, Nomura K, Oguma E. A novel sonographic sign of paradoxical move-

- ment of diaphragmatic paralysis in pediatric patients after cardiovascular surgery. *Radiol Case Rep.* 2021;16(4):777–84. <https://doi.org/10.1016/j.radcr.2021.01.033>.
41. Kim WY, Suh HJ, Hong SB, Koh Y, Lim CM. Diaphragm dysfunction assessed by ultrasonography: influence on weaning from mechanical ventilation. *Crit Care Med.* 2011;39(12):2627–30. <https://doi.org/10.1097/CCM.0b013e3182266408>.
 42. DiNino E, Gartman EJ, Sethi JM, McCool FD. Diaphragm ultrasound as a predictor of successful extubation from mechanical ventilation. *Thorax.* 2014;69(5):431–5. <https://doi.org/10.1136/thoraxjnl-2013-204111>.
 43. Ferrari G, De Filippi G, Elia F, Panero F, Volpicelli G, Aprà F. Diaphragm ultrasound as a new index of discontinuation from mechanical ventilation. *Crit Ultrasound J.* 2014;6(1):8. <https://doi.org/10.1186/2036-7902-6-8>.
 44. Xue Y, Zhang Z, Sheng C-Q, Li Y-M, Jia F-Y. The predictive value of diaphragm ultrasound for weaning outcomes in critically ill children. *BMC Pulm Med.* 2019;19(1):270. <https://doi.org/10.1186/s12890-019-1034-0>.
 45. Abdel Rahman DA, Saber S, El-Maghraby A. Diaphragm and lung ultrasound indices in prediction of outcome of weaning from mechanical ventilation in pediatric intensive care unit. *Indian J Pediatr.* 2020;87(6):413–20. <https://doi.org/10.1007/s12098-019-03177-y>.
 46. Palkar A, Narasimhan M, Greenberg H, Singh K, Koenig S, Mayo P, Gottesman E. Diaphragm excursion-time index: a new parameter using ultrasonography to predict extubation outcome. *Chest.* 2018;153(5):1213–20. <https://doi.org/10.1016/j.chest.2018.01.007>.
 47. Spadaro S, Grasso S, Mauri T, Dalla Corte F, Alvisi V, Ragazzi R, Cricca V, Biondi G, Di Mussi R, Marangoni E, et al. Can diaphragmatic ultrasonography performed during the T-tube trial predict weaning failure? The role of diaphragmatic rapid shallow breathing index. *Crit Care.* 2016;20(1):305. <https://doi.org/10.1186/s13054-016-1479-y>.
 48. Abbas A, Embarak S, Walaa M, Lutfy SM. Role of diaphragmatic rapid shallow breathing index in predicting weaning outcome in patients with acute exacerbation of COPD. *Int J Chron Obstruct Pulmon Dis.* 2018;13:1655–61. <https://doi.org/10.2147/COPD.S161691>.
 49. Pirompanich P, Romsaiyut S. Use of diaphragm thickening fraction combined with rapid shallow breathing index for predicting success of weaning from mechanical ventilator in medical patients. *J Intensive Care.* 2018;6(1):6. <https://doi.org/10.1186/s40560-018-0277-9>.
 50. Soilemezi E, Savvidou S, Sotiriou P, Smyrniotis D, Tsagourias M, Matamis D. Tissue Doppler imaging of the diaphragm in healthy subjects and critically ill patients. *Am J Respir Crit Care Med.* 2020;202(7):1005–12. <https://doi.org/10.1164/rccm.201912-2341OC>.
 51. Maurizio R, Rinaldi VE, Camerini PG, Salvatori C, Leonardi A, Bini V. Right diaphragmatic peak motion velocities on pulsed wave tissue Doppler imaging in neonates: method, reproducibility, and reference values. *J Ultrasound Med.* 2019;38(10):2695–701. <https://doi.org/10.1002/jum.14974>.
 52. Ye X, Xiao H, Bai W, Liang Y, Chen M, Zhang S. Two-dimensional strain ultrasound speckle tracking as a novel approach for the evaluation of right hemidiaphragmatic longitudinal deformation. *Exp Ther Med.* 2013;6(2):368–72. <https://doi.org/10.3892/etm.2013.1133>.
 53. Orde SR, Boon AJ, Firth DG, Villarraga HR, Sekiguchi H. Diaphragm assessment by two dimensional speckle tracking imaging in normal subjects. *BMC Anesthesiol.* 2016;16(1):43. <https://doi.org/10.1186/s12871-016-0201-6>.
 54. Oppersma E, Hatam N, Doorduyn J, van der Hoeven JG, Marx G, Goetzenich A, Fritsch S, Heunks LMA, Bruells CS. Functional assessment of the diaphragm by speckle tracking ultrasound during inspiratory loading. *J Appl Physiol.* 2017;123(5):1063–70. <https://doi.org/10.1152/jappphysiol.00095.2017>.
 55. Turton P, ALAidarous S, Welters I. A narrative review of diaphragm ultrasound to predict weaning from mechanical ventilation: where are we and where are we heading? *Ultrasound J.* 2019;11(1):2. <https://doi.org/10.1186/s13089-019-0117-8>.
 56. Flatres A, Aarab Y, Nougaret S, Garnier F, Larcher R, Amalric M, Klouche K, Etienne P, Subra G, Jaber S, et al. Real-time shear wave ultrasound elastography: a new tool for the evaluation of diaphragm and limb muscle stiffness in critically ill patients. *Crit Care.* 2020;24(1):34. <https://doi.org/10.1186/s13054-020-2745-6>.
 57. Fossé Q, Poulard T, Niérat M-C, Virolle S, Morawiec E, Hogrel J-Y, Similowski T, Demoule A, Gennisson J-L, Bachasson D, et al. Ultrasound shear wave elastography for assessing diaphragm function in mechanically ventilated patients: a breath-by-breath analysis. *Crit Care.* 2020;24(1):669. <https://doi.org/10.1186/s13054-020-03338-y>.
 58. Bachasson D, Dres M, Niérat M-C, Gennisson J-L, Hogrel J-Y, Doorduyn J, Similowski T. Diaphragm shear modulus reflects transdiaphragmatic pressure during isovolumetric inspiratory efforts and ventilation against inspiratory loading. *J Appl Physiol.* 2019;126(3):699–707. <https://doi.org/10.1152/jappphysiol.01060.2018>.
 59. Chino K, Ohya T, Katayama K, Suzuki Y. Diaphragmatic shear modulus at various submaximal inspiratory mouth pressure levels. *Respir Physiol Neurobiol.* 2018;252–253:52–7. <https://doi.org/10.1016/j.resp.2018.03.009>.
 60. Silva S, Ait Aissa D, Cocquet P, Hoarau L, Ruiz J, Ferre F, Rousset D, Mora M, Mari A, Fourcade O, et al. Combined thoracic ultrasound assessment dur-

- ing a successful weaning trial predicts postextubation distress. *Anesthesiology*. 2017;127(4):666–74. <https://doi.org/10.1097/ALN.0000000000001773>.
61. Haji K, Haji D, Canty DJ, Royse AG, Green C, Royse CF. The impact of heart, lung and diaphragmatic ultrasound on prediction of failed extubation from mechanical ventilation in critically ill patients: a prospective observational pilot study. *Crit Ultrasound J*. 2018;10(1):13. <https://doi.org/10.1186/s13089-018-0096-1>.
 62. Luo L, Li Y, Chen X, Sun B, Li W, Gu W, Wang S, Zhao S, Lv Y, Chen M, et al. Different effects of cardiac and diaphragm function assessed by ultrasound on extubation outcomes in difficult-to-wean patients: a cohort study. *BMC Pulm Med*. 2017;17(1):161. <https://doi.org/10.1186/s12890-017-0501-8>.
 63. Llamas-Álvarez AM, Tenza-Lozano EM, Latour-Pérez J. Diaphragm and lung ultrasound to predict weaning outcome. *Chest*. 2017;152(6):1140–50. <https://doi.org/10.1016/j.chest.2017.08.028>.
 64. Tenza-Lozano E, Llamas-Alvarez A, Jaimez-Navarro E, Fernández-Sánchez J. Lung and diaphragm ultrasound as predictors of success in weaning from mechanical ventilation. *Crit Ultrasound J*. 2018;10(1):12. <https://doi.org/10.1186/s13089-018-0094-3>.



Clinical Applications in Lung Point-of-Care Ultrasound Assessment in Neonates

Nadya Yousef and Daniele De Luca

Contents

Introduction	164
Technical Considerations	164
Clinical Applications of Lung Ultrasound for the Diagnosis of Neonatal Respiratory Diseases	164
Transitional Period	164
Congenital Diaphragmatic Hernia	169
Functional Use of Lung Ultrasound	170
Lung Ultrasound Scores	170
Lung Ultrasound Scores in RDS	170
Integrating Lung Ultrasound into POCUS Protocols	173
Conclusion	173
References	173

N. Yousef (✉)
Division of Pediatrics and Neonatal Critical Care
“A. Bécclère” Medical Center, Paris Saclay University
Hospitals, APHP, Paris, France
e-mail: nadya.yousef@aphp.fr

D. De Luca
Division of Pediatrics and Neonatal Critical Care
“A. Bécclère” Medical Center, Paris Saclay University
Hospitals, APHP, Paris, France

Physiopathology and Therapeutic Innovation
Unit-INSERM U999, Paris Saclay University,
Paris, France

Introduction

The field of neonatal lung point-of-care ultrasound (POCUS) is rapidly expanding. Lung POCUS is a safe and rapid bedside tool used for the diagnosis of the most common acute respiratory diseases in the newborn period. In addition, lung POCUS can be used to monitor postnatal adaptation, predict the need for ventilation and/or surfactant, and evolving chronic lung disease (CLD) [1]. Lung POCUS is especially attractive in neonates because of concerns about the potential long-term effects of radiation from repeated X-rays during their hospitalization stay in the neonatal intensive care unit [2, 3]. LU is used as an adjunct to the clinical examination and it must be always interpreted in light of available clinical findings and laboratory data [4]. The described findings for specific neonatal respiratory disorders are therefore only valid for the neonatal period when these pathologies are present.

Technical Considerations

The lungs are superficial organs. Since newborns have small chests with little subcutaneous tissue, almost any ultrasound transducer can be used to perform lung ultrasound. In order to obtain good quality images of the neonatal lung, high-frequency linear or micro-linear probes, usually with a frequency of 10 MHz or above, are most frequently utilized [5–7]. Since lung POCUS is based on the analysis of artifacts, machine settings need to be adjusted to minimize filters and facilitate the analysis of pleural sliding and artifacts as discussed in Chap. 10.

Clinical Applications of Lung Ultrasound for the Diagnosis of Neonatal Respiratory Diseases

Transitional Period

The transitional period from fetus to neonate is a unique period in life that involves complex physi-

ological processes that must occur within a short period of time. The use of lung POCUS has helped clinicians gain additional insight into the pulmonary transition.

In healthy term and near-term neonates, lung aeration and partial airway fluid clearance occur within the first few minutes of life and complete fluid clearance is usually accomplished within 3–4 hours after birth [8, 9]. A significant decrease in the number of B-lines, as an estimation of lung fluid, is observed over the first 24 hours after birth and is associated with an increase in static lung compliance [10]. Regional differences in airway clearance have been observed and may be quantified using a lung ultrasound score [11].

Most infants quickly and smoothly complete the adaptation process, but some will experience delay and present signs of distress and/or underlying disease. Lung POCUS emerges as a promising tool for the early identification of infants at risk for pulmonary maladaptation. Raimondi et al. demonstrated that early use of lung POCUS using a simple 3-point classification based on ultrasound patterns (type-1, white lung; type-2, black/white lung; type-3, normal lung) predicts the need for NICU admission for respiratory support in term and near-term infants [12]. Poerio et al. confirmed the reliability of lung POCUS performed at 30 min after birth to predict NICU admission for term and near-term infants born by cesarian section [13]. These findings may have practical implications in the management of infants born in facilities without a NICU on-site when decisions regarding transfer to another facility and separation of mother and child are required.

Transient Tachypnea of the Newborn

Transient tachypnea of the newborn (TTN) is a common cause of respiratory distress in the immediate newborn period. Lung edema observed in TTN is the result of delayed alveolar fluid resorption and clearance during the transitional period. Copetti and Cattarossi first described LU signs in TTN characterized by

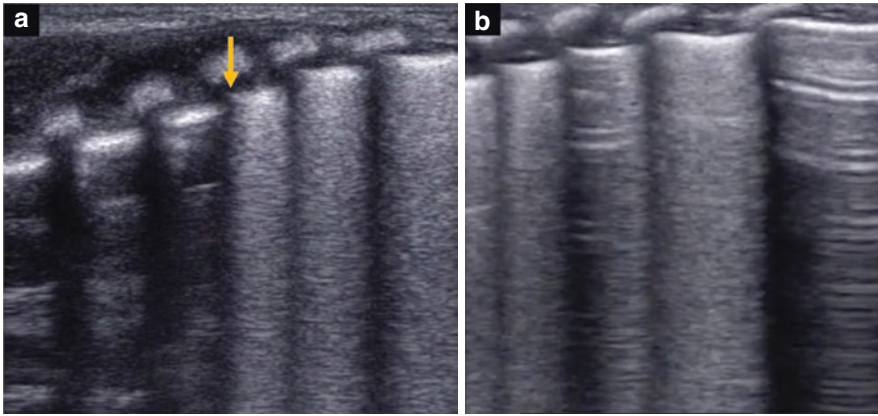


Fig. 1 Transient tachypnea of the newborn (TTN). The lung shows a mix of A- and B-lines with a well-defined pleural line. Areas with B-lines alternate with intercostal spaces with multiple A-lines and a “double lung point”

(DLP) (arrow) may be observed sharply separating both areas. The DLP is not necessary for diagnosis as shown in panel **b**

areas of B-lines (interstitial syndrome) in the lower lung fields with normal or almost normal areas (A-lines) in the upper lung fields [14]. A sharp transition between the two patterns called the “double lung point” (DLP) is typical for TTN and has not been described for any other neonatal respiratory diseases [14] (Fig. 1a). The presence of spared areas (with A-lines) in a late preterm or term neonate, with mild to moderate respiratory failure, is suggestive of TTN [14]. A regular pleural line with no consolidation is a consistent finding in TTN and may be a reliable sign to exclude other lung disorders [15]. However, future studies are needed to determine the diagnostic accuracy of these signs. Raimondi et al. demonstrated that although the presence of a DLP is a specific finding in TTN, it is not necessary for its diagnosis [15–17] (Fig. 1b). In these studies, DLP was present in roughly 50% of patients, and serial scanning showed that it could present later in the course of the disease [15]. A lung ultrasound aeration score correlates with the work of breathing in TTN and may be useful to monitor changes in lung aeration throughout the course of the disease [15].

Respiratory Distress Syndrome

Respiratory distress syndrome (RDS), originally called hyaline membrane disease, is primarily observed in preterm infants and is the result of

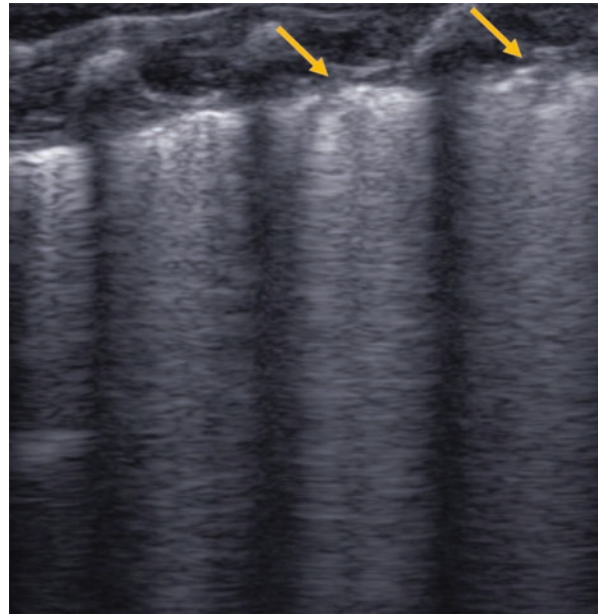
insufficient surfactant production. The risk and severity of RDS is inversely proportional to gestational age. Surfactant deficiency leads to reduced pulmonary compliance and increased alveolar surface tension leading to alveolar collapse and reduced surface area for gas exchange. RDS may present with other conditions including pneumonia, early onset sepsis, and/or air leaks [1].

Lung ultrasound imaging in RDS reflects the underlying pathophysiology with loss of aeration and decreased air/fluid ratio in the lungs. The lungs show severe diffuse alveolo-interstitial syndrome with an irregular pleural line, microconsolidations (“subpleural consolidations”), and uncountable, “confluent” B-lines giving rise to a bilateral uniform “white lung” appearance as first described by Copetti et al. [6] (Fig. 2). There are no spared areas, i.e., no areas with A-pattern, in severe RDS. Lung sliding is preserved. Other findings include “subpleural” microconsolidations and/or an irregular pleural line [6]. An adapted neonatal lung ultrasound score may be used to predict the need for surfactant in preterm infants with RDS and guide surfactant administration (see below).

Lung Ultrasound in RDS and TTN

Lung POCUS can accurately and reliably diagnose and differentiate TTN and RDS and little

Fig. 2 Respiratory distress syndrome (RDS). The lung has a “white” lung appearance with no spared areas. The pleural line is thick and irregular with “subpleural” microconsolidations (arrows)



previous experience is needed to achieve a high level of inter-operator concordance. From a pathophysiological point of view, RDS is a more severe and homogeneously diffuse condition than TTN. The absence of spared areas (with A-pattern) on lung ultrasound is the main difference between RDS when compared to TTN. Furthermore, ultrasound findings in RDS do not show short-term changes as is the case with TTN [15]. Interestingly, there appears to be a mixed-type RDS/TTN respiratory condition when fluid retention is associated with partial surfactant deficiency [1]. The clinical picture in these mixed cases is often more severe than the “classic” TTN, with longer recovery times, high noninvasive respiratory support and, occasionally, the need for surfactant administration [1]. Lamellar body count for these babies with mixed-type RDS/TTN is decreased, and although spared areas on lung POCUS are seen, these are often limited to a few areas compared with the “classic” TTN [18]. A semi-quantitative lung ultrasound aeration score correlates well with the quality of available endogenous surfactant and may be an interesting tool in studying this patient subgroup [19].

Pneumothorax

The diagnosis of pneumothorax in neonates is based on the same signs described in the adult literature and described in Chap. 10 [20]:

1. Loss of lung sliding and lung pulse with the presence of the “stratosphere sign” on the M-mode
2. The exclusive presence of A-lines with the absence of any other artifact (e.g., B-lines, Z-lines or consolidation)
3. The presence of a lung point (which may not be found in a large pneumothorax)

Lung POCUS can be used to rapidly diagnose or rule out tension pneumothorax in the newborn and shows excellent diagnostic accuracy which is superior to chest X-rays a time to diagnosis that is significantly shorter [21–23]. The diagnostic accuracy of lung POCUS for the diagnosis of pneumothorax in newborns appears to be higher than in adults. A meta-analysis performed by Dahamarde showed a sensitivity of 96.7% (88.3–99.6%), a specificity of 100% (97.7–100%), with an odds ratio of 1343.1% (167.20–10788.9) in neonates compared to a sensitivity of 82.9%

(78.3–86.9%), a specificity of 98.2% (97.0–99.0%), and an odds ratio of 423.13% (45.222–3959.1) in adults [24]. According to current recommendations, lung POCUS should be used to not only diagnose pneumothorax in children and neonates but also to provide guidance for thoracentesis [25].

Meconium Aspiration Syndrome

Meconium aspiration syndrome (MAS) is a common cause of neonatal respiratory distress which carries variable severity. The presence of meconium in the airways leads to airway obstruction and alveolar collapse, while the chemical properties of meconium induce lung tissue inflammation, chemical alveolar injury, and surfactant damage [26]. When lung injury is sufficiently severe and diffuse, it may lead to a severe oxygenation deficit fulfilling the criteria for neonatal acute respiratory distress syndrome (nARDS) [27]. The heterogeneous nature of MAS is reflected in the lung POCUS findings (Fig. 3) with signs of airway obstruction by meconium plugs (atelectasis and/or consolidation) and lung inflammation (interstitial syndrome and consolidation) [28, 29]. Mild or moderate pleural effusion may also be present. Images for the same patient may include normal lung areas, interstitial pattern, alveolar pattern, and consolidations with bronchograms and atelectasis [28, 29]. These

images are dynamic and change rapidly over the course of the disease. The lung ultrasound score (LUS) in MAS shows a significant negative correlation with the quality of available endogenous surfactant [30].

Pneumonia

Diagnosis of congenital pneumonia currently relies on clinical, biological, and radiological findings. Adding lung POCUS to the investigation of a newborn with suspected congenital pneumonia may increase the specificity of the diagnosis, especially for complicated cases [31]. The typical lung POCUS signs of pneumonia are the presence of consolidations with air bronchograms, and an irregular pleural line with areas of B-lines with or without pleural effusion (Fig. 4). These signs have a high diagnostic accuracy according to the study performed by Liu et al. [32]. Similar results were found by Chen et al. in a larger cohort of 3405 Chinese neonates who were routinely scanned using lung ultrasound [33]. This is consistent with data from the pediatric population where a meta-analysis of eight diagnostic studies (765 patients including both neonates and children) yielded a sensitivity and a specificity of 96 and 93%, respectively, which is superior to the accuracy of chest X-rays and comparable to that obtained combining radiology and laboratory exams [34].

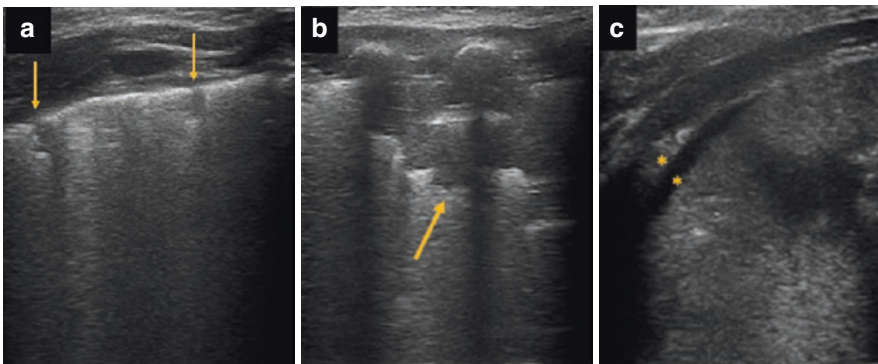
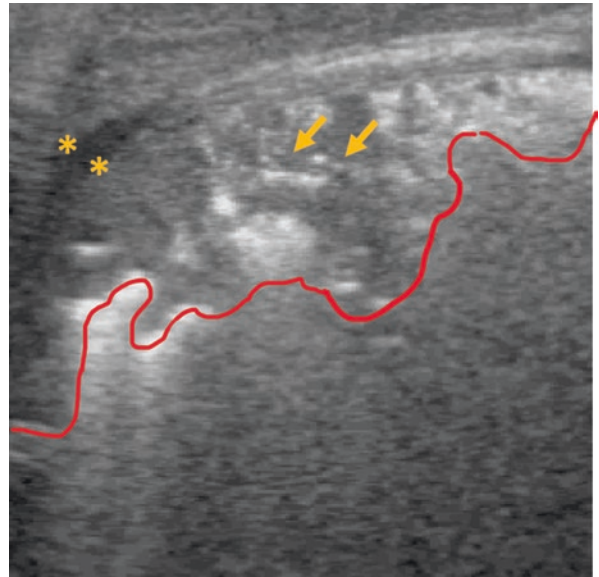


Fig. 3 Meconium aspiration syndrome (MAS). Lung ultrasound images from a neonate presenting with severe MAS. Lung ultrasound reveals heterogeneous findings related to injury and obstruction by meconium. Panel **a**: scan of the anterior chest wall showing an irregular pleural line with small consolidations (arrows) and multiple

B-lines. Panel **b**: scan of the lateral chest wall showing multiple B-lines and a large consolidation with irregular borders (arrow). Panel **c**: horizontal (transcostal) scan of the posterior chest wall showing consolidation with a rim of pleural effusion (*)

Fig. 4 Pneumonia. Horizontal (transcostal) scan of the anterolateral region of the chest. Typical signs of pneumonia are shown and include consolidation with shred sign (traced in red) with air bronchograms (arrows), areas with B-lines, and pleural effusion (*)



Many questions still remain unanswered regarding the diagnosis of neonatal pneumonia. For example, the abovementioned lung ultrasound signs are typically associated with pneumonia, but congenital pneumonia may also present with an alveolar-interstitial pattern, and an irregular pleural line with or without small consolidations [35]. These findings will need to be confirmed in larger studies. Lung POCUS may also be an interesting tool in the diagnosis and management of neonatal ventilator-associated pneumonia (VAP) as described in a recent study by Tusor et al. [36]. The proposed multiparametric score including clinical variables and lung ultrasound findings demonstrates promising predictive values for diagnosis of VAP in neonates with underlying CLD but needs further testing in larger patient populations under prospective, multicenter clinical trial settings.

Bronchopulmonary Dysplasia

Bronchopulmonary dysplasia (BPD) remains a major negative outcome of prematurity. BPD is a continuum starting soon after, or even before birth, and potentially continuing throughout infancy as chronic respiratory morbidity. BPD is characterized by its evolutive nature and its variable clinical severity [37]. Lung POCUS can document the evolving changes of BPD that include pleural line

abnormalities, areas with B-lines, and consolidations and reflect the non-homogenous nature of the disease. The characteristic lung POCUS finding of BPD is the presence of a thick pleural line with areas of interstitial-alveolar syndrome, in some cases a “white lung” appearance, with or without consolidations [35, 38]. Lung ultrasound can reliably predict progression towards BPD starting shortly after birth (see below).

Neonatal Acute Respiratory Distress Syndrome

ARDS is an acute and life-threatening respiratory disease characterized by extensive lung tissue inflammation, endothelial injury, and secondary surfactant dysfunction that leads to loss of lung aeration [27]. Pediatric (pARDS) and neonatal ARDS (nARDS) share the same biological and pathophysiological aspects as adult ARDS. However, nARDS may have different pathophysiology that presents specifically in the neonatal period, such as MAS, pulmonary hemorrhage, sepsis, perinatal asphyxia, pneumonia, and/or necrotizing enterocolitis [1].

Lung POCUS findings show bilateral, irregular, diffuse loss of aeration that may vary from a diffuse interstitial pattern to an irregular alveolar pattern with consolidations, air bronchograms, and atelectasis [1, 39]. The Montreux diagnostic definition of

nARDS officially requires chest radiographic findings defined as “diffuse, bilateral and irregular opacities or infiltrates, or complete opacification of the lungs, which are not fully explained by local effusion, atelectasis, RDS, TTN, or congenital lung anomalies,” but lung POCUS is used reliably for the diagnosis of ARDS in adults [40], and is considered suitable in neonates when sufficient clinical expertise is available for interpretation [41]. Further research is necessary to define the use of lung POCUS in pARDS and nARDS.

Congenital Lung and Airway Malformations

Congenital pulmonary adenomatous malformation (CPAM) and pulmonary sequestration (PS) are usually diagnosed prenatally. Although most of the babies are asymptomatic at birth, some may present with respiratory distress and/or hemodynamic compromise and require critical care and early surgical resection [42]. Chest CT and CT-angiography remain the gold standard for postnatal management of CPAM and PS, but lung

POCUS seems promising as an additional bedside tool for diagnosis, follow-up, and management. Several case series show that lung POCUS can be used to confirm lung lesions in infants with an antenatal diagnosis of CPAM [43–45]. The main lung ultrasound findings for CPAM are the presence of single or multiple cystic lesions, with or without consolidation, and have not been described for any other neonatal lung disease [43] (Fig. 5). In PS, the search for evidence of a systemic feeding vessel is essential [45].

Congenital Diaphragmatic Hernia

Congenital diaphragmatic hernia (CDH) is a complex condition with considerable associated mortality and morbidity rates. The congenital defect of the diaphragm leads to herniation of abdominal organs into the thorax and compromise of the ipsilateral as well as contralateral lung leading to lung hypoplasia and pulmonary hypertension. The role of lung POCUS in the

Fig. 5 Congenital pulmonary adenomatous malformation (CPAM). Vertical scan of a CPAM lesion. The presence of one or more cystic lesions (arrows) in the lung parenchyma is characteristic of CPAM and has not been described for other neonatal respiratory diseases

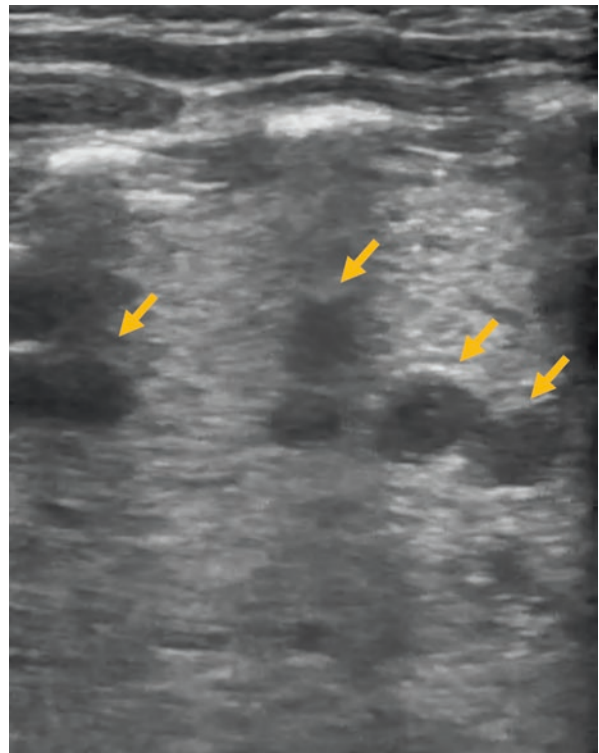
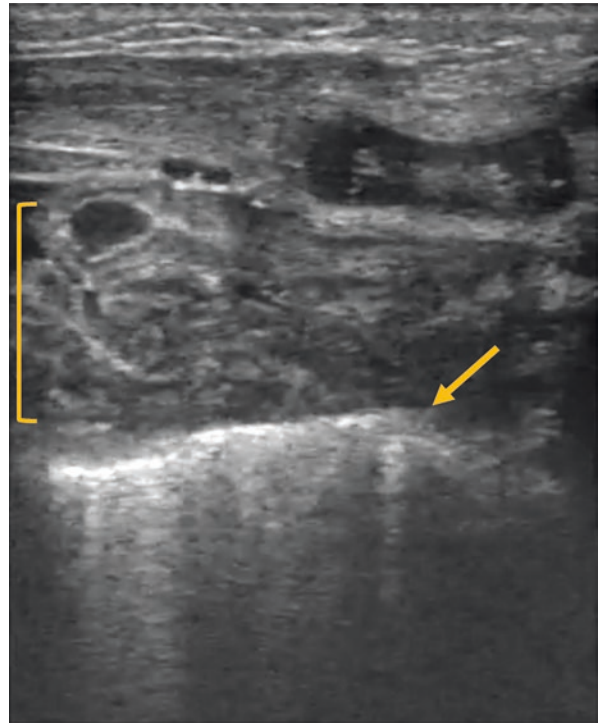


Fig. 6 Congenital diaphragmatic hernia (CDH). Vertical scan of the left anterior chest wall. In this image, loops of small bowel (bracket) are seen above the pleural line (arrow)



diagnosis and management of CDH seems promising but remains to be determined [35, 46]. Postnatal data on lung POCUS findings are scarce and limited to case descriptions. Thoracic ultrasound shows a defect in the diaphragm, with partial absence of the pleural line and absence of A-lines in the affected hemithorax, and the presence of a multilayered area with hyperechoic dynamic content (bowel) with or without abdominal organs in the thoracic cavity [46]. (Fig. 6).

Functional Use of Lung Ultrasound

Lung POCUS is a valuable tool for the diagnosis of the most common respiratory diseases shown in the sections above. In addition, lung POCUS can be used to guide respiratory therapeutic interventions and help in clinical decision-making as shown below.

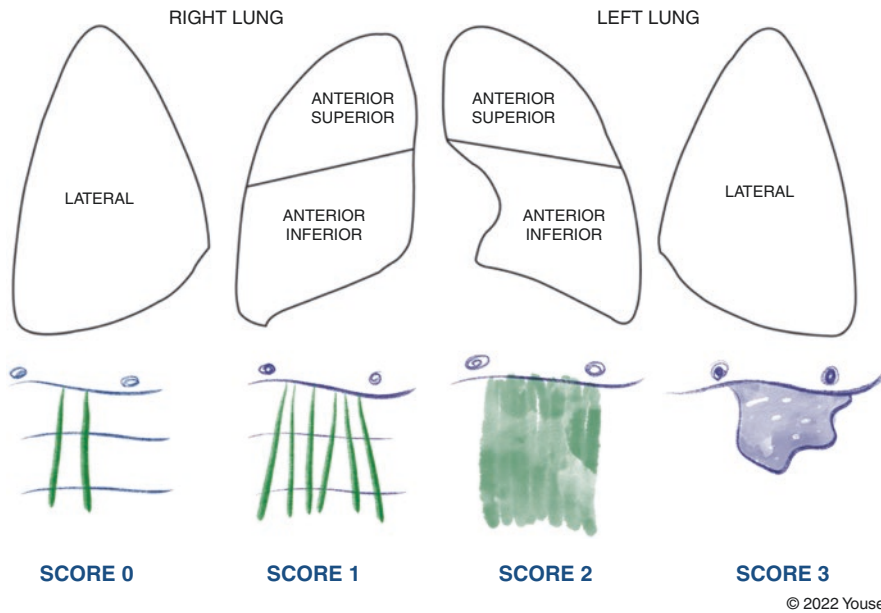
Lung Ultrasound Scores

Lung POCUS is an excellent tool for the evaluation of loss of lung aeration as it detects the arti-

facts generated when the fluid/air ratio in the lungs increases. The decrease in aeration leads to an increase in B-lines and/or a progression towards consolidation seen with complete loss of aeration. Multiple quantitative lung aeration scores have been developed based on this concept and are widely used in adult critical medicine to guide ventilation and lung recruitment, as well as for other applications [47, 48]. Quantitative and semi-quantitative LUS are fairly recent techniques in pediatric and neonatal critical care and are based on the same principles as adult scores [1]. The following subsections will discuss a few main applications of LUS in newborn (Fig. 7).

Lung Ultrasound Scores in RDS

The lung in RDS is characterized by a loss of aeration as a result of alveolar collapse due to surfactant deficiency. A quantitative LUS first published by Brat et al. is a simplified version of the adult lung ultrasound aeration scores [7]. The LUS is specifically adapted for newborn and correlates significantly with the quality of available surfactant [19]. Each lung is divided into three



© 2022 Yousef

Fig. 7 The LUS score. © 2022 Yousef. All rights reserved with permission. The lung ultrasound score allows for a quantitative evaluation of lung aeration in the newborn. Each lung is divided into three regions. A score of 0–3 is given for each region and added to give a total score of

0–18; 0 is given for <3 B-lines per intercostal space, 1 >3 B-lines per intercostal space, 2 when there are uncountable B-lines and disappearance of A-lines, and 3 is given for consolidation. The LUS is the sum of the regional scores and is inversely correlated with lung aeration

regions (anterior superior and inferior, and lateral) and a score from 0 to 3 is given to each region according to the degree of lung aeration (Fig. 8). The LUS is calculated as the sum of regional scores (maximal score of 18) and shows high accuracy in predicting surfactant need in CPAP-treated preterm and extremely preterm infants [7, 49] with a meta-analytical AUC of 0.952 (95% CI: 0.951–0.953) for LUS cutoff value between 6 and 8, and a higher diagnostic accuracy than chest X-rays [50, 51]. Although most authors use the score described by Brat et al., some include the posterior field in the evaluation for a total of three to six areas of each lung [50].

Another simplified semi-quantitative approach has been proposed to evaluate the loss of aeration and utilizes three basic pattern classifications: Type 1 or white lung (severe alveolo-interstitial pattern), Type 2 or white and black lung (moderate alveolo-interstitial pattern), and Type 3 or black lung (A-line pattern; normal lung) [52]. Both proposed methods show good

diagnostic accuracy for the early prediction of the need for surfactant replacement, especially for younger preterm infants compared with late preterm and term infants as shown in two recent meta-analyses [50, 53].

Surfactant administration should ideally be performed within the first 2–3 hours after birth to reduce mortality and morbidity [54]. LUS-guided surfactant replacement (also known as (Echography-guided Surfactant THERapy (ESTHER)) significantly increases the number of patients treated within the optimal 3 hours time frame, reduces oxygen exposure early in life, and improves oxygenation after surfactant dosing, without increasing the use of surfactant or changing cost/benefit ratios [55–57].

Lung Ultrasound Scores in BPD

Early prediction of the respiratory clinical course and progression towards BPD are promising applications of functional lung POCUS in very low birth weight infants. Quantitative LUS allows

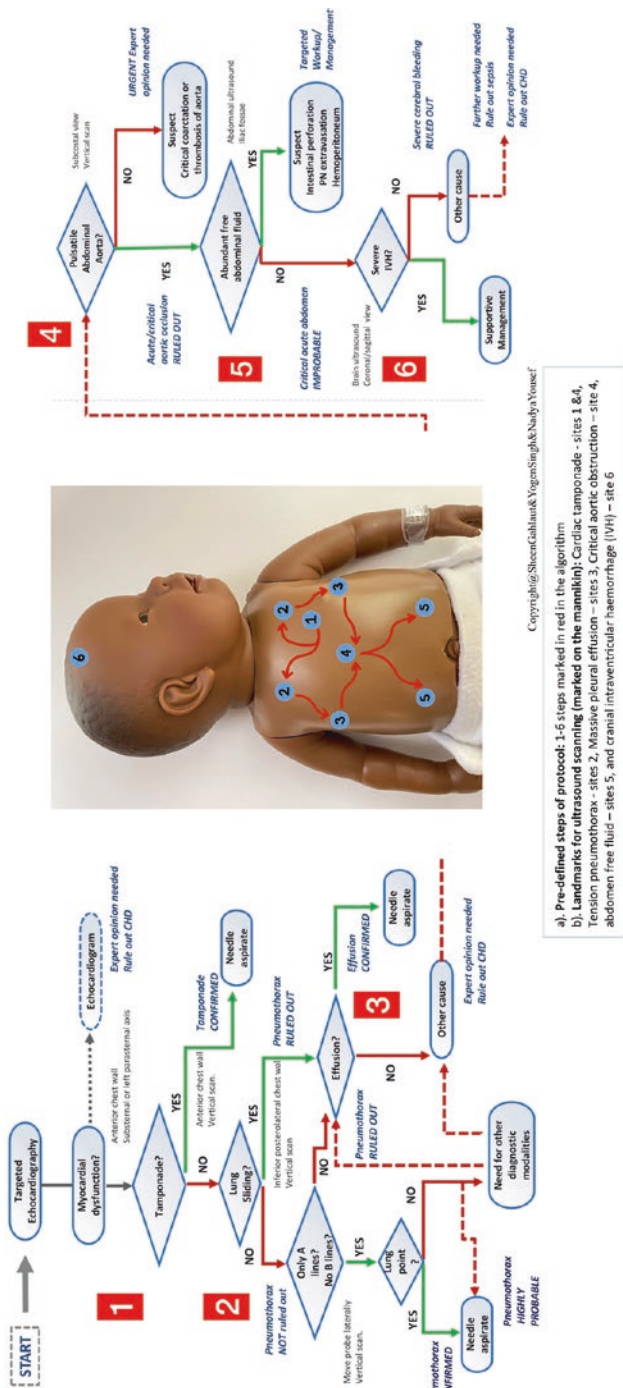


Fig. 8 The SAFE-R ultrasound protocol. © 2021 Gahlaut, Singh and Yousef. All rights reserved with permission. The SAFE-R protocol is specifically designed for the neonatologist faced with a suddenly decompensating NICU infant when no apparent cause is evident. The protocol starts at the upper left with the most urgent intra-thoracic causes: cardiac tamponade, tension pneumothorax, and pleural effusion, then includes extra-thoracic causes at the right hand of the figure with critical aortic occlusion, abdominal complication, and severe intraventricular hemorrhage. An important reminder of the possibility of congenital heart disease (CHD) needing a full echocardiogram by an expert is indicated on both sides of the panel since for the neonatal population this remains an important differential diagnosis. The step-by-step ultrasound protocol uses a single probe, at standardized SAFE points and a simple rule-in/rule-out approach. The decision tree is designed by urgency, and the order of the standardized points allows for a logical and easy use of the ultrasound probe from the thorax to the abdominal aorta, the iliac fossae, and then the head

a). Pre-defined steps of protocol: 1-6 steps marked in red in the algorithm
 b). Landmarks for ultrasound scanning (marked in red in the algorithm): Cardiac tamponade - sites 1 & 4, Tension pneumothorax - sites 2, 3, 4, Massive pleural effusion - sites 3, Critical aortic obstruction - site 4, Abdomen free fluid - sites 5, and cranial intraventricular haemorrhage (IVH) - site 6

Copyright © Sheem Gahlaut & Yogesh Singh & Nadiyah Yousef

to monitor changes in lung aeration and lung function in extremely preterm infants over time.

Serial studies in preterm infants demonstrate a significant difference in the trajectory of LUS in infants who later develop BPD and those who do not [58–60]. This difference is observed as early as 1 week after birth. LUS are accurate for early prediction of BPD and moderate to severe BPD, in an average population of preterm infants <32 weeks' gestation as shown in a recent analysis by Pezza et al. [61]. These authors evaluated the use of LUS (the LUS described by Brat et al. and eLUS, an extended LUS including posterior lung regions) for the prediction of progression towards BPD diagnosed at 36 weeks gestational age. Seven studies (1027 neonates) were meta-analyzed. Both LUS and eLUS showed good diagnostic accuracy in predicting BPD at 7 and 14 days after birth (AUC 0.85–0.87; pooled sensitivity, 70–80%; pooled specificity, 80–87%) [61]. There is currently no specific treatment for BPD, but the ability to predict BPD at an early stage may have practical implications for the management of at-risk infants in the future.

Integrating Lung Ultrasound into POCUS Protocols

Targeted emergency ultrasound protocols are widely used in adult medicine in many situations, e.g., dyspnea [62], shock [62, 63], and cardiac arrest [63, 64]. There is a need for specific and adapted ultrasound protocols for the neonatal population. SAFE-R (Sonographic Assessment of liFe-threatening Emergencies—Revised) is the first ultrasound protocol specifically designed for the neonatologist faced with a suddenly decompensating infant in the NICU and aims to help guide initial management and resuscitation efforts [65].

SAFE-R uses standardized ultrasound points and a simple one-probe rule-in/rule-out approach and needs minimal training to perform (Fig. 8). SAFE-R allows for rapid screening for the most common life-threatening complications needing immediate attention, thereby allowing the clinician to quickly initiate treatment, or in the case of

a negative screen, to promptly assess for other neonatal conditions such as sepsis, decompensation of metabolic or endocrine disorders, or critical congenital heart disease needing urgent comprehensive echocardiography.

The SAFE-R protocol requires prospective evaluation as have similar adult critical care ultrasound protocols [62]. Although any probe can be used, the optimal probe needs to be determined for each specific study [5]. International collaborative efforts are ongoing to develop and evaluate targeted multiorgan ultrasound protocols.

Conclusion

The integration of lung POCUS into clinical practice promises to transform the field of neonatology. Neonatal lung POCUS has evolved from being a purely descriptive tool for qualitative diagnosis of neonatal respiratory diseases to a functional bedside tool to quantitatively evaluate lung aeration and guide respiratory interventions. The literature on neonatal lung ultrasound has seen a rapid increase in recent years, but there persists a significant knowledge gap compared with adult critical care. Collaborative efforts and multicenter studies using rigorous methodology will hopefully contribute to increase experience and knowledge regarding applications in the coming years.

References

1. Raimondi F, Yousef N, Migliaro F, Capasso L, De Luca D. Point-of-care lung ultrasound in neonatology: classification into descriptive and functional applications. *Pediatr Res*. 2018.
2. Cattarossi L, Copetti R, Poskurica B. Radiation exposure early in life can be reduced by lung ultrasound. *Chest*. 2011;139(3):730–1.
3. Escourrou G, De Luca D. Lung ultrasound decreased radiation exposure in preterm infants in a neonatal intensive care unit. *Acta Paediatr*. 2016;105(5):e237–9.
4. Raimondi F, Migliaro F, De Luca D, Yousef N, Rodríguez FJ. Clinical data are essential to validate lung ultrasound. *Chest*. 2016;149(6):1575.

5. Gomond-Le Goff C, Vivalda L, Foligno S, Loi B, Yousef N, De Luca D. Effect of different probes and expertise on the interpretation reliability of point-of-care lung ultrasound. *Chest*. 2020;157(4):924–31.
6. Copetti R, Cattarossi L, Macagno F, Violino M, Furlan R. Lung ultrasound in respiratory distress syndrome: a useful tool for early diagnosis. *Neonatology*. 2008;94(1):52–9.
7. Brat R, Yousef N, Klifa R, Reynaud S, Shankar Aguilera S, De Luca D. Lung ultrasonography score to evaluate oxygenation and surfactant need in neonates treated with continuous positive airway pressure. *JAMA Pediatr*. 2015;169(8):e151797.
8. Blank DA, Rogerson SR, Kamlin COF, Fox LM, Lorenz L, Kane SC, et al. Lung ultrasound during the initiation of breathing in healthy term and late preterm infants immediately after birth, a prospective, observational study. *Resuscitation*. 2017;114:59–65.
9. Blank DA, Gaertner VD, Kamlin COF, Nyland K, Eckard NO, Dawson JA, et al. Respiratory changes in term infants immediately after birth. *Resuscitation*. 2018;130:105–10.
10. Martelius L, S uviri L, Jan er C, Helve O, Kaskinen A, Kirjavainen T, et al. Lung ultrasound and static lung compliance during postnatal adaptation in healthy term infants. *Neonatology*. 2015;108(4):287–92.
11. Guo BB, Wang KK, Xie L, Liu XJ, Chen XY, Zhang F, Chen C, Wu CJ. Comprehensive Quantitative Assessment of Lung Liquid Clearance by Lung Ultrasound Score in Neonates with No Lung Disease during the First 24 Hours. *Biomed Res Int*. 2020;24:2020:6598348. <https://doi.org/10.1155/2020/6598348>. PMID: 32185213; PMCID: PMC7060879.
12. Raimondi F, Migliaro F, Sodano A, Umbaldo A, Romano A, Vallone G, et al. Can neonatal lung ultrasound monitor fluid clearance and predict the need of respiratory support? *Crit Care*. 2012;16(6):R220.
13. Poerio A, Galletti S, Baldazzi M, Martini S, Rollo A, Spinedi S, et al. Lung ultrasound features predict admission to the neonatal intensive care unit in infants with transient neonatal tachypnoea or respiratory distress syndrome born by caesarean section. *Eur J Pediatr*. 2021;180(3):869–76.
14. Copetti R, Cattarossi L. The “double lung point”: an ultrasound sign diagnostic of transient tachypnea of the newborn. *Neonatology*. 2007;91(3):203–9.
15. Raimondi F, Yousef N, Rodriguez Fanjul J, De Luca D, Corsini I, Shankar-Aguilera S, et al. A multicenter lung ultrasound study on transient tachypnea of the neonate. *Neonatology*. 2019;115(3):263–8.
16. Vergine M, Copetti R, Brusa G, Cattarossi L. Lung ultrasound accuracy in respiratory distress syndrome and transient tachypnea of the newborn. *Neonatology*. 2014;106(2):87–93.
17. Liu J, Chen XX, Li XW, Chen SW, Wang Y, Fu W. Lung Ultrasonography to Diagnose Transient Tachypnea of the Newborn. *Chest*. 2016;149(5):1269–75.
18. Machado LU, Fiori HH, Baldisserotto M, Ramos Garcia PC, Vieira ACG, Fiori RM. Surfactant deficiency in transient tachypnea of the newborn. *J Pediatr*. 2011;159(5):750–4.
19. Autilio C, Echaide M, Benachi A, Marfaing-Koka A, Capoluongo ED, P erez-Gil J, et al. A noninvasive surfactant adsorption test predicting the need for surfactant therapy in preterm infants treated with continuous positive airway pressure. *J Pediatr*. 2017;182:66–73.e1.
20. Lichtenstein DA. Lung ultrasound in the critically ill. *Ann Intensive Care*. 2014;4(1):1.
21. Raimondi F, Rodriguez Fanjul J, Aversa S, Chirico G, Yousef N, De Luca D, et al. Lung ultrasound for diagnosing pneumothorax in the critically ill neonate. *J Pediatr*. 2016;175:74–78.e1.
22. Alrajab S, Youssef AM, Akkus NI, Caldito G. Pleural ultrasonography versus chest radiography for the diagnosis of pneumothorax: review of the literature and meta-analysis. *Crit Care*. 2013;17(5):R208.
23. Cattarossi L, Copetti R, Brusa G, Pintaldi S. Lung ultrasound diagnostic accuracy in neonatal pneumothorax. *Can Respir J*. 2016;2016:6515069.
24. Dahmarde H, Paroie F, Salarzaei M. Accuracy of ultrasound in diagnosis of pneumothorax: a comparison between neonates and adults—a systematic review and meta-analysis. *Can Respir J*. 2019;2019:5271982.
25. Singh Y, Tissot C, Fraga MV, Yousef N, Cortes RG, Lopez J, et al. International evidence-based guidelines on point of care ultrasound (POCUS) for critically ill neonates and children issued by the POCUS Working Group of the European Society of Paediatric and Neonatal Intensive Care (ESPNIC). *Crit Care*. 2020;24(1):65.
26. Kopincova J, Calkovska A. Meconium-induced inflammation and surfactant inactivation: specifics of molecular mechanisms. *Pediatr Res*. 2016;79(4):514–21.
27. De Luca D, van Kaam AH, Tingay DG, Courtney SE, Danhaive O, Carnielli VP, et al. The Montreux definition of neonatal ARDS: biological and clinical background behind the description of a new entity. *Lancet Respir Med*. 2017;5(8):657–66.
28. Piastra M, Yousef N, Brat R, Manzoni P, Mokhtari M, De Luca D. Lung ultrasound findings in meconium aspiration syndrome. *Early Hum Dev*. 2014;90(Suppl 2):S41–3.
29. Liu J, Cao HY, Fu W. Lung ultrasonography to diagnose meconium aspiration syndrome of the newborn. *J Int Med Res*. 2016;44(6):1534–42.
30. Autilio C, Echaide M, Shankar-Aguilera S, Bragado R, Amidani D, Salomone F, et al. Surfactant injury in the early phase of severe meconium aspiration syndrome. *Am J Respir Cell Mol Biol*. 2020;63(3):327–37.
31. Meau-Petit V, Fox GF. Atypical presentation of congenital pneumonia: value of lung ultrasound. *J Adv Pediatr Child Health*. 2021;4(1):033–4.

32. Liu J, Liu F, Liu Y, Wang HW, Feng ZC. Lung ultrasonography for the diagnosis of severe neonatal pneumonia. *Chest*. 2014;146(2):383–8.
33. Chen SW, Fu W, Liu J, Wang Y. Routine application of lung ultrasonography in the neonatal intensive care unit. *Medicine (Baltimore)*. 2017;96(2):e5826.
34. Pereda MA, Chavez MA, Hooper-Miele CC, Gilman RH, Steinhoff MC, Ellington LE, et al. Lung ultrasound for the diagnosis of pneumonia in children: a meta-analysis. *Pediatrics*. 2015;135(4):714–22.
35. ESPNIC textbooks [Internet]. ESPNIC. [cited 2022 May 4]. <https://www.espnic.eu/education/textbooks/>.
36. Tumor N, De Cunto A, Basma Y, Klein JL, Meau-Petit V. Ventilator-associated pneumonia in neonates: the role of point of care lung ultrasound. *Eur J Pediatr*. 2021;180(1):137–46.
37. De Luca D. The promise of lung ultrasound to monitor evolution of chronic respiratory morbidity in preterm infants. *Chest*. 2021;160(3):799–800.
38. Aldecoa-Bilbao V, Velilla M, Teresa-Palacio M, Esponera CB, Barbero AH, Sin-Soler M, et al. Lung ultrasound in bronchopulmonary dysplasia: patterns and predictors in very preterm infants. *Neonatology*. 2021;118(5):537–45.
39. Bellani G, Mauri T, Pesenti A. Imaging in acute lung injury and acute respiratory distress syndrome. *Curr Opin Crit Care*. 2012;18(1):29–34.
40. Rivello ED, Kiviri W, Twagirumugabe T, Mueller A, Banner-Goodspeed VM, Officer L, et al. Hospital incidence and outcomes of the acute respiratory distress syndrome using the Kigali modification of the Berlin definition. *Am J Respir Crit Care Med*. 2016;193(1):52–9.
41. De Luca D, van Kaam AH, Tingay DG, Courtney SE, Danhaive O, Carnielli VP, et al. Lung ultrasound and neonatal ARDS: is Montreux closer to Berlin than to Kigali?—authors' reply. *Lancet Respir Med*. 2017;5(11):e32.
42. Stanton M, Njere I, Ade-Ajayi N, Patel S, Davenport M. Systematic review and meta-analysis of the postnatal management of congenital cystic lung lesions. *J Pediatr Surg*. 2009;44(5):1027–33.
43. Yousef N, Mokhtari M, Durand P, Raimondi F, Migliaro F, Letourneau A, et al. Lung ultrasound findings in congenital pulmonary airway malformation. *Am J Perinatol*. 2018;35(12):1222–7.
44. Merli L, Nanni L, Curatola A, Pellegrino M, De Santis M, Silvaroli S, et al. Congenital lung malformations: a novel application for lung ultrasound? *J Ultrasound*. 2021;24(3):349–53.
45. Quercia M, Panza R, Calderoni G, Di Mauro A, Laforgia N. Lung ultrasound: a new tool in the management of congenital lung malformation. *Am J Perinatol*. 2019;36(S2):S99–S105.
46. Corsini I, Parri N, Coviello C, Leonardi V, Dani C. Lung ultrasound findings in congenital diaphragmatic hernia. *Eur J Pediatr*. 2019;178(4):491–5.
47. Mongodi S, De Luca D, Colombo A, Stella A, Santangelo E, Corradi F, et al. Quantitative lung ultrasound: technical aspects and clinical applications. *Anesthesiology*. 2021;134(6):949–65.
48. Bouhemad B, Brisson H, Le-Guen M, Arbelot C, Lu Q, Rouby JJ. Bedside ultrasound assessment of positive end-expiratory pressure-induced lung recruitment. *Am J Respir Crit Care Med*. 2011;183(3):341–7.
49. De Martino L, Yousef N, Ben-Ammar R, Raimondi F, Shankar-Aguilera S, De Luca D. Lung ultrasound score predicts surfactant need in extremely preterm neonates. *Pediatrics*. 2018;142(3):e20180463.
50. De Luca D, Autilio C, Pezza L, Shankar-Aguilera S, Tingay DG, Carnielli VP. Personalized medicine for the management of RDS in preterm neonates. *Neonatology*. 2021;118(2):127–38.
51. Perri A, Riccardi R, Iannotta R, Di Molfetta DV, Arena R, Vento G, et al. Lung ultrasonography score versus chest X-ray score to predict surfactant administration in newborns with respiratory distress syndrome. *Pediatr Pulmonol*. 2018;53(9):1231–6.
52. Raimondi F, Migliaro F, Sodano A, Ferrara T, Lama S, Vallone G, et al. Use of neonatal chest ultrasound to predict noninvasive ventilation failure. *Pediatrics*. 2014;134(4):e1089–94.
53. Razak A, Faden M. Neonatal lung ultrasonography to evaluate need for surfactant or mechanical ventilation: a systematic review and meta-analysis. *Arch Dis Child Fetal Neonatal Ed*. 2020;105(2):164–71.
54. Bahadue FL, Soll R. Early versus delayed selective surfactant treatment for neonatal respiratory distress syndrome. *Cochrane Database Syst Rev*. 2012;11:CD001456.
55. Raschetti R, Yousef N, Vigo G, Marseglia G, Centorrino R, Ben-Ammar R, et al. Echography-guided surfactant therapy to improve timeliness of surfactant replacement: a quality improvement project. *J Pediatr*. 2019;212:137–143.e1.
56. Rodríguez-Fanjul J, Jordan I, Balaguer M, Batista-Muñoz A, Ramon M, Bobillo-Perez S. Early surfactant replacement guided by lung ultrasound in preterm newborns with RDS: the ULTRASURF randomised controlled trial. *Eur J Pediatr*. 2020;179(12):1913–20.
57. De Luca D, Yousef N. Pharmaceutical expenditure is unchanged with ultrasound-guided surfactant administration. *Am J Perinatol*. 2022;39(5):562–6.
58. Abdelmawla M, Louis D, Narvey M, Elsayed Y. A lung ultrasound severity score predicts chronic lung disease in preterm infants. *Am J Perinatol*. 2019;36(13):1357–61.
59. Alonso-Ojembarrena A, Serna-Guerediaga I, Aldecoa-Bilbao V, Gregorio-Hernández R, Alonso-Quintela P, Concheiro-Guisán A, et al. The predictive value of lung ultrasound scores in developing bronchopulmonary dysplasia: a prospective multicenter diagnostic accuracy study. *Chest*. 2021;160(3):1006–16.
60. Loi B, Vigo G, Baraldi E, Raimondi F, Carnielli VP, Mosca F, et al. Lung ultrasound to monitor extremely preterm infants and predict bronchopulmonary dysplasia. A multicenter longitudinal cohort study. *Am J Respir Crit Care Med*. 2021;203(11):1398–409.

61. Pezza L, Alonso-Ojembarrena A, Elsayed Y, Yousef N, Vedovelli L, Raimondi F, et al. Meta-analysis of lung ultrasound scores for early prediction of bronchopulmonary dysplasia. *Ann Am Thorac Soc*. 2022;19(4):659–67.
62. Lichtenstein DA. BLUE-protocol and FALLS-protocol: two applications of lung ultrasound in the critically ill. *Chest*. 2015;147(6):1659–70.
63. Milne J, Atkinson P, Lewis D, Fraser J, Diegelmann L, Olszynski P, et al. Sonography in hypotension and cardiac arrest (SHoC): rates of abnormal findings in undifferentiated hypotension and during cardiac arrest as a basis for consensus on a hierarchical point of care ultrasound protocol. *Cureus*. 2016;8(4):e564.
64. Lichtenstein D, Malbrain MLNG. Critical care ultrasound in cardiac arrest. Technological requirements for performing the SESAME-protocol—a holistic approach. *Anaesthesiol Intensive Ther*. 2015;47(5):471–81.
65. Yousef N, Singh Y, De Luca D. “Playing it SAFE in the NICU” SAFE-R: a targeted diagnostic ultrasound protocol for the suddenly decompensating infant in the NICU. *Eur J Pediatr*. 2022;181(1):393–8.

Part IV

Abdominal Assessment



Abdominal Point-of-Care Ultrasound in Neonatal and Pediatric Populations

Yasser Elsayed and Vidit Bhargava

Contents

Introduction	179
Upper Abdomen (Liver, Spleen, and Stomach)	180
Lower Abdomen (Bowel, Peritoneal Cavity, and Abdominal Blood Vessels)	184
Renal and Bladder Ultrasound	192
Conclusion	195
Appendix: Intestinal Ultrasound Findings in Bowel Injury or Ischemia	195
References	202

Introduction

A broad spectrum of critical abdominal pathological conditions occurring in neonates and children warrants a real-time sonographic assessment. Abdominal radiographs have limited value with low sensitivity and specificity in many conditions, particularly in assessing bowel perfusion and microcirculation [1]. The advantages of abdominal point-of-care ultrasound

(POCUS) include that it is noninvasive, readily available, can provide information in real-time, and can guide therapeutic intervention (such as paracentesis). Thus, abdominal POCUS is an important tool for use in neonatal and pediatric abdominal emergencies [2, 3]. However, it should still be considered an adjunct rather than replacing abdominal radiographs due to its limitations and operator constraints [3].

Y. Elsayed (✉)

Section of Neonatology, Department of Pediatrics,
University of Manitoba, Winnipeg, MB, Canada

Royal College of Physicians and Surgeons,
Ottawa, ON, Canada
e-mail: yelsayed@hsc.mb.ca

V. Bhargava

Division of Pediatric Critical Care, University of
Alabama at Birmingham, Birmingham, AL, USA

Upper Abdomen (Liver, Spleen, and Stomach)

The upper abdomen can be divided into right and left sides. The right upper abdomen contains the right lobe of the liver, pylorus, and duodenum, and the left upper abdomen has the left lobe of the liver and body of the stomach. The right posterior upper abdomen contains the right lobe of the liver, and the left posterior upper abdomen contains the spleen. Figure 1 demonstrates the organs in the upper abdomen and plans for ultrasound assessment.

Liver

The recommended probe for assessment of the liver includes curvilinear and phased array transducers. The optimal patient positioning is either supine or left lateral decubitus.

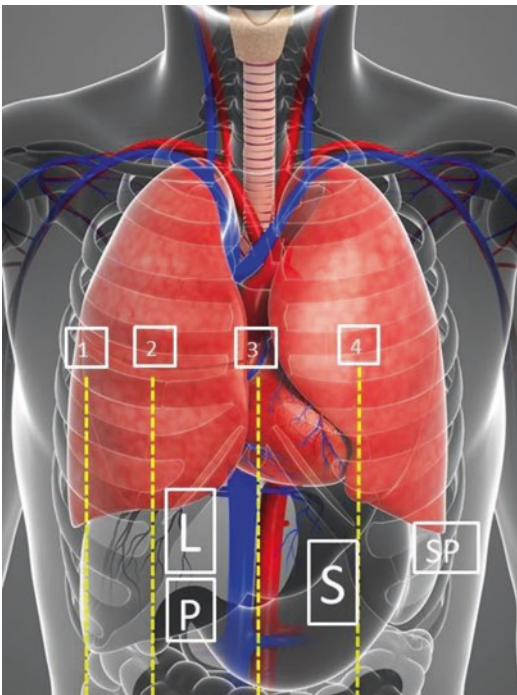


Fig. 1 The organs of the upper abdomen that can be assessed by ultrasound; the transparency of the organs reflects the anteroposterior arrangement of the organs. The ultrasound planes from right to left include (1) right anterior axillary line, (2) right midclavicular line, (3) midline, (4) left midclavicular line. *L* liver, *S* stomach, *P* pylorus, *SP* spleen

The liver can be assessed from ventral and lateral approaches, and sometimes the posterior approach is necessary for improved visualization. Providers should start with a sweep through the entire liver in sagittal and axial sections. From there they should follow the course of major blood vessels (portal vein, hepatic veins), assess the gall bladder, and eventually add Doppler if indicated.

The anterior upper right abdomen should be assessed in at least two plains: the anterior axillary and midclavicular line. All other regions of the abdomen can typically be assessed in one plain: the posterior right abdomen at the posterior axillary line, the upper left abdomen at the midclavicular line, and the posterior left abdomen at the posterior axillary line. Providers should perform 2D sagittal and axial sections in all plains and add color Doppler or pulse wave Doppler (PWD) whenever necessary.

Liver parenchyma is characterized by homogeneous echos of medium echogenicity and smooth margins. Physiologically, the left liver lobe is larger relative to the right lobe in neonates. The left lobe of a neonate gradually decreases in size after the closure of ductus venosus [4]. Figure 2 demonstrates the three-dimensional segmentation of liver and hepatic vasculature.

The ligamentum falciforme hepatis and ligamentum teres hepatis are usually only seen

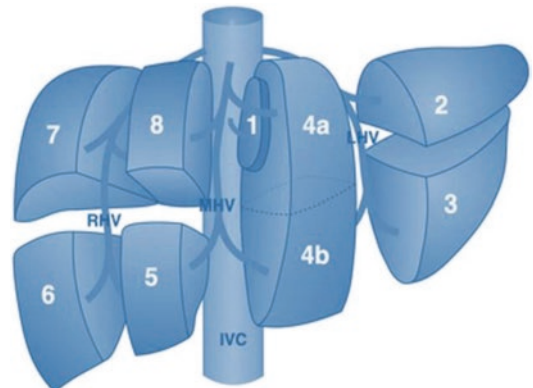


Fig. 2 Three-dimensional diagram demonstrating the relationship between the 8 liver segments. *RHV* right hepatic vein, *MHV* main hepatic vein, *LHV* left hepatic vein, *IVC* inferior vena cava

when patients have ascites. Hepatic veins converge cranially to drain into the subdiaphragmatic inferior vena cava (IVC) or the right atrium. Usually, three main hepatic veins drain into the subdiaphragmatic IVC. However, there may be other veins with insertions at different levels of the intrahepatic IVC that exist as normal variants.

The portal vein enters at the hepatic hilus and should not show signs of tapering (a sign of portal hypertension). The portal vein branches into the left and right portal veins centrally in the liver. Periportal regions become enlarged and more echogenic in various conditions or may appear prominent with decreased echogenicity of liver parenchyma. During the first few days of life in neonates, communication may persist between ductus venosus and the IVC or right atrium but should obliterate spontaneously. A persistent ductus venosus usually indicates underlying liver disease with increased peripheral liver resistance.

The hepatic artery can be followed from its origin at the celiac trunk as it branches into the left and right hepatic arteries. Usually, color Doppler enables easy identification and differentiation from other tubular structures, particularly in the liver periphery, where differentiation between the hepatic artery and pathologic dilation of intrahepatic bile ducts is otherwise difficult.

The gall bladder is positioned on the lower surface of the liver and centrally positioned close to the hilus on the right side. The gallbladder is a thin-walled structure with anechoic contents. Its size can vary depending on the time of the last enteral intake. The gallbladder is best visualized in a subcostal oblique view at the midclavicular line. Thickening of the gallbladder wall may indicate pathology, though note that an empty or poorly filled gall bladder, particularly if relatively large when filled, may show a falsely thickened wall.

Common Pathological Conditions

Liver Congestion

Liver congestion occurs in conditions characterized by increased right atrial pressure

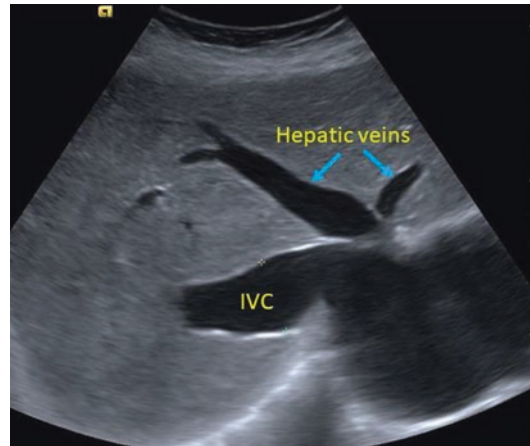


Fig. 3 Liver congestion with dilated IVC and hepatic veins (blue arrows), making the moose head sign

(e.g., secondary to congenital heart diseases or pulmonary hypertension) or hypervolemia [5].

Figure 3 demonstrates characteristic ultrasound findings in patients with liver congestion. The initial findings of liver congestion typically include an enlarged liver with reduced echogenicity, though chronic conditions may demonstrate increased echogenicity. The congested liver has a smooth surface with a rounded lower margin and dilated hepatic veins that can be followed into the liver periphery. The hepatic veins will typically empty into a dilated IVC, creating an image similar to a moose head. Patients with liver congestion may also have ascites, splenomegaly, omental thickening, and edematous thickening of the congested bowel wall. Color Doppler may demonstrate increased vascular flow into the liver periphery triggered by atrial contractions.

Tricuspid insufficiency may also be identified on cardiac imaging secondary to volume or pressure overload conditions.

Liver Hematoma

A simple hematoma or subcapsular hemorrhage is usually not life-threatening. However, the condition may become more severe if the liver capsule ruptures and significant free peritoneal fluid is visualized. It is important to recognize that free peritoneal fluid or blood appearing like complicated ascites can be found anywhere in the abdomen and does not necessarily correlate with the injury site [6].

A hematoma or subcapsular hemorrhage may have the same echogenicity as liver parenchyma. However, the disruption of other structures within the liver, such as vessels or the general contour of the liver, may be an early sign of injury. A subcapsular hemorrhage will typically appear as hypoechoic fluid around the liver (Fig. 4) [6].

Liver Contusion

A liver contusion is more challenging to diagnose compared to a hemorrhage and will often appear triangular within subcapsular regions.

Contusions are initially difficult to visualize, and their echogenicity changes from hyperechoic to hypoechoic over time (Fig. 5). Color Doppler may improve the detection of contusions by demonstrating abnormal vessel color signals in regions in which focal disruption of normal vascular architecture has occurred.

Bile Duct Gas

Identifying bile duct gas indicates an infection or distal obstruction, though it may also be transient without an identified pathophysiologic process. The bile duct is assessed from its insertion in the duodenum and inspected for any small and mobile hyperechoic foci within the lumen indicating the presence of air.

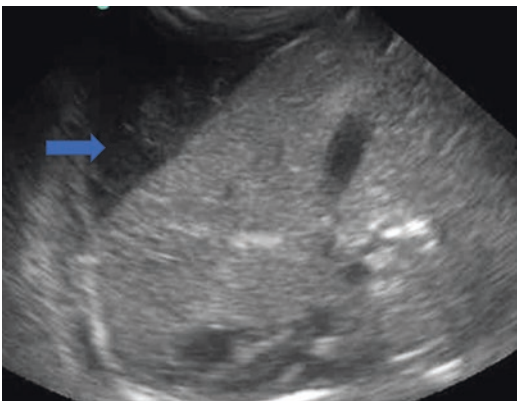


Fig. 4 Subcapsular hemorrhage with hypoechoic subcapsular collection of fluid (blue arrow)

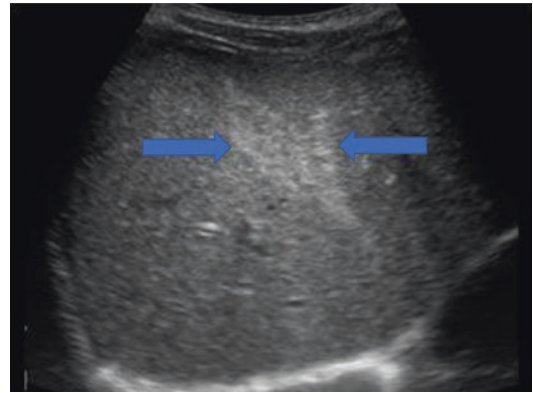


Fig. 5 Liver contusion, still hyperechoic (blue arrows)

Portal Venous Gas

Hyperechoic abnormalities “floating” in the portal venous system indicate concerning pathophysiologic abnormalities of the gastrointestinal tract, including necrotizing enterocolitis, ischemic bowel, and food protein-induced enterocolitis. The condition may also be idiopathic though the severity of conditions predisposing patients to develop portal-free air requires an extensive evaluation to rule out conditions with high morbidity and mortality [7, 8].

Most commonly, gas gathers in the dependent areas (anterior aspects of the liver in the supine position). Portal gas can be seen as tiny mobile echogenic foci (sometimes with comet-tail-like reverberation artifacts) visualized in central portal venous structures (Fig. 6) [9].

Color Doppler may demonstrate bidirectional spikes on spectral tracing identifying vascular structures, which can help differentiate between biliary and vascular air. Ultrasound is the most sensitive method for detecting air, even in mild cases that cannot be visualized using radiography. An immediate and thorough ultrasound investigation of the gastrointestinal tract is indicated if free air is identified. The finding of venous gas can be nonspecific. Therefore, the diagnosis of venous gas should integrate these ultrasound findings with other clinical data [3, 10].

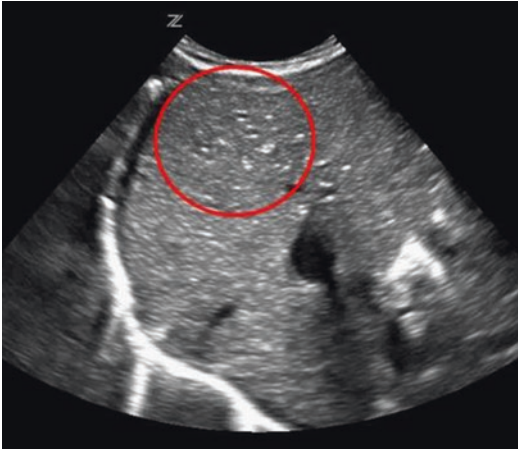


Fig. 6 Liver image with portal venous gases, more prominent inside the red circle

Spleen

An enlarged spleen on palpation is a frequent indication for abdominal ultrasound and may indicate systemic diseases, including oncologic processes, infections, or portal hypertension. The recommended probe for assessment of the spleen is typically curvilinear or phased array probe. Linear transducers can be used for detailed analysis, especially in younger children and infants with thin abdominal walls. Patients are optimally positioned in a right lateral decubitus position [4]. The spleen is also often interrogated during trauma assessments, and this is likely the most common reason for evaluation by acute care providers. Splenic injury resulting in hemorrhage can be common in blunt abdominal trauma in children and may also be present due to birth trauma. Children are capable of hemodynamic compensation even in the presence of severe hemorrhage. Thus, they are at risk of sudden deterioration at the extremes of physiologic perturbation rendering a thorough ultrasound investigation of the abdomen particularly valuable to rule out bleeding from splenic injury [4].

Splenic injury may result in increased spleen size due to subcapsular hematoma, which sometimes cannot be discriminated from normal spleen tissue in the early post-trauma stages of injury. Peri-splenic fluid, either simple or complex due to the sedimentation of erythrocytes,

may be present and indicative of hemorrhage. Contusions without hemorrhage often only exhibit regionally heterogeneous abnormalities without the demarcation present with a hematoma. With splenic laceration, the contour of the parenchyma is disrupted, and free fluid is often visualized. With splenic injury, there may also be evidence of reduced diaphragmatic motion.

Stomach

The stomach is optimally assessed in a fasted patient or patient with full stomach contents since any air will preclude the transmission of ultrasound waves. Due to the frequent presence of gas in the stomach, this organ can be difficult to image using ultrasound. Typically, patients are initially positioned in the supine position, though positioning maneuvers, including moving patients to the right or left lateral decubitus positions, may aid in the visualization of structures.

Near-field structures such as the pylorus and ventral wall of the stomach can be best visualized using high-resolution linear (or curved array) transducers [11]. The indications for gastric ultrasound include non-bilious vomiting, the assessment of gastric contents, and its inclusion in upper abdominal ultrasound protocols.

Stomach imaging includes ultrasound interrogation of the subxiphoid, median, or upper left abdomen. Images may be improved by using the left lobe of the liver as a window for acquisition. A focused assessment of the gastroduodenal outlet (pylorus) may utilize windows from the upper right quadrant. Systematic assessment localizes either the gastroesophageal entrance or pylorus with axial scanning through the stomach before transitioning to the longitudinal plane. The longitudinal plane is the optimum view for identifying inlet or outlet abnormalities. Ultrasonographers can assess for reflux or intermittent herniation towards the thoracic space at the gastroesophageal junction and can assess functionality in transitioning stomach contents into the duodenal bulb at the pylorus.

A normal stomach demonstrates a collapsed distal esophagus and gastroesophageal junction which should not measure more than 5–7 mm in young infants. The gastric wall, similar to the

bowel wall, has five layers and a wall thickness typically less than 3–4 mm. The inner mucosa is echogenic and appears thin. The contour of inner mucosa and gastric folds can be visualized if the stomach is sufficiently filled with anechoic fluid or other medium, allowing for ultrasound wave transmission. The ultrasound appearance of stomach contents varies depending on fluid or food content and the amount of air. The pylorus usually shows a slight thickening of the muscular wall compared to the stomach [11].

Common Pathological Conditions

Gastroesophageal Reflux (GER)

Reflux of stomach contents to the esophagus is characterized by small amounts of intermittent regurgitation through the gastroesophageal junction and can be physiologic in the first 6 months of life. The assessment can incorporate the provision of reflux by drinking formula or using a water test in older children. Optimal images can be acquired by placing the patient in the left lateral decubitus position with slight pressure on the abdomen with a transducer.

Abnormal findings include regurgitation of fluid from the stomach into the esophagus with variable dilation of the gastric inlet. Abnormalities can be quantified and qualified by assessing the number and duration of reflux episodes with the concurrent characterization of esophageal clearance and wall thickness. The presence of gastric structure herniation into the thoracic cavity can also be evaluated within the scope of this exam [12].

Hypertrophic Pyloric Stenosis

Clinically, pyloric stenosis is characterized by episodic abdominal pain with propulsive non-bilious vomiting and most commonly occurs in boys aged 4–12 weeks of age. Pyloric stenosis is typically treated surgically, though conservative medical management may be an option in early and mild disease as well as in patients with high surgical risk [11, 13].

Figure 7 demonstrates ultrasound findings consistent with pyloric stenosis. These include

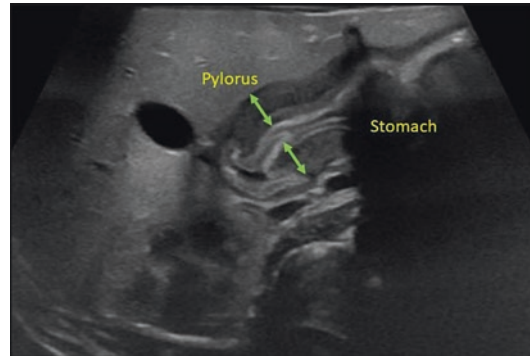


Fig. 7 The thickening of the muscular layer in hypertrophic pyloric stenosis (green arrows)

pyloric enlargement of the length (>15 mm), thickness (>3 mm), axial diameter (≥ 12 mm), and wall-to-lumen ratio (>2:1). There will be a change in wall thickness from the stomach to the pylorus with a typical shoulder-like contour at the pyloric entrance. Often the pylorus will be displaced and gastric enlargement with residual volume will present in fasted children.

Lower Abdomen (Bowel, Peritoneal Cavity, and Abdominal Blood Vessels)

Visualizing the bowel is easier after feeding and with less air content; therefore, neonates are an optimal population for interrogation since the bowel is full of fluid and meconium immediately after birth. A saline enema may help visualize the colon and can be used therapeutically in meconium ileus [14, 15].

There are numerous indications for bowel ultrasound in children, most notably to evaluate concerns for bowel obstruction and/or ischemic processes, including unique (or more prevalent) conditions found in pediatric populations, including necrotizing enterocolitis, intussusception, volvulus, intestinal Henoch–Schoenlein purpura, appendicitis, food protein-induced enterocolitis or in pediatric abdominal trauma.

To interrogate the lower abdomen patients are usually positioned supine and with relaxed abdominal wall musculature as tolerated (sometimes optimized by support to the knees flexed crani-

ally). In general, higher frequency linear transducers optimize image resolution in younger patients. Curvilinear and phased array probes allow for better scanning depths. Therefore, the optimal probe and frequency for assessment often depend upon the patient age and position of the targeted bowel segment. 2D Imaging of abdominal regions can be complemented by using color Doppler imaging, and the bowel should be assessed in sagittal and axial sectional sweeps [3, 10, 16].

The first step in assessing lower abdominal contents is identifying well-defined structures (e.g., pylorus, cecum, and rectum). Follow respective loops continuously from distal to proximal or the opposite direction. The jejunum occupies the upper left quadrant of the abdomen, while the ileum typically occupies the lower right quadrant (Fig. 8). The jejunal wall is thicker and mucosa is characterized by luminal folds called plicae circularis, while the ileum wall is thinner with smoother mucosa. The colonic wall demonstrates dome-shaped colonic haustra and is generally smooth and thin. Figure 9 is a cartoon simulating the ultrasound view of different bowel structures [16].

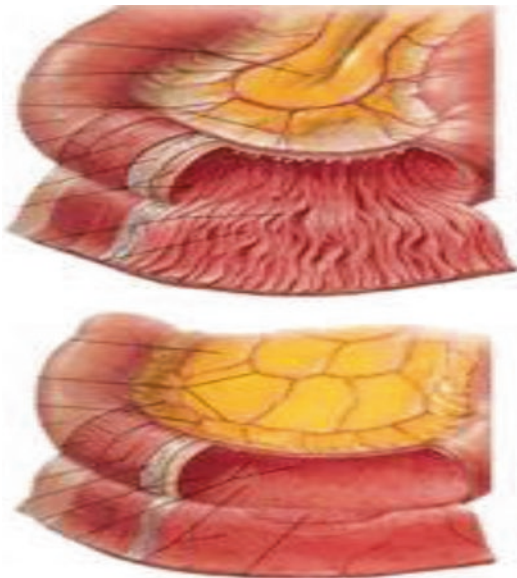


Fig. 8 The lumen of the jejunum is thick and rich in mucosal folds; the ileum wall is thin with a smooth mucosal surface

Imaging any portion of the bowel allows for assessment of wall structure and thickness, size (including concerning regions of stenosis), compressibility, and presence of peristalsis and its direction. Providers can assess the lumen for content and longitudinal sections to describe the inner contour for segment differentiation (Fig. 10) and the presence of stenosis.

Adding color Doppler can be an important component of assessing bowel wall vasculature and perfusion. Assessment of the mesenteric artery/vein orientation and celiac trunk is helpful to determine the presence of malrotation. Normal bowel will demonstrate a characteristic “intestinal signature” with at least three, but frequently all five layers of muscle and mucosa (Figs. 11 and 12) [10, 17, 18].

Normal small bowel is smooth, with clear layered walls, most lumens collapsed, and obvious peristalsis. It contains fluid, gas, and stool with variable echogenicity (Fig. 11). The five layers of the bowel wall can be identified in a high-quality image as in Fig. 12.

As general rules, a well-perfused intestine is hypoechoic with a normal intestinal signature, and an ischemic intestine is echogenic and often with an absent intestinal signature. Significant sonographic findings associated with pathophysiologic processes in neonates and children include (Appendix):

1. The presence of linear or punctate echogenic foci outside of the bowel with multiple A-line artifacts (Fig. 13) indicating pneumoperitoneum.
2. Focal fluid collections with complex echoes or septations within the fluid collections.
3. Bowel wall thickening greater than 2.6 mm or greater.
4. Bowel wall thinning less than 11.0 mm.
5. Loss of intestinal wall signature with an overall increase in mural echogenicity.
6. Pneumatosis intestinalis defined by the presence of punctate echogenic foci within the bowel wall in absence of artifact shadows.
7. Portal venous gas identified by the presence of punctate or linear moving echogenic foci within the portal vessels.

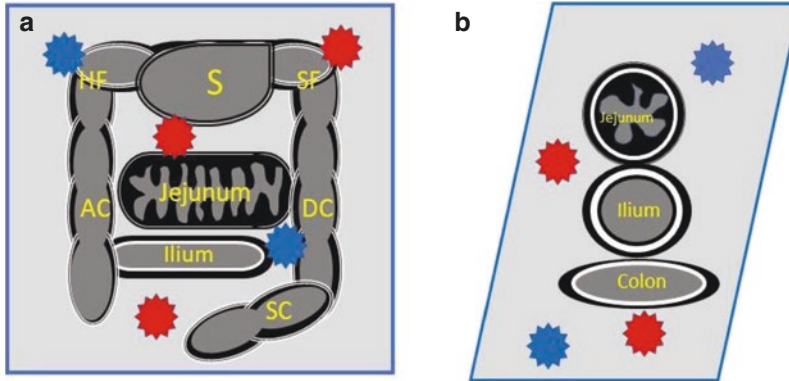


Fig. 9 Cartoon simulating the normal ultrasound images of bowel structures in sagittal section (a), and axial section (b). (a) S stomach which may overlap the transverse colon, HF hepatic flexure, SF splenic flexure, AC ascending colon, DC descending colon, SC sigmoid colon. The jejunum is representing the upper left part of lower abdomen, it has a thick wall and mucosal folds, and ilium is the lower right part, it has a thin smooth wall. Colonic wall is

also smooth and thin but also has haustra design, the color Doppler appear as small speckles, 3–9 speckle in each 2×2 color box. (b) The axial section of jejunum which has a thicker wall compared to ilium and colon, and wall in all views has multiple layers which gives the normal wall signature. The red and blue stars are representing normal speckles of color Doppler

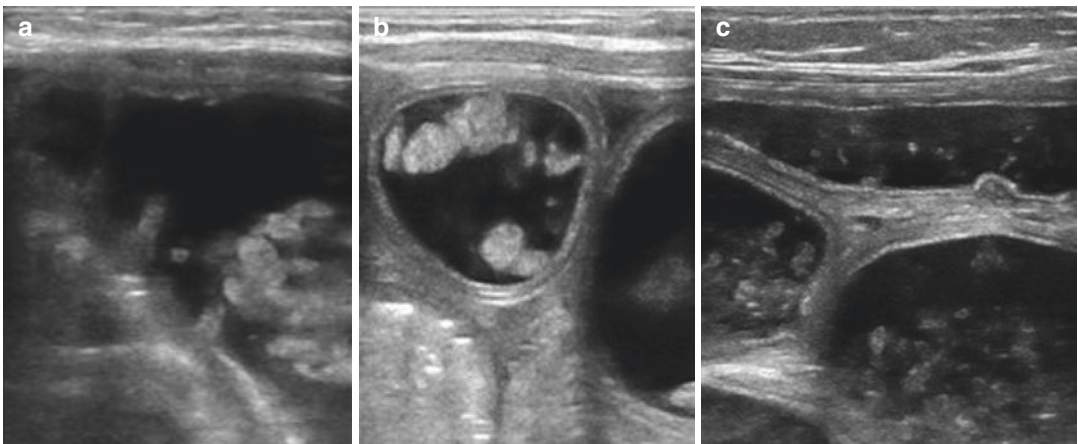


Fig. 10 The left image (a) is jejunum in sagittal section with internal mucosal folds, the middle image (b) is axial section of ileum with smooth internal surface, and the

right image (c) of colon with haustra. Notice the multilayers of the normal walls

8. Increased perfusion identified by an abnormal color Doppler pattern signifying hyperemia. Of note, a normal bowel color Doppler pattern is the presence of 3–9 small, scattered speckles within one assessment frame (Fig. 11).
9. Absent flow within a loop of bowel on color Doppler imaging.
10. Absent peristalsis defined as no bowel movement on a recorded clip for 60 seconds.
11. Dilated bowel with anechoic contents defined by the presence of anechoic fluid within bowel with a diameter equal to or greater than two vertebral body heights (as measured on radiography; this can be used as a convenient internal control for size) [16, 19].

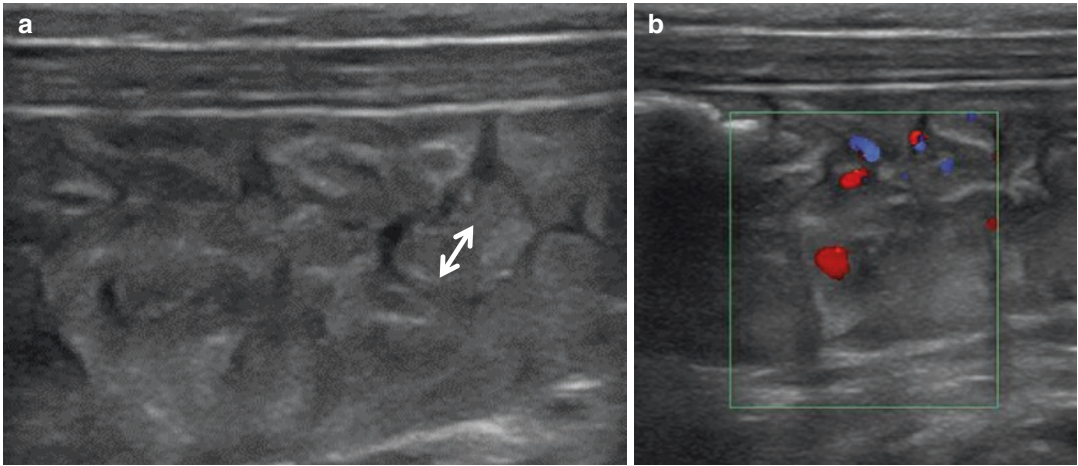


Fig. 11 The left image (a) is the gray or hypochoic appearance of normal bowels. They appear crowded, with no peritoneal fluid, and would demonstrate active peristal-

sis in a live clip. The white arrow represents the thickness of a loop of bowel. The right image (b) is normal appearance of color Doppler over healthy bowel

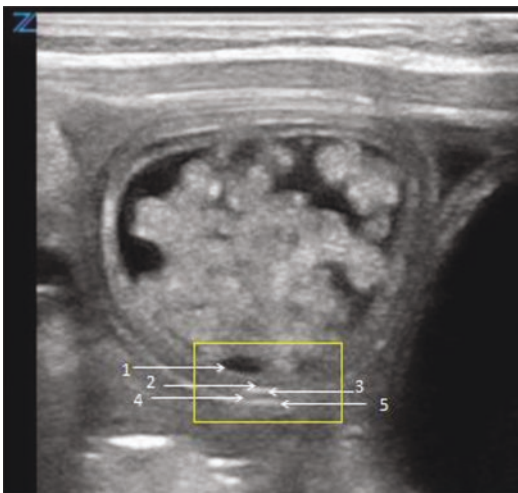


Fig. 12 The five layers of normal intestinal walls (“intestinal signature”): (1) mucosal interface with the lumen and it is echogenic layer, (2) hypochoic true mucosa, (3) echogenic submucosa, (4) hypochoic muscularis, (5) echogenic serosa

To assess suspected bowel injury, the provider can work systematically by beginning with the assessment of the liver. The liver echotexture can be evaluated by sweeping both right and left lobes in sagittal and axial sections which is important to detect portal venous gas as described previously. Further, the provider can assess for clots in the hepatic or portal veins, and evaluate the gall bladder for abnormalities. The bowel can

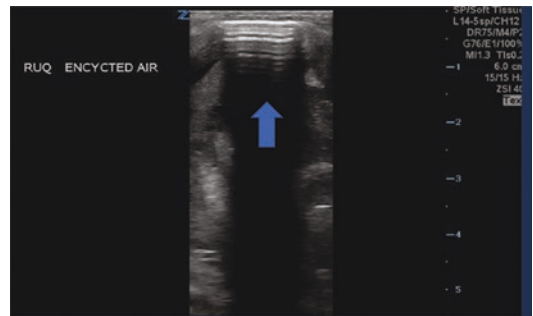


Fig. 13 Perforated bowel with encysted air collection presented as echogenic parallel artifact A-lines with a shadow underneath (blue arrow)

then be systematically inspected for the 11 ultrasound abnormalities discussed above. The colon is best assessed in the subhepatic area and lateral flanks and can be distinguished by colonic haustra.

Figure 14 shows the 4 abdominal quadrants that should be assessed by ultrasound including the right upper quadrant (containing part of the right lobe of the liver, right hepatic flexure of colon, gall bladder, pylorus, duodenum, and part of jejunum), right lower quadrant (containing the ascending colon, cecum, ilium, and appendix), left upper quadrant (containing the splenic flexure, descending colon, and jejunum), and left lower quadrant (containing portions of the jeju-

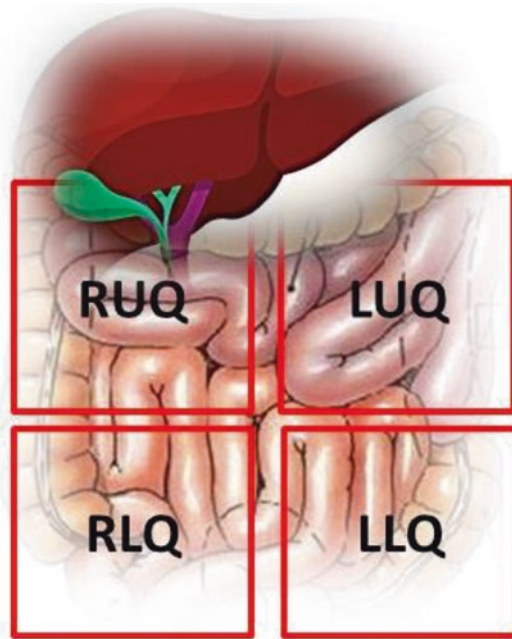


Fig. 14 Assessment of bowel should include 4 different quadrants. Notice the liver overlap part of the right upper quadrant. *RUQ* right upper quadrant, *RLQ* right lower quadrant, *LUQ* left upper quadrant, *LLQ* left lower quadrant

num, ileum, descending colon, and sigmoid colon) [9, 16, 19, 20].

Abnormalities identified above may be incorporated into clinical diagnostics to support or refute the presence of clinical pathophysiologic processes. Appendix identifies the different ultrasound findings in varied types of bowel injuries that are briefly discussed below.

Common Pathological Conditions

Necrotizing Enterocolitis

Necrotizing enterocolitis (NEC) is a multifactorial disease most frequently identified in preterm infants, with a peak incidence around corrected gestational ages of 29–32 weeks. In this population, NEC can be triggered by delayed feeding or periods of nil per os (NPO) as well as prolonged use of antibiotics. The presence of any of the 11 described ultrasound abnormalities should be assessed in each quadrant separately. NEC restricted to 1–2 quadrants may be considered mild to moderate and can be recognized versus

more severe progression with findings in 3–4 quadrants [21]. The presence of bowel wall thickening or thinning, absent peristalsis, and evidence of poor perfusion on color Doppler are associated with an increased odds ratio of surgical intervention and correlate with pathological changes of the bowel. Bowel wall echogenicity has been reported in early-stage NEC and presents prior to portal venous gas or perforation [8, 22–25]. Figures 15 and 16 are cartoon representations of ultrasound findings in mild versus severe NEC.

Food Protein-Induced Enterocolitis

Food protein-induced enterocolitis (FPIE) is poorly described in the neonatal population and is commonly misdiagnosed and treated as NEC since ultrasonographic features frequently overlap. Differentiation between FPIE and NEC is crucial as management is different between the two conditions. FPIE is non-IgE-induced bowel injury due to sensitivity to food protein and occurs more frequently with artificial formula but might occur with breast milk. Recent literature suggests patients with NEC may have more global dysfunction of bowel motility compared to the regional abnormalities seen in FPIE [26].

Hypoxic/Ischemic Bowel

Ischemic bowel injury might be associated with severe hypoxic ischemic encephalopathy (HIE) or associated with compromised oxygen delivery due to severe anemia, shock, congenital heart diseases with compromised systemic blood flow, or severe hypoxemia. Compromised blood flow secondary to an anatomical “twist” of the bowel as in patients with malrotation, volvulus, or intussusception requires urgent surgical intervention [24, 25] as discussed later in this chapter.

Henoch–Schönlein Purpura

Henoch–Schönlein Purpura is a systemic vasculopathy that may affect the bowel, kidneys, and other organs. Ultrasound findings are nonspecific and may demonstrate an echogenic and thickened bowel wall (particularly the mucosa). The lumen may also contain echogenic content due to hemorrhage or hyperemia [6, 27].

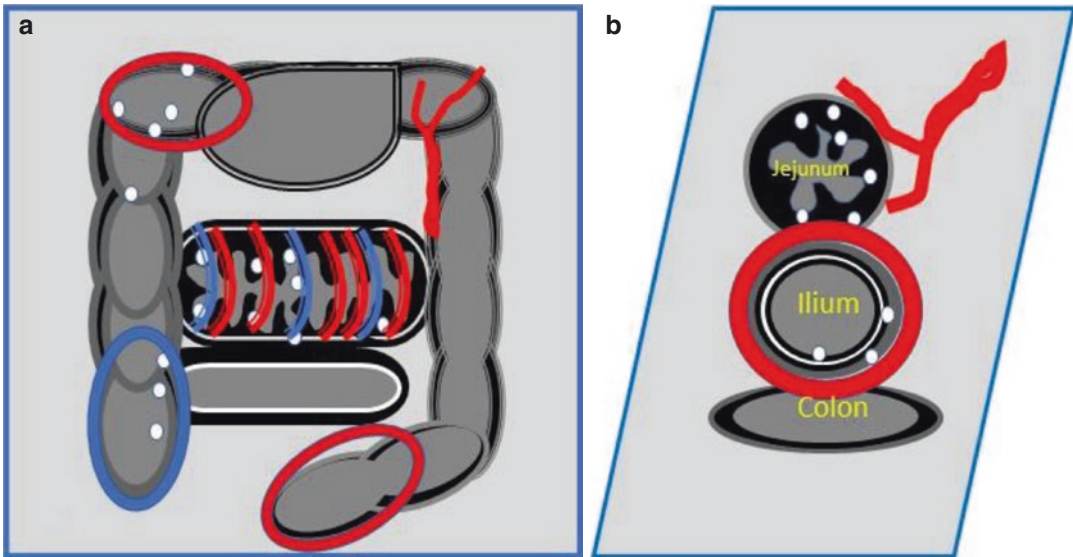


Fig. 15 Cartoon simulation of ultrasound changes in mild necrotizing enterocolitis: (a) in sagittal section, thickening walls, pneumatosis intestinalis as white tiny

dots, hyperemia as circular hyperemia, or zebra at the jejunal loops; (b) in axial section, circular and Y shaped hyperemia, thickening walls

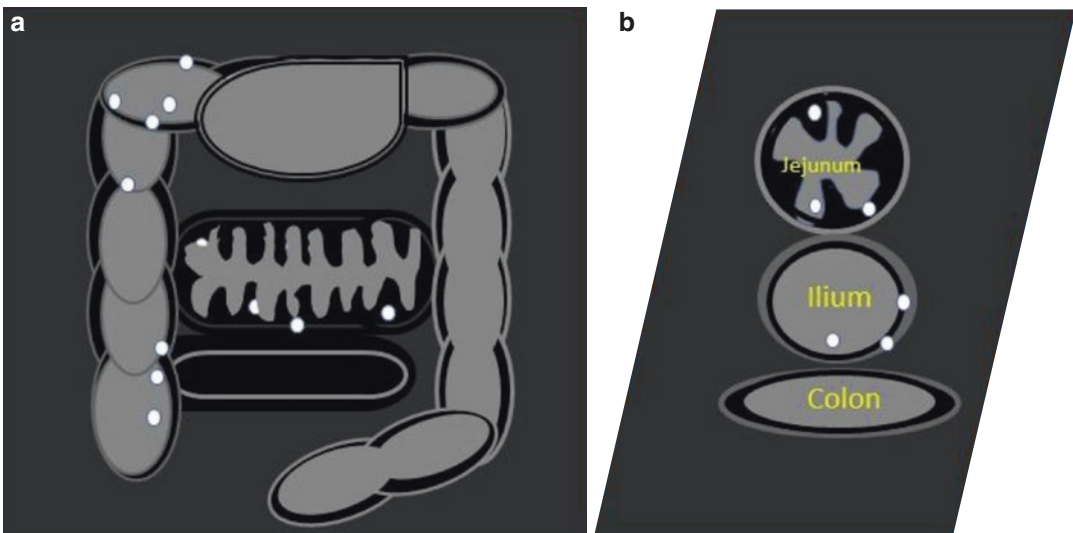


Fig. 16 Cartoon simulation of ultrasound changes in severe necrotizing enterocolitis: (a) in sagittal section, thinning walls, pneumatosis intestinalis as white tiny dots,

ischemia as absent signals of color Doppler, absent intestinal signature, floating loops in ascitic fluids; (b) in axial section, similar findings

Atresia

Congenital atresia is defined by the occlusion of bowel lumen. Ultrasound findings proximal to the atretic bowel demonstrate fluid-filled distended bowel loops with a sudden change in diameter at the site of obstruction. Distal to the obstruction, the bowel loops appear collapsed. In “high” atre-

sia (i.e., duodenum, jejunum) meconium may be present distal to the obstruction. In distal atresia the bowel will be without meconium and appear narrow, referred to as “empty bowel.” Figure 17 is an ultrasound image at the RUQ with a microcolon secondary to ileal atresia [28, 29].

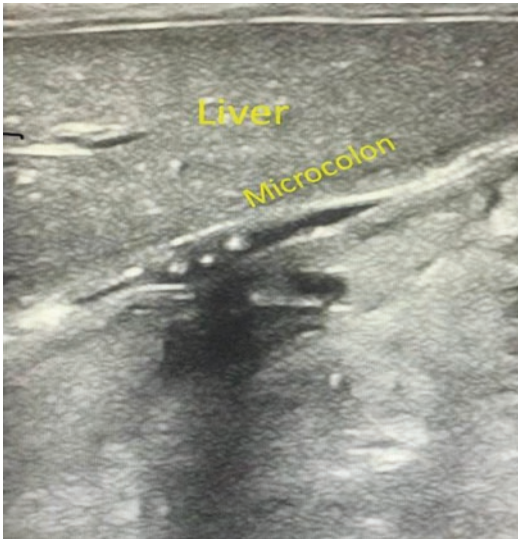


Fig. 17 Ultrasound image of the RUQ with microcolon secondary to ileal atresia

Malrotation

Malrotation is an atypical rotation or abnormal fixation of bowel presenting with obstructive symptoms and due to the incomplete fetal rotation of the foregut. A characteristic ultrasound finding is the inverse orientation of the superior mesenteric artery relative to the superior mesenteric vein. The atypical position of mesenteric vessels may not be diagnostic as rotation anomalies may coexist with normal vessel orientation, and normal rotation may be present despite inverse vessel orientation. The finding of an abnormal position of the duodenum-jejunal flexure by ultrasound or fluoroscopy can provide supportive evidence of malrotation [30–32].

Volvulus

Volvulus is the twisted torsion of the upper small bowel around the mesenteric root resulting in vascular compromise, bowel ischemia, and hemorrhagic infarction. Volvulus commonly presents in the first weeks of life as a surgical emergency [30, 33]. Volvulus is characterized by the presence of a dilated, fluid-filled duodenum with abrupt disruption due to the clockwise-twisted dilated superior mesenteric vein which curls around the more centrally positioned superior mesenteric artery. This is known ultrasonograph-

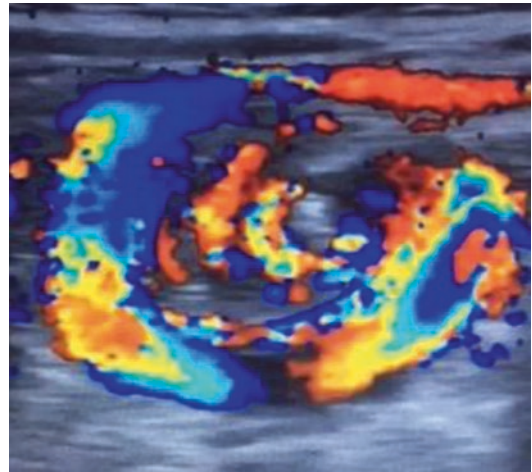


Fig. 18 Whirlpool sign which is an important color Doppler marker in the diagnosis of volvulus

ically as “whirlpool sign” (Fig. 18). Similar to other bowel pathological processes, the presence of 2D ultrasound findings depends upon the severity and duration of the volvulus. In more severe cases ultrasound may reveal the presence of peritoneal fluid and thickened echogenic bowel wall with hemorrhage and edema. Twisted bowel may appear donut-shaped (Fig. 19). Ultrasound is reliable for diagnosing volvulus and, once the whirlpool sign is visualized, time is critical for successful surgical intervention. In equivocal situations, emergency fluoroscopy should be performed to establish the diagnosis [30].

Hirschsprung Disease

Hirschsprung disease and other neuropathies of the bowel including neuronal intestinal dysplasia are caused by a lack of appropriate bowel innervation with the absence of peristalsis resulting in progressive constipation and bowel dilatation [33, 34]. Ultrasound findings include impressive dilatation of stool-filled colon (megacolon) with the ultimate diagnosis made by biopsy and histology.

Meconium Ileus

A meconium ileus results from obstruction of bowel by inspissated meconium. This condition is commonly seen in preterm infants, after dehy-

dration, or secondary to cystic fibrosis [32]. Ultrasound findings include dilated small bowel loops with highly echogenic content (typical for meconium). Passage of meconium results in a sudden luminal change from dilated to very narrow bowel (Fig. 20).

Intussusception

Intussusception is the telescopic invagination of a proximal bowel segment (intussusceptum) into a more distal segment (intussusciens). Small bowel intussusceptions are associated with a number of conditions including gastroenteritis or hyperperistalsis and most frequently occur at the junction of the small and large bowel [2, 35].

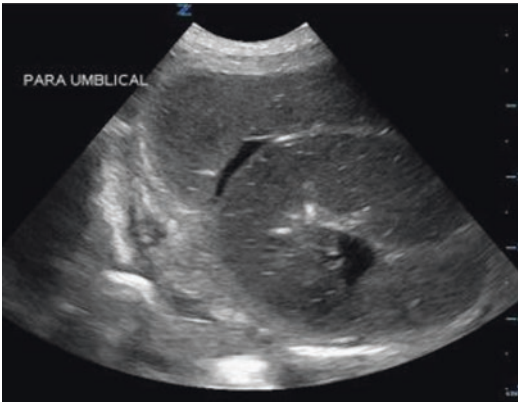
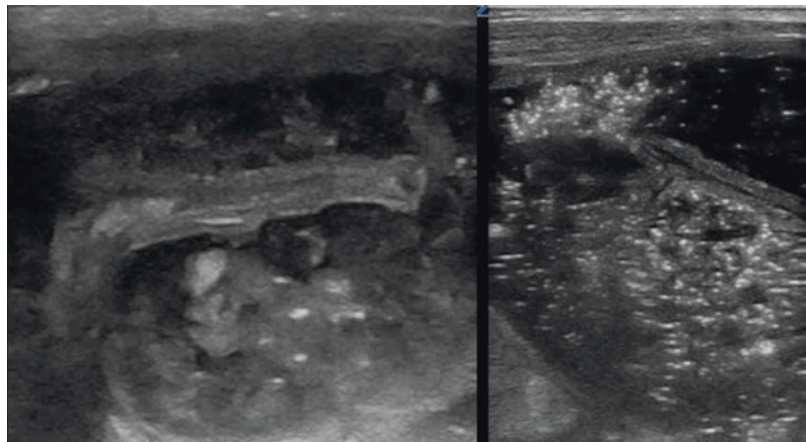


Fig. 19 Midgut ultrasound image with donut-shaped loop and thin wall. This portion of the bowel was necrosed secondary to intrauterine volvulus in a newborn and surgically removed shortly after this ultrasound

Fig. 20 Ultrasound image of an infant with meconium ileus. Dilated small bowel is present in the image on the left. The image on the right demonstrates echogenic contrast filling the dilated bowel following barium upper gastrointestinal study



Ultrasound is a reliable method of diagnosis. The invaginated portion appears as a double-walled “loop” in both sagittal and axial sections with disrupted blood flow identified by color Doppler (Fig. 21).

Appendicitis

Appendicitis is the inflammation of the appendix which risks perforation, abscess, peritonitis, and fistulae formation [6, 36]. Typically located in the right lower quadrant, the inflamed appendix can commonly be found with careful inspection around the cecal pole and the lower margin of the liver. The normal appearance of the appendix is a blind-ending tubular structure with a typical bowel wall appearance, commonly without content. The appendix is compressible with ultrasound palpation and this compression should be painless. The normal diameter of an appendix in children is 3–6 mm and, with the inflammation of appendicitis, becomes enlarged with an outer diameter >6 mm. The inflamed appendix will also be aperistaltic and non-compressible, sometimes with a hyperechoic appendicolith with posterior shadowing (Fig. 22).

Abdominal Bleeding

Ultrasound has a higher sensitivity compared to radiography in assessing and localizing abdominal bleeding and can be performed upon any infant or child suspected of having anemic shock due to traumatic or non-traumatic hemorrhage [6, 14, 37]. Ultrasound can identify blood as an

Fig. 21 Ultrasound image of an infant with intussusception before surgery. The image on the left is the axial view and on the right is the sagittal view. The blue arrow is pointing to the inner loop and red arrow is to the outer loop in both images

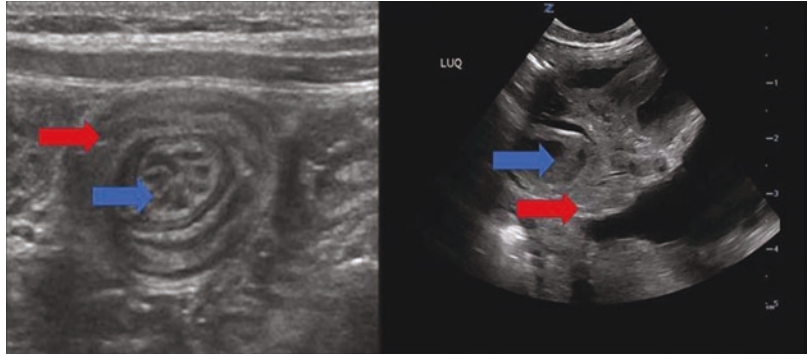
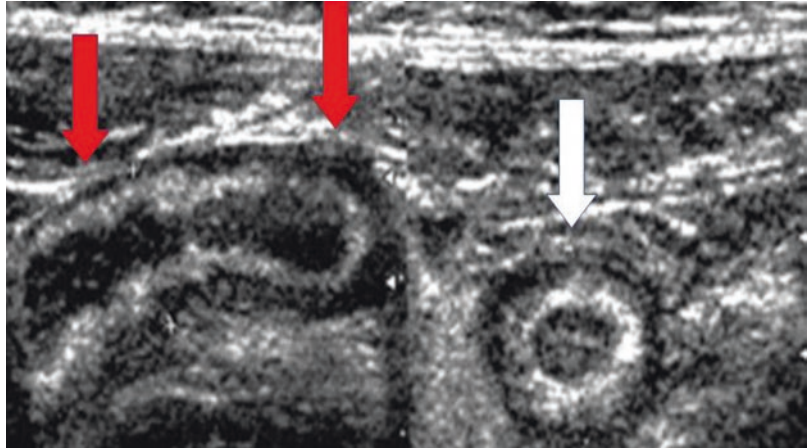


Fig. 22 Ultrasound image of a patient with appendicitis. Notice the thickened edematous wall and fluid-filled lumen (possibly pus) in sagittal section (red arrows, image on left), and axial section (white arrow, image on right)



anechoic collection of fluid around bowel loops or in dependent regions of the abdomen. Clinical correction is important as ultrasound does not differentiate hemorrhagic ascites from other types of free fluid [6].

Renal and Bladder Ultrasound

Renal and bladder ultrasound (RBUS) is quick, reliable, easily available, inexpensive, and has a rapid and steep learning curve facilitating basic interrogation even by novice sonographers [38]. RBUS is particularly valuable in the initial investigation of a child or neonate with oliguria/anuria [39]. Its role in the evaluation of flank pain has been explored, but an overall paucity of literature precludes recommendation for its use in all patients.

Renal Ultrasound

A low-frequency, curvilinear, or phased array probe is preferred for interrogation of both the kidneys and the urinary bladder. However, in infants and neonates a linear probe may be sufficient given the superficial positioning of the organs. The native kidney is imaged in at least two orthogonal planes. The probe is placed in the right and left upper quadrants and a sagittal plane in the mid-posterior axillary line with the probe marker oriented cranially for right and left kidney evaluation, respectively. The kidneys are retroperitoneal and require the probe to be directed posteriorly compared to the interrogation of the liver and spleen. The left kidney is usually higher and more posterior than the right kidney. The clinician must then rotate the probe in a transverse plane with a probe marker directed towards the patient's right side to further examine the kidney.

The depth should be adjusted to ensure that the kidneys are centered on the screen. The gain is adjusted to ensure that the renal calyx appears anechoic (black).

The kidney is divided into outer cortex with outer rim of tissue and columns of cortical tissue (hyperechoic) descending in between the medullary pyramids (anechoic). The apex of medullary pyramids projects into cup-shaped structures known as calyx which can be enlarged and dilated to a variable degree in patients with hydronephrosis or more accurately known as urinary tract dilation (UTD) [40]. The measurement of renal pelvis diameter, calyceal dilation, and the thickness and appearance of parenchyma allows the grading of UTD into mild, moderate, and severe. The involvement of the ureteropelvic junction with sparing of the renal parenchyma is classified as mild UTD, dilation of medullary pyramids with some involvement of parenchyma

is classified as moderate UTD, while severe dilation of the medullary pyramids with almost total obliteration of the cortical tissue is severe UTD [40] (Fig. 23). UTD can be distinguished from renal vasculature with the use of color doppler, which would demonstrate no flow over areas of UTD.

UTD can be seen with or without obstructive pathology of the urinary tract and is helpful in acute care settings to delineate pathology in patients presenting with oliguria/anuria and/or flank pain. A few examples of its clinical utility are described here:

1. UTD in an infant with oliguria/anuria, elevated creatinine, and blood urea nitrogen (BUN) with or without growth abnormalities should trigger a comprehensive radiological evaluation for congenital anomalies of the kidney and urinary tract (CAUKT).

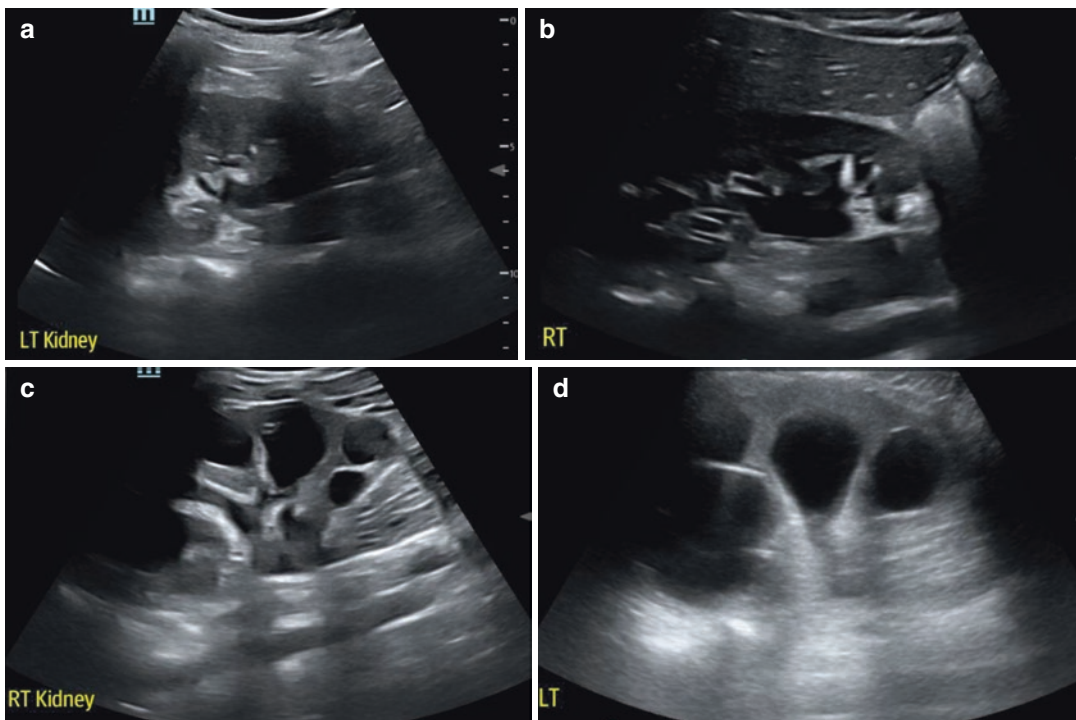


Fig. 23 (a): Normal kidney; (b): mild urinary tract dilation (UTD); (c): moderate UTD; (d): severe UTD. (Images courtesy of Dr. Michael McWay and the Children's

Hospital of Philadelphia Pediatric Emergency Medicine point-of-care ultrasound image library)

2. UTD in a patient with anuria and a dilated urinary bladder may indicate lower urinary tract obstruction and requires bladder decompression with further interrogation for the causes of obstruction.
3. UTD in a patient with a neurogenic bladder and a previously normal RBUS indicates the need for more frequent bladder catheterizations to avoid urinary retention. Pre- and post-void bladder volume estimation can demonstrate incomplete bladder emptying.
4. UTD in a neonate/infant with a large urinary bladder should trigger consideration for a posterior urethral valve [41].

Pediatric clinicians assessing patients with renal colic may identify renal abnormalities, including hydronephrosis, by using ultrasound thereby avoiding the need for diagnostic CT and its accompanying radiation exposure [42]. The consideration of other urinary tract pathologies requires a comprehensive radiological examination. However, in the hands of a skilled sonographer, ultrasound can be utilized for the diagnosis of kidney stones, pyonephrosis, renal or bladder tumors, congestive nephropathy, and renal hypertrophy or atrophy.

Numerous studies have evaluated the feasibility and the diagnostic performance of RBUS by bedside clinicians for the evaluation of oliguria/anuria and/or flank pain. In New Zealand, 28 rural physicians practicing in environments with limited imaging resources learned RBUS techniques to triage and expedite care. Physician-performed ultrasounds had >90% sensitivity and specificity for the diagnosis of hydronephrosis and 100% accuracy for bladder distension further supporting ease of use and clinical relevance [43]. In a study performed in an urban pediatric emergency department, the accuracy of RBUS in diagnosing hydronephrosis was evaluated. In 433 visits for urinary tract infections, the sensitivity and specificity for the diagnosis of hydronephrosis were 76.5% (95% confidence interval: 58.1–94.6%) and 97.2% (95.2–99.2%), respectively [44].

Bladder Ultrasound

The urinary bladder is a fluid-filled structure amenable to ultrasound interrogation. The learning curve is rapid and utilized by physicians as well as nurses [45]. Similar to renal ultrasound, a low-frequency, curvilinear, or phased array probe is preferred. However, the bladder is usually superficial and amenable to examination with a high frequency, linear probe. The probe is placed in the suprapubic area, in a transverse plane, with the probe marker oriented towards the patient's right. It is then rotated 90 degrees into a longitudinal plane with a probe marker oriented cranially. The probe is fanned/tilted anterior-posterior and side to side, respectively to image the bladder. Posterior acoustic enhancement through the bladder impedes visualization of free fluid behind the bladder and should be corrected by reducing the far field gain. The depth is adjusted to ensure that the bladder is centered on the screen. The bladder volume is calculated by measuring bladder length and width in the transverse plane and height in the longitudinal plane. One formula commonly used for the assessment of bladder volume in pediatric patients is length \times width \times height \times 0.53 (correction factor for the shape of a pediatric bladder) [46]. Many ultrasound machines allow automated bladder volume estimation.

Bladder evaluation is useful in acute care settings in multiple ways. Simple qualitative eyeballing can reveal important clinical information. For example, bladder ultrasound performed prior to suprapubic aspiration and bladder catheterization improves the success of both procedures in the pediatric emergency department [47, 48]. Manually performed ultrasound measurements also allow a more accurate assessment of bladder volume compared to automated bladder ultrasound devices [49]. Urinary catheters can be visualized within the bladder using ultrasound (Fig. 24). When a urinary catheter is in place, but the bladder is distended with fluid, either the catheter is obstructed or malpositioned. The presence of free fluid around the bladder in a patient with blunt abdominal trauma

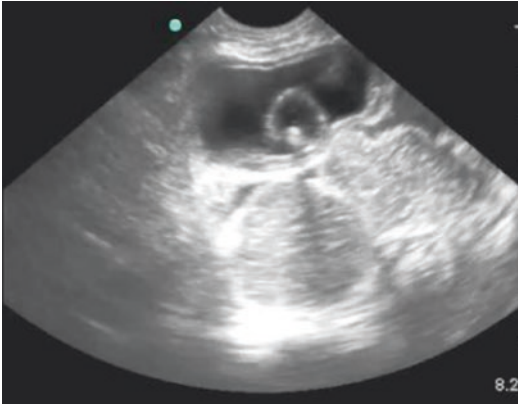



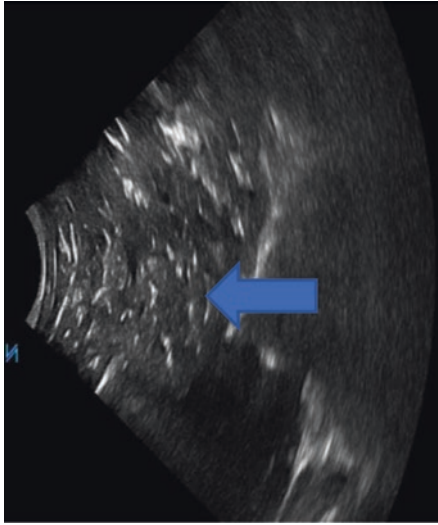
Fig. 24 Urinary catheter balloon visualized in the bladder

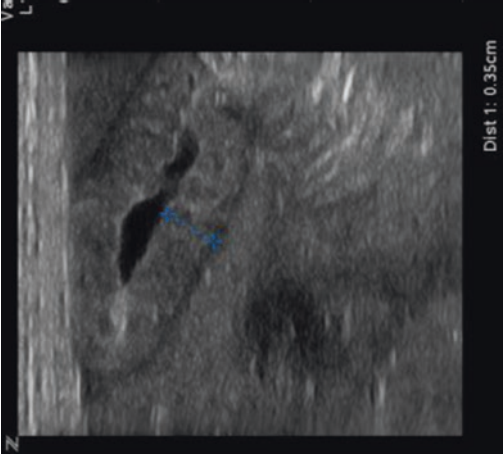
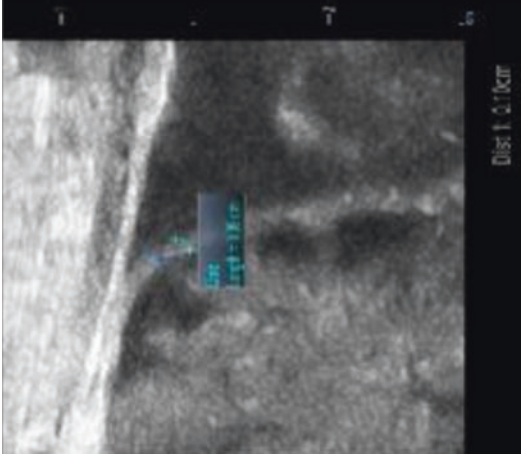
suggests intraperitoneal bleeding and need for further action. In a tachycardiac, critically ill, intubated child with oliguria/anuria, a paucity of volume in the bladder suggests intravascular volume depletion whereas a phenotypically similar child with a distended bladder may be tachycardic from the discomfort of medication-induced urinary retention, relieved by the placement of a urinary catheter. A distended bladder due to obstruction may also result in hydronephrosis which can be visualized and graded using ultrasound as described in the previous section [40].

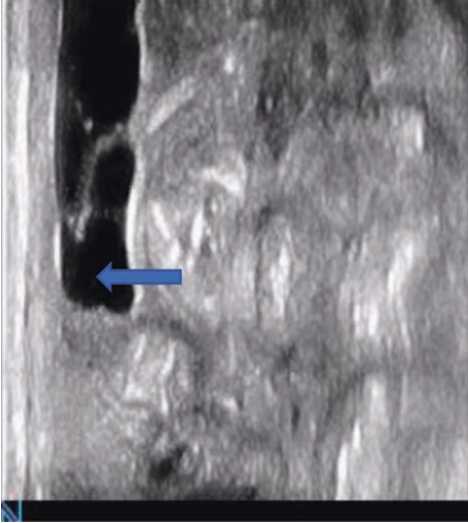
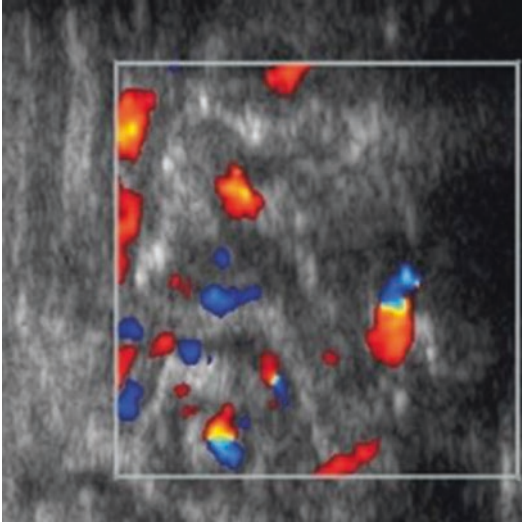
Conclusion

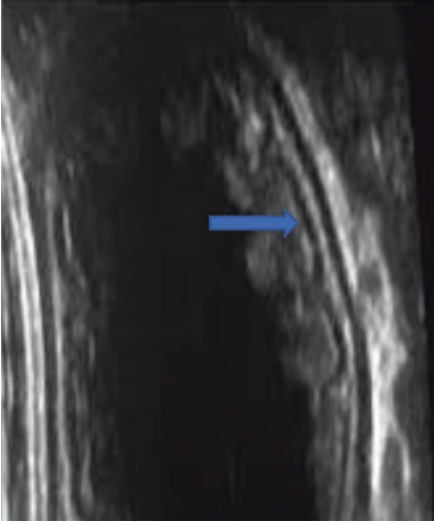
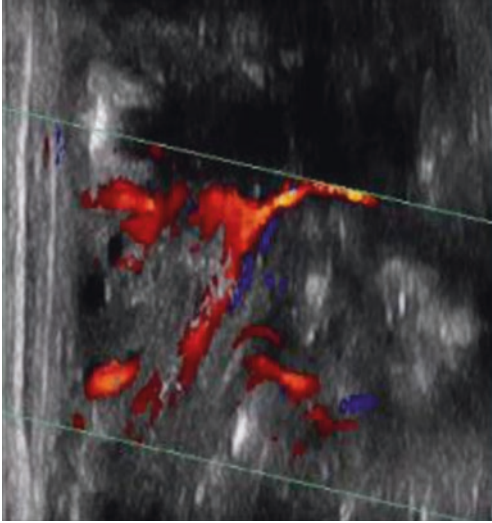
Numerous abdominal ultrasound applications are relevant to assessing pathophysiological processes and guiding diagnostics relevant to children. As with all POCUS applications, the benefit of the technology depends on the context of its use. First, defining abdominal ultrasound applications relevant to practice depends on patient populations and frequency of clinical presentations. Second, the technology requires provider skill development to a competency threshold, a topic discussed in later chapters. Finally, the need for this skill development within identified abdominal applications may differ based on access to local radiology specialists. Providers in low-resourced settings may seek to learn more diagnostic applications than those with 24-h/7 days per week radiology services. Understanding the scope of abdominal ultrasound applications may be less important than understanding the needs of patients within each of our practice environments.

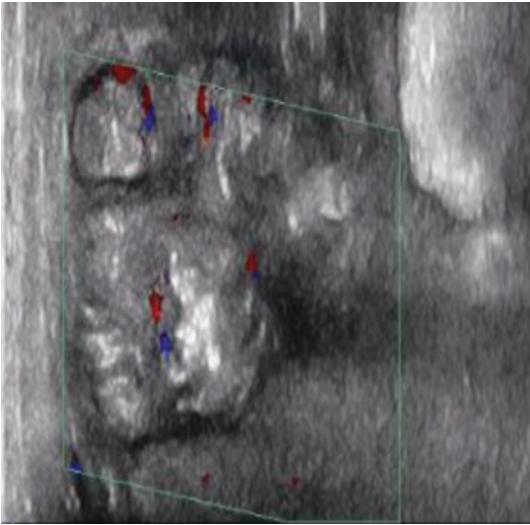
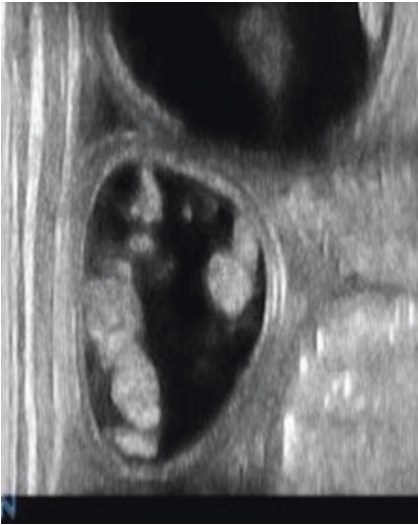
Appendix: Intestinal Ultrasound Findings in Bowel Injury or Ischemia

Intestinal ultrasound			
Ultrasound finding	Technique	Special considerations	Image
Pneumatosis intestinalis (arrow)	Use a linear probe in all 4 abdominal quadrants. Sweep in 2 perpendicular planes	It is sometimes difficult to differentiate pneumatosis intestinalis from artifact luminal air bubbles	
Portal venous gas (arrow)	Use a convex probe in the subcostal position. Sweep in 2 perpendicular planes	Usually seen only in early neonatal enterocolitis and may disappear within 24–48 h	

<p>Intestinal ultrasound Ultrasound finding Thickened bowel wall</p>	<p>Technique Use a linear probe in all 4 abdominal quadrants. Sweep in 2 perpendicular planes</p>	<p>Special considerations Experience is required to differentiate small from large bowel</p>	<p>Image </p>
<p>Thinned bowel wall</p>	<p>Technique Use a linear probe in all 4 abdominal quadrants. Sweep in 2 perpendicular planes</p>	<p>Special considerations Experience is required to differentiate small from large bowel</p>	<p>Image </p>

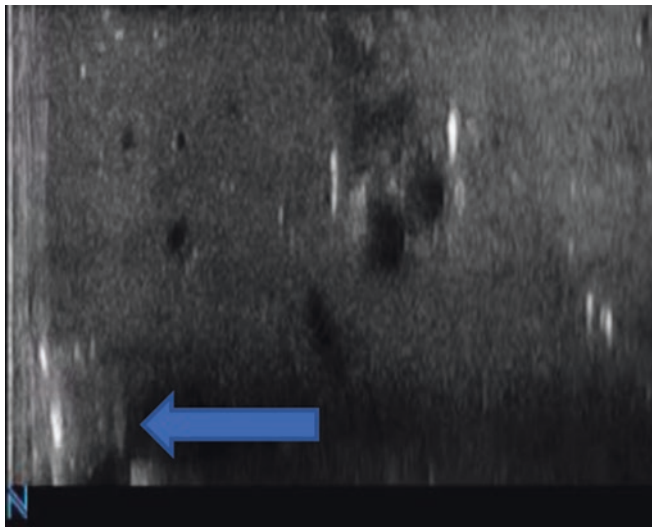
<p>Intestinal ultrasound</p> <p>Ultrasound finding</p> <p>Peritoneal ascitic fluid (arrow)</p>	<p>Technique</p> <p>Use a linear probe in all 4 abdominal quadrants. Sweep in 2 perpendicular planes</p>	<p>Special considerations</p> <p>Simple peritoneal fluid is commonly present in preterm infants</p>	<p>Image</p> 
<p>Peristalsis</p>	<p>Technique</p> <p>Use a linear probe in all 4 abdominal quadrants. Sweep in 2 perpendicular planes</p>	<p>Special considerations</p> <p>One minute of observation in all 4 quadrants is needed to diagnose absence of peristalsis (The image is of normal looking bowel with color Doppler)</p>	

<p>Intestinal ultrasound</p>	<p>Ultrasound finding</p>	<p>Intestinal signature (arrow)</p>	<p>Technique</p>	<p>Special considerations</p>	<p>Image</p>
			<p>Use a linear probe in all 4 abdominal quadrants. Sweep in 2 perpendicular planes</p>	<p>Different layers of bowel wall can be differentiated by zooming in on any loop. There are a total of 5 layers: 3 echogenic and 2 hypoechoic (the mucosa and muscularis)</p>	
			<p>Use a linear probe in all 4 abdominal quadrants with color Doppler box 2 x 2 cm with low gain</p>	<p>Mild hyperemia as an isolated feature could be normal, especially if speckle in shape</p>	
	<p>Hyperemia</p>				

<p>Intestinal ultrasound</p>	<p>Ultrasound finding</p>	<p>Ischemia</p>	<p>Technique Use a linear probe in all 4 abdominal quadrants with a color Doppler box with low gain</p>	<p>Special considerations Ischemia could be a sign of neonatal enterocolitis or secondary to circulatory arrest</p>	<p>Image</p> 
<p>Dilated loops</p>			<p>Use a linear probe in all 4 abdominal quadrants. Sweep in 2 perpendicular planes</p>	<p>This finding could represent intestinal obstruction</p>	

<p>Intestinal ultrasound</p>	<p>Ultrasound finding</p>	<p>Pneumoperitoneum</p>																								

Image



Special considerations

Ultrasound is not the modality of choice for this marker

Technique

Air reverberation artifact between the abdominal wall and liver in the decubitus position

References

1. Rehan VK, Seshia MM, Johnston B, Reed M, Wilmot D, Cook V. Observer variability in interpretation of abdominal radiographs of infants with suspected necrotizing enterocolitis. *Clin Pediatr (Phila)*. 1999;38(11):637–43. <https://doi.org/10.1177/000992289903801102>. PMID: 10587782.
2. Martínez Biarge M, García-Alix A, Luisa del Hoyo M, Alarcón A, Sáenz de Pipaón M, Hernández F, Pérez J, Quero J. Intussusception in a preterm neonate; a very rare, major intestinal problem—systematic review of cases. *J Perinat Med*. 2004;32(2):190–4. <https://doi.org/10.1515/JPM.2004.036>. PMID: 15085900.
3. Alexander KM, Chan SS, Opfer E, Cuna A, Fraser JD, Sharif S, Khashu M. Implementation of bowel ultrasound practice for the diagnosis and management of necrotizing enterocolitis. *Arch Dis Child Fetal Neonatal Ed*. 2021;106(1):96–103. <https://doi.org/10.1136/archdischild-2019-318382>. Epub 2020 May 12. PMID: 32398270; PMCID: PMC7788207.
4. Kumar S, Bansal VK, Muduly DK, Sharma P, Misra MC, Chumber S, Singh S, Bhardwaj DN. Accuracy of focused assessment with sonography for trauma (FAST) in blunt trauma abdomen—a prospective study. *Indian J Surg*. 2015;77(Suppl 2):393–7. <https://doi.org/10.1007/s12262-013-0851-2>. Epub 2013 Jan 31. PMID: 26730032; PMCID: PMC4692944.
5. Capozzi G, Santoro G. Patent ductus arteriosus: pathophysiology, hemodynamic effects and clinical complications. *J Matern Fetal Neonatal Med*. 2011;24(Suppl 1):15–6. <https://doi.org/10.3109/14767058.2011.607564>. Epub 2011 Sep 6. PMID: 21892883.
6. Gale HI, Gee MS, Westra SJ, Nimkin K. Abdominal ultrasonography of the pediatric gastrointestinal tract. *World J Radiol*. 2016;8(7):656–67. <https://doi.org/10.4329/wjr.v8.i7.656>. PMID: 27551336; PMCID: PMC4965350.
7. Kim JH, Sampath V, Canvasser J. Challenges in diagnosing necrotizing enterocolitis. *Pediatr Res*. 2020;88(Suppl 1):16–20. <https://doi.org/10.1038/s41390-020-1090-4>. PMID: 32855507.
8. Tracy SA, Lazow SP, Castro-Aragon IM, Fujii AM, Estroff JA, Parad RB, Staffa SJ, Zurakowski D, Chen C. Is abdominal sonography a useful adjunct to abdominal radiography in evaluating neonates with suspected necrotizing enterocolitis? *J Am Coll Surg*. 2020;230(6):903–911.e2. <https://doi.org/10.1016/j.jamcollsurg.2020.01.027>. Epub 2020 Feb 17. PMID: 32081753.
9. Muchantef K, Epelman M, Darge K, Kirpalani H, Laje P, Anupindi SA. Sonographic and radiographic imaging features of the neonate with necrotizing enterocolitis: correlating findings with outcomes. *Pediatr Radiol*. 2013;43(11):1444–52. <https://doi.org/10.1007/s00247-013-2725-y>. Epub 2013 Jun 15. PMID: 23771727.
10. Cuna AC, Reddy N, Robinson AL, Chan SS. Bowel ultrasound for predicting surgical management of necrotizing enterocolitis: a systematic review and meta-analysis. *Pediatr Radiol*. 2018;48(5):658–66. <https://doi.org/10.1007/s00247-017-4056-x>. Epub 2017 Dec 19. PMID: 29260286; PMCID: PMC5895673.
11. SK P, Kandasamy D, Jana M, Sharma R, Gupta AK. Pediatric stomach and duodenal imaging. *J Gastrointest Abdom Radiol*. 2021;4(2):94–108. <https://doi.org/10.1055/s-0041-1723926>.
12. McCarten KM. Ultrasound of the gastrointestinal tract in the neonate and young infant with particular attention to problems in the neonatal intensive care unit. *Ultrasound Clin*. 2010;5(1):75–95. <https://doi.org/10.1016/j.cult.2009.11.010>.
13. Iqbal CW, Rivard DC, Mortellaro VE, Sharp SW, St. Peter SD. Evaluation of ultrasonographic parameters in the diagnosis of pyloric stenosis relative to patient age and size. *J Pediatr Surg*. 2012;47(8):1542–7. <https://doi.org/10.1016/j.jpedsurg.2012.03.068>. PMID: 22901914.
14. Singh Y, Tissot C, Fraga MV, Yousef N, Cortes RG, Lopez J, Sanchez-de-Toledo J, Brierley J, Colunga JM, Raffaj D, Da Cruz E, Durand P, Kenderessy P, Lang HJ, Nishisaki A, Kneyber MC, Tissieres P, Conlon TW, De Luca D. International evidence-based guidelines on point of care ultrasound (POCUS) for critically ill neonates and children issued by the POCUS Working Group of the European Society of Paediatric and Neonatal Intensive Care (ESPNIC). *Crit Care*. 2020;24(1):65. <https://doi.org/10.1186/s13054-020-2787-9>. PMID: 32093763; PMCID: PMC7041196.
15. Conlon TW, Nishisaki A, Singh Y, Bhombal S, De Luca D, Kessler DO, Su ER, Chen AE, Fraga MV. Moving beyond the stethoscope: diagnostic point-of-care ultrasound in pediatric practice. *Pediatrics*. 2019;144(4):e20191402. <https://doi.org/10.1542/peds.2019-1402>. Epub 2019 Sep 3. PMID: 31481415.
16. Dördelmann M, Rau GA, Bartels D, Linke M, Derichs N, Behrens C, Bohnhorst B. Evaluation of portal venous gas detected by ultrasound examination for diagnosis of necrotizing enterocolitis. *Arch Dis Child Fetal Neonatal Ed*. 2009;94(3):F183–7. <https://doi.org/10.1136/adc.2007.132019>. Epub 2008 Sep 11. PMID: 18786962.
17. Miller LE, Stoller JZ, Fraga MV. Point-of-care ultrasound in the neonatal ICU. *Curr Opin Pediatr*. 2020;32(2):216–27. <https://doi.org/10.1097/MOP.0000000000000863>. PMID: 31851056.
18. Raghuvver TS, Lakhota R, Bloom BT, Desilet-Dobbs DA, Zarchan AM. Abdominal ultrasound and abdominal radiograph to diagnose necrotizing enterocolitis in extremely preterm infants. *Kans J Med*. 2019;12(1):24–7. PMID: 30854167; PMCID: PMC6396957.
19. Janssen Lok M, Miyake H, Hock A, Daneman A, Pierro A, Offringa M. Value of abdominal ultrasound in management of necrotizing enterocolitis: a sys-

- tematic review and meta-analysis. *Pediatr Surg Int*. 2018;34(6):589–612. <https://doi.org/10.1007/s00383-018-4259-8>. Epub 2018 May 2. PMID: 29721677.
20. Shebrya NH, Amin SK, El-Shinnawy MA, Imam SS. Abdominal ultrasonography in preterm necrotizing enterocolitis. Is it superior to plain radiography? *Egypt J Radiol Nucl Med*. 2012;43(3):457–63. <https://doi.org/10.1016/j.ejrnm.2012.06.001>.
 21. Elsayed Y, Seshia M. A new intestinal ultrasound integrated approach for the management of neonatal gut injury. *Eur J Pediatr*. 2022;181(4):1739–49. <https://doi.org/10.1007/s00431-021-04353-z>. Epub 2022 Jan 4. PMID: 34981184.
 22. Silva CT, Daneman A, Navarro OM, Moineddin R, Levine D, Moore AM. A prospective comparison of intestinal sonography and abdominal radiographs in a neonatal intensive care unit. *Pediatr Radiol*. 2013;43(11):1453–63. <https://doi.org/10.1007/s00247-013-2777-z>. Epub 2013 Sep 13. PMID: 24026851.
 23. Chen S, Hu Y, Liu Q, Li X, Wang H, Wang K, Zhang A. Application of abdominal sonography in diagnosis of infants with necrotizing enterocolitis. *Medicine (Baltimore)*. 2019;98(28):e16202. <https://doi.org/10.1097/MD.00000000000016202>. PMID: 31305401; PMCID: PMC6641777.
 24. Chen S, Hu Y, Liu Q, Li X, Wang H, Wang K. Comparison of abdominal radiographs and sonography in prognostic prediction of infants with necrotizing enterocolitis. *Pediatr Surg Int*. 2018;34(5):535–41. <https://doi.org/10.1007/s00383-018-4256-y>. Epub 2018 Mar 30. PMID: 29602968.
 25. Neu J, Pammi M. Necrotizing enterocolitis: the intestinal microbiome, metabolome and inflammatory mediators. *Semin Fetal Neonatal Med*. 2018;23(6):400–5. <https://doi.org/10.1016/j.siny.2018.08.001>. Epub 2018 Aug 17. PMID: 30172660.
 26. Neu J. Necrotizing enterocolitis: the future. *Neonatology*. 2020;117(2):240–4. <https://doi.org/10.1159/000506866>. Epub 2020 Mar 10. PMID: 32155645.
 27. Nchimi A, Khamis J, Paquot I, Bury F, Magotteaux P. Significance of bowel wall abnormalities at ultrasound in Henoch-Schönlein purpura. *J Pediatr Gastroenterol Nutr*. 2008;46(1):48–53. <https://doi.org/10.1097/01.mpg.0000304453.99799.8c>. PMID: 18162833.
 28. Hao J, Zhang Y, Tianyu L, Bo S, Shu F, Feng S, Chao J, Ying H. Preliminary investigation of the diagnosis of neonatal congenital small bowel atresia by ultrasound. *Biomed Res Int*. 2019;2019:7097159. <https://doi.org/10.1155/2019/7097159>. PMID: 31662992; PMCID: PMC6791188.
 29. Virgone C, D'antonio F, Khalil A, Jonh R, Manzoli L, Giuliani S. Accuracy of prenatal ultrasound in detecting jejunal and ileal atresia: systematic review and meta-analysis. *Ultrasound Obstet Gynecol*. 2015;45(5):523–9. <https://doi.org/10.1002/uog.14651>. PMID: 25157626.
 30. Zhang W, Sun H, Luo F. The efficiency of sonography in diagnosing volvulus in neonates with suspected intestinal malrotation. *Medicine (Baltimore)*. 2017;96(42):e8287. <https://doi.org/10.1097/MD.00000000000008287>. PMID: 29049228; PMCID: PMC5662394.
 31. Marine MB, Karmazyn B. Imaging of malrotation in the neonate. *Semin Ultrasound CT MR*. 2014;35(6):555–70. <https://doi.org/10.1053/j.sult.2014.08.004>. Epub 2014 Aug 9. PMID: 25454052.
 32. Orzech N, Navarro OM, Langer JC. Is ultrasonography a good screening test for intestinal malrotation? *J Pediatr Surg*. 2006;41(5):1005–9. <https://doi.org/10.1016/j.jpedsurg.2005.12.070>. PMID: 16677901.
 33. Casaccia G, Trucchi A, Spiridakis I, Giorlandino C, Aite L, Capolupo I, Catalano OA, Bagolan P. Congenital intestinal anomalies, neonatal short bowel syndrome, and prenatal/neonatal counseling. *J Pediatr Surg*. 2006;41(4):804–7. <https://doi.org/10.1016/j.jpedsurg.2005.12.022>. PMID: 16567197.
 34. Chen SW, Fu W, Liu J, Wang Y. Routine application of lung ultrasonography in the neonatal intensive care unit. *Medicine (Baltimore)*. 2017;96(2):e5826. <https://doi.org/10.1097/MD.00000000000005826>. PMID: 28079811; PMCID: PMC5266173.
 35. Petaros P, Giglio L, Oretti C, Demarini S. Small bowel intussusception in a very-low-birthweight infant. *Acta Paediatr*. 2006;95(2):250–1. <https://doi.org/10.1080/08035250500369619>. PMID: 16449035.
 36. Ashkenazi I, Zeina AR, Olsha O. Early ultrasound in acute appendicitis avoids CT in most patients but delays surgery and increases complicated appendicitis if nondiagnostic—a retrospective study. *Am J Surg*. 2020;219(4):683–9. <https://doi.org/10.1016/j.amjsurg.2019.05.013>. Epub 2019 May 25. PMID: 31153584.
 37. Lichtenstein DA. BLUE-protocol and FALLS-protocol: two applications of lung ultrasound in the critically ill. *Chest*. 2015;147(6):1659–70. <https://doi.org/10.1378/chest.14-1313>. PMID: 26033127.
 38. Watkins S, Bowra J, Sharma P, Holdgate A, Giles A, Campbell L. Validation of emergency physician ultrasound in diagnosing hydronephrosis in ureteric colic. *Emerg Med Australas*. 2007;19(3):188–95. <https://doi.org/10.1111/j.1742-6723.2007.00925.x>. PMID: 17564683.
 39. Steimle MD, Plumb J, Corneli HM. Point-of-care ultrasound to assess anuria in children. *Pediatr Emerg Care*. 2016;32(8):544–8. <https://doi.org/10.1097/PEC.0000000000000871>. PMID: 27490729.
 40. Nguyen HT, Benson CB, Bromley B, Campbell JB, Chow J, Coleman B, Cooper C, Crino J, Darge K, Herndon CD, Odibo AO, Somers MJ, Stein DR. Multidisciplinary consensus on the classification of prenatal and postnatal urinary tract dilation (UTD classification system). *J Pediatr Urol*. 2014;10(6):982–98.

41. Gillon JT, Cohen SG. Diagnosis of posterior urethral valves in an infant using point-of-care ultrasound. *Pediatr Emerg Care*. 2021;37(8):435–6. <https://doi.org/10.1097/PEC.0000000000002393>. PMID: 34397679.
42. Ng C, Tsung JW. Avoiding computed tomography scans by using point-of-care ultrasound when evaluating suspected pediatric renal colic. *J Emerg Med*. 2015;49(2):165–71. <https://doi.org/10.1016/j.jemermed.2015.01.017>. Epub 2015 Apr 29. PMID: 25934378.
43. Nixon G, Blattner K, Muirhead J, Kerse N. Rural point-of-care ultrasound of the kidney and bladder: quality and effect on patient management. *J Prim Health Care*. 2018;10(4):324–30. <https://doi.org/10.1071/HC18034>. PMID: 31039961.
44. Guedj R, Escoda S, Blakime P, Patteau G, Brunelle F, Cheron G. The accuracy of renal point of care ultrasound to detect hydronephrosis in children with a urinary tract infection. *Eur J Emerg Med*. 2015;22(2):135–8. <https://doi.org/10.1097/MEJ.000000000000158>. PMID: 24858915.
45. Schallom M, Prentice D, Sona C, Vyders K, Arroyo C, Wessman B, Ablordeppey E. Accuracy of measuring bladder volumes with ultrasound and bladder scanning. *Am J Crit Care*. 2020;29(6):458–67. <https://doi.org/10.4037/ajcc2020741>. PMID: 33130866; PMCID: PMC8141281.
46. Hwang JY, Byun SS, Oh SJ, Kim HC. Novel algorithm for improving accuracy of ultrasound measurement of residual urine volume according to bladder shape. *Urology*. 2004;64(5):887–91. <https://doi.org/10.1016/j.urology.2004.06.054>. PMID: 15533471.
47. Mahdipour S, Saadat SNS, Badeli H, Rad AH. Strengthening the success rate of suprapubic aspiration in infants by integrating point-of-care ultrasonography guidance: a parallel-randomized clinical trial. *PLoS One*. 2021;16(7):e0254703. <https://doi.org/10.1371/journal.pone.0254703>. PMID: 34265015; PMCID: PMC8282064.
48. Chen L, Hsiao AL, Moore CL, Dziura JD, Santucci KA. Utility of bedside bladder ultrasound before urethral catheterization in young children. *Pediatrics*. 2005;115(1):108–11. <https://doi.org/10.1542/peds.2004-0738>. PMID: 15629989.
49. Bevan C, Buntsma D, Stock A, Griffiths T, Donath S, Babl FE. Assessing bladder volumes in young children prior to instrumentation: accuracy of an automated ultrasound device compared to real-time ultrasound. *Acad Emerg Med*. 2011;18(8):816–21. <https://doi.org/10.1111/j.1553-2712.2011.01130.x>. PMID: 21843216.

Part V

Neurosonology



Focused Cranial Ultrasound for Neurointensive Care

Marlina Lovett, Kerri LaRovere, and Nicole O'Brien

Contents

Introduction	208
Transcranial Doppler Ultrasound	208
Basic Principles and Techniques	208
Basic Principles and Techniques for Imaging Duplex TCD	210
Clinical Applications	210
Traumatic Brain Injury: Prognosis	213
Traumatic Brain Injury: Noninvasive Assessment of Intracranial Pressure (ICP)	214
Traumatic Brain Injury: Noninvasive Assessment of Cerebral Perfusion Pressure (CPP)	215
Screening for Vasospasm in Children	215
Hypoxic-Ischemic Encephalopathy: Prognosis and Detection of Perfusion Disorders	215
Cardiorespiratory Support with Extracorporeal Membrane Oxygenation: Changes Concerning Hemorrhage or Ischemia and Emboli Monitoring	216
Arterial Ischemic Stroke: Progression or Regression of Steno-Occlusive Disease	216
Bacterial Meningitis: Detection of Perfusion Disorders (Oligemia or Hyperemia)	216
Cerebral Circulatory Arrest	218
Midline Shift	218
Limitations of TCD as a POCUS Tool	219
Ocular Ultrasonography	219
Basic Principles and Technique	219
Clinical Applications: Optic Nerve Sheath Diameter to Investigate ICP	220
Clinical Application: Identification of Retinal Trauma	220

M. Lovett · N. O'Brien (✉)

Division of Critical Care Medicine, Department of Pediatrics, Nationwide Children's Hospital and The Ohio State University, Columbus, OH, USA
e-mail: marlina.lovett@nationwidechildrens.org;
Nicole.obrien@nationwidechildrens.org

K. LaRovere

Department of Neurology, Harvard Medical School and Boston Children's Hospital, Boston, MA, USA
e-mail: kerri.larovere@childrens.harvard.edu

Neonatal Cranial Ultrasound	221
Basic Principles and Technique	221
Clinical Application	221
POCUS Neurosonography Integration	221
Conclusion	221
References	222

Introduction

The recent incorporation of point of care ultrasound (POCUS) into clinical practice by neonatal and pediatric critical care providers has, in many ways, begun to transform the field. This bedside performance and interpretation of scans to achieve specific procedural goals or to answer focused diagnostic questions are now powerful adjuncts to common clinical assessments arising in pediatric acute care environments including the neonatal (NICU) or pediatric intensive care unit (PICU). To date, POCUS in these settings has largely focused on the attainment of vascular access, lung and abdominal ultrasound, and goal-directed cardiac POCUS for the child in shock [1].

Pediatric acute care providers have not routinely employed neurosonography as a POCUS application. Comprehensive brain ultrasound studies performed by registered technologists can provide a full assessment of the structural and functional status of the brain and cerebrovasculature [2]. However, critically ill children at risk of or with known or suspected neurologic issues often experience clinical deterioration rapidly and repeatedly from diverse causes. Assessment or frequent re-assessment with formal ultrasound in these situations may not be feasible. Focused neurosonography by the bedside clinician may provide information that impacts clinical decision making [3–5].

In 1982, Rune Aaslid and colleagues used low-frequency ultrasound waves to measure cerebral blood flow velocities (CBFVs) in the major cerebral arteries [6]. This procedure is now known as Transcranial Doppler ultrasonography (TCD). In pediatric practice, the use of TCD is

well-established in children with sickle cell anemia. In this clinical situation, TCD has been used to identify children with cerebral vasculopathy and reduce stroke risk through the initiation of chronic transfusion therapy [7, 8]. As TCD is noninvasive, portable, inexpensive, and able to give repeated real-time assessments, it may also be an ideal point of care tool to evaluate cerebral circulation in children with critical illness. Its use as a prognostic, diagnostic, and neuromonitoring tool has been reported in 93% ($n = 27/29$) of surveyed hospitals that provide pediatric neurocritical care services [9]. Seventy-four percent of these centers reported that TCD studies were performed by a vascular sonographer. Therefore, more than a quarter of responding institutions have practicing clinicians (radiologists, neurologists, neurosurgeons, anesthesiologists, or intensivists) performing TCD, potentially as a point of care tool in some situations. Outside of TCD, clinical providers also use standard portable ultrasound machines for neurosonographic POCUS applications including measurement of the optic nerve sheath diameter (ONSD) in children and to evaluate the brain parenchyma in neonates with open fontanelles [5, 10, 11].

Transcranial Doppler Ultrasound

Basic Principles and Techniques

Two general types of TCD equipment are currently available: non-duplex (non-imaging) and duplex (imaging) devices [2, 12]. In the non-imaging technique, specific vessel identification is “blind” but assumptions are made based on the cranial window used, orientation of the probe,

depth of sample volume, direction of blood flow identified, the spectral display, and the characteristic sound of each vessel (Fig. 1) [6]. Imaging TCD combines pulsed wave doppler ultrasound with a cross-sectional view of the area being evaluated, which allows the identification of the arteries in relation to various anatomic locations [13, 14]. An advantage of imaging TCD includes an ability to identify structural perturbations, including the presence of masses and/or midline shift. The equipment used to perform imaging TCD is likely more readily available to the ICU provider as portable ultrasounds that are commonly available and used in critical care for other POCUS applications are now being equipped with imaging TCD capabilities. Imaging TCD therefore has the potential to become the pre-

dominant form of TCD in critical care. However, to date, the literature describing the use of TCD in the PICU has generally been done using non-imaging TCD devices. Thus, the focus of this chapter will be on this approach.

The non-imaging TCD examination is performed using a low-frequency (2 MHz) ultrasound probe. This probe is capable of penetrating thin regions of the skull termed acoustic windows. In general, four main acoustic windows have been described (Fig. 2). The transtemporal window can be used to evaluate the anterior circulation (including the middle cerebral artery (MCA), anterior cerebral artery, posterior cerebral artery, and intracranial portion of the internal carotid artery) [14–16]. The transorbital window evaluates the ophthalmic vessels and the carotid

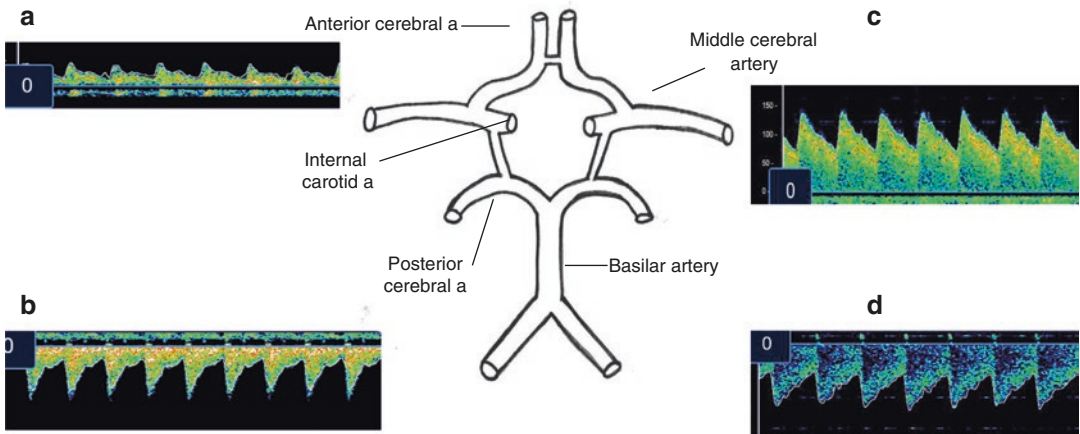


Fig. 1 Representative waveforms and schematic of the major cerebral arteries. (a) Anterior cerebral artery, (b) posterior cerebral artery, (c) middle cerebral artery, (d) basilar artery

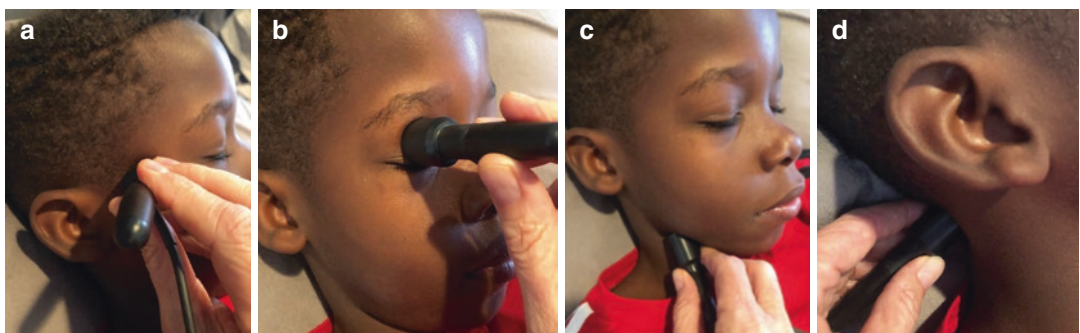


Fig. 2 The acoustic windows allowing for TCD insonation. (a) Transtemporal, (b) transorbital, (c) submandibular, and (d) suboccipital/transforaminal

siphon. The submandibular window evaluates the extracranial carotid arteries (Ex-ICA), and the suboccipital/transforaminal window is used to assess the posterior circulation (the vertebrobasilar system). A focused POCUS examination in a critical care setting will largely evaluate the MCAs, the Ex-ICA, and possibly the vertebral artery (VA)/basilar artery (BA) depending on the clinical question being evaluated. MCA flow will be towards the probe at depths of 50–60 mm (midline) to 30–35 mm (end of vessel) in adolescents and at shallower depths in younger children [17]. Ex-ICA flow will be away from the probe at depths of 35–40 mm. VA and BA flow will be away from the probe beginning at depths around 50 mm for the VA that transitions to BA flow at approximately 65 mm through 80 mm for adolescents. Again, these vessels are commonly identified at decreased depths in younger children.

Measurements should be taken every 2 mm along the length of the vessel to identify any focal pathology [16]. Cerebral blood flow increases through early childhood and peaks around age 6 years and declines to adult levels by adolescence. Thus, when interpreting any TCD examination in a pediatric patient, it is necessary to compare values to published normative values for age [18]. Measured CBFVs greater than or less than 2 standard deviations (SD) from the age published normal should be considered abnormal [16]. However, multiple physiologic parameters can affect measured CBFVs and these must be taken into account when interpreting any TCD examination in the ICU given the common occurrence of deranged systemic physiology in this patient population (Table 1) [17]. Furthermore, the interpreter should realize that sedative medications commonly used in the intensive care unit may be associated with reduced CBFV even in the absence of cerebral pathology [17]. Without careful consideration of these factors, the clinician performing a POCUS examination at the bedside could inappropriately interpret the findings on TCD.

Basic Principles and Techniques for Imaging Duplex TCD


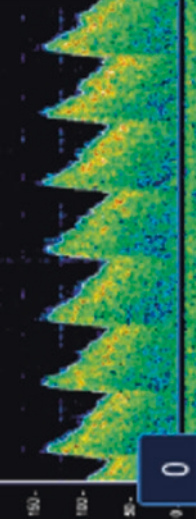

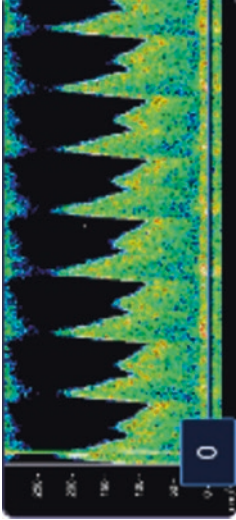

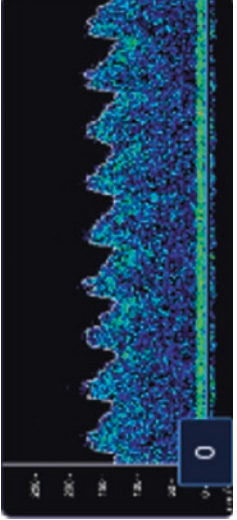
The foundations and skillset required for successfully obtaining TCD using non-imaging and imaging TCD are similar. The same cranial windows are insonated and the bedside provider should identify the waveform similarly with the aid of characteristic acoustic sounds. However, with imaging TCD one can visualize brain anatomy to help identify the desired individual vessels. When performing imaging TCD in the transtemporal window, the provider aims to identify the mesencephalon. The mesencephalon is identified as a low-echo butterfly-shaped structure surrounded by high echo borders representing the basal systems [19]. From this location, with the use of color, the individual vessels of the circle of Willis will be visible and the examiner may then evaluate the waveform of the vessel of interest (Fig. 3). An additional application that is available on duplex TCD that is not available on non-imaging TCD is the detection of midline shift.

Standardized approaches to scanning protocols, interpretation, and documentation of TCD examinations in the PICU have been recommended for formal examinations [16]. Standardization is necessary to ensure that high-quality TCD images are captured, interpreted, and reported using consistent nomenclature. Similar established recommendations for TCD performed as a point of care examination are lacking. Providers using TCD at the bedside should be familiar with these recommendations and consider the incorporation of relevant aspects into their practice.

Clinical Applications


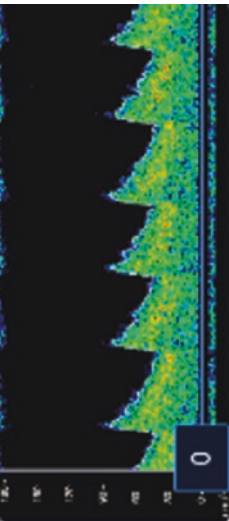

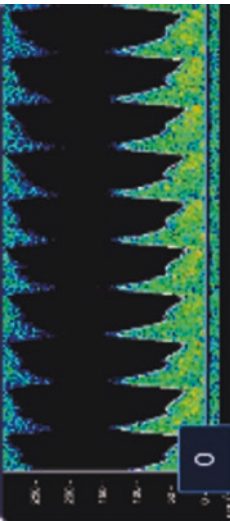
It is important to remember that POCUS by a clinician at the bedside in the ICU is different than a complete diagnostic study by a trained practitioner. POCUS involves a focused assessment to

Table 1 Common TCD abnormalities

TCD category	Clinical situation	Location of physiologic alteration	TCD Waveform
Normal	N/A		 <p>(Vs/Vd/Vm ± 2 SD in all vessels; PI 0.6–1.2)</p>
Hyperemia	Fever Anemia Hypertension ↑ cardiac output		 <p>(Vm ≥ 2 SD in all vessels; ↑ carotid artery flow, LR < 3)</p>
	↑ pCO ₂ Seizures		 <p>(Vm ± or ≥ 2 SD from normative value in all vessels; increased Vd, increased carotid artery flow)</p>

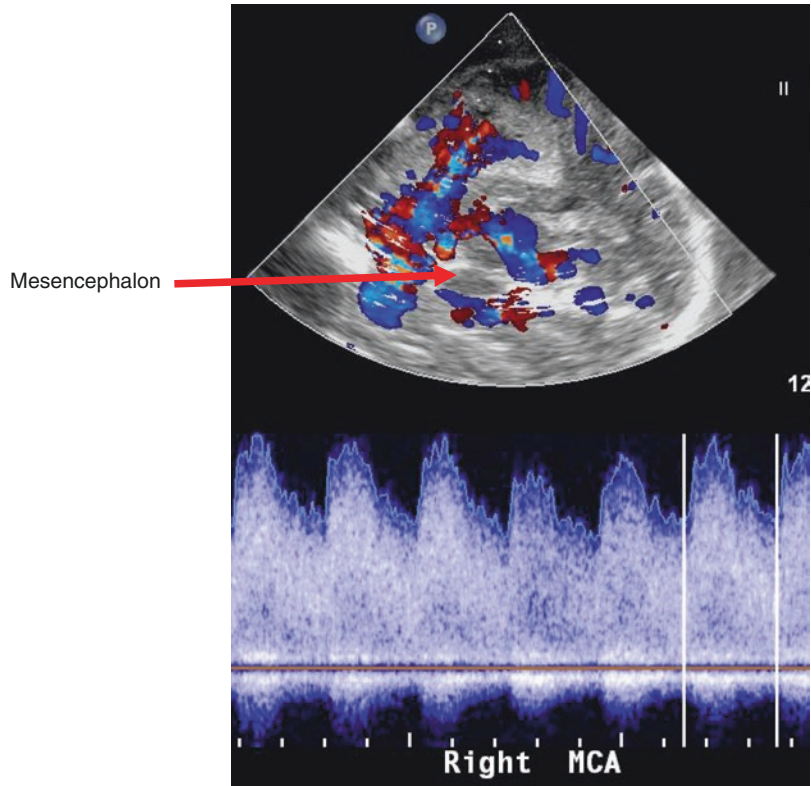
(continued)

Table 1 (continued)

TCD category	Clinical situation	Location of physiologic alteration	TCD Waveform
Decreased cerebral blood flow	Sedation Mechanical ventilation Shock ↓cardiac output		 <p>($V_m \leq 2$ SD in all vessels, $PI < 1.2$)</p>
	Hypocapnia		 <p>($V_m \pm$ or ≤ 2 SD in all vessels, PI variable but often > 1.2)</p>

pCO_2 partial pressure of carbon dioxide, PI pulsatility index (defined by: $[V_s \text{ PLUS_SPI } V_d/N_m]$), V_s systolic flow velocity, V_d diastolic flow velocity, LR Lindgaard Ratio

Fig. 3 Mesencephalon seen on duplex TCD



answer specific questions. It is more dynamic with a clinical provider performing and rapidly interpreting studies, integrating information into the clinical setting they are facing, and then repeating the study to identify changes associated with any attempted interventions. Neurosonography being used as a point of care tool is not different. Therefore, the following discussion is not comprehensive to all potential applications for TCD in the acute care setting but rather is focused on likely uses by a practitioner at the bedside. Additionally, there is a paucity of clear supportive data for clinical scenarios where TCD would have a definitive diagnostic or therapeutic benefit in the management of a critically ill child. Thus, the recommendations made here are largely based on the opinions of the authors.

Possible uses of POCUS TCD in the ICU are found in Table 2. There are additional reports of PICU practitioners using TCD in other clinical scenarios including the evaluation of hepatic encephalopathy, cerebral venous infarction, hydrocephalus, sepsis, and diabetic ketoacidosis that are not covered here [20, 21].

Traumatic Brain Injury: Prognosis

TCD may predict which patients are at risk of poor neurologic outcome following trauma [22–25]. Trabold et al. used TCD to evaluate CBFVs in the emergency room in 36 children with moderate to severe TBI. Multivariate and receiver operating characteristic (ROC) analyses revealed that MCA end-diastolic flow velocity (Vd) <25 cm/s and pulsatility index (PI) > 1.31 were associated with poor prognosis [26]. In another pediatric study, 69 infants and children with moderate to severe brain injury were enrolled and underwent daily TCD examination [27]. MCA flow velocities <2 SD from age-based normative values were identified in 6% of patients, all of whom had a poor 12-month neurologic outcome. In summary, the data is limited but suggests that children with decreased CBFV following trauma may be at increased risk of poor outcome. Once this association and specific cut-off values are further established with high-quality research, identification of high-risk children with POCUS may be possible. Future work may then determine if the use of volume or vasopressors to aug-

Table 2 The role of transcranial Doppler in various clinical scenarios

Clinical scenario	Potential role of TCD
Traumatic brain injury	Evaluate cerebrovascular hemodynamics for: Prognostication Detection of altered CBFV suggestive of perfusion disorders (oligemia or hyperemia) which may guide BP or CPP management Identifying increased intracranial pressure Effect of hyperventilation Screening for vasospasm
Hypoxic-ischemic encephalopathy	Evaluate cerebrovascular hemodynamics for: Prognostication Detection of altered CBFV suggestive of perfusion disorders (oligemia or hyperemia) which may guide BP or CPP
Cardiorespiratory support with extracorporeal membrane oxygenation	Evaluate cerebrovascular hemodynamics for: Changes concerning hemorrhage or ischemia Emboli monitoring
Subarachnoid hemorrhage	Screening for vasospasm
Arterial ischemic stroke	Evaluate cerebrovascular hemodynamics for: Progression or regression of steno-occlusive disease
Bacterial meningitis	Evaluate cerebrovascular hemodynamics for: Detection of abnormal CBFV suggestive of perfusion disorders (oligemia or hyperemia) which may guide BP or CPP management
Other/Multiple	Evaluate changes from previous exam that would lead to formal head imaging Evaluate for flow patterns concerning cerebral circulatory arrest Evaluate for midline shift

TCD transcranial Doppler, CBFV cerebral blood flow velocity, BP blood pressure, CPP cerebral perfusion pressure

ment cerebral perfusion pressure and CBFV could decrease secondary ischemic injury. Additionally, identification of this pattern by a practitioner on a POCUS examination may limit

the desire to perform even mild hyperventilation that would further reduce cerebral blood flow and potentially worsen the outcome.

Traumatic Brain Injury: Noninvasive Assessment of Intracranial Pressure (ICP)

The most recent guidelines for the management of severe traumatic brain injury (TBI) in children give a level III recommendation to ICP measurement [28]. Conventionally, this requires placement of an invasive monitor, with risks of infection, hemorrhage, malfunction, or malposition. TCD has been explored as a noninvasive method to assess ICP and to determine which individual’s risk-to-benefit ratio favors placement of a monitor. An increase in ICP leads to a more rapid reduction in flow velocity in the diastolic phase than in the systolic phase. This results in a pronounced difference between peak systole and the end of diastole. The pulsatility index (PI) is a value that is calculated by the TCD software according to the following equation: $(V_s - V_d)/V_m$ [29]. Therefore, as ICP rises, there is theoretically a progressive reduction in the measured Vd and an increase in PI [30–33].

Figaji et al. performed 291 TCD recordings on 34 children with severe TBI and an invasive ICP monitor and found that $ICP \geq 20$ mmHg could be detected with only 25% sensitivity and 80% negative predictive value using a PI cut-off of 1.0 (TCD was performed on a median of post-injury day 3). A slightly higher PI value did not improve sensitivity [34]. On the other hand, Melo et al. evaluated 117 severely head-injured children on admission. An initial abnormal TCD (evidence of reversal of flow, no flow, $V_d < 25$ cm/s or $PI > 1.31$) had a 94% sensitivity for predicting $ICP > 20$ mmHg [35]. O’Brien et al. reported that in 36 children with severe TBI undergoing 148 TCD examinations, a $PI \geq 1.3$ on post-injury day 0–1 had a 100% sensitivity and 82% specificity in predicting an $ICP \geq 20$ mmHg [36]. During this time frame, a moderately strong relationship was observed between the MCA PI and actual ICP ($r = 0.611, p = 0.01$). When using a threshold of < 25 cm/s, post-injury day 0–1 Vd had a 56% sensitivity to predict an $ICP \geq 20$ mmHg. Beyond the initial 24 h from injury, the sensitivity of $PI \geq 1.3$ to detect an $ICP \geq 20$ mmHg fell to 47%, and a weak relationship

between actual ICP values and PI ($r = 0.376$, $p = 0.01$) and Vd ($r = -0.284$, $p = 0.01$) was found.

Based on the limited literature, identification of MCA PI ≥ 1.3 on the early point of care TCD (within 24 h of injury) may suggest intracranial hypertension. However, this literature is limited by single-center studies with small sample sizes. Additional investigation is needed to further clarify specific associations of TCD values with ICP data, and at this point in time, TCD cannot be recommended as a replacement for the use of an invasive ICP monitor.

Traumatic Brain Injury: Noninvasive Assessment of Cerebral Perfusion Pressure (CPP)

In the setting of severe TBI, the bedside clinician aims to maintain an appropriate cerebral perfusion pressure [CPP = mean arterial pressure (MAP) – ICP]. Investigators have begun to investigate whether TCD can be used to noninvasively estimate CPP. There are several formulas suggested to calculate the estimated CPP (CPPe). The formula most frequently cited in the literature was published by Czosnyka et al.: $CPPe = [MAP \times (Vd / Vmean) \text{ PLUS_SPI } 14]$ [22]. Using continuous TCD, invasive monitoring of arterial blood pressure, and mathematical calculations in adults with head injury, the correlation between CPP and CPPe was 0.73, with an average absolute error of 6.5 mmHg. In one small study of 23 children with severe TBI, the authors attempted a simplified approach using one-time measurements of ICP/ CPP and TCD data to calculate a CPPe based on the Czosnyka et al. formula [37]. Bland-Altman analysis showed an average discrepancy of 3.7 mmHg but revealed limits of agreement of –17 to PLUS_SPI 25 mmHg. These wide limits of agreement limit the use of a single POCUS TCD to estimate CPPe. There have been several small studies using similar mathematical formulas, complex modeling, and continuous TCD examination to estimate CPP successfully [38, 39]. However, given the complexities inherent in these models, point of care integration of TCD for estimation of CPP cannot easily or reliably be used in children with TBI at this time.

Screening for Vasospasm in Children

Cerebral vasospasm can lead to critical reductions in cerebral blood flow, delayed cerebral ischemia, and increased morbidity and mortality. Adult criteria for the diagnosis of vasospasm were initially developed by correlating TCD flow velocities to the degree of vasospasm on conventional angiography [40]. Current vasospasm criteria in adults include: MCA mean flow velocity > 120 cm/s with Lindegaard Ratio (LR: $MCA \text{ Vm} / \text{External-ICA Vm}$) ≥ 3 (anterior circulation vasospasm) and basilar artery mean flow velocity > 90 cm/s (suggestive of posterior circulation vasospasm) [41–44].

In children, there are no angiographically validated TCD-based criteria to define the presence or absence of vasospasm. Adult-based criteria cannot be extrapolated to children since baseline flow velocities in children are elevated compared to adults and their use would grossly overestimate the true incidence of vasospasm in children. Thus, recent consensus guidelines for the use of TCD to evaluate for cerebral vasospasm in the PICU state: “Using specific cut-offs for diagnosing, grading, or determining the clinical significance of vasospasm in the MCAs cannot be recommended. However, following CBFVs and LR values over time may have clinical utility to determine trends in vascular diameter” [16]. In clinical practice, the authors perform POCUS TCD in children at risk for cerebral vasospasm [TBI, subarachnoid hemorrhage (SAH)], if CBFVs are >2SD above age-based normative values and the LR is >3–4. If new neurologic deficits are present on clinical examination, confirmation with an additional imaging modality may be considered (MRI, CT, angiogram). Once confirmed, TCD may be utilized at the bedside to follow trends and response to interventions [45–48].

Hypoxic-Ischemic Encephalopathy: Prognosis and Detection of Perfusion Disorders

There is very limited literature reporting the use of TCD in children with hypoxic-ischemic injury (HIE). Lovett et al. performed serial TCDs on 26 children with HIE [49]. Extreme flow velocity alterations (defined as either less than or greater

than 2SD from age-based normative values) within 48 h of injury were associated with poor neurologic outcome. No patient in the favorable outcome group had extreme CBFV alterations on day 1 whereas 38% of patients in the unfavorable group had extreme CBFV alterations on day 1 ($p = 0.03$). Children with favorable outcomes also had more periods of intact cerebral autoregulation evaluated by TCD compared to those with unfavorable outcome. Current paradigms in the management of HIE increasingly focus on improving neurologic resuscitation by meticulously targeting blood pressure optimizing vasoreactivity [50]. In the future, bedside TCD may serve as a tool to continuously determine optimal cerebral perfusion pressure in these children.

Cardiorespiratory Support with Extracorporeal Membrane Oxygenation: Changes Concerning Hemorrhage or Ischemia and Emboli Monitoring

Extracorporeal membrane oxygenation (ECMO) is an important strategy in the treatment of children with severe cardiorespiratory failure refractory to conventional management. Cerebral ischemia and intracranial hemorrhage remain prevalent complications of pediatric ECMO and result in an increased risk of mortality [51]. However, monitoring the development of these complications is difficult. Three studies have reported on the utility of TCD performed at the bedside to assist with this [51–53]. Across all studies, CBFVs during ECMO were significantly lower than published values for age-matched healthy and critically ill children. Regional asymmetries in CBFVs and increased pulsatility index were markers for ischemic injury in all studies. Only one study included a significant number of children suffering intracranial hemorrhage. Patients who developed clinically evident cerebral hemorrhage had higher Vs, Vd, and Vm than age normative values: 123% \pm 8% predicted, 130% \pm 18% predicted, and 127% \pm 9% predicted. These alterations were noted 2–6 days before the clinical recognition of hemorrhage [51]. Microemboli due to thrombosis within the circuit or cannula can lead to ischemic stroke in ECMO patients and can be monitored in real time with TCD [54]. To date, no study has evaluated the fre-

quency or significance of embolic signals in children on ECMO. In summary, POCUS with TCD may be considered by clinicians taking care of children on ECMO as a regular screening tool for acute neurologic complications as well as for rapid evaluation in the setting of neurologic deterioration. Identified TCD abnormalities could prompt neuroimaging if patients are stable for transport to the radiology suite.

Arterial Ischemic Stroke: Progression or Regression of Steno-Occlusive Disease

Arterial ischemic stroke associated with cerebral vasculitis, arteriopathy, and/or prothrombotic disorders is an important cause of morbidity and mortality in children [55–60]. TCD can play a pivotal role as an adjunct tool in the acute management of children with ischemic stroke associated with these conditions. On admission to the ICU, baseline TCD data may be procured and then flow velocities can be followed in real time for either improving perfusion or progressive stenosis/occlusion with worsening perfusion [20]. The clinician may then determine, based on these different flow profiles, to alter blood pressure, ventilation, fluid management, and head of bed positioning accordingly. However, supportive data for these approaches to care remain limited.

Bacterial Meningitis: Detection of Perfusion Disorders (Oligemia or Hyperemia)

Bacterial meningitis (BM) results in significant morbidity and mortality worldwide. Poor outcomes occur in approximately half of the children and are largely attributable to intracranial complications. Ischemic stroke is one such event occurring in 20–25% of patients with BM. The predominant pathological change to the neurovasculature on angiogram in these patients is cerebral arterial narrowing [61–63]. While the underlying etiology for this narrowing is still not completely understood, vasculitis, vasospasm, intra-arterial thrombosis, and external compression of vessels by purulent material in the subarachnoid space have all been implicated. The early identification of poor or deteriorating cerebral hemodynamics secondary to vascular narrowing in patients with

BM may create a therapeutic window in which measures to increase cerebral perfusion pressure (CPP) are undertaken. When CPP-targeted treatment using an invasive ICP monitor was provided indiscriminately to a group of children with CNS infection in India, those with BM had a 90-day mortality reduction from 41 to 10% ($p < 0.01$) [64]. However, the empiric augmentation of CPP requires significant resources, is likely not necessary for some patients, and may be dangerous to others. Thus, identifying patients with compromised cerebral hemodynamics due to vascular narrowing that are most likely to benefit from such therapy may be beneficial.

Ducharme et al. reported TCD findings in a cohort of children with mixed etiologies of CNS infection [65]. Ten children with BM had TCD performed in the acute phase of illness. Two chil-

dren with BM had a normal TCD (compared to age-based normative value), 7 had increased CBFV, and 1 had low CBFV. Across the entire cohort, the presence of hypoperfusion in at least one vessel due to vasospasm (defined as $V_m > 120$ cm/s with $LR > 3$ or absolute $V_m > 200$ cm/s) or low flow ($< 1SD$ from age normal) was associated with acquired ICU morbidity ($p = 0.04$) and death ($p = 0.03$). In 47 African children with bacterial meningitis, admission of TCD was normal in 10 (21%) [66]. High flow with a normal pulsatility index (PI) was seen in 20 (43%) and high flow with a low PI was identified in 7 (15%). Ten (21%) had low flow. All children with a normal TCD had a good outcome. Patients with a high-risk TCD flow pattern (high flow/low PI or low flow) were more likely to have a poor outcome (82% vs 38%, $p = 0.001$) (Fig. 4). These findings taken together

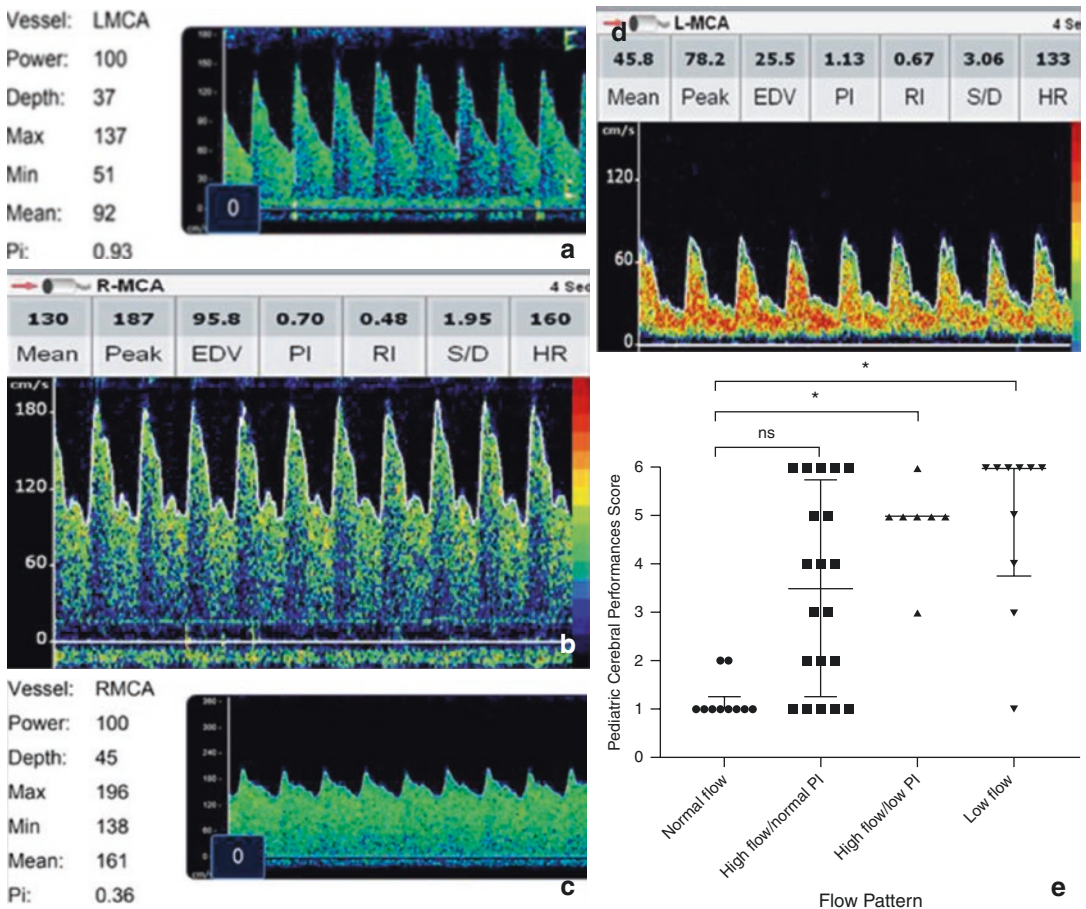


Fig. 4 TCD pattern classification in bacterial meningitis. (a) Normal flow, (b) high flow/normal PI, (c) high flow/low PI, (d) low flow, (e). Flow pattern association with pediatric cerebral performance score. *PI* pulsatility index

suggest that point of care TCD may be a useful tool to identify children with compromised cerebral perfusion in the setting of bacterial meningitis and serve to monitor response to therapy.

Cerebral Circulatory Arrest

TCD findings compatible with a clinical diagnosis of brain death evolve through phases (reduced diastolic flow > oscillatory flow > systolic spikes or no signal) in adults [3, 13, 67]. Similar patterns have been identified in children (Fig. 5). However, TCD has important limitations in the determination of brain death in infants and children, and therefore cannot be used as a confirmatory test at this time. Both false positives and false negatives are of significant concern in newborns and infants with open fontanelles up to age 12 months. Normative diastolic flow in newborns is 12 ± 7 cm/s, which to an inexperienced operator can look very similar to absent diastolic flow/oscillatory flow and could potentially lead to an inappropriate diagnosis of cerebral circulatory arrest. The elastic skull and open fontanelle in this age group oppose rising ICP that usually results in

cerebral circulatory arrest, and persistence of cerebral blood flow despite the infant meeting clinical diagnosis of brain death has also occurred [68]. In older children, the presence of congenital heart disease with cardiac shunts or aortic insufficiency can also limit the usefulness of TCD to aid in the confirmation of brain death as diastolic flow can appear absent in these clinical scenarios [69]. It remains unclear if TCD can be used as an ancillary test for the diagnosis of cerebral circulatory arrest in children older than age 1 year without congenital heart disease. In clinical practice, the authors have used TCD as a point of care tool to determine when to pursue perfusion studies when ancillary testing was necessary. If TCD reveals the presence of cerebral flow without clear evidence of an oscillatory pattern or systolic spikes, it may be reasonable to delay transporting critically ill children to the radiology suite until this pattern develops.

Midline Shift

The detection of midline shift (MLS) is an application of imaging (duplex) TCD which cannot be performed on non-imaging TCD machines. The

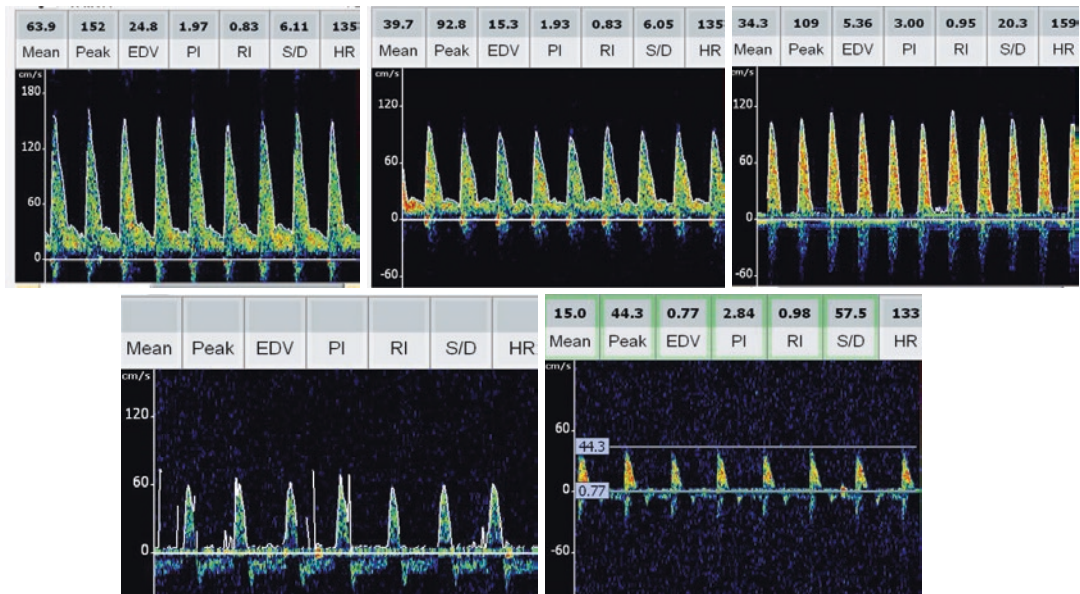


Fig. 5 TCD findings seen in the progression to cerebro-circulatory arrest. As images progress notice the reduction of end-diastolic flow velocity, the absence of end-diastolic

flow velocity with isolated systolic peaks, followed by reversal of flow

detection of midline shift is of interest to a POCUS provider at the bedside because of the potential implications of reducing time to a life-saving intervention and neuroprotective therapies. To calculate midline shift, one must first identify the third ventricle on ultrasound using the transtemporal window. This appears as a hyperechogenic image over the midbrain [70]. Once identified, the distance between the external bone table (duraplasty may be used as a bone surrogate in the setting of decompressive hemicraniectomy) and the center of the third ventricle can be measured bilaterally. The difference between the bilateral measurements, divided by 2 gives the measure of MLS. Therefore, $MLS = (B - A)/2$, where B is the measurement on the right side, and A is the measurement on the left side [71]. A positive or negative number will then denote whether the mass effect is present on the right or the left. When defining a significant MLS as >0.5 cm, this method had a correlation coefficient of 0.58–0.65 compared to CT scan in a study of 52 adults with varying neurosurgical conditions (~60% with severe TBI) [70]. However, when using 0.35 cm for the detection of MLS, the sensitivity was 84.2%, specificity was 84%, and the positive likelihood ratio was 5.56. Similarly, in 41 adults with TBI, the correlation coefficient between MLS measured by CT scan and imaging TCD was 0.88 [71]. This is a potentially useful application of imaging-based TCD but has yet to be described in children and research is needed before the authors can recommend making clinical decisions based on this aspect of POCUS.

Limitations of TCD as a POCUS Tool

Potential barriers to the adoption of TCD in pediatric critical care are twofold: equipment and personnel. Non-imaging TCD is only available on devices intended for this purpose and is often not available to the clinician. Imaging TCD is easily accessible on commonly available ultrasound machines but this technique requires familiarity

with not only TCD waveform interpretation, but also knowledge and recognition of the appropriate structures on ultrasound imaging. There is also no credentialing path for clinicians to perform POCUS TCD. Until these are developed, learners are encouraged to seek out opportunities to participate in proctored practical hands-on sessions with knowledgeable providers to gain the substantial technical and analytical skills that are unique to TCD compared to other POCUS studies. Lastly, there is a paucity of strong evidence surrounding when and how to use TCD in critically ill children limiting its utility at this time.

Ocular Ultrasonography

Basic Principles and Technique

Ocular ultrasonography is an emerging application of POCUS. The optic nerve sheath is continuous with the meninges and directly communicates with the subarachnoid space. Therefore, measurement of the optic nerve sheath diameter (ONSD) may provide additional insight into intracranial pathology. To measure the ONSD, a high-frequency linear transducer on a portable ultrasound machine (using preset ophthalmic settings) can be placed on a closed eyelid. The globe appears anechoic and in the axial plane the optic nerve can be visualized posterior to the globe [72, 73]. An image of the optic nerve can be saved and electronic calipers are then used to measure 3 mm posterior to the retina along the course of the optic nerve. Digital cursors are then used to measure the optic nerve sheath diameter at that location, defined as the distance between the outer hyperechogenic borders of the subarachnoid space (Fig. 6) [72]. To minimize intra-observer variability, each measurement should be performed three times and the mean value derived [74]. It is important to note that this procedure should not be performed if the patient has experienced bilateral ocular trauma/fracture. If unilateral injury has occurred, measurements can be performed on the uninjured side.

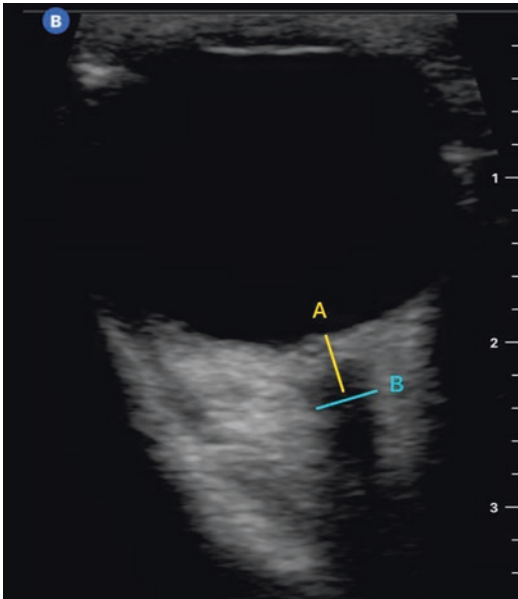


Fig. 6 Identification and measurement of the optic nerve sheath diameter on ocular ultrasonography. (A) represents 3 mm posterior to the retina and (B) represents measurement of the optic nerve sheath diameter

Clinical Applications: Optic Nerve Sheath Diameter to Investigate ICP

As intracranial pressure rises, this increases the amount of cerebral spinal fluid (CSF) around the optic nerve, resulting in dilation of the optic nerve sheath. POCUS evaluation of ONSD has been studied as a method to identify increased ICP. Using a cut-off of 5 mm, ONSD had a > 85% sensitivity in detecting increased ICP in a meta-analysis of adult patients [75]. Data supporting the use of ONSD to detect elevated ICP in children is less clear [76]. A study by Le et al. using ONSD to screen children at risk for elevated ICP in the emergency department found that increased ONSD had 83% sensitivity and 38% specificity for detecting increased ICP [77]. In another study of children over age 1 year, the ONSD value with the best diagnostic accuracy for detecting an ICP ≥ 20 mmHg was 5.75 mm, with 85.9% sensitivity, 70.4% specificity, a positive predictive value of 77.5%, a negative predictive value of 80.9%, and an area under the receiver

operating curve (AUROC) of 0.78 [78]. In a small study of 16 patients with 136 ONSD measurements, ONSD was not significantly associated with ICP ($p = 0.51$) and had AUROC of 0.52 to determine ICP > 20 mmHg [79]. Lastly, ICP/ONSD measurements were compared in a group of 30 children. Of the 144 observations, 106 were obtained when ICP ≥ 20 mmHg, and 38 were obtained when ICP < 15 mmHg. The AUC for the ONSD cut-off values reflecting an ICP ≥ 20 mmHg was 0.976, and an ONSD value of 4.0 mm for the detection of ICP ≥ 20 mmHg had 98% sensitivity, 75% specificity, 75% positive predictive value, and 97% negative predictive value. When a cut-off of 4.7 mm was used, there was 94% sensitivity, 92% specificity, 91% positive predictive value, and 95% negative predictive value [80]. Often the pediatric literature is limited by small sample sizes and heterogenous disease states. Given the absence of a clearly validated ONSD threshold to accurately diagnose intracranial hypertension in critically ill children, its use in the PICU cannot be recommended. In clinical practice, the authors often perform repeat examinations that allow for intra-subject comparison in serial measurements over time. Upward trends in this ONSD may prompt consideration of additional imaging.

Clinical Application: Identification of Retinal Trauma

When applying the same principles used in measuring ONSD, it is possible to evaluate for traumatic retinoschisis, of particular importance in children with suspected abusive head trauma. Riggs et al. were able to identify traumatic retinoschisis in children as smooth, dome-shaped, elevated layers in the posterior retina [81]. In the 11 children evaluated in this study, findings on ultrasound corresponded with formal ophthalmic exam. POCUS has the opportunity to potentially identify these injuries days before a formal dilated eye exam can occur in a child with severe neurologic injury. However, POCUS for the evaluation of retinoschisis should not replace a formal eye examination performed by an experienced ophthalmologist.

Neonatal Cranial Ultrasound

Basic Principles and Technique

Cranial ultrasound can readily image the newborn brain through the open fontanelles [82–84]. Using a portable ultrasound machine and a 5–10 Hz curved or linear array transducer, several views of the brain parenchyma can be obtained: coronal (front to back), sagittal (left to right), and axial (posterior fossa). These views provide information on the general architecture of the brain and the lateral ventricles. The frequency of ultrasound transmitted may be increased for optimal visualization of superficial structures like subcortical white matter and venous sinuses; this will increase resolution at the expense of penetration. Lower ultrasonic frequency may be used for visualization of deeper structures in the posterior fossa. More extensive discussion regarding cranial ultrasound is found in Chap. 16.

Clinical Application

The ability of cranial ultrasound to evaluate for and grade the degree of intraventricular hemorrhage in the hands of vascular technologists and radiologists is well-established [82, 83]. POCUS of the cranium is a particularly useful tool for the neonatologist to evaluate for germinal matrix hemorrhage, post-hemorrhagic ventricular dilation, or hydrocephalus when an infant acutely decompensates or when radiology support is not immediately available [82, 84, 85]. Neonatologists are quite familiar with viewing and interpreting cranial ultrasounds that are routinely followed on daily clinical rounds. Portable ultrasound equipment for these evaluations is also widely available. Thus, training programs focused on image acquisition skills for neonatologist have the potential to expand the field of point of care neurosonography in the NICU.

POCUS Neurosonography Integration

As highlighted in this chapter, point of care neurosonography is an emerging method of assessing critically ill children with acute neu-

rologic illness or injury. The supportive evidence for this topic is sparse, and before strong recommendations for clinical use can be made, the evidence base needs to evolve. However, there is an opportunity for POCUS neurosonography to transform the acute care of a child. Imagine admitting an infant with altered mental status and a questionable history of trauma who is intubated. With the same ultrasound machine that you use to place central venous access, one can use a high-frequency linear probe to evaluate for traumatic retinoschisis, then measure ONSD and trend that value over time as the clinical trajectory evolves. In the transtemporal acoustic window one could use TCD to measure CBFV in the MCAs, measure the pulsatility index, and evaluate for midline shift, all potential meaningful biomarkers that can be followed over time to provide additional insight into cerebrovascular hemodynamics. While the authors recognize the limitations of the literature, providers are encouraged to become familiar with POCUS neurosonography, gain experience with both image acquisition and interpretation, and use confirmatory imaging to verify findings when appropriate.

Conclusion

TCD is a noninvasive physiological monitor of cerebral hemodynamics that can be performed as a point of care examination in the PICU for a number of applications. Optic nerve sheath diameter evaluation using POCUS has a limited but evolving role in evaluating for intracranial hypertension in pediatric patients. Point of care cranial ultrasound performed by bedside providers to evaluate for intraventricular hemorrhage or hydrocephalus in the NICU may assist in the early identification of pathology and allow for rapid decisions. Development and implementation of focused point of care neurosonography training are necessary for both the pediatric and neonatal acute care provider.

References

- Singh Y, Tissot C, Fraga MV, Yousef N, Cortes RG, Lopez J, et al. International evidence-based guidelines on point of care ultrasound (POCUS) for critically ill neonates and children issued by the POCUS Working Group of the European Society of Paediatric and Neonatal Intensive Care (ESPNIC). *Crit Care*. 2020;24(1):65. <https://doi.org/10.1186/s13054-020-2787-9>.
- Sloan MA, Alexandrov AV, Tegeler CH, Spencer MP, Caplan LR, Feldmann E, et al. Assessment: transcranial Doppler ultrasonography: report of the therapeutics and technology assessment Subcommittee of the American Academy of Neurology. *Neurology*. 2004;62(9):1468–81. <https://doi.org/10.1212/wnl.62.9.1468>.
- Ducrocq X, Hassler W, Moritake K, Newell DW, von Reutern GM, Shiohagi T, et al. Consensus opinion on diagnosis of cerebral circulatory arrest using Doppler-sonography: task force group on cerebral death of the Neurosonology Research Group of the World Federation of Neurology. *J Neurol Sci*. 1998;159(2):145–50. [https://doi.org/10.1016/s0022-510x\(98\)00158-0](https://doi.org/10.1016/s0022-510x(98)00158-0).
- Kalanuria A, Nyquist PA, Armonda RA, Razumovsky A. Use of transcranial Doppler (TCD) ultrasound in the Neurocritical Care Unit. *Neurosurg Clin N Am*. 2013;24(3):441–56. <https://doi.org/10.1016/j.neuc.2013.02.005>.
- Lau VI, Arntfield RT. Point-of-care transcranial Doppler by intensivists. *Crit Ultrasound J*. 2017;9(1):21. <https://doi.org/10.1186/s13089-017-0077-9>.
- Aaslid R, Markwalder TM, Nornes H. Noninvasive transcranial Doppler ultrasound recording of flow velocity in basal cerebral arteries. *J Neurosurg*. 1982;57(6):769–74. <https://doi.org/10.3171/jns.1982.57.6.0769>.
- Adams RJ, McKie VC, Hsu L, Files B, Vichinsky E, Pegelow C, et al. Prevention of a first stroke by transfusions in children with sickle cell anemia and abnormal results on transcranial Doppler ultrasonography. *N Engl J Med*. 1998;339(1):5–11. <https://doi.org/10.1056/NEJM199807023390102>.
- Adams R, McKie V, Nichols F, Carl E, Zhang DL, McKie K, et al. The use of transcranial ultrasonography to predict stroke in sickle cell disease. *N Engl J Med*. 1992;326(9):605–10. <https://doi.org/10.1056/NEJM199202273260905>.
- LaRovere KL, Tasker RC, Wainwright M, Reuter-Rice K, Appavu B, Miles D, et al. Transcranial Doppler ultrasound during critical illness in children: survey of practices in Pediatric Neurocritical Care Centers. *Pediatr Crit Care Med*. 2020;21(1):67–74. <https://doi.org/10.1097/PCC.0000000000002118>.
- Kluckow M, Evans N. Low superior vena cava flow and intraventricular haemorrhage in preterm infants. *Arch Dis Child Fetal Neonatal Ed*. 2000;82(3):F188–94. <https://doi.org/10.1136/fn.82.3.f188>.
- Papile LA, Burstein J, Burstein R, Koffler H. Incidence and evolution of subependymal and intraventricular hemorrhage: a study of infants with birth weights less than 1,500 gm. *J Pediatr*. 1978;92(4):529–34. [https://doi.org/10.1016/s0022-3476\(78\)80282-0](https://doi.org/10.1016/s0022-3476(78)80282-0).
- Brandi G, Bechir M, Sailer S, Haberthur C, Stocker R, Stover JF. Transcranial color-coded duplex sonography allows to assess cerebral perfusion pressure noninvasively following severe traumatic brain injury. *Acta Neurochir*. 2010;152(6):965–72. <https://doi.org/10.1007/s00701-010-0643-4>.
- Purkayastha S, Sorond F. Transcranial Doppler ultrasound: technique and application. *Semin Neurol*. 2012;32(4):411–20. <https://doi.org/10.1055/s-0032-1331812>.
- Blanco P, Abdo-Cuza A. Transcranial Doppler ultrasound in neurocritical care. *J Ultrasound*. 2018;21(1):1–16. <https://doi.org/10.1007/s40477-018-0282-9>.
- Moppett IK, Mahajan RP. Transcranial Doppler ultrasonography in anaesthesia and intensive care. *Br J Anaesth*. 2004;93(5):710–24. <https://doi.org/10.1093/bja/aeH205>.
- O'Brien N, Reuter-Rice K, Wainwright M, Kaplan S, Appavu B, Erklauer J, et al. Practice recommendations for transcranial Doppler ultrasonography in critically ill children in the pediatric intensive care unit: a multidisciplinary expert consensus statement. *J Pediatr Intensive Care*. 2021;10(2):133–42.
- O'Brien NF. Reference values for cerebral blood flow velocities in critically ill, sedated children. *Childs Nerv Syst*. 2015;31(12):2269–76. <https://doi.org/10.1007/s00381-015-2873-5>.
- Bode H, Wais U. Age dependence of flow velocities in basal cerebral arteries. *Arch Dis Child*. 1988;63(6):606–11. <https://doi.org/10.1136/adc.63.6.606>.
- Zipper S, DSapostnik G, Weber S. Transcranial color-coded sonography (TCCS): a helpful tool in clinical neurology. *Internet J Intern Med*. 2000;2(1).
- LaRovere KL. Transcranial Doppler ultrasound in children with stroke and cerebrovascular disorders. *Curr Opin Pediatr*. 2015;27(6):712–8. <https://doi.org/10.1097/MOP.0000000000000282>.
- LaRovere KL, O'Brien NF. Transcranial Doppler sonography in pediatric neurocritical care: a review of clinical applications and case illustrations in the pediatric intensive care unit. *J Ultrasound Med*. 2015;34(12):2121–32. <https://doi.org/10.7863/ultra.15.02016>.
- Czosnyka M, Matta BF, Smielewski P, Kirkpatrick PJ, Pickard JD. Cerebral perfusion pressure in head-injured patients: a noninvasive assessment using transcranial Doppler ultrasonography. *J Neurosurg*. 1998;88(5):802–8. <https://doi.org/10.3171/jns.1998.88.5.0802>.
- Martin NA, Patwardhan RV, Alexander MJ, Africk CZ, Lee JH, Shalmon E, et al. Characterization of cerebral hemodynamic phases following severe head trauma: hypoperfusion, hyperemia, and vasospasm. *J*

Neurosurg. 1997;87(1):9–19. <https://doi.org/10.3171/jns.1997.87.1.0009>.

24. Ojha BK, Jha DK, Kale SS, Mehta VS. Trans-cranial Doppler in severe head injury: evaluation of pattern of changes in cerebral blood flow velocity and its impact on outcome. *Surg Neurol.* 2005;64(2):174–9; discussion 9. <https://doi.org/10.1016/j.surneu.2004.11.030>.
25. Moreno JA, Mesalles E, Gener J, Tomasa A, Ley A, Roca J, et al. Evaluating the outcome of severe head injury with transcranial Doppler ultrasonography. *Neurosurg Focus.* 2000;8(1):e8. <https://doi.org/10.3171/foc.2000.8.1.1702>.
26. Trabold F, Meyer PG, Blanot S, Carli PA, Orliaguett GA. The prognostic value of transcranial Doppler studies in children with moderate and severe head injury. *Intensive Care Med.* 2004;30(1):108–12. <https://doi.org/10.1007/s00134-003-2057-8>.
27. O'Brien NF, Maa T, Moore-Clingenpeel M, Rosenberg N, Yeates KO. Relationships between cerebral flow velocities and neurodevelopmental outcomes in children with moderate to severe traumatic brain injury. *Childs Nerv Syst.* 2018;34(4):663–72. <https://doi.org/10.1007/s00381-017-3693-6>.
28. Kochanek PM, Tasker RC, Carney N, Totten AM, Adelson PD, Selden NR, et al. Guidelines for the management of pediatric severe traumatic brain injury, third edition: update of the brain trauma foundation guidelines, Executive summary. *Pediatr Crit Care Med.* 2019;20(3):280–9. <https://doi.org/10.1097/PCC.0000000000001736>.
29. Gosling RG, King DH. Arterial assessment by Doppler-shift ultrasound. *Proc R Soc Med.* 1974;67(6 Pt 1):447–9.
30. de Riva N, Budohoski KP, Smielewski P, Kasprowitz M, Zweifel C, Steiner LA, et al. Transcranial Doppler pulsatility index: what it is and what it isn't. *Neurocrit Care.* 2012;17(1):58–66. <https://doi.org/10.1007/s12028-012-9672-6>.
31. Bellner J, Romner B, Reinstrup P, Kristiansson KA, Ryding E, Brandt L. Transcranial Doppler sonography pulsatility index (PI) reflects intracranial pressure (ICP). *Surg Neurol.* 2004;62(1):45–51; discussion. <https://doi.org/10.1016/j.surneu.2003.12.007>.
32. Kashif FM, Verghese GC, Novak V, Czosnyka M, Heldt T. Model-based noninvasive estimation of intracranial pressure from cerebral blood flow velocity and arterial pressure. *Sci Transl Med.* 2012;4(129):129ra44. <https://doi.org/10.1126/scitranslmed.3003249>.
33. Schmidt B, Czosnyka M, Raabe A, Yahya H, Schwarze JJ, Sackeler D, et al. Adaptive noninvasive assessment of intracranial pressure and cerebral autoregulation. *Stroke.* 2003;34(1):84–9. <https://doi.org/10.1161/01.str.0000047849.01376.ae>.
34. Figaji AA, Zwane E, Fieggen AG, Siesjo P, Peter JC. Transcranial Doppler pulsatility index is not a reliable indicator of intracranial pressure in children with severe traumatic brain injury. *Surg Neurol.* 2009;72(4):389–94. <https://doi.org/10.1016/j.surneu.2009.02.012>.
35. Melo JR, Di Rocco F, Blanot S, Cuttaree H, Sainte-Rose C, Oliveira-Filho J, et al. Transcranial Doppler can predict intracranial hypertension in children with severe traumatic brain injuries. *Childs Nerv Syst.* 2011;27(6):979–84. <https://doi.org/10.1007/s00381-010-1367-8>.
36. O'Brien NF, Maa T, Reuter-Rice K. Noninvasive screening for intracranial hypertension in children with acute, severe traumatic brain injury. *J Neurosurg Pediatr.* 2015;16(4):420–5. <https://doi.org/10.3171/2015.3.PEDS14521>.
37. O'Brien NF, Lovett ME, Chung M, Maa T. Noninvasive estimation of cerebral perfusion pressure using transcranial Doppler ultrasonography in children with severe traumatic brain injury. *Childs Nerv Syst.* 2020;36(9):2063–71. <https://doi.org/10.1007/s00381-020-04524-7>.
38. Fanelli A, Vonberg FW, LaRovere KL, Walsh BK, Smith ER, Robinson S, et al. Fully automated, real-time, calibration-free, continuous noninvasive estimation of intracranial pressure in children. *J Neurosurg Pediatr.* 2019;1–11. <https://doi.org/10.3171/2019.5.PEDS19178>.
39. Abecasis F, Cardim D, Czosnyka M, Robba C, Agrawal S. Transcranial Doppler as a non-invasive method to estimate cerebral perfusion pressure in children with severe traumatic brain injury. *Childs Nerv Syst.* 2020;36(1):125–31. <https://doi.org/10.1007/s00381-019-04273-2>.
40. Lindegaard KF, Normes H, Bakke SJ, Sorteberg W, Nakstad P. Cerebral vasospasm diagnosis by means of angiography and blood velocity measurements. *Acta Neurochir.* 1989;100(1–2):12–24. <https://doi.org/10.1007/bf01405268>.
41. Aaslid R, Huber P, Normes H. Evaluation of cerebrovascular spasm with transcranial Doppler ultrasound. *J Neurosurg.* 1984;60(1):37–41. <https://doi.org/10.3171/jns.1984.60.1.0037>.
42. Burch CM, Wozniak MA, Sloan MA, Rothman MI, Rigamonti D, Permutt T, et al. Detection of intracranial internal carotid artery and middle cerebral artery vasospasm following subarachnoid hemorrhage. *J Neuroimaging.* 1996;6(1):8–15. <https://doi.org/10.1111/jon1996618>.
43. Langlois O, Rabehoina C, Proust F, Freger P, Tadie M, Creissard P. [Diagnosis of vasospasm: comparison between arteriography and transcranial Doppler. A series of 112 comparative tests]. *Neurochirurgie.* 1992;38(3):138–140.
44. Grosset DG, Straiton J, du Trevou M, Bullock R. Prediction of symptomatic vasospasm after subarachnoid hemorrhage by rapidly increasing transcranial Doppler velocity and cerebral blood flow changes. *Stroke.* 1992;23(5):674–9. <https://doi.org/10.1161/01.str.23.5.674>.
45. Sert A, Aydin K, Pirgon O, Emlik D, Ustun ME. Arterial spasm following perimesencephalic nonaneurysmal subarachnoid hemorrhage in a pediatric patient. *Pediatr Neurol.* 2005;32(4):275–7. <https://doi.org/10.1016/j.pediatrneurol.2004.09.011>.

46. Gillis H, Lovett M, O'Brien N. Novel treatment of cerebral vasospasm following aneurysm rupture in a pediatric patient. *Crit Care Med.* 2019;47(1):370.
47. O'Brien NF, Maa T, Yeates KO. The epidemiology of vasospasm in children with moderate-to-severe traumatic brain injury. *Crit Care Med.* 2015;43(3):674–85. <https://doi.org/10.1097/CCM.0000000000000745>.
48. O'Brien NF, Reuter-Rice KE, Khanna S, Peterson BM, Quinto KB. Vasospasm in children with traumatic brain injury. *Intensive Care Med.* 2010;36(4):680–7. <https://doi.org/10.1007/s00134-009-1747-2>.
49. Lovett ME, Maa T, Chung MG, O'Brien NF. Cerebral blood flow velocity and autoregulation in paediatric patients following a global hypoxic-ischaemic insult. *Resuscitation.* 2018;126:191–6. <https://doi.org/10.1016/j.resuscitation.2018.02.005>.
50. Lee JK, Brady KM, Chung SE, Jennings JM, Whitaker EE, Aganga D, et al. A pilot study of cerebrovascular reactivity autoregulation after pediatric cardiac arrest. *Resuscitation.* 2014;85(10):1387–93. <https://doi.org/10.1016/j.resuscitation.2014.07.006>.
51. O'Brien NF, Hall MW. Extracorporeal membrane oxygenation and cerebral blood flow velocity in children. *Pediatr Crit Care Med.* 2013;14(3):e126–34. <https://doi.org/10.1097/PCC.0b013e3182712d62>.
52. O'Brien NF, Buttram SDW, Maa T, Lovett ME, Reuter-Rice K, LaRovere KL, et al. Cerebrovascular physiology during pediatric extracorporeal membrane oxygenation: a multicenter study using transcranial Doppler ultrasonography. *Pediatr Crit Care Med.* 2018;20:178. <https://doi.org/10.1097/PCC.0000000000001778>.
53. Rilinger JF, Smith CM, deRegnier RAO, Goldstein JL, Mills MG, Reynolds M, et al. Transcranial Doppler identification of neurologic injury during pediatric extracorporeal membrane oxygenation therapy. *J Stroke Cerebrovasc Dis.* 2017;26(10):2336–45. <https://doi.org/10.1016/j.jstrokecerebrovasdis.2017.05.022>.
54. Polito A, Ricci Z, Di Chiara L, Giorni C, Iacoella C, Sanders SP, et al. Cerebral blood flow during cardiopulmonary bypass in pediatric cardiac surgery: the role of transcranial Doppler—a systematic review of the literature. *Cardiovasc Ultrasound.* 2006;4:47. <https://doi.org/10.1186/1476-7120-4-47>.
55. Burgin WS, Malkoff M, Felberg RA, Demchuk AM, Christou I, Grotta JC, et al. Transcranial doppler ultrasound criteria for recanalization after thrombolysis for middle cerebral artery stroke. *Stroke.* 2000;31(5):1128–32. <https://doi.org/10.1161/01.str.31.5.1128>.
56. Felberg RA, Christou I, Demchuk AM, Malkoff M, Alexandrov AV. Screening for intracranial stenosis with transcranial Doppler: the accuracy of mean flow velocity thresholds. *J Neuroimaging.* 2002;12(1):9–14. <https://doi.org/10.1111/j.1552-6569.2002.tb00083.x>.
57. Barnes C, Deveber G. Prothrombotic abnormalities in childhood ischaemic stroke. *Thromb Res.* 2006;118(1):67–74. <https://doi.org/10.1016/j.thromres.2005.05.021>.
58. Morgenlander JC, McCallum RM, Devlin T, Moore MS, Gray L, Alberts MJ. Transcranial doppler sonography to monitor cerebral vasculitis. *J Rheumatol.* 1996;23(3):561–3.
59. Razumovsky AY, Wityk RJ, Geocadin RG, Bhardwaj A, Ulatowski JA. Cerebral vasculitis: diagnosis and follow-up with transcranial Doppler ultrasonography. *J Neuroimaging.* 2001;11(3):333–5. <https://doi.org/10.1111/j.1552-6569.2001.tb00059.x>.
60. Bojinova V, Dimova P, Belopitova L. Clinical manifestations of cerebrovascular hypoplasias in childhood. *J Child Neurol.* 2000;15(3):166–71. <https://doi.org/10.1177/088307380001500305>.
61. Ries S, Schminke U, Fassbender K, Daffertshofer M, Steinke W, Hennerici M. Cerebrovascular involvement in the acute phase of bacterial meningitis. *J Neurol.* 1997;244(1):51–5. <https://doi.org/10.1007/s004150050050>.
62. Moller K, Larsen FS, Qvist J, Wandall JH, Knudsen GM, Gjørup IE, et al. Dependency of cerebral blood flow on mean arterial pressure in patients with acute bacterial meningitis. *Crit Care Med.* 2000;28(4):1027–32. <https://doi.org/10.1097/00003246-200004000-00019>.
63. Sigmon J, Ball A, Namen A, Tucker K. Treatment of vasospasm in bacterial meningitis with hemodynamic augmentation. *Neurol Disord Therap.* 2017;1(4):1–5.
64. Kumar R, Singhi S, Singhi P, Jayashree M, Bansal A, Bhatti A. Randomized controlled trial comparing cerebral perfusion pressure-targeted therapy versus intracranial pressure-targeted therapy for raised intracranial pressure due to acute CNS infections in children. *Crit Care Med.* 2014;42(8):1775–87. <https://doi.org/10.1097/CCM.0000000000000298>.
65. Ducharme-Crevier L, Mills MG, Mehta PM, Smith CM, Wainwright MS. Use of transcranial Doppler for management of central nervous system infections in critically ill children. *Pediatr Neurol.* 2016;65:52–8.e2. <https://doi.org/10.1016/j.pediatrneurol.2016.08.027>.
66. Fonseca Y, Tshimanga T, Ray S, Malhotra H, Pongo J, Bodi Mabilia J, et al. Transcranial Doppler ultrasonographic evaluation of cerebrovascular abnormalities in children with acute bacterial meningitis. *Front Neurol.* 2021;11:558857.
67. American Institute of Ultrasound in Medicine (AIUM); American College of Radiology (ACR); Society of Radiologists in Ultrasound (SRU). AIUM practice guideline for the performance of a transcranial Doppler ultrasound examination for adults and children. *J Ultrasound Med.* 2012;31:1489–500.
68. Vicenzini E, Pulitano P, Cicchetti R, Randi F, Papov P, Spadetta G, et al. Transcranial Doppler for brain death in infants: the role of the fontanelles. *Eur Neurol.* 2010;63(3):164–9. <https://doi.org/10.1159/000286232>.
69. Rodríguez RA, Hosking MC, Duncan WJ, Sinclair B, Teixeira OH, Cornel G. Cerebral blood flow

velocities monitored by transcranial Doppler during cardiac catheterizations in children. *Catheter Cardiovasc Diagn.* 1998;43(3):282–90. [https://doi.org/10.1002/\(sici\)1097-0304\(199803\)43:3<282::aid-ccd9>3.0.co;2-5](https://doi.org/10.1002/(sici)1097-0304(199803)43:3<282::aid-ccd9>3.0.co;2-5).

70. Motuel J, Biette I, Srairi M, Mrozek S, Kurrek MM, Chaynes P, et al. Assessment of brain midline shift using sonography in neurosurgical ICU patients. *Crit Care.* 2014;18(6):676. <https://doi.org/10.1186/s13054-014-0676-9>.
71. Llompарт Pou JA, Abadal Centellas JM, Palmer Sans M, Perez Barcena J, Casares Vivas M, Homar Ramirez J, et al. Monitoring midline shift by transcranial color-coded sonography in traumatic brain injury. A comparison with cranial computerized tomography. *Intensive Care Med.* 2004;30(8):1672–5. <https://doi.org/10.1007/s00134-004-2348-8>.
72. Lochner P, Czosnyka M, Naldi A, Lyros E, Pelosi P, Mathur S, et al. Optic nerve sheath diameter: present and future perspectives for neurologists and critical care physicians. *Neurol Sci.* 2019;40(12):2447–57. <https://doi.org/10.1007/s10072-019-04015-x>.
73. Ballantyne J, Hollman AS, Hamilton R, Bradnam MS, Carachi R, Young DG, et al. Transorbital optic nerve sheath ultrasonography in normal children. *Clin Radiol.* 1999;54(11):740–2. [https://doi.org/10.1016/s0009-9260\(99\)91176-5](https://doi.org/10.1016/s0009-9260(99)91176-5).
74. Betcher J, Becker TK, Stoyanoff P, Cranford J, Theyyanni N. Military trainees can accurately measure optic nerve sheath diameter after a brief training session. *Mil Med Res.* 2018;5(1):42. <https://doi.org/10.1186/s40779-018-0189-y>.
75. Lee SH, Kim HS, Yun SJ. Optic nerve sheath diameter measurement for predicting raised intracranial pressure in adult patients with severe traumatic brain injury: a meta-analysis. *J Crit Care.* 2020;56:182–7. <https://doi.org/10.1016/j.jcrc.2020.01.006>.
76. Young AM, Guilfoyle MR, Donnelly J, Scoffings D, Fernandes H, Garnett M, et al. Correlating optic nerve sheath diameter with opening intracranial pressure in pediatric traumatic brain injury. *Pediatr Res.* 2017;81(3):443–7. <https://doi.org/10.1038/pr.2016.165>.
77. Le A, Hoehn ME, Smith ME, Spentzas T, Schlappy D, Pershad J. Bedside sonographic measurement of optic nerve sheath diameter as a predictor of increased intracranial pressure in children. *Ann Emerg Med.* 2009;53(6):785–91. <https://doi.org/10.1016/j.annemergmed.2008.11.025>.
78. Padayachy LC, Padayachy V, Galal U, Pollock T, Fieggen AG. The relationship between transorbital ultrasound measurement of the optic nerve sheath diameter (ONSD) and invasively measured ICP in children. Part II: age-related ONSD cut-off values and patency of the anterior Fontanelle. *Childs Nerv Syst.* 2016;32(10):1779–85. <https://doi.org/10.1007/s00381-016-3068-4>.
79. Biggs A, Lovett M, Moore-Clingenpeel M, O'Brien N. Optic nerve sheath diameter does not correlate with intracranial pressure in pediatric neurocritical care patients. *Childs Nerv Syst.* 2020;37:951. <https://doi.org/10.1007/s00381-020-04910-1>.
80. Sharawat IK, Kasinathan A, Bansal A, Sahu JK, Sodhi KS, Dogra MR, et al. Evaluation of optic nerve sheath diameter and transcranial Doppler as noninvasive tools to detect raised intracranial pressure in children. *Pediatr Crit Care Med.* 2020;21(11):959–65. <https://doi.org/10.1097/PCC.0000000000002523>.
81. Riggs BJ, Trimboli-Heidler C, Spaeder MC, Miller MM, Dean NP, Cohen JS. The use of ophthalmic ultrasonography to identify retinal injuries associated with abusive head trauma. *Ann Emerg Med.* 2016;67(5):620–4. <https://doi.org/10.1016/j.annemergmed.2015.09.027>.
82. Rath C, Suryawanshi P. Point of care neonatal ultrasound—head, lung, gut and line localization. *Indian Pediatr.* 2016;53(10):889–99. <https://doi.org/10.1007/s13312-016-0954-5>.
83. Dudink J, Jeanne Steggerda S, Horsch S, eurUS.brain group. State-of-the-art neonatal cerebral ultrasound: technique and reporting. *Pediatr Res.* 2020;87(Suppl 1):3–12. <https://doi.org/10.1038/s41390-020-0776-y>.
84. Govaert P, Roehr CC, Gressens P. Cranial ultrasound by neonatologists. *Pediatr Res.* 2020;87(Suppl 1):1–2. <https://doi.org/10.1038/s41390-020-0779-8>.
85. Subramaniam S, Chen AE, Khwaja A, Rempell R. Identifying infant hydrocephalus in the emergency department with transfontanelar POCUS. *Am J Emerg Med.* 2019;37(1):127–32. <https://doi.org/10.1016/j.ajem.2018.10.012>.



Cranial Ultrasound

Pradeep Suryawanshi, Reema Garegrat,
and Yogen Singh

Contents

Introduction	227
Technical Considerations	228
Clinical Indications	232
Cranial Ultrasonography in Brain Pathologies	232
Conclusion	239
References	239

P. Suryawanshi (✉)

Department of Neonatology, BVU Medical College,
Pune, India

Pediatrics and Neonatology, Sahyadri Hospital,
Pune, India

Neonatology, Noble Hospital, Pune, India

Department of Pediatrics, BLDE University,
Bijapur, Karnataka, India

R. Garegrat

Department of Neonatology, BVU Medical College,
Pune, India

Y. Singh

Department of Pediatrics, Division of Neonatology,
Loma Linda University School of Medicine,
California, USA

Department of Pediatrics, Division of Neonatal and
Developmental Medicine, Stanford University School
of Medicine, California, UK

Department of Pediatrics, Division of Neonatology,
University of Southern California, California, UK

ESPNIC Cardiovascular Dynamics Section and
POCUS Working Group, Geneva, Switzerland

Introduction

Cranial Ultrasound (CUS) is the most common imaging modality utilized in the neonatal intensive care unit (NICU) worldwide to evaluate the neonatal brain. It is routinely used in preterm and at-risk infants for screening purposes. The advent of more advanced radiodiagnostics cannot overshadow the ease, the cost, and the safety of this imaging modality. Besides, with more advances in technology, modern portable ultrasound machines provide faster processing and higher resolution. The newer higher frequency transducers also help in visualizing both superficial as well as deep areas of the brain.

This chapter will discuss the utility of neonatal CUS in evaluating different pathologies and the basic neurosonographic anatomy with its technical aspects.

Technical Considerations

Ultrasound Probe Selection for Neonatal Cranial Ultrasound

The selection of the probe is a vital aspect to acquire high quality cranial sonographic images. The minimum requirement for a probe includes that transducer footprint is appropriate for the size of the fontanelle. The ideal frequency is 8–12 MHz, usually as a multifrequency probe and preferably a curvilinear (curved or microconvex) probe, although a phased array sector probe can be used. Higher frequency probes (such as linear probes) provide better near-view resolution but loose optimal penetration power. The frequency of the probe may be increased (8–12 MHz) for optimal visualization of superficial structures like subcortical white matter and venous sinuses but this will be at the expense of the penetration. Likewise, for the deeper structures (such as brainstem and cerebellum) lower frequency probes (6–8 MHz) may be used.

Normal Neonatal Brain Anatomy

An in-depth knowledge of neonatal brain anatomy is mandatory before we discuss CUS along with an overview of the relative echogenicity of the intracranial structures. Calvarium, cerebellar vermis, and choroid plexus are the most echogenic structures of the neonatal brain. The reason for the echogenicity of these structures may be either due to large vascular structure pulsations or the arachnoid trabeculations [1, 2].

Choroid plexus is most prominent in the trigone of the lateral ventricles. It extends from the trigone to the caudothalamic notch or groove. The lateral

ventricles are at times asymmetrical, more so appreciable in preterm neonates [3]. They are horse-shoe shaped, placed around the cerebral peduncles, thalamus, and caudate nucleus. The lateral ventricles are separated by the septum pellucidum.

In premature infants, the septum pellucidum often appears as a fluid-filled space called cavum septum pellucidum, which is usually open at birth and closes around 3–6 months of age. It is also called the fifth ventricle. A deep pocket of ependyma contains a friable blood vessel collection called the germinal matrix which is not usually seen in a normal preterm neonate unless bleeding has occurred. The involution of this tissue normally is completed by 32 weeks of gestation. The appearance of the Sylvian fissures may vary with the gestational age [4, 5].

Cranial Ultrasound Views

Standard and supplementary windows exist during the neonatal period which can be used to acquire detailed images of the different intracranial structures with accuracy.

For standard CUS views enabling an optimal visualization of the supratentorial structures, the anterior fontanelle is used as an acoustic window where both coronal and sagittal planes can be obtained. This allows visualization and assessment of anatomical structures.

Coronal plane: To acquire images in the coronal plane, the probe is placed on the anterior fontanelle with the marker to the right of the patient and sweeping from orbits to occiput (anterior to posterior) obtaining views at three different levels (Fig. 1). The areas visualized in the order from

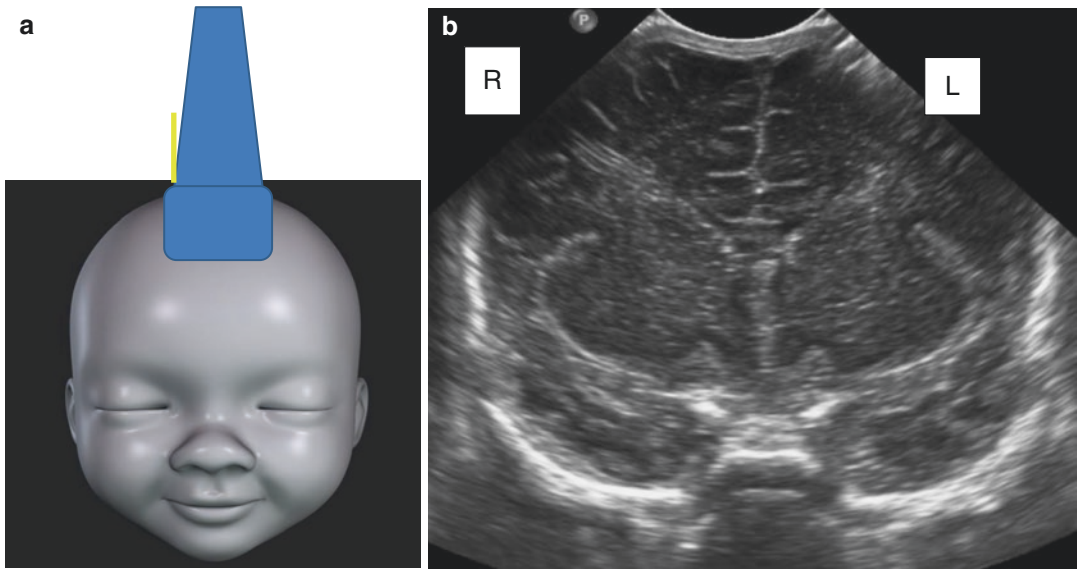


Fig. 1 (a) Adequately fitting linear ultrasound probe, positioned onto the anterior fontanelle. The yellow mark indicates the marker on the probe pointing to the right of the patient. (b) Coronal ultrasound image using a curvilinear

ear probe with the marker positioned in the top left corner of the screen, this way and by convention the right side of the brain is projected on the left side of the image

anterior to posterior are the frontal cortex and frontal horns of the lateral ventricles, deep nuclei and trigone and posterior horns of the lateral ventricles, and occipital cortex as shown in Fig. 2.

Sagittal plane: To acquire images in the sagittal plane, the probe is placed on the anterior fontanelle and swept from midline to either side of the brain. Marker points to the mid-face/nose (Fig. 3). The main areas visualized in the sagittal midline are corpus callosum, cavum septum pellucidum, third ventricle, brain stem, foramen of Monro, and fourth ventricle (Fig. 4).

Supplementary windows: For comprehensive CUS supplementary windows are routinely used by the radiologists or specialists in neonatal neurosonography. However, for the cranial point-of-care ultrasound imaging is performed only through the anterior fontanelle. For supplemental windows, scanning is performed through the posterior fontanelle to enable the detection of blood flow in the occipital horns of the lateral ventricles, cerebellar hemorrhage, and posterior fossa malformations. Mastoid fontanelles can also be used for visualization of the posterior fossa (Fig. 5).

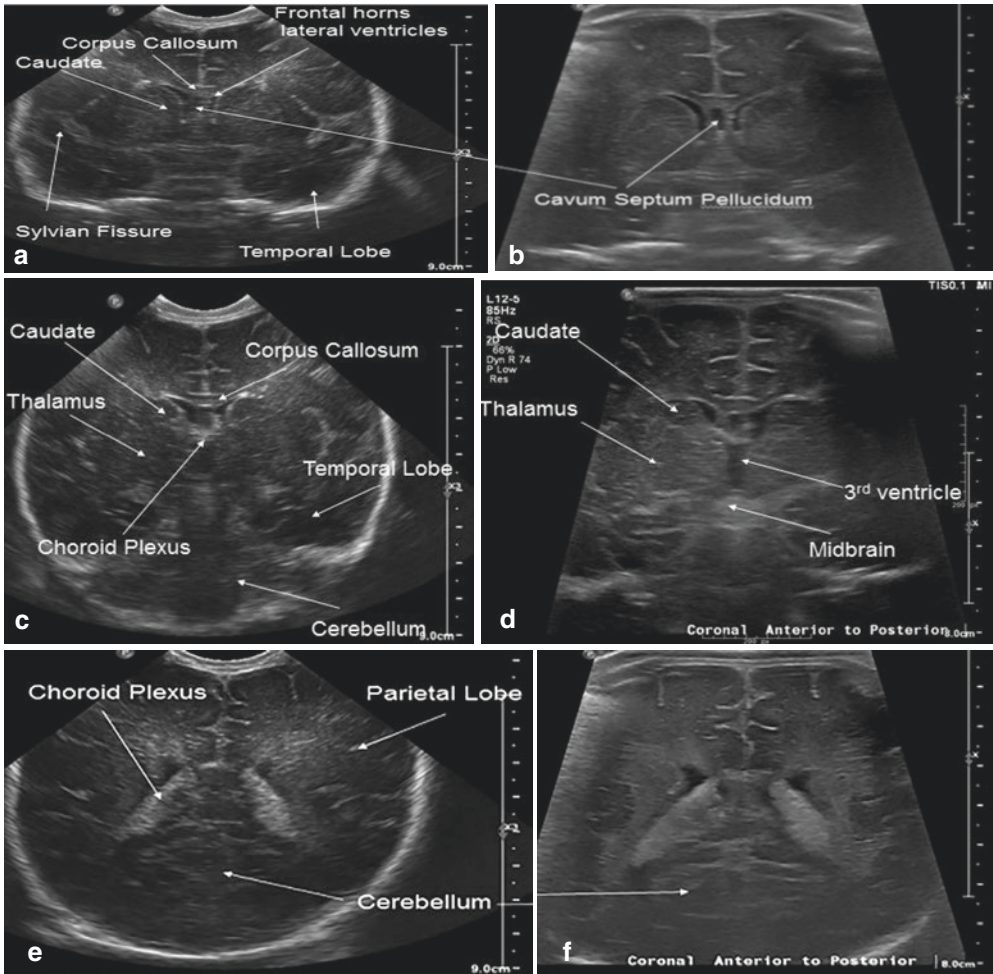


Fig. 2 Coronal planes comparing curvilinear with linear probes at the three different levels. (a and b) Coronal plane through the frontal horns of the lateral ventricles, (c and d) Coronal plane at the level of the deep nuclei, and (e and f) Coronal plane at the level of the trigone and posterior horns of the lateral ventricles

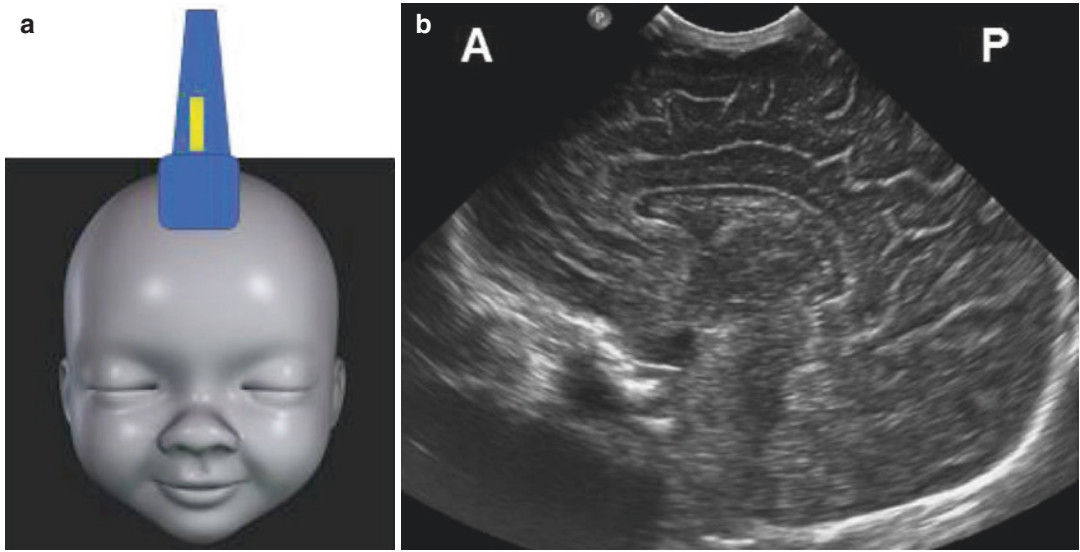


Fig. 3 (a) Probe positioning for obtaining sagittal plane with marker directed towards the nose. (b) The anterior part of the brain will be projected on the left of the image and the posterior part on the right

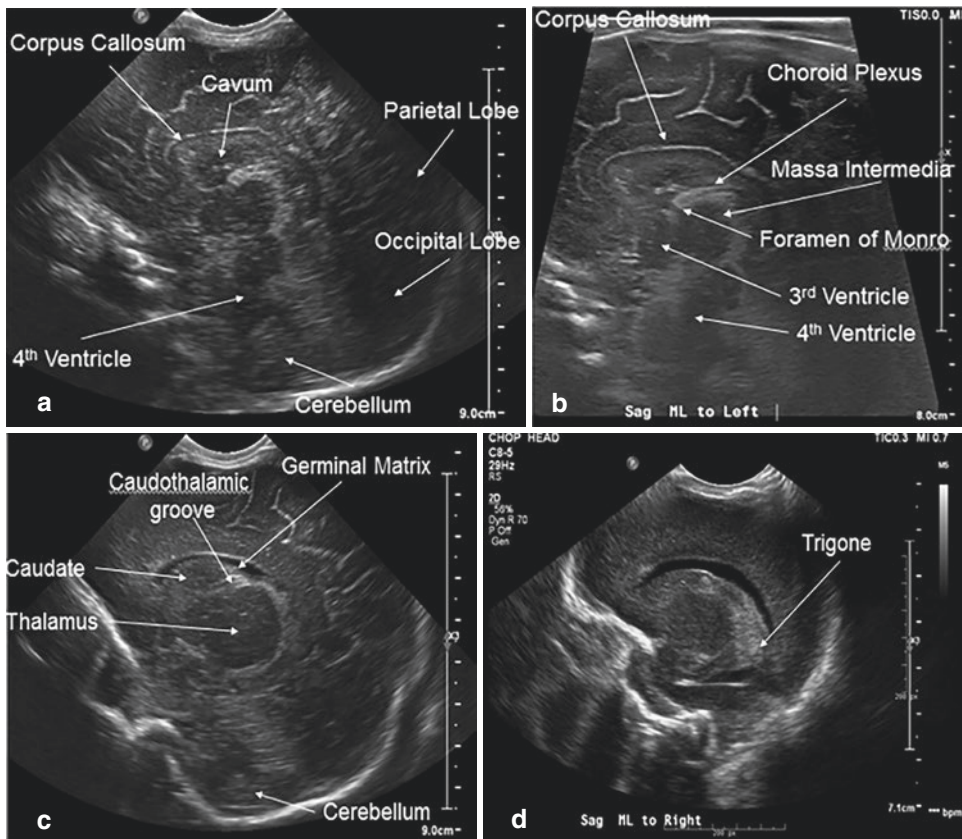


Fig. 4 Sagittal planes comparing curvilinear with linear probes at two different levels. Midline sagittal view demonstrating echogenic choroid plexus cranially and the ver-

mis caudally in the midline, confirming a true sagittal plane (a and b) and parasagittal through the lateral ventricles and the trigone (c and d)

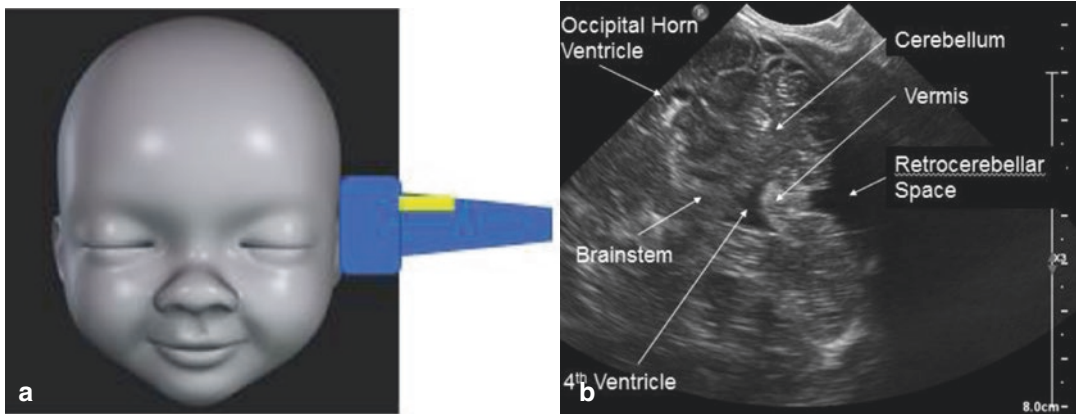


Fig. 5 (a) Probe positioned in the mastoid fontanelle showing the marker pointing upwards towards the anterior fontanelle, and (b) The mastoid coronal view for visualizing the posterior fossa abnormalities

Clinical Indications

CUS is recommended for the routine screening of all preterm neonates <32 weeks of gestational age, for very small infants with birth weight <1500 g, for infants with hypoxic ischemic encephalopathy (HIE) or perinatal asphyxia, and for all neonates with suspected congenital malformations and congenital infections [6–8]. Sick neonates with unexplained acute anemia should be screened first with CUS to rule out intraventricular hemorrhage (IVH) and cerebellar hemorrhage. Neonates born after a traumatic delivery and those with a suspicion of subgaleal hemorrhage warrant a neurosonographic evaluation.

Other indications for cranial ultrasound in neonates are: hypoxic ischemic meningitis, neonatal seizures to rule out congenital malformations and hydrocephalus to monitor ventricular dilatation over time.

Cranial Ultrasonography in Brain Pathologies

Intraventricular Hemorrhage

The majority of intracranial hemorrhages in preterm infants are in the germinal matrix [6]. This

matrix is specific to mammals and embryologically appears along the lateral ventricular margins [7]. It is deeply vascularized and highly metabolically active due to the abundance of proliferating neuroectodermal cells. Beyond 32 weeks of gestation, these cells migrate into the cerebral cortex followed by the disappearance of the germinal matrix. The vascular bed of the germinal matrix is extremely fragile containing vessels with a single layer of endothelial cells resembling capillaries and the paucity of supporting stroma makes them vulnerable to rupture during periods of hemodynamic instability, respiratory failure, and stress [8].

The presence of severe hemorrhage may indicate trans-ependymal rupture, parenchymal extension, or obliterative arachnoiditis may occur. Along with physiological factors, mechanical factors like stasis, compression or tearing of the fragile capillaries also play a role in the pathogenesis of germinal matrix hemorrhage [9, 10]. Disease processes like hypernatremia, disseminated intravascular coagulation, or excessive fibrinolytic activity are the commonly known triggers. But the base for the initiation of the germinal matrix hemorrhage (GMH) includes prematurity, metabolically active and fragile subependymal cells, poor autoregulation,

increased blood supply, increased cerebral venous pressure and endothelial damage.

The most commonly used IVH classifications by Volpe and Papille have been described in Tables 1 and 2, respectively. The Papille's classification is currently the most widely used grading system for IVH. With grade 1 and grade 2 IVH, good neurodevelopmental outcome are expected with only a 5% risk of ventricular dilatation. Conversely, grade 3 IVH carries 10–20% mortality and 30–40% risk of cognitive and motor delay. The risk of ventricular dilatation is high at 20–55% in presence of grade 3 IVH and risk is even higher at 80% for grade 4 IVH. Almost all infants with periventricular infarction have a poor neurodevelopmental outcome [11].

Table 1 Volpe's classification of intraventricular hemorrhage

Grade 1	GMH with no or minimal IVH (<10% of ventricular area on parasagittal view)
Grade 2	IVH (10–50% of ventricular area on parasagittal view)
Grade 3	IVH (>50% of ventricular area on parasagittal view, dilating the lateral ventricle)
Separate notation	Concomitant periventricular echodensity referred as IPE (intraparenchymal echodensity), periventricular hemorrhagic parenchymal infarction, or venous infarction

Table 2 Grading of intraventricular hemorrhage by Papille et al.

Grade 1	Small hemorrhage confined to the Germinal matrix and without effect on adjacent parenchyma (Fig. 6a)
Grade 2	Hemorrhage originating within the Germinal matrix and extending into the lateral ventricle, without ventricular dilatation (Fig. 6b)
Grade 3	Hemorrhage originating into the Germinal matrix and extending into the lateral ventricle leading to acute ventricular dilatation (Fig. 6c)
Grade 4	Large hemorrhage extending to the brain parenchyma with infarction of the periventricular white matter (Fig. 6d)

Post-Hemorrhagic Ventricular Dilatation

Post-hemorrhagic ventricular dilatation (PHVD) usually develops after a grade 3 or grade 4 IVH. It is defined as ventricular enlargement that exceeds the 97th percentile for the gestational age [12] (Fig. 7). Clinical parameters are not reliable for its diagnosis and serial cranial ultrasonography is the imaging of choice to monitor its progression [12–14].

The commonly used measurements for documenting ventriculomegaly are ventricular index, anterior horn width, thalamo-occipital distance (TOD), ventricular height, and frontal horn ratio [15] (Table 3).

Periventricular Leukomalacia

In neonates, the site of ischemic damage varies with gestational age. In term neonates, anoxia or severe hypoxia damages the grey matter and basal ganglia resulting in cerebral atrophy whereas in preterm neonates, ischemia damages the periventricular white matter.

Periventricular leukomalacia (PVL) is the result of infarction in the arterial boundary zones, better called as watershed zones.

This white matter injury can be cystic with macroscopic focal necrosis evolving to cysts or non-cystic with multiple focal areas of necrosis eventually ending up in glial scars and lastly diffuse astrogliosis without focal necrosis [16–20] as seen in Fig. 9.

The well-known classification by De Varies only focuses on cystic white matter injury which is less common than diffuse PVL (diffuse white matter gliosis). Diffuse PVL is not easily discernible by CUS [21].

De Varies et al. in 1992 classified periventricular leukomalacia into the following grades (Table 4):

Grade 1: Transient periventricular echo densities persisting for >7 days

Grade 2: Small, localized frontoparietal cysts.

Grade 3: Periventricular echo densities evolving into extensive periventricular cystic lesions

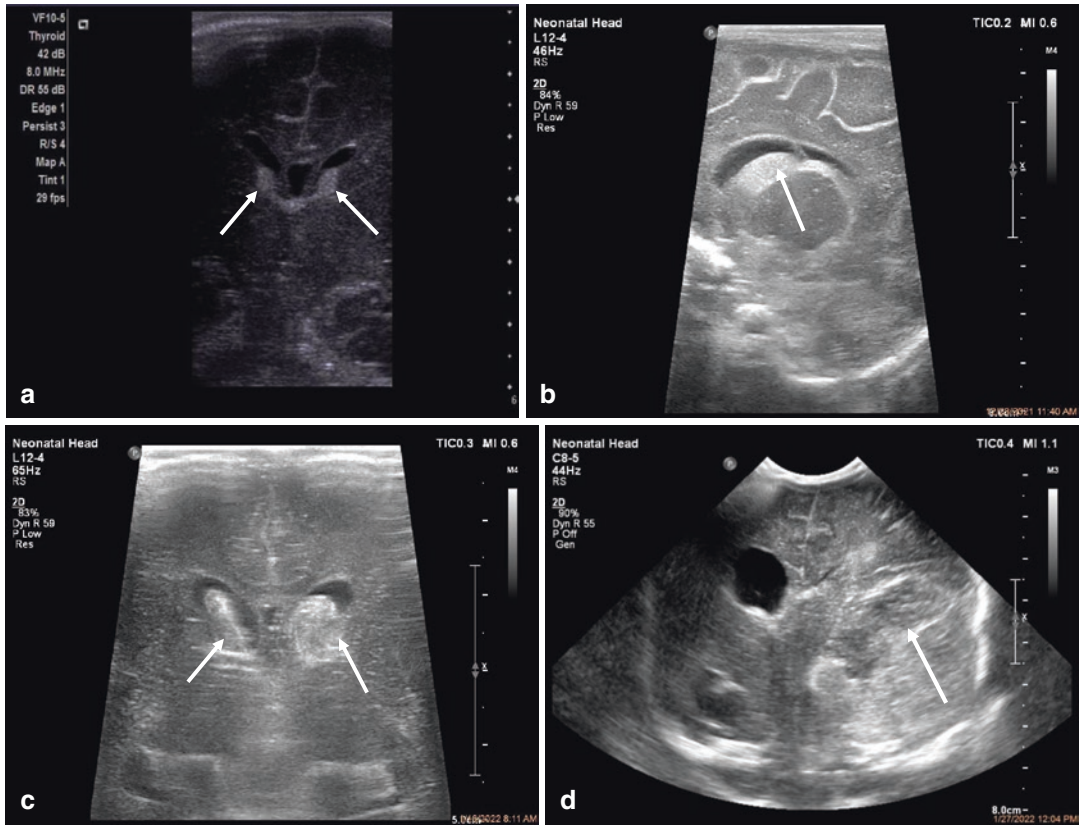


Fig. 6 (a) Coronal ultrasound image in a preterm neonate at the level of frontal horns of the lateral ventricles, showing bilateral germinal matrix hemorrhage (arrows; grade 1 IVH), (b) Parasagittal ultrasound scan through right lateral ventricle showing IVH grade 2 (arrow), and (c) Coronal ultrasound image in a preterm neonate with grade

3 IVH (arrows), showing dilatation of frontal and temporal horns of lateral ventricles (d) Grade 4 IVH implies extension of echogenicity out of the vicinity of the caudate nucleus into the periventricular white matter shown in the left parietotemporal region of the coronal scan (arrow)

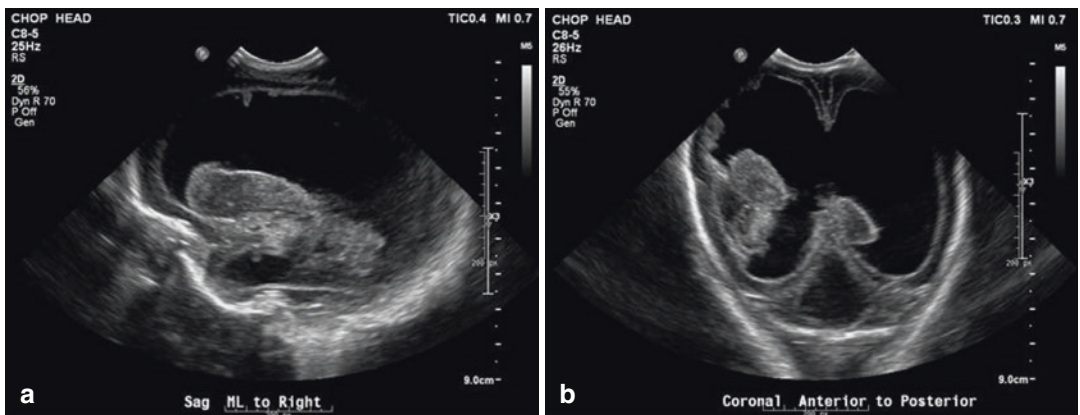


Fig. 7 (a and b) Post hemorrhagic dilatation of the ventricles on parasagittal and coronal views respectively

Table 3 Sonographic indexes to assess ventriculomegaly (Fig. 8)

Sonographic index	Advantages	Measurements
Ventricular index	Most widely used >4 mm of the 97th centile-poor prognosis Correlates well only for term neonates Misses out on early hydrocephalus	– Measured in coronal view (Foramen of Monro view) – Distance from Falx/midline to lateral wall of the body of the ventricle
Anterior horn width	Identifies early hydrocephalus No variation with change in gestational age >4 mm is abnormal	– Measured diagonally in coronal plane (Foramen of Monro view)
Thalamo-occipital distance	Absence of increased TOD is an important negative finding as it can be the only site of dilatation. >26 mm is abnormal It is a less meaningful marker due to its difficult visualization and considerable variation. Isolated dilatation exists in normal preterms infants	– Measured in sagittal plane – >26 mm is abnormal (or >1 mm over then 97th centile)
Third ventricular width	Measurement of the third ventricle assists in differentiating communicating and non-communicating hydrocephalus	– Measured in coronal plane – >3 mm is abnormal (or >1 mm over the 97th centile)

Grade 4: Densities extending into deep white matter evolving into extensive cystic lesions

The two phases in the evolution of cystic PVL are as follows:

Early acute phase	Occurs in the late antenatal and early postnatal period. Approximately from the end of first week to 10 days of life
Late chronic phase	Appears as swiss cheese multicystic pattern on neurosonogram and evolves over 4–6 weeks

Sequelae in Periventricular Leukomalacia

1. Cystic change of the affected white matter also called as Swiss Cheese appearance of brain parenchyma: Bilateral cysts in the fronto-parietal-occipital or parieto-occipital regions (Fig. 9) are associated with a high risk of cerebral palsy, mostly being spastic diplegia or quadriplegia.
2. Cystic encephalomalacia: Grade 4 or subcortical periventricular leukomalacia which often affects near-term infants has a poor prognosis (Fig. 10)
3. Porencephalic cyst: Porencephalic cavitation due to venous infarction associated with germinal matrix intraventricular hemorrhage or arterial infarction of a branch of a perforator artery.
4. Cognitive deficits: Intellectual disability is commonly associated with spastic diplegia, quadriplegia and/or cerebral visual impairment may occur due to the involvement of optic radiation [22, 23]. Behavioral and social-emotional problems are commonly seen in children born very preterm with white matter injury [23].

Perinatal Asphyxia and Hypoxic Ischemic Encephalopathy

A screening CUS is performed on day 1 of life in babies diagnosed with perinatal asphyxia. In addition, if severe forms of asphyxia causing intracranial hemorrhage are suspected, CUS should be obtained and serially repeated to monitor the progression. Doppler evaluation in cases of perinatal depression is also valuable as a prognostic factor.

The patterns of injury are variable in hypoxic ischemic encephalopathy. The neurosonographic findings can include cerebral edema (Fig. 11), periventricular injury, basal ganglia injury or focal ischemic lesions, and intracranial bleeds (Table 5) [24].

Neonatal Infections

Intrauterine infections occurring early in gestation result in congenital malformations while

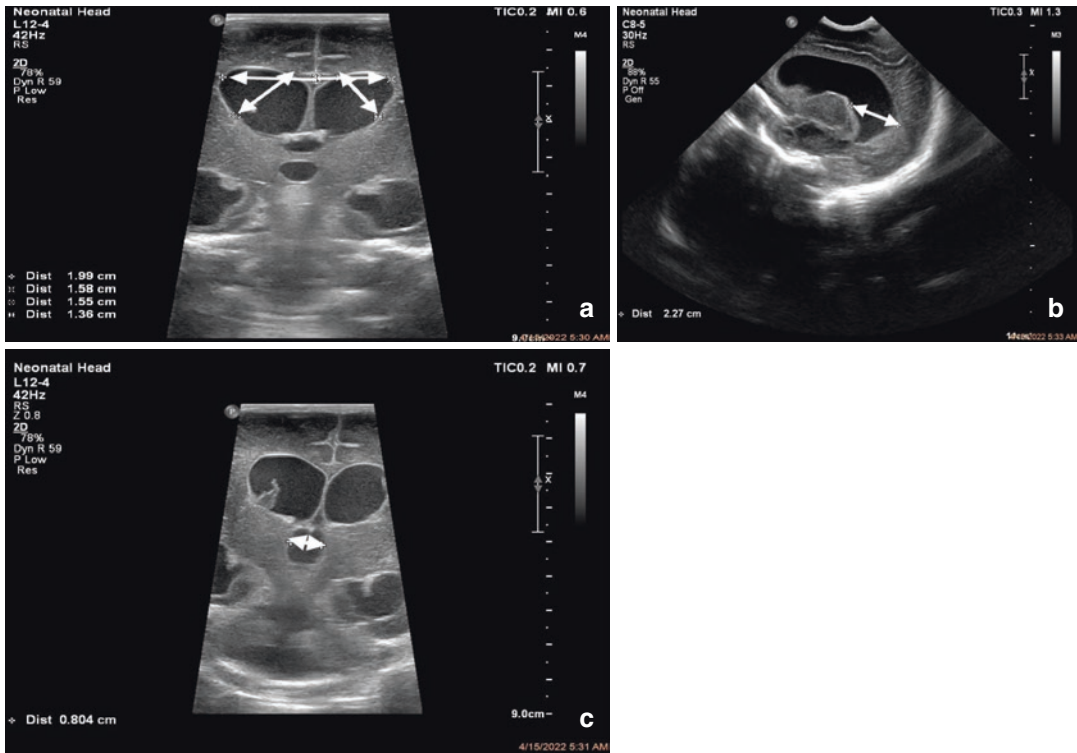


Fig. 8 (a) Single arrow showing the ventricular index of Levene while the double arrow denotes the anterior horn width, (b) Thalamo-occipital distance with double arrows, and (c) Third ventricular width with two arrowheads

those occurring later can cause the destruction of normal brain parenchyma. The neurosonographic findings in TORCH infections are: periventricular calcifications, cerebral atrophy, hydrocephalus, subependymal cysts, and lenticulostriate vasculopathy (LSV).

1. Lenticulostriate vasculopathy (LSV): It refers to the sonographic appearance of increased echogenicity of the lenticulostriate vessels arising from the middle cerebral arteries supplying the basal ganglia and portions of the internal capsule [25]. This may be unilateral/bilateral branching, punctate/linear, or thalamic echogenicity. The common infectious causes of LSV are congenital infections (cytomegalovirus, rubella, syphilis, human immunodeficiency virus, toxo-

plasmosis, varicella), bacterial meningitis, and rotavirus. Symptomatic cytomegalovirus (CMV) infected infants have central nervous system insults in the form of lissencephaly, polymicrogyria, microcephaly, ventriculomegaly, LSV, and cerebral calcifications, (Fig. 12) [26–28].

2. Meningitis: Neurosonographic findings in neonatal meningitis can be extensive in the form of subdural fluid collections, ventriculomegaly, ventriculitis, cerebritis, brain abscess, and echogenic sulci (Fig. 13). Echogenic sulci is the earliest finding discernible on CUS projecting as a sulcal thickness > 2 mm. Findings consistent with ventriculitis vary depending on the course of the disease as shown in Table 6

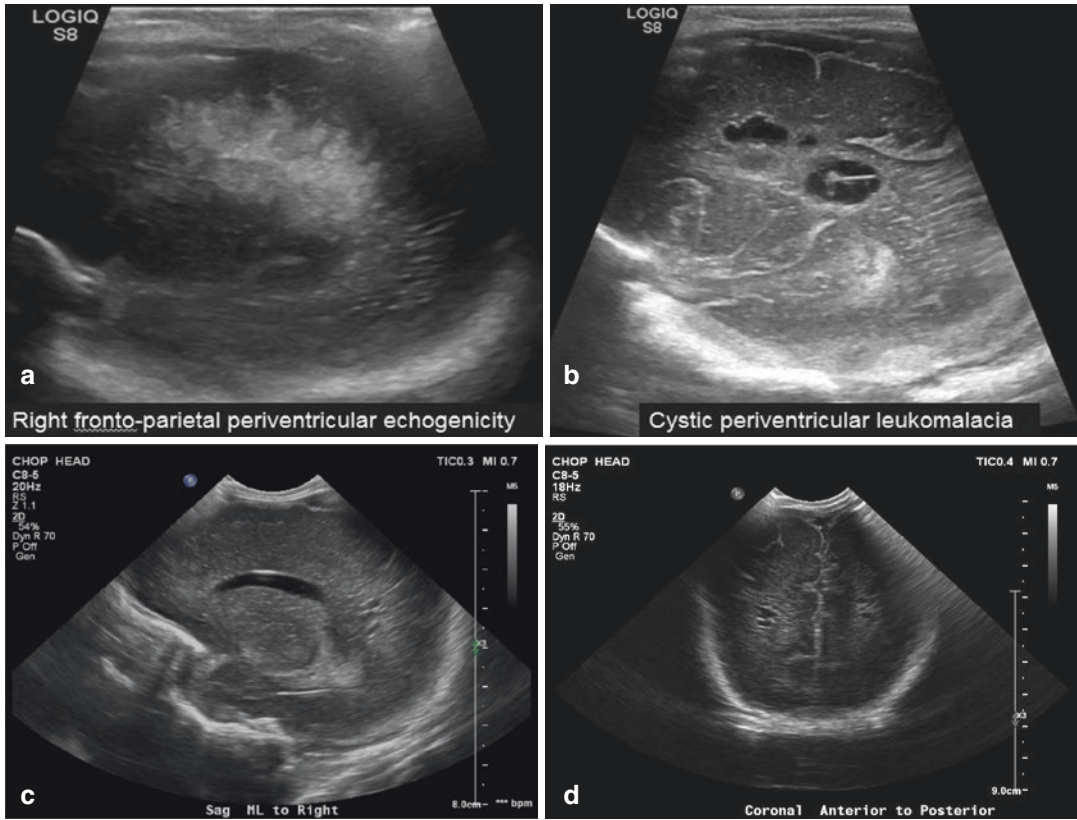


Fig. 9 (a) Transient periventricular echodensity seen in the fronto-parietal region on sagittal view, (b) Small localized fronto-parietal cysts seen in the sagittal plane, and (c) and (d) Deep cystic lesions in sagittal and coronal planes, respectively

Table 4 Neonatal cranial ultrasound findings in PVL

Grade 1 PVL	Peritrigonal blush-frontal horns, parieto-occipital junction of lateral ventricles
Grade 2 PVL	White matter cysts within flare-localized, few in number
Grade 3 PVL	Cysts representing total tissue necrosis, widespread along fronto-parieto-occipital region
Grade 4 PVL	Periventricular and cortical cysts—Subcortical leukomalacia

Fig. 10 Cystic encephalomalacia at 2 months follow up in a neonate who suffered from perinatal asphyxia

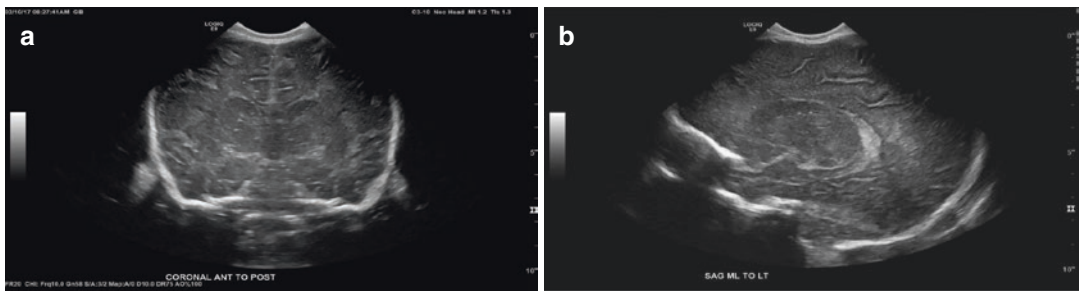
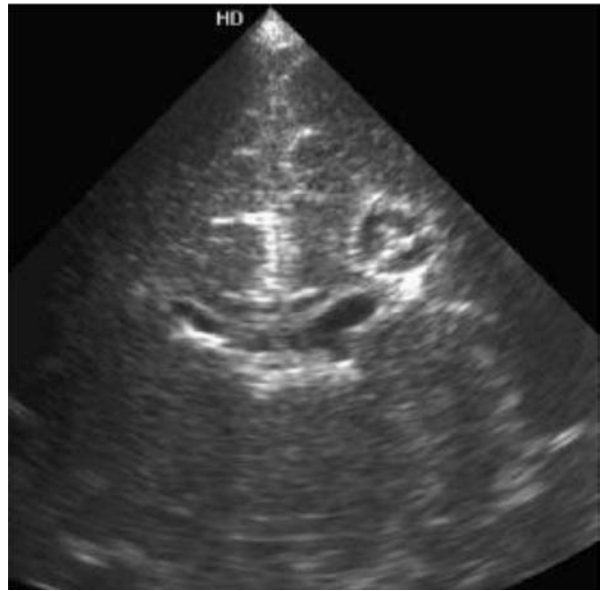


Fig. 11 (a and b) Early stage of perinatal asphyxia with gross cerebral edema and chinked lateral ventricles on coronal view and parasagittal view

Table 5 Different forms of injury known to occur in HIE

Periventricular injury	Visible as periventricular flare, cysts, or with progressive ventricular dilatation
Cerebral edema	Chinked lateral ventricles with loss of normal brain architecture.
Intracranial bleed	May be either a cerebellar bleed, parenchymal bleed, or an intraventricular hemorrhage
Basal ganglia injury	Echodense lesions in hemorrhagic necrosis or echolucent lesions in non-hemorrhagic necrosis
Focal ischemic lesions	Seen as echodensities in vascular network with loss of pulsations in the involved vessel
Structural malformations	Porencephaly



Fig. 12 Widespread punctate hyperechogenicities suggestive of cerebral calcifications

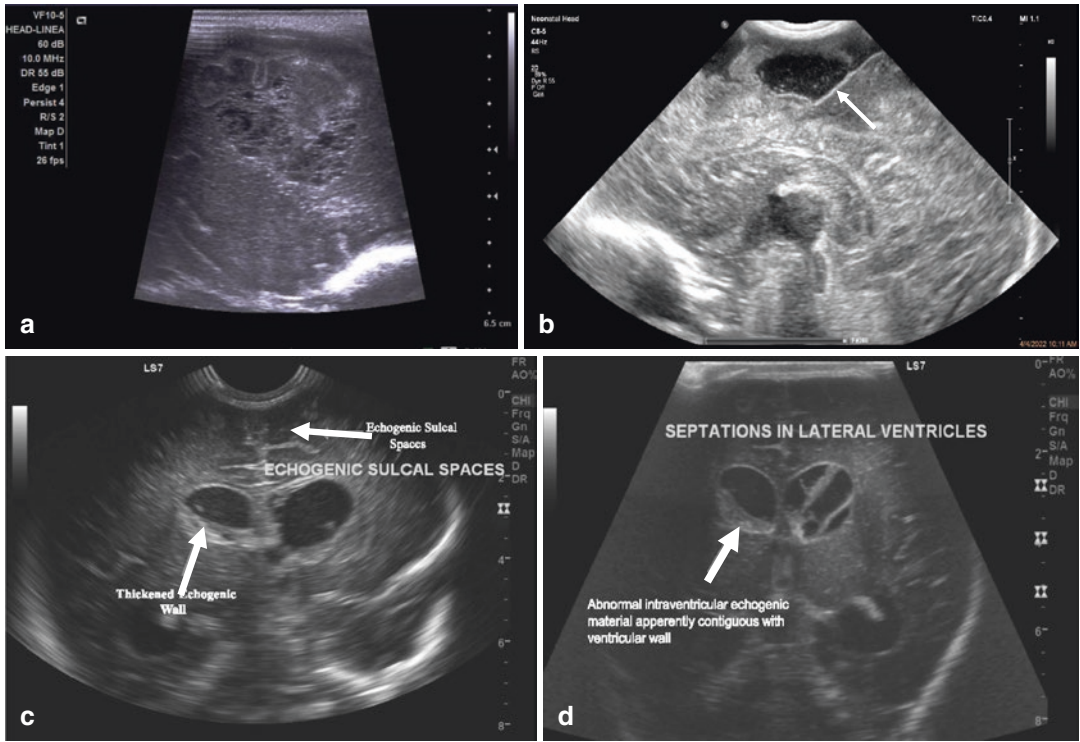


Fig. 13 (a) Brain abscess on sagittal view in a neonate suffering from *Burkholderia cepacia* meningoencephalitis, (b) Subdural empyema in sagittal plane in a term neonate suffering from *E. coli* meningitis, and (c and d) Changes seen in ventriculitis in early phase and late stages in the form of septations, respectively

Table 6 Cranial ultrasonography findings in neonatal meningitis

Early findings (under 2 weeks)	Late findings (after 2 weeks)
Irregular ventricular margins	Ventricular dilatation
Echogenic sulcal spaces	Intraventricular septations
Echogenic particles in ventricles	

Conclusion

Cranial ultrasound, an easily sought tool in neonatal intensive care assist to identify major comorbidities in neonates such as IVH, PVHD, and cystic PVL with excellent accuracy in real time and at the patient’s bedside. Cranial POCUS can be extremely helpful for diagnostic and prognostic purposes, and it can help neonatologists in making timely and accurate clinical decisions.

nate suffering from *E. coli* meningitis, and (c and d) Changes seen in ventriculitis in early phase and late stages in the form of septations, respectively

The list of its utilities is enormous but it does not replace the role of radiologists in this field and all infants with abnormal CUS on POCUS assessment should be consulted with pediatric radiologist and have a formal imaging evaluation by the radiologist.

References

1. Pigadas A, Thompson J, Grube G. Normal infant brain anatomy: correlated real-time sonograms and brain specimens. *AJNR*. 1981;2:339–44.
2. Grant E, Schellinger D, Richardson J. Real-time ultrasonography of the posterior fossa. *J Ultrasound Med*. 1983;2:73–87.
3. Horbar J, Leahy K, Lucey J. Ultrasound identification of lateral ventricular asymmetry in the human neonate. *JCU*. 1983;11:67–9.
4. Dorovini-Zis K, Dolman C. Gestational development of brain. *Arch Pathol Lab Med*. 1977;101:192–5.
5. Jeanty P, Chervenak F, Romero R, Michiels M, Hobbins J. The sylvian fissure: a commonly mis-

- labeled cranial landmark. *J Ultrasound Med.* 1984;3:15–8.
6. Leech RW, Kohlen P. Subependymal and intraventricular hemorrhages in the newborn. *Am J Pathol.* 1974;77:465–75.
 7. Rorke LB. Hemorrhages. In: Rorke LB, editor. *Pathology of perinatal brain injury.* Raven, New York; 1982. p. 15.
 8. Newton TH, Gooding CA. Compression of superior sagittal sinus by neonatal calvarial molding. *Radiology.* 1975;115:635–9.
 9. Kosmetatos N, Williams ML. Effect of positioning and head banding on intracranial pressure in the premature infant. *Pediatr Res.* 1978;12:553.
 10. Volpe JJ Intracranial hemorrhage: germinal matrix-intraventricular hemorrhage of the premature infant. In: *Neurology of the newborn.* 5th ed. Saunders Elsevier.
 11. Levene MI. Measurement of the growth of the lateral ventricles in preterm infants with real-time ultrasound. *Arch Dis Child.* 1981;56:900–4.
 12. Ingram MC, Huguenard AL, Miller BA, Chern JJ. Poor correlation between head circumference and cranial ultrasound findings in premature infants with intraventricular haemorrhage. *J Neurosurg Pediatr.* 2014;14:184–9.
 13. Muller WD, Urlesberger B. Correlation of ventricular size and head circumference after severe intraperiventricular haemorrhage in preterm infants. *Childs Nerv Syst.* 1992;8:33–5.
 14. Anderson N, Allan R, Darlow B, et al. Diagnosis of intraventricular hemorrhage in newborns: value of sonography via posterior fontanelle. *AJR.* 1994;163:893–6.
 15. Blumenthal I. Periventricular leukomalacia: a review. *Eur J Pediatr.* 2004;163:435–42.
 16. Volpe JJ. Cerebral white matter injury of the premature infant—more common than you think. *Pediatrics.* 2003;112:176–80.
 17. Khwaja O, Volpe JJ. Pathogenesis of cerebral white matter injury of prematurity. *Arch Dis Child Fetal Neonatal Ed.* 2008;93:F153–61.
 18. Back SA. White matter injury in the preterm infant: pathology and mechanisms. *Acta Neuropathol.* 2017;134:331–49.
 19. Buser JR, et al. Arrested preoligodendrocyte maturation contributes to myelination failure in premature infants. *Ann Neurol.* 2012;71:93–109.
 20. Hamrick SEG, et al. Trends in severe brain injury and neurodevelopmental outcome in premature newborn infants: the role of cystic periventricular leukomalacia. *J Pediatr.* 2004;145:593–9.
 21. Fawer CL, Diebold P, Calame A. Periventricular leukomalacia and neurodevelopmental outcome in preterm infants. *Arch Dis Child.* 1987;62:30–6.
 22. Resch B, et al. Risk factors and determinants of neurodevelopmental outcome in cystic periventricular leukomalacia. *Eur J Pediatr.* 2000;159:663–70.
 23. Aarnoudse-Moens CSH, et al. Meta-analysis of neurobehavioral outcomes in very preterm and/or very low birth weight children. *Pediatrics.* 2009;124:717–28.
 24. Neonatal neurosonography module', 1st National Basic Neonatal Neurosonography Workshop for the neonatologist, organized by National Neonatology Forum, India, December 2012. ©DrPradeepSuryawanshi, et al.
 25. Wang HS, Kuo MF, Chang TC. Sonographic lenticulostriate vasculopathy in infants: some associations and a hypothesis. *AJNR Am J Neuroradiol.* 1995;16:97–102.
 26. de Vries LS, Gunardi H, Barth PG, Bok LA, Verboon-Maciolek MA, Groenendaal F. The spectrum of cranial ultrasound and magnetic resonance imaging abnormalities in congenital cytomegalovirus infection. *Neuropediatrics.* 2004;35:113–9.
 27. Capretti MG, Lanari M, Tani G, Ancora G, Sciutti R, Marsico C, et al. Role of cerebral ultrasound and magnetic resonance imaging in newborns with congenital cytomegalovirus infection. *Brain Dev.* 2014;36:203–11.
 28. Ben-Ami T, Yousefzadeh D, Backus M, Reichman B, Kessler A, Hammerman-Rozenberg C. Lenticulostriate vasculopathy in infants with infections of the central nervous system: sonographic and Doppler findings. *Pediatr Radiol.* 1990;20:575–9.

Part VI

Use of Point of Care Ultrasound in Transport Setting



Role of Point of Care Ultrasound in the Transport Setting for Evaluating Infants and Children with Shock

Sajeev Job, Michael J. Griksaitis, and Yogen Singh

Contents

Introduction	243
Role of Point of Care Ultrasound in Critical Care Transport	244
Diagnostic Role of Point of Care Ultrasound in Transport	244
Role of Point of Care Ultrasound in Transport in Assessing Response to Intervention	246
Procedural Role of Point of Care Ultrasound in Transport	247
Role of Point of Care Ultrasound in Transport in Improving Communication Among the Teams	247
The Ideal Ultrasound Device for Critical Care Transport	247
Summary	248
References	248

S. Job (✉)

Department of Pediatrics, Cambridge University Hospitals NHS Foundation Trust, Cambridge, UK
e-mail: Sajeev.Job@addenbrookes.nhs.uk

M. J. Griksaitis

Department of Pediatrics, Southampton Children's Hospital, Southampton, UK

University of Southampton, Southampton, UK
e-mail: Michael.Griksaitis@uhs.nhs.uk

Y. Singh

Department of Pediatrics, Division of Neonatology, Loma Linda University School of Medicine, California, USA

Department of Pediatrics, Division of Neonatal and Developmental Medicine, Stanford University School of Medicine, California, UK

Department of Pediatrics, Division of Neonatology, University of Southern California, California, UK

ESPNIC Cardiovascular Dynamics Section and POCUS Working Group, Geneva, Switzerland
e-mail: YSingh@llu.edu

Introduction

The last two decades have witnessed the growth and recognition of neonatal and pediatric transport services as an integral part of the primary stabilization of critically unwell neonate and children. The same period of time has also seen published international guidelines on use of POCUS in neonates and children [1–7]. Training framework with specific guidelines for neonates and children, and the use of improved portable equipment and advances in telemedicine have enabled the teams to utilize POCUS in transport medicine [8–10].

Ultrasound was traditionally a tool used only by the specialist-trained sonographers and radiologists. Following the evolution of focused assessment sonography in trauma (FAST) scan-

ning in emergency medicine, interest developed in using bedside point-of-care ultrasound (POCUS) for a wider variety of patients. The use of bedside POCUS in the transport setting however was limited for years as the available ultrasound machines were large and not suitable for transport teams to apply in the transport setting.

The development of handheld and easily portable ultrasound devices has aided the adaptation and bedside utilization of POCUS in transport medicine. This was very much the need of the hour as it helped the clinician understand the physiology and aided in delivering target-specific intervention in the management of the critically sick infant and child. This has been further supported by several contributing factors among which include standardized guidelines and literature to support its use by other health professionals and its increasing recognition as a valuable diagnostic tool in aiding the bedside management of a critically ill patient. The other contributing factors include ease of use with training, portability, durability, affordability, and available probes for the ultrasound machines [11].

Role of Point of Care Ultrasound in Critical Care Transport

One benefit of POCUS is the ability of the clinician to carry out the assessment at the bedside, using their POCUS findings to augment their own clinical assessment and clinical decision-making. This is no different from its use in the neonatal or pediatric intensive care unit. However, the advancement of smaller and more portable POCUS devices benefits the transport team, as an ultrasound machine can be taken with the team on each transport.

Its roles include (Fig. 1):

1. Diagnostics
2. Assessment of interventions made
3. Procedural support
4. Improved communication

Each of these points will be discussed below.

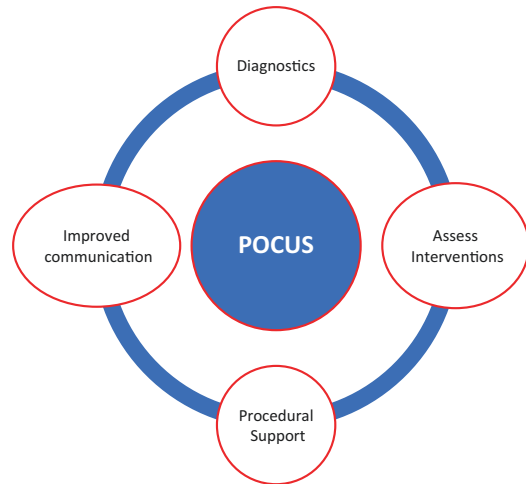


Fig. 1 Role of point of care ultrasound in infants and children in the transport setting

Diagnostic Role of Point of Care Ultrasound in Transport

The use of POCUS as a diagnostic tool in the stabilization of an infant and child is very different from the traditional radiology ultrasound or structural echocardiography [12–14]. The purpose of POCUS in transport is to answer predefined questions to identify the etiology of the shock and/or respiratory distress, perhaps in environments without access to expertise in ultrasound (for example, in the back of an ambulance or in a remote hospital with limited expertise availability).

The use of POCUS to make important diagnoses requires a sequential assessment, while incorporating your physiological data, clinical assessment, laboratory results, and other additional investigations. The aim is to understand deranged anatomical, physiological, or hemodynamic abnormality and then to treat any reversible causes [12–14]. The POCUS assessment should not delay resuscitation measures.

A schematic approach to using POCUS in identifying common causes of shock is shown in Fig. 2. POCUS can also be used to monitor the disease progression when you have made a diagnosis.

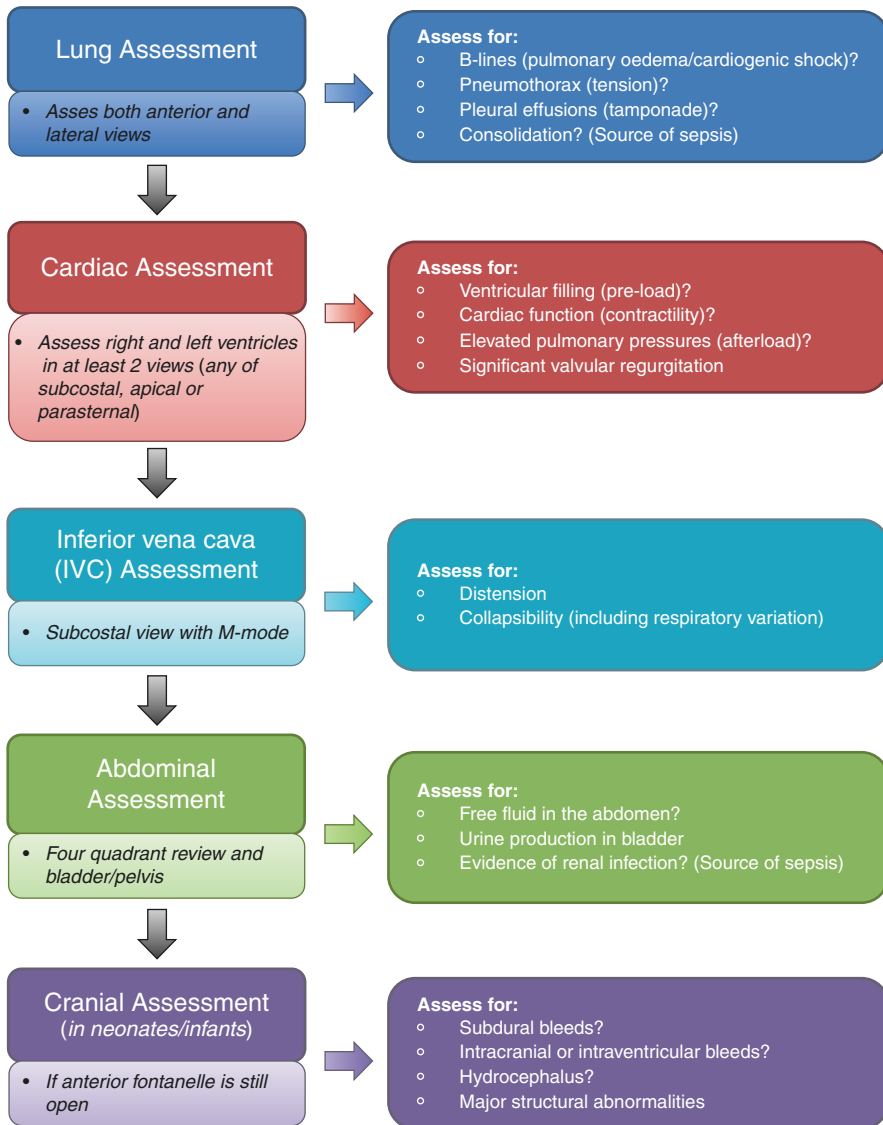


Fig. 2 A structured approach to using POCUS when approaching the infant or child with undifferentiated shock. [Modified from Hardwick JA, Griksaitis

MJ. Fifteen-minute consultation: Point of care ultrasound in the management of paediatric shock. Arch Dis Child Ed & Practice. August 2020] [13]

POCUS can also play an important role in the resuscitation of infants and children not responding to the standard treatment protocols. POCUS can be utilized to find the underlying cause by applying the ultrasound probe at predefined set points to rule out or recognize common causes of collapse in infants and children (SAFE-R protocol) [14].

While the specific findings on POCUS to diagnose these pathologies are discussed in the cardiac section of the book, this chapter emphasizes on cardiac POCUS in the transport setting.

The cardiac POCUS findings can be considered using the 5 “Fs” (Fig. 3).

Cardiac POCUS can help in differentiating the underlying cause among these five categories.

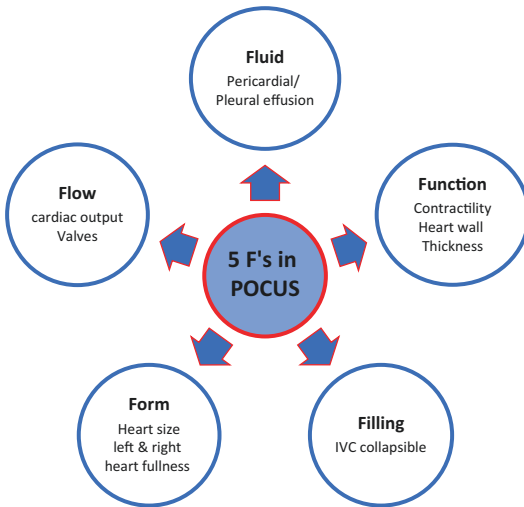


Fig. 3 5 F's in an infant or child with shock

Simplifying this further, considering the factors that determine cardiac output can help in targeting specific intervention:

- **Pre-Load:**
 - Volume status—do the ventricles look full/distended?
 - Is the inferior vena cava (IVC) distended or collapsed?
- **Contractility:**
 - Are the ventricles moving adequately?
- **Afterload:**
 - Is there a pericardial effusion?
 - Is the right ventricle (RV) hypertrophied and/or dilated/are there any signs of pulmonary hypertension?

However, one should remember POCUS should never be used as a screening tool for congenital heart diseases and when applied in the above-described manner it is not targeted to diagnose or rule out the critical congenital heart disease, *which should always be a differential in a collapsed infant, especially during the neonatal period.*

Lung POCUS has a very useful diagnostic role in the transport setting, and in conjunction with cardiac POCUS this becomes even more valuable for the assessment of sick infant [15–20]. While this has been discussed in the applica-

tions of lung ultrasound section of this book, it is important to understand that an infant or child presenting with respiratory distress, or deteriorating while on a ventilator in transport, could benefit from the use of lung POCUS. In fact, getting an urgent chest X-ray may not be available or may take longer time, especially in the community or outside the hospital, and a lung POCUS may be crucial in those situations in managing sick infants and children with possible lung pathologies. Lung POCUS can be used to diagnose:

- Atelectasis/Consolidation
- Pneumothorax
- Pleural effusions
- Pulmonary edema
- Acute respiratory distress syndrome (ARDS)
- Misplaced endotracheal tubes

The systematic approach to lung POCUS is described in the chapter on lung POCUS (*Please refer to the lung POCUS section of this book for further details.*)

Role of Point of Care Ultrasound in Transport in Assessing Response to Intervention

One benefit of POCUS is the ability to repeat the assessment several times to monitor the evolving pathology and in evaluating the impact of intervention or treatment provided. It can also help in identifying detrimental interventions. For example, following a fluid bolus clinician may now see a dilated ventricle with impaired contractility (on cardiac POCUS) and new B-lines (suggestive of pulmonary edema on lung POCUS), which would suggest volume is now no longer beneficial and it would be time to move on to other forms of cardiovascular support.

In a child with shock with hemodynamic instability, the aim of cardiac POCUS is to optimize pre-load (either fluid therapy for hypovolemia or diuretics for the failing heart), contractility (either with inotropes or vasopressor support), and afterload (e.g., potential need for inhaled

nitric oxide) (*Please refer to the cardiac section of this book for further details*).

Lung POCUS can also be used to review the resolution of a pneumothorax or pleural effusion following the insertion of a chest drain without the need for a repeat chest X-ray [15–20].

This has been discussed in detail in the lung ultrasound chapter of this book.

Procedural Role of Point of Care Ultrasound in Transport

Many procedures were traditionally taught with landmark techniques. This can be associated with a higher procedural failure rate, longer procedure time, and additional complications, particularly in smaller children. The introduction of ultrasound in critical care units (e.g., vascular access) is commonplace, and this technique can be used in transport [21].

When a neonate or child is in shock, ultrasound can make procedures quicker, easier, and less stressful if used properly [22, 23]. While the focus is often on using ultrasound to obtain vascular access, many other useful examples are shown in Table 1.

Table 1 Procedural role of POCUS in infants and children in the transport setting

Body cavity	Procedural support
Cranial Ultrasound	<ul style="list-style-type: none"> • Ventricular taps • Subdural taps
Thoracic Ultrasound	<ul style="list-style-type: none"> • Chest drain insertion • Pleural taps • Lung recruitment
Cardiac Ultrasound	<ul style="list-style-type: none"> • Pericardiocentesis • Identifying central line tip position • Guiding cardiac procedures (e.g., balloon atrial septostomy, ECMO cannulation)
Vascular Ultrasound	<ul style="list-style-type: none"> • Arterial line insertion • Peripheral intravenous cannulation • Central venous cannulation
Abdominal Ultrasound	<ul style="list-style-type: none"> • Ascitic tap • Peritoneal drain insertion • Suprapubic aspiration
Musculoskeletal Ultrasound	<ul style="list-style-type: none"> • Fracture manipulation • Nerve blocks • Lumbar punctures

Role of Point of Care Ultrasound in Transport in Improving Communication Among the Teams

A shocked neonate/child has a wide range of pathologies. The use of POCUS can help narrow this down, and therefore help determine which critical care unit is most appropriate to transport the patient to. For example, a POCUS demonstrating very severe left ventricular dysfunction may best be managed in a cardiac critical care unit with access to extracorporeal life support. The early decision-making by the transport team can reduce unnecessary transport of the patient and supply the receiving unit with more specific and physiologic information to be prepared for the incoming admission.

With the advances in telemedicine, some POCUS images could be transferred to specialist units for expert review and allow further advice to be given to the transport team in managing the child en route to the receiving center.

The Ideal Ultrasound Device for Critical Care Transport

Many devices exist on the market for POCUS, and some are more suitable than others for critical care transport. Many factors need to be considered when selecting the ultrasound machine for a transport service [24]. The ideal machine would be:

- Small/light-weight
- Handheld
- Robust if dropped
- Long battery life
- Suitable for all body systems (ideally one probe with the ability to alternate between linear, phased array, and curvilinear high and low frequencies)
- Ability to record and store images
- Ability to transmit images to other users for immediate review
- Probe size suitable for all ages of children (particularly for vascular access)
- Cost-efficient
- Probe/machine does not overheat
- Quick and easy to turn on and initiate scanning

Summary

POCUS has many roles in the diagnosis, assessing treatment effect, supporting procedures, and improving communication with clinical teams when dealing with a neonate or child with undifferentiated shock. All these roles are particularly beneficial for the transport teams, given the portable nature of handheld ultrasound devices and the limited access to other imaging modalities in circumstances such as a deterioration in the back of the ambulance or in a remote hospital with limited facilities or expertise. In fact, POCUS may be the ideal tool for managing a critically sick infant and child in these setting limited resources or expertise. The POCUS interpretation is unchanged from its use in a critical care unit or on transport.

References

- Singh Y, Tissot C, Fraga MV, Yousef N, et al. International evidence-based guidelines on Point of Care Ultrasound (POCUS) for critically ill neonates and children issued by the POCUS Working Group of the European Society of Paediatric and Neonatal Intensive Care (ESPNIC). *Crit Care*. 2020;24(1):65.
- Ma IWY, Arishenkoff S, Wiseman J, Desy J, Ailon J, et al. Internal medicine point-of-care ultrasound curriculum: consensus recommendations from the Canadian Internal Medicine Ultrasound (CIMUS) Group. *J Gen Intern Med*. 2017;32:1052–7.
- Frankel HL, Kirkpatrick AW, Elbarbary M, Blaivas M, Desai H, Evans D, et al. Guidelines for the appropriate use of bedside general and cardiac ultrasonography in the evaluation of critically ill patients—part I: general ultrasonography. *Crit Care Med*. 2015;43:2479–502.
- Mertens L, Seri I, Marek J, Arlettaz R, Barker P, McNamara P, et al. Targeted neonatal echocardiography in the neonatal intensive care unit: practice guidelines and recommendations for training. *J Am Soc Echocardiogr*. 2011;24:1057–78.
- Evans N, Gournay V, Cabanas F, Kluckow M, Leone T, Groves A, et al. Point-of-care ultrasound in the neonatal intensive care unit: international perspectives. *Semin Fetal Neonatal Med*. 2011;16:61–8.
- Singh Y, Gupta S, Groves AM, Gandhi A, Thomson J, Qureshi S, et al. Expert consensus statement ‘neonatologist-performed echocardiography (NoPE)’—training and accreditation in UK. *Eur J Paediatr*. 2016;175:281–7.
- de Boode WP, Singh Y, Gupta S, Austin T, Bohlin K, Dempsey E, et al. Recommendations for neonatologist performed echocardiography in Europe: consensus statement endorsed by European Society for Paediatric Research (ESPR) and European Society for Neonatology (ESN). *Pediatr Res*. 2016;80:465–71.
- Vignon P, Dugard A, Abraham J, Belcour D, Gondran G, Pepino F, et al. Focused training for goal-oriented hand-held echocardiography performed by noncardiologist residents in the intensive care unit. *Intensive Care Med*. 2007;33:1795–9.
- Hilbert-Carius P, Struck MF, Rudolph M, Knapp J, POCUS in HEMS Collaborators. Point-of-care ultrasound (POCUS) practices in the helicopter emergency medical services in Europe: results of an online survey. *Scand J Trauma Resusc Emerg Med*. 2021;29:124.
- Carmo KB. The history of ultrasound and its use at point of care: neonatal ultrasound in transport. *Curr Treat Options Pediatr*. 2017;3:305–12.
- Baribeau Y, Sharkey A, Chaudhary O. Handheld point-of-care ultrasound probes: the new generation of POCUS. *J Cardiothoracic Vasc Anesth*. 2020;34(11):3139–45.
- Longjohn M, Wan J, Joshi V, Pershad J. Point-of-care echocardiography by pediatric emergency physicians. *Pediatr Emerg Care*. 2011;27:693–6.
- Hardwick JA, Griksaitis MJ. Fifteen-minute consultation: point of care ultrasound in the management of paediatric shock. *Arch Dis Child Edu Pract Ed*. 2021;106(3):136–41. edpract-2019-317972.
- Yousef N, Singh Y, De Luca D. “Playing it SAFE in the NICU” SAFE-R: a targeted diagnostic ultrasound protocol for the suddenly decompensating infant in the NICU. *Eur J Pediatr*. 2022;181(1):393–8.
- Liu DM, et al. Utilization of ultrasound for the detection of pneumothorax in the neonatal special-care nursery. *Pediatr Radiol*. 2003;33(12):880–3.
- Brat R, et al. Lung ultrasonography score to evaluate oxygenation and surfactant need in neonates treated with continuous positive airway pressure. *JAMA Pediatrics*. 2015;169(8):e151797.
- Liu J, et al. Lung ultrasonography to diagnose transient tachypnea of the newborn. *Chest*. 2016;149(5):1269–75.
- Potter SK, Griksaitis MJ. The role of point-of-care ultrasound in pediatric acute respiratory distress syndrome emerging evidence for its use. *Ann Transl Med*. 2019;7(19):507.
- Ord HL, Griksaitis MJ. Fifteen-minute consultation: using point of care ultrasound to assess children with

- respiratory failure. *Arch Dis Child Educ Pract Ed.* 2019;104(1):2–10.
20. Supino MC, Buonsenso D, Scatani S, Scialanga B, Mesturino MA, Bock C, Chiaretti A, Giglioni E, Reale A, Musolino AM. Point-of-care lung ultrasound in infants with bronchiolitis in the pediatric emergency department: a prospective study. *Eur J Pediatr.* 2019;178(5):623–63.
 21. Katheria AC, Fleming SE, Kim JH. A randomized controlled trial of ultrasound-guided peripherally inserted central catheters compared with standard radiograph in neonates. *J Perinatol.* 2013;33(10):791–4.
 22. Karber BC, et al. Optimal radiologic position of an umbilical venous catheter tip as determined by echocardiography in very low birth weight newborn. *J Neonatal Perinatal Med.* 2017;10(1):55–61.
 23. Fleming SE, Kim JH. Ultrasound-guided umbilical catheter insertion in neonates. *J Perinatol.* 2011;31(5):344–9.
 24. European Society of Radiology (ESR). ESR statement on portable ultrasound devices. *Insights Imaging.* 2019;10(1):89.

Part VII

Procedural Ultrasound



Vascular Access Considerations in Children and Neonates

Mark D. Weber, Benjamin Kozyak,
and María Victoria Fraga

Contents

Introduction	254
Ultrasound-Guided Vascular Access: Basic Principles	254
Probe Selection	254
Probe Orientation	254
Identification of Structures	255
Assessment of Vessel Diameter	256
Dynamic Needle Tip Positioning	259
Central Venous Access	259
Internal Jugular Vein	259
Subclavian and Brachiocephalic Veins	261
Axillary Vein	263
Common Femoral Vein	265
Epicutaneo-Caval Catheters and Peripherally Inserted Central Catheters	265
Peripheral Venous Access	266
Arterial Access	267
Radial and Ulnar Arteries	268
Dorsalis Pedis and Posterior Tibial Arteries	268
Ultrasound-Guided Umbilical Venous Cannulation	270
POCUS for Central Line Position Evaluation	272
References	273

M. D. Weber
Department of Anesthesiology and Critical Care
Medicine, Children's Hospital of Philadelphia,
Philadelphia, PA, USA

B. Kozyak
Division of Cardiac Critical Care Medicine,
Department of Anesthesiology and Critical Care
Medicine, Children's Hospital of Philadelphia,
Perelman School of Medicine, University of
Pennsylvania, Philadelphia, PA, USA

M. V. Fraga (✉)
Department of Pediatrics, Division of Neonatology,
Children's Hospital of Philadelphia, Perelman School
of Medicine, University of Pennsylvania,
Philadelphia, PA, USA
The Children's Hospital of Philadelphia,
Philadelphia, PA, USA
e-mail: fragam@chop.edu

Introduction

The evidence for the use of Point-of-Care Ultrasound (POCUS) for procedural and vascular access guidance in children and neonates can no longer be disputed. The recent growth of supportive evidence makes a strong case for using POCUS for pediatric interventions such as vascular access [1]. Procedural ultrasound guidance has improved procedural success, provider performance, and patient safety [2]. National and international consensus have been developed supporting the use of ultrasound in vascular access [3, 4]. Consequently, the American Academy of Pediatrics and the Society of Critical Care Medicine have endorsed ultrasound use within the scope of pediatric procedural performance [5, 6]. Despite the strong evidence and recommendations by multiple pediatric societies, the use of ultrasound guidance for vascular access has not yet been universally adopted, especially in neonates, due to many barriers to its implementation. However, the increased availability of POCUS training modules and courses, as well as the introduction of POCUS curriculums in medical school, will make POCUS implementation for procedural guidance soon the standard of care in all pediatric and neonatal practices. This chapter describes the use of POCUS for vascular access guidance.

Ultrasound-Guided Vascular Access: Basic Principles

Probe Selection

When utilizing POCUS for vascular access guidance, proper probe selection will be crucial for procedural success. The primary probe that will be used is the linear probe due to its high frequency providing optimal image resolution. Linear probe frequencies range from 8 to 33 MHz (Fig. 1). The footprint of the linear probe is flat and the crystals are aligned in a linear fashion which provides a square image on the screen. The size of the patient will also determine the probe selection. Larger patients may require a lower

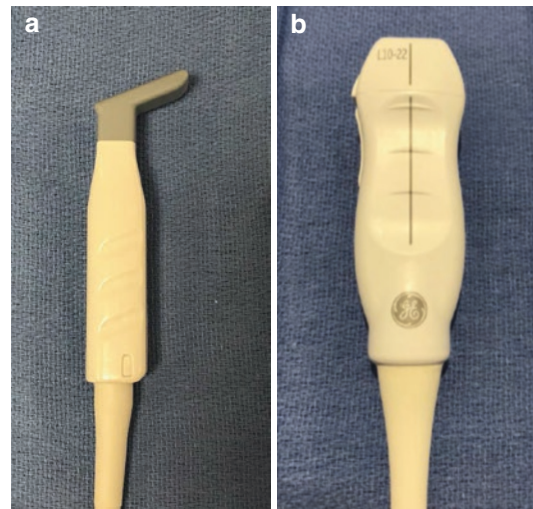


Fig. 1 High-frequency linear probes: (a) 7–15 MHz “Hockey-Stick”. (b) 10–22 MHz

frequency probe around the 12 MHz range so that the probe can penetrate the deeper structures. The hockey-stick probe has a much smaller footprint with a higher frequency range making it useful for smaller patients (Fig. 1a).

Probe Orientation

A vessel can be assessed in different views with POCUS. The three main orientations are short axis, where the plane of the probe is perpendicular to the vessel; long axis, where the plane of the probe is parallel to the vessel and oblique axis (Fig. 2a–c). From there the needle can be inserted in-plane, which is parallel to the plane of the probe or out-of-plane, which is perpendicular to the plane of the probe [7]. Each approach has its pros and cons. When accessing a vessel on the short axis with the needle out-of-plane the surrounding structures can be easily identified but following the needle tip can be challenging. Alternatively, when accessing a vessel on the long axis with the needle in-plane, the needle tip can be easily followed but visualization of surrounding structures is not possible and inadvertent probe manipulations can place the probe over an artery instead of an intended vein. Furthermore, the probe has to be kept perfectly

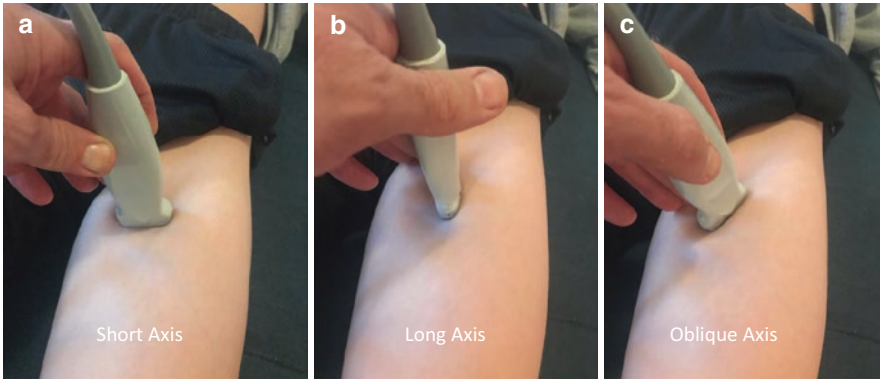


Fig. 2 Probe positioning for femoral vein view in short axis (a), long axis (b), and oblique axis (c)

aligned and in-plane over the needle which makes it a difficult maneuver when dealing with small neonatal vessels or unседated, noncooperative patients.

Identification of Structures

When performing an initial scan it is important to clearly identify the anticipated structures including arteries, veins, nerves, lymph nodes, and muscle. The first step is the differentiation of arteries from veins. Veins have thin walls and are compliant under gentle probe pressure (Figs. 3 and 4). Arteries will have thicker walls and will demonstrate pulsatility under gentle probe pressure.

Color doppler can be applied to the image to show the directionality of flow within the vessels. In the conventional setting of color doppler the flow that is moving away from the probe is blue and flow moving towards the probe is red (Fig. 5). The simple mnemonic of BART can be applied as *Blue Away Red Towards*. In an ideal state, the color doppler will work best when the ultrasound beam is parallel to the direction of blood flow. This is referred to as the angle of insonation being the difference of degrees between the beam and the blood

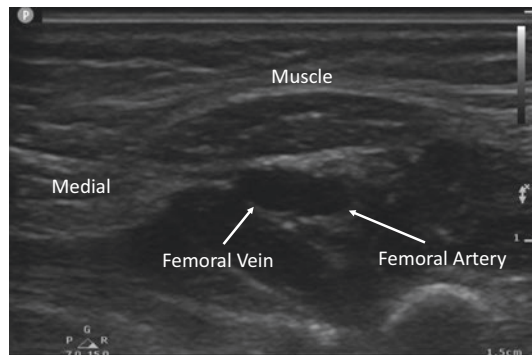


Fig. 3 Normal anatomy of the left femoral vessels in short axis

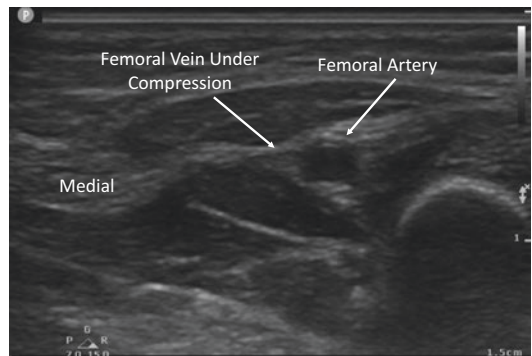


Fig. 4 Short axis view of left femoral vein under external compression demonstrating venous collapsibility

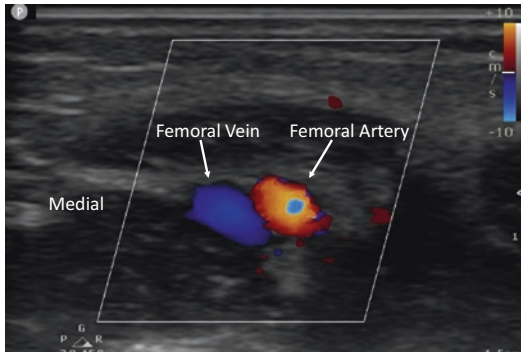
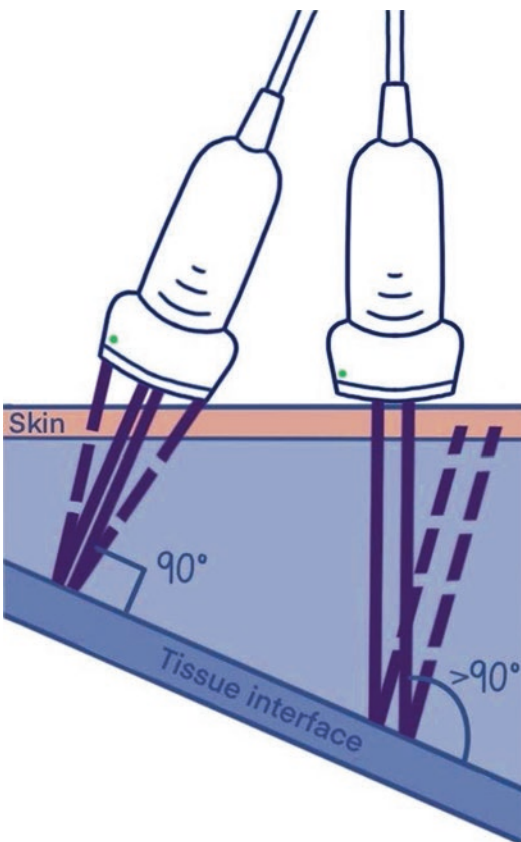


Fig. 5 Color doppler of left femoral vessels demonstrating directionality of flow. Red: flow towards the probe. Blue: flow away from the probe



Copyright@SheenGahlaut&YogenSingh

Fig. 6 Illustration demonstrating probe positioning to reduce angle of insonation

vessel of interest (Fig. 6). The probe is placed over the vessels and the tail of the probe can be fanned so that the ultrasound beam is as parallel as possi-

ble to the direction of blood flow. An angle of insonation of $<60^\circ$ is optimal for vascular ultrasound. However, an angle of insonation close to 90° is best for needle tip visualization (see below).

A second way to differentiate arteries from veins is by interrogating the vessel with spectral doppler or pulsed wave doppler (PWD). The gate of the doppler can be placed within the vessel. Again, this method works best when the angle of insonation is $<60^\circ$. The PWD will then display a waveform based on the flow characteristic of the vessel. The characteristics of a pulsatile arterial (Fig. 7) tracing can be differentiated from the phasic venous tracing (Fig. 8).

Nerves can be identified as hypoechoic structures that have the appearance of a honeycomb on the short axis. The individual nerve fascicles are surrounded by hyperechoic connective tissue known as the epineurium [8] (Fig. 9). Nerves generally lie near a main artery among the neurovascular bundle. Nerves will not compress under gentle pressure but may shift to the side. Lymph nodes can also be identified by ultrasound as having the appearance of a hypoechoic oval structure with smooth, well-defined margins (Fig. 10). Lastly, the surrounding muscle should be identified and avoided if possible. Muscles will appear as hypoechoic structures with bright surrounding fascia and linear perimysial stranding within.

Assessment of Vessel Diameter

During POCUS assessment of the vessel, an anterior-posterior measurement should be acquired. The probe is held on the short axis and an image of the vessel is captured at the anticipated point of cannulation. Care must be taken to support the hand on the patient so as not to compress the vessels with the probe (Fig. 11). The measurement calipers on the POCUS machine are then used to measure the inner diameter of the vessel (Fig. 12). For peripherally inserted central line placements the measurement should be acquired without a tourniquet in place. A catheter-to-vein ratio of less than 33–45% is suggested to decrease the risk of deep vein thrombosis [9, 10].

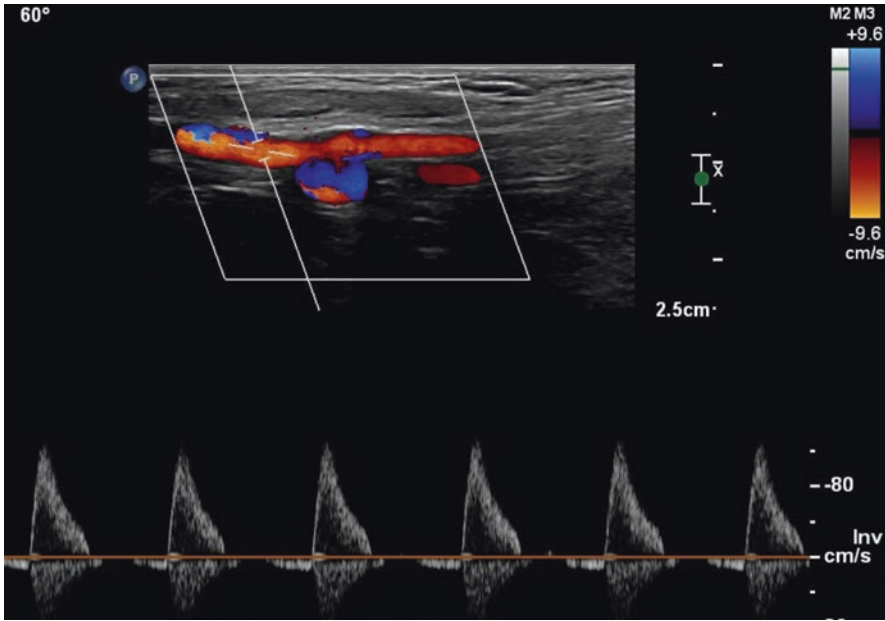


Fig. 7 Pulsed wave doppler of the femoral artery displays the classic pulsatile arterial tracing

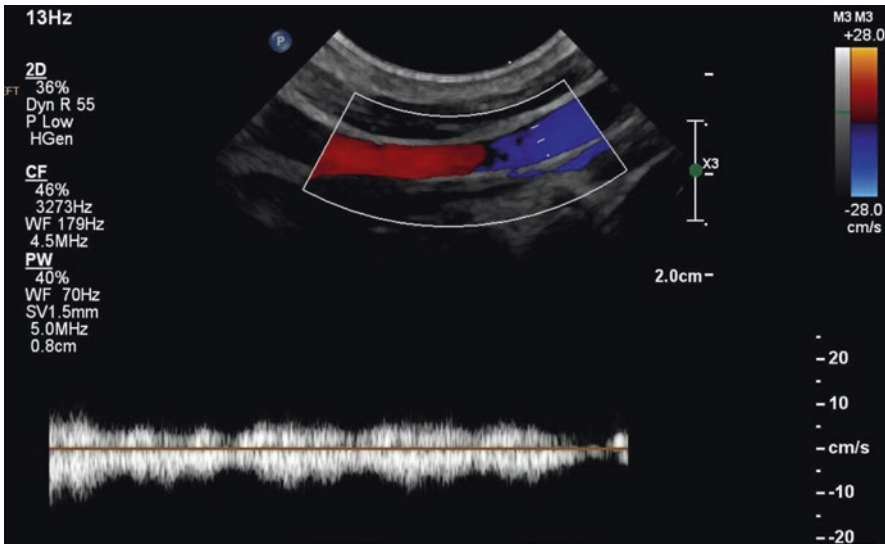


Fig. 8 Pulsed wave doppler of the jugular vein displays the classic continuous venous flow

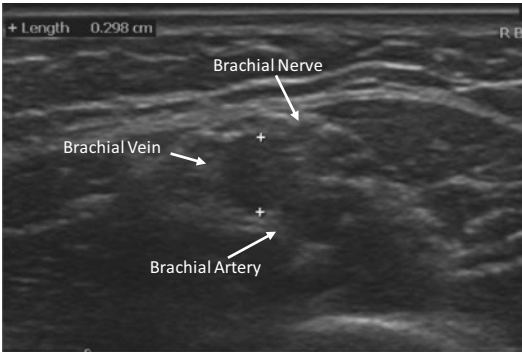


Fig. 9 Ultrasound view of the brachial nerve



Fig. 11 Image demonstrating how to hold the probe by the thumb and first finger while the other fingers are fanned out and resting on the patient to avoid external compression of the vessel

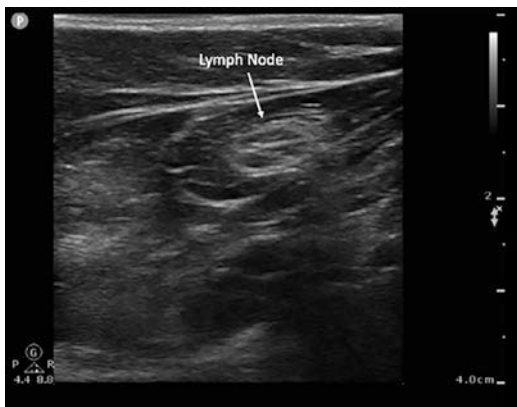


Fig. 10 Ultrasound image of a lymph node

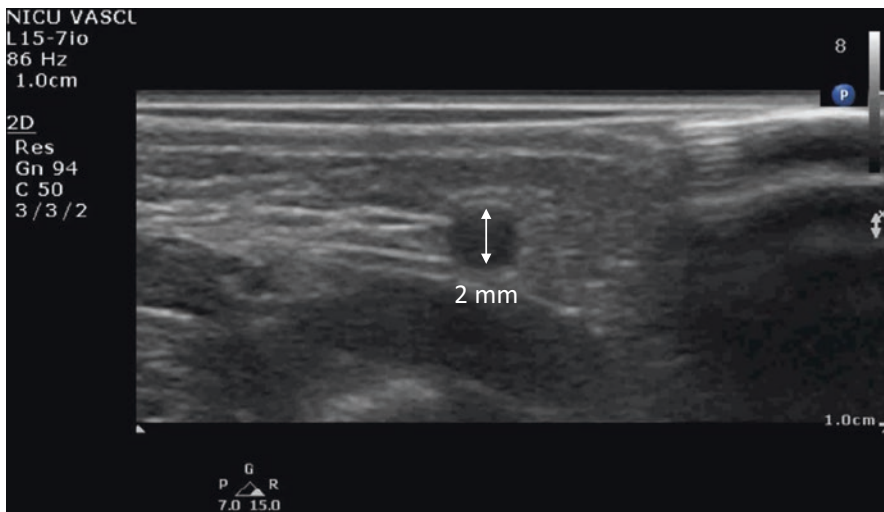


Fig. 12 Vessel measurement prior to line insertion

Dynamic Needle Tip Positioning

When accessing a vessel, it is important to be continually aware of the needle tip location in reference to surrounding structures and the target vessel. The needle tip and the shaft of the needle will both appear as a bright echogenic dot on the screen. The key to locating the needle tip is to identify the transition where the needle starts and ends. The best way to accomplish this is by using the step-down technique which is also known as dynamic needle tip positioning (DNTP) [11, 12].

During DNTP the probe is centered over the vessel with a short axis view. The vessel should remain centered on the ultrasound screen and the imaging depth should be set such that the vessel is approximately in the middle of the screen. The needle is inserted under the center of the probe and pierces the skin. An out-of-plane approach will be used while accessing the vessel. Once the needle is under the skin, the probe can be fanned so that the tail is away from the proceduralist and the POCUS beam is oriented 90 degrees to the plane of the needle (angle of insonation). The needle will appear as a bright echogenic dot on the screen. The probe is then slowly advanced to the point where the needle tip disappears. Next, the needle is slowly advanced towards the vessel. Just as the needle tip appears on the screen the needle advancement stops, and the probe is advanced a small step until the needle tip disappears again. This procedure is repeated until the needle has compressed the anterior wall of the vessel. At this point, it may be necessary to decrease the angle of the needle so as not to puncture the posterior wall of the vessel during cannulation (Fig. 13).

Subtle back and forth fanning may be required during this process. The POCUS image is best when the angle of insonation is optimized maintaining the ultrasound beam at 90° to the vessel of interest. When the probe is fanned so that the angle of insonation is perpendicular to the plane of the needle, the vessel will not be as clear. To view the vessel the probe is then fanned so that the beam is perpendicular to the vessel, then fanned back to the needle.

Central Venous Access

Internal Jugular Vein

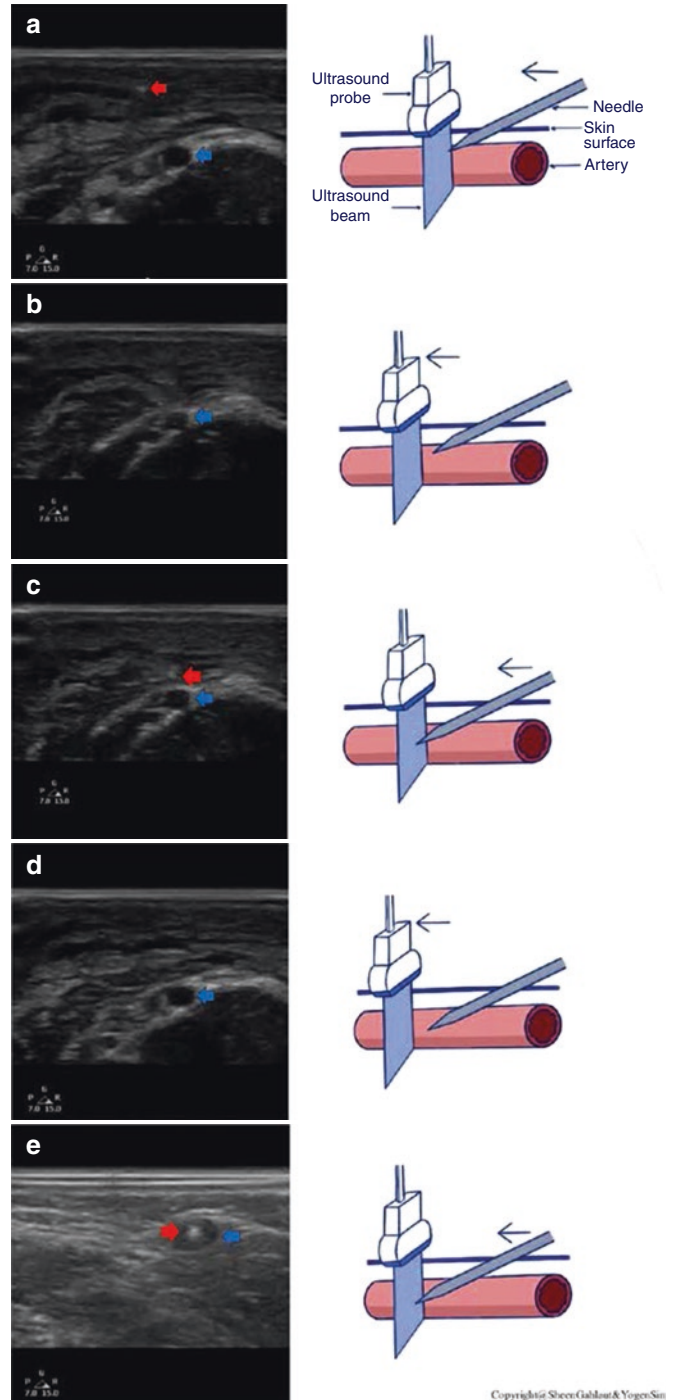
The internal jugular vein (IJV) is a commonly accessed vessel that runs lateral to the carotid artery (Fig. 14). In pediatric patients, the anatomy of the IJV relative to the carotid artery is variable. In 50% of the patients the IJV overlaps the carotid artery at the level of the apex of the sternocleidomastoid muscle whereas in 25% of patients this overlap occurs higher in the neck, at the level of the cricoid [13]. The head position should be adjusted to allow the most direct access to the IJV while avoiding the internal carotid artery. This may require the head to be midline or turned to the contralateral side of line placement [14]. The patient can be positioned in Trendelenburg in order to improve the diameter of the vessel.

Both the right and left IJVs should be assessed prior to the procedure to rule out thrombosis, stenosis, or suboptimal anatomy. The IJV can be visualized in a short axis, long axis, or oblique axis view. Upon assessment, the diameter of the vessel should be measured to optimize the catheter-to-vein ratio, keeping the catheter less than 33–45% of the vessel diameter [15]. For the IJV this measurement becomes critical in infants where a large bore hemodialysis catheter may be placed.

Traditionally the IJV is accessed through a short axis out-of-plane approach where the needle is inserted at the apex of the sternocleidomastoid with a 45–60° angle (Fig. 15). When the site of insertion is located, the proceduralist can advance the probe to the clavicle to get a sense of the vessel trajectory. The probe is then brought back to locate the needle and the DNTP approach is employed to follow the needle tip until the vessel is accessed.

Alternatively, an in-plane approach can be used with the probe in the short axis or oblique axis orientation (Fig. 16). The benefit of this approach is the ability to follow the entire needle as the vessel is cannulated. Additionally, it pro-

Fig. 13 Illustration demonstrating dynamic needle tip positioning technique for vascular access



Copyright © Shree-Gabaur & Yogen-Sin

vides optimal placement of the catheter hub away from the ear and hairline. Each of the three views offers the same result in first-pass success but the

oblique axis view may decrease the risk of carotid artery puncture compared to the short axis view [16, 17].

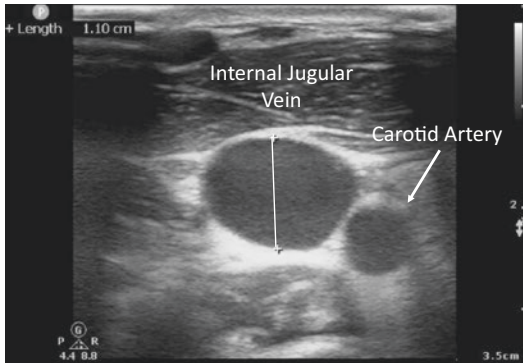


Fig. 14 Short axis view of the internal jugular vein and carotid artery with calipers measuring vessel diameter



Fig. 15 Short axis out-of-plane approach to access the internal jugular vein



Fig. 16 Short axis in-plane approach to access the internal jugular vein

Subclavian and Brachiocephalic Veins

The subclavian vein (SCV) begins just as the axillary vein passes over the first rib under the region of the clavicle. Due to the clavicle's passage over the distal end of the SCV, it can only be assessed with POCUS in the supraclavicular region. The patient should be positioned supine or in Trendelenburg with the head turned away from the insertion site. In smaller children, a neck roll can be utilized to further expose the supraclavicular region [18].

The SCV will be accessed using a long axis in-plane approach. First, the IJV is viewed with a short axis approach. The probe is slid down towards the clavicle and may need to be fanned so that the tail of the probe is towards the patient's head (Fig. 17). In this view, the IJV can be seen merging with the SCV and inserting it into the brachiocephalic vein (BCV). The probe is then manipulated so that the SCV is seen in a long axis view. The vessel should be interrogated with pulsed wave doppler and color doppler to confirm that the subclavian artery is not being viewed [19]. Additionally, valves within the vessel can help confirm venous anatomy as opposed to arterial (Fig. 18). The proceduralist can then access the vessel by inserting the needle under the foot of the probe



Fig. 17 Long axis in-plane supraclavicular approach to access the subclavian or brachiocephalic vein

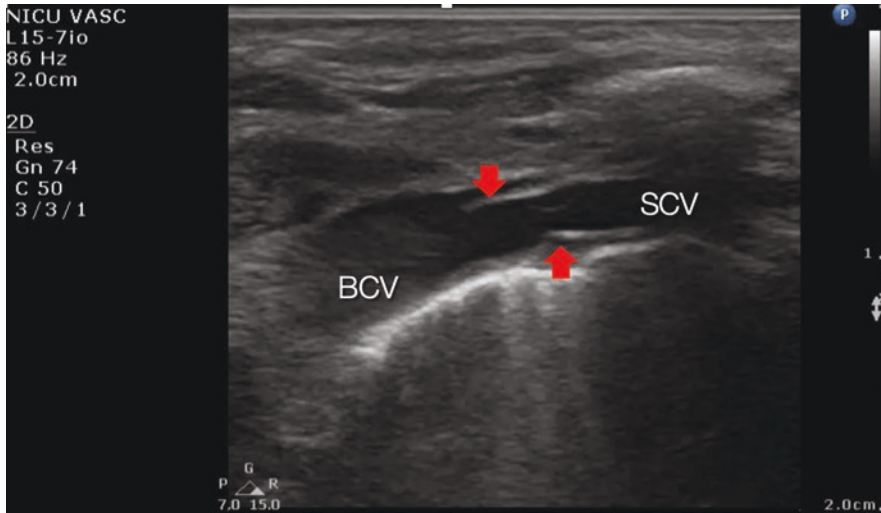


Fig. 18 Venous Valves (red arrows) in Subclavian vein. *SCV* Subclavian Vein, *BCV* Brachiocephalic Vein

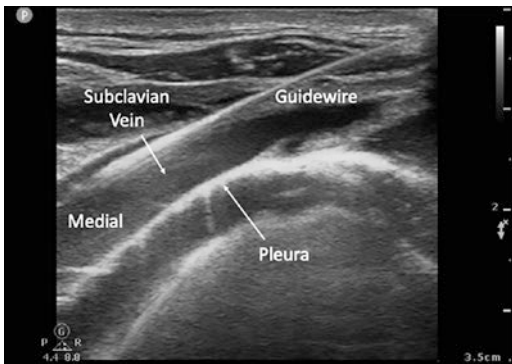


Fig. 19 Long axis view of the subclavian vein visualizing the pleura and guidewire

using an in-plane approach while following its trajectory on the POCUS screen (Fig. 19). It is important to keep the probe immobilized over

the SCV so that it does not drift over the subclavian artery. If the needle is not seen on the POCUS screen the needle trajectory should be adjusted rather than adjusting the probe.

In this view, the brachiocephalic vein (BCV) can also be seen as the IJV and SCV insert into it (Fig. 20). Cannulation of the BCV is similar to the supraclavicular SCV approach. The patient should be positioned supine with the head turned away from the insertion site (Fig. 21). The probe is again positioned so that the SCV is seen in the long axis view. The probe is fanned towards the frontal plane to capture the SCV merging with the BCV [20]. The vessel can be accessed with a 21 g needle or a 24 g angiocath based on the size of the patient. In the neonatal population, this approach has been successful in children down to 550 g [21] (Fig. 22).

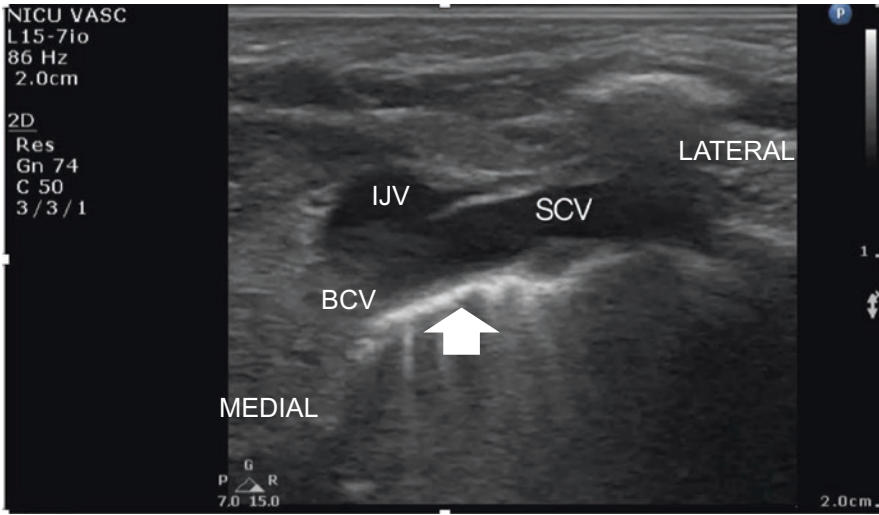


Fig. 20 IJV joining SCV to form BCV. Arrow showing pleural line



Fig. 21 Optimal position for BCV cannulation

Axillary Vein

The axillary vein (AxV) can be viewed on the anterior chest as it approaches the clavicle prior to coursing under the clavicle and becoming the SCV. The AxV lies just caudal to the axillary artery with the pleura posterior as they head towards the clavicle. For cannulation, the patient should be supine in a subtle Trendelenburg position of no more than 5° [22]. The arm can be abducted to position the clavicle more cephalad allowing more room to access the vessel [23]. To access the AxV the probe can be held in the short axis, long axis, or oblique axis views [24, 25] (Figs. 23 and 24). If the short axis or out-of-plane approach is used, DNTP can be employed to access the vessel while paying

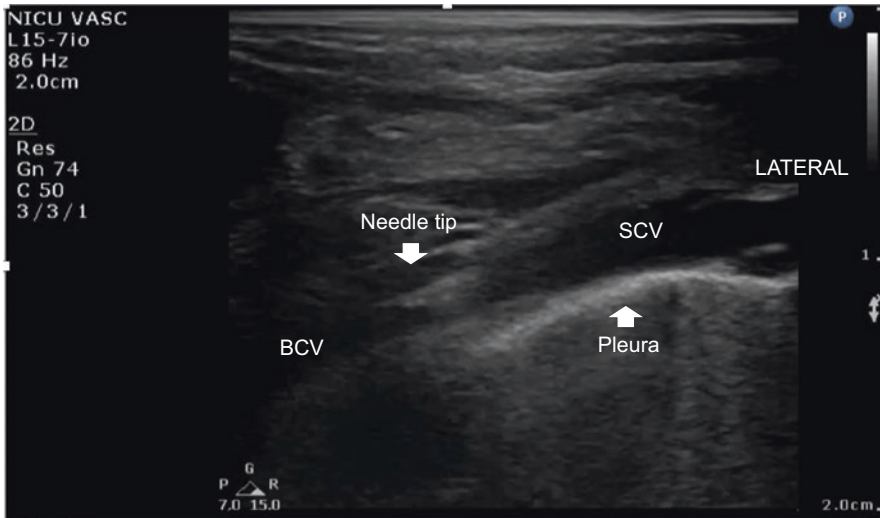


Fig. 22 Long axis view of the needle insertion in BCV cannulation



Fig. 23 Long axis in-plane approach to access the axillary vein

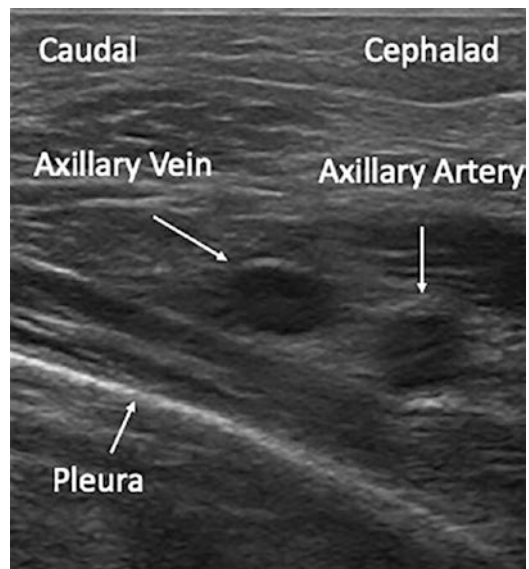


Fig. 25 Relationship between the axillary vessels and the pleura



Fig. 24 Short axis out-of-plane approach to access the axillary vein

close attention to avoiding the pleura (Fig. 25). Care must be taken to access the vessel before the clavicle obstructs the view. The long or oblique axis or in-plane approach can also be employed. This view allows better visualization of the needle tip in relation to the pleura.

Common Femoral Vein

Utilizing POCUS for common femoral vein (CFV) access increases first attempt success [26]. For pediatric temporary CVC site selection the CFV is frequently used. The access point lies just distal to the inguinal ligament. At that region, the CFV is medial to the femoral artery and the femoral nerve is lateral to the femoral artery (Fig. 3). Above the level of the inguinal ligament the CFV becomes the external iliac vein. In pediatric patients, the femoral artery will have a significant overlap of the CFV 3 cm distal to the inguinal ligament as opposed to relatively no overlap 1 cm distal to the inguinal ligament [27]. The patient should be placed in a supine position. For smaller children, placing the bed in reverse Trendelenburg can aid in distending the CFV. The use of a towel roll under the hips can aid in opening up the inguinal fold to assist in line placement. A linear probe should be placed over the vein distal to the inguinal ligament to view the vessel in short axis (Fig. 26). The legs can be positioned straight in

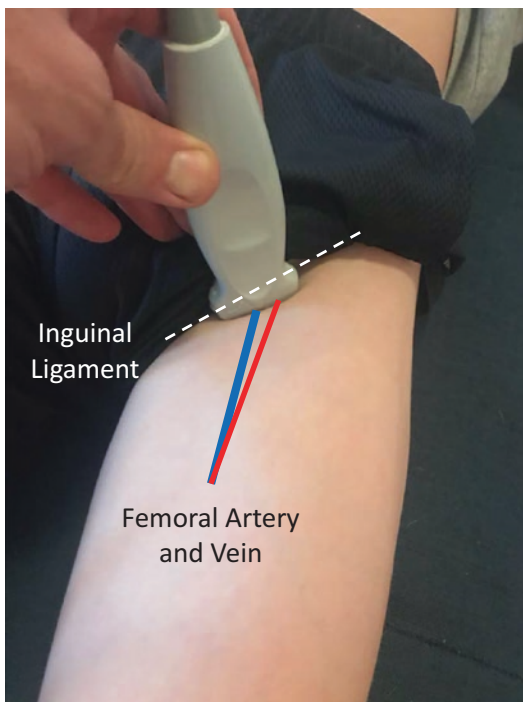


Fig. 26 Relationship between the inguinal ligament and the femoral vessels

older pediatric patients or in a frog-legged position in infants, with the hips flexed and externally rotated to expose the inguinal area and to assess the overlap of the CFV with the femoral artery in both positions. Structures to identify will be the femoral artery, femoral vein, femoral nerve, and lymph nodes. The vessel diameter should be measured to ensure the catheter-to-vein ratio is appropriate, although this can be challenging for novice providers [28].

The CFV can be accessed just distal to the inguinal ligament. In the most common approach, the operator holds the probe on the short axis and uses an out-of-plane approach with the needle. Once the vessel is centered on the screen the needle can be inserted and advanced to the vessel utilizing DNTP. The insertion angle will be steeper for older patients and shallower for infants. Alternatively, the vessel can be accessed with the probe in the long axis view using an in-plane approach. It is recommended to start with the short axis view and advance the needle to the anterior vessel wall before rotating the probe to the long axis view thereby minimizing the risk of inadvertent arterial puncture.

Epicutaneo-Caval Catheters and Peripherally Inserted Central Catheters

Critically ill newborns often require a central line for infusion of fluids, long-term parenteral nutrition, and drugs that are not appropriate for peripheral administration. While it has become frequent to place large caliber centrally inserted central catheters (CICCs) in neonates, the insertion of 1–2.6 Fr catheters into peripheral veins remains very common. Epicutaneo-caval catheters (ECCs) are the most common central lines used in neonates usually after umbilical lines are removed. ECCs are inserted in upper or lower extremity peripheral superficial veins (veins that lie less than 7 mm below the skin). A common target vessel for ECC placement is the great saphenous vein as it courses along the anteromedial aspect of the lower leg. Peripherally inserted central catheters (PICCs) are also common central lines in new-

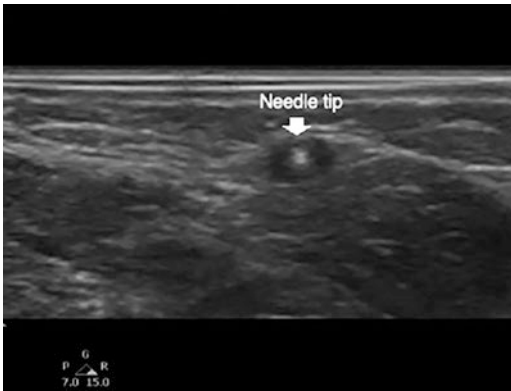


Fig. 27 PICC insertion in the basilic vein

borns, inserted in upper or lower extremity peripheral deep veins (veins that lie more than 7 mm below the skin). The most common vein used for PICC line insertion is the basilic vein (Fig. 27). Data on catheter diameter, vessel size, and risk of thrombosis suggest that limiting the external catheter diameter to one-third of the vessel's internal diameter may reduce the incidence of thrombosis [9, 29, 30]. It is strongly recommended to measure the vessel diameter to decide on the appropriate catheter size before central line insertion. The peel-away technique is the most common method used for ECC/PICC placement. With a short axis approach, a peel-away introducer is advanced into the vein under ultrasound guidance. When blood is visualized along the introducer or in the hub, the catheter is advanced into the vein while the needle is stabilized. The needle is removed and the ECC or PICC is threaded through the introducer. Prior to securing the central line, a second provider can evaluate the catheter tip position and adjust it in real-time using ultrasound (see the section below on POCUS for central line position evaluation). POCUS offers a tool to improve success rates during line placement and to accurately position the catheter tip at the superior or inferior cavo-atrial junction. Similar to other age groups, ultrasound guidance improves success and safety for PICC and ECC placement [1]. Although no randomized controlled trials comparing

ultrasound-guided versus landmark-guided PICC or ECC placement in preterm or full-term neonates exist, given the strong evidence already available favoring ultrasound use, equipoise may be nowadays impossible to achieve.

Peripheral Venous Access

POCUS adds tremendous value to the insertion of peripheral venous catheters. POCUS has been shown to decrease insertion attempts and time to cannulation [31]. Patients in whom peripheral veins may not be identified with palpation or visualization may have additional points of access identified with POCUS. Vessels greater than 1.2 cm below the skin should be avoided as most peripheral catheters may not have sufficient length leading to catheter dislodgement [32].

When accessing a peripheral vessel the limb of interest should be placed on a stable surface. The entire limb should be assessed looking for a straight vessel free of intraluminal thrombus or stenosis.

Both a short axis out-of-plane and long axis in-plane approach can be used to access the vessel. When accessing the vessel using a short axis out-of-plane approach DNTP should be utilized. The angle of insertion will depend on the depth of the vessel. A vessel that is greater than 1 cm deep may require an insertion angle of 45–60°. Once the catheter is advanced into the vessel the angle of approach should be decreased so that the catheter is parallel to the plane of the vessel. DNTP is used to advance the catheter a few more millimeters before the catheter is threaded off the needle. With the use of DNTP vessels <1 mm in diameter can be successfully accessed [12]. Novice providers have increased success with the short axis out-of-plane approach but as experience grows the long axis in-plane approach can be beneficial [33]. The long axis approach can help to limit posterior wall puncture on insertion and can be used to confirm appropriate placement.

Arterial Access

Arterial access is essential for the management of critically ill infants and children, enabling continuous measurement of blood pressure and facilitating frequent laboratory assessment of gas exchange as well as biochemical and hematologic parameters. In both pediatric and adult critical care, the use of ultrasound has been shown to significantly improve the success of arterial catheterization, reducing the number of attempts and procedure time and mitigating the effect of patient and trainee variables [34, 35]. As is the case with venous access, arterial catheters may be placed in either peripheral or central vessels. Peripheral arterial sites are typically preferred for several reasons: redundant arterial supply, lower consequences of thrombotic complications, and lower infectious risk [36]. Therefore, peripheral arterial line placement will be discussed in this chapter.

Site selection depends on a number of patient factors, including age, size, perfusion, anatomy, and vessel patency, including the history of arterial access. Despite the fact that arteries, in contrast to veins, are pulsatile and noncompressible, this is not always the case, particularly in infants and patients with hypotension, marginal cardiac output, or upstream stenosis or occlusion. Therefore, vessels of interest should always be

interrogated by ultrasound using both B-mode and Doppler imaging. While application of light pressure may serve to accentuate pulsatility, careful attention must be paid to minimizing external compression of the vessel. A high-frequency linear transducer for vascular access should be used as discussed above along with a 22 g or 24 g arterial catheter. Prior to entering the skin with a needle beneath, a straight section of the vessel should be identified for cannulation. Vessel straightness may be determined using POCUS, by orienting the probe on short axis and sliding it along the length of the vessel from distal to proximal. The vessel should remain centered on the ultrasound screen and the imaging depth should be set such that the vessel is approximately in the middle of the screen. DNTP improves the success of US-guided pediatric arterial catheterization [37]. As the arteries of interest may be quite superficial in neonates and infants, the skin should be entered at a very shallow angle to avoid inadvertently injuring the vessel, approximately 0.5 cm distal to the planned insertion site. Once the needle tip tents the anterior surface of the artery, the needle is again adjusted to enter the artery at a shallower angle, which facilitates cannulation and guidewire introduction (Fig. 28). The needle should then be advanced a few more millimeters using DNTP techniques to avoid exiting the posterior wall of the artery (Fig. 29).

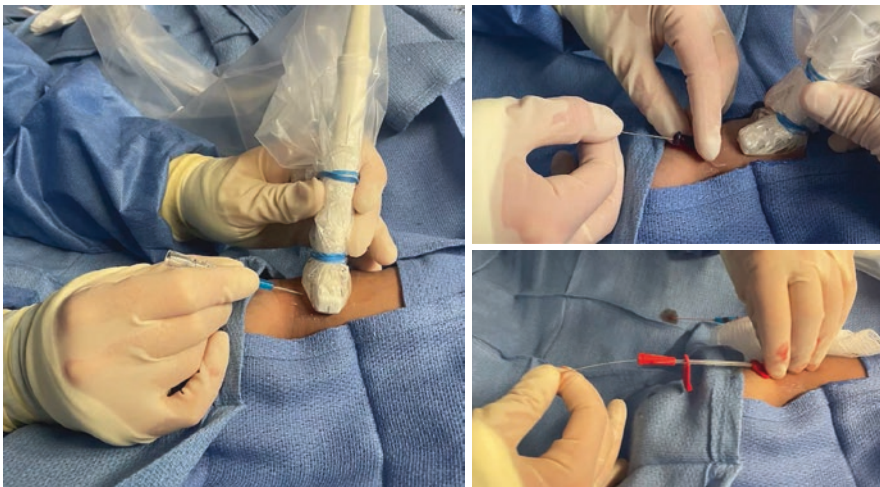


Fig. 28 Arterial line placement technique under ultrasound guidance

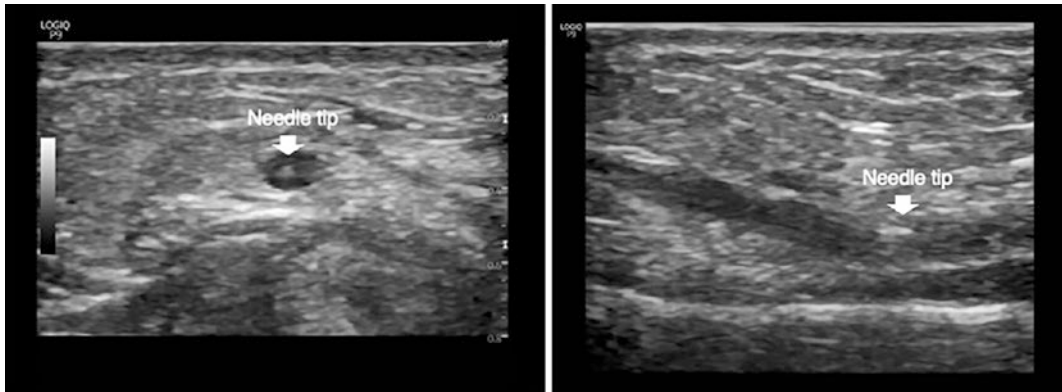


Fig. 29 DNTP in short axis and long axis during cannulation of the radial artery

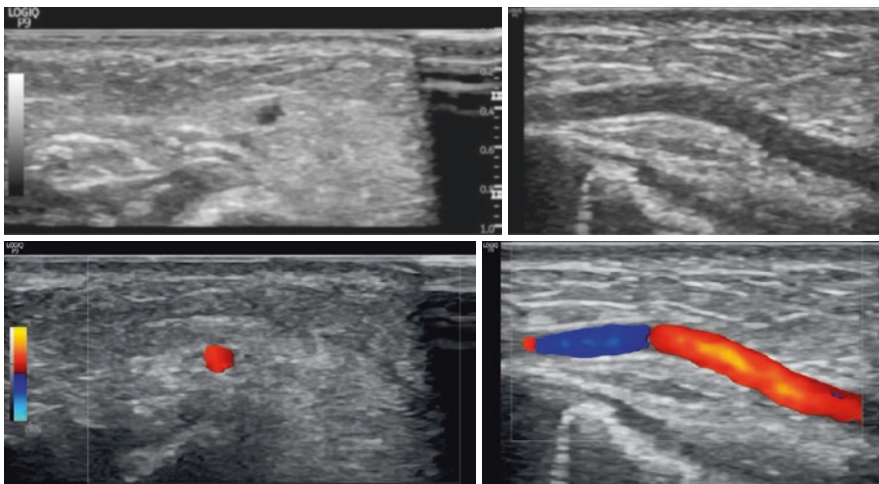


Fig. 30 2D image and color doppler of the radial artery in short and long axis views

Radial and Ulnar Arteries

In most patients, the upper extremity is the preferred site of peripheral arterial line placement. Arteries in the forearm are proximal and straight, therefore arterial catheters are less prone to dislodgement.

When evaluating the upper extremity arteries for cannulation, a combination of traditional physiologic techniques as well as POCUS should be utilized. The Modified Allen Test has been the standard of care for many years and should still be performed, and correlated with pulse oximetry and ultrasound-based evaluation [38, 39]. B-mode imaging, color, and pulse-wave doppler should be used to evaluate for pulsatile, antegrade blood flow in *both* the vessel of interest and the vessel responsible for collateral flow (Fig. 30).

This ensures that perfusion of the extremity remains intact in the event of an access-associated arterial occlusion.

Once a vessel has been selected for cannulation, position the forearm with the wrist gently extended. Avoid over-extension as this is uncomfortable and has the tendency to stretch the vessel longitudinally, decreasing its AP diameter.

Dorsalis Pedis and Posterior Tibial Arteries

Although upper extremities are generally preferred, the arteries of the foot offer a good alternative for peripheral sites, particularly in infants. However, arterial lines in the foot are more difficult to secure and more likely to become dis-

lodged in active patients with a tendency to kick. As with the arteries of the forearm, POCUS improves the success of dorsalis pedis and posterior tibial artery catheterization in infants and children [40].

The two most appropriate locations for peripheral arterial cannulation in the foot are the dorsalis pedis artery, a branch of the anterior tibial artery located on the dorsum of the foot and the posterior tibial artery, which courses through the posterior compartment of the leg and enters the foot after passing posterior to the medial malleolus. Patency of both arteries should be demon-

strated to ensure collateral flow before a catheter is placed.

The dorsalis pedis artery runs very superficially; therefore, care must be taken not to compress the artery with the transducer, which occurs with minimal pressure in neonates and infants.

This vessel should be approached at a shallow angle of about 20° under POCUS using DNTP in a short axis view (Figs. 31 and 32).

The posterior tibial artery takes a relatively straight course in the distal leg and is readily accessed just posterior to the medial malleolus.



Fig. 31 Foot positioning for arterial cannulation of the dorsalis pedis artery

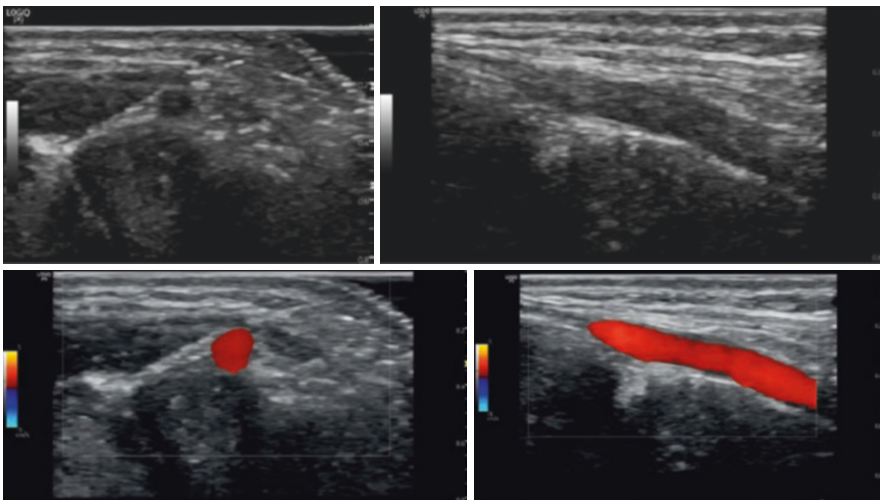


Fig. 32 2D image and color doppler of the dorsalis pedis artery in short and long axis views

The POCUS-guided approach to cannulation is very similar to that utilized for radial and ulnar catheterization, as described above.

Ultrasound-Guided Umbilical Venous Cannulation

Umbilical venous cannulation is the most common approach to obtaining central venous access in critically ill neonates. Unfortunately, the traditional blind insertion technique fails in 25–50% of newborns and has not meaningfully evolved in many years. A novel, ultrasound-augmented technique has recently been described, which takes advantage of the superior acoustic properties of the liver and provides the operator with real-time feedback on catheter position. Using this technique, informed manipulations of the catheter and portal venous anatomy can be made throughout the access procedure, markedly improving success [41].

Prior to beginning the procedure, the ductus venosus (DV) should be assessed and patency confirmed. For intra-procedural imaging, a 4–12 MHz linear array probe is recommended, as it affords high spatial resolution and a wide field of view. A cardiac phased array probe is also useful for assessing DV patency, as it often offers improved color signal. The probe is placed in the midline, just below the xiphoid and in a sagittal orientation (Fig. 33). The umbilical vein (UV) can be seen anteriorly, running superiorly to meet the portal sinus (PS) in the liver. Numerous left and right portal veins, identified by their bright endothelium, branch off from the PS and are the typical sites of UVC malposition. The DV takes off obliquely from the portal sinus, running superiorly, posteriorly, and slightly rightward to meet the inferior vena cava at the inferior cavo-atrial junction. Imaging of the PS and DV may be improved by rotating the transducer slightly counterclockwise and tilting the tail slightly to the left. Patency of the DV is performed using color Doppler imaging or agitated saline contrast (Fig. 34).



Fig. 33 Sagittal probe positioning for ultrasound-guided UVC placement

The infant is positioned in the manner typical for umbilical access. A wide sterile field should be prepped from hips to nipples and out to the anterior axillary lines. This allows for sterile transabdominal imaging during catheter manipulation, using a sterile transducer sleeve. Alternatively, a second provider may image non-sterilely under the drapes. Ultrasound provides visual feedback that enables the operator to make informed manipulations of the liver and catheter. Vascular alignment may be improved by using gentle posterior compression of the abdomen, flattening the course from the UV through the PS to the DV. Lateral mobilization of the liver away from the side of malposition may also be helpful. In addition to improving alignment, these manipulations may also be used to occlude the orifices of left portal veins, discouraging the catheter from entering them and favoring successful central UVC placement (Fig. 35).

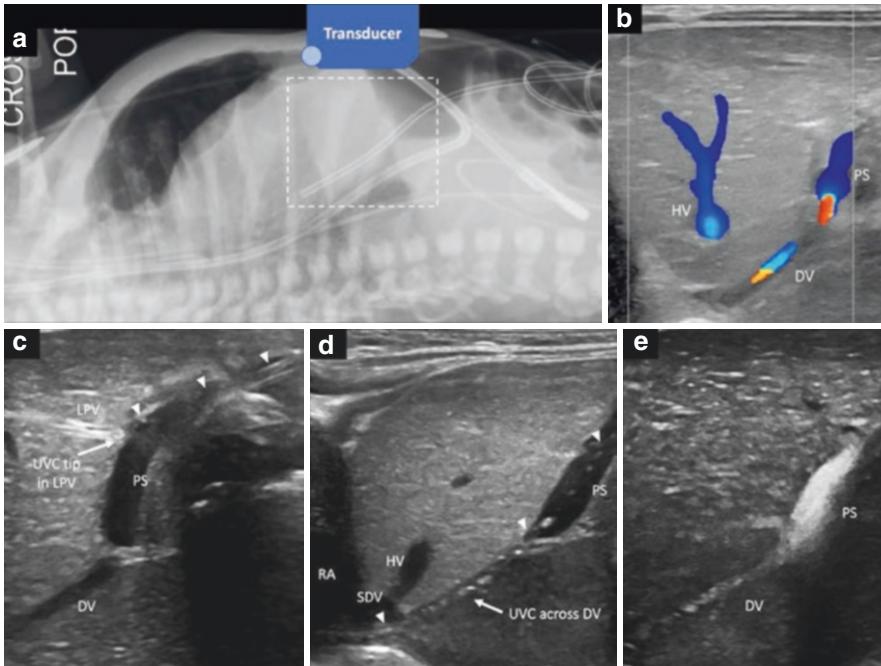


Fig. 34 Ultrasound-guided umbilical venous cannulation. (a) lateral X-ray demonstrating the path of a correctly positioned umbilical venous catheter. White box corresponds to ultrasound imaging shown in panels b–e. (b, e) Color doppler (b) and agitated saline contrast (e) demonstrate ductus venosus patency; (c, d) Sagittal ultrasound images demonstrating an umbilical venous catheter

passing into a left portal vein (c) and through the ductus venosus into the right atrium (d). Note the flattening of the trajectory from portal sinus to ductus venosus that occurs with posteriorly directed liver pressure. Arrowheads indicate the umbilical venous catheter (UVC). DV ductus venosus, HV hepatic vein, LPV left portal vein, PS portal sinus, RA right atrium, SDV subdiaphragmatic vestibule

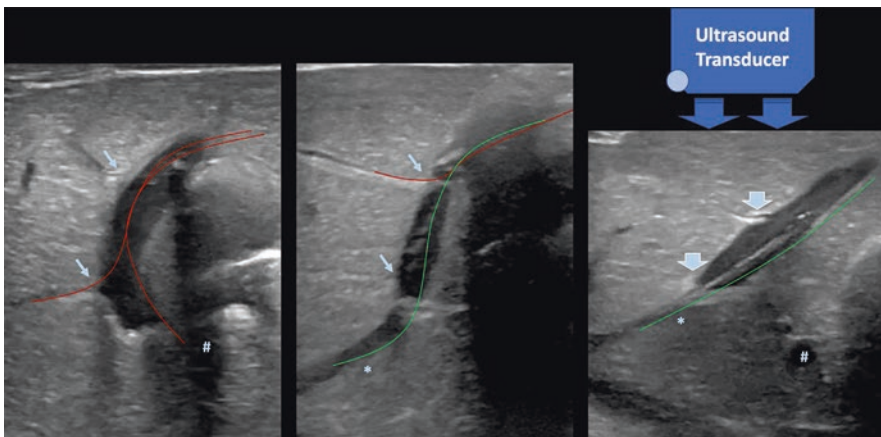


Fig. 35 Technique to avoid portal veins and improve alignment. Red lines indicate course of malpositioned UVC into the left portal veins (small arrows) or right portal veins (#). The green line indicates the desired course of

the UVC through the portal sinus and into the ductus venosus (*). Posterior compression of the abdomen as seen in the right panel improves vascular alignment and occludes the left portal vein orifices

POCUS for Central Line Position Evaluation

Several studies have questioned X-ray accuracy, reporting a discordance of 20–40% when compared to ultrasound assessment [42–45]. The location of the central line tip by X-ray is based on the relationship between the projection of the tip and non-vascular radiological landmarks, such as the carina, the vertebral bodies, and/or the diaphragm. Therefore, radiography can be misleading. POCUS can detect the position of the tip inside the vasculature with precision and should be considered as a standard practice for revealing the central line tip position and catheter migration [2]. Furthermore, acute clinical decompensation with impending cardiac arrest, where pericardial or pleural effusion is suspected due to central line malposition, makes radiological assessment extremely challenging. POCUS can reliably provide this information in real time [46–48]. For all these reasons, several studies and guidelines recommend to adopt real-time ultra-

sound as the “gold standard” to confirm correct tip position [49–52].

ECCs and PICCs are often used in neonates and the use of POCUS for their placement and monitoring has been associated with fewer catheter-related complications [20, 53]. The catheter is placed in upper or lower extremity veins and the tip position can be accurately found in the superior or inferior cavo-atrial junction respectively (Fig. 36). The catheter can be flushed with normal saline to sonographically visualize microbubbles from the tip, and thus accurately confirm the tip position [42].

Centrally inserted central venous catheters under ultrasound guidance are very common in pediatric critical care and are becoming more common in neonates since their placement is technically possible even in extremely preterm neonates as the vein diameter is sufficient even in these tiny babies [20]. These catheters overcome the aforementioned limitations of the ECCs and PICCs and seem at lower risk of infection and thrombosis while requiring a certain skill and ultrasound proficiency [29].

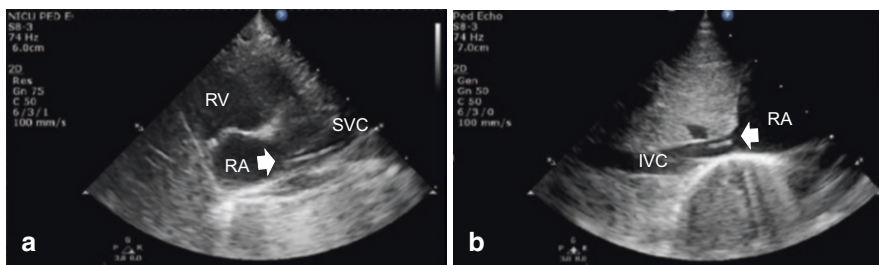


Fig. 36 (a) Long axis view of Superior Vena Cava. White arrow shows PICC line tip at the superior atrio-caval junction. (b) Long axis view of the Inferior Vena Cava. White

arrow shows PICC line tip at the inferior atrio-caval junction

References

1. De Souza TH, Brandao MB, Hersan Nadal JA, Negrao Nogueira RJ. Ultrasound guidance for pediatric central venous catheterization: a meta-analysis. *Pediatrics*. 2018;142(5):e20181719. <https://doi.org/10.1542/peds.2018-1719>.
2. Fraga MV, Stoller JZ, Glau CL, De Luca D, Rempell RG, Wenger JL, et al. Seeing is believing: ultrasound in pediatric procedural performance. *Pediatrics*. 2019;144(5):e20191401. <https://doi.org/10.1542/peds.2019-1401>.
3. Lamperti M, Bodenham AR, Pittiruti M, Blaivas M, Augoustides JG, Elbarbary M, et al. International evidence-based recommendations on ultrasound-guided vascular access. *Intensive Care Med*. 2012;38(7):1105–17. <https://doi.org/10.1007/s00134-012-2597-x>.
4. National Institute for Clinical Excellence. NICE technology appraisal guidance no 49: guidance on the use of ultrasound locating devices for placing central venous catheters. London: NICE; 2002. www.nice.org.uk/pdf/ultrasound_49_GUIDANCE.pdf.
5. Marin JR, Lewiss RE, et al. Point-of-care ultrasonography by pediatric emergency medicine physicians. Policy statement. *Ann Emerg Med*. 2015;65(4):472–8. <https://doi.org/10.1016/j.annemergmed.2015.01.028>.
6. Frankel HL, Kirkpatrick AW, Elbarbary M, Blaivas M, Desai H, Evans D, et al. Guidelines for the appropriate use of bedside general and cardiac ultrasonography in the evaluation of critically ill patients—part I: general ultrasonography. *Crit Care Med*. 2015;43(11):2479–502. <https://doi.org/10.1097/CCM.0000000000001216>.
7. Biasucci DG, La Greca A, Scoppettuolo G, Pittiruti M. Ultrasound-guided central venous catheterization: it is high time to use a correct terminology. *Crit Care Med*. 2015;43(9):e394–6. <https://doi.org/10.1097/CCM.0000000000001069>.
8. Martinoli C, Bianchi S, Derchi LE. Ultrasonography of peripheral nerves. *Semin Ultrasound CT MR*. 2000;21(3):205–13. [https://doi.org/10.1016/s0887-2171\(00\)90043-x](https://doi.org/10.1016/s0887-2171(00)90043-x).
9. Nifong TP, McDevitt TJ. The effect of catheter to vein ratio on blood flow rates in a simulated model of peripherally inserted central venous catheters. *Chest*. 2011;140(1):48–53. <https://doi.org/10.1378/chest.10-2637>.
10. Sharp R, Cummings M, Fielder A, Mikocka-Walus A, Grech C, Esterman A. The catheter to vein ratio and rates of symptomatic venous thromboembolism in patients with a peripherally inserted central catheter (PICC): a prospective cohort study. *Int J Nurs Stud*. 2015;52(3):677–85. <https://doi.org/10.1016/j.ijnurstu.2014.12.002>.
11. Clemmesen L, Knudsen L, Sloth E, Bendtsen T. Dynamic needle tip positioning—ultrasound guidance for peripheral vascular access. A randomized, controlled and blinded study in phantoms performed by ultrasound novices. *Ultraschall Med*. 2012;33(7):E321–E5. <https://doi.org/10.1055/s-0032-1312824>.
12. Takeshita J, Yoshida T, Nakajima Y, Nakayama Y, Nishiyama K, Ito Y, et al. Superiority of dynamic needle tip positioning for ultrasound-guided peripheral venous catheterization in patients younger than 2 years old: a randomized controlled trial. *Pediatr Crit Care Med*. 2019;20(9):e410–e4. <https://doi.org/10.1097/PCC.0000000000002034>.
13. Mallinson C, Bennett J, Hodgson P, Petros AJ. Position of the internal jugular vein in children. A study of the anatomy using ultrasonography. *Paediatr Anaesth*. 1999;9(2):111–4. <https://doi.org/10.1046/j.1460-9592.1999.9220329.x>.
14. Purohit G, Setlur R, Dhar M, Bhasin S. Assessment of head and neck position for optimal ultrasonographic visualisation of the internal jugular vein and its relation to the common carotid artery: a prospective observational study. *J Anaesthesiol Clin Pharmacol*. 2020;36(1):62–5. https://doi.org/10.4103/joacp.JOACP_330_18.
15. Spencer TR, Mahoney KJ. Reducing catheter-related thrombosis using a risk reduction tool centered on catheter to vessel ratio. *J Thromb Thrombolysis*. 2017;44(4):427–34. <https://doi.org/10.1007/s11239-017-1569-y>.
16. Maitra S, Bhattacharjee S, Baidya DK. Comparison of long-, short-, and oblique-axis approaches for ultrasound-guided internal jugular vein cannulation: a network meta-analysis. *J Vasc Access*. 2020;21(2):204–9. <https://doi.org/10.1177/1129729819868927>.
17. Miao S, Wang X, Zou L, Zhao Y, Wang G, Liu Y, et al. Safety and efficacy of the oblique-axis plane in ultrasound-guided internal jugular vein puncture: a meta-analysis. *J Int Med Res*. 2018;46(7):2587–94. <https://doi.org/10.1177/0300060518765344>.
18. Merchaoui Z, Lausten-Thomsen U, Pierre F, Ben Laiba M, Le Sache N, Tissieres P. Supraclavicular approach to ultrasound-guided brachiocephalic vein cannulation in children and neonates. *Front Pediatr*. 2017;5:211. <https://doi.org/10.3389/fped.2017.00211>.
19. Lausten-Thomsen U, Merchaoui Z, Dubois C, Dit Trolli SE, Le Sache N, Mokhtari M, et al. Ultrasound-guided subclavian vein cannulation in low birth weight neonates. *Pediatr Crit Care Med*. 2017;18(2):172–5. <https://doi.org/10.1097/PCC.0000000000001028>.
20. Barone G, Pittiruti M, Ancora G, Vento G, Tota F, D'Andrea V. Centrally inserted central catheters in preterm neonates with weight below 1500 g by ultrasound-guided access to the brachiocephalic vein. *J Vasc Access*. 2021;22(3):344–52. <https://doi.org/10.1177/1129729820940174>.
21. Breschan C, Graf G, Arneitz C, Stettner H, Feigl G, Neuwersch S, et al. Feasibility of the ultrasound-guided supraclavicular cannulation of the brachiocephalic vein in very small weight infants: a case series. *Paediatr Anaesth*. 2020;30(8):928–33. <https://doi.org/10.1111/pan.13928>.

22. Ford DR, Witting MD, Vora MV, Sommerkamp SK, Euerle BD. No effect of Valsalva maneuver or Trendelenburg angle on axillary vein size. *J Emerg Med.* 2013;45(3):452–7. <https://doi.org/10.1016/j.jemermed.2012.12.020>.
23. T S, Kulandyan I, Velraj J, Murugesan R, Srinivasan P. Sonographic visualization and cannulation of the axillary vein in two arm positions during mechanical ventilation: a randomized trial. *J Vasc Access.* 2020;21(2):210–6. <https://doi.org/10.1177/1129729819869504>.
24. Sharma A, Bodenham AR, Mallick A. Ultrasound-guided infraclavicular axillary vein cannulation for central venous access. *Br J Anaesth.* 2004;93(2):188–92. <https://doi.org/10.1093/bja/ae187>.
25. Brescia F, Biasucci DG, Fabiani F, Favarato M, Costa F, Longo F, et al. A novel ultrasound-guided approach to the axillary vein: oblique-axis view combined with in-plane puncture. *J Vasc Access.* 2019;20(6):763–8. <https://doi.org/10.1177/1129729819826034>.
26. Brass P, Hellmich M, Kolodziej L, Schick G, Smith AF. Ultrasound guidance versus anatomical landmarks for subclavian or femoral vein catheterization. *Cochrane Database Syst Rev.* 2015;1:CD011447. <https://doi.org/10.1002/14651858.CD011447>.
27. Bhatia N, Sivaprakasam J, Allford M, Guruswamy V. The relative position of femoral artery and vein in children under general anaesthesia—an ultrasound-guided observational study. *Paediatr Anaesth.* 2014;24(11):1164–8. <https://doi.org/10.1111/pan.12486>.
28. Good RJ, Levin M, Feder S, Loi MM, Kim JS, Branchford BR, et al. Accuracy of bedside ultrasound femoral vein diameter measurement by PICU providers. *Pediatr Crit Care Med.* 2020;21(12):e1148–e51. <https://doi.org/10.1097/PCC.0000000000002439>.
29. Barone G, D’Andrea V, Vento G, Pittiruti M. A systematic ultrasound evaluation of the diameter of deep veins in the newborn: results and implications for clinical practice. *Neonatology.* 2019;115(4):335–40. <https://doi.org/10.1159/000496848>.
30. Gnannt R, Waespe N, Temple M, Amirabdi A, Liu K, Brandao L, et al. Increased risk of symptomatic upper-extremity venous thrombosis with multiple peripherally inserted central catheter insertions in pediatric patients. *Pediatr Radiol.* 2018;48:1013–20. <https://doi.org/10.1007/s00247-018-4096-x>.
31. Gopalingam N, Obad DS, Kristensen BS, Lundgaard P, Veien M, Gjedsted J, et al. Ultrasound-guidance outperforms the palpation technique for peripheral venous catheterisation in anaesthetised toddlers: a randomised study. *Acta Anaesthesiol Scand.* 2017;61(6):601–8. <https://doi.org/10.1111/aas.12901>.
32. Fields JM, Dean AJ, Todman RW, Au AK, Anderson KL, Ku BS, et al. The effect of vessel depth, diameter, and location on ultrasound-guided peripheral intravenous catheter longevity. *Am J Emerg Med.* 2012;30(7):1134–40. <https://doi.org/10.1016/j.ajem.2011.07.027>.
33. Gottlieb M, Holladay D, Peksa GD. Comparison of short- vs long-axis technique for ultrasound-guided peripheral line placement: a systematic review and meta-analysis. *Cureus.* 2018;10(5):e2718. <https://doi.org/10.7759/cureus.2718>.
34. Kantor DB, Su E, Milliren CE, Conlon TW. Ultrasound guidance and other determinants of successful peripheral artery catheterization in critically ill children. *Pediatr Crit Care Med.* 2016;17(12):1124–30. <https://doi.org/10.1097/PCC.0000000000000936>.
35. Gu WJ, Tie HT, Liu JC, Zeng XT. Efficacy of ultrasound-guided radial artery catheterization: a systematic review and meta-analysis of randomized controlled trials. *Crit Care.* 2014;18(3):R93. <https://doi.org/10.1186/cc13862>.
36. Mignini MA, Piacentini E, Dubin A. Peripheral arterial blood pressure monitoring adequately tracks central arterial blood pressure in critically ill patients: an observational study. *Crit Care.* 2006;10(2):R43. <https://doi.org/10.1186/cc4852>.
37. Takeshita J, Takayuki Y, Nakajima Y, Nakayama Y, Nishiyama K, Ito Y, Shimizu Y, Takeuchi M, Shime N. Dynamic needle tip positioning for ultrasound-guided arterial catheterization in infants and small children with deep arteries: a randomized controlled trial. *J Cardiothorac Vasc Anesth.* 2019;33(7):1919–25. <https://doi.org/10.1053/j.jvca.2018.12.002>.
38. Barbeau GR, Arsenault F, Dugas L, Simard S, Larivière MM. Evaluation of the ulnopalmar arterial arches with pulse oximetry and plethysmography: comparison with the Allen’s test in 1010 patients. *Am Heart J.* 2004;147(3):489–93. <https://doi.org/10.1016/j.ahj.2003.10.038>.
39. Ruengsakulrach P, Brooks M, Hare DL, Gordon I, Buxton BF. Preoperative assessment of hand circulation by means of doppler ultrasonography and the modified Allen test. *J Thorac Cardiovasc Surg.* 2001;121(3):526–31. <https://doi.org/10.1067/mtc.2001.112468>.
40. Takeshita J, Takayuki Y, Nakajima Y, Nakayama Y, Nishiyama K, Ito Y, Shimizu Y, Takeuchi M, Shime N. Ultrasound-guided dynamic needle tip positioning versus conventional palpation approach for catheterisation of posterior tibial or dorsalis pedis artery in infants and small children. *Br J Anaesth.* 2021;126(4):e140–2. <https://doi.org/10.1016/j.bja.2020.11.033>.
41. Kishigami M, Shimokaze T, Enomoto M, Shibasaki J, Toyoshima K. Ultrasound-guided umbilical venous catheter insertion with alignment of the umbilical vein and ductus venosus. *J Ultrasound Med.* 2020;39(2):379–83. <https://doi.org/10.1002/jum.15106>.
42. Nguyen J. Ultrasonography for central catheter placement in the neonatal intensive care unit—a review of utility and practicality. *Am J Perinatol.* 2016;33(6):525–30. <https://doi.org/10.1055/s-0035-1569987>.
43. Jain A, McNamara PJ, Ng E, El-Khuffash A. The use of targeted neonatal echocardiography to confirm placement of peripherally inserted central catheters in

- neonates. *Am J Perinatol*. 2012;29(2):101–6. <https://doi.org/10.1055/s-0031-1295649>.
44. Tauzin L, Sigur N, Joubert C, Parra J, Hassid S, Moulies ME. Echocardiography allows more accurate placement of peripherally inserted central catheters in low birthweight infants. *Acta Paediatr*. 2013;102(7):703–6. <https://doi.org/10.1111/apa.12245>.
 45. Ohki Y, Tabata M, Kuwashima M, Takeuchi H, Nako Y, Morikawa A. Ultrasonographic detection of very thin percutaneous central venous catheter in neonates. *Acta Paediatr*. 2010;89:1381–4. <https://doi.org/10.1080/080352500300002615>.
 46. Katheria AC, Fleming SE, Kim JH. A randomized controlled trial of ultrasound-guided peripherally inserted central catheters compared with standard radiograph in neonates. *J Perinatol* [Internet]. 2013;33(10):791–4. <https://doi.org/10.1038/jp.2013.58>.
 47. Labovitz AJ, Noble VE, Bierig M, Goldstein SA, Jones R, Kort S, et al. Focused cardiac ultrasound in the emergent setting: a consensus statement of the American Society of Echocardiography and American College of Emergency Physicians. *J Am Soc Echocardiogr*. 2010;23(12):1225–30. <https://doi.org/10.1016/j.echo.2010.10.005>.
 48. Vieillard-Baron A, Slama M, Cholley B, Janvier G, Vignon P. Echocardiography in the intensive care unit: from evolution to revolution? *Intensive Care Med* [Internet]. 2008 [cited 2012 Mar 18];34(2):243–9. <https://doi.org/10.1007/s00134-007-0923-5>.
 49. George L, Waldman JD, Cohen ML, Segall ML, Kirkpatrick SE, Turner SW, et al. Umbilical vascular catheters: localization by two-dimensional echocardiography. *Pediatr Cardiol*. 1982;2:237–43. <https://doi.org/10.1007/BF02332115>.
 50. Ades A, Sable C, Cummings S, Cross R, Markle B, Martin G. Echocardiographic evaluation of umbilical venous catheter placement. *J Perinatol*. 2003;23:24–8. <https://doi.org/10.1038/sj.jp.7210851>.
 51. Garg AK, Houston AB, Laing JM, MacKenzie JR. Positioning of umbilical arterial catheters with ultrasound. *Arch Dis Child*. 1983;58:1017–8. <https://doi.org/10.1136/adc.58.12.1017>.
 52. Mertens L, Seri I, Marek J, Arlettaz R, Barker P, McNamara PJ, et al. Targeted neonatal echocardiography in the neonatal intensive care unit: practice guidelines and recommendations for training: writing group of the American Society of Echocardiography (ASE) in collaboration with the European association of echocardiograph. *Eur J Echocardiogr*. 2011;45:131. <https://doi.org/10.1016/j.echo.2011.07.014>.
 53. Oulego-Erroz I, Fernández-García A, Álvarez-Juan B, Terroba-Seara S, Quintela PA, Rodríguez-Núñez A. Ultrasound-guided supraclavicular cannulation of the brachiocephalic vein may reduce central line-associated bloodstream infection in preterm infants. *Eur J Pediatr*. 2020;179(11):1655–63. <https://doi.org/10.1007/s00431-020-03663>.



Ultrasound-Guided Procedures Beyond Vascular Access

Jesse Wenger and Grace Chong

Contents

Introduction	277
Lumbar Puncture	278
Thoracentesis	280
Pericardiocentesis	283
Paracentesis	284
Suprapubic Bladder Aspiration and Urethral Catheterization	286
Conclusion	287
References	287

Introduction

Before the use of bedside ultrasound for procedures, landmark techniques guided the proceduralist in choosing the optimal location for needle puncture, with the goal of avoiding important unseen structures and decreasing the likelihood of complications. The use of real-time ultrasound

guidance during minimally invasive procedures reduces failure rates, need for multiple attempts, and complications while procedural success improves.

The improved success and safety of ultrasound-guided vascular access techniques utilizing direct visualization of vessel location and catheter placement have been well-demonstrated in the pediatric population. Data to support ultrasound guidance of nonvascular access procedures is more limited in pediatrics; however, using the available pediatric data and more abundant adult data, a proceduralist can confidently use bedside ultrasound to improve the safety of nonvascular access procedures in children.

J. Wenger (✉)

Division of Pediatric Critical Care Medicine,
Seattle Children's Hospital, University of
Washington, Seattle, WA, USA
e-mail: Jesse.Wenger@seattlechildrens.org

G. Chong

Division of Pediatric Critical Care Medicine,
Comer Children's Hospital, The University of
Chicago School of Medicine, Chicago, IL, USA
e-mail: gchong@uchicagomedicine.org

Lumbar Puncture

A lumbar puncture (LP) is a common procedure performed in pediatrics to aid in the diagnosis of infection, inflammation, or malignancy or to provide therapeutic interventions for diseases of the central nervous system. Traditionally, the surface landmark technique has been used to obtain cerebrospinal fluid (CSF), but failure rates of up to 65% have been reported with first-pass LPs [1, 2]. The inability to palpate landmarks such as the iliac crest (corresponding to the L3–L4 space) can lead to ineffective CSF acquisition, defined as the inability to obtain CSF from the subarachnoid space, or to obtain bloody CSF from a traumatic puncture. LP failure places patients at risk for multiple and/or traumatic LPs, extended pain, longer hospital stays, prolonged antibiotic use, and other complications such as headaches, hematomas, and CSF leaks [3–5]. The use of bedside ultrasonography however offers a safe alternative method of landmark identification for improved procedural success.

Bedside ultrasonography is a rapid and effective tool used to identify and optimize interspinous and subarachnoid spaces via direct visualization of these anatomic landmarks. In particular, ultrasound guidance can be useful in infants who have incomplete ossification of bony structures that surround the spinal canal. Furthermore, ultrasound imaging can also be used to identify anatomic structures or pathophysiological processes necessary to avoid—such as the conus medullaris or an intrathecal hematoma—in order to achieve LP success. Though the literature for the use of ultrasound guidance for LP in pediatrics is limited, several studies have demonstrated reduced numbers of LP attempts, fewer traumatic LPs, decreased pain and lower complications rate, and improved identification of insertion sites with the use of ultrasound [5–8]. However, these are single-centered studies that require further investigation to confirm reproducibility and generalizability.

Due to the size and reduced ossification of infant vertebrae, it is often possible to identify spinal anatomic features such as the posterior dura, epidural fat, ligamentum flavum, cauda

equina, conus medullaris, and subarachnoid fluid during preprocedural sonographic assessment within this population (Fig. 1). Capturing these images, the distance between interspinous processes and the width of the subarachnoid space can determine the depth of needle insertion and angle of entry [9–13]. Images of vertebral structures will be more limited in older children and particularly those with obesity, though appreciation of anatomy and alignment will still allow for approximation of required needle insertion depth and direction.

The technique to perform an ultrasound-guided LP involves the following steps [6, 14, 15]:

1. Position the patient in a lateral decubitus position with neck and hip flexion or a sitting position with flexed hips. In one study of neonates and children, a seated position versus the lateral recumbent position was found to provide the maximally positioned lumbar spine [16].
2. Place the ultrasound probe midline over the spine in the transverse plane at the level of the iliac crests (Fig. 2a). On ultrasound, the spinous process is outlined by a crescent-shaped hyperechoic line with posterior acoustic shadowing (Fig. 2b). Mark transverse lines along the plane of the probe. Providers may choose to define where the end of the conus is as well as where the spinal canal narrows for locating optimal regions for cerebrospinal fluid acquisition. If the probe has a centerline

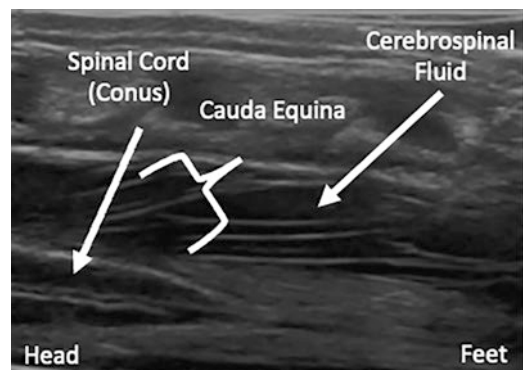


Fig. 1 Ultrasound image of longitudinal view of basic spinal anatomy



Fig. 2 (a) Transverse probe position for lumbar puncture with markings. (b) Ultrasound image of lower lumbar spine in transverse view with transverse processes (arrows) and visualized cerebral spinal fluid (asterisk). (c)

Longitudinal probe position for lumbar puncture with markings. (d) Ultrasound image of lower lumbar spine in longitudinal view. (e) Interconnected markings identifying optimal location for cerebrospinal fluid acquisition

marker, a mark can be made to identify longitudinal plane for planning.

3. Next, rotate the probe into the longitudinal plane with the probe indicator toward the

patient's head (Fig. 2c). In this plane, the space between the spinous processes is the interspinous space. Distal to the spinal process and epidural fat lies in the posterior dura,

a bright echogenic line separating the epidural space from the intrathecal space (Fig. 2d). Depth can be measured effectively in this stage of procedural planning.

4. Remove the ultrasound probe and extend the markings from the transverse and longitudinal planes until they intersect. This intersection represents the ideal location for needle insertion (Fig. 2e).

In addition to infants, ultrasound guidance of LPs can be useful in patients with abnormal anatomy or history of recent failed attempts. The width of the subarachnoid space varies by location and using ultrasonographic markings allows for midline identification with more precision, taking care to avoid epidural vessels that travel laterally to the spinal canal.

Thoracentesis

Pediatric and neonatal intensivists often need to perform a thoracentesis to evacuate a pneumothorax or pleural effusion to improve source control, pulmonary physiology, or hemodynamics. Pleural effusions in children most commonly present as parapneumonic effusions or empyemas but other common causes of pleural effusions in children are malignancy, renal disease, trauma, heart failure, and systemic diseases [17] (e.g., sepsis). Pneumothoraces are more frequent events in neonates and very premature infants compared to older children but when tension physiology is present it is a medical emergency for both populations [18, 19].

Assessment of suspected lung pathology requiring drainage commonly utilizes chest radiography. Interestingly, chest radiographs have a sensitivity as low as 38% for detecting pleural effusions and 46% for pneumothoraces but with good to excellent specificity for both abnormalities [20, 21]. A study by Lichtenstein et al. found higher diagnostic accuracy with ultrasound (93%) compared to physical exam (61%) and chest radiography (47%). These data support the increased use of lung ultrasound at the bedside to improve the diagnosis of pleural effusions and

pneumothorax. Beyond improved diagnostic accuracy, other benefits of ultrasonography include the absence of radiation exposure as well as convenience given its relative ubiquitous presence and portability in current acute care settings [22]. Potential limitations of lung ultrasound include the availability of trained personnel, operator-dependent image acquisition, and limited image acquisition secondary to subcutaneous air or body habitus.

Pediatric data on ultrasound-guided thoracentesis and thoracostomy is limited. However, multiple adult studies support the use of ultrasound to guide thoracentesis and improve procedural success and decrease complications, mainly defined as post-procedural pneumothorax [23–25]. The British Thoracic Society states that ultrasound must be used to confirm the presence of a pleural fluid collection for the management of pleural infection in children, and that ultrasound should be used to guide thoracentesis and/or thoracostomy tube placement [26].

Depending on the size of the patient, different transducers may provide better visualization of a pleural effusion. Small patients are likely best visualized with a linear transducer when only a depth of several centimeters is needed. Larger patients are likely to be better served with a phased array or microconvex transducer which allows for visualization of deeper structures as well as the advantage of a footprint that easily fits between ribs. While the decision to perform a thoracentesis is more frequently based on clinical indications, estimation of pleural fluid volume has been performed using ultrasound. One approach described in adult literature is to measure the height of the effusion (from the diaphragm to the meniscus of the effusion) and add this to the distance from the lung base to the apex of the diaphragm cupola. The sum of these measurements in centimeters is multiplied by 70 to obtain an estimated volume. One study found this equation to have an accuracy of 83% with good interclass correlation, although it was found to over-estimate the volume of left-sided effusions [27].

When drainage of pleural fluid is indicated, it can be both diagnostic and therapeutic. In general, there are three approaches to thoracentesis:

(1) blind landmark, (2) ultrasound marking or static ultrasound guidance, and (3) real-time ultrasound guidance. The “blind landmark” technique uses the triangle of safety to define a safe zone in which to perform the thoracentesis. The triangle of safety is defined by the lateral pectoralis major anteriorly, the lateral latissimus dorsi posteriorly, fifth intercostal space inferiorly, and the base of the axilla superiorly. Performing a thoracentesis within this triangle allows the proceduralist to be confident that they are above the diaphragm and away from vascular structures when the needle is passed above the superior aspect of the rib, avoiding the neurovascular bundle which runs along the inferior aspect of the rib. However, this technique is associated with higher rates of complications when compared to the ultrasound-guided technique [23, 25]. The second technique, “ultrasound marking,” involves either sending the patient to radiology to have an ultrasound performed or performing the ultrasound at bedside after which a “mark” is placed at the site assessed to be best for accessing the fluid [26]. It was noted in one study that there were similar rates of pneumothorax between radiology marking with ultrasound and the “blind landmark” technique [24], potentially related to changes in patient position between when the marking was performed and when the procedure was performed. Thus, we suggest marking take place immediately prior to procedure performance.

The ultrasound-guided technique is where the proceduralist uses ultrasound at the bedside to identify the optimal location for drainage and directly visualizes needle entry into the pleural space. The first step is to position the patient so that the fluid accumulates in a dependent and easily accessible area. This is usually done using one of two different methods: to have the patient supine in a semi-recumbent or lateral decubitus position, or in a seated position. A semi-recumbent or lateral decubitus position is often necessary in a critical care setting when patients may be intubated or immobile and allows for accessing the fluid along the mid-axillary line. A posterior “zone of safety” can be defined as maintaining a safe distance from the spine (about

5 cm in an adult-sized patient), staying above the ninth rib, and being posterior to the posterior axillary line. The proceduralist should choose the position that optimizes their chance of procedural success, patient comfort and should be made with consideration of other factors (e.g., age, mobility of patient, sedation strategy, comfort of proceduralist, respiratory support, and decision of thoracentesis alone or thoracentesis with thoracostomy tube placement, etc.).

Regardless of positioning choice, the proceduralist uses ultrasound to assess the triangle or zone of safety with the patient in the same position as when the procedure will be performed. The proceduralist chooses the appropriate transducer for the patient size, chooses the appropriate preset (an abdominal preset is often ideal) on the ultrasound machine, and assures that the machine is plugged in and cleaned. By convention, the probe position indicator is oriented toward the patient’s head and the position indicator on the screen should be on the upper left-hand side. This means that when looking at the ultrasound screen, superior objects (e.g., patient’s head) are located on the left side of the screen and inferior objects (patient’s feet) are located on the right side of the screen. Similarly, anterior structures (structures closest to the transducer) will be at the top of the screen while posterior structures will be toward the bottom of the screen. Starting with the fifth intercostal space, the proceduralist verifies that the diaphragm is indeed at that level and if not, carefully identifies the location of the diaphragm. Next, the effusion is identified, most easily as a large anechoic space above the diaphragm, sometimes with additionally seen atelectatic lung (Fig. 3a). The site of aspiration should contain at least 1–2 cm of pleural fluid depth, be absent of intervening lung during inspiration and minimize risk of puncturing other structures by attempted direct visualization (heart, liver, spleen) [28]. It can be helpful to mark the level of the diaphragm at exhalation with a pen as well as mark the chosen site of aspiration (Fig. 3b).

While acquiring images, the proceduralist should adjust the gain and depth so that fluid remains anechoic (not over-gained) and that the depth allows visualization of any lung deep to the

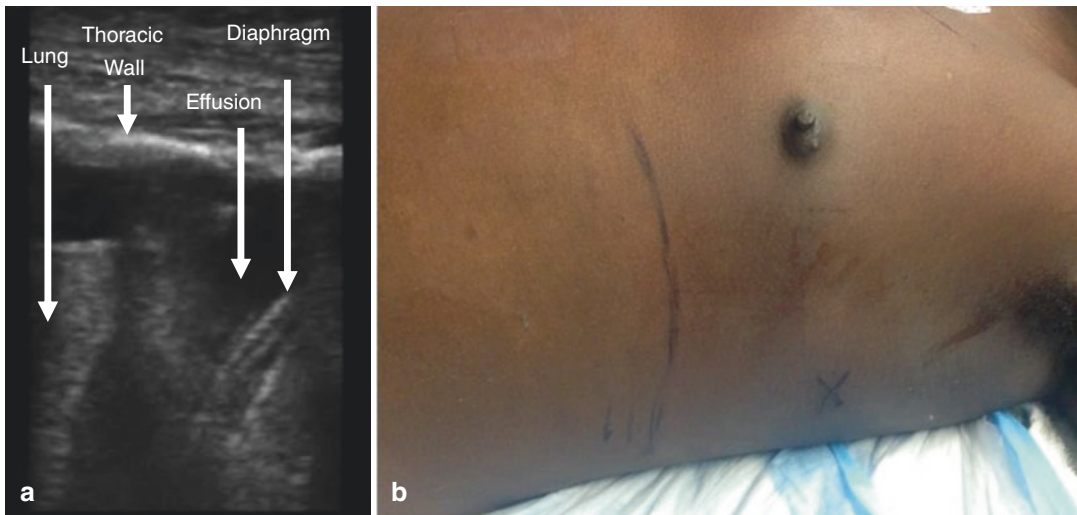


Fig. 3 (a) Ultrasound image of pleural effusion with anatomic landmarks. (b) Marking on a patient of diaphragm location and optimal site for needle insertion

pleural effusion. From here, the proceduralist moves the transducer increasingly superiorly, assessing the quality of the effusion and determining the optimal rib space which maximizes fluid removal while maintaining safety above the diaphragm. An orthogonal view should be obtained at the rib space chosen for thoracentesis to assess the effusion in a different dimension. Care should be taken while obtaining images that the transducer remains perpendicular to the chest wall in order to capture images that truly reflect the size and depth of the pleural effusions and proximity to other structures. If the patient requires repositioning between the initial ultrasound assessment and performing the procedure, the proceduralist should make sure to reassess the triangle or zone of safety and choice of puncture site. In addition to documenting ultrasound clips of the pleural effusion, the proceduralist should acquire bilateral anterior lung ultrasound images with the patient in a supine position, preferably with a linear transducer. These images provide a comparison of images acquired after the procedure which may help determine if there is a post-procedure pneumothorax.

Next, the proceduralist should prepare the patient for the thoracentesis with or without thoracostomy tube as per their institutional standard and determine a sedation and/or analgesia plan.

After adequate sedation/analgesia is achieved, the proceduralist is ready to perform the thoracentesis. As opposed to vascular access, most thoracenteses are done with static ultrasound guidance and not with real-time dynamic ultrasound guidance [29, 30]. Currently, there is not enough data to recommend real-time ultrasound guidance for thoracentesis for increased safety. However, there may be a benefit to real-time guidance for small or difficult-to-access pleural effusions [30, 31]. To use real-time ultrasound guidance, the proceduralist can switch to a linear transducer (if not used previously) and place it in the chosen intercostal space. If desired, a small lidocaine needle can then be slowly advanced—using a similar technique to vascular access—either in-plane or out-of-plane to numb the track for the thoracentesis. As the needle advances, the proceduralist continue to aspirate and then inject lidocaine until there is aspiration of pleural fluid. The needle can be directly viewed entering the pleural space using this technique and provides validation of the appropriateness of aspiration site. A similar process can be used to advance the thoracentesis needle with ultrasound guidance.

There are no clear guidelines for how much fluid can be safely drained in a pediatric thoracentesis. There are adult studies that support the removal of less than 1.5 L to reduce complica-

tions including re-expansion pulmonary edema [32]. Removal of greater than 2 L of fluid was associated with 3–6 times higher rates of complications in one study [32]. Additional findings to limit fluid removal or to stop the procedure include increased resistance to fluid removal, patient intolerance, coughing, tachycardia, or tachypnea.

A tension pneumothorax is a medical emergency and requires rapid diagnosis and treatment. Bedside ultrasound can provide a rapid assessment and diagnosis of a pneumothorax. Two articles reported 100% sensitivity and specificity of lung ultrasound to diagnose pneumothorax in term and premature infants [33, 34]. With this improved diagnostic assistance, a provider can move more confidently to perform an urgent or emergent needle decompression, using the usual approach of an angiocath (often a 20 g will work well), three-way stopcock, and large syringe in the midclavicular line of the second intercostal space. This approach can allow for rapid evacuation of air and improved hemodynamics while preparing for definitive treatment with a thoracostomy tube.

Pericardiocentesis

Cardiac tamponade is a life-threatening complication when pericardial fluid accumulation leads to increased intrapericardial pressures and circulatory collapse [35]. While the clinical signs and symptoms of cardiac tamponade include elevated jugular venous pressures, muffled heart tones, hypotension, tachycardia, dyspnea, and pulsus paradoxus, the clinical presentation is predetermined by the rapidity and/or volume of fluid accumulation and the etiology of the underlying disease [36]. For these reasons, prompt recognition is essential for directing treatment that favors beneficial outcomes.

Echocardiography is the standard of care to confirm the presence of pericardial effusion and its hemodynamic impact [37]. 2D echocardiography or focused cardiac ultrasound can unveil characteristic features of cardiac tamponade including right atrial collapse in late diastole/early systole, right ventricular collapse during

early diastole, exaggerated mitral and tricuspid valve in-flow velocities, and a plethoric IVC with minimal change with respiratory variation [35, 37, 38].

Pericardiocentesis under echocardiographic/ultrasound guidance is the definitive treatment for the management of symptomatic pericardial effusions. Simple and safe, ultrasound-guided percutaneous pericardial puncture can be performed rapidly at the bedside for unstable patients under emergency conditions. In adults, the use of ultrasound to visualize adjacent structures, determine the optimal site of puncture, estimate distance from chest wall to effusion, and guide needle advancement yields a higher rate of success and a lower rate of complications when compared with traditional landmark techniques [39, 40]. When pericardiocentesis is performed without sonographic or fluoroscopic guidance, mortality is relatively high (6%) and the risk of complications such as pneumothorax, cardiac wall perforation, and damage to other vital organs is even higher (20–50%) [40–42]. In contrast, among large-center observational studies, the rate of major complications reported for ultrasound- or fluoroscopic-guided pericardiocentesis is 0.3–3.9% and the rate of minor complications reported is 0.4–20% [40, 43, 44]. Death, perforation of the cardiac chambers, laceration of coronary or intercostal vessels, puncture to the lung or abdominal viscera, ventricular arrhythmias, and pericardial decompression syndrome are the most serious complications after pericardiocentesis. Minor complications include transient hypotension and bradycardia, supraventricular arrhythmias, pneumothorax without tension physiology, and pleuro-pericardial fistulas.

Tsang et al. demonstrated that echocardiographically guided pericardiocentesis was found to be safe and effective for pediatric patients with a 99% success rate (93% on the first attempt) and 1% major complication rate [45]. Despite these data, small children present a challenge to safely perform pericardiocentesis. Additionally, relatively small effusions that cause hemodynamic compromise leave little space between the outer rim of the effusion and the myocardium for safe needle entry [46].

The technique to perform an ultrasound-guided pericardiocentesis involves the following steps:

1. Position the patient in a semi-recumbent position at a 30°–45° angle, allowing the heart to come closer to the anterior chest wall.
2. Use the cardiac phased array ultrasound transducer to evaluate the size, distribution, and hemodynamic impact of the pericardial effusion.
3. There are several sites for pericardial access in the left chest. The three main approaches are (1) apical, (2) parasternal, or (3) subxiphoid [40, 41, 43, 44, 47–49]. In adults, pericardial access is most frequently obtained in the apical (63%) approach over the subxiphoid (15%) or parasternal (14%) approaches and several observational studies showed that the left chest approach was superior to the traditional subxiphoid approach [40, 46, 49, 50]. In infants and children, the ultrasound technique most commonly employed for puncture involves the subxiphoid approach, as the parasternal and apical approaches have not been studied in this population [45, 51].
 - (a) Apical: The ultrasound transducer is placed at the point of maximal impulse and aimed toward the patient's right shoulder. The needle insertion site is 1–2 cm lateral to the apex of the heart, within the fifth to seventh intercostal space, taking care to enter above the rib to avoid the neurovascular bundle. Advance the needle over the superior border of the rib to avoid intercostal vessels and nerves [52].
 - (b) Subxiphoid: The needle insertion site is between the xiphisternum and the left costal margin. Once inserted, lower the angle to 15°–30° and direct the ultrasound transducer to the patient's left shoulder [52].
 - (c) Parasternal: The needle insertion site is next to the sternal margin in the fifth intercostal space. Ensure the needle enters above the rib to avoid the neurovascular bundle. Locate and avoid the internal mammary arteries which are lateral to the sternum. Advance the needle perpendicular to the skin [52].
4. Among these puncture sites, use the ultrasound probe to locate the point where the effusion is closest to the transducer and the fluid collection is the most extensive, to minimize the risk of cardiac perforation and injury to other neighboring structures [41].
5. The needle trajectory is defined by the angulation of the transducer, and a direct trajectory is chosen to avoid vital organs such as the myocardium, liver, and lung.
6. For immediate evacuation of pericardial fluid and after appropriate disinfection, insert a long 18–22 gauge needle attached to a saline syringe in the direction of the pericardial fluid, continually aspirating as the needle is advanced. Advance the needle 1–2 mm at a time until fluid is aspirated. Confirm needle tip position in the pericardial space via direct visualization under ultrasound. Once confirmed, advance the cannula into the pericardial space, attach a three-way stopcock, and remove fluid. For indwelling pericardial catheter placement, seek expert consultation for placement via Seldinger technique.

Echocardiography/ultrasound-guided pericardiocentesis is the first-line therapy for life-threatening cardiac tamponade. It can be performed swiftly and adeptly at the bedside and is a clinical tool that provides a simple safe alternative to less effective traditional landmark techniques, with fewer complications and proven success.

Paracentesis

Paracentesis is less frequently performed in pediatrics compared to adults. In fact, best practices around pediatric paracentesis are usually dictated by individual or institutional experience since there is limited pediatric data to guide practice guidelines. In adults, paracentesis is infrequently associated with complications [53–55], but com-

plications may have significant effects on clinical outcomes. The necessity of preprocedural ultrasound has not been established in pediatrics, [54, 56] however adult literature has shown a benefit to ultrasound guidance and recommends its use when available [56–58].

Using the landmark technique, the child is placed in the supine position and the proceduralist percusses the abdomen to assess for dullness representing fluid. The abdomen should be assessed for surgical scars and these should be avoided to reduce the risk of puncturing potential underlying bowel adhesions. The needle insertion site is usually located either in the right or left lower quadrant identified by two fingerbreadths medial and cephalad to the anterior iliac spine, or is done in the midline through the avascular linea alba about half-way between the umbilicus and pubic symphysis. It is important to choose a site, which will avoid the inferior epigastric arteries (IEA), whose anatomic course is 2 cm lateral from midline under the rectus abdominis in the adult patient.

Ultrasound can augment the landmark approach and allow the proceduralist to assess and optimize the needle insertion site and guide the paracentesis for successful aspiration of fluid and decreased likelihood of complications. Nazeer et al. demonstrated a 95% success rate with ultrasound versus 63% success rate without ultrasound use, respectively [59]. Ultrasound can help identify the largest pocket of fluid and validate that the fluid is free floating in the abdomen and not contained in a cystic structure (e.g., fluid-filled bowel, bladder, or bladder cyst). The largest pocket of fluid can be assessed for the absence of bowel, vascular structures, enlarged spleen, or other organs that could overlay the fluid. The chosen puncture site should be viewed in two orthogonal planes and the depth of the ascites, thickness of the abdominal wall, and positioning of other important structures should be noted. The IEAs can be directly visualized and avoided [60, 61] instead of relying solely on anticipated anatomy. Using a high frequency or linear transducer, the IEA may be visualized in the lower abdomen in the mid-inguinal line and proceeding superomedially toward the umbilicus [61]. The

IEAs usually appear as round, pulsatile hypoechoic structures flanked by two inferior epigastric veins (Fig. 4). Color or pulse wave doppler can be placed over these structures to help confirm the artery. Once identified, a marker can be used to trace out the course of the IEA to assure the proceduralist of its location.

A Z-tract technique can be used to decrease the likelihood of a fluid leak post-procedures [54]. If using ultrasound for dynamic needle guidance, the needle can be introduced obliquely from a lateral approach into the peritoneal cavity with the probe oriented longitudinally over the needle. Similar to the Z-tract approach, the oblique approach helps to reduce the chance of leakage. A temporary catheter can be placed once the fluid space is accessed using a modified Seldinger technique. After placement, the catheter can be visualized in the abdominal cavity with ultrasound to confirm positioning. (Fig. 5).

Some of the most serious complications of a paracentesis are inadvertent puncture of the IEA, other peritoneal blood vessels, or underlying bowel. Mercaldi et al. showed in adults that the overall risk of bleeding complications in paracentesis could be lowered even further with ultrasound guidance from 1.25 to 0.27%. In this same study, bleeding complications from paracentesis were associated with a more costly hospital stay and with a mortality of 12.9% versus 3.7% for those receiving a paracentesis without bleeding complication [57].

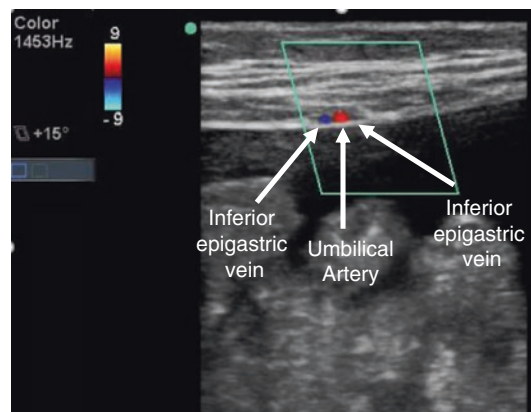


Fig. 4 Inferior epigastric artery and veins

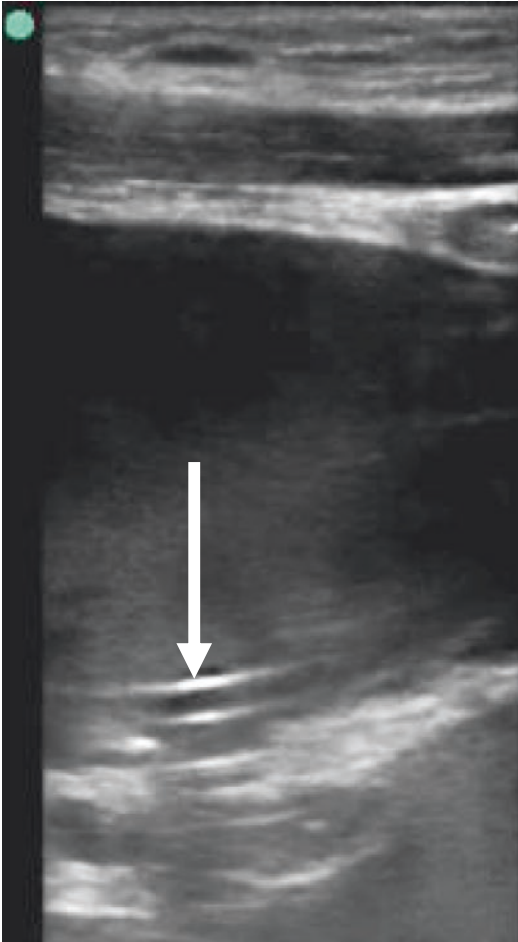


Fig. 5 Abdominal drainage catheter (arrow) visualized within the peritoneal cavity

Suprapubic Bladder Aspiration and Urethral Catheterization

Diagnostic evaluation of febrile neonates or young children often requires a clean sample of urine, which can be obtained through urethral catheterization (UC) or suprapubic bladder aspiration (SPA). Both of these procedures are invasive and uncomfortable. For both UC and SPA, multiple studies have found that the use of ultrasound improves the likelihood of obtaining urine on the first attempt merely by making sure that there is urine in the bladder before an attempt is made. Reported improvement in first-time success rates of UC or SPA, increased from 52–72% without ultrasound to 79–100% with ultrasound [62–67].

When urine is unable to be obtained from UC, SPA can be performed to obtain sterile urine for culture. The bladder usually lies posterior to the pubic symphysis and anterior to the uterus/rectum. An SPA with ultrasound guidance should be avoided in patients with genitourinary abnormalities, infections of the abdominal wall, clinically significant coagulopathy, and massive organomegaly.

This is one approach to performing a suprapubic aspiration:

1. Choose a transducer which can best visualize the entire bladder. Often a low-frequency curvilinear or phased array transducer will work best.
2. Use the transducer to visualize the bladder and confirm that there is enough urine present to optimize success.
 - (a) Place the child in a frog-leg position and place ultrasound gel about 1–2 cm above the pubic symphysis
 - (b) Place the transducer just above the pubic symphysis and fan down into the pelvis to view the bladder
 - (c) Obtain a view of the bladder in short (anterior/posterior) and long (superior/inferior) axis. Many ultrasound machines have calculation packages which will calculate the urine volume by measuring height, width, and depth (Fig. 6a, b). One study used a 1 cm × 1 cm measurement of the bladder as a minimum for performing an SPA in neonates [66] but some providers recommend that the bladder measure at least 2 cm in all dimensions to ensure having an adequate volume for needed urine studies [68].
3. Sterilely prepare the abdomen and anesthetize the anticipated access site
4. Use a small needle (e.g., 23 gauge) attached to a syringe. Visualize the bladder in short axis with the ultrasound transducer about 1–2 cm above the pubic symphysis. Insert the needle just inferior to the transducer maintaining a perpendicular angle to the abdomen (which may appear to be about a 10–20° angle from true vertical).

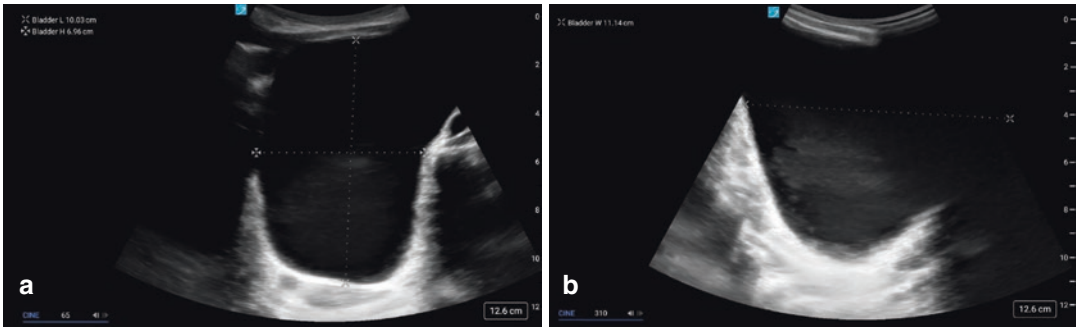


Fig. 6 (a) Bladder measurements in transverse view of the bladder (height and width). (b) Bladder measurement in longitudinal view of the bladder (depth)

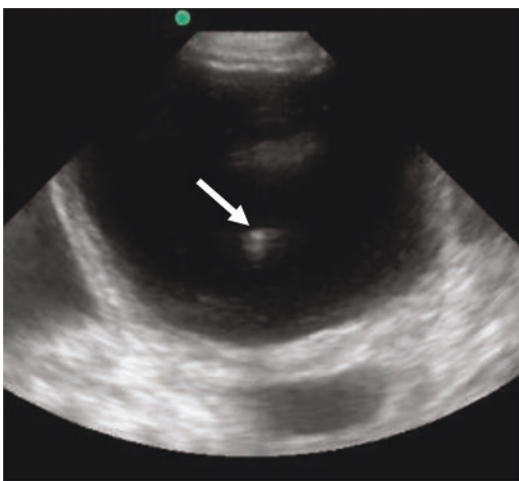


Fig. 7 Ultrasound of the needle tip (arrow) within the bladder during suprapubic aspiration

5. Use a similar technique to IV or central line placement (e.g., “step-down” technique), and slowly advance the needle until it is seen puncturing the bladder with the return of urine. The needle tip should be easily visualized if the bladder is obstructed and therefore fluid-filled (Fig. 7).

Conclusion

Critical care providers continue to need to weigh the risks and benefits of performing various procedures in critically ill children. Evidence in both pediatric and adult patients supports the use of ultrasound to guide procedures beyond vascular

access to improve provider performance and patient safety. Proceduralists should continue to develop ultrasound skills to assess anatomy and pathophysiology and to guide their needle across commonly performed procedures within respective domains of clinical practice.

References

1. Nigrovic LE, Kuppermann N, Neuman MI. Risk factors for traumatic or unsuccessful lumbar punctures in children. *Ann Emerg Med.* 2007;49:762–71.
2. Shah KH, Richard KM, Nicholas S, Edlow JA. Incidence of traumatic lumbar puncture. *Acad Emerg Med.* 2003;10(2):151–4.
3. Glatstein MM, Zucker-Toledano M, Arik A, et al. Incidence of traumatic lumbar puncture: experience of a large, tertiary care pediatric hospital. *Clin Pediatr.* 2011;50:1005–9.
4. Pingree EW, Kimia AA, Nigrovic LE. The effect of traumatic lumbar puncture on hospitalization rate for febrile infants 28 to 60 days of age. *Acad Emerg Med.* 2015;22:240–3.
5. Olowoyeye A, Fadahunsi O, Okudo J, Opaneye O, Okwundu C. Ultrasound imaging versus palpation method for diagnostic lumbar puncture in neonates and infants: a systematic review and meta-analysis. *BMJ Paediatr Open.* 2019;3(1):e000412.
6. Neal JT, Kaplan SL, Woodford AL, et al. The effect of bedside ultrasonographic skin marking on infant lumbar puncture success: a randomized controlled trial. *Ann Emerg Med.* 2017;69:610–619.e1.
7. Özdamar E, Özkaya AK, Güler E, Cantay B, Karabel N, Göksüğü Y, Çetinkaya A, Emre Ö. Ultrasound-assisted lumbar puncture in pediatric emergency department. *Pediatr Emerg Care.* 2017;33(8):e21–3.
8. Gorn M, Kunkov S, Crain EF. Prospective investigation of a novel ultrasound-assisted lumbar punc-

- ture technique on infants in the pediatric emergency department. *Acad Emerg Med.* 2017;24:6–12.
9. Fraga MV, Stoller JZ, Glau CL, et al. Seeing in believing: ultrasound in pediatric procedural performance. *Pediatrics.* 2019;144(5):e20191401.
 10. Gottlieb M, Holladay D, Peksa GD. Ultrasound-assisted lumbar punctures: a systematic review and meta-analysis. *Acad Emerg Med.* 2019;26(1):85–96.
 11. Coley BD, Shiels WE II, Hogan MJ. Diagnostic and interventional ultrasonography in neonatal and infant lumbar puncture. *Pediatr Radiol.* 2001;31(6):399–402.
 12. Oulego-Erroz I, Mora-Matilla M, AlonsoQuintela P, et al. Ultrasound evaluation of lumbar spine anatomy in newborn infants: implications for optimal performance of lumbar puncture. *J Pediatr.* 2014;165(4):862–865.e1.
 13. Furness G, Reilly MP, Kuchi S. An evaluation of ultrasound imaging for identification of lumbar intervertebral level. *Anaesthesia.* 2002;57(3):277–80.
 14. Muthusami P, Robinson AJ, Shroff MM. Ultrasound guidance for difficult lumbar puncture in children: pearls and pitfalls. *Pediatr Radiol.* 2017;47:822–30.
 15. Kessler D, Pahalyants V, Kriger J, et al. Preprocedural ultrasound for infant lumbar puncture: a randomized clinical trial. *Acad Emerg Med.* 2018;25:1027–34.
 16. Abo A, Yamamoto LG, Itoman EM, et al. Positioning for lumbar puncture in children evaluated by bedside ultrasound. *Pediatrics.* 2010;125:e1149–53.
 17. Cashen K, Petersen TL. Pleural effusions and Pneumothoraces. *Pediatr Rev.* 2017;38(4):170–81.
 18. Bhatia R, Davis PG, Doyle LW, Wong C, Morley CJ. Identification of pneumothorax in very preterm infants. *J Pediatr.* 2011;159(1):115–120.e1.
 19. Dotson K, Johnson LH. Pediatric spontaneous pneumothorax. *Pediatr Emerg Care.* 2012;28(7):715–20.
 20. Lichtenstein DA. Ultrasound examination of the lungs in the intensive care unit. *Pediatr Crit Care Med.* 2009;10(6):693–8.
 21. Ebrahimi A, Yousefifard M, Mohammad Kazemi H, Rasouli HR, Asady H, Moghadas Jafari A, Hosseini M. Diagnostic accuracy of chest ultrasonography versus chest radiography for identification of pneumothorax: a systematic review and meta-analysis. *Tanaffos.* 2014;13(4):29–40.
 22. Islam S, Calkins CM, Goldin AB, Chen C, Downard CD, Huang EY, Cassidy L, Saito J, Blakely ML, Rangel SJ, Arca MJ, Abdullah F, St Peter SD, APSA Outcomes and Clinical Trials Committee, 2011–2012. The diagnosis and management of empyema in children: a comprehensive review from the APSA Outcomes and Clinical Trials Committee. *J Pediatr Surg.* 2012;47(11):2101–10.
 23. Gordon CE, et al. Pneumothorax following thoracentesis: a systematic review and meta-analysis. *Arch Intern Med.* 2010;170(4):332–9.
 24. Raptopoulos V, Davis LM, Lee G, Umali C, Lew R, Irwin RS. Factors affecting the development of pneumothorax associated with thoracentesis. *AJR Am J Roentgenol.* 1991;156(5):917–20.
 25. Mercaldi CJ, Lanes SF. Ultrasound guidance decreases complications and improves the cost of care among patients undergoing thoracentesis and paracentesis. *Chest.* 2013;143(2):532–8.
 26. Balfour-Lynn IM, Abrahamson E, Cohen G, Hartley J, King S, Parikh D, Spencer D, Thomson AH, Urquhart D, Paediatric Pleural Diseases Subcommittee of the BTS Standards of Care Committee. BTS guidelines for the management of pleural infection in children. *Thorax.* 2005;60 Suppl 1(Suppl 1):i1–i21.
 27. Hassan M, Rizk R, Essam H, Abouelnour A. Validation of equations for pleural effusion volume estimation by ultrasonography. *J Ultrasound.* 2017;20(4):267–71.
 28. Havelock T, Teoh R, Laws D, Gleeson F. BTS Pleural Disease Guideline Group. Pleural procedures and thoracic ultrasound: British Thoracic Society pleural disease guideline 2010. *Thorax.* 2010;65 Suppl 2:ii61–76.
 29. Lichtenstein D. Lung ultrasound in the critically ill. *Curr Opin Crit Care.* 2014;20(3):315–22.
 30. Dancel R, Schnobrich D, Puri N, Franco-Sadud R, Cho J, Grikis L, Lucas BP, El-Barbary M, Society of Hospital Medicine Point of Care Ultrasound Task Force, Soni NJ. Recommendations on the use of ultrasound guidance for adult thoracentesis: a position statement of the Society of Hospital Medicine. *J Hosp Med.* 2018;13(2):126–35.
 31. Bass C, Morris A. UW WISH. Thoracic ultrasonography for bedside thoracentesis [Video]. YouTube. 2019. https://youtube.com/IUAn_1R7V3E.
 32. Josephson T, Nordenskjold CA, Larsson J, Rosenberg LU, Kaijser M. Amount drained at ultrasound-guided thoracentesis and risk of pneumothorax. *Acta Radiol.* 2009;50(1):42–7.
 33. Raimondi F, Rodriguez Fanjul J, Aversa S, Chirico G, Yousef N, De Luca D, Corsini I, Dani C, Grappone L, Orfeo L, Migliaro F, Vallone G, Capasso L, Lung Ultrasound in the Crashing Infant (LUCI) Protocol Study Group. Lung ultrasound for diagnosing pneumothorax in the critically ill neonate. *J Pediatr.* 2016;175:74–78.e1.
 34. Liu J, Chi JH, Ren XL, Li J, Chen YJ, Lu ZL, Liu Y, Fu W, Xia RM. Lung ultrasonography to diagnose pneumothorax of the newborn. *Am J Emerg Med.* 2017;35(9):1298–302.
 35. Tsang TS, Oh JK, Seward JB. Diagnosis and management of cardiac tamponade in the era of echocardiography. *Clin Cardiol.* 1999;22(7):446–52.
 36. Imazio M, Adler Y. Management of pericardial effusion. *Eur Heart J.* 2013;34(16):1186–97.
 37. Tsang TS, Oh JK, Seward JB, Tajik AJ. Diagnostic value of echocardiography in cardiac tamponade. *Herz.* 2000;25(8):734–40.
 38. Alerhand S, Carter JM. What echocardiographic findings suggest a pericardial effusion is causing tamponade? *Am J Emerg Med.* 2019;37(2):321–6.
 39. Adler Y, Charron P, Imazio M, et al. 2015 ESC guidelines for the diagnosis and management of pericardial diseases: the task force for the diagnosis and management of pericardial diseases of the European Society of Cardiology (ESC) endorsed by the European

- Association for Cardio-Thoracic Surgery (EACTS). *Eur Heart J*. 2015;36:2921–64.
40. Tsang TS, Enriquez-Sarano M, Freeman WK, et al. Consecutive 1127 therapeutic echocardiographically guided pericardiocentesis: clinical profile, practice patterns, and outcomes spanning 21 years. *Mayo Clin Proc*. 2002;77:429–36.
 41. Tsang TS, El-Najdawi EK, Seward JB, et al. Clinical and echocardiographic characteristics of significant pericardial effusions following cardiothoracic surgery and outcomes of echo-guided pericardiocentesis for management: Mayo Clinic experience, 1979–1998. *Chest*. 1999;116:322–31.
 42. Wong B, Murphy J, Chang CJ, et al. The risk of pericardiocentesis. *Am J Cardiol*. 1979;44:1110–4.
 43. Maggiolini S, Gentile G, Farina A, et al. Safety, efficacy, and complications of pericardiocentesis by real-time echo-monitored procedure. *Am J Cardiol*. 2016;117:1369–74.
 44. Akyuz S, Zengin A, Arugaslan E, et al. Echo-guided pericardiocentesis in patients with clinically significant pericardial effusion. Outcomes over a 10-year period. *Herz*. 2015;40(suppl2):153–9.
 45. Tsang TS, El-Najdawi EK, Seward JB, et al. Percutaneous echocardiographically guided pericardiocentesis in pediatric patients: evaluation of safety and efficacy. *J Am Soc Echocardiogr*. 1998;11:1072–7.
 46. Law MA, Borasino S, Kalra Y, et al. Novel, long-axis in-plane ultrasound-guided pericardiocentesis for postoperative pericardial effusion drainage. *Pediatr Cardiol*. 2016;37:1328–33.
 47. Flint N, Siegel RJ. Echo-guided pericardiocentesis: when and how should it be performed? *Curr Cardiol Rep*. 2020;22:71.
 48. Callahan JA, Seward JB. Pericardiocentesis guided by two-dimensional echocardiography. *Echocardiography*. 1997;14:497–504.
 49. Cho BC, Kang SM, Kim DH, et al. Clinical and echocardiographic characteristics of pericardial effusion in patients who underwent echocardiographically guided pericardiocentesis: Yonsei Cardiovascular Center experience, 1993-2003. *Yonsei Med J*. 2004;45:462–8.
 50. Hanaki Y, Kamiya H, Todoroki H, et al. New two-dimensional, echocardiographically directed pericardiocentesis in cardiac tamponade. *Crit Care Med*. 1990;18:750–3.
 51. Molkara D, Tejman-Yarden S, El-Said H, et al. Pericardiocentesis of noncircumferential effusions using nonstandard catheter entry sites guided by echocardiography and fluoroscopy. *Congen Heart Dis*. 2011;6:461–5.
 52. De Carlini CC, Maggiolini S. Pericardiocentesis in cardiac tamponade: indications and practical aspects. *E-journal Cardiol Pract*. 2017;15(19). <https://www.escardio.org/Journals/E-Journal-of-Cardiology-Practice/Volume-15/Pericardiocentesis-in-cardiac-tamponade-indications-and-practical-aspects>.
 53. Gieffer MJ, Murray KF, Colletti RB. Pathophysiology, diagnosis, and management of pediatric ascites. *J Pediatr Gastroenterol Nutr*. 2011;52:503–13.
 54. Kramer RE, Sokol RJ, Yerushalmi B, et al. Large-volume paracentesis in the management of ascites in children. *J Pediatr Gastroenterol Nutr*. 2001;33:245–9.
 55. Runyon BA. Paracentesis of ascitic fluid: a safe procedure. *Arch Intern Med*. 1986;146:2259–61.
 56. Lane ER, Hsu EK, Murray KF. Management of ascites in children. *Exp Rev Gastroenterol Hepatol*. 2015;9:1281–92.
 57. Mercaldi CJ, Lanes SF. Ultrasound guidance decreases complications and improves the cost of care among patients undergoing thoracentesis and paracentesis. *Chest*. 2013;143:532–8.
 58. Millington SJ, Koenig S. Better with ultrasound: paracentesis. *Chest*. 2018;154:177–84.
 59. Nazeer SR, Dewbre H, Miller AH. Ultrasound-assisted paracentesis performed by emergency physicians vs the traditional technique: a prospective, randomized study. *Am J Emerg Med*. 2005;23:363–7.
 60. Sekiguchi H, Suzuki J, Daniels CE. Making paracentesis safer: a proposal for the use of bedside abdominal and vascular ultrasonography to prevent a fatal complication. *Chest*. 2013;143:1136–9.
 61. Stone JC, Moak JH. Feasibility of sonographic localization of the inferior epigastric artery before ultrasound-guided paracentesis. *Am J Emerg Med*. 2015;33:1795–8.
 62. Baumann BM, McCans K, Stahmer SA, et al. Volumetric bladder ultrasound performed by trained nurses increases catheterization success in pediatric patients. *Am J Emerg Med*. 2008;26:18–23.
 63. Buntsma D, Stock A, Bevan C, et al. Success rate of BladderScan-assisted suprapubic aspiration. *Emerg Med Australas*. 2012;24:647–51.
 64. Chen L, Hsiao AL, Moore CL, et al. Utility of bedside bladder ultrasound before urethral catheterization in young children. *Pediatrics*. 2005;115:108–11.
 65. Gochman RF, Karasic RB, Heller MB. Use of portable ultrasound to assist urine collection by suprapubic aspiration. *Ann Emerg Med*. 1991;20:631–5.
 66. Kiernan SC, Pinckert TL, Keszler M. Ultrasound guidance of suprapubic bladder aspiration in neonates. *J Pediatr*. 1993;123:789–91.
 67. Milling TJ Jr, Van Amerongen R, Melville L, et al. Use of ultrasonography to identify infants for whom urinary catheterization will be unsuccessful because of insufficient urine volume: validation of the urinary bladder index. *Ann Emerg Med*. 2005;45:510–3.
 68. Marin JR, Shaikh N, Docimo SG, Hickey RW, Hoberman A. Lectures for you. Suprapubic bladder aspiration [Video]. YouTube. 2015. <https://www.youtube.com/watch?v=QRHOYcVC1-E>.



Use of Ultrasound in ECMO

Ivanna Maxson and Erik Su

Contents

Introduction	291
Precannulation	292
Venous Cannulation	292
Arterial Cannulation	293
Cannulation	293
ECMO Complications	294
Myocardial Function	294
Tamponade	294
Pulmonary Consolidation, Pneumothorax, and Effusions	295
Thrombosis and Spontaneous Contrast	295
De-Escalation of ECMO	296
Conclusion	296
References	297

Introduction

The use of point-of-care ultrasound (POCUS) for evaluating patients receiving extracorporeal membrane oxygenation (ECMO) support is controversial. Loading conditions of the heart change on venoarterial ECMO and cardiac motion measured using traditional echocardiography reflects not just myocardial health but rate of blood removal from the heart. This consequently affects quanti-

tative measurements, limiting its diagnostic assessment of cardiac function, a common indication for echocardiography on ECMO patients [1]. Despite limitations to quantitative physiologic assessment, ultrasound readily visualizes ECMO cannulas. Further, cardiac anatomic considerations and diagnostic applications in evaluating ECMO complications are nonquantitative applications that are clinically meaningful.

The American Society of Echocardiography has described multiple indications for echocardiographic assessment of the ECMO patient [2]. These include:

I. Maxson · E. Su (✉)
Division of Critical Care Medicine, Department of
Pediatrics, Baylor College of Medicine, Texas
Children's Hospital, Houston, TX, USA
e-mail: erik.su@bcm.edu

1. Precannulation diagnosis of reversible causes of hemodynamic instability
2. Cannula positioning
3. Identification of septal defects
4. Identification of complications including tamponade, thrombosis, left atrial and left ventricular decompression
5. Monitoring during ECMO weaning including the assessment of valvular function and changes in ventricular function

These applications suggest arenas where echocardiography, and potentially POCUS as employed by the intensivist, could facilitate routine ECMO management in conjunction with other assessment modalities throughout all phases of caring for an ECMO patient.

Precannulation

In the precannulation setting, ultrasound can be instrumental in helping identify important issues pertinent to ECMO candidacy. This includes the identification of vessel patency for candidate cannulation sites. Candidate vessels should be able to accommodate appropriately sized cannula at their narrowest cross-sectional dimension. The decision to dilate narrowed vessels is left to the

discretion of the provider performing cannulation.

Another fundamental ultrasound application in ECMO candidacy is identifying life-threatening bleeding in potential spaces such as the thorax, peritoneum, and potentially the extra-axial space around the brain if hematoma volumes are sufficient and visualizable.

Venous Cannulation

Venous cannulation with a single or dual-lumen cannula can be assisted using traditional transverse or longitudinal views on ultrasound of the internal jugular vein. Similarly, femoral cannulation using a single lumen cannula is also possible using these views. In both percutaneous and cut-down approaches, estimates regarding appropriate cannula size can be performed with ultrasound. Diameter measurements of venous structures are challenging due to their cylindrical shapes. Accurate measurements are best achieved by ensuring the probe is perpendicular to the axis of the vessel from external inspection and measuring the circumference of the vessel using measurement tools commonly available on ultrasound equipment (Fig. 1). Since this circumferential measurement ($\text{Circumference} = \pi \times \text{Diameter}$)

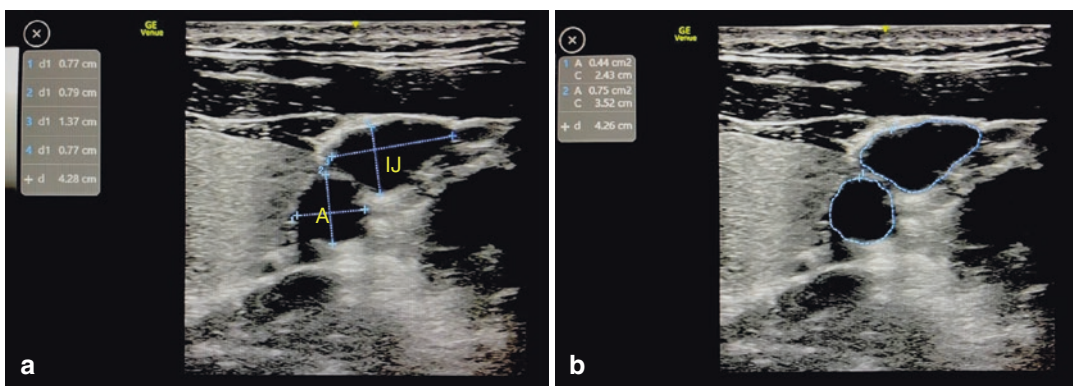


Fig. 1 Transverse measurements of right internal jugular (IJ) vein and carotid artery dimensions at the level of the bifurcation of the head of the sternocleidomastoid muscles. **(a)** Linear dimensions demonstrate approximate horizontal (1) and vertical (2) measurements of the carotid artery **(a)** consistent with a diameter of approximately 7.8 mm (~24F) and discrepant IJ horizontal (3) and verti-

cal (4) measurements of 13.7 mm and 0.77 mm, respectively. **(b)** Circumferential measurements of the vessels yield a carotid circumference of 24.3 mm, identical to the French size estimated with the diameter measurement above, and an IJ diameter of 35.2 mm which suggests a 35F device would fit in the vessel in the area visualized

approximates French size (equal to $3 \times$ Diameter), it will more likely give a sense of appropriate cannula dimension than a simple linear diameter measurement. The course of the vessel should be visualized as much as possible transcutaneously. Visualization of the superior vena cava (SVC) and right atrium (RA) is facilitated by transesophageal echocardiography using mid-esophageal and transgastric views. During ultrasound-guided percutaneous cannulation, providers can identify posterior luminal wall puncture of the vein which may increase the risk of bleeding complications in the event of converting to a cut-down approach. In the case of needing to access or repair the venotomy in the future, selecting a site where vascular puncture is cephalad enough in the neck for a surgical approach should be considered.

Arterial Cannulation

Arterial cannulation in venoarterial ECMO can be approached with ultrasound in a similar manner to venous cannulation with the exception that a simple diameter measurement, multiplied by three, is sufficient for approximation of the carotid or femoral artery dimension given that the profile of the artery is more circular. Exceptions may exist in situations of atypical or distorted anatomy, where sizing is at the discretion of the cannulating operator.

Cannulation

During cannulation, transthoracic echocardiography is often impractical without prior coordination with the cannulating team. Transesophageal echocardiography is possible with an experienced operator. Transthoracic imaging can be performed below a sterile field by an ultrasound operator or above the sterile field by the surgical team.

A right ventricular (RV) inflow view (Fig. 2) is helpful for identifying a venous side cannula and its depth of insertion into the heart. Subcostal inferior vena cava (IVC) longitudinal and trans-

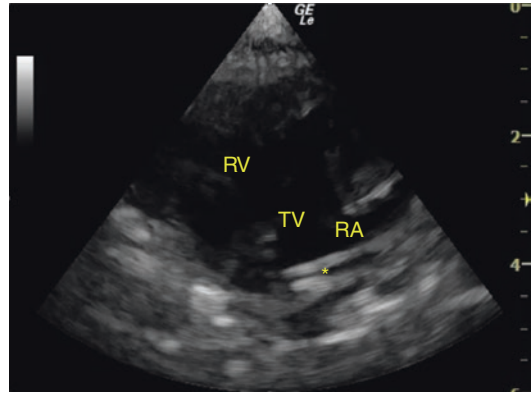


Fig. 2 Right ventricular inflow view with venous side cannula inserted from the right internal jugular vein. Cannula is marked with asterisk (*). RV Right Ventricle, RA Right Atrium, TV Tricuspid Valve

verse views are useful for identifying the position of the cannula tip as it approaches the inferior cavoatrial junction. Conventions for depth of insertion are often center-dependent and may vary between the placement of the tip above the cavoatrial junction to several centimeters distal in the IVC. Color Doppler is instrumental in assuring that the return jet from a dual-lumen cannula is aimed at the tricuspid valve using both sagittal (RV inflow) and axial (subcostal transverse IVC) views. Ultrasound can also be used to visualize femoral cannulation as the cannula ascends the IVC to terminate near the inferior cavoatrial junction (Fig. 3). Views of the central veins may be possible from the right neck down to the cavoatrial junction in cases of severe pulmonary consolidation or effusions, chest masses, and other situations where air has been evacuated from the thoracic space overlaying the SVC.

Views of the aorta can be obtained for venoarterial cannulation as well. High parasternal cervical views are often not possible during cannulation due to proximity to the cannula insertion site. To visualize the aortic arch, the probe can be placed in the patient's left or right parasternal region at the level of the sternal angle. The probe should be oriented longitudinally to capture the entire course of the ascending aorta, and with the probe face pointing towards the patient's left scapula if they have a normal arch orientation (Fig. 4). If the arch is not visualizable from this plane, a

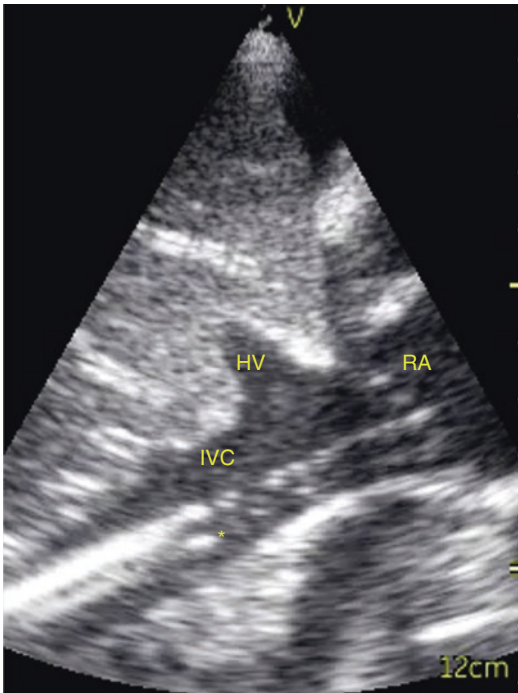


Fig. 3 IVC view of venous side cannula inserted via common femoral vein. Cannula is marked with asterisk (*). *IVC* Inferior Vena Cava, *HV* Hepatic Vein, *RA* Right Atrium

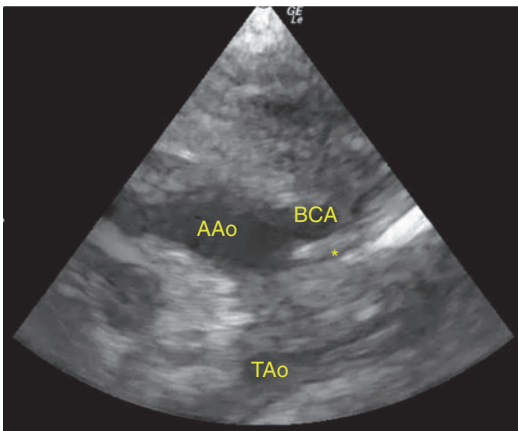


Fig. 4 Aortic arch view of the arterial cannula. Cannula is marked with asterisk (*). *AAo* Ascending Aorta, *BCA* Brachiocephalic Artery, *TAo* Transverse Aortic Arch

suprasternal view may be possible but extension of the neck for imaging is highly discouraged. The tip of the arterial return cannula should be positioned at the takeoff of the right brachioce-

phalic artery, which is the first branching artery of the aorta above the coronaries. A low cannula that propels blood against the aortic valve is deleterious to cardiac recovery.

ECMO Complications

Myocardial Function

Left ventricular (LV) failure on ECMO is a recognized complication caused by an inability of the ventricle to tolerate afterload and is characterized by progressive dilation and dysfunction with resultant increased wall stress and ischemia. This may progress to the point at which recovery is improbable. To mitigate this, ECMO teams may employ one of several interventions. These include Rashkind atrial septostomy in the young patient, and central LA venting through a sternotomy. Identification of an atrial septal defect depends upon a detailed examination of the atrial septum using multiple views and comprehensive diagnostic echocardiography is recommended for this assessment. Other proposed interventions have included pulmonary artery cannula placement for which some ventricular assist devices and ECMO cannula options are available.

In evaluating this phenomenon, the left heart will be unable to eject against the blood pressure necessary to sustain life and standard cardiac ultrasound views from the parasternal, apical, and subcostal windows reveal progressive left ventricular and atrial dilatation and myocardial dysfunction progressing to cardiac standstill irrespective of the function of the right heart. Cardiac ultrasound provides a readily accessible assessment tool at the bedside for serial monitoring of cardiac motion and chamber dilatation.

Tamponade

Tamponade physiology due to pericardial effusion is potentially challenging on ECMO as traditional signs of tamponade are potentially obscured by issues related to ECMO. For instance, the presence of cannulas at the inferior

cavoatrial junction may interfere with the assessment of IVC distention. Right atrial pressures may not be elevated in venoarterial ECMO, and ventilatory strategy and lung compliance may affect the assessment of atrioventricular valve inflow velocity. In contrast, circuit performance is potentially reassuring on venovenous ECMO in spite of hemodynamic instability [3]. In the published literature, tamponade often appears confirmed by precipitous hemodynamic insufficiency [4, 5]. In these cases, ultrasound is frequently a confirmatory modality for making a time-sensitive diagnosis in cases where other clinical data was unclear, particularly in cases of cardiac perforation by the ECMO cannula [6].

Pulmonary Consolidation, Pneumothorax, and Effusions

Extremes of pulmonary aeration are readily visualizable using ultrasound. Consolidation, particularly in patients receiving ECMO for respiratory reasons, may be dramatic and can appear as extensive hepatization of the pulmonary parenchyma permitting visualization of intrathoracic structures with little air artifact. A pneumothorax can be visualized and diagnosed with ultrasound as well, though pleural sliding might either become less apparent due to decreased lung compliance and movement with tidal volume or more apparent because consolidation permits easier visualization. Radiographic correlations are recommended for procedural intervention for pneumothoraces and effusions to assess the depth of device insertion, though ultrasound can provide real-time guidance in percutaneous procedures that may reduce the likelihood of an inadvertent bleeding injury.

Similar to pneumothorax, ultrasound applications for identifying pleural and pericardial effusions can also be applied to assess patients before or after cannulation (Fig. 5). Procedures for addressing these collections also benefit from correlating X-rays, as well as active procedural guidance for percutaneous drainage while on ECMO.

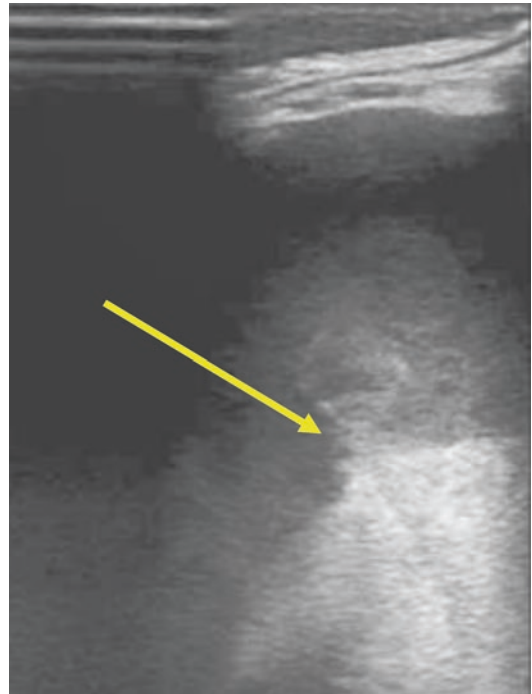


Fig. 5 Hemothorax in a child on ECMO with acute hypotension. Ultrasound identified a location of pulsatile bleeding from the lung which was the source of the acute hemothorax and etiology of hemodynamic instability

Thrombosis and Spontaneous Contrast

Ultrasound reflections occur at boundaries between media that differ in acoustic impedance, which in turn is dependent on density and speed of sound in the medium. Within blood, presuming the speed of sound is approximate throughout the volume, a primary factor affecting its echogenicity is therefore density. Changes in blood density from infusions or coagulation are visualizable using ultrasound. Acute changes can occur from both continuous and bolus infusions, as well as from sluggish flow leading to the increasing density of pooled or static blood. This can result in echogenicity in the blood known as *spontaneous contrast* (Fig. 6). This is commonly seen in infusions as particulate-appearing bright echogenic speckles in the blood flow and it may also appear in areas where blood is pooling with little flow as may be the case in severe LV failure

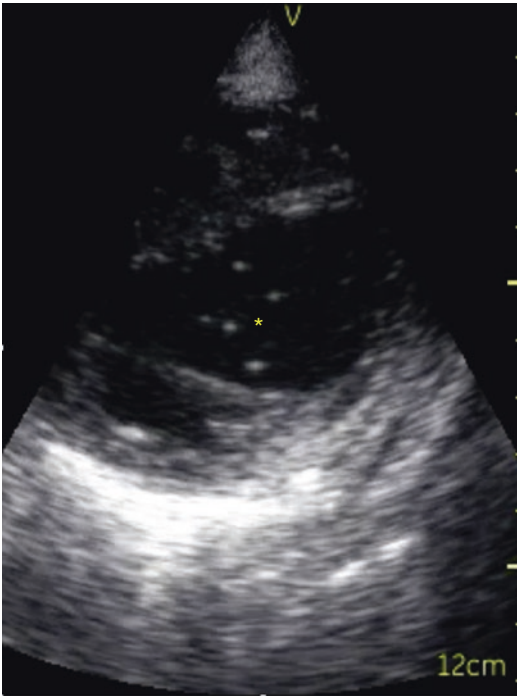


Fig. 6 Spontaneous contrast in the LV of a patient with severely depressed LV systolic function denoted by asterisk (*), modified subcostal 4-chamber view

or cardiac arrest. Air may also appear as echogenic speckles in the blood flow from infusions and commonly travels away from gravity and casts air artifact below it.

Blood pooling in cardiac chambers may progress to echogenic masses and early-on might remain liquid, as evidenced by postmortem examination, but remain indicative of the severity of illness [7]. In vascular spaces, thrombosis may appear at varying levels of echogenicity and brief and limited compression is recommended for elucidating whether the clot is solid. Repeated compression may cause thrombosis to embolize and is therefore discouraged. Blood stasis is the first part of Virchow's Triad as a significant risk factor for thrombosis, and in hemodynamic failure necessitating ECMO thrombi can of course appear anywhere in the circulation. Anticoagulation has a fundamental role in ECMO management. Therefore, ultrasound assessments for thrombi throughout the vascular system are useful and akin to other deep vein thrombosis

visualization techniques used in non-ECMO patients. Ultrasound of ventricular assist devices [8] has also been proposed for device monitoring including membrane function and valve competence. Findings of thrombi require multidisciplinary management in ECMO and therefore full diagnostic imaging by consulting services is likely helpful in cases where a suspected thrombus is identified.

De-Escalation of ECMO

Weaning ECMO with ultrasound guidance is relevant primarily in ECMO for hemodynamic causes in the absence of right heart failure. A stepwise de-escalation of support incorporating periodic serial imaging for evaluation of left and right heart function, and aortic valve opening in accordance with institutional protocol is a generally accepted approach. Findings consistent with worsening heart failure during reduction of support would be suspicious for a wean failure. Use of apical windows permits monitoring the function of each side of the heart, as well as the freedom to Doppler both ventricular inflows and outflows. Regarding quantitative measures useful for ECMO, a 21 patient prospective series of children receiving ECMO for hemodynamic support demonstrated that only augmentation of LV outflow tract velocity integral with ECMO support wean was predictive of cardiac survival in comparison to other quantitative 2D markers and strain [1]. Similar findings have been noted in adult ECMO patients as well [9].

Conclusion

Ultrasound is well-suited to imaging of an ECMO patient in terms of practicality and relative operational safety. Multiple applications in hemodynamic and respiratory support evaluating cardiac and pulmonary health are useful for caring for the ECMO patient. Clinicians should interpret full quantitative echocardiography findings with caution given alterations in cardiac loading status while on ECMO however this is a developing

field. Additional investigation is warranted into the efficacy and utility of ultrasound, including both traditional echocardiography as well as POCUS applications guided by the intensivist, in augmenting care of the pediatric ECMO patient.

References

1. Punj R, Axelrod DM, Sherman-Levine S, Roth SJ, Tacy TA. Predictors of mortality in pediatric patients on venoarterial extracorporeal membrane oxygenation. *Pediatr Crit Care Med*. 2014;15(9):870–7. <https://doi.org/10.1097/PCC.0000000000000236>.
2. Platts DG, Sedgwick JF, Burstow DJ, Mullany DV, Fraser JF. The role of echocardiography in the management of patients supported by extracorporeal membrane oxygenation [published correction appears in *J Am Soc Echocardiogr*. 2012 Apr;25(4):427]. *J Am Soc Echocardiogr*. 2012;25(2):131–41. <https://doi.org/10.1016/j.echo.2011.11.009>.
3. Yates AR, Duffy VL, Clark TD, et al. Cardiac tamponade: new technology masking an old nemesis. *Ann Thorac Surg*. 2014;97(3):1046–8. <https://doi.org/10.1016/j.athoracsur.2013.06.126>.
4. Basilio C, Fontoura A, Fernandes J, Roncon-Albuquerque R Jr, Paiva JA. Cardiac tamponade complicating extracorporeal membrane oxygenation: a single-centre experience. *Heart Lung Circ*. 2021;30(10):1540–4. <https://doi.org/10.1016/j.hlc.2021.05.078>.
5. Zhang Z. Echocardiography for patients undergoing extracorporeal cardiopulmonary resuscitation: a primer for intensive care physicians. *J Intensive Care*. 2017;5:15. Published 2017 Feb 2. <https://doi.org/10.1186/s40560-017-0211-6>.
6. Hirose H, Yamane K, Marhefka G, Cavarocchi N. Right ventricular rupture and tamponade caused by malposition of the Avalon cannula for venovenous extracorporeal membrane oxygenation. *J Cardiothorac Surg*. 2012;7:36. Published 2012 Apr 20. <https://doi.org/10.1186/1749-8090-7-36>.
7. Cui Y, Wang R, Yang F, Hou X. Spontaneous echo contrast mimicking left ventricular thrombus in a patient on extracorporeal membrane oxygenation support. *Chest*. 2021;159(6):e437–9. <https://doi.org/10.1016/j.chest.2020.06.090>.
8. Di Molfetta A, Iacobelli R, Ferrari G, et al. A new 2D echocardiographic approach to evaluate the membrane and valve movement of the Berlin heart EXCOR VAD chamber in pediatric VAD patients. *Artif Organs*. 2018;42(4):451–6. <https://doi.org/10.1111/aor.13122>.
9. Aissaoui N, Luyt CE, Leprince P, et al. Predictors of successful extracorporeal membrane oxygenation (ECMO) weaning after assistance for refractory cardiogenic shock. *Intensive Care Med*. 2011;37(11):1738–45. <https://doi.org/10.1007/s00134-011-2358-2>.

Part VIII

**Programmatic Considerations and Moving
Forward**



POCUS Guidelines, Training Curriculum, and Education

Thomas Conlon, Sam Rosenblatt,
Adam S. Himebauch, Christie Glau,
Yogen Singh, and Akira Nishisaki

Contents

Introduction	301
Problem Identification and General Needs Assessment	302
Targeted Needs Assessment	302
Goals and Objectives	304
Educational Strategies	306
Conclusion	306
References	306

T. Conlon (✉)

Department of Anesthesiology and Critical Care
Medicine, Children's Hospital of Philadelphia,
Perelman School of Medicine University of
Pennsylvania, Philadelphia, PA, USA

The Children's Hospital of Philadelphia,
Philadelphia, PA, USA
e-mail: Conlont@chop.edu

S. Rosenblatt · A. S. Himebauch
C. Glau · A. Nishisaki
Department of Anesthesiology and Critical Care
Medicine, The Children's Hospital of Philadelphia,
Philadelphia, PA, USA

Perelman School of Medicine, University of
Pennsylvania, Philadelphia, PA, USA
e-mail: Rosenblatts@chop.edu;
Himebaucha@chop.edu; GlauC@chop.edu;
Nishisakia@chop.edu

Y. Singh
Department of Pediatrics, Division of Neonatology,
Loma Linda University School of Medicine,
California, USA

Introduction

Use of point of care ultrasound (POCUS) has exponentially grown across pediatric non-imaging disciplines including neonatal and pediatric critical care medicine, emergency medicine, and ambulatory pediatric medicine. Recently evidence-based international guidelines, endorsed by the European Society of Pediatric and Neonatal Intensive Care (ESPNIC), on the use of POCUS in neonatal and pediatric intensive care units have been published.

Department of Pediatrics, Division of Neonatal and
Developmental Medicine, Stanford University School
of Medicine, California, UK

Department of Pediatrics, Division of Neonatology,
University of Southern California, California, UK

ESPNIC Cardiovascular Dynamics Section and
POCUS Working Group, Geneva, Switzerland
e-mail: YSingh@llu.edu

Table 1 Translating the Kern model of curricular development to focused ultrasound curricular development

Kern model	Ultrasound curricular considerations
1. Problem identification and general needs assessment	Identify the role of ultrasound in local clinical practice (<i>why</i>)
2. Targeted needs assessment	Assess the needs of the patient and the provider within practice context (<i>what</i>)
3. Goals and objectives	Goals and objectives to encompass provider, patient, and program
4. Educational strategies	Embrace adult learning theory to develop provider competence (<i>how</i>)
5. Implementation	Building an infrastructure to translate training to clinical practice (<i>structure, process</i>)
6. Evaluation and feedback	Outcome measures for providers, patients, and programs

These guidelines emphasize the need to develop training curriculum and certification/accreditation process specifically for neonatologists and pediatric intensivists. Yet, *how* to train providers is dependent upon *what* to train providers. Thus, the first step in training is to define relevant applications which will lead to curricular learning objectives. Educators tasked with developing curriculum early in the adoption of focused ultrasound relied upon their own knowledge of ultrasound and their respective context of practice to determine applications and objectives.

Education necessarily embraces elements beyond simply defining the scope of clinical practice. The *Kern model* of curricular development can be used to outline key requirements for effective educational delivery [1]. This model highlights six important elements in medical curricular design that are adaptable to bedside ultrasound training for pediatric critical care providers (Table 1) and is a useful framework for developing an ultrasound educational model. Data suggest that POCUS education is most effectively delivered when programs have robust infrastructural support mechanisms as discussed in Chap. 22: “Current and Future Challenges to Ultrasound Adoption in Clinical Practice”. Thus, this chapter will focus on the first four elements within Kern’s model.

Problem Identification and General Needs Assessment

The first element in designing a curriculum is problem identification and general needs assessment which helps to identify how ultrasound might impact our clinical practice. Once a cohesive argument can be made that ultrasound is likely to improve provider performance and patient outcomes within a domain of practice, there can be buy-in from stakeholders at all levels including the provider, division, department, and institution. This multilevel, multidisciplinary approach to structuring and implementing an ultrasound program likely offers the greatest opportunity for success and sustainability. We believe that the content of this book speaks for itself. Point of care ultrasound in the hands of non-radiology-based clinicians (i.e., non-cardiology, non-radiology specialists) indisputably impacts and improves the care we provide patients, with new applications tailored to varied practice domains constantly evolving. Thus, the “*why*” of POCUS use is decreasing as a barrier to widespread educational development.

Targeted Needs Assessment

Ultrasound performance must be tailored to the patients encountered within the clinical setting and the needs of the providers in that setting. Three characteristics render a procedural or diagnostic application conducive to ultrasound training for incorporation in patient care: (1) the procedure or diagnosis is *frequent*, i.e., commonly encountered in the respective clinical setting; (2) the procedure or diagnosis is *amenable* to ultrasound technology, i.e., performance of a procedure can be augmented by concurrent ultrasound use or a diagnosis can be elucidated through ultrasound interrogation; and (3) the procedure or diagnosis has *discrete* outcomes, i.e., success/failure, present/absent, normal/mild/moderate/severe, etc. Curricular design for the translation of POCUS training to clinical care should embrace applications that can be frequently utilized within the context of a

provider’s care. For example, the American College of Emergency Physicians has published and updated core applications for the adult emergency medicine ultrasound curriculum [2]. While an abdominal aortic aneurysm is something frequently encountered in adult populations, this disease process does not occur in pediatric populations and likely would not be an appropriate application within a basic pediatric POCUS educational curriculum. Further, the emphasis on training in cranial ultrasound may differ in institutions where neonatology and pediatric critical care providers are housed within separate divisions. POCUS technology adoption is heavily influenced by its environment. Thus, modifications to core applications should be specialty-specific, as has been suggested within

pediatric critical care (Fig. 1) [3]. Finally, the current educational curricula available to providers, their baseline knowledge, and baseline skills should be assessed in order to understand their specific needs and help guide the educational efforts in the most appropriate direction.

With the increasing adoption of POCUS in clinical practice across traditionally non-imaging specialties, respective Societies are developing guidelines, statements, and policies outlining pediatric specialty-specific curriculum and considerations to develop best practice parameters (Table 2) [4–9]. Existing literature supports that POCUS image acquisition and interpretation skills by novices improve rapidly after short focused training when discrete measures are employed during interpretation [10–12]. We

Fig. 1 Modifying Adult Emergency Medicine Core Applications to Pediatrics Using Critical Care as an Example

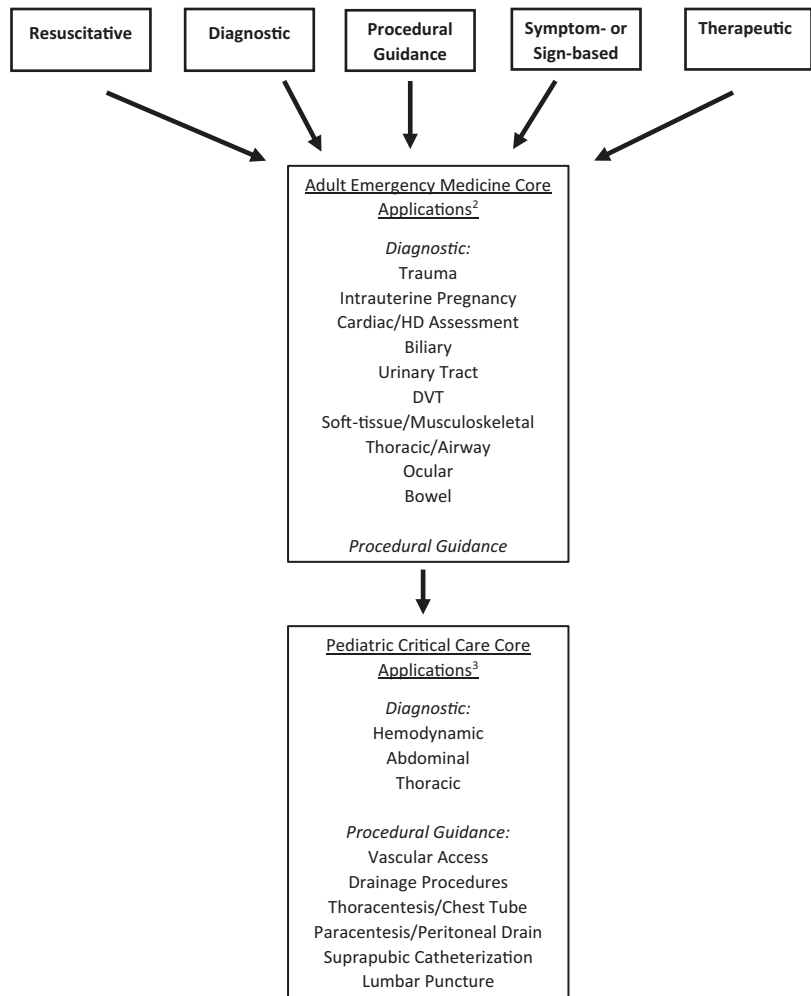


Table 2 Guidelines, policies, and statements from societies regarding pediatric focused ultrasound

Pediatric society	Specialty	Year of publication	Endorsements	Methodology	Content	Notes
European Society of Paediatric and Neonatal Intensive Care [4]	Critical Care and Neonatology	2021		GRADE, RAND	Guidelines across all focused ultrasound applications	Does not discuss incorporation into practice
American Academy of Pediatrics [5]	Emergency Medicine	2015	SAEM, ACEP, WINFOCUS	Descriptive	Statement describing the incorporation of focused ultrasound in clinical practice	Does not discuss specific applications
Society of Critical Care Medicine [6, 7]	Critical Care	2015, 2016		GRADE, RAND	Pediatric considerations within adult critical care-focused ultrasound guidelines	Limited pediatric guidelines
AAP Section of Emergency Medicine Fellowship Directors Subcommittee [8]	Emergency Medicine	2013		Consensus	Suggested clinical applications and programmatic elements for incorporation of focused ultrasound in clinical practice	
WINFOCUS [9]	Neonatology	2020	Lung Ultrasound Training Base of China, Chinese College of Critical Ultrasound	Literature review among experts	Development of a standardized lung ultrasound protocol	Limited to lung ultrasound

AAP American Academy of Pediatrics, WINFOCUS World Interactive Network Focused on Critical Ultrasound, SAEM Society for Academic Emergency Medicine, ACEP American College of Emergency Physicians, GRADE Grading of Recommendations Assessment, Development, and Evaluation

must also be cautious when defining what *is* and *is not* amenable to point of care ultrasonography. For many years clinicians believed that ultrasound of the lung would be an irrelevant practice since the well-aerated lung is inhospitable to ultrasound wave transduction. Yet Lichtenstein, among others, identified and expanded lung ultrasound clinical use [13], and we now use lung POCUS to diagnose the etiology of respiratory failure, guide therapies, and titrate supportive strategies (*see* Chap. 13 “Clinical Applications in Focused Thoracic Assessment in

Neonates”). What is “true” now may not always remain that way, and there must be frequent revisitation of clinical applications as our skills and ultrasound technologies evolve together.

Goals and Objectives

When developing an educational platform, whether for POCUS use or another area of clinical inquiry, it is important to recognize that defining educational goals/outcomes is crucial to success-

ful educational delivery. The *Halstedian model* embracing “*see one, do one, teach one*” is an oversimplification of complex interactions between providers, technologies, and patients. Use of POCUS incorporates different domains of competence for providers (knowledge, psychomotor, and interpretative), domains of performance for the technology (comparisons to gold standards), interactions between provider and technology (feasibility and interrater reliability), and domains of patient outcomes (direct and indirect impact of POCUS within clinical care).

Once applications are defined within a scope of clinical practice, educators must develop objectives for training. These objectives should be measurable, focused and specify processes and outcomes relevant to the application. Bloom’s taxonomy of learning progresses from basic evaluation of knowledge and comprehension, then advances to understanding, application, and then analyzing educational objectives [14]. For example, objectives for the assessment of the inferior vena cava for volumetric assessment might describe requisite views (transverse \pm longitudinal) and might build to interpretative methodology (morphology, inferior vena cava-to-aorta ratio, qualitative respiratory variation, quantitative respiratory variation) based upon the goal of study performance. As providers gain experience and new data emerges within the ultrasound landscape, similar to core applications themselves, respective goals and objectives may change and become more complex moving up the pyramid of learning. Goals and objectives should also be periodically revisited and updated accordingly if and when needed.

Applications and respective learning objectives likely have variable difficulty in knowledge, psychomotor, and interpretative skill development. Some groups have suggested creating “Basic” and “Advanced” applications, recognizing discrepancies in either the ease of uptake or frequency of use between applications. There may even be utility in distinguishing between evaluative domains for learners as discussed above (knowledge, psychomotor, interpretative)

and recognition that within an application, a knowledge domain may be taught at the *Basic level* though its corresponding psychomotor and interpretative domain remain *Advanced*. For example, discussing the methodology of measuring ejection fraction using Simpson’s method as a means of determining left ventricular systolic function may be relevant to the Basic learner. Such a discussion teaches (1) how using two planes of a two-dimensional image can be integrated to model a three-dimensional structure, (2) how three-dimensional modeling may overcome *some* limitations inherent in two-dimensional assessment, and (3) how three-dimensional modeling continues to have its own limitations in functional assessment due to load dependence as well as challenges in measurement. In developing a curriculum that includes left ventricular systolic assessment as a core application, educators may define basic knowledge objectives to understand qualitative evaluation or fractional shortening measurements, psychomotor objectives for learners to obtain adequate images, and finally combine the knowledge and psychomotor objectives into *interpretive objectives* to be able to appropriately interpret the images obtained. Knowledge of Simpson’s method can further support an understanding of the strengths and limitations of qualitative evaluation and fractional shortening without necessarily being required as a component of Basic psychomotor and interpretative performance.

We should also recognize that learners themselves may have different rates at which they achieve targeted objectives. Individualized learning curves have been used across many areas of educational assessment [15]. Utilization of such curves requires a targeted outcome, though, which should define *competence* within the educational domain. *Competence* in critical care ultrasound is defined as the implicit, internalized knowledge of bedside ultrasound for clinical benefit [16]. Yet we do not have well-defined thresholds of competence in pediatric POCUS applications or objectives as they translate to clinical care. This is an area of particular interest

and importance in the neonatal and pediatric POCUS community.

Educational Strategies

Educational strategies for ultrasound training should be devised to integrate adult learning theory. Trainee's independence and experience should be respected and embraced. The educational structure should be problem-centered and emphasis should be placed on how this newly acquired knowledge will be utilized in the learner's daily practice [17].

Though there are no POCUS education outcome data regarding longitudinal curriculum, we know that educational outcomes in ultrasound training are dependent upon the educational methods employed. Recent literature suggests that knowledge retention is optimized through shorter, case-based lectures on focused ultrasound topics, though overall retention by novice learners is poor 2 weeks following training [18]. In our institution, POCUS studies by trainees fulfilling criteria for hemodynamic US competency showed statistically significant improvement in image interpretation score compared with those not completing criteria for competency using a pediatric cardiologist as a reference standard [19]. Further, the literature also suggests that maintaining ultrasonography skills requires ongoing utilization in the clinical setting [20]. Borrowing knowledge from other simulation-based studies including ultrasound-guided central vascular access, we favor adapting "mastery training" techniques to our POCUS educational paradigm [21–23]. Use of the deliberate practice model is helpful to obtain mastery learning in which learners deliberately choose portions of focused ultrasound to practice after self-reflection and assessment to understand their individual needs [24, 25]. With deliberate practice, learners could use an ultrasound simulator to focus on particularly challenging views to obtain, spending extra time on this area of need rather than spending time on obtaining and practicing a full POCUS evaluation.

More robust studies evaluating the optimization of both initial and maintenance training are required to better evaluate optimal training methods. And we need to recognize that a "one-size-fits-all" mentality towards educational standardization is likely insufficient in overcoming local barriers to training. But there are likely common themes to successful POCUS educational programs and such themes should continue to be explored [26].

Conclusion

Developing a standardized training curriculum is an essential first step towards training competent providers in the use of POCUS in neonates and children followed by a structured training program and certification/accreditation process while ensuring robust clinical governance and quality assurance. The question "why" use POCUS in clinical practice is now obviated by the robust literature supporting its use within and across traditionally non-imaging disciplines. Specialties must now define the "what" and the "how" of effectively translating education into practice. Kern's framework for curricular development can structure our approach to developing meaningful education. Outcomes relevant to providers, the technology, and our patient populations are currently poorly defined and will require careful consideration as the use of POCUS increases across the spectrum of pediatric care.

References

1. Kern DE, Thomas PA, Howard DM, Bass EB. Curriculum development for medical education: a six-step approach. Baltimore: Johns Hopkins University Press; 2006.
2. Ultrasound guidelines: emergency, point-of-care and clinical ultrasound guidelines in medicine. *Ann Emerg Med.* 2017;69:e27–e54.
3. Conlon TW, Himebauch AS, Fitzgerald JC, et al. Implementation of a pediatric critical care focused bedside ultrasound training program in a large academic PICU. *Pediatr Crit Care Med.* 2015;16:219–26.
4. Singh Y, Tissot C, Fraga MV, et al. International evidence-based guidelines on point of care ultrasound

- (POCUS) for critically ill neonates and children issued by the POCUS Working Group of the European Society of Paediatric and Neonatal Intensive Care (ESPNIC). *Crit Care*. 2020;24:65.
5. Marin JR, Lewis RE. Point-of-care ultrasonography by pediatric emergency medicine physicians. *Pediatrics*. 2015;135:e1105–6.
 6. Frankel HL, Kirkpatrick AW, Elbarbary M, et al. Guidelines for the appropriate use of bedside general and cardiac ultrasonography in the evaluation of critically ill patients—Part I: general ultrasonography. *Crit Care Med*. 2015;43:2479–502.
 7. Levitov A, Frankel HL, Blaivas M, et al. Guidelines for the appropriate use of bedside general and cardiac ultrasonography in the evaluation of critically ill patients—Part II: cardiac ultrasonography. *Crit Care Med*. 2016;44:1206–27.
 8. Vieira RL, Hsu D, Nagler J, et al.; American Academy of Pediatrics. Pediatric emergency medicine fellow training in ultrasound: consensus educational guidelines. *Acad Emerg Med*. 2013;20:300–306.
 9. Liu J, Copetti R, Sorantin E, et al. Protocol and guidelines for point-of-care lung ultrasound in diagnosing neonatal pulmonary diseases based on international expert consensus. *J Vis Exp*. 2019;(145).
 10. Pershad J, Myers S, Plouman C, et al. Bedside limited echocardiography by the emergency physician is accurate during evaluation of the critically ill patient. *Pediatrics*. 2004;114:e667–71.
 11. Longjohn M, Wan J, Joshi V, et al. Point-of-care echocardiography by pediatric emergency physicians. *Pediatr Emerg Care*. 2011;27:693–6.
 12. Spurney CF, Sable CA, Berger JT, et al. Use of hand-carried ultrasound device by critical care physicians for the diagnosis of pericardial effusions, decreased cardiac function, and LV enlargement in pediatric patients. *J Am Soc Echocardiogr*. 2005;18:313–9.
 13. Lichtenstein DA. Lung ultrasound in the critically ill. *Ann Intensive Care*. 2014;4(1):1.
 14. Bloom BS (editor), Engelhart MD, Furst EJ, Hill WH, Krathwohl DR. Taxonomy of educational objectives, handbook I: the cognitive domain. New York, David McKay, 1956.
 15. Pusic MV, Boutis K, Hatala R, et al. Learning curves in health professions education. *Acad Med*. 2015;90:1034–42.
 16. Levitov A, Mayo PH, Slonim AD. Training of the critical care physician as sonographer. In: Levitov A, Mayo PH, Slonim AD (editors) *Critical care ultrasonography*. 1st ed. New York: McGraw-Hill; 2009. pp. 45–57.
 17. Kaufman DM. Applying educational theory in practice. *BMJ*. 2003;326:213. McKay Co Inc.
 18. Hempel D, Stenger T, Dell’Orto MC, et al. Analysis of trainees’ memory after classroom presentations of didactical ultrasound courses. *Crit Ultrasound J*. 2014;6(1):10. Copyright Hempel et al. Licensee Springer 2014.
 19. Conlon TW, Ishizuka M, Himebauch AS, et al. Hemodynamic bedside ultrasound image quality and interpretation after implementation of a training curriculum for pediatric critical care medicine providers. *Pediatr Crit Care Med*. 2016;17(7):598–604.
 20. Kimura BJ, Sliman SM, Waalen J, Amundson SA, Shaw DJ. Retention of ultrasound skills and training in “point-of-care” cardiac ultrasound. *J Am Soc Echocardiogr*. 2016;29(10):992–7.
 21. Barsuk JH, Cohen ER, Williams MV, et al. Simulation-based mastery learning for thoracentesis skills improves patient outcomes: a randomized trial. *Acad Med*. 2018;93:729–35.
 22. Barsuk JH, McGaghie WC, Cohen ER, et al. Simulation-based mastery learning reduces complications during central venous catheter insertion in a medical intensive care unit. *Crit Care Med*. 2009;37:2697–701.
 23. Barsuk JH, Cohen ER, Wayne DB, et al. A comparison of approaches for mastery learning standard setting. *Acad Med*. 2018;93:1079–84.
 24. Ericsson KA. Deliberate practice and the acquisition and maintenance of expert performance in medicine and related domains. *Acad Med*. 2004;79(10 Suppl):s70–81.
 25. van de Wiel MWJ, Van den Bossche P, Janssen S, et al. Exploring deliberate practice in medicine: how do physicians learn in the workplace? *Adv Health Sci Educ*. 2011;16:81–95.
 26. LoPresti CM, Schnobrich DJ, Dversdal RK, et al. A road map for point-of-care ultrasound training in internal medicine residency. *Ultrasound J*. 2019;11:10.



Current and Future Challenges to Ultrasound Adoption in Clinical Practice

Thomas Conlon, Yogen Singh, Cécile Tissot, and María Victoria Fraga

Contents

Introduction	309
The Technology: Learning from History	310
The Processes: The Need for Programmatic Development	311
Putting the Pieces Together: Credentialing, Privileging, and Outcomes	314
How to Support the Individual Provider	314
Exploring the Final Competency Domain: Treatment Methods and the Protocolization of Bedside Ultrasound	316
References	317

T. Conlon (✉)

Department of Anesthesiology and Critical Care Medicine, Children's Hospital of Philadelphia, Philadelphia, PA, USA

Perelman School of Medicine, University of Pennsylvania, Pennsylvania, PA, USA
e-mail: Conlont@chop.edu

Y. Singh

Department of Pediatrics, Division of Neonatology, Loma Linda University School of Medicine, California, USA

Department of Pediatrics, Division of Neonatal and Developmental Medicine, Stanford University School of Medicine, California, UK

Department of Pediatrics, Division of Neonatology, University of Southern California, California, UK

ESPNIC Cardiovascular Dynamics Section and POCUS Working Group, Geneva, Switzerland
e-mail: YSingh@llu.edu

C. Tissot

Department of Pediatrics, Clinique des Grangettes, Chêne-Bougeries, Geneva, Switzerland

Introduction

The era of pediatric point of care ultrasound (POCUS) is upon us. Ultrasound technology is now ubiquitous in most acute care practice settings and both procedural and diagnostic ultrasound applications challenge previously defined standards of care. Ultrasound education is embedded within medical school curriculum and available to novice trainees as well as experienced clinicians practicing within non-imaging-based specialties. With the abundance of literature

M. V. Fraga

Department of Pediatrics, Division of Neonatology, Children's Hospital of Philadelphia, Perelman School of Medicine, University of Pennsylvania, Philadelphia, PA, USA

The Children's Hospital of Philadelphia, Pennsylvania, PA, USA

e-mail: fragam@chop.edu

supporting the use of ultrasound to improve the quality of care delivered at the bedside, why is its use not more widespread?

The delivery of care at the bedside of acutely ill children requires the integration of *technologies, processes, and people* [1]. This chapter focuses on the technologies and processes, but readers will identify that the people required for successful programmatic build and dissemination in practice are varied and include (but are not limited to) specialist clinicians, hospital administrators, and local information technologists. Delivery of *quality* care ensures that the interaction between technologies, processes, and people adhere to the idealized aims of our medical profession, as discussed in Chap. 1: “Introduction to Point of Care Ultrasound” [2, 3]. These ideals may be subtly different given local, regional, national, or international cultural differences, but regardless of their specifics, should serve as guideposts for care delivery.

The Technology: Learning from History

Changes in *technology*, as well as access to that technology, has been a constant in medicine and continues to evolve with time. We should expect that changes in technology at the bedside of care are not rapidly adopted. Indeed, over 200 years ago, a disruptive technology called “the stethoscope” confronted medicine and would change practice to this day [4].

How do we assess new technologies? If you attend any medical conference, you are likely to encounter the “newest and greatest” gadgets promoted by sales representatives who declare proprietary technological (and clinical outcome) superiority to current practice. So how do companies decide to pursue the production of technological innovations? They first ask a few basic questions about the characteristics and attributes of the technology (Table 1) [5]. Companies seek to answer these questions to optimize their return on investment. As clinicians integrate new technology in delivering clinical care, we should also seek a high return on our investment, specifically

Table 1 Characteristics and attributes of successful new technologies

Characteristics	<ul style="list-style-type: none"> • Is the technology a radical departure or improvement from previous technologies? • Does it stand alone as unique? • Is it simple to learn? Is implementation straightforward? • Can you add ideas to enhance its performance?
Attributes	<ul style="list-style-type: none"> • What are important performance measures and how does it perform? • What are the benefits to the user? • Is the technology easy to adopt?

by improving our clinical practice. Thus, we should ask many of the same questions asked by the business models within our defined framework of quality care.

Ultrasound has characteristics and attributes optimal for integration in clinical care. The technology stands alone in real-time visualization of anatomy and physiology both in procedural and diagnostic applications and represents a radical departure from prior methods of palpation and auscultation. The technology is already present in our units and, as highlighted throughout this book, we can adapt the technology to fit the needs of providers (clinicians) across varied clinical specialties. Thus, we can say that ultrasound has impressive *face validity* when it comes to incorporation within our practice.

We have many examples of technologies with robust face validity and considerable impact on our practice. Bioengineers developed pulse oximetry in the 1970s with clinical adoption in the 1980s [6]. Some technologies have such high face validity that there is no equipoise regarding integration in practice [7]. Despite the absent data of proven efficacy, pulse oximetry is considered the standard of care across diverse patient populations within varied clinical settings.

Face validity and equipoise need to be carefully considered words, though, when integrating technologies at the bedside. Critical care learned this through its experience with the pulmonary arterial catheter (PAC). PAC technology was also developed in the 1970s and had such face validity in the minds of criticologists that, by the mid-

1980s, PAC data guided the care of 40% of all ICU patients [8]. In the next 10 years, published studies emerged demonstrating problems with clinician interpretation of the data as well as PAC inaccuracies. Most notably, PACs used in clinical management resulted in worse patient outcomes [9]. Studies identified problems in technology, processes, and people resulting in the delivery of inferior care. The experience with the PAC remains important. Clinicians should combine face validity with relevant outcome data before widespread adoption of technologies within care delivery.

Throughout this book, the authors have provided supportive literature demonstrating that focused ultrasound applications: (1) are easily taught to novice providers, (2) are accurate in the identification of varied pathophysiologic processes, (3) provide timely diagnosis, (4) identify new, clinically relevant information, (5) change medical management, and (6) improve patient outcomes. Thus, the data support a wider adoption of ultrasound in acute care practice. Yet, we remain slow to universally adopt it in routine care.

The Processes: The Need for Programmatic Development

If we accept ultrasound as a safe and impactful technology to adopt in practice, then we need to assess the *processes* of translating ultrasound education into delivery of care. Institutional or governmental regulations often shape processes of care, and we define commonly used regulatory words relevant to focused ultrasound translation in Table 2. Despite a multitude of focused ultrasound courses delivered locally, nationally, and internationally, experience (and data) suggest that few learners will translate education into actual clinical practice [10]. If the goal of training is to develop reliable skills for ultrasound use in the clinical setting, then a provider should develop a level of *competency*. Unfortunately, there is no definition of competency in the practice of POCUS.

Competency is the presence of sufficient knowledge or skill [11]. Competency in POCUS

Table 2 Definitions of regulatory terms relevant to ultrasound practice

Licensing: Regulatory agency recognition that an individual clinician has completed qualifications to practice ultrasound. Licensing also involves ongoing continued education or training and potentially reexamination.

Credentialing: Employer recognition that an individual has completed qualifications to practice ultrasound. Credentialing can be independent of ultrasound applications or be considered within the scope of other credentialed activities. Credentialing is institution-specific and may be periodically updated.

Privileging: Employer recognition of a global skill set, which can include ultrasound, defining an individual's scope of practice within an institution. Credentials are assessed as a component of the privileging process.

Accreditation: Independent organization recognition that a healthcare entity/program has met defined standards.

Certification: Independent organization recognition that an individual has met defined standards in a skill outside of their current specialty-specific scope of practice. In ultrasound, certification by external agencies suggests that there has been training with oversight to a level of competency often verified through formal testing.

depends on the application and the definition of a minimum standard (what our community would consider “sufficient”). Competency should also result in clinical effectiveness, which incorporates not only meeting a performance standard but also avoiding underuse and misuse. Thus, each application should have a standard for assessing competency in performance and education should include indications, contraindications, and limitations to its use. There are likely similar competency domains across varied applications, including knowledge, psychomotor, interpretative, and medical decision-making domains [12]. Thus, even prior to receiving training or addressing competency, a provider should identify their *scope of practice* within their clinical domain. Ultrasound applications should address clinical questions that are frequently encountered, are amenable to ultrasound interrogation, have discrete qualitative or semi-quantitative measures (present/absent, small/moderate/large, normal/abnormal, mild/moderate/severe, etc.), and impact medical manage-

ment. For example, a pediatric emergency medicine clinician may greatly benefit from learning how to evaluate an abscess since this is a frequently encountered pathophysiology in their practice setting. The incorporation of ultrasound assessment by an emergency medicine provider will expedite quality care in the practice setting, and exposure to recurrent pathophysiologic processes will allow for longitudinal experiences providing depth and breadth to skill development and maintenance. In contrast, critical care clinicians infrequently encounter clinically relevant abscesses resulting in limited opportunities to develop clinically relevant skills that would impact care provided to patients. Critical care development of competency in abscess assessment may waste valuable time better spent in learning applications relevant to their specialty. As discussed in Chap. 21: “POCUS Guidelines, Training Curriculum, and Education”, pediatric specialty-specific guidelines will be invaluable in curricular design for learners.

Once pediatric specialties identify ultrasound applications and define competency standards, training alone is insufficient without complementary structural elements to ensure the translation

to quality care. *Implementation science* is a relatively new discipline promoting the systematic uptake of research and evidence-based practice to deliver quality and effective care [13]. Component-based implementation science models emphasize the need for environmental structural elements for the successful adoption of practice [14]. Thus, effective translation of ultrasound skill from education to the bedside requires a programmatic build for individual success (Fig. 1).

The American College of Emergency Physicians (ACEP) has been a leading organization in both developing coherent specialty-based guidelines as well as outlining the processes and structural elements required to translate education to quality care at the bedside [15]. ACEP guidelines identify five key structural elements for implementation: *Training, Documentation, Image Storage, Quality Assurance, and Credentialing*.

Chapter 21: “POCUS Guidelines, Training Curriculum, and Education” as well as earlier discussion within this chapter describes current thoughts regarding *training* in relevant applications and its requisite goals of competency development across evaluative domains. *Documentation* is the process by which provid-

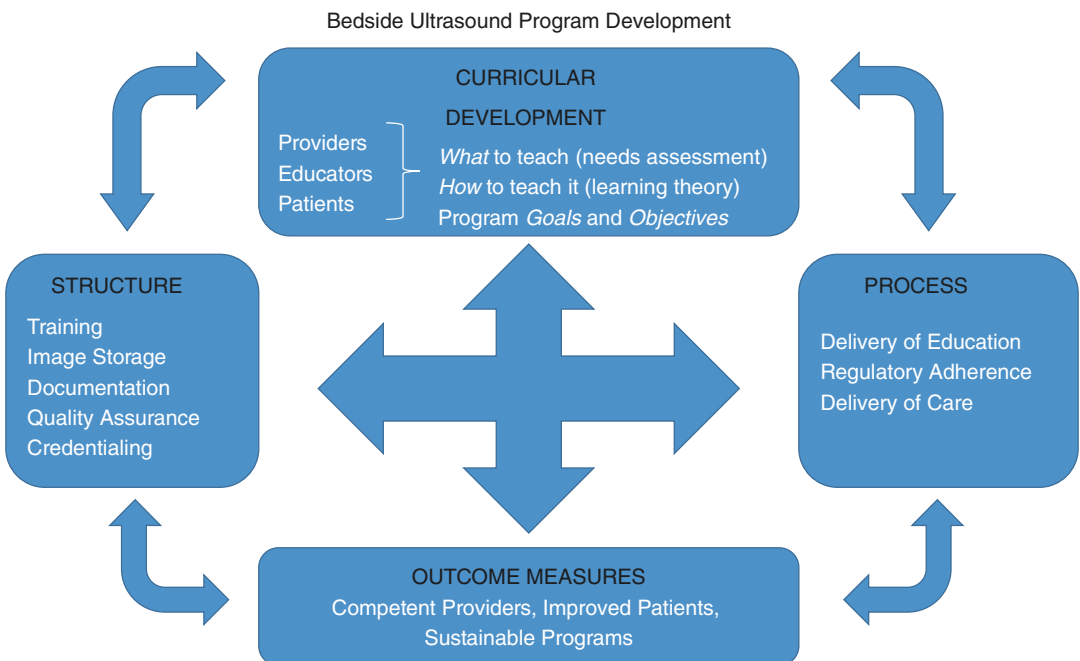


Fig. 1 Bedside Ultrasound Program Development

ers record their findings. During training, documentation for a learner is essential for iterative feedback regarding interpretative accuracy, one of the important domains within competency assessment. Appropriate documentation processes extend beyond training and have obvious implications in patient care. Local leadership should collaborate with administrators regarding policies involving documentation in clinical care, specifically within the patient's medical record. Performance of a bedside ultrasound in the clinical context always has the potential to identify important information, whether previously known or unknown. Thus, documentation with an accurate interpretation within the medical record of a patient is important to both their short-term and long-term care, and the development and growth of electronic medical records add to the need for standardized approaches consistent with local regulations. The individual providing any documentation of focused ultrasound interpretation in the medical record should have institutional authorization for providing focused ultrasound interpretations. We also suggest standardization of documentation in the medical record for consistency of reporting and ease of reading. Reports should also include the diagnostic limitations of focused ultrasound. In the United States, billing for studies requires specific documentation elements included in reports [16].

Image Storage is another recommended structural element in ultrasound program build. Storage solutions frequently require collaboration with local institutional information technology and/or radiology specialists with insights into current institutional storage platforms. Both proprietary and non-proprietary picture archiving and communication systems exist. Should there not be an institutional image storage solution, both trainees as well as those experienced in POCUS should identify a personal method of image storage adherent to patient information regulations. The *Quality Assurance* process, discussed further below, utilizes these saved images for assessment of developed and maintained competency in the image acquisition domain. Most all machines have, at minimum, a

universal serial bus (USB) port whereby portable USB drives can upload stored images. Studies solely for education have not always required incorporation within a patient's health record, though one should be familiar with local and national regulatory standards [17]. Many institutions consider *all* acquired images collected as within the scope of patient care, even if solely for the purpose of education, since they provide data regarding a patient's anatomy and physiology.

Quality assurance is the process whereby a program safeguards the translation of training to quality care delivery. Reviewers assess focused ultrasound studies performed in the educational or clinical setting for image quality and interpretation accuracy through this process. Providers with expertise in POCUS applications relevant to the studies assessed lead these structured review sessions. Early in programmatic development, there may not be an expert in POCUS applications within a division or department. Thus, developing programs should seek local imaging specialists (i.e., radiology or cardiology colleagues, or other POCUS specialists including emergency medicine colleagues) or remote tele-expertise. Anyone providing assessment of image acquisition and interpretation during review sessions should be familiar with the purpose of performed studies, have the clinical context of the study, and be aware of the application objectives and limitations as defined by local curriculum or specialty-specific guidelines.

A quality assurance process should also prioritize effective two-way communication between study performers and reviewers. Study performers should communicate the clinical setting of acquired studies, as well as any challenges encountered during study performance. They should also be able to provide contextual relevance of the study and impact in their assessment and management. Expert reviewers should be able to provide relevant feedback regarding study image acquisition and interpretation including suggestions for improvement. Importantly, quality assurance is not only for novice learners but also for those experienced in POCUS. Longitudinal quality assurance promotes contin-

ued education within this specialized area of clinical care delivery and provides another layer of safety for patients, providers, and institutions.

Putting the Pieces Together: Credentialing, Privileging, and Outcomes

Credentialing is institution-specific and is a pre-determined threshold of training and experience in a specific area of clinical practice. *Privileging* is the institutional allowance of care delivery in that clinical practice. Thus, credentialing represents the structure of institutionally-defined competency in practice, with privileging the end result of program build. Structured didactic and experiential training in defined specialty-specific applications should have oversight by providers experienced in respective imaging domains. Appropriate documentation and imaging solutions, adherent to local, national, and international standards, support quality assurance processes to assess development and longitudinal translation of skill to care delivery. Target thresholds of experience should define competency and be assessed through this quality assurance process. Once competency in a POCUS application is achieved, institutional Credentialing Committees should recognize developed skills through their credentialing process. Once an institution credentials an individual in a skill, they will often require documentation of maintenance of the skill.

Structural elements within programmatic build, and the implementation processes they support, often require multidisciplinary collaboration and significant effort in their construction. However, we have strong evidence that building this infrastructure results in programmatic success and the delivery of quality care. By structuring emergency medicine residency-focused ultrasound training programs in this fashion, diagnostic and procedural ultrasound applications are now components of Accreditation Council for Graduate Medical Education core competencies for emergency medicine residencies in the United States. Thus, the performance

of ultrasound is a component of *what it is to be* a modern emergency medicine physician. Evidence exists that structuring an ultrasound program in such a manner can be successful in other specialties. The Children's Hospital of Philadelphia developed a training program in critical care and neonatal-focused ultrasound based on ACEP guidelines. Program leaders modified core applications for appropriateness in the pediatric critical care setting, and multidisciplinary support by institutional leaders resulted in a credentialing process for clinicians [18].

Relevant outcomes should assess how the technologies, processes, and people interact in the delivery of high-quality care. Outcomes for successful programmatic build are broad and extend across an entire institution, including assessment of trainee skill development, departmental revenue generation (where applicable), and institutional medical-legal exposure. Most importantly, structural elements solidifying programmatic build allow for measures of improvement in patient outcomes. Though this book has described many of the impressive benefits of ultrasound in clinical care, we should continue to seek outcome data regarding its incorporation in daily clinical practice.

How to Support the Individual Provider

This chapter details the infrastructure suggested for effective focused ultrasound programmatic build. We also recognize that many institutions will be unable to support the time and energy required to develop and maintain these structural elements. A recent survey of United States pediatric critical care fellowship programs found that 67% of divisions were performing diagnostic-focused ultrasound studies, while <25% of institutions had documentation, image storage, or quality assurance processes in place [19]. Structural elements for program build were acknowledged by respondents to have a high *impact* on program development but also required high *effort*. Solutions to focused ultrasound integration in care require dedicated time and finan-

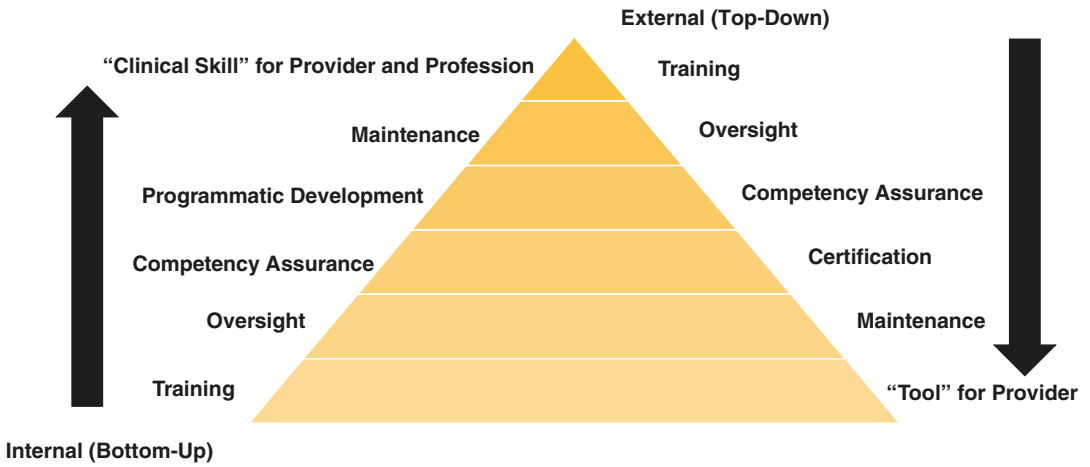


Fig. 2 Top-Down Versus Bottom-Up Approach to Individual Translation of Skill

cial investment. We suggest that solutions can be shared, thus reducing effort and cost to both providers and institutions. We also suggest two approaches to the large-scale development of individual skill that can translate to clinical care, what we will term a “top-down” (external) and a “bottom-up” (internal) approach (Fig. 2).

The top-down approach recognizes the potential contribution of societies, or external agencies, in supporting and validating training processes. Training supported by external agencies should include both initial as well as longitudinal support and have a mechanism for quality assurance across prespecified domains of competency. Formal testing of knowledge and/or psychomotor skill follows the completion of requisite steps within longitudinal training. Completion of longitudinal training and performance above the threshold on the test will result in *certification* by that external agency. Local institutions may then adopt certification as a component of credentialing and privileging individual providers. Longitudinal maintenance of skills can be locally developed or supported through an external agency as well.

An example of a successful translation of a “new” technology by the top-down approach is the introduction of perioperative transesophageal echocardiography (PTE) by adult anesthesiologists. PTE grew in practice among anesthesiologists in the early 1980s, emerging as a potentially

important technology for guiding perioperative therapies [20]. In 1988, the American Society of Echocardiography (ASE) realized the unique benefit of PTE in clinical care and the need for separate training for anesthesiologists [21]. In 1993, The American Society of Anesthesiologists (ASA) and the Society for Cardiothoracic Anesthesiologists (SCA) partnered to define essential knowledge, skill, and training objectives within basic and advanced PTE platforms [22]. Following this, the ASA and SCA partnered with the American Society of Echocardiography. In 1998 the groups created the National Board of Echocardiography to develop and administer echocardiographic exams including the adult special competency in echocardiography examination (ASCeXAM) and perioperative TEE examination (PTE-examination). Thus, pathways to certification by an external agency exist in PTE for individual providers.

The benefit of the top-down approach is that there is a centralized and standardized approach to developing a skill. Developing a certification process through an external agency may shift the burden of oversight away from local departments unable to support the time and effort required for training. However, there are challenges with such a system [23]. First, certification through formalized testing and external oversight is often expensive. Recently, the Society of Critical Care Medicine worked with NBE to develop the

Examination of Special Competence in Critical Care Echocardiography (CCEeXAM) at a current cost of approximately \$1000 USD. This does not include costs such as an initial training course or subsequent test preparatory review courses which will also run costs into the thousands of USD. Second, certification by an external agency frequently *still* requires local training solutions. Using the same example, the CCEeXAM requires an experiential component developed either through supervised clinical training (typically residency or fellowship) or through what is termed a “Practice Experience Pathway” whereby clinical exams are logged and supervised by local experts [24]. In this example, regardless of the pathway (supervised training vs. practice experience) there is a requirement for local infrastructural support.

Emergency medicine successfully embraced the bottom-up approach in the incorporation of the Focused Assessment with Sonography in Trauma (FAST) exam within clinical practice. The FAST exam was first developed in Europe in the 1970s as a rapid method of evaluating the presence of blood in the abdomen or pericardial space following abdominal trauma [25]. From the 1970s thru the 1980s, the growing literature suggested that the technology had superior test characteristics compared to prior gold standards of clinical assessment and non-imaging-based clinicians were reliable in performance and interpretation [26, 27].

Interestingly, the emergence of the FAST exam by clinicians coincided with the development of emergency medicine as a specialty. In 1979, the American Board of Medical Specialties (ABMS) recognized emergency medicine as an independent discipline following American Board of Emergency Medicine incorporation in 1976 [28]. It is not surprising that ultrasound use in emergent clinical conditions arose alongside the growth of the emergency medicine profession. The FAST exam remains well entrenched within emergency medicine ultrasound guidelines and serves as an example of the power of ultrasound in the hands on non-traditionally imaging-based clinicians. The importance of the FAST exam in shaping quality care has allowed

for continued explorations of applications beneficial to providers and patients alike.

The bottom-up approach supports standardization in practice across a specialty, though allows for local influences on training and practice. This approach requires a local program built to support translation of skill to clinical practice. It does not create pathways to certification, though external agency testing can complement efforts. Local programmatic build results in defining specialty-specific requirements for a specialty-specific physician, or stated a different way, defines *what it is to be* a specialty-specific physician. Ultrasound applications adopted in this manner become part of training platforms within specialty residency and fellowship programs as evidenced by ACGME requirements in training for adult emergency medicine and critical care [29, 30].

Exploring the Final Competency Domain: Treatment Methods and the Protocolization of Bedside Ultrasound

Throughout this chapter, we have focused on two elements of competency: image acquisition quality and study interpretation accuracy. The third domain of competency is delivering appropriate treatment following ultrasound study. Clinicians frequently equate protocols with the appropriateness of treatment in the current era of practice embracing quality and safety ideals. Indeed, the medical field has learned about the benefits of standardization and protocolization since Early Goal Directed Therapy (EGDT) demonstrated mortality benefits assigned to well-structured care processes [31]. EGDT also taught us that the individual elements within protocols (for example, central venous pressure, mixed venous oxygen saturation, hemoglobin levels, and mean arterial pressure) leading providers to their treatment decisions may not actually be the causal elements of outcomes [32]. Thus, protocols may improve care, but we should be mindful to study the individual elements within protocols and maintain the intellectual and clinical flexibility to

modify our actions when improved methods of assessment are available.

For example, the previously discussed FAST exam had important outcome benefits when incorporated into the adult management of trauma. Yet, in many pediatric institutions, clinicians do not employ the FAST exam as a first-line method of trauma assessment due to poor performance characteristics within this specific population (see Chap. 14 “Abdominal Point-of-Care Ultrasound in Neonatal and Pediatric Populations”) [33]. Protocols are only as strong as the elements upon which they are constructed and the technologies/policies/people gathering the data. Protocols are not infallible and may not represent current evidence-based best practice.

Certainly, in this era emphasizing quality and safety, protocols and structure are essentials of care delivery. Thus, an ultrasound performed within clinical applications should have consistency in performance. In procedural ultrasound, pre- and post-procedural checklists improve provider performance and patient safety [34]. In diagnostic ultrasound there are numerous adult protocols for assessing pathophysiologic processes beyond the previously discussed FAST exam [35–40]. Applications described in prior chapters have single-study methodologies demonstrating beneficial outcomes, but widespread adoption of pediatric-specific non-imaging specialty applications remain absent from practice.

Without well-studied protocols, how do we assess appropriateness of our therapeutic decisions? This last domain of competency is the most difficult to assess, whether in focused ultrasound or *any* clinical practice. Therapies may align with protocols, but therapeutic outcomes alone define therapeutic appropriateness. We should not cease from working towards this domain of competency for this is, in fact, the ultimate challenge we have as clinicians.

With the lack of high-quality evidence around the use of POCUS during neonatal or pediatric resuscitation, and in managing neonatal and pediatric emergencies, it is a challenge to introduce them in acute care protocols in pediatric practice. However, such protocols already exist

in adult practice as well as pediatric emergency medicine, and clearly show benefit in understanding pathophysiology and targeting specific interventions earlier. Hence, we believe that despite current and future challenges it is time to develop POCUS training curriculum, develop training programs, and adopt its use in neonatal and pediatric emergency protocols.

References

1. Slonim AD, Pollack MM. Integrating the Institute of Medicine’s six quality aims into pediatric critical care: relevance and applications. *Pediatr Crit Care Med*. 2005;6(3):264–9.
2. IOM (Institute of Medicine). *Crossing the quality chasm: a new health system for the 21st century*. Washington, DC: National Academy Press; 2001.
3. Schlander M. *Health technology assessments by the National Institute for Health and Clinical Excellence*. New York: Springer Science+Business Media; 2007.
4. *A treatise on the diseases of the chest by R.T.H. Laennec, Translated from French to English by John Forbes, Translator’s Preface by John Forbes, Start Page i, Quote Page xviii–xix, Printed for T. and C. Underwood, London. [Facsimile of the London 1821 Edition Published in 1962 by Hafner Publishing, New York]*.
5. <http://www.trilogyassociates.com/pdf/TechAssessment.pdf> as found on 1/20/2021.
6. Van Meter A, Williams U, Zavala A, et al. Beat to beat: a measured look at the history of pulse oximetry. *J Anesth Hist*. 2017;3:24–6.
7. Smith GC, Pell JP. Parachute use to prevent death and major trauma related to gravitational challenge: systematic review of randomised controlled trials. *BMJ*. 2003;327:1459–61.
8. Marik PE. Obituary: pulmonary artery catheter 1970–2013. *Ann Intensive Care*. 2013;3:38.
9. Connors AF, Speroff T, Dawson NV, et al. The effectiveness of right heart catheterization in the initial care of critically ill patients. *JAMA*. 1996;276:889–97.
10. Conlon T, Su E, Hirshberg E, et al. Benefits and barriers to bedside ultrasound: a survey of the SCCM Pediatric Ultrasound Course. (Abstract). *Crit Care Med*. 2016;44:175.
11. <https://www.merriam-webster.com/dictionary/competency> as found on 1/25/2021.
12. Costantino T, Burton J, Tayal V. Ultrasound competency and practice: what’s in a number? *Acad Emerg Med*. 2015;22:597–9.
13. Damschroder LJ, Aron DC, Keith RE, et al. Fostering implementation of health services research findings

- into practice: a consolidated framework for advancing implementation science. *Implement Sci.* 2009;4:50.
14. Villalobos Dintrans P, Bossert TJ, Sherry J, Kruk ME. A synthesis of implementation science frameworks and application to global health gaps. *Glob Health Res Policy.* 2019;4:25.
 15. Ultrasound guidelines: emergency, point-of-care and clinical ultrasound guidelines in medicine. *Ann Emerg Med.* 2017;69:e27-e54.
 16. Facep SH, Facep ED. Ultrasound coding and reimbursement document 2009 Table of Contents.
 17. Dougherty M, Washington L. Defining and disclosing the designated record set and the legal health record. *J AHIMA.* 2008;79(4):65–8.
 18. Conlon TW, Himebauch AS, Fitzgerald JC, et al. Implementation of a pediatric critical care focused bedside ultrasound training program in a large academic PICU. *Pediatr Crit Care Med.* 2015;16:219–26.
 19. Conlon TW, Kantor DB, Su ER, et al. Diagnostic bedside ultrasound program development in pediatric critical care medicine: results of a national survey. *Pediatric Crit Care Med.* 2018;19:e561–8.
 20. Aronson S, Thys DM. Training and certification in perioperative transesophageal echocardiography: a historical perspective. *Anesth Analg.* 2001;93:1422–7.
 21. Pearlman AS, Gardin JM, Martin RP, et al. Guidelines for physician training in transesophageal echocardiography: recommendation of the American Society of Echocardiography Committee for Physician Training in Echocardiography. *J Am Soc Echocardiogr.* 1992;5:187–94.
 22. Practice guidelines for perioperative transesophageal echocardiography. A report by the American Society of Anesthesiologists and the Society of Cardiovascular Anesthesiologists Task Force on Transesophageal Echocardiography. *Anesthesiology* 1996; 84:986–1006.
 23. Cormican D, Winter D, Sheu R. Practice patterns for the use of perioperative transesophageal echocardiography: a practice not yet made perfect. *J Cardiothorac Vasc Anesth.* 2019;33:134–6.
 24. https://echoboards.org/docs/CCEeXAM-Cert_App-2020.pdf as found on 1/25/2021.
 25. Kristensen JR, Bueman B, Keuhl E. Ultrasonic scanning in the diagnosis of splenic haematomas. *Acta Chir Scand.* 1971;137:653–7.
 26. Tiling T, Bouillon B, Schmid A. Ultrasound in blunt abdominotoracic trauma. In: Border J, Algoewer M, Reudi T, editors. *Blunt multiple trauma.* New York: Marcel Dekker; 1990.
 27. Ma OJ, Mateer JR, Ogata M, et al. Prospective analysis of a rapid trauma ultrasound examination performed by emergency physicians. *J Trauma.* 1995;38:879–85.
 28. Suter RE. Emergency medicine in the United States: a systemic review. *World J Emerg Med.* 2012;3(1):5–10.
 29. As found on: <https://www.acgme.org/Portals/0/PDFs/Milestones/EmergencyMedicineMilestones.pdf?ver=2015-11-06-120531-877>; as found on January 28, 2021.
 30. As found on: file:///C:/Users/conlon/Desktop/SCCM/FUSED/Book/CriticalCareMedicineSupplementalGuide.pdf; as found on January 28, 2021.
 31. Rivers E, Nguyen B, Havstad S, et al. Early goal-directed therapy in the treatment of severe sepsis and septic shock. *N Engl J Med.* 2001;345:1368–77.
 32. Nguyen HB, Jaehne AK, Jayaprakash N, et al. Early goal-directed therapy in severe sepsis and septic shock: insights and comparisons to ProCESS, ProMISE, and ARISE. *Crit Care.* 2016;20:160.
 33. Holmes JF, Kelley KM, Wootton-Gorges SL, et al. Effect of abdominal ultrasound on clinical care, outcomes, and resource use among children with blunt torso trauma: a randomized clinical trial. *JAMA.* 2017;317:2290–6.
 34. Barsuk JH, McGaghie WC, Cohen ER, et al. Use of simulation-based mastery learning to improve the quality of central venous catheter placement in a medical intensive care unit. *J Hosp Med.* 2009;4:397–403.
 35. Holm JH, Frederiksen CA, Juhl-Olsen P, et al. Perioperative use of focus assessed transthoracic echocardiography (FATE). *Anesth Analg.* 2012;115:1029–32.
 36. Oveland NP, Bogale N, Waldron B, et al. Focus assessed transthoracic echocardiography (FATE) to diagnose pleural effusions causing haemodynamic compromise. *Case Rep Clin Med.* 2013;2:189–93.
 37. Atkinson PR, McAuley DJ, Kendall RJ, et al. Abdominal and cardiac evaluation with sonography in shock (ACES): an approach by emergency physicians for the use of ultrasound in patients with undifferentiated hypotension. *Emerg Med J.* 2009;26:87–91.
 38. Breikreutz R, Walcher F, Seeger FH. Focused echocardiographic evaluation in resuscitation management: concept of an advanced life support-conformed algorithm. *Crit Care Med.* 2007;35:S150–61.
 39. Breikreutz R, Price S, Steiger HV, et al. Focused echocardiographic evaluation in life support and periresuscitation of emergency patients: a prospective trial. *Resuscitation.* 2010;81:1527–33.
 40. Ghane MR, Gharib M, Ebrahimi A, et al. Accuracy of early rapid ultrasound in shock (RUSH) examination performed by emergency physician for diagnosis of shock etiology in critically ill patients. *J Emerg Trauma Shock.* 2015;8:5–10.



Correction to: Echocardiographic Evaluation of Left Ventricular Function and Hemodynamic Status

Cécile Tissot, Nicole Sekarski, and Yogen Singh

Correction to:
Chapter 5 in: Y. Singh et al. (eds.), *Point-of-Care Ultrasound for the Neonatal and Pediatric Intensivist*,
https://doi.org/10.1007/978-3-031-26538-9_5

In Chapter 5: Echocardiographic Evaluation of Left Ventricular Function and Hemodynamic Status, in the formulas, the **X (multiply sign) has been incorrectly replaced by the ? symbol**, which has now been corrected.

The publisher apologizes to the Editors and to their readers.

The updated original version of this chapter can be found at
https://doi.org/10.1007/978-3-031-26538-9_5

Appendix: Learning Outcomes

Basics in Critical Care and Neonatal Focused Ultrasound

Learning Outcomes Chapter 1: Introduction to Focused Ultrasound in Neonates and Children (Thomas Conlon, Cécile Tissot, Maria V Fraga, Yogen Singh)

- Discuss the history of ultrasound technology and its integration in medical practice.
- Identify factors related to the dissemination of ultrasound practice across traditionally non-imaging specialties.
- Describe current challenges to ultrasound implementation in pediatric acute care settings.

Learning Outcomes Chapter 2: Physics, Knobology and Probes—Imaging Optimization (Jason Z. Stoller, Yogen Singh, Cécile Tissot)

- Describe how to select the appropriate probe for your study.
- Discuss how ultrasound waves are transmitted and received so as to create images on a screen, including the various echogenic characteristics of tissues.

- Describe how to adjust and optimize the quality of ultrasound images.
- Identify how “artifacts” are created and recognize how they help us interpret anatomy and pathology.
- Explain the various modes of ultrasound imaging including appropriate clinical applications of B-mode, M-mode, and Doppler modalities.
- Discuss proper maintenance of an ultrasound machine.

Cardiovascular System Assessment

Learning Outcomes Chapter 3: Basic Echocardiographic Views for the Pediatric Intensivist (Cécile Tissot, Yogen Singh)

- Explain how a basic echocardiographic assessment can assist in the assessment and management of children with critical illness.
- Describe strengths and weaknesses of the core views of an echocardiographic assessment for the pediatric intensivist.
- Discuss the probe position for acquisition and correct plane for assessment of each basic view.
 - Basics of Cardiac Anatomy/Physiology
 - Ultrasound Views
 - Assessment of Pathophysiology

Learning Outcomes Chapter 4: POCUS in Shock and Volume Status (Saul Flores, Fabio Savorgnan, David Kantor)

- Define fluid responsiveness.
- Differentiate between static and dynamic measures of fluid responsiveness and describe methods of assessing fluid responsiveness using.
- Integrate volume status and cardiac assessment in a standardized approach to the management of pediatric shock.
 - Physiology
 - Ultrasound Views
 - Assessment of Pathophysiology

Learning Outcomes Chapter 5: Assessing Left Ventricular Function (Cécile Tissot, Nicole Sekarski, Yogen Singh)

- Differentiate qualitative and quantitative methods of left ventricular function.
- Describe strengths and limitations of basic cardiac views for left ventricular functional assessment.
- Discuss how preload and afterload conditions impact varied measures of left ventricular function.
 - Anatomy/Physiology of the Left Ventricle
 - Ultrasound Views
 - Assessment of Pathophysiology

Learning Outcomes Chapter 6: Focused Ultrasound in Right Ventricular Function, Pulmonary Hypertension (Shazia Bhombal, Shahab Noori, Yogen Singh, Maria V Fraga)

- Describe the morphology of the right ventricle and implications in assessing right ventricular function.
- Describe methods of assessing qualitative and quantitative right ventricular functional assessment.

- Discuss methods of assessing the presence of pulmonary hypertension using basic cardiac views and introduce advanced views for qualitative and quantitative assessment of pulmonary hypertension.
 - Anatomy/Physiology
 - Ultrasound Views
 - Assessment of Pathophysiology

Learning Outcomes Chapter 7: Focused Assessment of Pericardial Effusion and Cardiac Tamponade (Yogen Singh, Farha Vora, Cécile Tissot)

- Identify optimal cardiac views for assessing the presence of pericardial effusion.
- Discuss the underlying physiology characterizing tamponade.
- Describe echocardiographic findings associated with hemodynamic perturbations associated with tamponade physiology.
 - Anatomy/Physiology
 - Ultrasound Views (including procedural)
 - Assessment of Pathophysiology

Learning Outcomes Chapter 8: Advanced Functional Echocardiographic Views Including PDA Assessment and Hemodynamic Evaluation (Yogen Singh, Sebastien Joye, Cécile Tissot)

- Describe how to acquire and optimize views of the PDA.
- Discuss the interpretation of the PDA and implications in medical management.
- Describe superior vena cava view acquisition and flow interpretation in the context of critical illness.
 - Anatomy/Physiology of the PDA
 - Ultrasound Views
 - Assessment of Pathophysiology

**Learning Outcomes Chapter 9:
Comprehensive Echocardiography and
Diagnosis of Major Common Congenital
Heart Defects (Nicole Sekarski, Cécile
Tissot, Yogen Singh)**

- Describe cardiac embryology and associations with congenital heart defects.
- Identify the roles of comprehensive echocardiography and focused echocardiography in the identification of congenital heart defects.
- Discuss a structured approach to screening for clinically relevant cardiac defects in the neonatal time period.
 - Anatomy
 - Ultrasound Views
 - Assessment of Pathophysiology

**Learning Outcomes Chapter 11: Airway
Ultrasound in Children and Neonates
(Erik Su, Bereketeab Haileselassie)**

- Discuss airway anatomy and impact on acquisition of ultrasound images.
- Describe direct and indirect techniques to assess endotracheal and transtracheal intubation using ultrasound.
- Identify indications and methods to assess vocal cord function in children.
 - Anatomy
 - Ultrasound Views
 - Assessment of Pathophysiology

Thoracic Assessment

**Learning Outcomes Chapter 10: Basic
Focused Lung Ultrasound for the Intensivist
(Adam S. Himebauch, Akira Nishisaki)**

- Discuss methods of ultrasound interrogation of the thoracic cavity.
- Describe how artifacts assist in assessing lung pathophysiologic processes including pneumothorax.
- Differentiate effusions from atelectatic or consolidated lung.
 - Anatomy/Physiology
 - Ultrasound Views
 - Assessment of Pathophysiology (pneumonia, bronchiolitis, reactive airway disease)

**Learning Outcomes Chapter 12:
Diaphragmatic Ultrasound (Joel K. B. Lim,
Jan Hau Lee, Mark D. Weber)**

- Describe the functional anatomy of the diaphragm and conditions associated with diaphragmatic dysfunction.
- Identify methods of qualifying and quantifying diaphragmatic weakness in critical illness as well as clinical significance of these findings.
- Describe indications and methods to assess diaphragm paralysis.
 - Anatomy
 - Ultrasound Views
 - Assessment of Pathophysiology

Learning Outcomes Chapter 13: Clinical Applications in Focused Thoracic Assessment in Neonates and Children (Nadya Yousef, Daniele De Luca)

- Describe the lung ultrasound score.
- Discuss applications of the lung ultrasound score in adult critical illness.
- Identify how lung ultrasound score can be employed in the assessment and management of pediatric ARDS and neonatal RDS.
 - Special Anatomic Considerations in Neonates
 - Scoring Systems Using Views
 - Unique Thoracic Pathophysiologies with Treatments Guided by Ultrasound

Abdominal Assessment

Learning Outcomes Chapter 14: Basic Abdominal Focused Ultrasound (Yasser Elsayed, Vidit Bhargava)

- Describe indications for critical care ultrasound assessment of the abdomen including the FAST or free fluid examination.
- Discuss the spectrum of findings in neonatal enterocolitis and other bowel pathophysiologic processes.
- Describe the assessment of the bladder including and evidence of abnormalities within varied clinical contexts.
 - Anatomy
 - Ultrasound Views
 - Assessment of Pathophysiology

Neurosonology

Learning Outcomes Chapter 15: Focused Cranial Ultrasound for Neurointensive Care (Marlina Lovett, Kerri LaRovere, Nicole O'Brien)

- Identify neuroanatomy accessible by ultrasound interrogation.
- Identify indications for TCD in pediatric populations and literature supporting the role of both imaging and non-imaging TCD in clinical applications.
- Discuss the current state of optic nerve sheath diameter measurements for elevated intracranial pressure as well as a guided retinal exam for identification of retinal hemorrhages, retinoschisis, retinal detachment, vitreous hemorrhages, and vitreous detachment.
 - Anatomy
 - Ultrasound Views
 - Assessment of Pathophysiology

Learning Outcomes Chapter 16: Neonatal Brain Ultrasound (Pradeep Suryawanshi, Reema Garegrat, Yogen Singh)

- Discuss applications of basic head ultrasound in pediatric/neonatal critical care.
- Demonstrate a standardized approach to evaluation using head ultrasound.
- Discuss pathological processes and findings within head ultrasound studies.
 - Anatomy
 - Ultrasound Views
 - Assessment of Pathophysiology

Focused Ultrasound in Transport Setting

Learning Outcomes Chapter 17: Rapid Focused Ultrasound Assessment of a Crashing Infant and Child in Transport Setting (Sajeev Job, Michael J. Griksaitis, Yogen Singh)

- Defer learning objectives.

- Describe the technique for performing lumbar-puncture using ultrasound as an adjunct technology.
 - Anatomy
 - Ultrasound Views
 - Assessment of Pathophysiology

Procedural Ultrasound

Learning Outcomes Chapter 18: Vascular Access Considerations in Children and Neonates (Mark D. Weber, Benjamin Kozyak, Maria V Fraga)

- Describe the proper technique of central and peripheral venous and arterial vascular access using ultrasound and literature supporting its use.
- Contrast the strengths and limitations of the short and long axis approaches to vascular access.
- Discuss the importance of maintaining needle tip visualization throughout procedures and the use of the step-down technique.
- Discuss strengths and limitations to ultrasound use in procedural applications.
 - Anatomy
 - Ultrasound Views

Learning Outcomes Chapter 20: Considerations in Pediatric and Neonatal ECMO Cannulation (Ivanna Maxson, Erik Su)

- Describe optimal ultrasound views for transthoracic assessment of appropriate ECMO cannula placement and positioning.
- Discuss clinical scenarios in which ultrasound may assist in troubleshooting ECMO circuit challenges in pediatric and neonatal critical illness.

Anatomy
 Ultrasound Views
 Assessment of Pathophysiology

Programmatic Considerations and Moving Forward

Learning Outcomes Chapter 21: POCUS Guidelines, Training curriculum and Education (Thomas Conlon, Sam Rosenblatt, Adam S. Himebauch, Christie Glau, Akira Nishisaki, Yogen Singh)

- Describe the need for bedside ultrasound training programs in pediatric practice.
- Discuss experience- and literature-based approaches to successful ultrasound education for both novice and experienced learners.

Learning Outcomes Chapter 19: Ultrasound-Guided Procedures Beyond Vascular Access (Jesse Wenger, Grace Chong)

- Discuss translating landmark techniques to ultrasound-guided techniques in drainage procedures including thoracentesis, paracentesis, pericardiocentesis, and suprapubic catheterization.

Learning Outcomes Chapter 22: Future Developments: Certification, Accreditation, Continued Medical Education (CME), Advances in POCUS Technology and Future Protocols (Thomas Conlon, Yogen Singh, Cécile Tissot, Maria V Fraga)

- Define 3Cs: competence, certification, and credentialing important in the development of programmatic implementation.

- Discuss necessary components to develop and maintain a bedside ultrasound program within the context of the international critical care community.